# Vortices in high-temperature superconductors

## G. Blatter

*Theoretische Physik, Eidgenössische Technische Hochschule Zürich-Hönggerberg, CH-8093 Zürich, Switzerland\**
*and Asea Brown Boveri, Corporate Research, CH-5405 Baden, Switzerland*

## M. V. Feigel'man

*L. D. Landau Institute for Theoretical Physics, 117940 Moscow, Russia*
*and The Weizmann Institute of Science, Rehovot 76100, Israel*

## V. B. Geshkenbein

*Theoretische Physik, Eidgenössische Technische Hochschule Zürich-Hönggerberg, CH-8093 Zürich, Switzerland;*
*L. D. Landau Institute for Theoretical Physics, 117940 Moscow, Russia;*
*and The Weizmann Institute of Science, Rehovot 76100, Israel*

## A. I. Larkin

*L. D. Landau Institute for Theoretical Physics, 117940 Moscow, Russia*
*and The Weizmann Institute of Science, Rehovot 76100, Israel*

## V. M. Vinokur

*Argonne National Laboratory, Argonne, Illinois 60439*

With the high-temperature superconductors a qualitatively new regime in the phenomenology of type-II superconductivity can be accessed. The key elements governing the statistical mechanics and the dynamics of the vortex system are (dynamic) thermal and quantum fluctuations and (static) quenched disorder. The importance of these three sources of disorder can be quantified by the Ginzburg number $Gi = (T_c/H_c^2 \varepsilon \xi^3)^2/2$, the quantum resistance $Qu = (e^2/\hbar)(\rho_n/\varepsilon \xi)$, and the critical current-density ratio $j_c/j_0$, with $j_c$ and $j_0$ denoting the depinning and depairing current densities, respectively ($\rho_n$ is the normal-state resistivity and $\varepsilon^2 = m/M < 1$ denotes the anisotropy parameter). The material parameters of the oxides conspire to produce a large Ginzburg number $Gi \sim 10^{-2}$ and a large quantum resistance $Qu \sim 10^{-1}$, values which are by orders of magnitude larger than in conventional superconductors, leading to interesting effects such as the melting of the vortex lattice, the creation of new vortex-liquid phases, and the appearance of macroscopic quantum phenomena. Introducing quenched disorder into the system turns the Abrikosov lattice into a vortex glass, whereas the vortex liquid remains a liquid. The terms "glass" and "liquid" are defined in a dynamic sense, with a sublinear response $\rho = \partial E/\partial j|_{j \to 0}$ characterizing the truly superconducting vortex glass and a finite resistivity $\rho(j \to 0) > 0$ being the signature of the liquid phase. The smallness of $j_c/j_0$ allows one to discuss the influence of quenched disorder in terms of the weak collective pinning theory. Supplementing the traditional theory of weak collective pinning to take into account thermal and quantum fluctuations, as well as the new scaling concepts for elastic media subject to a random potential, this modern version of the weak collective pinning theory consistently accounts for a large number of novel phenomena, such as the broad resistive transition, thermally assisted flux flow, giant and quantum creep, and the glassiness of the solid state. The strong layering of the oxides introduces additional new features into the thermodynamic phase diagram, such as a layer decoupling transition, and modifies the mechanism of pinning and creep in various ways. The presence of strong (correlated) disorder in the form of twin boundaries or columnar defects not only is technologically relevant but also provides the framework for the physical realization of novel thermodynamic phases such as the Bose glass. On a macroscopic scale the vortex system exhibits self-organized criticality, with both the spatial and the temporal scale accessible to experimental investigations.

## CONTENTS

---

\*Permanent address.

## LIST OF SYMBOLS

| Symbol | Description | Ref. |
|---|---|---|
| $\mathbf{A}$ | vector potential | (2.1) |
| $\mathbf{A}^{(2)}$ | planar component of vector potential | (8.1) |
| $A_{ij}$ | bond vector potential | (7.4) |
| $a_\Delta$ | vortex lattice constant | (2.15) |
| $a_\circ$ | inverse square-root vortex density | (2.16) |
| $\mathbf{B}$ | magnetic induction | (2.1) |
| $B_{\mathrm{BG}}$ | Bose-glass field | Fig. 45 |
| $B_{\mathrm{dc}}$ | decoupling field | (8.147) |
| $B_{\mathrm{dp}}$ | lattice depinning field | (4.88) |
| $B^{\mathrm{ED}}$ | entanglement-disentanglement field | Fig. 23 |
| $B_m$ | lattice melting field | (4.107) |
| $B_{\mathrm{lb}}$ | large-bundle field | (4.51) |
| $B_{\mathrm{rb}}$ | bundle field (columnar defects) | (9.44) |
| $B_{\mathrm{sb}}$ | small-bundle field | (2.79) |
| $B_{\mathrm{sc}}$ | scaling field (anisotropy) | (4.115) |
| $B_\Phi$ | ion-flux equivalent field (columnar defects) | (9.44) |
| $B_{\mathrm{2D}}$ | 2D crossover field (layered sc) | (8.124) |
| $C$ | elastic modulus | (3.103) |
| $C$ | Euler constant | (3.69) |
| $c$ | constant | |
| $c$ | velocity of light | |
| $c_L$ | Lindemann number | (4.104) |
| $c_{11}$ | compression modulus | (3.31) |
| $\hat{c}_{11}$ | homogeneous compression modulus, $c_{11}(0)$ | |
| $c_{44}$ | tilt modulus | (3.31) |
| $\hat{c}_{44}$ | homogeneous tilt modulus, $c_{44}(0)$ | |
| $c_{66}$ | shear modulus | (3.32) |
| $d$ | layer distance | |
| $d$ | sample size | |
| $d_r$ | rod distance | |

| | | |
|---|---|---|
| $d_{TP}$ | twinning plane distance | |
| $\mathbf{E}$ | electric field | (2.52) |
| $E_d$ | disorder potential | (3.141) |
| $E_k$ | kink energy | (3.118) |
| $E_{pin}$ | pinning energy density (vortex lattice) | (3.89) |
| $\mathscr{E}_{pin}(L)$ | pinning energy (vortex segment) | (2.40) |
| $\mathscr{E}_{pin}(V)$ | pinning energy | (4.73) |
| $e_J$ | line energy (Josephson vortex) | (8.16) |
| $e_l$ | line energy | (2.13) |
| $F$ | free-energy density | |
| $F$ | force density | |
| $\mathscr{F}$ | free-energy functional | (2.31) |
| $\mathbf{F}_L$ | Lorentz force density (vortex lattice) | (3.92) |
| $\mathbf{F}_{pin}$ | pinning force density (vortex lattice) | (3.91) |
| $\mathscr{F}_{pin}(L)$ | pinning force (vortex segment) | |
| $\mathscr{F}_{pin}(V)$ | pinning force | |
| $\mathbf{F}_\eta$ | friction force density (vortex lattice) | (3.92) |
| $\mathbf{f}_L$ | Lorentz force (vortex line) | (2.19) |
| $f_{pin}$ | pinning force (single defect) | (2.43) |
| $\mathbf{f}_{pin}$ | pinning force (vortex line) | (2.29) |
| $G$ | Green's function | (2.114) |
| $G$ | Gibbs free-energy density | |
| $\mathscr{G}$ | Gibbs free-energy functional | (2.1) |
| $Gi$ | Ginzburg number | (2.47) |
| $Gi^{2D}$ | 2D Ginzburg number | (8.104) |
| $\mathbf{H}_a$ | applied magnetic field | (8.59) |
| $H_c$ | GL thermodynamic critical field | (2.7) |
| $H_{c_1}$ | lower critical field | (2.13) |
| $H_{c_2}$ | upper critical field | (2.17) |
| $H_{c\,BCS}$ | BCS thermodynamic critical field | (3.69) |
| $\mathbf{h}_{ac}$ | (ac) magnetic-field amplitude | (10.22) |
| $\mathscr{J}$ | stiffness constant | (8.70) |
| $J_{ij}$ | coupling constant | (7.1) |
| $j$ | current density | |
| $j_c$ | critical current density | (2.29) |
| $j_c^c$ | in-plane critical current density ($\mathbf{B}\|c$) | (2.151) |
| $j_{CDW}$ | CDW-type current density | (4.69) |
| $j_c^{in}$ | intrinsic critical current density ($\mathbf{B}\perp c$) | (8.158) |
| $j_{cr}$ | crossover current density (vortex liquid) | (6.43) |
| $j_c^{2D}$ | 2D critical current density ($\mathbf{B}\|c$) | (8.222) |
| $j_J$ | Josephson current density | (8.8) |
| $j_{lb}$ | large-bundle current density | (4.69) |
| $j_{pc}$ | pancake depinning current density | (8.218) |
| $j_{sb}$ | small-bundle current density | (2.78) |
| $j_{sv}$ | single-vortex critical current | (4.50) |

| | | |
|---|---|---|
| | density | |
| $j_x^{\pm}$ | crossover current density (scaling) | (7.42) |
| $j_o$ | depairing current density | (2.30) |
| $K_{BZ}$ | Brillouin-zone wave vector | (3.18) |
| $\mathbf{K}_\nu$ | reciprocal vortex lattice vector | (3.22) |
| $K_0$ | modified Bessel function | |
| $K_o$ | basic reciprocal lattice vector | (6.39) |
| $k_F$ | Fermi wave vector | (2.82) |
| $l$ | mean free path | (3.66) |
| $\mathscr{L}$ | Lagrange functional | (2.156) |
| $L_a$ | range of lattice order ($\|\mathbf{B}$) | (4.39) |
| $L^b$ | bundle length ($\|\mathbf{B}$) | (4.56b) |
| $L_c$ | collective pinning length (vortex line) | (2.45) |
| $L_c^b$ | collective pinning length (vortex bundle) | (4.18) |
| $L_E$ | entanglement length | (6.45) |
| $l_{hl}$ | half-loop hopping length (columnar defects) | (9.105) |
| $L_{opt}$ | optimal hopping length | (3.177) |
| $l_{loc}$ | localization length (columnar defects) | (9.70) |
| $l_{VRH}$ | variable-range hopping length (columnar defects) | (9.124) |
| $M$ | magnetization | |
| $m_l$ | vortex mass | (2.82) |
| $m_e$ | electron mass | |
| $m^*$ | effective mass | |
| $n$ | carrier density | (2.12) |
| $n_{dp}$ | dislocation pair density | (8.251) |
| $n_i$ | impurity density | (2.43) |
| $p$ | vortex form factor | (2.34) |
| $Qu$ | quantum resistance | (2.90) |
| $q$ | equilibrium spin-glass order parameter | (7.8) |
| $q_{EA}$ | Edwards-Anderson order parameter | (7.5) |
| $R_a$ | range of lattice order ($\perp\mathbf{B}$) | (4.39) |
| $R_c$ | collective pinning radius | (4.18) |
| $R_g$ | range of glassy order ($\perp\mathbf{B}$) | (4.161) |
| $\mathbf{R}_\nu$ | vortex lattice vector | (3.17) |
| $R_\|$ | parallel bundle dimension | (4.56) |
| $R_\perp$ | perpendicular bundle dimension | (4.56) |
| $r_c$ | radius of critical nucleus | (3.120) |
| $r_p$ | disorder length scale | (4.90) |
| $r_r$ | rod radius (columnar defects) | |
| $S$ | normalized relaxation rate | (2.77) |
| $S(\mathbf{K},t)$ | structure factor | (3.99) |
| $S_c$ | collective pinning action | |
| $S_c^b$ | tunneling action | (4.59) |
| $S_{CDW}$ | CDW-type action | (4.70) |
| $S_E$ | Euclidean action | (2.83) |
| $S_E^H$ | Euclidean action (Hall) | (2.92) |
| $S_E^{eff}$ | effective Euclidean action (diss.) | (2.87) |
| $S(j)$ | current dependent tunneling action | (4.68) |

| Symbol | Description | Ref. |
|---|---|---|
| $S_{lb}$ | large-bundle action | (4.70) |
| $S_{pc}$ | pancake action | (8.243) |
| $S_{sb}$ | small-bundle action | (4.70) |
| $S_{sv}$ | single-vortex action | (4.60) |
| $T$ | temperature | |
| $T_{BG}$ | Bose-glass temperature | Fig. 45 |
| $T_{BKT}$ | BKT temperature | (8.81) |
| $T_{cr}$ | 2D-3D crossover temperature | |
| $T_{dc}$ | decoupling temperature | (8.141) |
| $T_e$ | evaporation temperature | (8.131) |
| $T_{c_o}$ | mean-field transition temperature | (8.89) |
| $T_{dl}$ | rod delocalization temperature (columnar defects) | (9.72) |
| $\tilde{T}_{dl}$ | ($T$-dep.) rod delocalization energy (columnar defects) | (9.72) |
| $T_{dp}$ | lattice depinning temperature | (4.76) |
| $\tilde{T}_{dp}^{s}$ | vortex depinning energy | (2.128) |
| $T_{dp}^{s}$ | vortex depinning temperature | (2.130) |
| $T_{dp}^{lb}$ | bundle depinning temperature | Fig. 17 |
| $\tilde{T}_{dp}^{TP}$ | twinning plane depinning energy | (9.18) |
| $T_{dp}^{TP}$ | twinning plane depinning temperature | (9.19) |
| $T_{dp}^{r}$ | rod depinning temperature | (9.77) |
| $\tilde{T}_{dp}^{r}$ | ($T$-dep.) rod depinning energy | (9.77) |
| $T^{ED}$ | entanglement-disentanglement temperature | (6.48) |
| $T_g$ | glass temperature | |
| $T_k$ | "kink" temperature | (6.4) |
| $T_m$ | melting temperature | (4.104) |
| $T_m^{2D}$ | 2D melting temperature | (8.111) |
| $T_R$ | roughening temperature | (3.135) |
| $T_c$ | transition temperature | |
| $t$ | reduced temperature $T/T_c$ | |
| $t$ | hopping matrix element (columnar defects) | (9.114) |
| $t_c$ | collective tunneling time | (2.84) |
| $t_{pin}$ | pinning time | (6.4) |
| $t_{pl}$ | plastic relaxation time | (6.30) |
| $t_{th}$ | thermal relaxation time | (6.9) |
| $t_o$ | macroscopic time scale for creep | (10.33) |
| $U_c$ | collective pinning energy | (2.46) |
| $U_c^b$ | bundle activation energy | (4.57) |
| $U_{CDW}$ | CDW-type activation energy | (4.70) |
| $U_g$ | glassy barrier | (4.161) |
| $U_{hl}$ | half-loop activation energy (columnar defects) | (9.110) |
| $U_{in}$ | intrinsic pinning potential | (8.159) |
| $U(j)$ | current dependent activation energy | (4.67) |
| $U_{lb}$ | large-bundle activation energy | (4.70) |
| $U_{Mott}$ | activation energy, Mott limit (columnar defects) | (9.119) |
| $U_{nn}$ | nn percolation activation energy (columnar defects) | |
| $U_{pc}$ | pancake pinning energy | (8.219) |
| $U_{pin}$ | random pinning potential | (2.33) |
| $U_{pl}$ | plastic barrier | (6.2) |
| $U_{sb}$ | small-bundle activation energy | (4.70) |
| $U_{sv}$ | single-vortex activation energy | (4.58) |
| $U_r$ | correlated pinning potential (columnar defects) | (9.40) |
| $U_{VRH}$ | variable-range hopping activation energy (columnar defects) | (9.123) |
| $\mathbf{u}$ | vortex displacement | |
| $u_{hl}$ | half-loop hopping distance (columnar defects) | (9.106) |
| $u_{Mott}$ | variable-range hopping distance, Mott limit | (9.118) |
| $u_{opt}$ | optimal hopping distance | (3.178) |
| $u_p$ | pinning displacement | |
| $u_{th}$ | thermal displacement | |
| $u_{VRH}$ | variable-range hopping distance (columnar defects) | (9.121) |
| $V$ | volume | |
| $V$ | voltage | |
| $V_c$ | collective pinning volume | (4.45) |
| $V_{opt}$ | optimal hopping volume | |
| $\mathbf{v}$ | velocity | |
| $v_c$ | critical velocity | (3.88) |
| $v_F$ | Fermi velocity | (3.66) |
| $\mathbf{v}_s$ | superfluid velocity | (2.20) |
| $\mathbf{v}_v$ | velocity of vortex line | (2.20) |
| $W$ | mean pinning force density | (4.9) |
| $w_k$ | kink width (columnar defects) | |
| $z$ | relaxation time exponent (vortex glass) | (7.25) |
| $\alpha$ | GL parameter | (2.1) |
| $\alpha$ | nonlinearity parameter | (10.6) |
| $\alpha$ | constant of order unity | |
| $\alpha_l$ | Hall coefficient (vortex line) | (2.28) |
| $\beta$ | GL parameter | (2.1) |
| $\gamma$ | disorder parameter | (2.38) |
| $\gamma$ | disorder parameter | (9.164) |
| $\gamma$ | dispersion parameter | (9.115) |
| $\Delta$ | disorder correlator | (3.142) |
| $\Delta_{BCS}$ | BCS gap parameter | (3.69) |
| $\Delta_r$ | disorder correlator (columnar defects) | (9.42) |
| $\Delta^{(2)}$ | 2D Laplacian | |
| $\delta$ | dimensionless disorder parameter | (3.73) |
| $\delta_s$ | skin depth | (10.14) |
| $\varepsilon$ | anisotropy parameter | (2.2) |
| $\varepsilon_\vartheta$ | angular-dependent anisotropy parameter | (2.137) |
| $\varepsilon_F$ | Fermi energy | (3.64) |
| $\varepsilon_l$ | line tension | (2.18) |
| $\varepsilon_{pin}$ | pinning energy (vortex line) | (2.31) |
| $\varepsilon_r$ | rod potential well | (9.55) |
| $\varepsilon_{TP}$ | twinning plane potential well | (9.1) |

| | | |
|---|---|---|
| $\varepsilon_0$ | basic energy scale | (2.14) |
| $\zeta_{d,n}$ | wandering exponent | (3.143) |
| $\eta$ | friction coefficient (vortex lattice) | (3.86) |
| $\eta_J$ | friction coefficient (Josephson vortex) | (8.19) |
| $\eta_l$ | friction coefficient (vortex line) | (2.26) |
| $\theta$ | angle from the $c$ axis | Fig. 7 |
| $\theta$ | stiffness exponent | |
| $\theta_L$ | lock-in angle (columnar defects) | (9.173) |
| $\theta(\mathbf{r})$ | bond-angle field | (4.152) |
| $\theta_t$ | trapping angle (columnar defects) | (9.173) |
| $\vartheta$ | angle from the $ab$ plane | Fig. 7 |
| $\vartheta_L$ | lock-in angle (layered structure) | (8.63) |
| $\kappa$ | GL parameter ($\mathbf{H}\|c$) | |
| $\kappa_c$ | GL parameter ($\mathbf{H}\perp c$) | |
| $\lambda$ | GL penetration depth | (2.6) |
| $\Lambda$ | Josephson penetration depth | (8.9) |
| $\lambda_L$ | London penetration depth | (2.12) |
| $\mu$ | glassy exponent | (2.60) |
| $\nu$ | correlation exponent (vortex glass) | (7.26) |
| $\nu_s$ | transverse stiffness | (8.77) |
| $\xi$ | GL coherence length | (2.5) |
| $\xi_{BCS}$ | BCS coherence length | (3.69) |
| $\xi_{BKT}$ | BKT coherence length | (8.83) |
| $\xi_{VG}$ | vortex-glass correlation length | (7.25) |
| $\rho$ | resistivity | |
| $\rho_{flow}$ | flux-flow resistivity | |
| $\rho_n$ | normal-state resistivity | |
| $\rho_{peak}$ | (ac) peak resistivity | (10.21) |
| $\rho_s$ | superfluid density | |
| $\sigma(\omega)$ | conductivity | |
| $\tau_r$ | relaxation time | |
| $\tau_{VG}$ | vortex-glass relaxation time | (7.26) |
| $\Phi$ | magnetic flux | |
| $\Phi_0$ | unit flux | |
| $\Phi_{\alpha\beta}(\mathbf{k})$ | elastic matrix | (3.22) |
| $\Phi_{n+1,n}$ | gauge-invariant phase difference (layered sc) | (8.7) |
| $\varphi$ | phase of order parameter | |
| $\nabla\tilde{\varphi}$ | gauge-invariant phase gradient | (2.10) |
| $\varphi_L$ | lock-in angle (twinning planes) | (9.9) |
| $\varphi_t$ | trapping angle (twinning planes) | (9.5) |
| $\chi'$ | (ac) susceptibility (real part) | (10.18) |
| $\chi''$ | (ac) susceptibility (imaginary part) | (10.18) |
| $\chi_{d,n}$ | energy exponent | (3.144) |
| $\Psi$ | order parameter | (2.1) |
| $\psi_v$ | normalized vortex solution | (2.34) |
| $\Omega$ | crossover frequency (scaling) | (7.48) |
| $\omega_{peak}$ | (ac) peak frequency | (10.20) |
| $\nabla^{(2)}$ | 2D gradient | (8.1) |
| $\langle \cdots \rangle_{dis}$ | disorder average | |
| $\langle \cdots \rangle_{th}$ | thermal average | |

| | | |
|---|---|---|
| $\langle\!\langle \cdots \rangle\!\rangle$ | disorder and thermal average | |
| $\|$ | parallel to CuO planes (in-plane) | |
| $\perp$ | perpendicular to CuO planes (out-of-plane) | |
| $c$ | $\mathbf{B}\|c$ configuration | |
| (2) | planar component | |
| $\sim$ | dimensionally equal | |
| $\simeq$ | equal up to a numerical of order unity | |
| $\approx$ | approximately equal | |
| $=$ | equal | |
| $\propto$ | proportional | |

"Owl explained about *flux pinning* and *creep*. He had explained this to Pooh and Christopher Robin once before, and had been waiting ever since for a chance to do it again, because it is a thing you can easily explain twice before anybody knows what you are talking about."

A.A. Milne, *Winnie-the-Pooh*

# I. INTRODUCTION

The discovery of high-temperature superconductivity by Bednorz and Müller in 1986 opened a new chapter in the field of solid-state physics in general and in superconductivity in particular. This review deals with the phenomenological aspect of high-temperature superconductivity and, as such, it develops the physics of vortices as a new state of matter. In fact, thanks to a set of lucky circumstances, the new high-temperature superconductors set the stage for the physical realization and experimental accessibility of the entire statistical mechanics of vortices and thus, from a more general point of view, of interacting elastic strings. Furthermore, the coupling of the vortices to external currents and fields allows us to exert forces on these strings, accessing the wide field of their dynamical behavior to investigations. Finally, vortices are susceptible to disorder such that the statistical mechanics as well as the dynamical properties of this system have to be understood in the presence of a random environment. Given this outlook, it goes without saying that the present review does not represent the final knowledge in this field. Rather, the aim of this work is to collect, assemble, and interpret (what the authors believe to be) the main pieces of this puzzle as they are known today and to work out a consistent picture of our present knowledge.

The phenomenology of superconductivity is based on the Ginzburg-Landau theory (Ginzburg and Landau, 1950), which provides the starting variational functional (free energy) for the charged superconductor coupled to electromagnetism. The two fields determining the physics of the system are the superconducting order parameter $\Psi$ and the vector potential $\mathbf{A}$. In its simplest version, $\Psi = |\Psi|\exp(i\varphi)$ is a complex order parameter describing an $s$-wave superconductor, the system we shall deal with

throughout this review.[1] The new high-temperature superconductors are strongly type II and, as such, their phenomenology is dominated by the presence of vortices over most of the phase diagram. The mean-field version of the latter was constructed by Abrikosov back in 1957 and has proved over several decades to describe very accurately the phenomenological behavior of all the conventional low-temperature superconductors. This mean-field $H$-$T$ phase diagram comprises a Meissner phase characterized by complete flux expulsion at low magnetic fields $H < H_{c_1}$, separated from the mixed (or Schubnikov) phase at higher fields $H > H_{c_1}$, where the magnetic field penetrates the superconductor in the form of flux lines (or vortices); see Fig. 1. The lower critical field $H_{c_1}$ is mainly determined by the London penetration depth $\lambda$, which is the length scale determining the electromagnetic response of the superconductor. Since the superconducting state is a macroscopic quantum fluid, the magnetic flux enclosed in a vortex is quantized in units of $\Phi_0 = hc/2e \approx 2 \times 10^{-7}$ G cm$^2$, the flux quantum. With increasing field the density of flux lines (which form a triangular lattice) increases until the vortex cores overlap when the upper critical field $H_{c_2}$ is reached. Beyond this field we recover the normal metallic state. The upper critical field $H_{c_2}$ is determined by the coherence length $\xi$ of the superconductor, which represents the second fundamental length scale in the system and which determines the (spatial) response of the macroscopic quantum fluid $\Psi$ itself.

Now let us turn away from the mean-field phase diagram and discuss the dynamic properties of the vortex system (in order to keep the present introductory discussion simple we ignore here the possibility of a large Hall force). When an external current density $j$ is applied to the vortex system, the flux lines start to move under the action of the Lorentz force $\mathbf{F}_L = \mathbf{j} \wedge \mathbf{B}/c$ [or $\mathbf{f}_L = (\Phi_0/c)\mathbf{j} \wedge \mathbf{n}$ for a single vortex, where $\mathbf{n}$ denotes the unit vector along the vortex]. Within a perfectly homogeneous system the driving Lorentz force is counteracted only by the friction force $\mathbf{F}_\eta = -\eta \mathbf{v}$, where $\mathbf{v}$ is the steady-state velocity of the vortex system, $\mathbf{v} = \mathbf{j} \wedge \mathbf{B}/c\eta$.

---

[1]Recent experiments (see Wollman *et al.*, 1993; Brawner and Ott, 1994; Kirtley *et al.*, 1994) suggest that the microscopic mechanism in the new high temperature superconductors produces superconductivity with $d$-wave symmetry. Due to crystal field effects the representation is again one dimensional and the order parameter is a scalar complex field. The Ginzburg-Landau theory takes the same form as for an $s$-wave superconductor and the phenomenology remains essentially unchanged (apart from specific experiments tracing the symmetry of the order parameter). Corrections appear when relating the phenomenological parameters in the Ginzburg-Landau functional with the underlying microscopic parameters, with largest deviations occurring for the dynamical response coefficients due to the presence of zero-gap excitations in special directions.
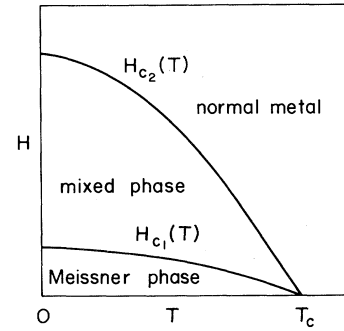
FIG. 1. Mean-field phase diagram comprising a normal-metallic phase at high fields and temperatures, separated by the upper critical-field line $H_{c_2}(T)$ from the mixed or Shubnikov phase, which in turn is separated by the lower critical-field line $H_{c_1}(T)$ from the Meissner-Ochsenfeld phase at low temperatures and fields.

The dissipation is due to the appearance of a finite electric field $\mathbf{E}$ as a consequence of the flux motion, $\mathbf{E} = \mathbf{B} \wedge \mathbf{v}/c$. Since both $\mathbf{j}$ and $\mathbf{E}$ run parallel, the power $P = (\mathbf{j} \wedge \mathbf{B})^2/c^2\eta$ is dissipated in the system and the superconducting property of dissipation-free current flow is lost. The friction coefficient $\eta$ can be obtained from an analysis of the dissipation processes inside and around the vortex cores, $\eta \approx BH_{c_2}/c^2\rho_n$ (Bardeen and Stephen, 1965; $\rho_n$ is the normal-state resistivity), hence $P = \rho_n j^2(B/H_{c_2})$ for $\mathbf{j} \perp \mathbf{B}$, and the dissipation is merely reduced by the fraction $B/H_{c_2}$ as compared with a normal metal. In order to recover the desired property of dissipation-free current flow, the flux lines have to be pinned such that $\mathbf{v} = 0$ in spite of $\mathbf{F}_L \neq 0$. In this case the driving Lorentz force is counteracted by the pinning force $\mathbf{F}_{pin}$. Fortunately, any static disorder affecting the superconducting order parameter will contribute to a finite pinning force density $\mathbf{F}_{pin}$, and thereby the technological usefulness of the type-II superconductors is reestablished. However, dissipation-free flow now has become a matter of optimizing the pinning force density $\mathbf{F}_{pin}$, since increasing the current density $j$ beyond $j_c = cF_{pin}/B$ (again we assume $\mathbf{j} \perp \mathbf{B}$) leads to the depinning of the vortices and hence to the reappearance of dissipation. The current density $j_c$ is the critical depinning current density, which is always bounded by the depairing current density $j_0 = cH_c/3\sqrt{6}\pi\lambda$ determined by the thermodynamic critical field $H_c$, $j_c < j_0$. The dimensionless critical current-density ratio $j_c/j_0$ is a measure of the strength of the pinning force density $F_{pin}$ and as such can be very conveniently used as the fundamental parameter in the phenomenology of type-II superconductors, characterizing the strength of the quenched disorder in the system. Disorder not only affects the dynamical behavior of the vortices, it also has important consequences for the $H$-$T$ phase diagram because the triangular vortex lattice is destroyed. As was shown by Larkin in 1970, in fewer than four dimensions quenched disorder

always destroys the translational long-range order of the Abrikosov vortex lattice.

We emphasize that the accurate description of quenched disorder and the understanding of its consequences are not merely an interesting scientific exercise, but technologically unavoidable: Superconductivity in type-I superconductors suffers from small thermodynamic critical fields $H_c$, and hence both large current flows (creating large self-fields) and large external fields are detrimental. Similarly, the Meissner phase in type II superconductors is bounded by the (even smaller) lower critical field $H_{c_1}$, hence all technologically relevant materials are hard type-II superconductors operating in the mixed state.

Once we understand that quenched disorder is a prerequisite for obtaining the (at least phenomenologically) fundamental property of dissipation-free flow, the question arises what effects other kinds of "disorder" might have on the vortex system. Going then beyond the traditional mean-field picture, the most obvious type of disorder is introduced into the system in the form of thermal fluctuations. A very crucial difference between quenched and thermal disorder is that the latter is dynamical whereas the former is static. Again, thermal disorder has severe consequences both for the phase diagram of the vortex system and for its dynamical properties. Regarding the statistical mechanics of the vortex lattice, one could think of a melting transition transforming the vortex solid into a vortex-liquid phase. Such a melting transition can be understood in terms of large thermal fluctuations [of the order of the lattice constant $a_0 \approx (\Phi_0/B)^{1/2}$] of the positions of the vortex lines and hence as fluctuations in the phase field $\varphi(\mathbf{r})$ of the superconducting order parameter $\Psi(\mathbf{r}) = |\Psi(\mathbf{r})| \exp[i\varphi(\mathbf{r})]$. Near the normal-superconducting transition, not only the phase but also the modulus of the order parameter is subject to large (thermal) fluctuations, thereby establishing the so-called critical region of the transition.

The inclusion of thermal fluctuations in the phenomenology of type-II superconductors also affects the dynamical behavior of the vortex system in various ways. First of all, the vortex lines can move due to thermally activated jumps over the pinning barriers, even at current densities $j < j_c$ (Anderson, 1962), leading to the famous creep phenomenon in type-II superconductors. Creep of vortex lines is equivalent to a small but finite directed motion of the vortex lines and thus reestablishes dissipation in the system. One then could ask if true "transverse" superconductivity exists at all in the thermodynamic sense (note that longitudinal superconductivity with $\mathbf{j} \| \mathbf{B}$ produces a force-free configuration, at least in the thermodynamic sense, with $j \to 0$ where self-fields can be neglected). The crucial question is whether creep persists down to the limit of zero driving force: Does the dissipation and hence the resistivity $\rho$ vanish in the limit $j \to 0$ or does a superconductor in the mixed phase finally end up in a resistive state? Note that probing the superconductor with a vanishing current density $j \to 0$

amounts to investigating the thermodynamic state of the vortex system. The kind of response the system develops for $j \to 0$ then determines whether the vortex system constitutes a glass, characterized by infinite barriers against creep and hence $\rho(j \to 0) \to 0$, or whether the vortex system is in a liquid state with finite creep barriers, allowing vortex motion at any nonzero temperature such that $\rho(j \to 0) > 0$.

The interplay between quenched and thermal fluctuations manifests itself in other ways than the phenomenon of creep. Thermal fluctuations of the individual vortex lines lead to a dynamical sampling and hence averaging of the disorder potential over the spatial extent of the thermal displacement $\langle u^2 \rangle_{\text{th}}^{1/2}$. Thermal disorder hence opposes quenched disorder via a smoothing of the disorder potential and thereby reduces the critical current density $j_c$ in the system. The smoothing of the quenched disorder potential due to thermal fluctuations has come to be known as *thermal depinning*, though one must understand that the phenomenon of thermal depinning is not an abrupt transition but rather a continuous crossover from a pinned to an unpinned situation.

It turns out that the fundamental parameter governing the strength of thermal fluctuations in all of the above phenomena is the Ginzburg number $Gi = [T_c / H_c^2(0)\varepsilon\xi^3(0)]^2 / 2$, which measures the relative size of the minimal $(T=0)$ condensation energy $H_c^2(0)\varepsilon\xi^3(0)$ within a coherence volume and the critical temperature $T_c$. A few examples illustrating the importance and universality of the Ginzburg number $Gi$ in describing phenomena related to thermal fluctuations can be found in the width of the critical regime, $|T_c - T| < T_c G_i$, in the melting line $B_m(T) \approx (5.6c_L^4/Gi)H_{c_2}(0)(1 - T/T_c)^2$, or in the depinning line $B_{\text{dp}}(T) \approx 8Gi\, H_{c_2}(0)(T/T_c)^2$. (Here $c_L \approx 0.2$ is the Lindemann number; for a derivation and discussion of these results, see below). With increasing Ginzburg number $Gi$ the critical fluctuation region and those parts of the $H$-$T$ phase diagram where the vortex lattice is melted or depinned become larger.

A third kind of "disorder" able to change the mean-field phase diagram as well as the dynamical behavior of the system are (macroscopic) quantum fluctuations. Similar to thermal fluctuations, quantum fluctuations can affect superconductivity via fluctuations in the order-parameter modulus as well as fluctuations in the phase of the order parameter, e.g., via quantum motion of vortices (quantum creep). In fact, classical and quantum processes can be mapped onto one another via the simultaneous interchange of the energy $U$ and the action $S$ of the process together with the exchange of the basic units $T$ and $\hbar$ governing classical and quantum fluctuations, respectively (here and in the following we measure the temperature in units of energy or vice versa, i.e., we set the Boltzmann constant $k_B$ equal to unity). With this point of view, a quantum process is a $(d+1)$-dimensional generalization of a $d$-dimensional classical process, where the

additional dimension describes nothing but the (imaginary) time evolution of the process. Since quantum processes are virtual, the appearance of the time evolution in the formalism can be naturally understood. Again, the importance of quantum fluctuations can be expressed by a dimensionless parameter. Since the time evolution of the process is relevant, this parameter depends on whether the dynamics of the system is massive, damped, or of the Hall type. For the massive case the fundamental parameter is given by the ratio $1/k_F\xi$, where $k_F$ denotes the Fermi wave vector in the underlying electronic system. In the overdamped limit the fundamental parameter governing the appearance of macroscopic quantum processes is the quantum resistance $Qu = (e^2/\hbar)(\rho_n/\varepsilon\xi)$. Since macroscopic quantum processes are usually strongly coupled to the environment, the overdamped limit is usually the physically most relevant case. However, in a super-clean system (with a mean free path $l > \xi\varepsilon_F/T_c$, where $\varepsilon_F$ is the Fermi energy) at low temperatures the Hall term dominates the vortex equation of motion, and the relevant parameter takes the form $Qu^H = 1/n\varepsilon\xi^3$, where $n$ denotes the carrier density.

With the three fundamental parameters quantifying the strengths of quenched disorder ($j_c/j_0$), of thermal fluctuations ($Gi$), and of quantum fluctuations ($Qu$), we are in a position to express the difference between the conventional low-$T_c$ superconductors and the new high-temperature superconductors in a very compact way: In conventional superconductors pinning is usually strong, $j_c/j_0 \simeq 10^{-2}-10^{-1}$, whereas both thermal and quantum fluctuations are weak, $Gi \simeq 10^{-8}$ and $Qu \simeq 10^{-3}$. In generic high-temperature superconductors such as $YBa_2Cu_3O_{7-y}$ (YBCO), pinning is usually weak, $j_c/j_0 \simeq 10^{-3}-10^{-2}$, whereas thermal and quantum fluctuations are large, $Gi \simeq 10^{-2}$ and $Qu \simeq 10^{-1}$ (similar considerations apply to the layered Bi- and Tl-based materials). This change in the relative importance of static and dynamic disorder is a consequence of the extreme material parameters characterizing the oxide superconductors: First of all, the transition temperature $T_c$ is very large and hence the coherence length $\xi \propto \hbar v_F/T_c$ is small. Since the oxide superconductors are doped insulators rather than generic metals, the electronic density is small, hence $v_F$ is small, and the resistivity $\rho_n$ as well as the penetration depth $\lambda$ tend to be large (provided we can still use Fermi-liquid concepts for these crude estimates). In addition, the layered structure of the oxides introduces a large uniaxial anisotropy in the system, which reduces the coherence length along the anisotropy axis (the $c$ axis of the material) by an additional factor $\varepsilon = (m/M)^{1/2} < 1$. Here, $m$ and $M$ denote the (small and large) effective electronic masses in the $ab$ plane and along the $c$ axis, respectively. The anisotropy strongly promotes the thermal and quantum fluctuations, since $Gi \propto 1/\varepsilon^2$ and $Qu \propto 1/\varepsilon$. All the above shifts in the material parameters tend to increase the importance of the fluctuations in the high-temperature superconductors. Whereas the mean-field description was quite sufficient for the understanding of

the conventional low-temperature superconductors, this is no longer the case for the new materials. In particular, the increase of $Gi$ by roughly six orders of magnitude implies that the vortex lattice should be melted over a large portion of the phase diagram (Nelson, 1988). The complete statistical mechanics description, including vortex fluctuations, becomes mandatory, and a phase transition between a vortex solid and a vortex-liquid phase not only is possible in principle but has probably been experimentally observed in the new materials (Farrell, Rice, and Ginsberg, 1991; Safar, Gammel, Huse, *et al.*, 1992). Similarly, the increase of $Qu$ by 2 orders of magnitude renders macroscopic quantum effects relevant and observable in the new superconductors (Fruchter *et al.*, 1991; Griessen *et al.*, 1991; Mota *et al.*, 1991). We wish to point out that these novel effects are not unique to high-temperature superconductivity; they are present as well in the conventional low-$T_c$ materials (Rossel *et al.*, 1991; Suenaga *et al.*, 1991; Berghuis and Kes, 1993). It is the special set of material parameters in the oxides, however, which render these phenomena physically important and accessible to experimental investigations.

The special material properties of high-temperature superconductors not only accentuate the importance of fluctuations, they also tend to render pinning in these materials weak. The weak pinning (small $j_c/j_0$) is a consequence both of the small coherence length $\xi$ and of the absence of generic extended pinning sites in these materials, such as precipitates or grain boundaries occurring in conventional superconductors. Again, this circumstance is a consequence of the oxides' being doped insulators rather than conventional metals; hence pinning centers are mainly provided by point defects, e.g., oxygen vacancies (Tinkham, 1988). An important exception are the twin boundaries in YBCO, which provide extended pinning sites upon proper alignment of the magnetic field, leading to enhanced pinning, as observed in several experiments (Gyorgy *et al.*, 1990; Kwok *et al.*, 1990; Liu *et al.*, 1991).

The weakness of the pinning in the high-temperature superconductors is extremely interesting from a theoretical point of view as it allows us to treat the effects of quenched disorder perturbatively. In particular, weak pinning implies the existence of a well-defined starting Hamiltonian in the form of a continuum elastic description of the vortex lattice, upon which effects due to disorder can be studied in a well-defined fashion. The dynamical behavior of the vortex system in the presence of quenched disorder then can be studied within the framework of the weak collective pinning theory introduced by Larkin and Ovchinnikov (1973 and 1979). Furthermore, if the pinning is weak enough in the sense $Gi_d \ll Gi$, where $Gi_d = (j_c/j_0)^3$, the melting transition between the vortex solid and the vortex-liquid phase will be only weakly perturbed by the presence of quenched disorder, allowing for the possibility of observing a generic melting transition in the vortex system.

From the above discussion we see that we can expect a

wealth of novel phenomena in type-II superconductors to be experimentally accessible for the first time and to be theoretically tractable in a well-defined fashion, allowing for a mutual exchange of experimental and theoretical results. On the experimental side, such novel phenomena include the broadening of the resistive transition in a finite magnetic field (Iye *et al.*, 1988; Palstra *et al.*, 1988b; Tinkham, 1988a), the existence of a distinct irreversibility line far below $H_{c_2}$ (Müller, Takashige, and Bednorz, 1987), which often is associated with a melting or glass transition (Koch, Foglietti, and Fisher, 1990; Farrell, Rice, and Ginsberg, 1991), the presence of giant creep (Yeshurun and Malozemoff, 1988; Yeshurun *et al.*, 1989) even at temperatures far below $T_c$, manifesting itself in a fast magnetic relaxation which furthermore proceeds nonlinearly in the time logarithm (Svedlindh *et al.*, 1991; Thompson, Sun, and Holtzberg, 1991), a rapid decrease in the critical current density $j_c$ with increasing temperature even far below the superconducting transition (Senoussi *et al.*, 1988), and the appearance of quantum effects on approaching zero temperature (Mota, Pollini, Visani, *et al.*, 1988; Lensink *et al.*, 1989; Fruchter *et al.*, 1991).

On the theoretical side, the statistical mechanics and the dynamics of individual vortices and of the vortex lattice are being studied in homogeneous and in disordered environments. These studies have led to the postulation of new phases such as the entangled and the disentangled vortex liquids (Nelson, 1988), the vortex-glass phase (Fisher, 1989), and the Bose-glass phase (Lyuksyutov, 1992, Nelson and Vinokur, 1992). The corresponding phase transitions have also been studied, e.g., via scaling analysis (Fisher, Fisher, and Huse, 1991) or numerical simulations (Huse and Seung, 1990; Hetzel, Sudbø, and Huse, 1992). The dynamical behavior of the vortices is very different in these various phases and therefore can be used as a possible characterization of the new vortex-liquid and vortex-glass phases (Feigel'man *et al.*, 1989; Nattermann, 1990; Vinokur *et al.*, 1990; Fisher, Fisher, and Huse, 1991; Fischer and Nattermann, 1991). The study of classical motion has also been extended to the quantum case (Blatter, Geshkenbein, and Vinokur, 1991).

A second source of novel phenomena is associated with the layered structure of the new oxides. Whereas the YBCO compound still can be described reasonably well within a continuum anisotropic model, the more strongly layered Bi- and Tl-based compounds have to be described by a discrete Lawrence-Doniach model. Superconductivity in these materials can then become quasi-two-dimensional over a large part of the $H$-$T$ phase diagram, and many experiments exhibit a characteristic Berezinskii-Kosterlitz-Thouless (BKT)-type behavior; see, for example, Artemenko, Gorlova, and Latyshev (1989a, 1989b) and Martin *et al.* (1989). Furthermore, the simple rectilinear vortex may have to be replaced by a more complicated object consisting of an array of two-dimensional (2D) pancake vortices interconnected by (coreless) Josephson vortices running parallel in between

two superconducting planes (Efetov, 1979; Doniach, 1990; Clem, 1991). Strong layering also introduces new features in the dynamical behavior of the vortices due to the appearance of intrinsic pinning and creep (Tachiki and Takahashi, 1989; Ivlev and Kopnin, 1990a; Roas, Schultz, and Saemann-Ischenko, 1990; Schmitt *et al.*, 1991). The statistical mechanics of the vortex system (Glazman and Koshelev, 1990) can be affected by layering, not only via the presence of large (quasi-2D) fluctuations, but also through the appearance or suppression of phase transitions, e.g., the possibility of a layer-decoupling transition for a field **H** directed perpendicular to the layers (Feigel'man, Geshkenbein, and Larkin, 1990; Glazman and Koshelev, 1991a) or the possible absence of a melting transition when **H** is directed parallel to the layers (intrinsic pinning; Korshunov, 1991; Mikheev and Kolomeisky, 1991).

Two additional fields of broad interest driven strongly by the technological relevance of high-temperature superconductors are attempts to increase the critical current density via the artificial introduction of strong pinning centers (e.g., columnar defects, Civale *et al.*, 1991) and the investigation of the macroscopic properties of the new materials. It is very exciting to notice that these seemingly technological issues illuminate a wealth of fundamental questions, e.g., the replacement of the vortex-glass phase by the Bose-glass phase in the case where the disorder is correlated. A second example is found in the connection of the macroscopic behavior of a type-II superconductor in a magnetic field with the idea of self-organized criticality (De Gennes, 1966; Vinokur, Feigel'man, and Geshkenbein, 1991), a concept that has attracted a lot of interest recently (Bak, Tang, and Wiesenfeld, 1988).

In order to give a theoretical description of these very diverse phenomena, one has to gather together various concepts and results from different branches of modern theoretical physics, such as the theory of elastic manifolds in quenched random media, polymer physics, spin-glass theory, fluctuation theory of phase transitions, strongly correlated quantum systems, disordered quantum Bose liquids, macroscopic quantum tunneling, hopping conductivity in semiconductors, and self-organized criticality. This list illustrates the richness and complexity we encounter when dealing with the physics of vortices in high-temperature superconductors.

The main philosophy followed in this review is to base all the discussions on some sort of "basic Hamiltonian." The requirement we impose on this Hamiltonian is that it describe the vortex system *accurately* in all its details and thus be close to *reality*. In particular, all the internal structure existing in the vortex system (e.g., the vortex lattice) as well as the interactions present in the system (e.g., between the vortices and the static disorder potential) shall be accurately described by the model Hamiltonian. Examples of the kind of "microscopic Hamiltonians" we consider in this review are the (continuous anisotropic) Ginzburg-Landau and London free-energy

functionals, the discrete Lawrence-Doniach model, and the continuum elastic free-energy functional for the vortex lattice. In our terminology the term "microscopic" refers to length scales $\gtrsim \xi$, with the coherence length $\xi$ denoting the smallest scale in our problem. The calculation of $\xi$ itself is the subject of truly microscopic considerations involving the solution of a very complicated many-body problem. Here we shall treat $\xi$ as a phenomenological parameter. We shall also require our starting Hamiltonians to describe a *minimal model*. In particular, we shall introduce the simplest possible type of disorder in the system which is of the short-ranged Gaussian type. It turns out that the physics described by such a minimal model is already extremely rich and in fact able to account for a wealth of experimental observations in a very consistent manner. Such an approach is in contrast to more phenomenological approaches, such as that developed by Hagen and Griessen (1989, see also Griessen, 1990) to account for problems related to pinning and creep, or the droplet model going back to Fisher, Fisher, and Huse (1991) and designed to give a description of the vortex-glass phase. It will be our aim to describe various diverse phenomena such as vortex-lattice melting, the resulting liquid phases, pinning and creep (classical as well as quantum), loss of long-range order, and glassiness, all within the same framework, starting from the most convenient of the set of (roughly equivalent) Hamiltonians mentioned above. Our approach is, moreover, not specific to the high-temperature superconductors, and the results obtained should equally well describe the conventional low-temperature superconductors if the correct limits are considered in parameter space. In this way the crucial differences between the conventional low- and the new high-$T_c$ superconductors can be accurately discussed.

Of course, starting out with these still very complex Hamiltonians we cannot hope to develop exact solutions to our questions. We thus have to resort to approximate methods in dealing with the vortex system, such as the method of dimensional estimates or perturbative methods such as the dynamic approach. Since a vortex system subject to quenched, thermal, and quantum disorder and possibly driven by external forces is an extremely complex object, the structure of the answers we derive below is not simple but involves many regimes in which the behavior of the system is different. The reader will be rewarded for his patience by the richness of the physics he will find in this system.

Let us turn, then, to the main results, i.e., the general picture we obtain for vortex systems in the high-temperature superconductors. We start out with a discussion of the statistical mechanics in a homogeneous system and discuss the various phase transitions, the form of the transition lines, and the physical properties of the resulting new phases. Next we introduce disorder into the system and discuss its effects on the (dynamic) properties of the various phases. The main additional new features appearing as a consequence of strong layer-

ing will be summarized as well. Third, we extend the discussion to the case in which the disorder is correlated and strong, e.g., the artificial introduction of pining centers in the form of columnar defects.

Let us begin with the statistical mechanics of the flux-line system in a homogeneous superconductor. We first have to specify the region of phase space where our results are valid, which lies outside the regime of critical fluctuations. The latter is determined by the Ginzburg number $Gi = (T_c / H_c^2 \varepsilon \xi^3)^2 / 2$. The largeness of $T_c$ and the smallness of the anisotropy parameter $\varepsilon$ enhance $Gi$ in the high-temperature superconductors by factors of $\sim 10^4 - 10^5$ and $\sim 10^2$, respectively (note that $\xi \propto 1/T_c$), and hence $Gi$ takes the value $\sim 10^{-2}$ in YBCO. The critical region at zero magnetic field then is of the order of 1 K wide and increases weakly with field, $Gi(H) \simeq Gi^{1/3}(H/H_{c_2})^{2/3}$. In spite of the largeness of $Gi$ the critical region around the mean-field transition line $H_{c_2}(T)$, where fluctuations in the amplitude of the order parameter become relevant, is still rather narrow. Outside of this region all the fluctuation degrees of freedom involve only the phase of the order parameter, which can be described by fluctuations in the positions of the vortices. It is this part of the phase diagram where our results can be applied. In the strongly layered Bi- and Tl-based superconductors, the situation is slightly complicated by the appearance of strong quasi-2D fluctuations. The 2D Ginzburg number $Gi^{2D}$ is given by the expression $Gi^{2D} = T_c / \sqrt{2} \varepsilon_o d$, with $\varepsilon_o = (\Phi_o / 4\pi\lambda)^2$, and is of the order of 0.1, implying that the critical region of strong 2D fluctuations is roughly 10 K wide. The 3D Ginzburg number $Gi$ then should be considered as a (still very useful, see below) combination of parameters.

The main new result in the statistical mechanics of vortices in the high $T_c$'s is the appearance of a vortex-liquid phase occupying a substantial portion of the phase diagram below the $H_{c_2}(T)$ line; see Figs. 2(a) and 2(b). A consistent theory for a 3D bulk melting transition is still lacking at present, so the position and the shape of the vortex-lattice melting line is usually determined by the Lindemann criterion $\langle u^2(T_m) \rangle_{th} \simeq c_L^2 a_o^2$. In the intermediate-field range $H_{c_1} \ll B \ll H_{c_2}$, the transition line takes the form $B_m(T) \approx (5.6 c_L^4 / Gi) H_{c_2}(0)(1 - T/T_c)^2$, where $c_L \simeq 0.1 - 0.4$ is the Lindemann number. The fact that the melting line is outside of the critical regime is merely the consequence of the Lindemann number $c_L$ being small. The large extent of the vortex-liquid phase, on the other hand, is due to the largeness of the Ginzburg number $Gi$. It is very interesting that the vortex lattice can melt not only as a consequence of increasing the temperature but also as a consequence of decreasing the magnetic field near $H_{c_1}(T)$; see Figs. 2(a) and 2(b). With decreasing field, the distance between the vortices increases and eventually grows beyond the London penetration depth $\lambda$. In this region, the vortex-vortex interaction is exponentially small, and consequent-
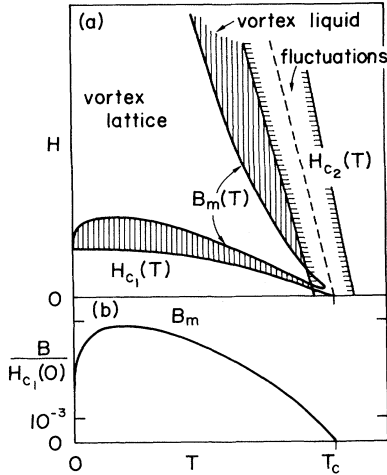
FIG. 2. Phenomenological phase diagram for the anisotropic high-temperature superconductors [parameters for YBCO, $H_{c_1}(0) \approx 730$ G, $H_{c_2}(0) \approx 230$ T, values extrapolated linearly to zero, see also Sec. II.C]: (a) The Abrikosov vortex lattice is melted over a substantial part of the phase diagram. The vortex lattice can melt with increasing temperature (thermal fluctuations) or with decreasing field (exponentially vanishing shear modulus), leading to a reentrant behavior of the melting line $B_m(T)$. The thermodynamic phase transition is shifted to the melting line $B_m(T)$, with the upper critical-field line $H_{c_2}(T)$ marking only a crossover line where the modulus of the order parameter increases rapidly. The regime of large critical fluctuations where the description in terms of vortex (phase) fluctuations breaks down and amplitude fluctuations become important is confined to a rather narrow ($\sim 1$ K wide) region close to $H_{c_2}(T)$. The drawing is not to scale, but emphasizes the main structures appearing in the phase diagram. (b) Shape of the melting line $B_m(T)$ for YBCO with parameters $\xi_{BCS} \approx 16$ Å, $\lambda_L \approx 1400$ Å, and an anisotropy parameter $\varepsilon^2 = M/m \approx 1/25$; drawing is to scale. Note that the extent of the dilute vortex-liquid phase along the field axis is only of the order of a few gauss.

ly the shear modulus $c_{66} \propto \exp(-a_0/\lambda)$ decays rapidly, leading to a melting of the flux-line lattice. As a result, the melting line develops the interesting reentrant behavior shown in Figs. 2(a) and 2(b). Note that the width of the vortex-liquid phase close to $H_{c_1}$ is extremely narrow, of the order of 1 G. Unfortunately, in the anisotropic YBCO superconductor we cannot trace out the entire melting line, as the latter enters the critical regime where fluctuations in the amplitude of the order parameter have to be considered [see Fig. 2(a)]. The corresponding part of the melting line is, however, rather small. Note that the $H_{c_2}(T)$ line now is merely a crossover line and no longer describes a thermodynamic phase transition. Nevertheless, close to the line $H_{c_2}(T)$ the modulus of the order parameter increases rapidly, so that the "jump" in the specific heat takes place near the crossover line $H_{c_2}(T)$.

In the more strongly layered Bi- and Tl-based super-

conductors, the extent of the vortex-liquid phase is even larger; see Figs. 3(a) and 3(b). Within the intermediate-field range $H_{c_1} \ll B \ll H_{c_2}$ the melting line consists of two parts, which join up at the characteristic field $B_{2D} \approx (\pi \Phi_0 / \Lambda^2) \ln(\Lambda / \xi)$. Here $\Lambda = d/\varepsilon$ denotes the Josephson screening length in the layered system, and $d$ is the layer separation. At low fields $H_{c_1} \ll B < B_{2D}$ the vortices constitute well-defined line objects, and the melting transition is of the 3D type with $Gi \simeq 1$. At higher fields $B_{2D} < B \ll H_{c_2}$ the melting transition is quasi-two-dimensional in nature and approaches the field-independent value $T_m^{2D} = \varepsilon_0 d / 4\sqrt{3}\pi \approx 25$ K.

The melting line $B_m(T)$ separates the vortex-lattice phase at low temperatures from the vortex-liquid phase above $B_m(T)$. It is interesting to note that, when going from the high-temperature normal-metallic phase to the Abrikosov vortex lattice, *two* symmetries are broken.
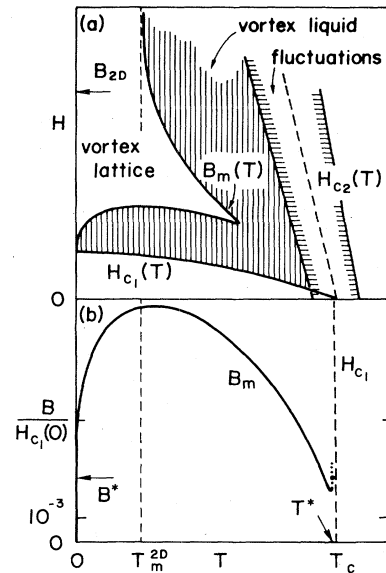


FIG. 3. Phenomenological phase diagram for the strongly layered high-temperature superconductors [parameters for BiSCCO, $H_{c_1}(0) \approx 650$ G, $H_{c_2}(0) \approx 100$ T, values extrapolated linearly to zero, see also Sec. II.C]: (a) The part of the phase diagram occupied by the liquid phase is substantially larger than for the anisotropic YBCO material. Furthermore, the phase diagram separates into two regimes, a low-field regime with $B < B_{2D}$ where the melting process is well described by a 3D continuous anisotropic model, and a high-field region with $B > B_{2D}$, where the melting is quasi-two-dimensional. $T_m^{2D}$ denotes the Berezinskii-Kosterlitz-Thouless dislocation-mediated melting temperature, which is the asymptotic for the melting line $B_m(T)$ at large fields. Drawing not to scale. (b) Shape of the melting lines $B_m(T)$ and the lower critical-field line $H_{c_1}(T)$ for BiSCCO, with parameters $\xi_{BCS} \approx 25$ Å, $\lambda_L \approx 1400$ Å, and an anisotropy parameter $\varepsilon^2 = M/m \approx 1/2500$; drawing is to scale. The point $(T^*, B^*)$ denotes the turning point of the lower melting line $B_m(T)$.

These two symmetries are the translation invariance, which is broken in the lattice phase, and the gauge symmetry producing longitudinal superconductivity (due to the absence of pinning in the present thermodynamic considerations, the response of the vortex lattice to a transverse current density $j\perp H$ is that of a normal metal). The question then arises whether these two symmetries are broken simultaneously or sequentially. If the latter possibility is realized, then the vortex-liquid phase appearing just above $B_m(T)$ will be a *disentangled* vortex liquid, which still exhibits longitudinal superconductivity. A second phase transition then is needed to transform this disentangled vortex-liquid phase into an *entangled* vortex liquid which is equivalent to the normal metallic phase; see Fig. 24 below. On the other hand, if the two symmetries are strictly coupled, then the vortex liquid appearing above the melting line $B_m(T)$ will directly be the entangled phase, and the system will develop a single phase transition only.

Again the situation is somewhat different in the case of strongly layered superconductors (see Fig. 39 below). At small fields $H_{c_1} \ll B < B_{2D}$ the situation is analogous to the anisotropic situation discussed above, since the system exhibits well-defined vortex lines. At higher fields, however, it appears that the two transitions discussed above may reverse their order. If this scenario is indeed realized in these materials, then the 3D lattice phase at low temperatures would undergo a decoupling transition in which longitudinal superconductivity is lost, while the long-range translational order of the vortex lattice survives. The latter then would disappear only at the melting transition close to $T_m^{2D}$. The two transition lines cross one another at $(\sim T_m^{2D}, B_{2D})$. The above discussion of the possible existence of intermediate liquid phases is still quite speculative at present, and more work is certainly needed to confirm or reject these ideas.

Next, let us introduce disorder into the system and study the consequences. The most simply accessible phenomenological parameter describing the strength of the disorder is the critical current-density ratio $j_c/j_0$. If $j_c/j_0$ is small, the disorder potential is weak, and the concept of weak collective pinning can be applied. The idea of weak collective pinning can be most easily illustrated using the example of a single vortex line subject to weak disorder; see Fig. 4 (we consider an isotropic superconductor here): Since the vortex line is an elastic object, the individual point pins acting on the flux line will compete with one another. When we sum up the individual pinning forces acting on the vortex line, the various pins will add up only randomly, i.e., only fluctuations in the density and force of the defects will pin the flux line in a definite position. Assuming a density $n_i$ of pins acting with an individual force $f_{pin}$ on the vortex line, the total force accumulated along a segment of length $L$ is $\mathcal{F}_{pin}(L) \simeq (f_{pin}^2 n_i \xi^2 L)^{1/2}$, where we have taken the coherence length $\xi$ to be the physical length scale of the disorder potential (the extent of the point pins themselves is
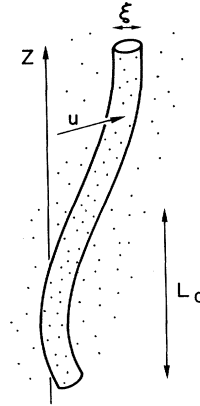


FIG. 4. Single vortex line pinned by the collective action of many weak pointlike pinning centers. Only fluctuations in the pin density are able to pin the vortex. In order to accommodate optimally to the pinning potential, the vortex line deforms by $\xi$ (the minimal transverse length scale the vortex core is able to resolve equals the scale of the pinning potential) on a longitudinal length scale $L_c$, the collective pinning length.

less than $\xi$; however, the vortex line cannot resolve lengths smaller than $\xi$).

The pinning force $\mathcal{F}_{pin}(L)$ competes with the Lorentz force $\mathcal{F}_L(L) \simeq j\Phi_0 L/c$, which grows *linearly* with distance, whereas $\mathcal{F}_{pin}(L) \propto \sqrt{L}$ shows only a square-root growth due to the random addition of the individual pinning forces. These dependencies would imply that, over long distances, the Lorentz force always wins and a (stiff) vortex would remain unpinned. On the other hand, as the vortex can accommodate itself to the pinning potential by elastic deformation, the flux line can bend in order to find the most favorable position in the random potential. Such a deformation will cost an elastic energy $\mathcal{E}_{el} \simeq \varepsilon_l(\xi/L)^2 L$, which in turn is in competition with the pinning energy $\mathcal{E}_{pin}(L) \simeq \mathcal{F}_{pin}(L)\xi$ [here $\varepsilon_l \simeq \varepsilon_0 = (\Phi_0/4\pi\lambda)^2$ is the vortex line tension]. At distances $L > L_c$, where the length $L_c$ is defined by the equality $\mathcal{E}_{el}(L_c) \simeq \mathcal{E}_{pin}(L_c)$, the vortex can readjust itself elastically to the optimal local configuration, and the square-root growth in $\mathcal{E}_{pin}(L)$ is cut off. The vortex then "breaks up" into segments of length $L_c$, each of which is pinned independently and competes as one unit with the Lorentz force $\mathcal{F}_L(L_c) \simeq j\Phi_0 L_c/c$. $L_c \simeq (\varepsilon_0^2 \xi^2/\gamma)^{1/3}$ is called the collective pinning length. Here $\gamma \simeq f_{pin}^2 n_i \xi^2$ parametrizes the disorder strength. Inserting $L_c$ back into $\mathcal{E}_{pin}$, we obtain the collective pinning energy $U_c \simeq (\varepsilon_0 \xi^4 \gamma)^{1/3}$ and equating $\mathcal{F}_{pin}(L_c)$ with the Lorentz force $\mathcal{F}_L(L_c)$ one finds the critical current density $j_c \simeq j_0(\xi\gamma/\varepsilon_0^2)^{2/3}$. Given the disorder parameter $\gamma$, the longitudinal and transverse lengths $L_c$ and $\xi$, the energy $U_c$, the action $S_c \simeq (\hbar/Qu)(L_c/\xi)$ for quantum processes, and the critical current density $j_c$ constitute a set of basic scales for

the discussion of the statistical mechanics and of the dynamics of the vortex line subject to a quenched disorder potential. Since the disorder parameter $\gamma$ is not directly accessible in an experiment, one usually considers the critical current-density ratio $j_c/j_0$ as the fundamental quantity characterizing the strength of the disorder potential. Expressing $L_c$ and $U_c$ in terms of $j_c/j_0$, one obtains $L_c \simeq \xi(j_0/j_c)^{1/2}$, $U_c \simeq H_c^2\xi^3(j_c/j_0)^{1/2} \simeq [j_c(1-t)/j_0\, Gi]^{1/2}T_c$, and $S_c \simeq (\hbar/Qu)(j_0/j_c)^{1/2}$, where $j_c/j_0 \ll 1$ is the weak pinning condition. The generalization of these results to the anisotropic case with $\mathbf{H}\|c$ is $L_c^c \simeq \varepsilon\xi(j_0/j_c)^{1/2}$, $U_c \simeq H_c^2\varepsilon\xi^3(j_c^c/j_0)^{1/2} \simeq [j_c^c(1-t)/j_0\, Gi]^{1/2}T_c$, and $S_c^c \simeq (\hbar/Qu)(j_0/j_c^c)^{1/2}$ ($j_c^c$ denotes the planar critical current density in the orthogonal configuration where $\mathbf{H}\|c$).

In the above illustrative example for the mechanism of collective pinning we have considered only the simplest case of an isolated vortex line. This case is actually realized for weak enough fields where the distance between the vortex lines is large and their mutual interaction is small as compared with the interaction between the vortices and the quenched random potential. At higher fields the intervortex interaction becomes dominant, and the collectively pinned object will be a three-dimensional vortex bundle. Whereas the starting point in the single-vortex case discussed above was the elastic string, the starting point at higher fields is the elastic vortex lattice with its well-defined compression, shear, and tilt properties. Considerations similar to those introduced above allow us to determine the transverse and longitudinal dimensions of the bundle $R_c$ and $L_c^b$, the collective pinning energy $U_c$, and the critical current density $j_c$. It turns out that the bundle volume $V_c \simeq R_c^2 L_c^b$ (i.e., $R_c$ and $L_c^b$) and the energy $U_c$ both increase with the magnetic-field strength, whereas the critical current density $j_c$ decreases with increasing field. The latter can be understood by noting that $U_c \propto \sqrt{V_c}$, whereas $j_c \propto U_c/V_c \propto 1/\sqrt{V_c}$. Note that the vortex-lattice order is still rather well preserved within the volume $V_c$ as distortions $u$ of the lattice which accumulated at the distances $R_c$ and $L_c^b$ are of the order of $\xi < a_0$, where $a_0$ is the lattice constant. The long-range order is lost only over larger distances $R_a \geq R_c$ and $L_a \geq L_c^b$, where $u(R_a, L_a) \simeq a_0$. This regime, however, lies outside of the perturbatively accessible region discussed above, and new scaling concepts have to be considered in order to treat distances beyond the lengths $R_c$ and $L_c^b$; see the discussion below.

One of the most fascinating issues in the physics of vortices is the interplay between quenched and thermal disorder. Thermal fluctuations will interfere with quenched disorder in two ways. First of all, small intravalley oscillations of the vortices will lead to an averaging of the disorder potential over the mean amplitude of thermal displacements $\langle u^2\rangle_{th}^{1/2}$. As this amplitude increases beyond the scale $\xi$ of the disorder potential, thermal fluctuations will smooth the disorder potential so that the pinning is reduced and the critical current densi-

ty rapidly decreases with increasing temperature. The condition $\langle u^2(T_{dp})\rangle_{th} \simeq \xi^2$ determines the so-called depinning line, which takes the form $B_{dp}(T) \approx 8Gi\, H_{c_2}(0)(T/T_c)^2$ in the $H$-$T$ phase diagram (see Fig. 18 below). Note that $B_{dp}(T)$ is not a transition line but marks the crossover to that region of phase space where thermal disorder strongly interferes with pinning. Again, the crucial parameter entering the expression for $B_{dp}$ is the Ginzburg number $Gi$. With increasing $Gi$, the region of phase space where the pinning properties of the vortex lattice are strongly affected by thermal fluctuations becomes larger. At small enough temperatures and fields, the depinning line enters the regime where the vortices are pinned individually. The depinning line then bends and becomes independent of the magnetic field, approaching the single-vortex depinning temperature $T_{dp}^s$; see Fig. 18. The extent of the single-vortex pinning regime depends on the strength of disorder and so does $T_{dp}^s$, $T_{dp}^s \approx 0.7(j_c/j_0\, Gi)^{1/2}T_c$. Above $T_{dp}^s$ the pinning of the vortices always involves vortex bundles, which expresses the fact that the interaction among the vortices is relevant and short-range lattice order persists over several lattice constants $R_a \geq R_c > a_0$. The weak pinning condition $j_c/j_0 < Gi$ then guarantees that the melting transition, with its characteristic length $a_0$, is only weakly perturbed by the quenched disorder, characterized by the elastic length $R_c$. Closer inspection shows that the weak-pinning condition for the melting line is even less stringent: Requiring that the single-vortex pinning regime nowhere touch the melting line and taking all the temperature dependencies into account, one obtains (for not too large $Gi$) the condition $j_c/j_0 < Gi^{1/3}/4 \simeq 5\times10^{-2}$ (parameters for YBCO), such that the weak-pinning condition can indeed be fulfilled in the high-temperature superconductors. Note that the above condition is difficult to fulfill in low-$T_c$ material where $Gi \sim 10^{-8}$. Further, it turns out that the reentrant part of the melting line near $H_{c_1}(T)$ is characterized by a thermal fluctuation parameter $Gi/\kappa^2 \ln\kappa$, which is smaller than $Gi$ by several orders of magnitude. The reentrant part of the melting line $B_m(T)$ then is always strongly affected by the quenched disorder potential.

Thermal fluctuations not only affect the pinning potential; most importantly they also change the dynamics in the system. Better, they produce a creep-type motion of the vortex system for current densities $j < j_c$ where the vortices still are pinned. Following the classical ideas of Anderson (1962) and of Anderson and Kim (1964), we see that thermal fluctuations induce intervalley hops of vortex segments and of vortex bundles so that the whole vortex system is driven by an external current density $j$ to move with a finite creep velocity $v \simeq 2v_0 \exp(-U_0/T)\sinh[(U_0/T)(j/j_0)]$. At small current densities $j \to 0$ we can expand and obtain $v \propto j$, i.e., the system shows Ohmic behavior with a resistance $\rho(T) \propto \rho_n \exp(-U_0/T)$. One can immediately think of

several limits which all seem to be realized and experimentally accessible in the high-temperature superconductors: If the pinning barriers[2] $U_o$ in the system become small as compared with the temperature $T$, $U_o \ll T$, the vortex motion is essentially unaffected by the disorder and can develop a free flow under the action of a driving force. The resistivity $\rho$ is then given by the flux flow resistivity $\rho \approx \rho_{\text{flow}} \approx \rho_n (B/H_{c_2})$; see Fig. 5. This flux flow (FF) behavior is the dynamic response of the *unpinned vortex liquid* at high temperatures near the $H_{c_2}(T)$ crossover line; see Fig. 6. For large pinning barriers $U_o \gg T$ the resistivity becomes exponentially small, $\rho(T) \simeq (\rho_{\text{flow}}/A)\exp(-U_o/T)$, $A \ll 1$, and shows an activated behavior. This is the dynamic response of the *pinned vortex liquid* at high temperatures near the melting line $B_m(T)$. The corresponding regime is now commonly known as the TAFF regime for thermally assisted flux flow (Kes *et al.*, 1989). Within this regime the vortex system is modeled as a very viscous liquid with a (plastic) relaxation time $t_{\text{pl}}$ that is large compared with the typical pinning time $t_{\text{pin}} \simeq a_o/v_c$ in the problem ($v_c$ is the critical velocity, where the current-voltage characteristic turns away from the linear behavior, $v_c \simeq j_c B/\eta c$). With increasing temperature the plastic relaxation time $t_{\text{pl}}$ decreases, and when $t_{\text{pl}} \simeq t_{\text{pin}}$ the TAFF regime crosses over to the FF regime.

The question then arises what type of barriers do we expect in the system at low temperatures below the melting line $B_m(T)$, where the elastic properties of the vortex lattice are established (i.e., the shear modulus $c_{66}$ of the vortex system becomes finite). It can be shown that, as a direct consequence of the elasticity, the pinning barriers in the vortex system diverge in the limit of vanishing current density $j \rightarrow 0$. In this case the small-current expansion, as used above in the traditional Anderson-Kim-type approach to vortex creep, cannot be done any more, and the response of the system to an external current density $j$ remains sub-Ohmic for all $j \rightarrow 0$. In fact, the current-voltage characteristic develops an essential singularity in the limit $j \rightarrow 0$, with the electric field $E$ vanishing according to $E \propto \exp[-(U_c/T)(j_c/j)^\mu]$. The vortex system is then in a *vortex-glass* phase, which can be characterized by the value of the glassy exponent $\mu$. Since $\rho(j \rightarrow 0) \rightarrow 0$, the vortex glass is a truly superconducting phase in the thermodynamic sense. Here we have defined the glass in a dynamic way, neither via the absence of long-range translational order nor via the appearance of some Edwards-Anderson-type order parameter. The crucial feature of the vortex-glass phase as we have introduced it here is the divergence of the barriers

---

[2]We avoid here identifying the barrier $U_o$ with the collective pinning barrier $U_c$, which is always of elastic origin; under certain conditions the relevant barriers against vortex motion can be due to other processes, e.g., plastic deformations of the vortex system, as is the case in a vortex liquid.
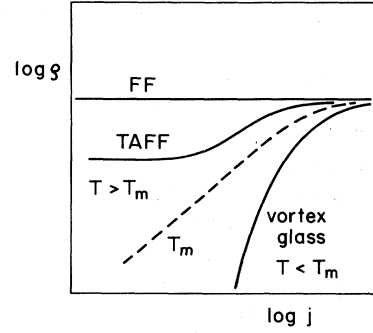
FIG. 5. Resistivity $\rho$ vs current density $j$ for three different regions within the phenomenological phase diagram. At large temperatures the barriers against vortex motion are small, $U_o \lesssim T$, and the vortex system is in the flux-flow (FF) regime with $\rho_{\text{flow}} \approx \rho_n (B/H_{c_2})$. Close to the melting line, $T \gtrsim T_m$, the barriers in the system become large but finite, $T \ll U_o < \infty$, and the system enters the thermally assisted flux-flow (TAFF) regime, where the finite linear-response resistivity is activated, $\rho \approx (\rho_{\text{flow}}/A)\exp(-U_o/T)$, with $A \ll 1$. Below the melting line, $T < T_m$, we enter the vortex-glass regime, where the barriers diverge, $U(j \rightarrow 0) \rightarrow \infty$, leading to a truly superconducting phase with $\rho(j \rightarrow 0) \rightarrow 0$.

$U(j)$ when the probing current density $j$ becomes vanishingly small (and hence does not alter the thermodynamic phase by its own presence). Note that the appearance of infinite dislocation loops (if thermodynamically possible at all) is not expected to renormalize the shear modulus to zero at large distances, since such elastic objects would
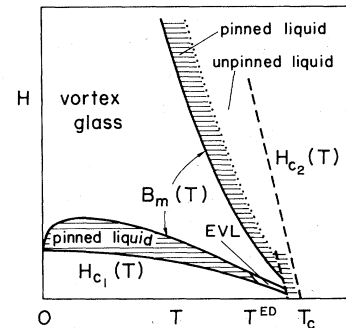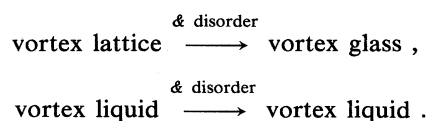


FIG. 6. Phenomenological phase diagram for the high-temperature superconductors including the effects of thermal fluctuations and of quenched disorder (pinning). For the vortex lattice with its finite shear modulus the disorder is relevant, and the lattice turns into a vortex glass, which is a true superconductor with $\rho(j \rightarrow 0) \rightarrow 0$. For the vortex liquid the disorder is perturbatively irrelevant, and the liquid remains a liquid. Close to the melting line $B_m(T)$ the (finite) barriers against vortex motion are still large, $T \ll U_o < \infty$, and the vortex liquid is pinned (TAFF regime), whereas close to the upper critical-field line $H_{c_2}(T)$ the barriers are small, $U_o \lesssim T$, and the vortex liquid cannot be pinned (FF regime). The low-field/low-temperature part of the dilute vortex liquid is probably in a pinned state, and an unpinned entangled vortex liquid (EVL) appears only close to $T_c$. Note that the importance of thermal fluctuations is strongly suppressed in the diluted vortex-liquid phase close to $H_{c_1}(T)$. Drawing is not to scale.

themselves be pinned by the underlying disorder potential. The theory of weak collective pinning, combined with the modern scaling concepts describing the behavior of elastic manifolds subject to a quenched disorder potential, appears to be particularly apt for the description of the vortex-glass phase. Whereas the (perturbative) collective pinning approach allows us to determine all the basic scales, such as $R_c$, $L_c^b$, $U_c$, and $S_c$, in the system, the (nonperturbative) scaling concepts applying to elastic manifolds in random media provide the relevant scaling exponents (e.g., the glassy exponent $\mu$) in the problem. The interplay of quenched and thermal disorder can be expressed most compactly by the following diagram (see also Figs. 2 and 6):

$$\text{vortex lattice} \xrightarrow{\& \text{ disorder}} \text{vortex glass} ,$$

$$\text{vortex liquid} \xrightarrow{\& \text{ disorder}} \text{vortex liquid} .$$

In other words, disorder transforms a vortex lattice into a vortex glass and hence is perturbatively relevant, whereas disorder is perturbatively irrelevant for the vortex-liquid phase, which remains a liquid.

In the strongly layered situation, the possibility arises that pinning and creep do not involve either vortex lines or vortex bundles, but that single pancake vortices can become pinned individually or that a 2D collective pinning regime appears. In fact, if pinning is strong enough that the collective pinning length $L_c$ drops below the interlayer distance $d$, the pancake vortices become individually pinned at low magnetic fields. When the magnetic field is increased, the interaction between the pancake vortices within one layer starts to dominate over the interaction between the pancake vortices and the disorder potential, and a 2D bundle of pancake vortices becomes pinned collectively. When the field is further increased, the dimension of these bundles increases and so does the (Josephson) coupling energy between 2D bundles in neighboring layers. Eventually the coupling into the third dimension becomes dominant, and the collectively pinned object takes the shape of a 3D vortex bundle again. If the weak-pinning condition $L_c > d$ is fulfilled, however, pinning and creep will mainly involve either lines or bundles, as in the continuous anisotropic case.

A second interesting feature of the strongly layered superconductors concerns glassiness at low temperatures. It turns out that in a two-dimensional vortex system the vortex-glass phase cannot exist at finite temperatures. This is due to the presence of dislocation pairs, which can carry a finite amount of flux and whose barriers against creep, being a zero-dimensional object, always remains finite. The finite barriers against plastic deformations therefore will always cut off glassiness in two dimensions. Note that the corresponding object is topologically forbidden in a 3D vortex lattice, since dislocation loops are bound to lie within the gliding plane of the edge dislocations and hence they cannot carry flux. In a layered superconductor the finite-temperature vortex-glass

phase is reestablished due to the finite Josephson coupling between the layers, which punishes dislocation pairs carrying flux within one layer with an infinite creation energy. Hence the layered case appears to be equal to the continuous anisotropic one, which in fact is true at low fields $B < B_{2D}$. For larger fields $B > B_{2D}$ the possibility arises of a decoupling transition's taking place *below* the melting transition. In this case, the glassy phase would give way to a liquid phase as soon as the temperature was raised above the decoupling transition line (see Fig. 42 below).

Finally, let us briefly discuss the main consequences of strong pinning, examples of which are given by the twin boundaries in YBCO, by screw dislocations produced in thin films during growth, or by artificially introduced columnar defects. The type of strong pinning that is technologically most relevant (and which is physically very interesting) is obtained by irradiating the material with high-energy ions. The linear tracks of damaged material then introduce strongly correlated disorder into the (aligned) vortex system. At low magnetic fields such that $a_0 \gg d_r$, where $d_r$ denotes the mean distance between the tracks, each vortex is individually pinned by a columnar defect. Since the pinning energy now grows linearly with distance, pinning becomes strong, and the critical current density $j_c$ takes values close to its upper bound, $j_c \lesssim j_0$. Whereas at low temperatures each vortex line is bound to its line defect, the vortices tend to delocalize with increasing temperature. As the mean thermal displacement $\langle u^2 \rangle_{th}^{1/2}$ becomes equal to the distance $d_r$ between the tracks, the vortex becomes collectively pinned by an assembly of line defects. Pinning then is reduced, since only fluctuations in the density of tracks lead to the pinning of the vortex line. It is interesting to compare the competition between quenched and thermal disorder for the two cases where a single vortex line is pinned collectively by uncorrelated (pointlike) disorder and by correlated disorder (line defects): A vortex line subject to uncorrelated pointlike disorder and thermal fluctuations is only marginally pinned in 3D, and thus the critical current density $j_c$ vanishes exponentially with increasing temperature. On the other hand, correlated disorder competes more efficiently with thermal fluctuations, resulting in a weaker algebraic decay of the critical current density with increasing temperature. Another interesting difference between uncorrelated and correlated disorder is that in the former case the statistical mechanics of the vortex is characterized by line wandering, whereas in the latter case the characteristic feature is localization.

When the temperature is further increased, the interaction between the vortex lines becomes important, and the collectively pinned object takes the form of a vortex bundle. It turns out that for typical parameter values (YBCO), the melting line of the pure system is situated close to the boundary of the single-vortex pinning regime. For the case in which the melting line lies entirely within the bundle pinning regime, the largest energy in the problem is given by the intervortex interaction, and

the disorder does not strongly perturb the melting transition of the vortex lattice. The actual situation depends rather sensitively on the numerical values of the parameters, and a strong-pinning situation turning the melting transition continuous can arise equally well. Finally, the investigation of the vortex system at high fields involves taking into account the interaction between the vortex lines from the beginning, and plastic as well as elastic barriers are relevant in different regimes.

The study of vortex creep in the presence of columnar defects reveals again a variety of cases, including a (nonglassy) percolation-type motion for a finite-thickness, low-disorder sample, a (glassy) variable-range hopping regime for more strongly disordered or thick samples, as well as plastic and collective creep regimes at higher fields where interaction between the vortices is relevant. In the thermodynamic limit the phase below the melting line is always a glass; however, its properties differ from the vortex-glass phase characteristic of the case of uncorrelated disorder. Whereas the latter promotes line wandering, the Bose-glass phase typical of the correlated disorder discussed here promotes localization of the flux lines. Also, the glassy exponent $\mu$ differs for these two cases.

Let us close this introduction with a summary of the contents of the review. The simplest system we can consider when studying vortices in the high-temperature superconductors is the single vortex. All the basic concepts of (weak collective) pinning and creep, thermal depinning, and the complications arising due to the anisotropy of the material can best be illustrated in a discussion of this simplest case. Furthermore, the physics of the individual vortex line is also realized in the low-field/low-temperature part of the $H$-$T$ phase diagram, and thus it is an important subject to be studied first. In Sec. III we introduce a set of general tools that will be used later in the discussion of the vortex system. These tools comprise the continuum elastic theory of the vortex lattice and the scaling approach to the problem of anisotropy. In this section we also study the origin and the size of the elementary pinning force, which is treated as a phenomenological parameter in the other sections of the review (the discussion is based on an $s$-wave BCS superconductor). It turns out that weak collective pinning by pointlike oxygen disorder is well able to account for the experimentally observed critical current densities in the high-$T_c$ superconductors. The dynamic approach discussed in Sec. III.D is one of the most important tools in the discussion of the physics of vortices subject to quenched disorder, as it allows us to obtain at least semiquantitative results. The statistical mechanics and the dynamics of elastic manifolds subject to periodic and random disorder are studied in Secs. III.E and F. The discussion in Sec. III.E illustrates that (dynamic) glassiness is a consequence of elasticity and not of randomness. The nonperturbative scaling approach to the statistical mechanics and dynamics of elastic manifolds subject to a disorder potential is thoroughly discussed in Sec. III.F. In particular, Sec.

III.F explains those concepts needed later in the discussion of the glassiness of the vortex system below the melting line. Section IV is devoted to the physics of the vortex lattice subject to quenched disorder, external force fields, and thermal as well as quantum fluctuations. The structure of this section is very similar to that of Sec. II, as it generalizes all the basic ideas introduced there to the case of the interacting vortex lattice. In addition, questions regarding the destruction of long-range order by the disorder potential are discussed in Sec. IV.E.

Section V deals with the thermodynamic properties of the vortex system. This section is rather independent of Secs. II and IV, but it draws from the ideas introduced in Secs. III.A and B. In Sec. V.A we present a detailed discussion of the phenomenon of vortex lattice melting and determine the shape of the melting line for the low-, intermediate-, and large-field regimes. The possible existence of two vortex-liquid phases is discussed in Sec. V.B.

In Sec. VI we investigate the consequences of the presence of quenched disorder on the vortex-liquid phase. The different role quenched disorder plays for the vortex-solid and vortex-liquid phases is clearly explained here, and the concepts of pinned and unpinned liquids (TAFF and FF regimes) are introduced and explained.

Section VII gives a discussion of the vortex-glass phase. The basic glass problematics are first summarized in Sec. VII.A, where we discuss various types of glasses, the spin, the gauge, and the vortex glass. Section VII.B is devoted to the idea of vortex-glass scaling close to the glass transition line, though gauge-glass scaling may actually be a more accurate heading for this section. Section VII.C finally discusses the various approaches to the vortex-glass phase and its dynamics away from the transition line. In particular, a thorough discussion is given of the relationship between the ideas of collective creep and the vortex glass.

Section VIII is devoted to layered superconductors. The first two sections treat the structure of the individual flux lines and of the vortex lattice (Sec. VIII.A), as well as the (quasi-two-dimensional) thermodynamic properties (Sec. VIII.B). The second part of the section then concentrates on pinning and creep, both intrinsic (Sec. VIII.C) and collective (Sec. VIII.D).

Strong pinning due to correlated disorder is discussed in Sec. IX, where we treat the two most relevant cases of pinning by twin boundaries and by columnar defects.

Section X deals with the macroscopic properties of type-II superconductors for the two cases in which the vortex system is in a liquid phase (Sec. X.A) or in a glass phase (Sec. X.B). The main issues discussed here are the ac-susceptibility experiments and their relation to the possible observation of the melting transition, and the decay of a trapped magnetic moment as a consequence of creep and its relation to the concept of self-organized criticality.

Finally, in Sec. XI we conclude with a list of unsolved problems. A summary of the main results has already

been given above. The main emphasis of this review is on the theory of the statistical mechanics and of the dynamics of vortices. Contact with experiments will be made only as an illustration of the theoretical results, and we make no attempt to present a complete list and discussion of the experimental situation.

$$\mathcal{G} = \int d^3r \left\{ \alpha |\Psi|^2 + \frac{\beta}{2} |\Psi|^4 + \sum_{\mu=1}^{3} \frac{1}{2m_\mu} \left| \left( \frac{\hbar}{i} \frac{d}{dx_\mu} + \frac{2e}{c} A_\mu \right) \Psi \right|^2 + \frac{B^2}{8\pi} - \frac{\mathbf{H} \cdot \mathbf{B}}{4\pi} \right\} , \qquad (2.1)$$

where $\Psi(\mathbf{r})$ is the order parameter, $\mathbf{A}$ is the vector potential, $\mathbf{B} = \nabla \wedge \mathbf{A}$ is the microscopic magnetic field, and $\mathbf{H}$ is the applied external field. The GL parameter $\alpha = -\alpha(0)(1 - T/T_c)$ changes sign at the transition temperature $T_c$, whereas $\beta$ is taken to be constant in temperature. We choose the charge unit $e$ to be positive, $e > 0$, and the charge of the electron therefore is $-e$. The parameters $m_\mu$, $\mu = 1, 2, 3$, denote the effective masses along the main axes of the crystal. Here we are interested in the two cases of isotropic and of uniaxially anisotropic material. Our interest in the isotropic case $(m_\mu = m$, $\mu = 1, 2, 3)$ derives mainly from the simplicity of the situation—new ideas and concepts can be developed without having to deal with complications due to additional parameters and reduced symmetry. On the other hand, when applying our results to the new high-temperature superconductors, we have to take the anisotropy of the material into account. For the sake of simplicity and because the oxide superconductors are within high accuracy uniaxial (axis $\| z$) materials, we choose $m_x = m_y = m$, $m_z = M$ and denote the mass anisotropy ratio by

$$\varepsilon^2 = m/M < 1 . \qquad (2.2)$$

In anisotropic materials an additional degree of freedom is the angle between the external magnetic field $\mathbf{H}$ and the superconducting planes. The external field $\mathbf{H}$ is then chosen to lie in the $yz$ plane and to enclose an angle $\vartheta_H (= \pi/2 - \theta_H)$ with the $y$ axis; see Fig. 7. Pinning is introduced into the model via spatial disorder in the GL coefficient $\alpha(\mathbf{r})$ describing disorder in the transition temperature $T_c$, and/or by spatial variation of the effective mass $m_\mu(\mathbf{r})$ describing disorder in the mean free path $l$. To be specific, we shall concentrate mainly on short-scale disorder characterized by Gaussian white noise: $\alpha(\mathbf{r}) = \alpha_0 + \delta\alpha(\mathbf{r})$ with $\langle \delta\alpha \rangle = 0$ and $\langle \delta\alpha(\mathbf{r})\delta\alpha(\mathbf{r}') \rangle = \gamma_\alpha \delta(\mathbf{r} - \mathbf{r}')$, and similarly $m_\mu(\mathbf{r}) = m_{0\mu} + \delta m_\mu(\mathbf{r})$ with $\langle \delta m_\mu \rangle = 0$ and $\langle \delta m_\mu(\mathbf{r})\delta m_\nu(\mathbf{r}') \rangle = \gamma_{m\mu}\delta_{\mu\nu}(\mathbf{r} - \mathbf{r}')$. Pinning by extended defects will be discussed in Sec. IX. In the following we shall consider the isotropic case and return to the anisotropic situation in Sec. II.C.

The homogeneous solutions of Eq. (2.1) are given by $\Psi_0 = 0$ (normal state) and $|\Psi_0|^2 = |\alpha|/\beta$ (superconducting state). The energy gain in the superconducting state $(\alpha < 0)$ is given by the condensation energy

## II. SINGLE-VORTEX PINNING

The basic frame for the phenomenological description of superconductivity is given by the Ginzburg-Landau (GL) free-energy functional

$H_c^2/8\pi = \alpha^2/2\beta$, with $H_c$ the thermodynamic critical field. Variation of the GL functional (2.1) with respect to the order parameter $\Psi^*$ and the vector potential $\mathbf{A}$ furnishes the equations determining the spatial variations of $\Psi = |\Psi| \exp(i\varphi)$ and $\mathbf{A}$ in the inhomogeneous situation,

$$\xi^2 \left[ \nabla + \frac{2\pi i}{\Phi_0} \mathbf{A} \right]^2 \Psi + \Psi - \frac{|\Psi|^2}{|\Psi_0|^2} \Psi = 0 , \qquad (2.3)$$

$$\lambda^2 \frac{|\Psi_0|^2}{|\Psi|^2} \nabla \wedge (\nabla \wedge \mathbf{A}) + \mathbf{A} = -\frac{\Phi_0}{2\pi} \nabla\varphi . \qquad (2.4)$$

These two differential equations are characterized by the GL coherence length $\xi(T)$ and the penetration depth $\lambda(T)$ determining the scale of variations in the order parameter and in the magnetic field, respectively. In terms of the GL parameters these length scales are given by

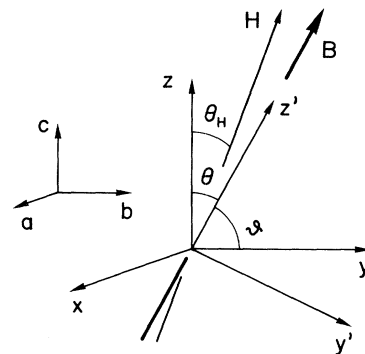$$\xi^2(T) = \frac{\hbar^2}{2m |\alpha(T)|} = \xi^2(0) \frac{1}{1 - T/T_c} \qquad (2.5)$$

and

FIG. 7. Main coordinate systems used throughout this review. The axes $x$, $y$, and $z$ are aligned with the crystal symmetry axes $a$, $b$, and $c$, with $c$ denoting the axis of (roughly) uniaxial anisotropy and the $ab$ plane containing the superconducting CuO planes. The magnetic field $\mathbf{H}$ lies in the $yz$ plane and encloses an angle $\theta_H = \pi/2 - \vartheta_H$ with the $c$ axis (an angle $\vartheta_H$ with the $ab$ plane). The induction $\mathbf{B}$ (also lying in the $yz$ plane) is in general not aligned with the magnetic field $\mathbf{H}$ and encloses an angle $\vartheta$ with the $ab$ plane. The coordinate system $x', y', z'$ is aligned with the induction $\mathbf{B}$ and has a common $x$ axis with the crystal system, $x' = x$.

$$\lambda^2(T) = \frac{mc^2}{16\pi e^2 |\Psi_0(T)|^2} = \lambda^2(0) \frac{1}{1 - T/T_c} \ . \qquad (2.6)$$

In the following we use the zero-temperature values of the length scales $\xi$ and $\lambda$ for the characterization of the superconductor rather than the original GL parameters. Note that we distinguish between the extrapolated zero-temperature parameters $\xi(0)$ and $\lambda(0)$ and the microscopic quantities $\xi_{BCS}[\approx 1.36\xi(0)]$ and $\lambda_L[\approx 1.41\lambda(0)]$; see Sec. III.C. The expression for the thermodynamic critical field takes the form

$$H_c = \frac{\Phi_0}{2\sqrt{2}\pi\lambda\xi} \ , \qquad (2.7)$$

where $\Phi_0 = hc/2e$ is the flux quantum.

In this review we focus on the class of strongly type-II materials characterized by a large Ginzburg-Landau parameter $\kappa = \lambda/\xi \gg 1$, to which the new oxide superconductors belong. In this case the London theory provides a good approximation to the phenomenological description of superconductivity. Within the London theory the free energy of the system is obtained by summation of the energy of the currents flowing in the superconductor and the magnetic-field energy $B^2/8\pi$. By variation of Eq. (2.1) with respect to the vector potential $\mathbf{A}$ we obtain for the current density the expression

$$\mathbf{j} = -\frac{e\hbar}{mi}[\Psi^*\nabla\Psi - \Psi\nabla\Psi^*] - \frac{4e^2}{mc}\Psi^*\Psi\mathbf{A} \ , \qquad (2.8)$$

$$= -\frac{2e\hbar}{m}|\Psi|^2\nabla\tilde{\varphi} \ , \qquad (2.9)$$

where we have introduced the gauge-invariant phase gradient

$$\nabla\tilde{\varphi} = \nabla\varphi + \frac{2\pi}{\Phi_0}\mathbf{A} \ . \qquad (2.10)$$

Within the London approximation we ignore the spatial variations in the modulus of the order parameter, and the London free-energy functional then takes the form

$$\mathcal{F}_L = \frac{1}{8\pi}\int d^3r[\lambda_L^2(\nabla\wedge\mathbf{B})^2 + B^2] \ , \qquad (2.11)$$

with the London penetration depth $\lambda_L$ given by

$$\lambda_L^2 = \frac{mc^2}{4\pi ne^2} \ , \qquad (2.12)$$

$n$ being the density of superconducting electrons. In contrast to the GL theory with its regime of applicability restricted near the superconducting transition temperature $T_c$, the London theory is valid within the whole temperature range $0 < T < T_c$, as long as the magnetic field does not lead to a significant suppression of the order parameter.

In a type-II superconductor the (mean-field) $H$-$T$ phase diagram is divided up into two phases with very different phenomenological properties, a Meissner regime at small applied fields below the lower critical field $H_{c_1}$ and the Abrikosov mixed phase above $H_{c_1}$; see Fig. 1. The lower

critical field is determined by the line energy $e_l$ of a single vortex, which is given by

$$e_l = \varepsilon_0 \ln\frac{\lambda}{\xi} = \frac{\Phi_0}{4\pi}H_{c_1} \ . \qquad (2.13)$$

Here we have introduced the important energy scale

$$\varepsilon_0 = \left[\frac{\Phi_0}{4\pi\lambda}\right]^2 \ , \qquad (2.14)$$

which determines the self-energy of the vortex lines as well as their mutual interaction. The isolated vortex line is a topological excitation of the superconductor characterized by a line singularity in the phase $\varphi$ of the order parameter: encircling the vortex line once, the phase $\varphi$ changes by $2\pi$. As a result, the order parameter $\Psi$ is suppressed within the core region extending a length $\xi$ away from the singularity. Second, the gauge-invariant phase gradient $\nabla\tilde{\varphi}$ drives a circular screening current $\mathbf{j} = -(2e\hbar/m)|\Psi|^2\nabla\tilde{\varphi}$ extending a distance $\lambda$ away from the core and trapping a flux $\Phi_0$. Above $H_{c_1}$ the external magnetic field penetrates into a homogeneous superconductor by setting up a triangular lattice of vortex lines with a lattice constant

$$a_\Delta = \left[\frac{2}{\sqrt{3}}\right]^{1/2}\left[\frac{\Phi_0}{B}\right]^{1/2} \ . \qquad (2.15)$$

For later convenience we also introduce the inverse square root of the vortex density,

$$a_0 = \left[\frac{\Phi_0}{B}\right]^{1/2} \ . \qquad (2.16)$$

For large external fields, the vortex cores start to overlap and superconductivity disappears above the upper critical field $H_{c_2}$,

$$H_{c_2} = \frac{\Phi_0}{2\pi\xi^2} \ . \qquad (2.17)$$

Let us now concentrate on a single vortex: In general terms, a vortex can be considered as an elastic string which, compared with a pointlike object, exhibits additional interesting static and dynamic properties due to its one-dimensional extended nature. The vortex line is an elastic object, and therefore we first have to determine its line tension, the quantity describing the elastic response. Consider, then, a vortex aligned with the $z$ axis of our coordinate system. In an isotropic material the elastic energy of a deformed vortex is simply determined by the increase of the vortex length,

$$\mathcal{F}_{el} = \int dz\, e_l\{[1 + (\partial_z\mathbf{u})^2]^{1/2} - 1\} \ ,$$

$$\approx \int dz\frac{e_l}{2}\left[\frac{\partial\mathbf{u}}{\partial z}\right]^2 \ ,$$

where $\mathbf{u}(z) = (u_x, u_y)$ denotes the displacement field of the vortex. We thus obtain the simple result that the (long-

wavelength) line tension $\varepsilon_l$ is equal to the line energy $e_l$ in an isotropic material, $\varepsilon_l = e_l$. This is no longer the case in an anisotropic material, where the line energy of the vortex depends on the angle $\vartheta$ between the vortex and the superconducting planes, thereby generating an additional contribution to the line tension (Sudbø and Brandt, 1991a, 1991b). Deviations from the simple expression (2.13) for the line tension are also possible in an isotropic material: a short-wavelength distortion with $k > 1/\lambda$ leads to a dispersive line tension (Brandt, 1977b)

$$\varepsilon_l(k) = \varepsilon_0 \ln \frac{1}{k\xi} \ . \tag{2.18}$$

This logarithmic dispersion has the following physical origin: The line energy of a vortex consists of a part due to the energy of the circular currents set up by the phase gradient $\nabla\tilde{\varphi}$ and a second contribution which originates from the magnetic-field energy. The contribution from the currents is largest near the vortex core and cut off due to screening at a distance $\lambda$ for the case of a straight vortex. A short-wavelength distortion of the vortex affects mainly the current pattern in the vicinity of the vortex core. The line tension is then due to this redistribution in the current density, which we have to cut off on the scale $1/k$, thereby producing the logarithmic dispersion (2.18). In the following we shall deal mainly with the problem of vortex pinning, which involves short-wavelength distortions $k \sim 1/L$ of the vortex line with $\xi < L \ll \lambda$. In this case we shall drop the logarithmic correction of order unity $\ln(1/k\xi)$ in the line tension (2.18) and use the approximation $\varepsilon_l(k \sim 1/L) \simeq \varepsilon_0$.

There are *three* main sources of force acting on an individual vortex line: *First,* a vortex at rest with respect to the laboratory frame of reference and exposed to a laminar current flow $\mathbf{j}$ is subject to the Lorentz force,

$$\mathbf{f}_L = \frac{\Phi_0}{c} \mathbf{j} \wedge \mathbf{n} \ . \tag{2.19}$$

Here, $\mathbf{n}$ is a vector of unit length along which the vortex is directed. As the vortex line starts to move, only velocity relative to the motion of the condensate contributes to the driving force, and by Galilean invariance we obtain (see, for example, Vinen, 1969)

$$\mathbf{f}_M = \rho_s \frac{\Phi_0}{c} (\mathbf{v}_s - \mathbf{v}_v) \wedge \mathbf{n} \ , \tag{2.20}$$

where $\rho_s = 2e|\Psi|^2$ denotes the charge density of the superconducting condensate and $\mathbf{v}_s$ and $\mathbf{v}_v$ are the velocities of the condensate and of the vortex line with respect to the laboratory frame, respectively. The force (2.20) can be derived from hydrodynamic considerations [and thus is also present in an uncharged superfluid (Vinen, 1969)] and is usually called the Magnus force. A very modern derivation of this force in terms of a Berry phase argument has recently been given by Haldane and Wu (1985) and by Ao and Thouless (1993). In a perfect system, (2.20) is the only force acting on the vortex. When a transport current density $\mathbf{j} = \rho_s \mathbf{v}_s$ is applied to the sys-

tem, the vortex simply is dragged along with the flow such that $\mathbf{f}_M = 0$.

The *second* class of forces acting on a vortex is due to the presence of (microscopic) scattering processes in an otherwise homogeneous system. The determination of the equation of motion for the vortex then becomes a very difficult issue, and the final answer in this matter is still unknown to date. A major problem, as yet unsolved, is a curious change of sign in the Hall voltage appearing in various materials as they enter the superconducting state. Such observations have been reported for various high-temperature superconductors (Galffy and Zirgiebl, 1988; Artemenko, Gorlova, and Latyshev, 1989c; Iye, Nakamura, and Tamegai, 1989b; Hagen et al., 1991) as well as for some conventional materials (in niobium: Van Beelen et al., 1967; in vanadium: Usui, Ogaswara, and Yasukochi, 1968; Usui et al., 1969). A microscopic derivation of the vortex equation of motion in the presence of scattering has been given by Kopnin and Kravtsov (1976a, 1976b) and by Kopnin and Salomaa (1991). In their equation the driving Lorentz force $(\Phi_0/c)\mathbf{j} \wedge \mathbf{n}$ is balanced against the sum of the friction force $\eta_l \mathbf{v}_v$ and the Hall force $\alpha_l \mathbf{v}_v \wedge \mathbf{n}$,

$$\frac{\Phi_0}{c} \mathbf{j} \wedge \mathbf{n} = \eta_l \mathbf{v}_v + \alpha_l \mathbf{v}_v \wedge \mathbf{n} \ . \tag{2.21}$$

The transport coefficients $\eta_l$ and $\alpha_l$ take the form

$$\eta_l = \frac{\Phi_0}{c} \rho_s \frac{\omega_0 \tau_r}{1 + \omega_0^2 \tau_r^2} \ ,$$
$$\alpha_l = \frac{\Phi_0}{c} \rho_s \frac{\omega_0^2 \tau_r^2}{1 + \omega_0^2 \tau_r^2} \ , \tag{2.22}$$

with the characteristic frequency $\omega_0$ given by the level separation of the quasiparticle states bound to the vortex core (see, for example, Caroli, de Gennes, and Matricon, 1964), where $\hbar\omega_0 \approx \delta\varepsilon^2/\varepsilon_F$, and $\tau_r$ is the scattering relaxation time. Here, $\delta\varepsilon = \hbar v_F/\pi\xi$ denotes the confinement energy, $v_F$ is the Fermi velocity, and $\varepsilon_F$ denotes the Fermi energy. Note that in Eq. (2.21) no term of the form $\eta_l' \mathbf{v}_s$ appears—such terms would lead to the deceleration of the superflow even for vortices at rest (Vinokur et al., 1993). Also, no term describing a vortex mass appears in Eq. (2.21). Such a term would involve taking the finite frequency response of the vortex into account; see, for example, Kopnin and Salomaa (1991).

We present a simple (heuristic) argument for the form of the vortex equation of motion (2.21) in the presence of scattering. The argument is based on the requirement that the resulting vortex velocity $\mathbf{v}_v$ be consistent with the carrier motion inside the vortex core (Bardeen and Sherman, 1975; Kopnin and Salomaa, 1991; Volovik, 1993). The latter is described by the generalized law of conductivity in the presence of both an electric ($\mathbf{E}$) and a magnetic ($\mathbf{B}$) field; for $\mathbf{B}\|\mathbf{n}$ and $\mathbf{j}$, $\mathbf{E}\perp\mathbf{n}$ we can write

$$\mathbf{j} = \sigma_\| \mathbf{E} + \sigma_\perp \mathbf{n} \wedge \mathbf{E} \ , \tag{2.23}$$

with

$$\sigma_\parallel = \sigma_n \frac{1}{1+v^2}, \quad \sigma_\perp = \sigma_n \frac{v}{1+v^2}, \quad (2.24)$$

and the conductivity is given by $\sigma_n = e^2 n \tau_r / m$. The relaxation time $\tau_r$ accounts for all the scattering processes, and the parameter $v = \omega_c \tau_r$ relates to the Hall effect with $\omega_c = eB/mc$ the cyclotron frequency. Rewriting the electric field $\mathbf{E}$ in terms of the vortex velocity $\mathbf{v}_v$, $\mathbf{E} = \mathbf{B} \wedge \mathbf{v}_v / c$ and taking the cross product of (2.23) with $\Phi_0 \mathbf{n}/c$, we obtain the force equation

$$\frac{\Phi_0}{c} \mathbf{j} \wedge \mathbf{n} = \tilde{\eta}_l \mathbf{v}_v + \tilde{\alpha}_l \mathbf{v}_v \wedge \mathbf{n}, \quad (2.25)$$

with the two transport coefficients $\tilde{\eta}_l = \pi \hbar n v / (1+v^2)$ and $\tilde{\alpha}_l = -\pi \hbar n v^2 / (1+v^2)$ describing the dissipative and the Hall component of the motion (we have used $\sigma_n \Phi_0 H / c^2 = \pi \hbar n$). For an electron in a magnetic field $B$, the parameter $v$ is determined by the cyclotron motion and hence involves the cyclotron frequency $\omega_c = eB/mc$. On the other hand, the corresponding frequency for an electron orbiting within the core of a vortex is given by the level spacing $\hbar \omega_0$. Substituting $\omega_c \to \omega_0$ and $-en \to \rho_s = 2e|\Psi_0|^2 (T=0)$ in the expressions for the coefficients $\tilde{\eta}_l$ and $\tilde{\alpha}_l$, we recover the result (2.21) and (2.22) derived from microscopic calculations [note that the substitution $-en \to \rho_s = 2e|\Psi_0|^2 (T=0)$ is consistent with the derivation of the phenomenological Ginzburg-Landau equations from the microscopic Gor'kov equations, as discussed below in Sec. III.C].

Let us briefly discuss the various types of motion a vortex can perform on the basis of Eq. (2.21). In most cases the parameter $\omega_0 \tau_r \ll 1$ is small, and the equation of motion is dominated by the dissipative term, with the viscous drag coefficient $\eta_l$ given by the Bardeen-Stephen (1965) expression

$$\eta_l \simeq \frac{\Phi_0 H_{c_2}}{\rho_n c^2}, \quad (2.26)$$

with $\rho_n$ the normal-state resistivity of the material. Equation (2.26) describes well the situation at low fields and low temperatures, whereas corrections become important near the transition temperature and for high magnetic fields (Gor'kov and Kopnin, 1973; Larkin and Ovchinnikov, 1986). In the limit $\alpha_l \ll \eta_l$, Eq. (2.21) then simplifies to

$$\eta_l \mathbf{v}_v = \frac{\Phi_0}{c} \mathbf{j} \wedge \mathbf{n}, \quad (2.27)$$

and the vortex moves at right angles to the external current density $\mathbf{j}$. On the other hand, in very pure material such that $\omega_0 \tau_r \gg 1$ [note that this corresponds to the super-clean limit $l \gg \xi (\varepsilon_F / \Delta)$, where $l = v_F \tau_r$ denotes the mean free path and $\Delta$ is the gap parameter, thus guaranteeing the existence of well-defined quasiparticle states in the core], the Hall term becomes the dominant one, with

$$\alpha_l = \frac{\Phi_0}{c} \rho_s. \quad (2.28)$$

In this case we recover the Magnus force (2.20) as the only force acting on the vortex, which thus is dragged along with the superflow (see also Vinen and Warren, 1967), the typical situation for a vortex in an uncharged superfluid.

The more conventional situation in a superconductor involves a large dissipative and only a small Hall component in the vortex motion. However, as shown in Sec. III.C, in the oxide superconductors the smallness of $\xi$ and $\varepsilon_F$ and the largeness of $l = v_F \tau_r$ and $\Delta$ open up the possibility that these materials may be close to or even within the super-clean limit, so that the Hall term becomes relevant. The Hall angle $\theta_{\text{Hall}}$ then describes the appearance of a field component $\mathbf{E}$ perpendicular to the current flow $\mathbf{j}$ and is determined by the ratio $\alpha_l / \eta_l$,

$$\tan \theta_{\text{Hall}} = \frac{v_v^\parallel}{v_v^\perp} = \frac{\alpha_l}{\eta_l}.$$

Here $v_v^\parallel$, $(v_v^\perp)$ denote the velocity component of the vortex parallel (perpendicular) to the current density $\mathbf{j}$. Usually $(\alpha_l \ll \eta_l)$ the Hall angle is small, $\theta_{\text{Hall}} \approx 0$, and becomes large $(\theta_{\text{Hall}} \to \pi/2)$ only in the super-clean limit. In the following, if not otherwise stated, we shall ignore the Hall effect and set $\theta_{\text{Hall}} = 0$. Note that the issue of a possible sign change in the Hall angle involves the calculation of the sign of $\alpha_l$ from microscopic considerations.

Finally, let us turn to the *third* type of force acting on a vortex: in an inhomogeneous material the vortex can become pinned by the action of the defects. This pinning allows for the formation of a static vortex density gradient, or Bean critical state (see Bean, 1962, 1964), which in turn is equivalent to a bulk-transport current density $\mathbf{j} = (c/4\pi) \nabla \wedge \mathbf{B}$ flowing free of dissipation, an important goal where applications are concerned. The maximal vortex density gradient is obtained when the pinning force $\mathbf{f}_{\text{pin}}$ acting on a vortex becomes equal to the driving Lorentz force, the resulting current density being the critical or depinning current density $j_c$,

$$\frac{\Phi_0}{c} \mathbf{j}_c \wedge \mathbf{n} = \mathbf{f}_{\text{pin}}. \quad (2.29)$$

Usually, this critical current density is considerably reduced with respect to the depairing current density $j_0$, which can be estimated from Maxwell's equation $\nabla \wedge \mathbf{B} = (4\pi/c)\mathbf{j}$ to be of the order of $j_0 \simeq cH_c/4\pi\lambda$. The exact result from GL theory is

$$j_0 = \frac{cH_c}{3\sqrt{6}\pi\lambda} = \frac{4}{3\sqrt{3}} \frac{c\varepsilon_0}{\xi\Phi_0}. \quad (2.30)$$

From a thermodynamic point of view the critical state is only a metastable state and thus bound to decay either by thermal activation or by tunneling, phenomena known under the name of "creep." The critical current density as well as the rates for classical and quantum creep de-

pend strongly on the strength of the pinning force. Since the Lorentz force actually is a force per unit length, pinning has to produce a force per unit length, too. Thus we are faced with a summation problem for individual pinning forces. For the case of weak pointlike pinning centers, this summation problem was first solved by Larkin and Ovchinnikov within their collective pinning theory (1973).[3] In the following sections, we determine the critical current density and the classical and quantum creep rates within weak collective pinning theory for the situation in which the interaction between vortices can be neglected. The results then apply to the regime of small fields and small temperatures within the $H$-$T$ phase diagram. The general situation treating both large fields and higher temperatures is discussed in Sec. IV below.

## A. Collective pinning theory

### 1. Single vortex in a random potential

Consider an isolated vortex line directed along the $z$ axis of our coordinate system in the presence of a weak random pinning potential $\varepsilon_{pin}$ and subject to the Lorentz force $\mathbf{f}_L = \Phi_0 \mathbf{j} \wedge \mathbf{e}_z / c$ with the current density $\mathbf{j} = (0, j_y, 0)$ directed along the $y$ axis. The Lorentz force is then directed along the $x$ axis. The free-energy functional describing this situation is

$$\mathcal{F}[\mathbf{u}] = \int dz \left[ \frac{\varepsilon_l}{2} (\partial_z \mathbf{u})^2 + \varepsilon_{pin}(z, \mathbf{u}) - \mathbf{f}_L \cdot \mathbf{u} \right] , \quad (2.31)$$

where $\mathbf{u}(z)$ denotes the displacement vector of the vortex line and $\varepsilon_l$ is the elastic tension. The random pinning potential $\varepsilon_{pin}$ acting on the vortex line can be characterized by a correlation function $\mathcal{H}$,

$$\langle \varepsilon_{pin}(z, \mathbf{u}) \varepsilon_{pin}(z', \mathbf{u}') \rangle = \mathcal{H}(z - z', \mathbf{u} - \mathbf{u}') . \quad (2.32)$$

The correlator $\mathcal{H}(z, \mathbf{u})$ depends on the nature of the disorder: When the disorder is produced by an extended defect, e.g., precipitates, twinning or grain boundaries, or columnar defects such as dislocation lines, the pinning potential is correlated over the size of the defect $r_p$, and hence $\mathcal{H}$ decays on this same length scale. We shall come back to this case in Sec. IX below. Here we assume that

pinning is due to point defects perturbing the superconductor on a scale smaller than the coherence length $\xi$. In the new oxide superconductors, such pinning sites are produced by oxygen defects (Tinkham, 1988b), and we shall show in Sec. III.C that this source of pinning can indeed account for the experimentally observed critical current densities. In this case the disorder correlation length along the vortex is given by the size of the defect, which we assume to be zero here. On the other hand, the smallest transverse length scale that can be resolved by the vortex core is the coherence length $\xi$, hence $r_p \simeq \xi$ defines the disorder correlation length in the transverse direction. To be more specific, let us compare Eq. (2.31) with the GL equation (2.1) and relate the pinning potential $\varepsilon_{pin}$ to the disorder in the coefficients $\alpha$ and $m$,

$$\varepsilon_{pin}(z, \mathbf{u}) = \int d^2R \ U_{pin}(\mathbf{r}) p(\mathbf{R} - \mathbf{u}) , \quad (2.33)$$

with $U_{pin}(\mathbf{r}) = |\Psi_0|^2 \delta\alpha(\mathbf{r})$ for the case of $\delta T_c$ disorder and $U_{pin}(\mathbf{r}) = \alpha |\Psi_0|^2 \delta m(\mathbf{r})/m$ for disorder in the mean free path $l$. We denote the two-dimensional coordinate in the plane orthogonal to the vortex by $\mathbf{R}$. Note that we denote the pinning potential acting on the vortex by $\varepsilon_{pin}(z, \mathbf{u})$, whereas $U_{pin}(\mathbf{r})$ describes the material defects generating the pinning. For the two kinds of disorder, the relevant form factors for a single vortex are

$$p(R) = \begin{cases} 1 - |\psi_v(R)|^2, & \delta T_c \text{ pinning}, \\ \xi^2 |\nabla \psi_v(R)|^2, & \delta l \text{ pinning} . \end{cases} \quad (2.34)$$

$\psi_v$ is the solution of the GL equations for a straight vortex aligned with the $z$ axis and normalized by the homogeneous solution $\Psi_0$. In future calculations involving $\psi_v$ we shall use a simple but very accurate model for the vortex core in a type-II superconductor which has been proposed by Schmid (1966; see also Clem, 1975) on the basis of a variational ansatz: In the large-$\kappa$ limit the model core function for a vortex directed along the $z$ axis takes the form $\psi_v(R) = f(R) \exp[i\varphi]$, with $f(R) = R / (R^2 + 2\xi^2)^{1/2}$. Note that for pinning due to short-scale disorder we can neglect the (long-range) screening effects by the vector potential in the form factor for $\delta l$ pinning.

Using Eq. (2.33) we obtain for the correlation function $\mathcal{H}$ the expression

$$\mathcal{H}(z - z', \mathbf{u} - \mathbf{u}') = \int d^2R \ d^2R' \langle U_{pin}(\mathbf{r}) U_{pin}(\mathbf{r}') \rangle p(\mathbf{R} - \mathbf{u}) p(\mathbf{R}' - \mathbf{u}')$$

$$= \gamma_U \delta(z - z') \int d^2R \ p(\mathbf{R} - \mathbf{u}) p(\mathbf{R} - \mathbf{u}') , \quad (2.35)$$

---

[3]This 1973 work took the dynamic approach. The scaling approach was introduced by Fukuyama and Lee (1978) in connection with the pinning problem in 1D charge-density-wave systems (see also Efetov and Larkin, 1977) and was applied to the vortex problem by Larkin and Ovchinnikov (1979) and to the 3D charge-density-wave system by Lee and Rice (1979).

where we have assumed short-scale correlated disorder in $U_{pin}$,

$$\langle U_{pin}(\mathbf{r}) U_{pin}(\mathbf{r}') \rangle = \gamma_U \delta(\mathbf{r} - \mathbf{r}') . \quad (2.36)$$

Evaluating the integral over the form function, we obtain the final result

$$\mathcal{H}(z, \mathbf{u}) = \gamma \xi^4 \delta(z) k(u) , \quad (2.37)$$

with

$$\gamma = \begin{cases} 2\pi \dfrac{\gamma_\alpha}{\alpha^2} \left[ \dfrac{H_c^2}{4\pi} \right]^2 & \text{for } \delta T_c \text{ pinning,} \\[4mm] \dfrac{14\pi}{15} \dfrac{\gamma_m}{m^2} \left[ \dfrac{H_c^2}{4\pi} \right]^2 & \text{for } \delta l \text{ pinning ,} \end{cases} \tag{2.38}$$

and

$$k(u) = \begin{cases} \dfrac{1}{\xi^2}, & u = 0, \\[4mm] \propto \left[ \dfrac{1}{u} \right]^2 \ln \dfrac{u}{\xi}, & u \to \infty . \end{cases} \tag{2.39}$$

Note that $k(u)$ differs for the two cases of $\delta T_c$ and $\delta l$ pinning, but is normalized to $1/\xi^2$ at $u = 0$ and shows the same asymptotic behavior as $u \to \infty$. Let us now consider the interaction of a *stiff* vortex line with a random pinning potential. In this case, the average pinning energy $\langle \mathscr{E}_{\text{pin}}(L) \rangle$ of a vortex segment of length $L$ is zero. On the other hand, the fluctuations of the pinning energy do not vanish, and using Eqs. (2.32) and (2.37) we obtain

$$\langle \mathscr{E}_{\text{pin}}^2(L) \rangle = \int dz \, dz' \langle \varepsilon_{\text{pin}}(z,0)\varepsilon_{\text{pin}}(z',0) \rangle \tag{2.40}$$

$$= \gamma \xi^2 L . \tag{2.41}$$

The sublinear growth of $\langle \mathscr{E}_{\text{pin}}^2(L) \rangle^{1/2}$ has its origin in the competition between the individual pinning centers. Let us characterize the disorder potential by the density of pins $n_i$ and the individual pinning force $f_{\text{pin}}$. Only defects within a distance $\xi$ away from the vortex core contribute to the pinning energy. Due to competition between the pins, the individual pinning forces add up only randomly within the volume $V \simeq \xi^2 L$, and the fluctuations in the pinning energy $\langle \mathscr{E}_{\text{pin}}^2(L) \rangle^{1/2}$ can be written as

$$\langle \mathscr{E}_{\text{pin}}^2(L) \rangle^{1/2} \simeq (f_{\text{pin}}^2 n_i \xi^2 L )^{1/2} \xi , \tag{2.42}$$

allowing us to relate the disorder parameter $\gamma$ to the individual pinning force $f_{\text{pin}}$ and the impurity density $n_i$,

$$\gamma \simeq f_{\text{pin}}^2 n_i \xi^2 . \tag{2.43}$$

Thus we have two possible alternatives for the determination of $\gamma$: First, the random potential producing the pinning can be described by short-scale disorder in the GL coefficients $\alpha$ and $m$. Our task then is to determine their spatial variation due to the point defects present in the material. This approach is followed in Sec. III.C below, where we determine the disorder parameter $\gamma$ from microscopic considerations. The second method is to calculate [again from microscopic considerations; see, for example, Thuneberg (1989)] the individual pinning force $f_{\text{pin}}$ of one defect and then use Eq. (2.43) for the determination of the pinning parameter $\gamma$. This approach has been taken by van der Beek and Kes (1991).

## 2. Basic idea of collective pinning theory

The result (2.41) implies that the pinning force acting on an individual stiff vortex grows only sublinearly. Since the driving Lorentz force increases linearly with length, we have to conclude that a *stiff* vortex is never pinned, and hence the critical current density vanishes in this limit. On the other hand, a real vortex is characterized by a *finite* elasticity such that the vortex line can accommodate to the pinning potential on some large enough length scale. The basic idea of weak collective pinning theory, then, is to cut off the sublinear growth in $\langle \mathscr{E}_{\text{pin}}^2(L) \rangle^{1/2}$ at the *collective pinning length* $L_c$ above which the displacement $u$ of the vortex increases beyond the characteristic length $r_p$ of fluctuations in the random potential $\varepsilon_{\text{pin}}$. Each vortex segment of length $L_c$ is then pinned independently, and balancing the Lorentz force against the pinning force acting on the individual segments generates a finite critical current density $j_c$. Our final task is to determine the collective pinning length $L_c$. This is accomplished by minimizing the free energy of the vortex with respect to the length $L$ over which the pinning forces add up randomly, and we shall do this by using the method of dimensional estimates. In particular, we shall consistently drop all numerical factors within this approach.

Let us consider the following simple estimate for the free energy (2.31): A vortex segment of length $L$ and distorted with an amplitude $u$ contributes an elastic energy $\varepsilon_0 u^2/L$ to the free energy of the string. Second, we have to add the energy gain $-(\gamma \xi^2 L)^{1/2}$ from the random pinning potential, and finally the contribution to Eq. (2.31) from the Lorentz force is $j\Phi_0 Lu/c$. Collecting all the terms, we obtain

$$\mathscr{F}(u,L) \simeq \varepsilon_0 \frac{u^2}{L} - (\gamma \xi^2 L)^{1/2} - j\frac{\Phi_0}{c} Lu . \tag{2.44}$$

The collective pinning length $L_c$ is obtained by minimizing the energy density $\mathscr{F}(u = \xi, L)/L$ with respect to $L$ at zero current density,

$$L_c \simeq \left[ \frac{\varepsilon_0^2 \xi^2}{\gamma} \right]^{1/3} , \tag{2.45}$$

and the resulting collective pinning energy is

$$U_c \simeq (\gamma \xi^2 L_c)^{1/2} \simeq (\gamma \varepsilon_0 \xi^4)^{1/3}$$

$$\simeq H_c^2 \xi^3 \frac{\xi}{L_c} \simeq T_c \left[ \frac{1-t}{Gi} \right]^{1/2} \frac{\xi}{L_c} , \tag{2.46}$$

where we have expressed $U_c$ via the elastic energy, $U_c \simeq \varepsilon_0 \xi^2/L_c$. Here $Gi$ denotes the Ginzburg number (Ginzburg, 1960),

$$Gi = \frac{1}{2} \left[ \frac{T_c}{H_c^2(0)\xi^3(0)} \right]^2$$

$$= \frac{16\pi^3\kappa^4}{\Phi_0^3} \frac{(T_c)^2}{H_{c_2}(0)} = 10^{-9} \frac{\kappa^4 T_c^2}{H_{c_2}(0)} , \tag{2.47}$$

as defined by the condition $|\delta\Psi/\Psi|^2(T_f)=1$, $(1-T_f/T_c)=Gi$. Here $\delta\Psi$ denotes the (critical) fluctuation of the superconducting order parameter; hence $Gi$ is a measure of the importance of thermal fluctuations. In Eq. (2.47), the thermodynamic field $H_c(0)$ is related via the equation $H_c(0)=H_{c_2}(0)/\sqrt{2}\kappa$ to the upper critical field $H_{c_2}(T\rightarrow0)$ *linearly* extrapolated to zero temperature. In the last formula, the transition temperature $T_c$ has to be expressed in Kelvin, and the upper critical field $H_{c_2}(0)$ is measured in Gauss. Whereas in conventional superconductors $Gi$ is a very small number, of the order of $10^{-7}$, the Ginzburg number is quite large in the new high-temperature superconductors, of the order of $10^{-2}$ (Lobb, 1987). Note that, for the anisotropic oxide superconductors, $Gi$ is enhanced by the anisotropy parameter $1/\varepsilon^2\gg1$,

$$Gi=\frac{1}{2}\left[\frac{T_c}{H_c^2(0)\varepsilon\xi^3(0)}\right]^2.\tag{2.48}$$

A very useful relation between the transition temperature $T_c$, the energy scale of the vortex interaction $\varepsilon_0$, and the Ginzburg number $Gi$ is

$$\left[\frac{\varepsilon\varepsilon_0\xi}{T_c}\right]^2=\frac{1-T/T_c}{8Gi}.\tag{2.49}$$

The results (2.45) and (2.46) apply to the limit of an isolated vortex, i.e., for weak enough magnetic fields that we can neglect the interaction between neighboring vortices. For this case, each segment of length $L_c$ of this vortex is pinned by the collective action of all the defects within the collective pinning volume $V_c\simeq\xi^2L_c$, which then act to produce a finite pinning potential $U_c$.

Experimentally, the collective pinning length $L_c$ is difficult to determine, one possibility being to investigate the thickness dependence of the critical curent density in a thin film (Wördenweber and Kes, 1985, 1986; Brandt, 1986a; Kes and Wördenweber, 1987). On the other hand, the collective pinning energy $U_c$ can be determined more directly in a relaxation experiment by measuring the creep rate. The simplest quantity to be determined in an experiment, however, is the critical current density $j_c$.

### 3. Critical current density

From the above considerations the critical current density $j_c$ is simply determined by equating the pinning force $(\gamma L_c)^{1/2}$ with the Lorentz force $j_c\Phi_0L_c/c$. We obtain

$$j_c\simeq\frac{c}{\Phi_0}\left[\frac{\gamma}{L_c}\right]^{1/2}\simeq j_0\left[\frac{\xi}{L_c}\right]^2,\tag{2.50}$$

with the depairing current density $j_0$ introduced above, Eq. (2.30). The regime of weak collective pinning is characterized by a large suppression of the critical current density $j_c$ with respect to the depairing value $j_0$,

$j_c\ll j_0$. Using Eq. (2.50), this implies that the collective pinning length $L_c$ should be much larger than the coherence length $\xi$, $L_c\gg\xi$. The latter condition is consistent with our use of elasticity theory in the determination of the collective pinning length. For $L_c\approx\xi$ the distortion of the vortex line is large, simple elasticity theory breaks down, and the pinning should be considered to be strong. According to the result (2.45) for the collective pinning length $L_c$, the condition for weak pinning is then fulfilled for a weak enough pinning potential characterized by a small disorder parameter $\gamma$.

A comparison of the critical current density $j_c$ with experimental results provides the simplest check for the validity of collective pinning theory. As already mentioned above, we are then forced to study the microscopic origin of the disorder in order to determine the parameter $\gamma$. Alternatively, we can take a more phenomenological point of view and regard $j_c$ as the simplest experimentally accessible quantity which we can use for the characterization of the disorder potential. Taking the latter point of view we express the collective pinning length $L_c$ and the collective pinning energy $U_c$ by the critical current density $j_c$ and obtain

$$L_c\simeq\xi\left[\frac{j_0}{j_c}\right]^{1/2},\tag{2.51a}$$

$$U_c\simeq H_c^2\xi^3\left[\frac{j_c}{j_0}\right]^{1/2}\simeq T_c\left[\frac{1-t}{Gi}\right]^{1/2}\left[\frac{j_c}{j_0}\right]^{1/2}.\tag{2.51b}$$

The plan, then, is to determine various physical quantities from weak collective pinning theory and to check whether a consistent picture emerges in the comparison with experimental data. Should we use the critical current density $j_c$ for the characterization of the disorder strength we in fact lose one of the possible "tests" of our theory. In Sec. III.C we shall show how the disorder strength can be determined from other experimental data outside the realm of collective pinning theory, and thus we recover this additional check on our theory.

### 4. Classical creep

The property of hard type-II superconductors that is technologically most interesting is their ability to carry a bulk current density **j** with essentially no dissipation. This current density is related via Maxwell's equation $\nabla\wedge\mathbf{B}=(4\pi/c)\mathbf{j}$ to the vortex density gradient which is the result of pinning. Therefore a sample carrying a macroscopic screening or transport current is in a state which, from a thermodynamic point of view, is only metastable and thus bound to decay due to thermally activated motion of the vortices. The latter phenomenon, known as creep, was introduced by Anderson (1962) and by Anderson and Kim (1964) (see also Kramers, 1940, for his pioneering work describing the decay of metastable states, as well as the review of Hänggi, Talkner, and Borkovec, 1990). The basic equations determining the decay

of the current density $j$ are given by Maxwell's equation, $\partial_t B = -c \partial_x E$, where we are using the same geometrical arrangement as above with the field $B \| z$, the current $j \| y$, and with the electric field generated by the vortex motion

$$\mathbf{E} = \frac{1}{c} \mathbf{B} \wedge \mathbf{v} \tag{2.52}$$

also parallel to the $y$ axis. The velocity of the vortices is parallel to the Lorentz force, $\mathbf{v} = (v, 0, 0)$. Using Eq. (2.52) in Faraday's law, we obtain the equation of continuity for the vortex lines,

$$\partial_t B = -\partial_x (vB) . \tag{2.53}$$

Relating the magnetic field and the current via $\nabla \wedge \mathbf{B} = (4\pi/c) \mathbf{j}$, we obtain the corresponding dynamic equation for the current,

$$\partial_t j = \frac{c}{4\pi} \partial_x^2 (vB) . \tag{2.54}$$

The dynamic equations (2.53) and (2.54) describe a non-linear diffusion process that we shall discuss in more detail in Sec. X. The important factor in the above equations is the velocity $v$ of the vortices, which is due to thermal activation over the pinning barrier $U(j)$,

$$v = v_0 e^{-U(j)/T} , \tag{2.55}$$

leading to a dynamic equation for the current density $j$ of the form

$$\partial_t j \simeq -\frac{j_c}{\tau_0} e^{-U(j)/T} . \tag{2.56}$$

(We measure energies in units of Kelvin and thus put the Boltzmann constant equal to unity.) The above equation can be solved with logarithmic accuracy, and we obtain (Geshkenbein and Larkin, 1989)

$$U(j) = T \ln \left[ 1 + \frac{t}{t_0} \right] , \tag{2.57}$$

with $t_0 = \tau_0 T/j_c |\partial_j U|$. From Eq. (2.57) we can find the time evolution of the screening current density $j(t)$ by simple inversion.

The important quantity that we need to know is the activation energy $U(j)$, in particular, its functional dependence on the current density $j$. The energy scale for the pinning barrier $U$ is determined by the collective pinning energy $U_c$. Furthermore, the dependence of $U$ on the transport current density $j$ is due to the Lorentz force, so that the barrier vanishes at the critical current density $j_c$,

$$U(j \to j_c) \simeq U_c \left[ 1 - \frac{j}{j_c} \right]^{\alpha} . \tag{2.58}$$

Up until now no theory has existed for the exponent $\alpha$, and its calculation poses a very interesting problem related to the theory of phase transitions and self-organized criticality. We shall comment on this point later (see Sec. III.E) since the interaction between the vortices is impor-

tant in the determination of $\alpha$. Using Eq. (2.58) with an exponent $\alpha = 1$ in accordance with Anderson's original proposal, we obtain the famous logarithmic time decay of the (diamagnetic) current,

$$j(t) = j_c \left[ 1 - \frac{T}{U_c} \ln \left[ 1 + \frac{t}{t_0} \right] \right] . \tag{2.59}$$

The temporal decay of the transport current is thus determined by the ratio $T/U_c$, which can be found experimentally by measuring the relaxation of the diamagnetic moment of a sample in the critical state. The activation energy $U_c$ is therefore an experimentally accessible quantity and provides one test for the validity of the weak collective pinning theory. Typical experimental results for the activation energy $U_c$, obtained in magnetic relaxation experiments at low temperatures, are in the range $U_c \sim 100$–$1000$ K (Yeshurun and Malozemoff, 1988; Yeshurun *et al.*, 1988, 1989; Hagen and Griessen, 1989; Campbell, Fruchter, and Cabanel, 1990; Lairson *et al.*, 1991; Malozemoff, 1991).

So far we have considered only the case in which $j$ is close to its critical value $j_c$, a restriction that happened to be reasonably justified in conventional hard type-II superconductors with typical decay coefficients $T/U_c$ of the order of $10^{-3}$ (Kim *et al.*, 1962; Beasley, Labusch, and Webb, 1969). In the new oxide superconductors, however, the corresponding decay coefficients turn out to be much larger, reaching values of the order of 5% at temperatures $T \simeq 20$ K (see, for example, Campbell, Fruchter, and Cabanel, 1990). These large logarithmic decay rates are a result of various factors, such as the high temperatures available in an experiment, the small pinning energies $U_c$, which in turn are a consequence of the small coherence length $\xi$, and the large anisotropy of the oxides; see Sec. C below. Combining the large decay coefficients with a typical logarithmic time factor $\ln(t/t_0)$ of the order of 20 (waiting time $t \simeq 1$ minute; see Sec. X for a discussion of the normalization time $t_0$), we have to conclude that the experimentally measured current density $j$ has been roughly halved due to creep, as compared with the critical current density $j_c$ even at such low temperatures as $T \sim 10$ K [see Eq. (2.59)]. Therefore, it is important to realize that the determination of the critical current density in the oxides is always affected by the presence of creep, and the condition $j_c - j \ll j_c$ is no longer fulfilled. The expression "giant creep" was therefore introduced by Yeshurun and Malozemoff (1988) to describe this phenomenon of very large creep rates characteristic of the oxide superconductors. From a scientific point of view, the case $j \ll j_c$ and in particular the limit $j \to 0$ is very interesting, too: If we wish to probe the thermodynamic state of the vortex structure, we should perturb the system only infinitesimally and record its response. For a truly superconducting state we would expect to observe a vanishing resistivity $\rho$ in the limit $j \to 0$ or, to put it somewhat differently, to see a sublinear "glassy" response of the

vortex structure. In fact, we shall see below that the barriers $U(j)$ against creep diverge algebraically with vanishing current density $j$,

$$U(j) \simeq U_c \left[ \frac{j_c}{j} \right]^\mu ,$$ (2.60)

which implies a strongly subohmic current-voltage characteristic of the form

$$V \propto \exp \left[ -\frac{U_c}{T} \left[ \frac{j_c}{j} \right]^\mu \right] .$$ (2.61)

The above ideas are susceptible to experimental verification if the sample can be prepared in a state characterized by a small transport current flow. A method for reaching small nonequilibrium transport current densities within experimentally accessible times was proposed by Feigel'man *et al.* (1989). Independently, the corresponding experiment was carried out by Maley *et al.* (1990): By warming up a sample in the critical state, one can increase the decay rate of the shielding current by several orders of magnitude, so that the current density $j$ drops far below its critical value $j_c$ within experimentally accessible time scales, and the small current regime $j \ll j_c$ can be probed. Let us then proceed with our analysis and consider the case $j \ll j_c$.

The classical creep-type motion of a vortex can be visualized as a thermal diffusion process in which different segments of the vortex move between metastable states. In the absence of an external current density $j$, a vortex segment lowers its energy by finding the optimal low-energy state among its neighboring metastable states. Under the action of an applied current density $j$, some other metastable state becomes more favorable and the vortex starts to move. The new optimal states are determined by the condition that the energy gain due to the driving Lorentz force be equal to the deformation and pinning energies of the vortex. For a current density near the critical value $j_c$ this condition is already fulfilled for the neighboring metastable state, which is a distance $\sim \xi$ away. However, when the current density $j$ is decreased, the Lorentz force is reduced and the next favorable metastable state is moved a larger distance away. As a consequence, the thermal motion of the vortex will involve hops of *larger* segments by *longer* distances in order to reach the next optimal low-energy state; see Fig. 8. For a quantitative analysis, then, we need to know more about the low-lying metastable states of the vortex in its random pinning environment.

Recently, considerable insight has been gained into the problem of diverse manifolds in quenched random media, of which our vortex is a typical example. Let us consider for the moment an elastic string ($d = 1$ denotes the dimension of the optimal manifold, which is one for the vortex) which can move in $n$ transverse directions (for a vortex in three-dimensional space, $n = 2$). Investigation of the statistical mechanics of this object has shown (for a recent overview, see Fisher and Huse, 1991) that, for di-
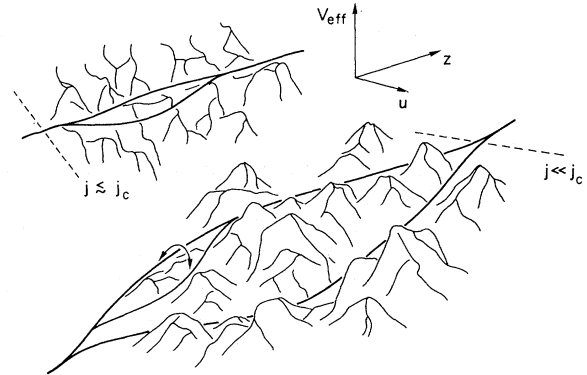


FIG. 8. Effective tilted random potential felt by the flux line in the presence of quenched disorder and of a driving transport current density $j$. The elastic vortex line relaxes into a low-lying metastable state. Close to the critical driving force, $j \lesssim j_c$, the next metastable state is very near the original state and separated from the latter by only a small barrier $U(j) \simeq U_c (1 - j/j_c)^\alpha$. At low driving currents $j \ll j_c$ the closest favorable metastable state is far away from the original state and separated from the latter by a large barrier, $U(j) \simeq U_c (j_c/j)^\mu$. Hops to the closest valleys are not favorable and represent only an intermediate step in the diffusion motion of the vortex to its next optimal state.

mensions $n \leq 2$, the string is always in a pinned phase characterized by a wandering exponent $\zeta > 1/2$,

$$\langle\langle [\mathbf{u}(L) - \mathbf{u}(0)]^2 \rangle\rangle \sim u_c^2 \left[ \frac{L}{L_c} \right]^{2\zeta} , \quad L > L_c ,$$ (2.62)

where $L$ is the distance along the vortex and $u_c$ and $L_c$ are transverse and longitudinal scaling parameters, respectively. For the single-vortex pinning problem discussed above, these two length scales are given by the characterized scale $r_p \simeq \xi$ of the disorder potential and the collective pinning length $L_c$. Here $\langle\langle \cdots \rangle\rangle = \langle\langle \cdots \rangle_{th} \rangle_{dis}$ denotes the full statistical average to be taken over dynamical variables first and then over the quenched variables describing the disorder. For $n = 1$ (vortex confined to move in a plane) it has been proven exactly (Huse, Henley, and Fisher, 1985; Kardar, 1987a) that $\zeta = \frac{2}{3}$, whereas numerical simulations (e.g., Wolf and Kertész, 1987; Forrest and Tang, 1990) suggest that for $n = 2$, $\zeta \approx \frac{3}{5}$. We shall come back to the question of the numerical values for the line-wandering exponents in Sec. III.F below, where we present additional supporting arguments for this value.

Furthermore, it has been found that competing metastable states that differ from one another on a length scale $L$ are separated by a typical distance

$$u(L) \sim u_c \left[ \frac{L}{L_c} \right]^\zeta , \quad L > L_c ,$$ (2.63)

and a typical energy barrier

$$\mathcal{E}(L) \sim U_c \left[ \frac{L}{L_c} \right]^{2\zeta-1} , \quad L > L_c , \tag{2.64}$$

with $U_c$ denoting the scaling parameter for the energy. In the single-vortex pinning problem this typical energy scale reduces to the collective pinning energy $U_c$. Note that the results (2.63) and (2.64) describe the *fluctuations* in position and energy of the string under variation over different *low-lying* metastable states. The result (2.64) can be understood rather simply by noting that the elastic energy change in going from one metastable minimum to the neighboring one is of the order of $\varepsilon_l u^2(L)/L$, where $\varepsilon_l$ denotes the appropriate elasticity of the string.

For dimensions $n > 2$, on the other hand, it has been found (Imbrie and Spencer, 1988) that there exists a high-temperature "free" phase in which the quenched disorder is irrelevant at long length scales, implying a minimal line-wandering exponent $\zeta = \frac{1}{2}$ characteristic of a random walk. At small enough temperatures the thermal fluctuations become irrelevant and the string becomes pinned by the quenched disorder (Cook and Derrida, 1989), leading to a finite "freezing" temperature. However, for the physically relevant case discussed here, $n = 2$, and a single vortex is always in a pinned or "glassy" state.

Let us return now to our original problem and apply the above results to the discussion of vortex creep. We normalize the scaling laws for the distance (2.63) and for the energy barrier (2.64) to take the values $\xi$ and $U_c$ at $L \sim L_c$, $u(L) \sim \xi (L/L_c)^\zeta$ and $\mathcal{E}(L) \sim U_c (L/L_c)^{2\zeta-1}$. The free-energy functional at low driving currents, $j \ll j_c$, becomes (see Fig. 9)

$$\mathcal{F}(L) \sim U_c \left[ \frac{L}{L_c} \right]^{2\zeta-1} - j \frac{\Phi_0}{c} L_c \xi \left[ \frac{L}{L_c} \right]^{\zeta+1} . \tag{2.65}$$
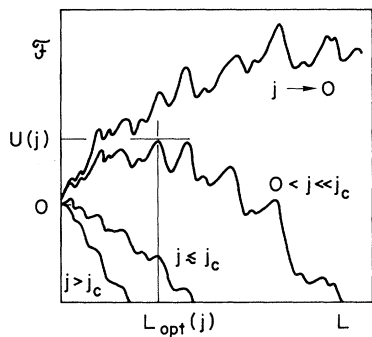


FIG. 9. Free-energy functional vs length $L$ of the hopping segment, which plays the role of a generalized coordinate. The free energy is made up of two terms, the barrier energy $U_c (L/L_c)^{2\zeta-1}$, growing slowly with $L$, and the energy gain due to the Lorentz force, $(j/j_c)U_c(L/L_c)^{1+\zeta}$, with a small prefactor $j/j_c \ll 1$ but a more rapid growth in $L$. For a fixed driving current density $j$, a minimal segment of length $L_{opt}(j)$ has to overcome the barrier $U(j)$ in order to reach the next favorable metastable state. With decreasing $j$, both the length of the optimal segment and the barrier diverge, $L_{opt}(j) \simeq L_c(j_c/j)^{1/(2-\zeta)}$ and $U(j) \simeq U_c(j_c/j)^\mu$, with $\mu = (2\zeta-1)/(2-\zeta)$.

Equation (2.65) reduces the present analysis to a simple nucleation problem (Langer, 1967): Whereas nuclei with lengths $L$ smaller than some critical length $L_{opt}$ will collapse back to zero length and thus are undercritical, all activated segments with a length $L > L_{opt}$ remain stable (due to pinning) and contribute to the motion of the vortex. The critical size of the nucleus is found by calculating the minimal barrier in Eq. (2.65) through the condition $\partial_L \mathcal{F}(L)|_{L=L_{opt}} = 0$, and we find the result

$$L_{opt}(j) \sim L_c \left[ \frac{j_c}{j} \right]^{1/(2-\zeta)} . \tag{2.66}$$

The size of the critical nucleus depends nontrivially on the driving current $j$. Inserting the result (2.66) back into the free-energy functional (2.65), we obtain the minimal barrier for creep increasing algebraically for decreasing driving current (see Fig. 9),

$$U(j) \sim U_c \left[ \frac{j_c}{j} \right]^\mu , \tag{2.67}$$

with

$$\mu = \frac{2\zeta-1}{2-\zeta} . \tag{2.68}$$

Correspondingly, the current-voltage characteristic shows the "glassy" behavior

$$V \propto \exp \left[ -\frac{U_c}{T} \left[ \frac{j_c}{j} \right]^\mu \right] . \tag{2.69}$$

Using the above estimate $\zeta \approx \frac{3}{5}$ for a single vortex in three dimensions, we obtain (Feigel'man *et al.*, 1989)

$$U(j) \sim U_c \left[ \frac{j_c}{j} \right]^{1/7} . \tag{2.70}$$

Note that the energy functionals (2.44) and (2.65) are very different. Whereas (2.44) is sufficient for determining the minimal hopping length $L_c$, which is the relevant length for current densities near $j_c$, we have to consider the more complicated functional (2.65) when treating the problem of creep away from the critical current density. A nonlinear increase of the creep barrier with decreasing current density has been observed experimentally by various groups, e.g., Zeldov *et al.* (1989), Maley *et al.* (1990), Lairson *et al.* (1991), Ossandon *et al.* (1992), and van der Beek, Kes, Maley, *et al.* (1992).

Combining Eqs. (2.67) and (2.57), we obtain a nonlinear logarithmic time decay of the current density,

$$j(t) \sim j_c \left[ \frac{T}{U_c} \ln \frac{t}{t_0} \right]^{-1/\mu} . \tag{2.71}$$

For current densities close to critical the result (2.59) is more appropriate, and interpolating between these two formulas we obtain the general behavior

$$j(t) \simeq j_c \left[ 1 + \frac{\mu T}{U_c} \ln \left[ 1 + \frac{t}{t_0} \right] \right]^{-1/\mu} , \tag{2.72}$$

which is valid close to $j_c$ as well as for $j \ll j_c$ (Geshkenbein *et al.*, 1989; Malozemoff and Fisher, 1990; Nattermann, 1990; Feigel'man *et al.*, 1991). Note that the slightly different forms of the above relaxation rates, (2.71) and (2.72), are due to the different extrapolation schemes used. The barrier $U(j)$ has been extrapolated to take the value $U_c$ at $j \simeq j_c$ in (2.70), whereas Eq. (2.72) produces a barrier $U_c/\mu$ in the extrapolation to $j \simeq j_c$, which differs from (2.70) by a numerical factor. A nonlinear logarithmic time decay of the trapped diamagnetic moment has indeed been observed in several experiments, e.g., Svedlindh *et al.* (1991), Thompson, Sun, and Holtzberg (1991), Sandvold and Rossel (1992).

Within the single-vortex pinning regime the exponent $1/\mu = 7$ is large and, for small enough temperatures or small enough times, we can rewrite the solution (2.72) in an exponential form,

$$j(t) \simeq j_c \exp\left[ -\frac{T}{U_c}\ln\frac{t}{t_\circ} \right], \quad T\ln\frac{t}{t_\circ} < 7U_c \ . \quad (2.73)$$

The time decay of the current then is roughly algebraic,

$$j(t) \simeq j_c \left[ \frac{t_\circ}{t} \right]^{T/U_c} , \quad (2.74)$$

with a temperature-dependent exponent $T/U_c$. On the other hand, Eq. (2.73) also predicts an interesting dependence of the screening current density on temperature:

$$j(T) \simeq j_c \exp\left[ -\frac{T}{T_\circ} \right] , \quad (2.75)$$

with

$$T_\circ \simeq \frac{U_c}{\ln(t/t_\circ)} \ . \quad (2.76)$$

A sample prepared in a critical state at $t=0$ will carry a strongly reduced screening current $j \ll j_c$ after only a few seconds of waiting time. The quantity measured in a relaxation experiment is not the critical current density $j_c$ but the strongly reduced value $j(T)$. Such an exponential decrease of the apparent critical current density has indeed been observed in the new oxide superconductors, and the characteristic temperature $T_\circ$ has been measured to be of the order of 10 K (Senoussi *et al.*, 1988). Typical experimental values for the activation energy $U_c$ are of the order of $10^2-10^3$ K (Yeshurun *et al.*, 1988, 1989; Maley *et al.*, 1990; Zavaritsky, 1992). Combining these results with a typical experimental waiting time $t/t_\circ \sim 10^{10}$ (see Sec. X for a discussion of the normalization time $t_\circ$), we find that the relation (2.76) between the characteristic temperature $T_\circ$ and the activation energy $U_c$ is fulfilled, thus providing an additional confirmation of the weak collective pinning idea.

Let us return to the more general result, Eq. (2.72), and determine the normalized creep rate $S = -d\ln j/d\ln t$, which differs from Anderson's result $T/U_c$ due to the nonlinear dependence of the activation barrier $U(j)$ on the current density $j$,

$$S \simeq \frac{T}{U_c + \mu T \ln(1 + t/t_\circ)} \ . \quad (2.77)$$

Equation (2.77) shows two very interesting features, which are a direct consequence of collective creep behavior with its characteristic strong increase of the pinning barrier (2.67) with decreasing current density: First, the decay rate $S$ decreases with increasing time, producing an upward curvature in a plot of the logarithmic time decay of the diamagnetic current (Svedlindh *et al.*, 1991, Thompson *et al.*, 1991). Second, the decay rate $S$ saturates for temperatures $T > U_c/\mu\ln(t/t_\circ)$, $S_{sat} \simeq 1/\mu\ln(t/t_\circ)$. Both these effects are due to the increase in the relevant barriers in the system as time evolves and the current density $j$ in the system decays due to creep. In fact, such a saturation in $S$ has been observed, and a careful analysis of a number of representative experimental results has been given by Malozemoff and Fisher (1990). However, we cannot expect this saturation to take place within the single-vortex pinning regime. Near saturation the ratio $\mu T \ln(t/t_\circ)/U_c$ in (2.72) has become larger than unity, so that the current density has decayed by a factor $\sim 10^{-2}$ by then. At such small current densities the interaction between neighboring vortices can no longer be neglected (see below), and the vortex motion proceeds by the diffusion of vortex bundles rather than independent single vortices. As we shall show in Sec. IV, creep due to vortex bundles is characterized by an exponent $\mu$ of order unity, such that we should expect a saturation to a level $S_{sat} \simeq 1/\ln(t/t_\circ)$ of a few percent, in agreement with experimental results. Moreover, experiments show a saturation appearing for temperatures $T > 10$ K, which is in agreement with a value of the collective pinning energy of the order of $10^2$ K, as obtained above. On the other hand, some experiments have been analyzed using the Anderson result $S \simeq T/U_c$. For an underlying collective creep mechanism, such an analysis produces a pinning barrier $U_c \simeq T/S$ which *increases* with temperature. An increase of the creep barrier with temperature has indeed been reported in several experimental studies using this kind of analysis (e.g., Stollman *et al.*, 1989; Xu *et al.*, 1989; Campbell, Fruchter, and Cabanel, 1990).

As we have already mentioned above, the analysis of collective creep in terms of individually moving vortices applies only for a limited regime of current densities $j$, the reason being that the pinning energy grows only sublinearly in the length $L$, whereas the interaction energy between neighboring vortices grows linearly in $L$. Thus with decreasing current density $j$ the relative importance of the interaction between the vortices grows. The length scale associated with intervortex interaction is the lattice constant $a_\circ$ and, as we shall show below (see Sec. D), the boundary of the single-vortex pinning regime is determined by the condition $L_{opt}(j_{sb}) \simeq a_\circ$. Using Eqs. (2.66), (2.51a), and the definition (2.17) of the upper critical field,

we obtain

$$j_{sb} \simeq j_c \left[ \frac{L_c}{a_0} \right]^{2-\zeta}$$

$$= j_c \left[ \frac{B}{\beta_{sb} H_{c_2}} \frac{j_0}{j_c} \right]^{(2-\zeta)/2} , \qquad (2.78)$$

and with $\zeta = \frac{3}{5}$ the exponent becomes $(2-\zeta)/2 = \frac{7}{10}$. The above analysis of single-vortex collective creep is then limited to currents $j_{sb} \lesssim j < j_c$. Note that the limiting current density $j_{sb}$ depends on the strength of the magnetic field $B$. For current densities $j \approx j_c$ the condition (2.78) transforms into a condition for the magnitude of the applied magnetic field. Using the definition

$$B_{sb} = \beta_{sb} \frac{j_c}{j_0} H_{c_2} , \qquad (2.79)$$

the single-vortex pinning regime is restricted to weak enough magnetic fields, $B < B_{sb}$. In principle the prefactor $\beta_{sb}$ can be estimated by keeping all the numerical factors in the above dimensional estimates. A more reliable result can be obtained within the framework of the dynamical approach (see Sec. VI.A.3 below), and the result of such an analysis gives $\beta_{sb} \approx 5$.

For smaller current densities, $j < j_{sb}$, or larger field values, $B > B_{sb}$, the interaction between vortices is important and the minimal barrier for flux motion is realized for a *small bundle* of vortices instead of a *single vortex*. The index "sb" for the crossover current density $j_{sb}$ and the crossover field $B_{sb}$ then indicates that we are entering the small-bundle regime upon decreasing the current density $j < j_{sb}$ or increasing the field $B > B_{sb}$. We shall come back to this question in Sec. D.

### 5. Quantum creep

We have analyzed above the decay of a vortex density gradient due to thermal activation of the vortices out of their metastable states. According to this classical picture, the decay rate $S$ should vanish in the zero-temperature limit; see Eq. (2.77). However, in a number of recent experiments the low-temperature relaxation rate has been found not to extrapolate to zero, suggesting the existence of vortex motion by quantum tunneling. Particularly careful experiments have been done on the oxide superconductors (Mota, Pollini, *et al.*, 1988; Lensink *et al.*, 1989; Griessen *et al.*, 1990 and 1991; Fruchter *et al.*, 1991; Mota, Juri, *et al.*, 1991) and on the organic superconductor $(BEDT\text{-}TTF)_2 Cu(NCS)_2$ (Mota, Pollini, *et al.*, 1990a; Mota, Juri, *et al.*, 1991). However, even before, similar results were reported for the Chevrel phase $PbMo_6 S_8$ (Mitin, 1987) and for the heavy-fermion compounds $CeCu_2 Si_2$ (Mota, Visani, *et al.*, 1988) and $UPt_3$ (Mota, Pollini, *et al.*, 1990b). The possibility of vortex motion by quantum tunneling in thin films was proposed by Glazman and Fogel (1984; see also Liu

*et al.*, 1992), and, quantum motion of vortices in Josephson-junction arrays was studied by Larkin, Ovchinnikov, and Schmid (1988). More recently, Fisher, Tokuyasu, and Young (1991) have discussed quantum creep of vortices in disordered thin-film superconductors and have found a variable-range hopping resistivity with a non-Arrhenius low-temperature behavior. Vortex tunneling in bulk superconductors has been analyzed by Blatter, Geshkenbein, and Vinokur (1991) within the framework of weak collective pinning theory. Furthermore, quantum motion of individual vortex lines across the intrinsic pinning barrier in layered superconductors ($H \| ab$-planes) has been studied by Ivlev, Ovchinnikov, and Thompson (1991) and more details concerning this interesting case are given in Sec. VIII.C below.

Macroscopic tunneling phenomena have always attracted a good deal of interest, as they touch the boundary between quantum and classical physics in a natural way. Macroscopic systems are always coupled to their environment and are therefore inherently dissipative. Up until now the most carefully studied system, both experimentally (see, for example, Martinis, Devoret, and Clarke, 1987) and theoretically (Caldeira and Leggett, 1981, 1983; Larkin and Ovchinnikov, 1983a, 1983b; Eckern, Schön, and Ambegaokar, 1984; Grabert, Weiss, and Hänggi, 1984) has been the (rf) superconducting quantum interference device (SQUID), which has become a model system in the field of macroscopic quantum tunneling. In particular, Caldeira and Leggett have shown that the quantum description can be extended to macroscopic systems, the main effect of dissipation being to suppress the probability of the tunneling process. Here we mainly follow their description, which we generalize to describe the tunneling of a string instead of a pointlike particle.

The decay of a metastable state due to tunneling is actually very similar to the classical decay process via thermal activation. The additional feature to be taken care of in a tunneling process is the time component of the motion. In the case of thermal activation, the time is irrelevant since the vortex is activated *over* the energy barrier, hence the process is real. The probability for the process then is given by the saddle-point solution of the free energy (2.31). During tunneling, the vortex moves *under* the barrier, hence the process is forbidden (virtual), and the longer the time that the string has to spend under the barrier, the fewer chances there are for the process to happen. The functional for which we have to find the saddle-point solution is the Euclidean action (Iordanskii and Finkel'shtein, 1972; Lifshitz and Kagan, 1972; Banks, Bender, and Wu, 1973; Callan and Coleman, 1977; Coleman, 1977; Caldeira and Leggett, 1983). The quantum problem then is a $(d+1)$-dimensional generalization of the $d$-dimensional classical problem, where $d$ again denotes the dimension of the object, which is $d=1$ for the string.

From the above discussion we conclude that the additional new feature that enters all quantum descriptions, be they statistical mechanical or dynamical as in the

present case, is the dynamics of the system. The most general equation of motion for a vortex in a superconductor comprises a massive ($m_l$), a dissipative ($\eta_l$), and a Hall ($\alpha_l$) term,

$$m_l \dot{\mathbf{v}}_v + \eta_l \mathbf{v}_v + \alpha_l \mathbf{v}_v \wedge \mathbf{n} = \mathbf{f}_{\text{ext}} , \qquad (2.80)$$

where $\mathbf{f}_{\text{ext}}$ denotes the sum of all the "external" forces acting on the vortex, such as the Lorentz force $\mathbf{f}_L = \Phi_0 \mathbf{j} \wedge \mathbf{n}/c$ or the pinning force $\mathbf{f}_{\text{pin}}$. The question then arises under what circumstances each of the three dynamical terms is the dominant one. In charged superconductors this is usually the dissipative term $\eta_l \mathbf{v}_v$, with $\eta_l$ given by the Bardeen-Stephen expression (2.26). However, as discussed in the introduction of Sec. II above, in super-clean material with a mean free path $l > \xi \varepsilon_F / \Delta$ the Hall term becomes the dominant one (here $\Delta$ denotes the gap parameter and $\varepsilon_F$ is the Fermi energy). It turns out (see Sec. III.C) that the high-temperature superconductors are indeed potential candidates for the realization of this super-clean limit: With $\varepsilon_F / \Delta \sim 20$ and $l$ of the order of a few hundred Å at low temperature (an estimate $l \approx 700$ Å is obtained in Sec. III.C), we obtain $l \Delta / \varepsilon_F \sim 35$ Å $\gtrsim \xi$. Finally, the massive term is small and usually can be neglected as compared to either the dissipative or the Hall term.

There are at least two reasons, however, to start our discussion below with the case of a massive dynamics: (i) The massive string is by far the simplest and most transparent example to treat, and we use it as an introduction to the new concepts associated with the phenomenon of quantum creep. (ii) In addition to the electronic contribution to the vortex mass, additional components of electromagnetic origin (Suhl, 1965; Coffey and Clem, 1991a) and due to strain fields (Coffey, 1994; Duan and Šimánek, 1994) can be found. Both these contributions are usually much smaller than the electronic contribution. However, the electromagnetic mass can become large under special circumstances, e.g., for a Josephson vortex in an individual junction or for an intrinsic pinning configuration in a layered superconductor where the magnetic field is aligned parallel to the layers. The vortex mass is then due to capacitive effects and can be enhanced by a large dielectric constant of the (insulating) buffer layers enclosing the superconducting layers/contacts. A related mechanism producing an enhanced electromagnetic vortex mass within a homogeneous superconductor close to the superconductor-insulator transition has been proposed by Doniach and Inui (1990). In the following we first discuss the tunneling of a massive string and then include the effects of dissipation. Next, we analyze the pure Hall tunneling case; the inclusion of dissipation for the Hall-dominated motion is more difficult, and we shall confine ourselves to qualitative considerations.

The Lagrangian generating the classical equation of motion for a massive vortex is

$$\mathcal{L}[\mathbf{u}] = \int dz \frac{m_l}{2} (\partial_t \mathbf{u})^2 - \mathcal{F}[\mathbf{u}] , \qquad (2.81)$$

with the free-energy functional $\mathcal{F}$ given by Eq. (2.31). The displacement vector $\mathbf{u}(z,t)$ plays the role of the microscopic variable. The new parameter $m_l$ denotes the mass per unit length of the vortex, which has to be found by going to a microscopic description. For example, an expression for the vortex mass $m_l$ can be obtained by calculating the kinetic energy of a moving vortex or by studying the response of the vortex to an external force. Using different kinds of time-dependent Ginzburg-Landau theories, corresponding calculations have been carried out by Suhl (1965) and by Kupriyanov and Likharev (1975) with similar results. Such an approach is strictly valid only for a gapless superconductor (Gor'kov and Eliashberg, 1968), the applicability of the results to a superconductor with a finite gap at low temperatures being unclear. However, a simple estimate of the vortex mass can be made involving very general arguments which should hold, as well, for a finite-gap superconductor at low temperatures, the situation we are interested in here. This rough estimate in fact reproduces the more elaborate results of Suhl and of Kupriyanov and Likharev: The basic idea is that the electronic contribution to the vortex mass is due to the local change in dispersion within the vortex core. The number of electrons experiencing this change is $2\pi \xi^2 N(\varepsilon_F) \delta \varepsilon$. Here $\delta \varepsilon \simeq \hbar v_F / \pi \xi$ is the change in energy due to confinement to the vortex core, $N(\varepsilon_F) = m_e k_F / 2\hbar^2 \pi^2$ is the density of states (per spin) at the Fermi level, $m_e$ denotes the effective mass, and $k_F$ and $v_F$ are the Fermi wave vector and Fermi velocity, respectively. The effective mass of the electrons confined to the core will be modified by an amount of the order of $m_e \delta \varepsilon / \varepsilon_F$, and we obtain the mass $m_l$ of the vortex

$$m_l = \frac{2}{\pi^3} m_e k_F , \qquad (2.82)$$

in agreement with the results of Suhl and of Kupriyanov and Likharev. In addition to this electronic contribution, a second term $m_{\text{em}} [= (\Phi_0 / 4\pi c \xi)^2]$ of electromagnetic origin contributes to the vortex mass (Suhl, 1965). Typically $m_{\text{el}} \gg m_{\text{em}}$, and in the following we use the estimate $m_l \simeq m_{\text{el}}$.

As already mentioned above, macroscopic quantum tunneling is always a dissipative process, and we should ask ourselves if the problem at hand belongs to the ballistic or to the dissipative limit. Below we compare the kinetic energy and the dissipative contribution to the action and show that, for the limit of weak pinning, we shall always find ourselves in the dissipative limit. Thus our qualitative estimate for the vortex mass will not influence the accuracy of our final results.

From Eq. (2.81) we immediately obtain the Euclidean action by going over to imaginary time, $t \to -it$,

$$\mathcal{S}_E = \int dt \left\{ \int dz \frac{m_l}{2} (\partial_t \mathbf{u})^2 + \mathcal{F}[\mathbf{u}] \right\} , \qquad (2.83)$$

for which we have to find the saddle-point solution. The

saddle-point solution is given by the classical bounce trajectory (Callan and Coleman, 1977, Coleman, 1977), where the string moves through the inverted potential and bounces back to its origin along a homoclinic orbit. Here we are interested in the scale of the action, i.e., we wish to determine the quantity corresponding to $U_c$, and thus we set the driving force equal to zero, $j=0$. Equation (2.83) then has to be minimized with respect to the form (length) and the duration of the bounce, and we do this using again the method of dimensional estimates. At this point we should note that the tunneling process involves the same initial and final states as encountered above in the determination of the classical creep rate. The additional new feature of the quantum problem is the relevance of the time evolution of the vortex motion. In fact, the determination of the optimal length for the bounce solution involves only the free-energy part of Eq. (2.83), and the result has been found above, Eq. (2.45). The optimal length of the bounce is the collective pinning length $L_c$. The estimate for the tunneling time $t_c$ is obtained by equating the elastic and the kinetic energy densities, $m_l(\xi/t_c)^2 \simeq \varepsilon_0(\xi/L_c)^2$,

$$t_c \simeq \left[\frac{m_l}{\varepsilon_0}\right]^{1/2} L_c , \qquad (2.84)$$

and the resulting minimal action for the tunneling process is

$$\frac{S_E}{\hbar} \simeq \frac{t_c}{\hbar} U_c \simeq \left[\frac{\varepsilon_0 m_l}{\hbar^2}\right]^{1/2} \xi^2 \sim (k_F \xi)^2 . \qquad (2.85)$$

Thus we find that, for vanishing dissipation, the action does not depend on the collective pinning length $L_c$ and hence is independent of the pinning potential. Note that if $T_c \sim \varepsilon_F$ or equivalently $\xi \sim 1/k_F$ the superconducting coherence will be destroyed due to strong quantum fluctuations, as has been recognized by Imry (1991).

Next we generalize our result to include dissipation in the model. Here we restrict ourselves to the simplest case of ohmic dissipation with the viscous drag coefficient (2.26). As shown by Caldeira and Leggett (1983), such an interaction with the environment can be accounted for by adding a term

$$\frac{\eta_l}{4\pi} \int dt \int dt' \int dz \left[\frac{\mathbf{u}(z,t)-\mathbf{u}(z,t')}{t-t'}\right]^2 \qquad (2.86)$$

to the Euclidean action (2.83), resulting in the so-called effective action $S_E^{\text{eff}}$ for the vortex. The expression (2.86) is nonlocal in time, and in order to treat this term we transform the effective action to Fourier space,

$$S_E^{\text{eff}} = \int \frac{d\omega}{2\pi} \int \frac{dq}{2\pi} \left\{\frac{1}{2}\left[m_l\left[1+\frac{\eta_l}{|\omega|m_l}\right]\omega^2 + \varepsilon_0 q^2\right]|\mathbf{u}(q,\omega)|^2 + \varepsilon_{\text{pin}}(q,\mathbf{u})\right\} . \qquad (2.87)$$

The friction is seen to produce an enhanced and dispersive effective mass $m_{\text{eff}} = m_l(1+\eta_l/|\omega|m_l) > m_l$. The inverse tunneling time $\omega_c$ is again determined by equating the kinetic and elastic energy densities, $m_{\text{eff}}(\omega_c)\xi^2\omega_c^2 \simeq \varepsilon_0\xi^2 q_c^2$, with $q_c \simeq 1/L_c$ the inverse length of the tunneling segment. In the most general case we have to solve a quadratic equation for $\omega_c$. However, the situation simplifies considerably if the dissipative part is dominant, $\eta_l/|\omega_c|m_l \gg 1$. In this case the equation for $\omega_c$ is trivially solved, and we obtain a tunneling time

$$t_c \simeq \frac{\eta_l}{\varepsilon_0} L_c^2 . \qquad (2.88)$$

Inserting this expression back into the equation for the mass enhancement factor and using the result (2.51a) for the collective pinning length, we obtain

$$\frac{\eta_l t_c}{m_l} \simeq \left[\frac{\hbar\pi^3}{e^2\rho_n k_F}\right]^2 (k_F\xi)^{-2}\frac{j_0}{j_c} . \qquad (2.89)$$

In the limit of weak pinning, $j_c \ll j_0$, the mass enhancement factor will be larger than unity, and the dissipative term in the action will be dominant. The final result for the effective Euclidean action in the dissipative limit becomes

$$\frac{S_E^{\text{eff}}}{\hbar} \simeq \frac{\eta_l\xi^2 L_c}{\hbar} \simeq \frac{\hbar}{e^2}\frac{\xi}{\rho_n}\left[\frac{j_0}{j_c}\right]^{1/2} \simeq \frac{1}{Qu}\left[\frac{j_0}{j_c}\right]^{1/2} , \qquad (2.90)$$

where we have used the definition $Qu = (e^2/\hbar)(\rho_n/\xi)$ for the dimensionless quantum resistance in the last equation. The normalized creep rate $S$ near $j_c$ takes the form

$$\frac{d \ln j}{d \ln t} \simeq -\frac{\hbar}{S_E^{\text{eff}}} . \qquad (2.91)$$

The main parameter determining the action and thereby also the tunneling rate is the ratio $\rho_n/\xi$. A small action favoring tunneling is obtained in materials characterized by a large normal-state resistivity $\rho_n$ and a small coherence length $\xi$. The quantum unit of resistance is $\hbar/e^2 \approx 4.1$ k$\Omega$. Thus the phenomenon of quantum creep should become experimentally observable for ratios $\rho_n/\xi \gtrsim 1$ k$\Omega$. Note, however, that the decrease of the effective action $S_E^{\text{eff}}$ with increasing ratio $\rho_n/\xi$ is cut off at the value $S_E$ as we cross over to the ballistic regime; see Eq. (2.89). The disorder potential enters the result (2.90) via the critical current density $j_c$. With the square-root dependence on $j_c$ the final result depends only weakly on the pinning potential.

An alternative viewpoint regarding the relevance of dissipation starts from a purely dissipative dynamic equa-

tion and considers the inertia of the vortex as a correction. In this approach we expand the dispersive friction coefficient $\eta_l(\omega)$ for small frequencies, $|\omega| \ll \Delta/\hbar$, and obtain a term of the form $[\eta_l(0)/2](1+\hbar|\omega|/\Delta)|\omega|u^2$ in the Euclidean Lagrangian. Inserting the tunneling time (2.88) into the second term, we find again that the ballistic contribution is irrelevant for a weak-pinning potential, $\hbar/\Delta t_c \simeq j_c/j_o \ll 1$. For a dirty superconductor the kinetic term in the expansion of $\eta_l(\omega)$ is consistent with Eq. (2.82) for the vortex mass $m_l$.

Let us now consider the case of a pure Hall-type dynamics for a vortex, as it is relevant in a super-clean superconductor (the Hall dynamics is also relevant for the tunneling of vortices in superfluid He; see Volovik, 1972). Here, we mainly follow the discussion of Feigel'man *et al.* (1993; see also Ao and Thouless, 1994). We then have to replace the dissipative dynamical term $\eta_l|\omega|u^2$ by the Hall term $\alpha_l\omega u^2$ in the action for the tunneling process. Proceeding on the level of dimensional estimates we immediately reproduce the result (2.90) above, but with $\eta_l$ replaced by $\alpha_l$,

$$\frac{S_E^H}{\hbar} \simeq \frac{\alpha_l\xi^2 L_c}{\hbar} \simeq n\xi^3 \left[\frac{j_o}{j_c}\right]^{1/2} . \tag{2.92}$$

There is a good deal of interesting physics associated with the Hall tunneling of vortices. In particular, the geometry of the "bounce" solution is very different from that found in the massive or in the dissipative situation. In the following we present a model calculation that highlights the important differences and that is also relevant for the tunneling motion of a (collectively) pinned vortex.

To keep the discussion simple, we first concentrate on the 2D situation, describing, for example, a vortex in a thin film (of thickness $d$) or a pancake vortex in a strongly layered superconductor (see Sec. VIII.A.2 below). When we rewrite the external force $\mathbf{f}_{\text{ext}}$ in Eq. (2.80) in terms of a potential $U(\mathbf{r})$, the equation of motion reads

$$\alpha_d \mathbf{v} \wedge \mathbf{n} = -\nabla U(\mathbf{r}) , \tag{2.93}$$

with $\alpha_d = \alpha_l d = \Phi_o\rho_s d/c$ [see Eq. (2.28)]. Equation (2.93) is the equation of motion of a charged ($e$) particle with zero mass in a magnetic field $\mathbf{B} = (0,0,\alpha_d c/e)$. Such a particle always follows the equipotential lines defined by the potential $U$, $\mathbf{v} = \nabla U \wedge \mathbf{n}/\alpha_d$. Expressing Eq. (2.93) in components, we obtain the set of equations

$$\alpha_d \frac{dx}{dt} = \frac{\partial U(x,y)}{\partial y} ,$$
$$\alpha_d \frac{dy}{dt} = -\frac{\partial U(x,y)}{\partial x} . \tag{2.94}$$

The action that produces the equation of motion (2.93) is

$$\mathcal{S} = \int dt\,[\alpha_d y\dot{x} - U(x,y)] , \tag{2.95}$$

where the first term is just the Lagrangian $\mathbf{j} \cdot \mathbf{A}/c$ of a charged particle moving in a magnetic field $\mathbf{B}$ produced by the vector potential $\mathbf{A} = (By,0,0)$. The interesting

feature is that the set (2.94) of dynamical equations is of the Hamiltonian form (see also Volovik, 1972, and Jain and Kivelson, 1987 and 1988, who have used the same approach in the calculation of a tunneling vortex in a superfluid and for a particle tunneling in the presence of a strong magnetic field). If we define the coordinate $q = \sqrt{\alpha_d}x$, the momentum $p = \sqrt{\alpha_d}y$, and the Hamiltonian $\mathcal{H}(q,p) = U(x,y)$, we find that (2.94) is equivalent to

$$\frac{dq}{dt} = \frac{\partial \mathcal{H}(q,p)}{\partial p} ,$$
$$\frac{dp}{dt} = -\frac{\partial \mathcal{H}(q,p)}{\partial q} . \tag{2.96}$$

The Hamilton equations (2.96) now describe a particle moving in one dimension with a dynamics defined by the $y$ dependence of the potential $U(x,y)$. The coordinates $x$ and $y$ play the role of canonical variables, and we can immediately quantize the theory by imposing the commutation relation

$$[x,y] = \frac{1}{\alpha_d}[q,p] = \frac{i\hbar}{\alpha_d} = \frac{i}{\pi n d} . \tag{2.97}$$

An alternative way to go over to a quantum description makes use of the action (2.95) in a path-integral formulation, and below we follow this line of thought.

In order to describe the tunneling motion of the vortex we have to go over to an imaginary-time formalism. However, a mere substitution $t \to -it$ in (2.95), as used in Eq. (2.83), leads us to an action describing a particle moving in an imaginary magnetic field [only *one* time derivative appears in the dynamical part of (2.95)]. On the other hand, if we perform a simultaneous rotation of both the time $t$ and the $y$ axis, $t \to -it$ and $y \to iy$, the dynamical term in (2.95) becomes real again. If additionally the potential $U(x,y)$ is even in the coordinate $y$, we recover a real Lagrangian. Finding a saddle point of the original action describing the decay of the metastable state then becomes equivalent once again to solving a real classical mechanical problem. In fact, this scheme for obtaining the desired saddle-point solution can be put on firmer ground by exploiting the equivalence between the original 2D Hall problem and the 1D Hamiltonian problem. We assume that the original potential $U(x,y)$ can be rewritten in a form $U(x,y) = (f/2)y^2 + U_x(x)$. The resulting 1D problem is that of a massive particle (with mass $m = \alpha_d/f$) in a potential $U_x(q/\sqrt{\alpha_d}) \equiv U_1(q)$. [Note that close to a (local) minimum we can expand any potential $U(x,y)$ into the above form if we choose the appropriate axes.] Writing down the action for the 1D particle problem,

$$\mathcal{S} = \int dt\left[\frac{1}{2m}\dot{q}^2 - U_1(q)\right] = \int dt\,[p\dot{q} - \mathcal{H}(q,p)] , \tag{2.98}$$

we can now easily go over to the imaginary-time formalism and obtain the Euclidean action ($t \to -it$)

$$\mathcal{S}_E = -iS(t \to -it) = \int dt \left[ \frac{1}{2m} \dot{q}^2 + U_1(q) \right]$$

$$= \int dt [p\dot{q} - \mathcal{H}_E(q,p)] , \tag{2.99}$$

with the definition $\mathcal{H}_E(q,p) = p^2/2m - U_1$. The usual Wick rotation within the Lagrangian formalism is equivalent to the combined rotation $t \to -it$ and $p \to ip$ in the Hamiltonian formalism. This follows simply from the fact that the substitution $t \to -it$ implies $p \to ip$. Equivalently, we can simply invert the potential $U_1(q) \to -U_1(q)$ in Eq. (2.98).

Returning to the original Hall tunneling problem in 2D, we can now set up the appropriate rule to go from the action

$$\mathcal{S} = \int dt [\alpha_d y\dot{x} - U(x,y)]$$

$$= \int dt \left[ \alpha_d y\dot{x} - \frac{f}{2}y^2 - U_x(x) \right] \tag{2.100}$$

to the imaginary-time expression $\mathcal{S}_E$. Remembering that the $y$ coordinate plays the role of the momentum $p$ in the 1D Hamiltonian problem, we obtain the Euclidean action

$$\mathcal{S}_E = -iS(t \to -it, \; y \to iy)$$

$$= \int dt \left[ \alpha_d y\dot{x} - \frac{f}{2}y^2 + U_x(x) \right] . \tag{2.101}$$

Alternatively, we can invert the potential; see Fig. 10. According to the above rule we should invert only the potential along the $x$ axis, $U_x \to -U_x$. Below we shall see that this partial inversion is crucial for obtaining an appropriate "bounce" solution for the tunneling action.

To proceed further, we choose an appropriate model potential describing a typical tunneling situation: The potential $U(x,y)$ should exhibit a local minimum (say at the origin) and should be connected via a saddle to free space along one direction (we choose this direction to be the $x$ axis). A model potential fulfilling this requirement and separable according to the above discussion $[U = (f/2)y^2 + U_x(x)]$ is

$$U(x,y) = U_c \left[ \frac{y^2}{\xi^2} + \frac{x^2}{\xi^2} - \frac{x^3}{\xi^3} \right] . \tag{2.102}$$

Here we have already used the parameters $U_c$ and $\xi$ for the potential shape as they result from a typical weak-pinning situation. The Hall tunneling problem then maps to the 1D particle problem with a particle mass
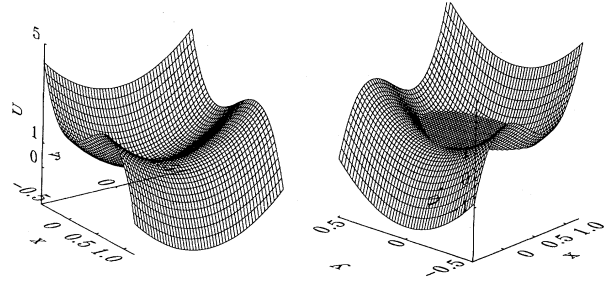


FIG. 10. Metastable potential $U = \frac{27}{4}[x^2 - x^3 + y^2]$ and its inversion $U_i = \frac{27}{4}[-x^2 + x^3 + y^2]$. A particle trapped at the origin escapes via Hall tunneling from its metastable state along an equipotential line, $\alpha_d \mathbf{v} = \nabla_\perp U_i$, with $\nabla_\perp = (\partial_y, -\partial_x)$. The Hall trajectory follows the boundary of the $U_i = 0$ equipotential surface shown in the plot.

$m = \alpha_d \xi^2/2U_c$ in the cubic potential $U(q) = U_0[(q/q_0)^2 - (q/q_0)^3]$, $U_0 = U_c$, $q_0 = \sqrt{\alpha_d}\xi$. The exact solution for the tunneling action of a massive particle in a cubic potential is well known, $S_E/\hbar = (8/15)q_0\sqrt{2mU_0}$ (see, for example, Caldeira and Leggett, 1983), and transforming this result back to the Hall problem we obtain the final result

$$\frac{S_E^H}{\hbar} = \frac{8}{15} \frac{\alpha_d}{\hbar} \xi^2 = \frac{8}{15} \pi n d \xi^2 . \tag{2.103}$$

The result (2.103) does not depend on the depth of the pinning potential, but only on its geometry. This can be readily understood if we consider the shape of the "bounce" solution. Inverting the $x$ component of (2.102), we obtain an inverted potential featuring an interchange of the minimum and the saddle, i.e., what used to be the saddle point for the decay path now becomes a local minimum. The trajectory describing the escape of the particle out of its metastable state follows the equipotential lines in the inverted potential and describes a circle-shaped curve of radius $\simeq \xi$. The resulting action $S = 2\int p\,dq \to 2\alpha_d \int y\,dx$ is a consequence of the "geometrical" quantization (2.97) and is determined solely by the encircled area, without any further dependence on the depth of the potential, in agreement with the result (2.103).

Next let us consider the more general situation in which both the dissipative and the Hall term are relevant in the equation of motion. Going over to imaginary time we obtain the Euclidean action

$$\mathcal{S}_E = \int dt \left[ i\alpha_d \dot{x}y + U(x,y) + \frac{\eta}{4\pi} \int dt' \frac{[x(t)-x(t')]^2 + [y(t)-y(t')]^2}{(t-t')^2} \right] . \tag{2.104}$$

The additional transformation $y \to iy$ again produces a real action, and the task then is to minimize the functional (2.104) for real trajectories $[x(t), y(t)]$. Note that the corresponding mechanical problem features an inverted potential along the $x$ axis and an "antifriction" term in the $y$ coordinate. Alternatively, we can proceed directly from Eq. (2.104)

and integrate over the $y$ variable. After Fourier transformation the effective action for the $x$ component then becomes

$$\mathscr{S}_E = \int \frac{d\omega}{2\pi} \left\{ \left[ \frac{\eta_d|\omega|}{2} + \frac{\alpha_d^2 \omega^2}{2(\eta_d|\omega| + 2U_c/\xi^2)} + \frac{U_c}{\xi^2} \right] x_\omega x_{-\omega} - \frac{U_c}{\xi^3} \int \frac{d\omega'}{2\pi} x_\omega x_{\omega'} x_{-\omega-\omega'} \right\} , \qquad (2.105)$$

and we end up with a one-dimensional problem with a dispersive kinetic term and a potential term nonlocal in $\omega$. An exact solution is complicated by the nonlocal term arising from the cubic potential, but we can easily understand a few qualitative features of the solution. The relevant frequency scale is given by $\omega \simeq (2U_c/\xi)/(\eta_d + |\alpha_d|)$. For vanishing dissipation $\eta_d = 0$ the trajectory is a circular one, which narrows along the $y$ direction as we enhance the friction. The scale along the $y$ direction is $y \simeq x\alpha_d\omega/(\eta_d|\omega| + 2U_c/\xi^2)$; inserting the result for $\omega$, we obtain the ratio $y/x \simeq 1/(1 + \eta_d/|\alpha_d|)$. Comparing the contributions to the dynamical term, we find the corrections to the pure Hall motion for small $\eta_d$ to be of order $\eta_d/\alpha_d$, whereas in the opposite case the Hall corrections to the dissipative motion are of order $\alpha_d^2/\eta_d^2$. The latter result follows from the general observation that $\alpha_d$ refers to an axial vector, and the lowest-order corrections should only involve $\alpha_d^2$, which is independent of the sign.

The generalization of the result (2.103) to three dimensions (tunneling of a vortex line) is straightforward: The area enclosed by the trajectory simply has to be replaced by the enclosed volume,

$$\frac{S_E^H}{\hbar} = \frac{\alpha_l}{\hbar} V = \pi n V . \qquad (2.106)$$

Within the framework of collective pinning (a vortex line segment of length $L_c$ tunneling through a distance $\sim \xi$), we immediately reproduce the result (2.92).

An important question is how to distinguish experimentally between the different types of tunneling. One possibility is to compare the various dependencies on the disorder potential. For the tunneling of a vortex line the result (2.85) for the massive case remains independent of the disorder potential, whereas for the dissipative case [Eq. (2.90)] and for Hall-type dynamics [Eq. (2.92)] we obtain the same dependence $S_E \propto L_c \propto (j_0/j_c)^{1/2}$ on disorder. A second distinction between the various dynamics can be made by considering the initial corrections of the tunneling action due to finite temperatures: For the nondissipative case the finite-temperature corrections to the $T = 0$ result show an exponential behavior $\propto \exp(-T_0/T)$, whereas for the dissipative situation the corrections are of order $(T/T_0)^2$ (see Larkin and Ovchinnikov, 1983; Grabert and Weiss, 1984; Hida, 1985; Blatter and Geshkenbein, 1993; Morais-Smith *et al.*, 1995). The relevant temperature scale is determined by the crossover temperature $T_0 \simeq \hbar U_c/S_E$.

Finally, let us consider the dependence of the action on

the current density $j$. Here we concentrate on the case $j_{sb} < j \ll j_c$, where the single-vortex tunneling concept can be applied. The situation very close to the critical current density is complicated by interaction among the vortices, and we shall comment on this problem in Sec. IV. Above we noticed a strong similarity between the problems of classical and quantum creep, where the latter is just a $(d+1)$-dimensional generalization of the classical $d$-dimensional problem. However, there are also important differences, for example, concerning the nature of the disorder potential, which fluctuates in space but not along the time axis in the $(d+1)$-dimensional extension of the problem. In fact, the solution of the quantum creep problem at low current densities differs in an important way from the corresponding classical analysis. Whereas the string *jumps over* the potential barriers for the classical creep motion, it has to *tunnel through* the potential landscape in order to reach its final state in the quantum case. As a consequence, the time needed for the jump is irrelevant for the classical case but does enter the quantum problem. This has an important effect on the barriers entering the motion. For the classical motion the string can choose *optimal* barriers, scaling with distance according to $U_c(L/L_c)^{2\zeta-1}$; see Eq. (2.64). This is no longer the case in the quantum creep problem, where the vortex has to tunnel under all the barriers within a finite time period, the latter entering the action for the tunneling process. The relevant barrier under which the vortex tunnels therefore scales like the *average* barrier $U_c(L/L_c)$ rather than the *optimal* barrier $U_c(L/L_c)^\chi$. To be specific, we concentrate first on the case of a massive string.

We consider a string trapped in a favorable minimum of the potential landscape. Due to the pinning, the line energy of the string is renormalized downwards by the value $\bar{\varepsilon}_{pin} \simeq -U_c/L_c$. Choosing this state as our zero-energy reference, we find that the potential landscape is given by $\varepsilon_{pin}(z, \mathbf{u}) - \bar{\varepsilon}_{pin}$ and the Euclidean action takes the form

$$\mathscr{S}_E = \int dz\, dt \left[ \frac{m_l}{2}(\partial_t \mathbf{u})^2 + \frac{\varepsilon_l}{2}(\partial_z \mathbf{u})^2 + \varepsilon_{pin}(z, \mathbf{u}) - \bar{\varepsilon}_{pin} \right] , \qquad (2.107)$$

where we have ignored the small tilt due to the driving force. We replace the time integral by an integration over the displacement field $u$, $dt = |\partial u/\partial t|^{-1} du$, and obtain

$$\mathcal{S}_E = \int dz\, du \frac{1}{|\partial_t u|} \left[ \frac{m_l}{2}(\partial_t \mathbf{u})^2 + \frac{\varepsilon_l}{2}(\partial_z \mathbf{u})^2 + \varepsilon_{\text{pin}}(z,\mathbf{u}) - \overline{\varepsilon}_{\text{pin}} \right]$$

$$\gtrsim \left[ \frac{mL_c}{U_c} \right]^{1/2} \int dz\, du \left[ \frac{m_l}{2}(\partial_t \mathbf{u})^2 + \frac{\varepsilon_l}{2}(\partial_z \mathbf{u})^2 + \varepsilon_{\text{pin}}(z,\mathbf{u}) - \overline{\varepsilon}_{\text{pin}} \right] , \qquad (2.108)$$

where we have replaced the velocity $|\partial_t u|$ by its short-wavelength limit $|\partial_t u|_{\max} \simeq \sqrt{U_c/mL_c}$ in the last equation. Now the $u$ integration over the random potential $\varepsilon_{\text{pin}}(z,\mathbf{u})$ averages to zero, and we are left with the expression

$$\mathcal{S}_E \gtrsim \left[ \frac{mL_c}{U_c} \right]^{1/2} \int dz\, du \left[ \frac{m_l}{2}(\partial_t \mathbf{u})^2 + \frac{\varepsilon_l}{2}(\partial_z \mathbf{u})^2 + \frac{U_c}{L_c} \right] , \qquad (2.109)$$

containing only positive terms and hence directly providing a lower estimate for the tunneling action. The remaining task is to find the scales $u$ and $L$ for the closest favorable metastable state. These quantities are determined by the usual consideration that optimal metastable states for segments of length $L$ are separated by a distance $u(L) \simeq \xi(L/L_c)^\zeta$. Combining this result with Eq. (2.109), we obtain the action

$$\mathcal{S}_E \simeq \frac{U_c}{L_c} \left[ \frac{mL_c}{U_c} \right]^{1/2} Lu(L) \simeq \mathcal{S}_E \left[ \frac{L}{L_c} \right]^{1+\zeta}$$

$$\simeq S_E \left[ \frac{j_c}{j} \right]^{(1+\zeta)/(2-\zeta)} . \qquad (2.110)$$

In the last equation we have used Eq. (2.66) relating the length $L$ of the hopping segment to the driving current density $j$, as it is the driving force $j\Phi_0 L/c$ which has to compensate for the elastic energy $\varepsilon_l u^2/L$. Using the line-wandering exponent $\zeta \simeq \frac{3}{5}$ for a string moving in three-dimensional space, we obtain the exponent $\frac{8}{7}$ for the dependence of the action (2.110) upon the current density $j$.

Within the present approximation the dynamics of the string enters the formalism only via the velocity $|\partial_t u|_{\max}$, which for the dissipative case takes the value $U_c/\eta_l \xi L_c$ and for the Hall motion has a corresponding result with $\eta_l$ replaced by the Hall parameter $\alpha_l$. As a result, the actions for the dissipative and for the Hall-type motion take the same form as for the massive case (2.110), with only the prefactor $S_E$ replaced by $S_E^{\text{eff}}$ and by $S_E^H$; see Eqs. (2.90) and (2.92). Note that the assumption of a constant "local" velocity implies that the total tunneling time scales with the distance $u$ between the metastable states, and the action involves the area $Lu(L)$ swept by the tunneling object. In Sec. VIII.C.2 we shall discuss the case of intrinsic quantum creep, both for the massive and for the dissipative string. The tunneling actions can be calculated to higher accuracy in this specific example, with the result that the actions differ by logarithmic factors, $S_E \propto j^{-1}$ and $S_E^{\text{eff}} \propto j^{-1} \ln j^{-1}$. The origin

of these log corrections can be traced back to the different dynamical terms $\sim M \int dt (\partial_t u)^2$ and $\sim \eta \int dt\, dt'(\partial_t u)(\partial_{t'} u) \ln|t-t'|$ in the actions, a feature independent of the specific pinning potential and hence very possibly a general result. We point out again that the regime of validity of the above results is limited to currents $j_{\text{sb}} \lesssim j < j_c$ with $j_{\text{sb}}$ given by Eq. (2.78).

The result (2.110) differs from that obtained in a preprint version of this work. Let us briefly recapitulate our previous approach in order to illuminate the difference in our present understanding of this problem. The most obvious approach to quantum collective creep *at low driving force* would be to generalize the concept of classical collective creep in a straightforward manner, i.e., to determine the tunneling time via equating the dynamical and elastic energies, for the massive case $m_l(u/t)^2 \simeq \varepsilon_l(u/L)^2$, from which follows $t \simeq \sqrt{m_l/\varepsilon_l}L \simeq t_c(j_c/j)^{1/(2-\zeta)}$, and to choose as the relevant tunneling barrier the optimal barrier $U(j) \simeq U_c(j_c/j)^\mu$. This approach assumes that the string can take advantage of the optimal barriers not only for the classical hopping process but also during tunneling. The action then scales with current according to $S \simeq S_c(j_c/j)^{2\zeta/(2-\zeta)}$, and the result depends on the specific dynamics chosen for the string. However, it turns out that this approach leads to conflicting results with known solutions in more regular situations, e.g., a massive elastic manifold trapped in a metastable state of a tilted washboard potential (a scaling law $S \propto r_c^{d-1/2}$ is obtained instead of the known result $S \propto r_c^d$, where $r_c$ is the radius of the critical nucleus; see Sec. III.E.1 below). A careful analysis of the same problem also shows that the manifold cannot profit by creating a thin-wall configuration in the tunneling process (Sec. III.E.1): the tunneling as a rigid object provides the same action as the tunneling via creation of a thin wall. A simple interpretation of these findings is that the manifold has to tunnel under the average potential and not under the optimal one. Second, since the manifold cannot take advantage of the global properties during tunneling, the tunneling time is not determined by the optimal scale $L$ for the tunneling segment but by the distance $u$. Note that the difficulties mentioned above arise within the context of tunneling at *low driving forces*, where a complicated potential landscape with many metastable states has to be considered and where the question of optimal barriers becomes relevant. Quantum creep close to criticality [see Eqs. (2.85), (2.90), and (2.92)] involves only the barrier to the neighboring metastable state, and thus the calculation of the appropriate action is not affected by these new considerations.

## B. Thermal depinning

The new oxide superconductors are characterized by a high transition temperature $T_c$, which implies that the experimentally accessible range of temperatures is large. Therefore we expect that thermal fluctuations of the vortex lines will become important at elevated temperatures. In general, we have to distinguish between two types of thermal motion of the vortex lines: Phonon-like small-amplitude fluctuations restricted to the individual pinning valleys (intravalley fluctuations) will lead to a smoothing of the pinning potential and thereby affect the pinning strength and the critical current density. This has to be contrasted with the large intervalley fluctuations that produce the phenomenon of flux creep discussed above in Sec. II.A.4. In the present section we concentrate on the intravalley motion and analyze the interplay between thermal fluctuations and quenched disorder in the single-vortex pinning regime, where we can neglect interactions between the vortices.

As already mentioned above, the relative importance of thermal fluctuations and of disorder depends on the dimensionality of the problem. Of course, at small length scales, thermal fluctuations are always dominant. At larger length scales, however, disorder can become relevant: For $n = 1$ (string confined to a plane) the disorder *always* becomes relevant at large length scales $L$ (see,

for example, Kardar, 1985). For $n = 3$ (string in four-dimensional space), disorder is irrelevant at high enough temperatures and thermal fluctuations determine the behavior of the string (Imbrie and Spencer, 1988). The most physical case, $n = 2$ (string in three-dimensional space), is special: Again, disorder *always* becomes relevant at large length scales, but its importance is only marginal. Below we shall see that this marginal relevance of disorder for $n = 2$ will lead to a considerable complication of the analysis, as the method of dimensional estimates turns out to be too rough to produce the desired results.

The important effect of thermal fluctuations is a smoothing of the quenched disorder potential producing the pinning. Due to thermal motion of the vortex line, the vortex core will sample the disorder potential over an extended spatial region. As the amplitude of the thermal fluctuations $\langle u^2 \rangle_{\mathrm{th}}^{1/2}$ increases beyond the extent of the vortex core, $\langle u^2 \rangle_{\mathrm{th}} > \xi^2$, the vortex will experience an averaged disorder potential, and thereby pinning will be reduced. Let us calculate the mean-squared pinning potential in the presence of thermal fluctuations. Before taking the average over the disorder potential [see Eq. (2.40)] we perform a time average

$$\langle \cdots \rangle_t = \frac{1}{t_\circ} \int_0^{t_\circ} dt \cdots$$

of the vortex position,

$$\langle\!\langle \mathscr{E}_{\mathrm{pin}}(L) \rangle_t^2 \rangle = \int \frac{dt}{t_\circ} dz \int \frac{dt'}{t_\circ} dz' \langle \varepsilon_{\mathrm{pin}}[z, \mathbf{u}(z,t)] \varepsilon_{\mathrm{pin}}[z', \mathbf{u}(z',t')] \rangle$$

$$= \gamma_U L \int \frac{dt}{t_\circ} \frac{dt'}{t_\circ} \int d^n R p[\mathbf{R} - \mathbf{u}(t)] p[\mathbf{R} - \mathbf{u}(t')] \ . \tag{2.111}$$

After Fourier transformation and using the relation

$$\int \frac{dt'}{t_\circ} e^{i\mathbf{K}\cdot[\mathbf{u}(t) - \mathbf{u}(t')]} = \exp[-\tfrac{1}{2} K^2 \langle u^2(t) \rangle_{\mathrm{th}}]$$

characteristic for Gaussian fluctuations, we obtain

$$\langle\!\langle \mathscr{E}_{\mathrm{pin}}(L) \rangle_t^2 \rangle = \gamma_U L \int \frac{d^n K}{(2\pi)^n} |p_K|^2 \exp[-\tfrac{1}{2} K^2 \langle u^2(t) \rangle_{\mathrm{th}}] \ .$$

$$\tag{2.112}$$

Here we have introduced the definition $\langle u^2(t) \rangle_{\mathrm{th}} = \langle [\mathbf{u}(t) - \mathbf{u}(0)]^2 \rangle_{\mathrm{th}}$ and we have taken the limit $t_\circ \to \infty$, i.e., in Eq. (2.112) we should take the asymptotic value of $\langle u^2(t) \rangle_{\mathrm{th}}$ at large times. The latter step can be done as long as the string remains pinned and does not diffuse away at large times, so that the Debye-Waller factor remains finite in the asymptotic limit. It remains to determine the amplitude of thermal fluctuations for which a simple dimensional estimate comparing the elastic energy $\varepsilon_l \langle u^2(L_c) \rangle_{\mathrm{th}}/L_c$ with the thermal energy $T$ gives the result $\langle u^2(L_c) \rangle_{\mathrm{th}} \simeq TL_c/\varepsilon_l$. A more rigorous derivation of this result is obtained by using the

fluctuation-dissipation theorem (Landau and Lifshitz, 1958b) relating the thermal amplitude $\langle u^2(t) \rangle_{\mathrm{th}}$ to the Green's function $G(q, \omega)$ for a single vortex,

$$\langle u^2(t) \rangle_{\mathrm{th}} = 2\hbar \int \frac{d\omega}{2\pi} [1 - \cos(\omega t)] \coth\frac{\hbar\omega}{2T} \mathrm{Im} G(z=0, \omega) \ ,$$

$$\approx 4T \int \frac{d\omega}{2\pi} [1 - \cos(\omega t)] \frac{1}{\omega} \mathrm{Im} G(z=0, \omega) \ .$$

$$\tag{2.113}$$

Here $\mathrm{Im} G$ denotes the imaginary part of $G$. Using the single-vortex Green's function,

$$G(q, \omega) = \frac{1}{-i\eta_l \omega + \varepsilon_l q^2} \ , \tag{2.114}$$

we obtain after integration over frequencies

$$\langle u^2(t) \rangle_{\mathrm{th}} = \frac{2T}{\varepsilon_l} \int \frac{dq}{2\pi} \frac{1}{q^2} \left[ 1 - \exp\left[ -\frac{\varepsilon_l}{\eta_l} q^2 t \right] \right] \ . \tag{2.115}$$

In the absence of disorder we have to integrate over all $q$ modes and find for the diffusion behavior of a string the

law

$$\langle u^2(t) \rangle_{\text{th}} \simeq T \left[ \frac{t}{\varepsilon_l \eta_l} \right]^{1/2}, \qquad (2.116)$$

which is suppressed as compared with the diffusion law for a pointlike object,

$$\langle u^2(t) \rangle_{\text{th}} \propto t .$$

If disorder is present, we should cut off the $q$ integration in Eq. (2.115) at the length $L_c(T)$ where the disorder becomes relevant, $q > 2\pi/L_c(T)$, and we obtain for the fluctuation amplitude in the limit $t \to \infty$

$$\langle u^2(L_c) \rangle_{\text{th}} \simeq \frac{T L_c(T)}{\varepsilon_l} . \qquad (2.117)$$

Inserting (2.117) back into our expression for the mean-squared pinning energy (2.112), we obtain the result

$$\langle\!\langle \mathscr{E}_{\text{pin}}(L_c) \rangle_t^2 \rangle \simeq \gamma L_c \left[ \frac{\xi^4}{\langle u^2(L_c) \rangle_{\text{th}}} \right]^{n/2}$$

$$\simeq \gamma L_c \left[ \frac{\xi^4 \varepsilon_l}{T L_c} \right]^{n/2}, \qquad (2.118)$$

where we have assumed $\langle u^2(t \to \infty) \rangle_{\text{th}} = \langle u^2(L_c) \rangle_{\text{th}} > \xi^2$ so that the short-wavelength cutoff in Eq. (2.112) is produced by the exponential factor $\exp[-K^2 \langle u^2(L_c) \rangle_{\text{th}}/2]$, hence $K < 1/\langle u^2(L_c) \rangle_{\text{th}}^{1/2}$. Note that, for the opposite case, $\langle u^2(L_c) \rangle_{\text{th}} < \xi^2$, the relevant cutoff is due to the factor $|p_K|^2$, i.e., $K < 1/\xi$, and we recover the zero-temperature result (2.41).

The final step consists in determining the temperature-dependent collective pinning length $L_c(T)$. For $n = 1$ the method of dimensional estimates works fine, and by equating the pinning energy (2.118) to the elastic energy $\varepsilon_0 \langle u^2(L_c) \rangle_{\text{th}}/L_c \simeq T$ we can easily obtain the collective pinning length

$$L_c(T) \simeq \frac{T^5}{\gamma^2 \varepsilon_0 \xi^4}, \quad n = 1 . \qquad (2.119)$$

Again, we have substituted the short-wavelength limit $\varepsilon_0$ for the dispersive line tension $\varepsilon_l[q \sim 1/L_c(T)]$. Defining the (temperature-dependent) depinning energy $\tilde{T}_{\text{dp}}^s = (\gamma \varepsilon_0 \xi^3)^{1/3}$ for a single vortex in two dimensions, we can rewrite Eqs. (2.117) and (2.119) in the simple form $\langle u^2(L_c) \rangle_{\text{th}} \simeq \xi^2 (T/\tilde{T}_{\text{dp}}^s)^6$ and $L_c(T) \simeq L_c(0)(T/\tilde{T}_{\text{dp}}^s)^5$, with $L_c(0) \simeq (\varepsilon_0^2 \xi^3/\gamma)^{1/3}$. A strong decrease in the pinning strength due to thermal smoothing is expected above the depinning temperature $T_{\text{dp}}^s$, which is defined by the self-consistency equation $T_{\text{dp}}^s = \tilde{T}_{\text{dp}}^s(T_{\text{dp}}^s)$, with $\tilde{T}_{\text{dp}}^s(T) = \tilde{T}_{\text{dp}}^s(0)(1 - T/T_c)^{1/3}$ (note that the disorder parameter $\gamma$ is itself also temperature dependent; see Sec.

III.C. The $T$ dependence given here applies to the case of $\delta T_c$ pinning). The temperature-dependent activation energy becomes $U_c(T > T_{\text{dp}}^s) \simeq T$, and the depinning critical current density decays with increasing temperature according to $j_c(T) \simeq j_0 [\xi/L_c(0)]^2 (\tilde{T}_{\text{dp}}^s/T)^7$ (Feigel'man, 1983; see also Ioffe and Vinokur, 1987).

On the other hand, for $n = 2$ the length $L_c$ drops out of the problem, and we cannot use the method of dimensional estimates for the determination of the collective pinning length. The deeper reason for this failure can be found in the marginal relevance of disorder for the three-dimensional single-vortex problem: The transverse fluctuations in the vortex position due to thermal disorder, $\langle u^2(L) \rangle_{\text{th}} = \langle [u(L,t) - u(0,t)]^2 \rangle_{\text{th}}$, compete with those due to quenched disorder, $\langle\!\langle u_p^2 \rangle\!\rangle = \langle\!\langle [u_p(L,t) - u_p(0,t)]^2 \rangle\!\rangle$, where $u_p$ denotes the displacement field due to the pinning potential. Of course, $\langle\!\langle u_p^2(L) \rangle\!\rangle > \langle u^2(L) \rangle_{\text{th}}$ for $L > L_c(T)$, since for $n \leq 2$ disorder is always relevant at large length scales. On the other hand, at small length scales, $L < L_c(T)$, thermal fluctuations are dominant, $\langle\!\langle u_p^2(L) \rangle\!\rangle < \langle u^2(L) \rangle_{\text{th}}$, and hence we expect that the disorder fluctuations $\langle\!\langle u_p^2(L) \rangle\!\rangle$ should grow faster with $L$ than the thermal fluctuations in this regime. Whereas $\langle\!\langle u_p^2(L) \rangle\!\rangle / \langle u^2(L) \rangle_{\text{th}} \propto L^{1/2}$ grows algebraically with distance $L < L_c(T)$ for $n = 1$, as we shall show below, the corresponding ratio depends only logarithmically on $L$ for the case of $n = 2$. This logarithmic dependence on $L$ is beyond the realm of the method of dimensional estimates. However, an alternative way to determine the collective pinning length $L_c(T)$ is to use the length dependence of the disorder fluctuations $\langle\!\langle u_p^2(L) \rangle\!\rangle$ themselves. As $L$ approaches $L_c(T)$ the disorder fluctuations $\langle\!\langle u_p^2(L) \rangle\!\rangle$ grow as large as the thermal fluctuations $\langle u^2(L) \rangle_{\text{th}}$, and hence the condition $\langle\!\langle u_p^2(L_c) \rangle\!\rangle = \langle u^2(L_c) \rangle_{\text{th}}$ determines the collective pinning length $L_c(T)$. The amplitude of thermal fluctuations has been calculated above [see Eq. (2.117) with $L$ substituted for $L_c$], and the remaining task is to determine the fluctuation amplitude $\langle\!\langle u_p^2(L) \rangle\!\rangle^{1/2}$ due to the pinning potential.

Again we can use the (real-space) single-vortex Green's function in order to relate the displacement field $\mathbf{u}_p(z,t)$ to the disorder potential $U_{\text{pin}}$,

$$\mathbf{u}_p(z,t) = \int d^n R' \, dz' \, dt' \, G(z,z';t,t')$$

$$\times U_{\text{pin}}(\mathbf{R}',z') \nabla_p [\mathbf{R}' - \mathbf{u}(z',t')] . \qquad (2.120)$$

We split the total displacement field $\mathbf{u}$ into a part $\mathbf{u}_{\text{th}}$ due to thermal fluctuations and a contribution $\mathbf{u}_p$ due to quenched disorder. For $L < L_c(T)$ the disorder can be treated as a perturbation, and we can expand the right-hand side of (2.120) in $\mathbf{u}_p$. To lowest order the mean-square displacement field then becomes

$$\langle\!\langle u_p^2(L) \rangle\!\rangle \approx \gamma_U \int d^n R' \, dz' \int dt' \, dt'' [G(L,z';t,t') - G(0,z';t,t')] \nabla_p [\mathbf{R}' - \mathbf{u}_{\text{th}}(z',t')]$$

$$\times [G(L,z';t,t'') - G(0,z';t,t'')] \nabla_p [\mathbf{R}' - \mathbf{u}_{\text{th}}(z',t'')] , \qquad (2.121)$$

and after Fourier transformation

$$\langle\langle u_p^2(L)\rangle\rangle \approx \gamma_U \int \frac{d^nK}{(2\pi)^n} \frac{dq}{2\pi} \int dt'\, dt'' \int \frac{d\omega}{2\pi} \frac{d\omega'}{2\pi} \frac{e^{-i\omega t'}}{-i\eta_l\omega+\varepsilon_l q^2} \frac{e^{-i\omega' t''}}{-i\eta_l\omega'+\varepsilon_l q^2}$$

$$\times [1-\cos(qL)]|p_K|^2 K^2 \exp[-\tfrac{1}{2}K^2\langle u^2(t'-t'')\rangle_{\mathrm{th}}]\, , \tag{2.122}$$

where we have used the definition of the single-vortex Green's function (2.114). Performing the (contour) integrations over the frequencies as well as one of the time integrals, we arrive at

$$\langle\langle u_p^2(L)\rangle\rangle \approx \frac{\gamma_U}{\eta_l\varepsilon_l} \int \frac{d^nK}{(2\pi)^n} \frac{dq}{2\pi} \int d\bar{t}\, \frac{1-\cos(qL)}{q^2} \exp\left[-\frac{\varepsilon_l}{\eta_l}q^2\bar{t}\right]|p_K|^2 K^2 \exp[-\tfrac{1}{2}K^2\langle u^2(\bar{t})\rangle_{\mathrm{th}}]\, . \tag{2.123}$$

For large enough temperatures the cutoff in the transverse wave vector $K$ is given by the amplitude of thermal fluctuations, and using the result Eq. (2.116) we find

$$\langle\langle u_p^2(L)\rangle\rangle \simeq \frac{\gamma\xi^4}{T^2} \int \frac{dq}{2\pi} d\bar{t}\, \frac{1-\cos(qL)}{q^2} \exp\left[-\frac{\varepsilon_l}{\eta_l}q^2\bar{t}\right] \begin{cases} \dfrac{1}{\xi^2}\left[\dfrac{T}{\sqrt{\varepsilon_l\eta_l}}\right]^{1/2}\dfrac{1}{\bar{t}^{3/4}} & \text{for } n=1\ , \\[2ex] \dfrac{1}{\bar{t}} & \text{for } n=2\ . \end{cases} \tag{2.124}$$

For the case $n=1$ all the remaining integrals converge, and we obtain for the fluctuations due to disorder the final expression

$$\langle\langle u_p^2(L)\rangle\rangle \simeq \gamma\xi^2 \left[\frac{L^3}{\varepsilon_l T^3}\right]^{1/2}\, , \quad n=1\ , \tag{2.125}$$

which indeed grows faster than the thermal fluctuations $\langle u^2(L)\rangle_{\mathrm{th}} \simeq TL/\varepsilon_l$ by a factor $\propto L^{1/2}$. Moreover, using the condition $\langle\langle u_p^2(L_c)\rangle\rangle \simeq \langle u^2(L_c)\rangle_{\mathrm{th}}$, we obtain the temperature-dependent pinning length $L_c(T) \simeq T^5/\gamma^2\varepsilon_0\xi^4$, in agreement with the previous result (2.119) based on the method of dimensional estimates. Note that for $L > L_c(T)$ our perturbative approach, which has been based on the smallness of $u_p$, $u_p < u_{\mathrm{th}}$, breaks down.

For the case $n=2$, we have to cut off the time integral in (2.124) at small times where $\langle u^2(\bar{t})\rangle_{\mathrm{th}} \simeq \xi^2$, as for smaller times the cutoff in the $K$ integration in (2.123) is provided by the factor $|p_K|^2$ rather than by the Debye-Waller factor. Using Eq. (2.116), we obtain a lower cutoff on the time integral in (2.124) given by $\bar{t} \simeq \eta_l\varepsilon_0\xi^4/T^2$. After subsequent integration over time $\bar{t}$ and wave vectors $q$, the disorder-induced mean-squared amplitude of fluctuations becomes

$$\langle\langle u_p^2(L)\rangle\rangle \simeq \frac{\gamma\xi^4}{T^2}L\ln\frac{TL}{\varepsilon_0\xi^2}, \quad n=2\ , \tag{2.126}$$

which is growing only logarithmically faster than the corresponding thermal amplitude. At the collective pinning length $L_c(T)$ disorder becomes dominant, and we find the result

$$L_c(T) \simeq \xi\frac{\varepsilon_0\xi}{T}\exp\left[\frac{T^3}{\gamma\varepsilon_0\xi^4}\right]$$

$$\simeq L_c(0)\frac{\tilde{T}_{\mathrm{dp}}^s}{T}\exp\left[c\left[\frac{T}{\tilde{T}_{\mathrm{dp}}^s}\right]^3\right], \quad n=2\ , \tag{2.127}$$

which grows exponentially in temperature. Here we have introduced the thermal depinning energy $\tilde{T}_{\mathrm{dp}}^s$,

$$\tilde{T}_{\mathrm{dp}}^s \simeq (\gamma\varepsilon_0\xi^4)^{1/3} \simeq U_c \simeq T_c\left[\frac{1-t}{Gi}\right]^{1/2}\left[\frac{j_c}{j_0}\right]^{1/2}, \tag{2.128}$$

for a single vortex embedded in three dimensions. In terms of the depinning energy $\tilde{T}_{\mathrm{dp}}^s$ the fluctuation amplitude at $L_c(T)$ takes the simple form

$$\langle u^2(L_c)\rangle_{\mathrm{th}} \simeq \xi^2\exp\left[c\left[\frac{T}{\tilde{T}_{\mathrm{dp}}^s}\right]^3\right]\, . \tag{2.129}$$

Again, the depinning temperature $T_{\mathrm{dp}}^s$ itself is given by the self-consistency equation

$$T_{\mathrm{dp}}^s = \tilde{T}_{\mathrm{dp}}^s(T_{\mathrm{dp}}^s)\ . \tag{2.130}$$

For $\delta T_c$ pinning we have $\tilde{T}_{\mathrm{dp}}^s(T) = \tilde{T}_{\mathrm{dp}}^s(0)(1-T/T_c)^{1/3}$; see Sec. III.C. Once the collective pinning length $L_c(T)$ has been determined, the calculation of the activation energy $U_c(T)$ for classical creep and the critical current density $j_c(T)$ is easy, and the results are (Feigel'man and Vinokur, 1990)

$$U_c(T) \simeq \frac{\varepsilon_0\langle u^2(L_c)\rangle_{\mathrm{th}}}{L_c(T)} \simeq T\ , \tag{2.131}$$

$$j_c(T) \simeq \frac{c}{\Phi_0}\frac{T}{\langle u^2(L_c)\rangle_{\mathrm{th}}^{1/2}}L_c(T)$$

$$\simeq j_c(0)\left[\frac{T}{\tilde{T}_{\mathrm{dp}}^s}\right]^2\exp\left[-\frac{3}{2}c\left[\frac{T}{\tilde{T}_{\mathrm{dp}}^s}\right]^3\right]\, , \tag{2.132}$$

with $c$ a constant of order unity. Note that $U_c(T=T_{dp}^s) \simeq T_{dp}^s = U_c$, in agreement with Eq. (2.46). With decreasing temperature the $T$ dependence in the above results has to be cut off at $T \simeq T_{dp}^s$, and we obtain a smooth crossover to the corresponding zero-temperature expressions. The most remarkable result of this section is the exponential decay of the critical current density with temperature, which is a consequence of the marginal relevance of disorder for a string in three-dimensional space.

Finally, we remark that the range of applicability of the single-vortex pinning results derived in this section is reduced with respect to the situation at zero temperature: Using the condition $L_c(T) < a_0$, we find that the above results are valid in a temperature-field region characterized by the relation

$$T < T_{dp}^s \left[ \ln \frac{j_c}{j_0} \frac{\beta_{sb} H_{c_2}}{B} \right]^{1/3} . \tag{2.133}$$

## C. Anisotropy

In this section we generalize to the anisotropic situation the concept of weak collective pinning theory developed above for the simplest case of an isotropic superconductor. This will enable us to make a direct comparison between our theoretical analysis and experimental results on the oxide superconductors with their pronounced anisotropy. The more extreme case of layered superconductivity will be extensively discussed in Sec. VIII. However, we wish to point out that, for many important questions, the layered structure of the material turns out to be irrelevant and a description in terms of an anisotropic GL theory based on Eq. (2.1) is appropriate. In particular, this is the case for single-vortex pinning and creep in layered superconductors within a wide angular regime when the direction of the magnetic field **H** is not too closely aligned with the superconducting planes. In this section we follow the work of Blatter and Geshkenbein (1992) and present the traditional approach for obtaining results in an anisotropic situation. This approach starts from the anisotropic GL functional (2.1) and calculates all the quantities following the same line of argument as in the isotropic case. In Sec. III.A we introduce a more elegant scaling approach due to Blatter, Geshkenbein, and Larkin (1992), which allows us to derive the results of this section in a much simpler way. However, we believe that the traditional approach also has its merits, as it is more physical and allows for a deeper understanding of the results.

Let us recall the anisotropic GL free-energy functional (2.1), which can be characterized by the two length scales $\xi$ and $\lambda$ describing the (planar) coherence of the condensate and the (planar) electromagnetic response, respectively, and the anisotropy ratio $\varepsilon^2 = m/M \ll 1$; see Eq. (2.2). In our notation, $\xi$ and $\lambda$ denote the characteristic scales within the superconducting planes, and we shall use the convention $\xi_c = \varepsilon \xi$ and $\lambda_c = \lambda/\varepsilon$ to describe the corresponding scales along the $c$ axis. Note that the penetration depth characterizes the decay length of currents rather than magnetic fields: a current density **j** directed along the $ab$ plane (along the $c$ axis) can be modified on a scale $\lambda$ ($\lambda_c$). The new oxide superconductors are characterized by the following set of parameters (at vanishing temperatures):

$$\text{YBa}_2\text{Cu}_3\text{O}_{7-y} \begin{cases} \lambda_L \approx 1400 \text{ Å}, \\ \xi_{BCS} \approx 12-18 \text{ Å}, \\ d \approx 12 \text{ Å}, \\ \varepsilon \approx \frac{1}{5} - \frac{1}{7} \end{cases} \tag{2.134}$$

(Cava, Batlogg, van Dover, *et al.*, 1987; Worthington *et al.*, 1987; Farrell *et al.*, 1988; Harshman *et al.*, 1989; Krusin-Elbaum *et al.*, 1989; Welp *et al.*, 1989),

$$\text{Bi}_2\text{Sr}_2\text{Ca}_1\text{Cu}_2\text{O}_{8+y} \begin{cases} \lambda_L \approx 1400-2000 \text{ Å}, \\ \xi_{BCS} \approx 20-40 \text{ Å}, \\ d \approx 15 \text{ Å}, \\ \varepsilon \approx \frac{1}{50} - \frac{1}{200} \end{cases} \tag{2.135}$$

(Hazen *et al.*, 1988; Naughton *et al.*, 1988; Palstra *et al.*, 1988a; Sunshine *et al.*, 1988; Farrell *et al.*, 1989; Uemura *et al.*, 1989; Chikumoto *et al.*, 1992a; Martínez *et al.*, 1992). The Ginzburg-Landau values extrapolated to zero temperature are obtained out of $\lambda_L$ and $\xi_{BCS}$ via the relations $\lambda^2(0) = \lambda_L^2/2$ and $\xi^2(0) = 0.54\xi_{BCS}^2$ (clean limit; see also Sec. III.C below). Here we have added the interplanar distance $d$ to the list of characteristic parameters. Note that $\varepsilon\xi_{BCS} < d$ for both materials, so that a description in terms of a Lawrence-Doniach model (1971) is actually more appropriate within a large temperature range. However, as already mentioned above, the anisotropic GL description is able to capture all of the essential physics in many important cases of interest.

### 1. Collective pinning length and energy

Let us consider an anisotropic superconductor characterized by the planar coherence length $\xi$, the in-plane London penetration depth $\lambda$, and a mass anisotropy ratio $\varepsilon^2 = m/M < 1$. We choose a coordinate system where the $z$ axis is aligned parallel to the crystal $c$ axis. A magnetic field **H** enclosing an angle $\vartheta_H$ with the $ab$ plane (an angle $\theta_H = \pi/2 - \vartheta_H$ with the $c$ axis) is applied to the sample; see Fig. 7. To be explicit, we assume **H** to lie in the $yz$ plane of our coordinate system. The magnitude of **H** is chosen to be much larger than the lower critical field $H_{c_1}(\theta_H)$. The correct angular dependence of $H_{c_1}(\theta_H)$ still seems to be a rather controversial issue. A particularly simple expression can be obtained within the London approximation (Balatskii, Burlachkov, and Gor'kov, 1986),

$$H_{c_1}(\theta_H) = \frac{\Phi_0}{4\pi\lambda^2} \frac{\varepsilon}{\varepsilon_{\theta_H}} \ln\left[\frac{\lambda}{\xi}\right] . \tag{2.136}$$

Here we have introduced the angle-dependent anisotropy parameter

$$\varepsilon_\vartheta^2 = \varepsilon^2(\vartheta) = \varepsilon^2\cos^2\vartheta + \sin^2\vartheta , \tag{2.137}$$

which is the main parameter describing the angular dependencies of physical quantities in an anisotropic superconductor. An analysis based on the Ginzburg-Landau theory provides the additional angular dependence in the logarithm (plus additional non-logarithmic corrections), which can lead to modifications of the above simple result (Klemm and Clem, 1980; Klemm, 1990, 1993). Whereas the following analysis does not rely on a precise value for $H_{c_1}$, the expression (2.136) allows for an order-of-magnitude estimate for the regime of applicability of our results.

In general, the direction of the external magnetic field $\vartheta_H$ deviates from the direction $\vartheta$ of the vortices, where the angle $\vartheta$ is again measured with respect to the *ab* plane; see Fig. 7. For an Abrikosov lattice in an equilibrium state, this deviation is given by (Balatskii, Burlachkov, and Gor'kov, 1986; Kogan, 1988; Bulaevskii, 1991)

$$\sin(\vartheta_H - \vartheta) = \frac{H_{c_1}^c}{H} \frac{\sin\vartheta\cos\vartheta}{\varepsilon_\vartheta}(1-\varepsilon^2)\frac{\ln[H_{c_2}(\vartheta)/B]}{2\ln(\lambda/\xi)} .$$

Here $H_{c_1}^c$ is the lower critical field along the *c* axis and

$$H_{c_2}(\vartheta) = \frac{\Phi_0}{2\pi\varepsilon_\vartheta\xi^2} \tag{2.138}$$

is the upper critical field along $\vartheta$. For large enough fields,

$$H \gg \frac{H_{c_1}^c}{\varepsilon_\vartheta} , \tag{2.139}$$

the relative difference between the external angle $\vartheta_H$ and the internal angle $\vartheta$ becomes small, and we can neglect this complication in the following analysis, where we express all quantities by the internal field variable $\vartheta$. For small field values the situation is more difficult. Here our main focus is on pinning, thus the vortices go into a metastable critical state rather than to a stable equilibrium configuration. The internal angle $\vartheta$ then depends on the condition under which the critical state is formed. If the field is switched off after field-cooling (magnetic remanence), initially the vortices are pinned in a direction parallel to the former external field. This initial angle is changed due to flux flow and creep as the metastable critical state evolves in time, as has been shown, for example, by Tuominen et al. (1990), who observe an alignment of the remanent diamagnetic moment with the *c* axis after the external field is switched off. On the other hand, in a zero-field-cooled situation vortices entering the sample will be directed along the external magnetic-field direction at the surface, though, it is unclear along which direction the vortices will point within the interior of the sample, as this is the result of flux flow and creep during the creation time of the critical state itself. In the following we shall concentrate on a specific part of this problem, which is the pinning and creep in anisotropic and layered material due to classical and quantum motion. We therefore express all quantities by the (local) internal field angle $\vartheta$ and leave the problem of relating internal and external angles under nonequilibrium conditions for future studies.

Vortices entering the sample will minimize their energies with respect to the weak random pinning potential $\varepsilon_{\text{pin}}$. Here we restrict our analysis to the case of scalar disorder as produced, for example, by a spatial fluctuation of the transition temperature $T_c$. As we shall show below (Sec. III.C), this type of disorder seems to predominate over the disorder in the mean free path, which in general is of tensorial character. Again, for not too large fields, the interaction between the vortices is small compared with the interaction of a single vortex with pinning centers, so that we can study the single-vortex free energy

$$\mathcal{F}[\mathbf{u}] = \int dz' \left[ \frac{\varepsilon_l^\parallel(\vartheta)}{2}(\partial_{z'}u_x)^2 + \frac{\varepsilon_l^\perp(\vartheta)}{2}(\partial_{z'}u_{y'})^2 \right.$$
$$\left. + \varepsilon_{\text{pin}}(z',\mathbf{u}) - \mathbf{f}_L\cdot\mathbf{u} \right] . \tag{2.140}$$

Equation (2.140) is the generalization of the single-vortex free-energy functional (2.31) to the anisotropic situation. Here we have introduced a rotated coordinate system with $z'$ pointing along the external field **H** and a common *x* axis, $x = x'$.

The elasticities $\varepsilon_l^\parallel(\vartheta)$ and $\varepsilon_l^\perp(\vartheta)$ for in-plane and for out-of-plane motion can be obtained in the following way: The line energy of a vortex segment of length $L$ enclosing an angle $\vartheta$ with the *ab* plane is

$$e_l(L,\vartheta) = \varepsilon_0\varepsilon_\vartheta L \ln\left[\frac{\lambda}{\varepsilon_\vartheta\xi}\right] , \tag{2.141}$$

(Klemm and Clem, 1980; Balatskii, Burlachkov, and Gor'kov, 1986) with $\varepsilon_0 = (\Phi_0/4\pi\lambda)^2$. The tilt modulus is determined by the increase in energy due to a transverse fluctuation of the vortex position. When the vortex is symmetrically deformed over a distance $2L$ by an amplitude $L\delta\phi$, the energy increase of one segment with length $L$ is

$$\delta e_l = \frac{\partial e_l}{\partial L}\delta L + \frac{\partial e_l}{\partial\vartheta}\delta\vartheta + \frac{1}{2}\frac{\partial^2 e_l}{\partial\vartheta^2}(\delta\vartheta)^2 . \tag{2.142}$$

For an out-of-plane tilt by an angle $\delta\phi = \delta\vartheta$, the length of the segment $L$ is increased by $\delta L \simeq L(\delta\vartheta)^2/2$. The out-of-plane elasticity is defined by the relation

$$\frac{1}{2}\varepsilon_l^\perp(\vartheta)L(\delta\vartheta)^2 = \frac{\partial e_l}{\partial L}\delta L + \frac{1}{2}\frac{\partial^2 e_l}{\partial\vartheta^2}(\delta\vartheta)^2 . \tag{2.143}$$

Here the linear term in (2.142) has dropped out as the total deformation involves two segments of length $L$ with opposite angular corrections $\pm \delta \vartheta$. After a few algebraic manipulations we obtain the result

$$\varepsilon_l^{\perp}(\vartheta) \simeq \frac{\varepsilon^2 \varepsilon_0}{\varepsilon_\vartheta^3} \ . \tag{2.144}$$

As before, we ignore the logarithmic dispersion (Brandt, 1977b) of the line tension here, since we are interested in pinning phenomena involving only short-wavelength distortions with $k \simeq 1/L_c$.

For an in-plane tilt by an angle $\delta\phi$, the length of the segment $L$ is increased by $\delta L \simeq L(\delta\phi)^2/2$, whereas the change in the angle $\vartheta$ is given by the equation $\tan(\vartheta + \delta\vartheta) = L \sin\vartheta/[(L \cos\vartheta)^2 + (L\delta\phi)^2]^{1/2}$, resulting in $\delta\vartheta = -(\tan\vartheta)(\delta\phi)^2/2$. The in-plane elasticity is defined by

$$\tfrac{1}{2}\varepsilon_l^{\parallel}(\vartheta)L(\delta\phi)^2 = \frac{\partial e_l}{\partial L}\delta L + \frac{\partial e_l}{\partial \vartheta}\delta\vartheta \ , \tag{2.145}$$

where we have dropped the term quadratic in $\delta\vartheta$, as the angular correction $\delta\vartheta$ is already of second order in $\delta\phi$. The final result for the in-plane elasticity is

$$\varepsilon_l^{\parallel}(\vartheta) \simeq \frac{\varepsilon^2 \varepsilon_0}{\varepsilon_\vartheta} \ . \tag{2.146}$$

Again, our task is to minimize the free-energy functional (2.140) and to find the collective pinning lengths and energies. In anisotropic materials we have to consider two types of relaxation: (i) the in-plane relaxation with $\mathbf{u} = (u_x, 0, 0)$ involving the elasticity modulus $\varepsilon_l^{\parallel}(\vartheta)$ and the length scale $\xi$, and (ii) the out-of-plane relaxation with $\mathbf{u} = (0, u_{y'}, 0)$, elasticity $\varepsilon_l^{\perp}(\vartheta)$, and the relevant length scale for pinning $\varepsilon_\vartheta\xi$; see Fig. 11. Pinning is due to fluctuations in the potential $\varepsilon_{\text{pin}}$, and in analogy with Eq. (2.41) above we obtain

$$\langle \varepsilon_{\text{pin}}^2(L) \rangle \simeq \gamma \varepsilon_\vartheta \xi^2 L \ . \tag{2.147}$$
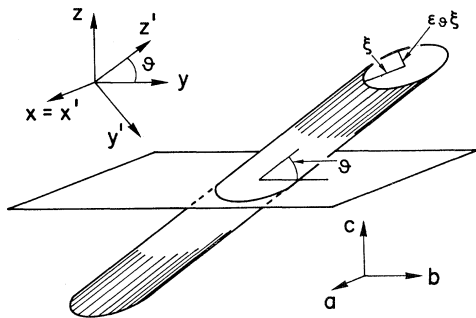


FIG. 11. Abrikosov vortex in an anisotropic superconductor tilted away from the main axis. The vortex core is deformed into an elliptic shape with the main axes extending a distance $\xi$ and $\varepsilon_\vartheta\xi$ along the $x$ and $y'$ axes, respectively. These two lengths then also define the relevant distances for the relaxation of the vortex to the pinning potential and for creep-type motion within the $ab$ plane ($x$ axis) and in the out-of-plane direction ($y'$ axis).

This result can also be obtained from an analysis similar to that leading to Eq. (2.42). For the case of in-plane relaxation the individual pinning force remains unchanged, the pinning volume is reduced to $V_c \simeq \varepsilon_\vartheta \xi^2 L$, and the length scale of the disorder is $\xi$. On the other hand, in the case of out-of-plane relaxation, the pinning force is enhanced, $f_{\text{pin}} \to f_{\text{pin}}/\varepsilon_\vartheta$, the pinning volume is again $V_c \simeq \varepsilon_\vartheta \xi^2 L$, and the disorder involves the reduced length scale $\varepsilon_\vartheta\xi$. Both relaxation modes then lead to the same result for the mean-squared pinning energy, which is identical with (2.147) if we use the equality (2.43).

Using the method of dimensional estimates, the collective pinning length is obtained by equating the mean pinning energy $\langle \varepsilon_{\text{pin}}^2(L) \rangle^{1/2}$ to the elastic energy accumulated along the length $L$. The relevant length scale for relaxation in the $ab$ plane is $\xi$, and thus the elastic energy becomes $\varepsilon_l^{\parallel}(\vartheta)\xi^2/L_c^{\parallel}$. Solving for the collective pinning length $L_c^{\parallel}$, we obtain

$$L_c^{\parallel} \simeq \left[ \frac{\varepsilon_0^2 \xi^2 \varepsilon^4}{\gamma \varepsilon_\vartheta^3} \right]^{1/3} \ . \tag{2.148}$$

The result (2.148) has to be compared with the out-of-plane relaxation mode, where the relevant length scale is given by $\varepsilon_\vartheta\xi$ and the elastic energy becomes $\varepsilon_l^{\perp}(\vartheta)(\varepsilon_\vartheta\xi)^2/L_c^{\perp}$. The collective pinning length $L_c^{\perp}$ then turns out to be identical to the result for in-plane motion. In general, the vortex relaxes to the pinning potential by choosing the mode characterized by the smaller collective pinning length. Here, the two collective pinning lengths for in-plane and for out-of-plane relaxation agree with each other, and thus the relaxation of the vortex involves both in-plane and out-of-plane motion. The final result for the collective pinning length in an anisotropic superconductor is

$$L_c(\vartheta) \simeq \frac{L_c^c}{\varepsilon_\vartheta}, \quad L_c^c \simeq \left[ \frac{\varepsilon_0^2 \xi^2 \varepsilon^4}{\gamma} \right]^{1/3} \ , \tag{2.149}$$

where $L_c^c$ denotes the collective pinning length for a field applied parallel to the $c$ axis of the crystal. Note that $L_c^c$ is reduced by a factor $\varepsilon^{4/3}$ with respect to the isotropic result (2.45). The collective pinning energy is

$$U_c^c \simeq (\gamma \xi^2 L_c^c)^{1/2} \simeq \varepsilon^{2/3}(\gamma \varepsilon_0 \xi^4)^{1/3}$$

$$\simeq H_c^2 \varepsilon \xi^3 \frac{\varepsilon\xi}{L_c^c} \simeq \left[ \frac{1-t}{Gi} \right]^{1/2} \frac{\varepsilon\xi}{L_c^c} \ , \tag{2.150}$$

which is independent of the angle $\vartheta$ and reduced by a factor $\varepsilon^{2/3}$ with respect to the isotropic result (2.46).

### 2. Critical current density

Once the collective pinning length $L_c(\vartheta)$, Eq. (2.149), and the pinning energy $U_c^c$, Eq. (2.150), have been determined, it is trivial to find the critical current densities. Let us first consider a current flowing in the $ab$ plane orthogonal to the field direction, i.e., along the $x$ axis. The

vortex density gradient is directed along the $y'$ axis and the relevant length scale of the pinning potential is $\varepsilon_\vartheta\xi$. The critical current density $j_c^\parallel$ is then found by equating the Lorentz force $j_c^\parallel\Phi_0 L_c^c/\varepsilon_\vartheta c$ to the pinning force $U_c^c/\varepsilon_\vartheta\xi$. The anisotropy parameter $\varepsilon_\vartheta$ drops out, and we obtain a planar critical current density that does not depend on the angle $\vartheta$,

$$j_c^\parallel \simeq j_c^c \simeq \frac{c}{\Phi_0}\left[\frac{\gamma}{L_c^c}\right]^{1/2} \simeq j_\circ \left[\frac{\varepsilon\xi}{L_c^c}\right]^2 , \qquad (2.151)$$

and that coincides with the in-plane critical current density $j_c^c$ for a magnetic field aligned with the $c$ axis. Here $j_\circ$ denotes the in-plane depairing current density (2.30). Note that the critical current density $j_c^c$ is enhanced by a factor of $\varepsilon^{-2/3}$ with respect to the isotropic result. Second, we consider the critical current density $j_c^\perp$ for a current flow along the $y'$ axis which has to cross the superconducting planes. The vortex density gradient is now directed along the $x$ axis. The length scale of the pinning potential is $\xi$, producing a pinning force $U_c^c/\xi$ independent of the angle $\vartheta$. The critical current density then becomes

$$j_c^\perp(\vartheta) \simeq \varepsilon_\vartheta j_c^c \qquad (2.152)$$

and thus is suppressed by a factor $\varepsilon$ for a field aligned with the superconducting planes. Note that in the latter case the current flow is parallel to the $c$ axis.

The above theoretical results for the critical current densities $j_c^\parallel$ and $j_c^\perp(\vartheta)$ have been experimentally observed by Gyorgy *et al.* (1989). Depending on the shape of the sample, the measurement of the diamagnetic moment determines the critical current density $j_c^\parallel$ (thin platelet-shaped sample) or $j_c^\perp$ ($\sim$square cross section perpendicular to the superconducting planes). Using a Bean critical state analysis for the diamagnetic moment, Gyorgy *et al.* found that $j_c^\parallel \approx j_c^c$ and $j_c^\perp(\vartheta) \approx j_c^c\sin\vartheta$, in agreement with our results (2.151) and (2.152).

Again, we can use the in-plane critical current density $j_c^c$ as a convenient phenomenological parameter for the characterization of the disorder potential $\varepsilon_{\rm pin}$. We should then express the collective pinning length $L_c^c$ and the pinning energy $U_c^c$ in terms of the ratio $j_c^c/j_\circ$, and the result is

$$L_c^c \simeq \varepsilon\xi\left[\frac{j_\circ}{j_c^c}\right]^{1/2} ,$$

$$U_c^c \simeq H_c^2\varepsilon\xi^3\left[\frac{j_c^c}{j_\circ}\right]^{1/2} \simeq T_c\left[\frac{1-t}{Gi}\right]^{1/2}\left[\frac{j_c^c}{j_\circ}\right]^{1/2} . \qquad (2.153)$$

Regarding the regime of validity, we should compare the interaction energy between the vortex and the pinning potential with the interaction energy between two neighboring vortices. This can be done, for example, by comparing the elastic tilt energy of one vortex with the shear energy within the volume $a_\circ^2 L_c(\vartheta)$. The result (see below) of such an analysis leads to the condition

$$L_c(\vartheta) < \frac{\varepsilon}{\varepsilon_\vartheta}\frac{a_\circ}{\sqrt{\varepsilon_\vartheta}} . \qquad (2.154)$$

Using Eqs. (2.149) and (2.151) for the collective pinning length and the in-plane critical current density, we find that Eq. (2.154) transforms to

$$B < \beta_{\rm sb}\frac{j_c^c}{j_\circ}H_{c_2}(\vartheta) . \qquad (2.155)$$

## 3. Creep

With the determination of the collective pinning energy $U_c^c$, Eq. (2.150), we have also found the activation energy for (classical) creep in an anisotropic superconductor. The main results here are the suppression of the activation energy by a factor $\varepsilon^{2/3}$, leading to a further enhancement of the classical creep rate, and the angular independence of the activation energy. The latter result shows that relaxation measurements on powdered or on polycrystalline material actually determine the same quantity $U_c^c$ as an experiment done on a single crystal (except for possible changes due to the presence of grain boundaries in polycrystalline material). Let us turn now to quantum motion. Similarly to Eq. (2.140) we have to generalize the Lagrangian generating the classical equation of motion for the vortex to the anisotropic situation,

$$\mathcal{L}[\mathbf{u}] = \int dz'\left[\frac{m_l^\parallel(\vartheta)}{2}(\partial_t u_x)^2 + \frac{m_l^\perp(\vartheta)}{2}(\partial_t u_{y'})^2\right] - \mathcal{F}[\mathbf{u}] . \qquad (2.156)$$

Equation (2.156) describes the limit of vanishing dissipation. The vortex masses $m_l^\parallel$ and $m_l^\perp$ for in-plane and out-of-plane motion can be determined, for example, by calculating the kinetic energy of a moving vortex. Indeed, it turns out to be rather simple to generalize Suhl's (1965) analysis to the anisotropic case: The electronic part of the mass is determined by the time-derivative term $l_t$ in the Lagrange density, which has the form (Suhl, 1965)

$$l_t \propto \int d^2R'|\partial_t\psi_v(\mathbf{R}'-\mathbf{v}'t)|^2 ,$$

where $\psi_v$ denotes the (normalized) order parameter in the presence of an Abrikosov vortex pointing along $z'$ and positioned at the origin of the (rotated) coordinate system. Here $\mathbf{v}'$ is the velocity of the vortex in the rotated frame of reference. Using $\partial_t = v_x\partial_x + v_{y'}\partial_{y'}$ and the approximations $|\partial_x\psi_v| \simeq 1/\xi$ and $|\partial_{y'}\psi_v| \simeq 1/\varepsilon_\vartheta\xi$ within the core region, we obtain the results

$$m_l^\parallel(\vartheta) = \varepsilon_\vartheta m_l^c, \quad m_l^\perp(\vartheta) = \frac{m_l^c}{\varepsilon_\vartheta} \qquad (2.157)$$

for the angular dependencies of the vortex masses. Here $m_l^c$ is the vortex mass for the case of a magnetic field applied parallel to the crystal $c$ axis,

$$m_I^c \simeq \frac{2}{\pi^3} m_e k_F^c \ , \tag{2.158}$$

with $k_F^c$ denoting the Fermi wave vector along the $c$ axis. The result (2.158) can be obtained by repeating the arguments leading to Eq. (2.82) above and noting that the density of states is given by $N(\varepsilon_F) = m_e k_F^c / 2\hbar^2\pi^2$. Again, $m_e$ denotes the planar effective mass of the electrons. The angular dependencies of the in-plane and out-of-plane masses (2.157) can be understood by noting the following two points: (i) The vortex core size $\varepsilon_\vartheta\xi^2$ depends on the angle $\vartheta$, so that the vortex mass is reduced by a factor $\varepsilon_\vartheta$ for motion along $x$. (ii) For motion along $y'$ the effective mass of the electrons is increased by a factor $\varepsilon_\vartheta^{-2}$, leading to an increase in the vortex mass by a factor $\varepsilon_\vartheta^{-1}$ for this case, in agreement with Eq. (2.157).

Let us turn now to the tunneling process. In the absence of dissipation we have to determine the saddle-point solution of the Euclidean action

$$\mathcal{S}_E = \int dt \left\{ \int dz' \left[ \frac{m_I^\|(\vartheta)}{2}(\partial_t u_x)^2 \right. \right.$$
$$\left. \left. + \frac{m_I^\perp(\vartheta)}{2}(\partial_t u_{y'})^2 \right] + \mathcal{F}[\mathbf{u}] \right\} \ . \tag{2.159}$$

Again we have to determine the geometrical shape and the duration of the bounce. The length of the tunneling segment has already been found above, Eq. (2.149), and the result has turned out to be independent of the type of

motion. It remains to determine the tunneling time, which can be obtained by equating the kinetic-energy density involved in the tunneling motion to the elastic-energy density. Performing these dimensional estimates for both in-plane and out-of-plane motion, we observe that all the angular dependencies $\varepsilon_\vartheta$ drop out, and we find a tunneling time $t_c^M$ that is independent of the angle $\vartheta$ and of the type of motion,

$$t_c^M \simeq \left[ \frac{m_I^c}{\varepsilon_0} \right]^{1/2} \frac{L_c^c}{\varepsilon} \ . \tag{2.160}$$

The Euclidean action for the bounce solution has the same characteristics—it is independent of the angle $\vartheta$ and of the direction of motion,

$$\frac{S_E^c}{\hbar} \simeq \frac{t_c^M}{\hbar} U_c^c \simeq \xi^2 \varepsilon k_F^c K_F \ . \tag{2.161}$$

Here we have used standard formulas to relate the London penetration depth $\lambda$ to the density of electrons $n = K_F^2 k_F^c / 3\pi^2$ (with $K_F$ denoting the in-plane Fermi wave vector). For a dirty superconductor an additional factor $(1/\xi)^{1/2}$ appears in the last expression in Eq. (2.161). For a free-electron-like parabolic dispersion, the above formula can be further simplified by using $\varepsilon k_F^c = K_F$.

The above discussion applies to the limit of vanishing dissipation. Coupling our macroscopic variable $\mathbf{u}(z,t)$ to the environment, we have to add a term

$$\int dt\, dt'\, dz' \left\{ \frac{n_I^\|(\vartheta)}{4\pi} \left[ \frac{u_x(z',t) - u_x(z',t')}{t-t'} \right]^2 + \frac{\eta_I^\perp(\vartheta)}{4\pi} \left[ \frac{u_{y'}(z',t) - u_{y'}(z',t')}{t-t'} \right]^2 \right\} \tag{2.162}$$

to the Euclidean action (2.159), where we have assumed that the dissipation is Ohmic. The viscous drag coefficients $\eta_I^\|(\vartheta)$ and $\eta_I^\perp(\vartheta)$ depend on the direction $\vartheta$ of the applied field and on the direction of motion. Again the two effects of vortex core size $\varepsilon_\vartheta\xi^2$ and of the electronic mass $m_e/\varepsilon_\vartheta^2$ compete with each other, resulting in

$$\eta_I^\|(\vartheta) = \varepsilon_\vartheta \eta_I^c, \quad \eta_I^\perp(\vartheta) = \frac{\eta_I^c}{\varepsilon_\vartheta} \ . \tag{2.163}$$

Here $\eta_I^c = \Phi_0^2 / 2\pi c^2 \xi^2 \rho_n$ is the viscous drag coefficient for a vortex aligned with the $c$ axis of the crystal, which agrees with the isotropic expression (2.26) if we simply interpret all the parameters as planar quantities. As we redirect the field along $\vartheta$, the vortex core size $\xi^2$ changes to $\varepsilon_\vartheta\xi^2$, producing a correction factor $\varepsilon_\vartheta^{-1}$. For the case

of out-of-plane motion the electric field generated by the moving vortex points along $x$, so that we have to use the in-plane resistivity $\rho_n$. On the other hand, in-plane motion of the vortex produces an electric field along $y'$, and we have to use the corresponding resistivity $\rho_n/\varepsilon_\vartheta^2$ in our expression for $\eta_I$. Here we assume that the anisotropy in the normal-state resistivity $\rho_n$ agrees with the anisotropy of the superconducting parameters $\xi$ and $\lambda$, an assumption that is fulfilled if the anisotropy is due to the effective mass anisotropy of the carriers. Experiments show that the anisotropy in the normal-state resistivity is usually somewhat larger (Tozer *et al.*, 1987; Martin *et al.*, 1988, 1990).

The correction (2.162) is nonlocal in time, and in order to treat this term we transform the effective action to Fourier space,

$$\mathcal{S}_E^{\text{eff}} = \int \frac{d\omega}{2\pi} \frac{dq}{2\pi} \left\{ \frac{1}{2} \left[ \left[ m_I^\|(\vartheta) + \frac{\eta_I^\|(\vartheta)}{|\omega|} \right] \omega^2 + \varepsilon_I^\|(\vartheta)q^2 \right] |u_x(q,\omega)|^2 \right.$$
$$\left. + \frac{1}{2} \left[ \left[ m_I^\perp(\vartheta) + \frac{\eta_I^\perp(\vartheta)}{|\omega|} \right] \omega^2 + \varepsilon_I^\perp(\vartheta)q^2 \right] |u_{y'}(q,\omega)|^2 + \varepsilon_{\text{pin}}(q,\mathbf{u}) \right\} \ . \tag{2.164}$$

The inclusion of dissipation leads to renormalized dispersive masses $M_{\text{eff}}^{\parallel} = m_i^{\parallel}(1 + \eta_i^{\parallel}/m_i^{\parallel}|\omega|)$ and $M_{\text{eff}}^{\perp} = m_i^{\perp}(1 + \eta_i^{\perp}/m_i^{\perp}|\omega|)$. Again, the tunneling times for in-plane and out-of-plane motion are obtained by equating the corresponding kinetic-energy and elastic-energy densities. For weak enough pinning, the dissipative contribution to the action is always dominant, and we concentrate on this limit here. As in the dissipation-free limit, the tunneling times turn out to be independent of the angle $\vartheta$ and the direction of motion,

$$t_c^{\eta} \simeq \frac{\eta_i^c}{\varepsilon_0}\left[\frac{L_c^c}{\varepsilon}\right]^2 . \tag{2.165}$$

The final expression for the effective action in an anisotropic superconductor is

$$\frac{S_E^{\text{eff},c}}{\hbar} \simeq \frac{t_c^{\eta}}{\hbar}U_c^c \simeq \frac{\hbar}{e^2}\frac{\varepsilon\xi}{\rho_n}\left[\frac{j_0}{j_c^c}\right]^{1/2} \simeq \frac{1}{Qu}\left[\frac{j_0}{j_c^c}\right]^{1/2} , \tag{2.166}$$

independent of the angle $\vartheta$ and the direction of motion. Note that $Qu \propto 1/\varepsilon$ in the anisotropic situation,

$$Qu = \frac{e^2}{\hbar}\frac{\rho_n}{\varepsilon\xi} . \tag{2.167}$$

For the Hall tunneling motion the result has the same structure as Eq. (2.166),

$$S_E^{H,c} = \frac{1}{Qu^H}\left[\frac{j_0}{j_c^c}\right]^{1/2} , \tag{2.168}$$

with $Qu^H = 1/n\varepsilon\xi^3$. As we did for the classical activation energy $U_c^c$, we find a suppression of the effective action due to anisotropy. Here the suppression factor $\varepsilon^{4/3}$ is even larger than for classical creep.

Equations (2.149)–(2.152), (2.161), (2.166), and (2.168) are the main results of our discussion of weak collective pinning theory in anisotropic superconductors. They apply to the single-vortex pinning regime at small enough temperatures and magnetic-field strengths and allow us to make direct comparison with experimental results on the new oxide superconductors for the first time. It is interesting to note that the activation energy $U_c^c$ and the actions $S_E^c$, $S_E^{\text{eff},c}$, and $S_E^{H,c}$ turn out to take such a simple form, independent of the angle $\vartheta$ and of the direction of motion. The deeper reason behind this result is the fact that these quantities are scalar objects and independent of the magnetic-field strength (within the single-vortex pinning regime). In our discussion of the scaling approach to the problem of anisotropy in Sec. III.A this interesting result will become clearer.

## D. Regime of applicability

In this section we have presented a detailed discussion of the theory of weak collective pinning for a single vortex interacting with a quenched random potential. In the presence of other vortices, the elastic tilt energy $\mathcal{E}_{\text{tilt}}$ accumulated along an individual vortex line competes with the energy of interaction with the other vortices. The latter becomes increasingly important with increasing magnetic-field strength $B$, as the distance $a_0$ between adjacent vortices shrinks. Let us estimate the interaction energy $\mathcal{E}_{\text{int}}$ between neighboring vortices. The energy scale determining the interaction (per unit length) between two neighboring vortices is $\varepsilon_0$, and the relevant length scale is the lattice constant $a_0$. Displacing a vortex by a distance $u$ out of its equilibrium position then involves an energy

$$\mathcal{E}_{\text{int}} \simeq \varepsilon_0 \left[\frac{u}{a_0}\right]^2 L , \tag{2.169}$$

which in fact is nothing but the shear energy, with $c_{66} \simeq \varepsilon_0/a_0^2$ an estimate for the shear modulus (see Sec. III.B below). On the other hand, the elastic tilt energy of an individual vortex subject to the same displacement field $u$ is

$$\mathcal{E}_{\text{tilt}} \simeq \varepsilon_0 \frac{u^2}{L} . \tag{2.170}$$

Comparing the two energies (2.169) and (2.170), we see that we have to take the interaction between the vortices into account on large length scales

$$L > a_0 . \tag{2.171}$$

Let us apply this result to the problems of pinning and creep. The relevant length scale for pinning, as well as the length determining creep near criticality, is the collective pinning length $L_c$. Applying the general result (2.171), we see that the interaction between the vortices becomes relevant for large enough fields with a lattice constant

$$a_0 < L_c . \tag{2.172}$$

With the help of Eqs. (2.16) and (2.51a), the condition (2.172) transforms to

$$B > \beta_{\text{sb}}\frac{j_c}{j_0}H_{c_2} = B_{\text{sb}} , \tag{2.173}$$

which is the result (2.79) cited above. The prefactor $\beta_{\text{sb}}$ can be estimated either by keeping track of all the factors in the dimensional estimates or, more reliably, by using the dynamic approach, in which case one obtains $\beta_{\text{sb}} \approx 5$; see Sec. VI.A.3 below. In order to generalize the result (2.172) to anisotropic materials, we have to determine the elastic shear energies for the two cases of in-plane and out-of-plane motion. The in-plane shear modulus $c_{66}^{\parallel}(\vartheta)$ is suppressed by a factor $\varepsilon_{\vartheta}^3$ (Kogan and Campbell, 1989) and the relevant lattice constant is rescaled to a value $\sqrt{\varepsilon_{\vartheta}}a_0$, leading to a shear energy

$$\mathcal{E}_{\text{int}} \simeq c_{66}\varepsilon_{\vartheta}^3\left[\frac{u}{\sqrt{\varepsilon_{\vartheta}}a_0}\right]^2 a_0^2 L \simeq c_{66}\varepsilon_{\vartheta}^2 u^2 L . \tag{2.174}$$

Second, the tilt energy $\mathscr{E}_{\text{tilt}}$ for an in-plane motion becomes

$$\mathscr{E}_{\text{tilt}} \simeq \varepsilon_0 \frac{\varepsilon^2}{\varepsilon_\vartheta} \frac{u^2}{L} \; . \tag{2.175}$$

Combining the two results (2.174) and (2.175), we obtain as the condition for the relevance of the vortex-vortex interaction

$$L > \frac{\varepsilon}{\varepsilon_\vartheta} \frac{a_0}{\sqrt{\varepsilon_\vartheta}} \; . \tag{2.176}$$

For the case of an out-of-plane shear motion, the (isotropic) shear modulus is enhanced by a factor $1/\varepsilon_\vartheta$, and the relevant lattice constant is equal to $a_0/\sqrt{\varepsilon_\vartheta}$. Similarly, the tilt modulus is enhanced by a factor $1/\varepsilon_\vartheta^2$. All these changes combine so as to leave the ratio of the two energies and hence the general condition (2.176) unchanged. Applying the result (2.176) to the pinning problem, we have to substitute the angular-dependent collective pinning length $L_c(\vartheta) \simeq L_c^c/\varepsilon_\vartheta$ [see Eq. (2.149)], for the length $L$, and the generalization of (2.172) to the anisotropic case becomes

$$\frac{\varepsilon}{\sqrt{\varepsilon_\vartheta}} a_0 < L_c^c \; . \tag{2.177}$$

When we include thermal fluctuations as well, Eqs. (2.172) and (2.173) are generalized to

$$\frac{\varepsilon}{\sqrt{\varepsilon_\vartheta}} a_0 < L_c^c(T) \; ,$$

$$B > \beta_{\text{sb}} H_{c_2}(\vartheta) \frac{j_c^c}{j_0} \left[ 1 + \frac{T}{\tilde{T}_{\text{dp}}^s} \right]^2 \exp \left[ -2c \left[ \alpha + \frac{T}{\tilde{T}_{\text{dp}}^s} \right]^3 \right]$$

$$= B_{\text{sb}}(\vartheta, T) \; , \tag{2.178}$$

where the single-vortex depinning energy in an anisotropic material is given by (2.175) with the characteristic lengths $\xi$ and $L_c(\vartheta)$ substituted for $u$ and $L$,

$$\tilde{T}_{\text{dp}}^s \simeq \varepsilon^2 \varepsilon_0 \frac{\xi^2}{L_c^c} \simeq \varepsilon^{2/3} \tilde{T}_{\text{dp}}^{s,\text{iso}} \; . \tag{2.179}$$

The parameter $\alpha$ is of order unity and has been introduced in order to produce the correct low-temperature correction to the $T = 0$ result (finite-temperature corrections appear in the form of a Debye-Waller factor, and its expansion produces a correction that is linear in $T$).

On the other hand, for smaller driving currents, $j \ll j_c$, the relevant length scale for *creep* is $L_{\text{opt}}(j) \simeq L_c(j_c/j)^{1/(2-\zeta)}$ [see Eq. (2.66)], and we obtain the condition

$$j < j_c \left[ \frac{L_c}{a_0} \right]^{2-\zeta} \simeq j_c \left[ \frac{j_0}{j_c} \frac{B}{\beta_{\text{sb}} H_{c_2}} \right]^{7/10} = j_{\text{sb}} \tag{2.180}$$

for the relevance of the interaction between the vortices in the creep process, which is the same result as Eq. (2.78). The general condition including anisotropy and thermal fluctuations depends on the direction of the current flow. For a current density flowing along the planes, we have to use the condition (2.177) in combination with the expression $L_{\text{opt}}(\vartheta, T, j) \simeq L_c(\vartheta, T)[j_c^c(T)/j]^{1/(2-\zeta)}$ for the optimal length of the hopping segment. The result is

$$j < j_c^c(T) \left[ \frac{\sqrt{\varepsilon_\vartheta}}{a_0} \frac{L_c^c(T)}{\varepsilon} \right]^{2-\zeta} \simeq j_c^c(T) \left[ \frac{j_0}{j_c^c} \frac{B}{\beta_{\text{sb}} H_{c_2}(\vartheta)} \left[ \frac{\tilde{T}_{\text{dp}}^s}{T} \right]^2 e^{2c(\alpha + T/\tilde{T}_{\text{dp}}^s)^3} \right]^{7/10} = j_{\text{sb}}^{\parallel}(\vartheta, T) \; . \tag{2.181}$$

For the case of an out-of-plane current flow, the optimal length is given by $L_{\text{opt}}(\vartheta, T, j) \simeq L_c(\vartheta, T)[\varepsilon_\vartheta j_c^c(T)/j]^{1/(2-\zeta)}$, and we obtain the condition

$$j < \varepsilon_\vartheta j_{\text{sb}}^{\parallel}(\vartheta, T) = j_{\text{sb}}^{\perp}(\vartheta, T) \; . \tag{2.182}$$

Thus we see that increasing the magnetic-field strength $B$, increasing the temperature $T$, or decreasing the driving current density $j$ eventually places the system in a regime where interaction between the vortices becomes fully as important as interaction with the disorder potential. This is the regime of pinning and creep of vortex bundles, which we are going to discuss in Sec. IV below.

## III. GENERAL TOOLS

In the last section we introduced most of the ideas and concepts that make up the modern theory of weak collective pinning. In order to keep the discussion simple, we restricted ourselves to the case of single-vortex pinning, which describes well the situation in the new high-temperature superconductors at low enough temperatures, $T < T_{\text{dp}}^s \{\ln[(\beta_{\text{sb}} H_{c_2}/B)(j_c/j_0)]\}^{1/3}$, and low enough fields, $B < (j_c/j_0)\beta_{\text{sb}} H_{c_2}$. At larger temperatures and fields the interaction between vortices becomes important, which implies that we have to generalize the concepts derived in Sec. II to the case of a vortex lattice. Our interest then moves from the physics of an elastic string to the behavior of a three-dimensional elastic medium. In this section we present some general and

preparatory material, which we shall use later in Sec. IV when we discuss the problem of pinning of vortex bundles. The topics treated include the scaling approach to the problem of anisotropy, Sec. III.A; the theory of elasticity of the vortex lattice, Sec. III.B; the determination of elementary pinning forces in the oxide superconductors, Sec. III.C; the dynamic approach to the calculation of the critical current density, Sec. III.D; the behavior of an elastic medium in a periodic pinning potential, Sec. III.E; and the behavior of an elastic medium in a quenched random potential, Sec. III.F.

## A. Anisotropy

With the discovery of high-temperature superconductivity, the phenomenology of type-II superconductors acquired a broader perspective in two respects. First of all, many new subjects for study have appeared in the physics of vortices in general, among which are the proposed new thermodynamic phases such as vortex glass (Fisher, 1989; Fisher, Fisher, and Huse, 1991) or different kinds of vortex liquids (Nelson, 1988; Nelson and Seung, 1989; Feigel'man, Geshkenbein, and Vinokur, 1990), the influence of thermal fluctuations leading to thermal depinning (Feigel'man and Vinokur, 1990) and vortex-lattice melting (Nelson, 1988; Brandt, 1989; Houghton, Pelcovits, and Sudbø, 1989), and the investigation of pinning and creep, both classical (Feigel'man, Geshkenbein, Larkin, and Vinokur, 1989; Kes, Aarts, van den Berg, Van der Beek, and Mydosh, 1989; Fisher, Fisher, and Huse, 1991) and quantum (Blatter, Geshkenbein, and Vinokur, 1991; Ivlev, Ovchinnikov, and Thompson, 1991). Second, since the new high-temperature superconductors are characterized by a large anisotropy, we are forced to develop the phenomenology for the case of anisotropic materials. The latter refers not only to the novel phenomena mentioned above, but also to more established aspects of the phenomenological theory of type-II superconductors, such as the theory of elasticity developed by Brandt (1977a–1977d) for the case of isotropic materials, which has been generalized to anisotropic materials only recently (Houghton, Pelcovits, and Sudbø, 1989; Kogan and Campbell, 1989; Sudbø and Brandt, 1991a, 1991b; Sardella, 1992). In this section we concentrate on the second of these two aspects and discuss a scaling approach to the problem of anisotropy developed by Blatter, Geshkenbein, and Larkin (1992), which allows us to generalize known results for isotropic superconductors to anisotropic materials in a simple way, including the case of an arbitrary direction of the magnetic field with respect to the anisotropic axes.

The traditional way to incorporate anisotropy into the phenomenological description of superconductivity is to introduce an anisotropic effective-mass tensor into the Ginzburg-Landau or London equations. In the conventional approach one then repeats all the calculations that usually have been done for the isotropic case before. We followed this conventional approach throughout all of

Sec. II, where we first derived the results for the isotropic situation and then rederived the corresponding results for anisotropic material along the same lines; see Sec. II.C. Due to the appearance of additional parameters and the breaking of spherical symmetry, the analysis becomes very tedious for the anisotropic problem. As a consequence, new results become available first for the isotropic case and then for the case of cylindrical symmetry, where the magnetic field is aligned with the *c* axis. Few results are known for the general case of arbitrary field direction. The scaling approach introduced below provides simple and direct access to the most general anisotropic result by rescaling the anisotropic problem to a corresponding isotropic one on the initial level of Ginzburg-Landau or London equations. The scaling rules extracted out of this mapping can be used to generalize the isotropic results to the anisotropic situation with essentially no effort. The two approaches are schematically illustrated in Fig. 12.

Let us consider the Gibbs free energy (2.1) for an anisotropic superconductor with $m_x = m_y = m$, $m_z = M > m$. As usual we denote the mass anisotropy ratio by $\varepsilon^2 = m/M < 1$ and we choose a coordinate system where the external field H is chosen to lie in the $yz$ plane, enclosing an angle $\vartheta$ with the $y$ axis; see Fig. 7. In addition, we shall make strong use of the angle-dependent anisotropy parameter $\varepsilon_\vartheta$, which is given in Eq. (2.137) above.

Several years ago, Klemm and Clem (1980) introduced a transformation that mapped Eq. (2.1) onto an isotropic form. Their approach allows us to isotropize all terms in the Gibbs energy, although the transformation is rather complicated and limited to unidirectional fields. In particular, Kogan (1981) pointed out that the magnetic field around a vortex also involves transverse components, which the scaling approach fails to take into account. Later, Kogan and Clem (1981) and Hao and Clem (1991) used a scaling transformation in their calculation of the
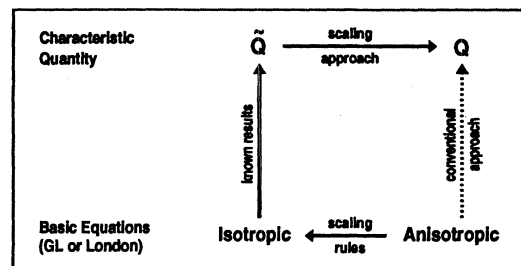


FIG. 12. Schematic comparison of the traditional and the new scaling approaches for obtaining physical results in the anisotropic situation. The traditional approach starts from an anisotropic Ginzburg-Landau or London free-energy functional and determines the desired quantity $Q$ by performing all the steps done previously for the isotropic case, but now under more difficult conditions. In the scaling approach the desired quantity $\tilde{Q}$ is obtained by a simple rescaling of the isotropic result $Q$. The scaling rules are determined only once by a rescaling of the anisotropic functional to an isotropic one.

reversible magnetization and of the torque. In particular, they showed that the scaling approach is valid for large $\kappa = \lambda/\xi$ and large magnetic fields, $H \gg H_{c_1}$. However, it is important to realize that, for strong type-II superconductors with $\kappa \gg 1$, fluctuations in the magnetic field can be neglected altogether in most applications. This idea allows us to use the scaling approach in a much wider context, as will be demonstrated below in detail.

In Eq. (2.1) the anisotropy enters only in the gauge-invariant gradient term. A simple rescaling of the coordinate axes (we denote a quantity $q$ in the rescaled isotropic system by $\tilde{q}$),

$$x = \tilde{x}, \quad y = \tilde{y}, \quad z = \varepsilon \tilde{z}, \tag{3.1}$$

together with a scaling of the vector potential,

$$A_x = \tilde{A}_x, \quad A_y = \tilde{A}_y, \quad A_z = \frac{\tilde{A}_z}{\varepsilon}, \tag{3.2}$$

will render this term isotropic. As a consequence, we obtain the following scaling rule for the magnetic field:

$$B_x = \frac{\tilde{B}_x}{\varepsilon}, \quad B_y = \frac{\tilde{B}_y}{\varepsilon}, \quad B_z = \tilde{B}_z. \tag{3.3}$$

Inserting this result back into the free-energy functional (2.1), we find that the last two terms describing the magnetic-field energy are transformed to

$$\mathcal{G}_m = \frac{1}{8\pi} \int d^3r \left[ \left[ \frac{\tilde{B}_\perp^2}{\varepsilon^2} + \tilde{B}_z^2 \right] - 2 \left[ \frac{\tilde{\mathbf{B}}_\perp \cdot \mathbf{H}_\perp}{\varepsilon} + \tilde{B}_z H_z \right] \right]. \tag{3.4}$$

In short, we have removed the anisotropy from the gradient term but reintroduced it in the magnetic-energy term. In general it is not possible to isotropize both terms in the Gibbs energy simultaneously. However, depending on the physical question addressed, we can neglect fluctuations in the magnetic field. For example, the problems of vortex pinning or of vortex-lattice melting involve the coherence length $\xi$ or the intervortex distance $a_0 = (\Phi_0/B)^{1/2}$ as their natural length scales. The latter are small compared with the scale of fluctuations of the magnetic field $\lambda$, if the superconductor is strongly type II or if the magnetic fields are large enough, with $a_0 < \lambda$, respectively. In such situations the magnetic field is uniform on the natural length scale of the problem, and we can adopt a mean-field decoupling scheme, in which we first minimize the magnetic-field energy $\mathcal{G}_m$ with respect to $\tilde{\mathbf{B}}$ and then insert the resulting uniform field back into the free energy. More rigorously, let us consider the case $\kappa \to \infty$ or, equivalently, charge $e \to 0$. The coupling between the order parameter $\Psi$ and the gauge field $\mathbf{A}$ is given by the gradient term $|[\nabla/i + (2e/\hbar c)\mathbf{A}]\Psi|^2$ and vanishes in the limit $e \to 0$. The external magnetic field then merely fixes the average density of vortices. Hence the approach is exact for the case of an uncharged superfluid.

Minimizing the magnetic-field energy $\mathcal{G}_m$, we obtain

$\tilde{\mathbf{B}} = (\varepsilon H_x, \varepsilon H_y, H_z)$, corresponding to $\mathbf{B} = \mathbf{H}$ in the original system. Thus in the rescaled system the magnetic field is reduced to

$$\tilde{B} = \varepsilon_\vartheta B, \tag{3.5}$$

as compared with the field in the original system. Next, let us transform energy and temperature. Since the volume scales as

$$V = \varepsilon \tilde{V}, \tag{3.6}$$

all energies $\mathcal{E}$ scale as

$$\mathcal{E} = \varepsilon \tilde{\mathcal{E}}, \tag{3.7}$$

and for the temperature determining the strength of thermal fluctuations we obtain the rule

$$T = \varepsilon \tilde{T}. \tag{3.8}$$

This rule can be easily understood from the invariance condition on the Boltzmann factor, $\exp(-\tilde{\mathcal{G}}/\tilde{T}) = \exp(\mathcal{G}/T)$. An interesting subtlety is the distinction between the microscopic temperature entering the Ginzburg-Landau functional via the parameter $\alpha$ and the fluctuation temperature $T$ entering in the Boltzmann factor. The appearance of an additional temperature dependence in the "effective Hamiltonian" ($=$Ginzburg-Landau functional) is a consequence of the partial summation over microscopic degrees of freedom in the partition function when going over from the microscopic formulation in terms of electronic degrees of freedom to the phenomenological description in terms of the order parameter $\Psi$. According to the above derivation it is only the fluctuation temperature $T$, determining the statistical mechanics of the macroscopic wave function $\Psi$, which is rescaled, whereas the microscopic temperature determining the size of $\alpha$ and hence of $\Psi_0$, $\lambda$, and $\xi$ remains unchanged.

Finally, we have to find the scaling rule for the disorder. We consider first the case of disorder in $T_c$, $\delta\alpha(\mathbf{r})$. In the isotropized system the correlator reads $\langle \delta\tilde{\alpha}(\tilde{\mathbf{r}})\delta\tilde{\alpha}(\tilde{\mathbf{r}}') \rangle = \langle \delta\alpha[\mathbf{r}(\tilde{\mathbf{r}})]\delta\alpha[\mathbf{r}(\tilde{\mathbf{r}}')] \rangle = (\gamma_\alpha/\varepsilon)\delta(\tilde{\mathbf{r}} - \tilde{\mathbf{r}}')$; thus the disorder strength $\gamma_\alpha$ scales as

$$\gamma_\alpha = \varepsilon \tilde{\gamma}_\alpha. \tag{3.9}$$

A second type of disorder is generated by the spatial variation of the mean free path (Larkin, 1970; Larkin and Ovchinnikov, 1979), which can be described by a variation of the effective masses $m(\mathbf{r})$ and $M(\mathbf{r})$. For a layered superconductor, the disorder in $m$ and $M$ is due to disorder within the conducting plane and between adjacent planes, respectively, and thus in general the two need not be the same after rescaling. The difference between the disorder in $m$ and $M$ is relevant only in the small-angle regime, $|\vartheta| < \varepsilon$, since for angles larger than $\varepsilon$ the vortices are redirected mainly along the $c$ axis after rescaling, and thus disorder in $M$ can be neglected. Except for this small-angle regime, the disorder in the mean free path can be treated as scalar and therefore transforms in the

same manner as the disorder in $T_c$. We then obtain the more general rule

$$\gamma = \varepsilon \widetilde{\gamma} \ , \tag{3.10}$$

which is valid as long as the discreteness of the layered structure is not important. Note that, when we define the scale transformation according to Eq. (3.1), the parameters $\lambda$ and $\xi$ are not rescaled, as the planar coordinates are not affected by the transformation,

$$\lambda = \widetilde{\lambda} \quad \text{and} \quad \xi = \widetilde{\xi} \ . \tag{3.11}$$

We are now in a position to set up the general scaling rule for transferring results from isotropic superconductors to anisotropic materials. Consider a uniaxially anisotropic superconductor (axis $\|z$) characterized by the planar coherence length $\xi$ and London penetration depth $\lambda$, the anisotropy $\varepsilon$, and the scalar disorder strength $\gamma$, in an applied magnetic field $\mathbf{H}$ enclosing an angle $\vartheta$ with the $xy$ plane, at a temperature $T$. Let $Q$ be the desired quantity for which the isotropic result $\widetilde{Q}$ is known. Then we obtain $Q$ for the anisotropic superconductor by the scaling rule:

$$Q(\vartheta,H,T,\xi,\lambda,\varepsilon,\gamma) = s_Q \widetilde{Q} \left[ \varepsilon_\vartheta H, \frac{T}{\varepsilon}, \xi, \lambda, \frac{\gamma}{\varepsilon} \right] \ . \tag{3.12}$$

Typical scaling factors are $s_V = s_E = s_S = s_T = \varepsilon$ for volumes, energies, actions, and temperatures, and $s_B = s_H = 1/\varepsilon_\vartheta$ for magnetic fields. The scaling rule (3.12) is the main result of this section.

We wish to point out that the scaling rule (3.12) is not unique. It is defined out of a mathematical construction, which renders the gauge-invariant gradient term in the Ginzburg-Landau functional isotropic. It is clear that there exist alternative transformation rules achieving the same goal. In particular, here we have chosen a transformation that leaves the main planar parameters $\xi$ and $\lambda$ of the superconductor invariant, with the consequence that volume, energy, temperature, and disorder are rescaled. Another transformation (that used by Klemm and Clem, 1980) leaves the volume (and hence also energy, temperature, and disorder) invariant, while rescaling the planar parameters $\xi$ and $\lambda$. The important point is that all these *consistent* sets of rescaling rules are *equivalent* to the original rule (3.12) [see also the discussion between Hao and Clem (1993) and Blatter, Geshkenbein, and Larkin (1993)].

In the remainder of this section we present a few illustrative examples of how to use the scaling formalism to transfer results from the isotropic to the anisotropic situation. In doing so, we concentrate mainly on the results obtained for the single-vortex pinning regime above and demonstrate how the expressions derived in Sec. II.C for the anisotropic material can be obtained in an elegant fashion by use of the scaling approach. Let us start with the elasticity coefficients for a single vortex. The elastic energy of a single vortex is given by Eq. (2.140). Transforming the in-plane tilt energy to the isotropic system,

we obtain the relation

$$\varepsilon_\|(\vartheta) \frac{(\delta u_x)^2}{\delta z'} = \varepsilon \widetilde{\varepsilon}_l \frac{(\delta \widetilde{u}_x)^2}{\delta \widetilde{z}'} \ . \tag{3.13}$$

Since $\lambda$ is invariant, $\widetilde{\varepsilon}_l \simeq (\Phi_0/4\pi\lambda)^2 = \varepsilon_0$, where we again concentrate on the short-wavelength limit of the elastic modulus. Furthermore, the amplitude $\delta u_x$ is not affected by the rescaling and therefore $\delta \widetilde{u}_x / \delta u_x = 1$. On the other hand, the length $\delta z'$ *is* affected by the transformation (3.1). Let us consider a segment of length $l_l$ directed along the $z'$ axis and let us transform this "longitudinal length" to the rescaled system. In the rescaled system we have $\widetilde{l}_l^2 = \widetilde{l}_x^2 + \widetilde{l}_y^2 + \widetilde{l}_z^2$. Using Eq. (3.1), we obtain $\widetilde{l}_l^2 = l_l^2(\cos^2\vartheta + \sin^2\vartheta/\varepsilon^2)$. Using the definition (2.137) for the angle-dependent anisotropy parameter $\varepsilon_\vartheta$, we find that all longitudinal lengths $l_l$ scale according to the rule

$$l_l = \frac{\varepsilon}{\varepsilon_\vartheta} \widetilde{l}_l, \quad l_l \| \mathbf{B} \ , \tag{3.14}$$

and therefore $\delta z'/\delta \widetilde{z}' = \varepsilon/\varepsilon_\vartheta$. The final expression for the in-plane elasticity is then $\varepsilon_\|(\vartheta) = \varepsilon_0 \varepsilon^2/\varepsilon_\vartheta$, in agreement with the result (2.146) of the conventional approach. When transforming the out-of-plane tilt energy, we should take care about the change of angles due to the scale transformation. The transformed vectors $\delta \widetilde{u} = \delta u_{y'}(0, -\sin\vartheta, \cos\vartheta/\varepsilon)$ and $\delta \widetilde{z} = \delta z'(0, \cos\vartheta, \sin\vartheta/\varepsilon)$ are no longer orthogonal. Orthogonalizing, we obtain

$$\varepsilon_l^\perp(\vartheta) \frac{(\delta u_{y'})^2}{\delta z'} = \varepsilon \widetilde{\varepsilon}_l \frac{|\delta \widetilde{u} \wedge \delta \widetilde{z}|^2}{\delta \widetilde{z}'^{\,3}} \ , \tag{3.15}$$

and the final expression for the out-of-plane line tension is then $\varepsilon_l^\perp(\vartheta) = \varepsilon_0 \varepsilon^2/\varepsilon_\vartheta^3$, in agreement with Eq. (2.144). Here we have used $\delta \widetilde{z} = \delta \widetilde{z}' = (\varepsilon_\vartheta/\varepsilon) \delta z'$. As an additional result, we obtain the scaling rule for "transverse lengths,"

$$l_t = \varepsilon_\vartheta \widetilde{l}_t, \quad l_t \perp \mathbf{B}, \quad \widetilde{l}_t \perp \widetilde{\mathbf{B}}, \quad l_t, \widetilde{l}_t \perp \mathbf{e}_x \ . \tag{3.16}$$

Next we discuss the problem of single-vortex pinning and creep in anisotropic superconductors. For isotropic superconductors we have found above that a vortex segment of length $L_c \simeq (\varepsilon_0^2 \xi^2/\gamma)^{1/3}$ is pinned collectively. We have determined the pinning potential to be $U_c \simeq (\gamma \xi^2 L_c)^{1/2}$, the effective action governing quantum motion to be $S_E^{\text{eff}} = (\hbar/e)^2(\xi/\rho_n)(j_0/j_c)^{1/2}$ (limit of strong damping), and the critical current density against depinning to be $j_c \simeq j_0 (\xi/L_c)^2$. Furthermore, the single-vortex pinning regime is limited to fields $B < B_{\text{sb}}$, with $B_{\text{sb}} \simeq (j_c/j_0) \beta_{\text{sb}} H_{c_2}$. Using our scaling rule (3.12) we obtain the following results for the anisotropic superconductor: The collective pinning length $L_c$ is a longitudinal length, therefore $L_c(\vartheta) = (\varepsilon/\varepsilon_\vartheta) \widetilde{L}_c$. In order to obtain $\widetilde{L}_c = (\widetilde{\varepsilon}_0^2 \widetilde{\xi}^2/\widetilde{\gamma})^{1/3}$ we have to express all rescaled material parameters $(\widetilde{\lambda}, \widetilde{\xi}, \widetilde{\gamma})$ by the original parameters $(\widetilde{\lambda} = \lambda, \widetilde{\xi} = \xi, \widetilde{\gamma} = \gamma/\varepsilon)$, hence $\widetilde{L}_c = (\varepsilon_0^2 \xi^2 \varepsilon/\gamma)^{1/3}$. We then obtain the final result $L_c(\vartheta) = L_c^c/\varepsilon_\vartheta$, where $L_c^c = (\varepsilon_0^2 \xi^2 \varepsilon^4/\gamma)^{1/3} = \varepsilon^{4/3} L_c^{\text{iso}}$ is the collective pinning

length for the case where the magnetic field is aligned with the $c$ axis, in agreement with Eq. (2.149) above. $L_c^{\text{iso}}$ denotes the collective pinning length in an equivalent isotropic material characterized by identical material parameters $\lambda$, $\xi$, and $\gamma$, but with $\varepsilon = 1$. The scaling factor for the pinning potential $U_c$ is $s_E = \varepsilon$. Rewriting $\tilde{U}_c$ in terms of the original material parameters, we obtain the result $U_c^c = \varepsilon^{2/3}(\gamma \varepsilon_0 \xi^4)^{1/3} = \varepsilon^{2/3} U_c^{\text{iso}}$, independent of the angle $\vartheta$ and in agreement with the previous result (2.150). Similarly, the action becomes $S_E^{\text{eff},c} = \varepsilon^{4/3} S_E^{\text{eff,iso}}$, again independent of $\vartheta$. In the anisotropic material we have to distinguish between two critical current densities, the in-plane critical current density $j_c^{\|} \| x$ involving a Lorentz force along $y'$, and $j_c^{\perp} \| y'$, the out-of-plane critical current density, pushing the vortices along the direction of the $x$ axis. The in-plane critical current density is obtained from rescaling the force balance equation between the pinning and the Lorentz force, $\tilde{j}_c \Phi_0 \tilde{L}_c \xi = \tilde{U}_c$. The in-plane critical current density then scales like a planar length and thus $j_c^{\|} = \tilde{j}_c = \varepsilon^{-2/3} j_c^{\text{iso}} = j_c^c$. On the other hand, for the out-of-plane critical current density we have to orthogonalize the Lorentz force after rescaling such that $j_c^{\perp}$ scales like a transverse length, therefore $j_c^{\perp} = \varepsilon_\vartheta \tilde{j}_c$, and we obtain the result $j_c^{\perp}(\vartheta) = \varepsilon_\vartheta j_c^c$. Finally, the field $B_{\text{sb}}$ limiting the regime of single-vortex collective pinning becomes $B_{\text{sb}}(\vartheta) \simeq (j_c^c/j_0)\beta_{\text{sb}} H_{c_2}(\vartheta)$, where we have used the scaling rule for magnetic fields (3.5) and the above result for the transformation of the in-plane critical current density $j_c^{\|}$.

Next, let us discuss collective creep at low driving forces, $j \ll j_c^c$, with $j$ flowing in the plane. Within the single-vortex pinning regime, the relevant length $L_{\text{opt}}(j)$ (size of the critical nucleus) increases with decreasing current density $j$ according to $L_{\text{opt}}(j) \simeq L_c(\vartheta)(j_c^c/j)^{5/7}$, and similar results apply for the thermal activation barrier (classical creep), $U(j) \simeq U_c^c(j_c^c/j)^{1/7}$, and for the tunneling action (quantum creep), for the overdamped case, $S(j) \simeq S_E^{\text{eff},c}(j_c^c/j)^{8/7}$. The boundary of the single-vortex pinning regime is reached when the current density $j$ drops below $j_{\text{sb}}(\vartheta, B) \simeq j_c^c(\sqrt{\varepsilon_\vartheta} L_c^c/\varepsilon a_0)^{7/5}$, a result obtained from rescaling the condition $L_{\text{opt}}(j) \simeq a_0$. If the vortex lattice is subject to an out-of-plane current density $j$ ($j \| y'$), the creep motion is directed along the superconducting planes. For this case we have to replace the in-plane current-density ratio $j_c^c/j$ in the above expressions, as well as the boundary $j_{\text{sb}}$, by their out-of-plane counterparts, $\varepsilon_\vartheta j_c^c/j$ and $\varepsilon_\vartheta j_{\text{sb}}$, respectively. All these results agree with those obtained following the conventional approach, but involve essentially no calculations at all.

In anisotropic materials an additional degree of freedom is the angle $\vartheta$ between the magnetic-field direction and the superconducting planes. Here the scaling rule (3.12) predicts the angular dependence of physical quantities to be expected due to the anisotropy of the material. For example, the scaling behavior of the in-plane resistivity as measured by Iye *et al.* (1989a) and interpreted by Kes *et al.* (1990) finds a natural explanation within

the scaling approach: The scaling factor for the in-plane resistivity is $s_\rho = 1$, and using Eq. (3.12) we obtain $\rho(\vartheta, H) = \rho(\varepsilon_\vartheta H) \simeq \rho(\sin \vartheta H)$, without making any special assumptions about a possible breakdown of the concept of a flux-line lattice in layered superconductors (Kes *et al.*, 1990). In addition, for $\vartheta > \varepsilon$, after rescaling, the magnetic field is directed mainly along the $c$ axis, and thus the Lorentz force is essentially independent of the direction of the current in the plane. Going back to the original system, one then expects that the in-plane resistivity *should be* independent of the angle between the magnetic field and the current. The latter observation offers a very natural explanation for the angular independence of the dissipation as reported by Iye, Nakamura, and Tamegai (1989a) for the case in which both the current and the magnetic field are aligned with the superconducting planes, if a slight misalignment of the field is assumed. Similarly, the anisotropy of the critical current density as measured by Roas, Schultz, and Saemann-Ischenko (1990) in $YBa_2Cu_3O_{7-y}$ and by Schmitt *et al.* (1991) in $Bi_2Sr_2CaCu_2O_{8+y}$ thin films exhibits all the features predicted by the scaling rule (3.12). In large magnetic fields, $H > B_{\text{sb}}$, the critical current density $j_c^c$ starts to decrease with increasing field strength $H$; see Sec. IV.B.1 below. Changing the direction of the magnetic field then leads to a dependence of the in-plane critical current density $j_c^{\|}$ on the angle $\vartheta$. In particular, the scaling rule (3.12) predicts that this angular dependence of the planar current density $j_c^{\|}(\vartheta)$ is only through the combination, $\varepsilon_\vartheta H$, $j_c^{\|}(\vartheta) = j_c^c(\varepsilon_\vartheta H)$, resulting in sharp maxima of $j_c^{\|}(\vartheta)$ when the field is aligned with the superconducting planes and a sharpening of these maxima with increasing field amplitude $H$ (see also Pokrovsky, Lyuksyutov, and Nattermann, 1992). A detailed discussion of the angular dependencies of thermodynamic and electromagnetic properties in anisotropic superconductors, as predicted by Eq. (3.12) and observed in various experiments, can be found in Hao and Clem (1992).

Regarding the regime of applicability, we wish to point out that, in spite of starting from a GL-type description, the scaling approach is not limited to the regime near $T_c$. In fact, the above scaling rules can be obtained as well by starting from the London equations, which are valid throughout the entire temperature regime. The scaling rules for the disorder will not be changed as long as the anisotropy in the penetration depths and in the vortex core size remain the same. Moreover, the scaling approach can be used for the case of layered superconductors as long as the discreteness of the structure is not important. The crossover between quasi-2D and 3D anisotropic behavior depends on the physical quantity of interest, although the regime in which the anisotropic description is valid is usually large.

Finally, the scaling rule (3.12) clarifies the following features of anisotropic superconductivity: First, the effect of anisotropy is to reduce the field component in the superconducting planes and to enhance the effective

strength of the pinning, both favorable effects in view of technological applications of the new materials. On the other hand, anisotropy increases the temperature of thermal fluctuations, favoring phenomena such as thermal depinning and melting of the vortex lattice, effects which are scientifically very interesting but rather undesirable in view of applications.

## B. Elasticity

### 1. Isotropic material

The theory of elasticity of a vortex lattice in an isotropic superconductor was worked out several years ago by Brandt (1977a, 1977b; see also 1977c, 1977d) using the GL description at high inductions, $B \gtrsim 0.6H_{c_2}$ (Brandt, 1977a), and the London theory for small fields, $B \lesssim 0.2H_{c_2}$ (Brandt, 1977b). These results were later confirmed by Larkin and Ovchinnikov (1979), who based their calculation on the BCS-Gor'kov theory and thus extended the validity of the results to the entire temperature range $0 < T < T_c$.

When a type-II superconductor is placed in a magnetic field $H > H_{c_1}$, the field starts to penetrate the superconductor in the form of vortices (or flux lines). In a homogeneous material, a triangular lattice with a lattice constant $a_\Delta$ given by Eq. (2.15) is formed. We assume the vortices to be aligned with the $z$ axis such that we can describe their equilibrium positions $\mathbf{R}_\nu = [n\sqrt{3}a_\Delta/2,$ $(2m+n)a_\Delta/2]$, $\nu = (m,n)$, by a planar coordinate. In general, the vortex lattice is not in its equilibrium configuration but in some distorted state, which we can characterize by the two-component displacement field $\mathbf{u}_\nu(z)$ or its Fourier transform $[\mathbf{r}_\nu \equiv (\mathbf{R}_\nu, z)]$,

$$\mathbf{u}(\mathbf{k}) = a_0^2 \int dz \sum_\nu e^{-i\mathbf{k}\mathbf{r}}\mathbf{u}_\nu(z) . \tag{3.17}$$

The transformation back to real space is then

$$\mathbf{u}_\nu(z) = \int_{BZ} \frac{d^3k}{(2\pi)^3} e^{i\mathbf{k}\mathbf{r}}\mathbf{u}(\mathbf{k}) , \tag{3.18}$$

where the integration runs over the two-dimensional Brillouin zone (BZ) of the vortex lattice, $K \lesssim K_{BZ} = \sqrt{4\pi}/a_0$ (= radius of the circularized BZ), and the integration along $k_z$ is cut off at the inverse core radius, $|k_z| \lesssim 2\pi/\xi$. Within linear elasticity theory the energy of such a distorted state is given by

$$\mathscr{F}[\mathbf{u}] = \frac{1}{2}\int_{BZ} \frac{d^3k}{(2\pi)^3}[u_\alpha(\mathbf{k})\Phi_{\alpha\beta}(\mathbf{k})u_\beta(-\mathbf{k})$$
$$-f_\beta(\mathbf{k})u_\beta(-\mathbf{k})] , \tag{3.19}$$

where $\Phi(\mathbf{k})$ denotes the elastic matrix of the vortex lattice and $\mathbf{f}(\mathbf{k})$ is the Fourier transform of the force field $\mathbf{f}_\nu(z)$ that generates the distortion $\mathbf{u}_\nu(z)$. We adopt the convention that indices appearing twice are summed

over. Variation of Eq. (3.19) with respect to $u_\beta(-\mathbf{k})$ provides us with the equation of motion

$$[-i\omega\eta\delta_{\alpha\beta} + \Phi_{\alpha\beta}(\mathbf{k})]u_\alpha(\mathbf{k}) = f_\beta(\mathbf{k}) , \tag{3.20}$$

from which we immediately obtain the Green's function for the vortex lattice by simple matrix inversion,

$$G_{\alpha\beta}(\mathbf{k},\omega) = [-i\omega\eta\mathbb{1} + \Phi(\mathbf{k})]_{\alpha\beta}^{-1} . \tag{3.21}$$

In Eq. (3.20) we have added a term $-i\omega\eta\mathbf{u}$ in order to account for the damped motion of the vortices. The viscous drag coefficient for the vortex lattice is $\eta = \eta_l/a_0^2$, with $\eta_l$ given by the Bardeen-Stephen formula (2.26).

It remains to determine the elastic matrix $\Phi_{\alpha\beta}(\mathbf{k})$, which is characterized by the following symmetries:

$$\Phi_{\alpha\beta}(\mathbf{k}) = \Phi_{\beta\alpha}(\mathbf{k}) = \Phi_{\alpha\beta}^*(\mathbf{k})$$
$$= \Phi_{\alpha\beta}(-\mathbf{k}) = \Phi_{\alpha\beta}(\mathbf{k}+\mathbf{K}_\nu) , \tag{3.22}$$

where $\mathbf{K}_\nu = 2\pi[(2n-m)/(\sqrt{3}a_\Delta), m/a_\Delta]$, $\nu = (m,n)$ is a reciprocal-lattice vector. For magnetic fields near the upper critical field, $B \gtrsim 0.6H_{c_2}$, the Abrikosov solution for the order parameter $\Psi_A$ can be used as a starting point, where $\Psi_A$ is a solution of the *linearized* GL equations. However, a simple shift of the zeros in $\Psi_A$ to the new positions $\mathbf{R}_\nu + \mathbf{u}_\nu(z)$ results in unphysical divergencies for long-wavelength distortions $\mathbf{u}(\mathbf{k})$ with $\mathbf{k} \to 0$. These divergencies can be removed by appropriately relaxing the new order parameter using a variational Ansatz and taking the quartic term in the GL functional into account (Brandt, 1977c). Evaluation of the free energy to second order in the displacement field $\mathbf{u}(\mathbf{k})$ then provides us with an expression for the elastic matrix (Brandt and Essmann, 1987; Brandt, 1991a).

A somewhat simpler approach can be taken at small fields, $B \lesssim 0.2H_{c_2}$, where the vortex cores do not overlap and therefore the London theory is applicable. For the new high-temperature superconductors this regime is large, covering most of the experimentally accessible field range, as $H_{c_2}$ is of the order of 50–150 T. The elastic energy stored in a distorted vortex lattice can then be found by an integration of the interaction potential $V^{int}$ over all pairs of vortex segments $d\mathbf{s}_\mu$,

$$\mathscr{F}[\mathbf{u}] = \frac{\varepsilon_0}{2}\sum_{\mu,\nu}\int d\mathbf{s}_\mu \cdot d\mathbf{s}_\nu V^{int}(\mathbf{s}_\mu - \mathbf{s}_\nu) , \tag{3.23}$$

where the $\mathbf{s}_\mu = \mathbf{r}_\mu + \mathbf{u}_\mu(z)$ denotes the positions of the vortices in the distorted state. Note that the terms $\mu = \nu$ are also included in the sum in Eq. (3.23) and produce the self-energies of the individual vortex lines. Within simple London theory, the interaction potential $V^{int}$ between two vortex segments takes the form

$$V^{int}(\mathbf{r}) = \frac{1}{r}e^{-r/\lambda} , \tag{3.24}$$

with an appropriate short-distance cutoff at small length scales $r < \xi$, provided, for example, by the model potential

$$V^{int}(\mathbf{r}) = 4\pi\lambda^2 \int \frac{d^3k}{(2\pi)^3} e^{i\mathbf{kr}} V^{int}(\mathbf{k}) ,$$

with

$$V^{int}(\mathbf{k}) = \frac{e^{-\xi^2 k^2}}{1+\lambda^2 k^2} . \tag{3.25}$$

Expansion of Eq. (3.23) in the small displacement field $\mathbf{u}_\mu(z)$ provides an expression for the elastic matrix,

$$\Phi_{\alpha\beta}(\mathbf{k}) = \frac{B^2}{4\pi} \sum_\nu [f_{\alpha\beta}(\mathbf{k}+\mathbf{K}_\nu) - f_{\alpha\beta}(\mathbf{K}_\nu)] , \tag{3.26}$$

with

$$f_{\alpha\beta}(\mathbf{k}) = (k_\alpha k_\beta + \delta_{\alpha\beta}k_z^2)V^{int}(\mathbf{k}) . \tag{3.27}$$

For large fields, the GL theory produces an expression for the elastic matrix that is similar to the London result (3.26) but that involves a double sum over reciprocal lat-

tice vectors $\mathbf{K}_\nu$ and $\mathbf{Q}_\nu$. Moreover, the reduction of the order parameter at large fields renormalizes the length scales $\lambda$ and $\xi$ to $\lambda' = \lambda/(1-b)^{1/2}$ and $\xi' = \xi/(1-b)^{1/2}$, with the reduced field $b \equiv B/H_{c_2}(T)$ (Brandt, 1986b, 1991a).

The result (3.26) provides us with expressions for all the elastic moduli for the vortex lattice. Various approximations can be adopted in dealing with this result, and we shall discuss them very briefly in the following. Within the *nonlocal continuum* limit, the elastic matrix is written in the form

$$\Phi_{\alpha\beta}(\mathbf{k}) = [c_{11}(\mathbf{k}) - c_{66}]K_\alpha K_\beta + \delta_{\alpha\beta}[c_{66}K^2 + c_{44}(\mathbf{k})k_z^2] , \tag{3.28}$$

with $c_{11}(\mathbf{k})$ and $c_{44}(\mathbf{k})$ denoting the *dispersive* compression and tilt moduli and $c_{66}$ the nondispersive shear modulus. Using Eq. (3.28), the elastic free energy (3.19) takes the simple form

$$\mathcal{F}[\mathbf{u}] = \frac{1}{2} \int \frac{d^3k}{(2\pi)^3} \{c_{11}(\mathbf{k})[\mathbf{K}\cdot\mathbf{u}(\mathbf{k})]^2 + c_{66}[\mathbf{K}_\perp\cdot\mathbf{u}(\mathbf{k})]^2 + c_{44}(\mathbf{k})[k_z\mathbf{u}(\mathbf{k})]^2 - \mathbf{f}(-\mathbf{k})\cdot\mathbf{u}(\mathbf{k})\} , \tag{3.29}$$

with $\mathbf{K}_\perp = (k_y, -k_x)$, and the elastic Green's function (3.21) becomes

$$G_{\alpha\beta}(\mathbf{k},\omega) = \frac{\mathcal{P}_{\alpha\beta}^L(\mathbf{K})}{-i\eta\omega + c_{11}(\mathbf{k})K^2 + c_{44}(\mathbf{k})k_z^2} + \frac{\mathcal{P}_{\alpha\beta}^T(\mathbf{K})}{-i\eta\omega + c_{66}K^2 + c_{44}(\mathbf{k})k_z^2} , \tag{3.30}$$

with the projection operators $\mathcal{P}_{\alpha\beta}^L(\mathbf{K}) = K_\alpha K_\beta/K^2$ and $\mathcal{P}_{\alpha\beta}^T(\mathbf{K}) = \delta_{\alpha\beta} - K_\alpha K_\beta/K^2$. Within the *continuum isotropic* approximation, we restrict the sum over reciprocal lattice vectors in Eq. (3.26) to the $\nu=0$ term and obtain for the compression and tilt moduli

$$c_{11}(\mathbf{k}) \simeq c_{44}(\mathbf{k}) \simeq \frac{B^2}{4\pi} \frac{1}{1+\lambda^2 k^2} . \tag{3.31}$$

Within this approximation ($\nu=0$) the shear modulus is zero, so this description applies to a vortex-liquid phase. The terms $\nu\neq 0$ then add up to produce a finite shear modulus

$$c_{66} \simeq \frac{\Phi_0 B}{(8\pi\lambda)^2} , \tag{3.32}$$

which is essentially nondispersive. In addition, the terms $\nu\neq 0$ produce a (nonisotropic) correction to the tilt and compression moduli as $\mathbf{K}$ approaches the BZ boundary, which reflects the hexagonal symmetry of the vortex lattice. This "geometric" dispersion depends only on the product $a_0 k$ and thus is much weaker than the "essential" dispersion which originates from the $\nu=0$ term and involves the parameter $\lambda k$. More important, when we take terms $\nu\neq 0$ into account the tilt modulus $c_{44}(\mathbf{k})$ crosses over to the single-vortex result in a large part of the Brillouin zone, $K > K_s = K_{BZ}/[\ln(1/\xi K_s)]^{1/2}$ (Brandt, 1977b; Sudbø and Brandt, 1991b),

$$c_{44}(\mathbf{k}) \simeq \frac{\varepsilon_0}{a_0^2} \ln\frac{1}{\xi k_z} , \tag{3.33}$$

so that we can write

$$c_{44}(\mathbf{k}) = c_{44}^0(\mathbf{k}) + c_{44}^c(\mathbf{k}) , \tag{3.34}$$

with $c_{44}^0(\mathbf{k})$ given by Eq. (3.31) and

$$c_{44}^c(\mathbf{k}) \simeq \begin{cases} \dfrac{B(H-B)}{4\pi} & \text{for } k\to 0 , \\[3mm] \dfrac{\varepsilon_0}{2a_0^2}\ln\dfrac{\kappa^2}{1+\lambda^2(K_{BZ}^2+k_z^2)} & \text{for } K > K_s . \end{cases} \tag{3.35}$$

Here the correction $B(H-B)/4\pi$ has been introduced in order to produce the correct expression $c_{44}(0)$ for the uniform tilt modulus, which can be obtained from thermodynamic considerations (Campbell and Evetts, 1972).

At very small field values, $B < H_{c_1}/\ln\kappa$, the compressional and shear moduli become exponentially small, $c_{11} = 3c_{66} \propto \exp(-a_0/\lambda)$ (Labusch, 1967, 1969; Larkin, 1970),

$$c_{66} = \left[\frac{\pi}{6}\right]^{1/2} \frac{\varepsilon_0}{\lambda^2} \left[\frac{\lambda}{a_0}\right]^{1/2} e^{-a_0/\lambda} , \tag{3.36}$$

whereas the tilt modulus goes over into the single-vortex expression (3.33). Finally, at large inductions the renormalization of the length scales due to the suppression of the order parameter should be taken into account and $\lambda'$ should be substituted for $\lambda$ in Eqs. (3.31) and (3.32). However, close to the upper critical field $H_{c_2}$ the shear

modulus vanishes as $(1-b)^2$, so that Eq. (3.32) with $\lambda'$ substituted for $\lambda$ should not be used beyond $b \simeq 0.5$ (Brandt, 1977b).

The dispersive behavior of the compression and tilt moduli $c_{11}(\mathbf{k})$ and $c_{44}(\mathbf{k})$ leads to a considerable softening of the vortex lattice. Near the BZ boundary, $K_{BZ} \simeq \sqrt{4\pi}/a_0$, a suppression factor $(\lambda K_{BZ})^2 \simeq B\ln\kappa/H_{c_1}$ is obtained with respect to the value at $k=0$ describing a uniform distortion. In the new high-temperature superconductors the GL parameter $\kappa$ is of the order of 100, the lower critical field $H_{c_1}$ is small, typically a few hundred Gauss, and thus the softening of the vortex lattice is an important effect in a large field range. On the other hand, the shear modulus is essentially free of dispersion and always small, in fact, $c_{66} \simeq (1/4)c_{11}(K_{BZ})$. The physical origin of the dispersion in $c_{11}$ and in $c_{44}$ is found in the long-range interaction potential $V^{int}$, Eq. (3.24): For fields $B > H_{c_1}/\ln\kappa$, the nearest-neighbor distance $a_0$ drops below the potential range $\lambda$ and the vortex-vortex interaction extends beyond the nearest neighbors. The *local* limit described by the functional

$$\mathcal{F}[\mathbf{u}] = \frac{1}{2} \int d^3r [c_{11}(0)(\nabla \cdot \mathbf{u})^2 + c_{66}(\nabla_\perp \cdot \mathbf{u})^2$$
$$+ c_{44}(0)(\partial_z \mathbf{u})^2] \, , \qquad (3.37)$$

with $\nabla_\perp = (\partial_y, -\partial_x)$ and $c_{11}(0) \simeq c_{44}(0) \simeq B^2/4\pi$, should therefore be used with caution. Since $c_{11}(0) \gg c_{66}$, Eq. (3.37) essentially describes an incompressible solid.

## 2. Anisotropic material

The generalization of the theory of elasticity to anisotropic superconductors is a rather tedious undertaking. As outlined in Sec. III.A above, we can follow the traditional approach and recalculate all the moduli starting from the Ginzburg-Landau or London free-energy functional or we can use the scaling approach and start directly from the isotropic results. Whereas the former method provides us, at least in principle, with the most general expressions for the elastic moduli, their derivation along this traditional path is very cumbersome, and not all the moduli have as yet been derived. On the other hand, the scaling approach allows one to find all the moduli in a simple and straightforward way, but the results obtained are limited to the regime $\lambda\tilde{k} > 1$ (here $\tilde{k}$ denotes the wave-vector modulus in the isotropized system), since it neglects fluctuations in the magnetic field. The limited applicability of the method to the dispersive regime is not a severe restriction, however, since this regime makes up a large part of the Brillouin zone, and furthermore the results for the uniform limit $k \to 0$ are known from thermodynamic considerations.

As the (internal) magnetic field is tilted away from the $c$ axis, the (equilateral) triangular lattice defining the equilibrium configuration is deformed and the new basis vectors become

$$\mathbf{R}'_v = [n\sqrt{3}a_\Delta/(2\sqrt{\varepsilon_\vartheta}), (2m+n)\sqrt{\varepsilon_\vartheta}a_\Delta/2]$$

with the corresponding lattice vectors $\mathbf{K}'_v = 2\pi[(2n-m)\sqrt{\varepsilon_\vartheta}/(\sqrt{3}a_\Delta), m/(\sqrt{\varepsilon_\vartheta}a_\Delta)]$ (Campbell, Doria, and Kogan, 1988). Here we have used the same coordinate system as was introduced in Sec. II above (see Fig. 7), with $\vartheta$ denoting the angle enclosed between the internal magnetic field and the superconducting planes. The angle-dependent anisotropy parameter $\varepsilon_\vartheta$ is given by Eq. (2.137). Rescaling of the transverse length $\tilde{y}' = y'/\varepsilon_\vartheta$ reproduces the equilateral triangular Abrikosov lattice at the rescaled field $\tilde{B} = B\varepsilon_\vartheta$, i.e., $\tilde{a}_\Delta = a_\Delta/\sqrt{\varepsilon_\vartheta}$. Note that the equilibrium lattice configuration is characterized by a short lattice vector $\mathbf{R}_{(1,0)}$ pointing along the $y'$ axis and that the planar rotational degeneracy present for $\mathbf{H}\|c$ is removed as the field is tilted away from the $c$ axis (Campbell, Doria, and Kogan, 1988). The above configuration describes the equilibrium state of the vortex lattice at large enough magnetic fields, $H > H_{c_1}^c/\varepsilon_\vartheta$. For low fields, $H < H_{c_1}^c/\varepsilon_\vartheta$, the equilibrium state for the tilted lattice is realized by the so-called chain state (Buzdin and Simonov, 1990; Grishin *et al.*, 1990; Bolle *et al.*, 1991; Ivlev and Kopnin, 1991; Gammel *et al.*, 1992; see also Ivlev, Kopnin, and Salomaa, 1991), where the vortex lines rearrange themselves into parallel running chains defining planes of high flux density oriented parallel to the $yz$ plane containing the $c$ axis and the magnetic-field vector. This instability arises from an attractive interaction between the tilted vortex lines, which has its origin in the tendency of the screening currents to flow in the $ab$ planes. It is interesting to realize that the transition line $H_{c_1}^c/\varepsilon_\vartheta$ between the usual triangular state and the chain state coincides with the boundary of the regime where the scaling approach to the problem of anisotropy can be used. In the following we concentrate on the elastic properties of the triangular lattice, which corresponds to the equilibrium state for large enough fields. Note that the elastic properties of the chain state are different. In particular, the relative shear between the planes containing the vortex chains is exponentially small due to the increase in the field homogeneity within the planes (Ivlev and Kopnin, 1991).

The elastic properties of the vortex lattice are known once we have found an expression for the elastic matrix $\Phi_{\alpha\beta}(\mathbf{k})$. The most compact formulation can be given within the London theory, which, for the new high-temperature superconductors with their large GL parameter $\kappa$, covers most of the experimentally accessible field range. For the anisotropic case the formulas (3.25) and (3.27) then have to be replaced by the more general expressions (Sudbø and Brandt, 1991a; Sardella, 1992)

$$V_{\alpha\beta}^{\text{int}}(\mathbf{k}) = \frac{e^{-(\xi^2 K^2 + \xi_c^2 k_z^2)}}{1 + \lambda^2 k^2} \left[ \delta_{\alpha\beta} - \frac{(\lambda_c^2 - \lambda^2) K_{\perp\alpha} K_{\perp\beta}}{1 + \lambda^2 k^2 + (\lambda_c^2 - \lambda^2) K^2} \right]$$ (3.38)

and

$$f_{\alpha\beta}(\mathbf{k}) = k_\alpha k_\beta V_{zz}^{\text{int}}(\mathbf{k}) + k_z^2 V_{\alpha\beta}^{\text{int}}(\mathbf{k}) - 2 k_z k_\beta V_{z\alpha}^{\text{int}}(\mathbf{k}) ,$$ (3.39)

with $\mathbf{K} = (k_x, k_y)$ and $K_\perp = \mathbf{k} \wedge \hat{c} = (k_y, -k_x)$, where $\hat{c}$ denotes the unit vector along the $c$ axis. We remind the reader that $\xi_c = \varepsilon \xi$ is the coherence length along the $c$ axis and $\lambda_c = \lambda/\varepsilon$ denotes the screening length for currents flowing parallel to the $c$ axis. In an anisotropic material the number of elastic moduli increases dramatically. The linear elastic energy within the nonlocal continuum approximation takes the form

$$\mathcal{F}[\mathbf{u}] = \frac{1}{2} \int \frac{d^3 k}{(2\pi)^3} [c_{11}^{\parallel}(\mathbf{k})(k_x u_x)^2 + c_{11}^{\perp}(\mathbf{k})(k_{y'} u_{y'})^2 + 2c_{11}^{\parallel\perp}(\mathbf{k})(k_x u_x k_{y'} u_{y'}) + c_{44}^{\parallel}(\mathbf{k})(k_{z'} u_x)^2 + c_{44}^{\perp}(\mathbf{k})(k_{z'} u_{y'})^2$$

$$+ 2c_{14}^{\perp}(\mathbf{k})(k_{y'} k_{z'} u_{y'}^2) + 2c_4^{\parallel\perp}(\mathbf{k})(k_x u_x k_{z'} u_{y'}) + c_{66}^{\parallel}(k_{y'} u_x)^2 + c_{66}^{\perp}(k_x u_{y'})^2 + 2c_{64}^{\parallel}(k_{y'} k_{z'} u_{x'}^2)] .$$ (3.40)

In addition, the vortex lattice in the anisotropic material exhibits rotational modes, which are discussed in the work of Kogan and Campbell (1989). Note that the $x$ axis is common to both the vortex- and lattice-related coordinate systems, hence $x = x'$.

The first anisotropic moduli were calculated by Kogan and Campbell (1989), who determined the soft in-plane shear modulus $c_{66}^{\parallel}(\vartheta)$ and the hard out-of-plane shear modulus $c_{66}^{\perp}(\vartheta)$ for all angles $\vartheta$. Basing their calculations on the London theory, they found

$$c_{66}^{\parallel}(\vartheta) = c_{66} \varepsilon_\vartheta^3, \quad c_{66}^{\perp}(\vartheta) = \frac{c_{66}}{\varepsilon_\vartheta} ,$$ (3.41)

with $c_{66} = \Phi_o B / (8\pi\lambda)^2$, the isotropic result evaluated with the planar screening parameter $\lambda$.

The tilt moduli $c_{44}^{\parallel}$ and $c_{44}^{\perp}$ for the in-plane and for the out-of-plane tilt modes have been determined for the special cases where the magnetic field is aligned with one of the main axes of the material by Houghton, Pelcovits, and Sudbø (1989; $\mathbf{B}\|c$, calculation based on the GL theory) and by Sudbø and Brandt (1991a; $\mathbf{B}\|c$ and $\mathbf{B}\perp c$, calculation based on the London theory). Very recently, Sardella (1992) calculated the full angular dependence of the tilt moduli within the London approximation. Again, the results can be written in a form $c_{44}(\mathbf{k}) = c_{44}^{\circ}(\mathbf{k}) + c_{44}^{c}(\mathbf{k})$, with $c_{44}^{\circ}(\mathbf{k})$ the strongly dispersive contribution arising from the term $\nu = 0$ in Eq. (3.26) and $c_{44}^{c}(\mathbf{k})$ denoting the correction due to the remaining terms in the sum. The results for $c_{44}^{\circ}(\mathbf{k})$ take the form (note that $\theta = \pi/2 - \vartheta$, $\varepsilon_\theta^2 = \varepsilon^2 \sin^2\vartheta + \cos^2\vartheta$)

$$c_{44}^{\circ\parallel}(\mathbf{k}) = \frac{B^2}{4\pi} \frac{1}{1 + \lambda_c^2 K^2 + \lambda^2 k_z^2} ,$$ (3.42a)

$$c_{44}^{\circ\perp}(\mathbf{k}) = \frac{1 + (\varepsilon_\theta \lambda_c k)^2}{1 + \lambda^2 k^2} c_{44}^{\circ\parallel}(\mathbf{k}) .$$ (3.42b)

For a uniform tilt, the isotropic result $c_{44}^{\circ}(\mathbf{k}=0) = B^2/4\pi$ is recovered. Note that again the out-of-plane tilt modulus $c_{44}^{\circ\perp}(\mathbf{k})$ is in general larger ("harder") than the corresponding in-plane quantity $c_{44}^{\circ\parallel}(\mathbf{k})$. The correction

term $c_{44}^c(\mathbf{k})$ again becomes important at large $\mathbf{k}$ vectors and essentially describes the crossover from the lattice modulus to the (dispersive) single-vortex line tension as the interaction between neighboring vortices becomes small, for $\mathbf{B}\|c$:

$$c_{44}^c(\mathbf{k} \to 0) = \frac{1}{4\pi} B(H - B) ,$$

$$c_{44}^c(k_z) \approx \frac{\varepsilon_o}{2a_o^2} \left[ \varepsilon^2 \ln \frac{\kappa_c^2}{1 + \lambda_c^2 K_{\text{BZ}}^2 + \lambda^2 k_z^2} + \frac{1}{\lambda^2 k_z^2} \ln \left( 1 + \frac{\lambda^2 k_z^2}{1 + \lambda^2 K_{\text{BZ}}^2} \right) \right] ,$$ (3.43)

where $\kappa_c = \kappa/\varepsilon$ (see Glazman and Koshelev, 1991a). The second term in Eq. (3.43) is due to the electromagnetic interaction. The first term is only weakly dispersive, depends strongly on the anisotropy $\varepsilon$, and vanishes in the limit $\varepsilon \to 0$; the electromagnetic contribution is strongly dispersive but independent of $\varepsilon$ and hence always remains finite.[4] A particularly interesting limit is the single-vortex line tension, which becomes strongly dispersive as a consequence of the anisotropy,

$$\varepsilon_l(k_z) \approx \varepsilon^2 \varepsilon_o \ln \left[ \frac{\kappa_c^2}{1 + \lambda^2 k_z^2} \right]^{1/2} + \varepsilon_o \frac{1}{\lambda^2 k_z^2} \ln(1 + k_z^2 \lambda^2)^{1/2} .$$ (3.44)

For large wave vectors, $k_z > 1/\varepsilon\lambda$, the line tension is small, $\varepsilon_l \simeq \varepsilon^2 \varepsilon_o$. Within the intermediate regime $1/\lambda < k_z < 1/\varepsilon\lambda$ the line tension rapidly increases, $\varepsilon_l \simeq \varepsilon_o / k_z^2 \lambda^2$, and reaches the long-wavelength limit

---

[4]Within the language of layered superconductors, the first term is due to the Josephson coupling between the layers and vanishes as the layers decouple; in contrast, the electromagnetic contribution remains finite even for a completely decoupled system.

$\varepsilon_l \simeq \varepsilon_0$ for $k_z < 1/\lambda$. This separation into a small line tension due to the Josephson coupling and a strongly dispersive component due to electromagnetic coupling is specific to the anisotropic situation. In the isotropic situation there is no suppression of the first term, and the dispersion is only weak. For additional details we refer the reader to the work of Sudbø and Brandt (1991; see also Brandt and Sudbø, 1991a) and of Glazman and Koshelev (1991a).

The compression moduli $c\|_{11}$, $c^{\perp}_{11}$, and $c\|^{;\perp}_{11}$ have been determined for the special cases mentioned above by Houghton, Pelcovits, and Sudbø (1989) and by Sudbø and Brandt (1991a), and the complete angular dependence has been obtained by Sardella (1992),

$$c\|_{11}(\mathbf{k}) = c^{\perp}_{11}(\mathbf{k}) = c\|^{;\perp}_{11}(\mathbf{k})$$
$$= \frac{1+(\varepsilon_\vartheta \lambda_c k)^2}{1+\lambda^2 k^2} c^{\circ}_{44}\|(\mathbf{k}) \ . \tag{3.45}$$

Finally, the mixed compression-tilt moduli $c^{\perp}_{14}$ and $c\|^{;\perp}_{14}$ have been found by Sardella to take the form

$$c^{\perp}_{14}(\mathbf{k}) = c\|^{;\perp}_{14}(\mathbf{k}) = \frac{\sqrt{\varepsilon_\vartheta^2 \varepsilon_\theta^2 - \varepsilon^2} \lambda_c^2 k^2}{1+\lambda^2 k^2} c^{\circ}_{44}\|(\mathbf{k}) \ . \tag{3.46}$$

The mixed shear-tilt modulus $c\|_{64}$ arises from terms $\boldsymbol{\nu} \neq 0$ in the sum (3.26). In addition, corrections to the above moduli due to the admixing of the shear mode to the tilt and compression modes can only be obtained by considering terms $\boldsymbol{\nu} \neq 0$ in the sum over reciprocal lattice vectors in Eq. (3.26). A complete analysis of these terms has not yet been carried out.

Let us turn now to the scaling approach introduced in Sec. III.A (Schönenberger, Geshkenbein, and Blatter, 1993). Using this very efficient method, we shall obtain all the desired results for the elastic moduli provided that after rescaling the condition $\lambda \tilde{k} > 1$ is fulfilled. This is not a severe restriction, since we already know the results for the uniform limit from thermodynamic considerations,

$$c_{11}(0) \simeq c_{44}(0) \simeq \frac{B^2}{4\pi} \ , \tag{3.47}$$

independent of the angle $\vartheta$ and the direction of the displacement vector. In order to obtain the elastic moduli in the anisotropic situation, we have to transform the isotropic elastic free-energy functional (3.29) to fit the anisotropic system with the help of the scaling rule (3.12). To begin with, let us rewrite (3.29) in the isotropized system,

$$\tilde{\mathscr{F}}[\tilde{\mathbf{u}}] = \frac{1}{2} \int \frac{d^3\tilde{k}}{(2\pi)^3} [\tilde{c}_{11}(\tilde{\mathbf{k}})(\tilde{\mathbf{K}} \cdot \tilde{\mathbf{u}})^2 + \tilde{c}_{66}(\tilde{\mathbf{K}}_{\perp} \cdot \tilde{\mathbf{u}})^2$$
$$+ \tilde{c}_{44}(\tilde{\mathbf{k}})(\tilde{k}_z \tilde{\mathbf{u}})^2] \ . \tag{3.48}$$

The goal is to express the above isotropized elastic energy by the parameters and variables of the original anisotropic system and to extract the elastic moduli for the anisotropic situation from a comparison with Eq. (3.40). To this end we first have to find the transformation rule for

the displacement field $\tilde{\mathbf{u}}$ and the wave vector $\tilde{\mathbf{k}}$. Let us define the rotation operator

$$\mathscr{R}(\alpha) = \begin{bmatrix} 1 & 0 & 0 \\ 0 & \cos\alpha & \sin\alpha \\ 0 & -\sin\alpha & \cos\alpha \end{bmatrix} \tag{3.49}$$

and the scaling operator

$$\mathscr{S}(s) = \begin{bmatrix} 1 & 0 & 0 \\ 0 & 1 & 0 \\ 0 & 0 & s \end{bmatrix} \ . \tag{3.50}$$

The transformation of the displacement vector $\tilde{\mathbf{u}} = (\tilde{u}_x, \tilde{u}_{y'})$ (expressed in the isotropized coordinate system with the $z'$ axis pointing along the field direction) to the displacement vector $\mathbf{u} = (u_x, u_{y'})$ (expressed in the original coordinate system with the $z'$ axis pointing along the field direction) involves the sequence of operations $(\theta = \pi/2 - \vartheta)$

$$\mathbf{u} = \mathscr{R}(-\theta)\mathscr{S}(\varepsilon)\mathscr{R}(\tilde{\vartheta})\tilde{\mathbf{u}} \ . \tag{3.51}$$

The angle $\tilde{\vartheta}$ in the isotropized system is related to the angle $\vartheta$ in the original system by

$$\tan\tilde{\vartheta} = \frac{1}{\varepsilon}\tan\vartheta \ . \tag{3.52}$$

Evaluating (3.51) and using the relations $\cos\tilde{\vartheta} = (\varepsilon/\varepsilon_\vartheta)\cos\vartheta$ and $\sin\tilde{\vartheta} = (1/\varepsilon_\vartheta)\sin\vartheta$ following from Eq. (3.52), we obtain the result

$$\tilde{u}_x = u_x \quad \text{and} \quad \tilde{u}_{y'} = \frac{1}{\varepsilon_\vartheta} u_{y'} \ . \tag{3.53}$$

In a similar way we transform the wave vector $\tilde{\mathbf{k}}$. The transformation rule now reads

$$\mathbf{k} = \mathscr{R}(-\theta)\mathscr{S}(1/\varepsilon)\mathscr{R}(\tilde{\vartheta})\tilde{\mathbf{k}} \ , \tag{3.54}$$

and we obtain, after trivial inversion,

$$\tilde{k}_x = k_x \ ,$$
$$\tilde{k}_{y'} = \varepsilon_\vartheta k_{y'} + \frac{\sqrt{\varepsilon_\vartheta^2 \varepsilon_\theta^2 - \varepsilon^2}}{\varepsilon_\vartheta} k_{z'} \ , \tag{3.55}$$
$$\tilde{k}_{z'} = \frac{\varepsilon}{\varepsilon_\vartheta} k_{z'} \ .$$

Next, we have to rescale the isotropized moduli $\tilde{c}_{11}$, $\tilde{c}_{44}$, and $\tilde{c}_{66}$. Using the scaling rule (3.12) we obtain

$$\tilde{c}_{11}(\tilde{\mathbf{k}}) \simeq \tilde{c}_{44}(\tilde{\mathbf{k}}) \simeq \frac{B^2}{4\pi} \frac{\varepsilon_\vartheta^2}{\lambda^2 \tilde{k}^2} \ ,$$
$$\tilde{c}_{66} \simeq \frac{\Phi_0 B \varepsilon_\vartheta}{(8\pi\lambda)^2} \ . \tag{3.56}$$

The rescaled wave vector $\tilde{k}^2$ is trivially obtained from the transformation rule (3.55) and reads

$$\tilde{k}^2 = k_x^2 + \varepsilon_\vartheta^2 k_{y'}^2 + \varepsilon_\theta^2 k_{z'}^2 + 2\sqrt{\varepsilon_\vartheta^2 \varepsilon_\theta^2 - \varepsilon^2} k_{y'} k_{z'}$$
$$= \varepsilon^2 k^2 + (1-\varepsilon^2)K^2 \ , \tag{3.57}$$

where the last equation has been obtained by expressing **k** in the lattice frame of reference with the $z$ axis parallel to the $c$ axis of the uniaxially anisotropic material. As usual, **K** denotes the planar component of **k**, $\mathbf{K}=(k_x,k_y)$. Finally, we combine (3.48) with Eqs. (3.53), (3.55), and (3.56) and compare the resulting expression with the free-energy functional (3.40). Dropping the small correction from the admixing of the shear mode with the compression mode, $\tilde{c}_{11}-\tilde{c}_{66}\simeq\tilde{c}_{11}$, we obtain the results

$$c_{44}^{\circ,\parallel}(\mathbf{k})\simeq\frac{B^2}{4\pi}\frac{1}{\lambda^2k^2+(\lambda_c^2-\lambda^2)K^2}\ ,\qquad(3.58)$$

$$c_{44}^{\circ,\perp}(\mathbf{k})\simeq\frac{\varepsilon_\theta^2}{\varepsilon^2}c_{44}^{\circ,\parallel}(\mathbf{k})\ ,\qquad(3.59)$$

$$c_{11}^{\parallel}(\mathbf{k})\simeq c_{11}^{\perp}(\mathbf{k})\simeq c_1^{\perp}(\mathbf{k})\simeq\frac{\varepsilon_\vartheta^2}{\varepsilon^2}c_{44}^{\circ,\parallel}(\mathbf{k})\ ,\qquad(3.60)$$

$$c_{14}^{\perp}(\mathbf{k})\simeq c_{14}^{\perp}(\mathbf{k})\simeq\frac{\sqrt{\varepsilon_\vartheta^2\varepsilon_\theta^2-\varepsilon^2}}{\varepsilon^2}c_{44}^{\circ,\parallel}(\mathbf{k})\ ,\qquad(3.61)$$

$$c_{66}^{\parallel}\simeq\varepsilon_\vartheta^4 c_{66}^{\perp}\simeq\frac{B\Phi_\circ}{(8\pi\lambda)^2}\varepsilon_\vartheta^3\ ,\qquad(3.62)$$

$$c_{64}^{\parallel}\simeq\frac{\sqrt{\varepsilon_\vartheta^2\varepsilon_\theta^2-\varepsilon^2}}{\varepsilon_\vartheta^2}c_{66}^{\parallel}\ .\qquad(3.63)$$

The comparison with Eqs. (3.42), (3.45), and (3.46) derived in the traditional way verifies that the two results agree within the dispersive regime. Finally, rescaling of the correction term $c_{44}^c(\mathbf{k})$, Eq. (3.33), provides the single-vortex line tensions already derived in Sec. A above. Taking the logarithmic correction factor into account, we obtain $\varepsilon_\parallel^l(k_{z'})\simeq(\varepsilon_\circ\varepsilon^2/\varepsilon_\vartheta)\ln(\varepsilon_\vartheta/\varepsilon k_{z'}\xi)$ and $\varepsilon_l^l(k_{z'})\simeq(\varepsilon_\circ\varepsilon^2/\varepsilon_\vartheta^3)\ln(\varepsilon_\vartheta/\varepsilon k_{z'}\xi)$, which is valid in the regime $k_{z'}>\varepsilon_\vartheta/\varepsilon\lambda$.

It is interesting to note that the ratio of the bulk tilt moduli $c_{44}^{\circ,\perp}/c_{44}^{\circ,\parallel}$ shows a different angular dependence from that of the single-vortex tilt moduli $\varepsilon_l^l/\varepsilon_\parallel^l$: whereas $c_{44}^{\circ,\perp}/c_{44}^{\circ,\parallel}=\varepsilon_\theta^2/\varepsilon^2$, the single-vortex result is $\varepsilon_l^l/\varepsilon_\parallel^l=1/\varepsilon_\vartheta^2$. This difference is due to the admixing of the bulk modulus with the tilt mode $c_{44}^{\circ,\perp}$. It is important to note that the elastic theory for an anisotropic superconductor for angles $\vartheta$ away from the main axes is very cumbersome, since the elastic energy is no longer diagonal in the vortex frame of reference. Consider as an example the study of single-vortex pinning as carried out in Sec. II.C above. In view of the difference in the angular dependence of the lattice and the single-vortex tilt moduli, one may ask where the crossover from lattice to single-vortex-type behavior takes place. Is the physics at low fields determined by the single-vortex tilt modulus or by the lattice tilt modulus? At first sight it appears that the regime where the single-vortex line tension dominates the physics is only small. On the other hand, when going over to the isotropized system, the regime where the single-vortex elasticity dominates is rather large. How

can this apparent discrepancy be understood? Within the isotropized system the relevant wave vectors at crossover all are large and of the same order, $\sim1/\tilde{a}_\circ$. Mapping back to the anisotropic system, again both $k_{y'}$ and $k_{z'}$ become large but of opposite sign. Hence the energies arising from the bulk tilt, compression, and mixed tilt-compression modes all are large but roughly cancel one another, since the contribution from the mixed mode is negative. What remains is the single-vortex energy, which determines the relevant physics as discussed in Sec. II.C above. In order to extract the relevant physics, it is therefore much more convenient to study the problem within the isotropized system than to carry out the analysis in the anisotropic-vortex frame of reference, where the elastic energy is no longer diagonal.

### C. Elementary pinning forces

In the previous section we have determined a number of important quantities characterizing flux motion in type-II superconductors under low-temperature/low-field conditions: the collective pinning length $L_c$, the activation energy $U_c$, and the action $S_E^{\mathrm{eff}}$ for creep, as well as the critical current density $j_c$. These characteristic quantities have been calculated within weak collective pinning theory, where the pinning potential is due to weak short-range disorder. In the high-$T_c$ superconductors this type of disorder is expected to occur as a consequence of oxygen doping, producing point defects interacting weakly with the vortex cores (Tinkham, 1988b). The above results for the pinning length $L_c$, the pinning energy $U_c$, the action $S_E^{\mathrm{eff}}$, and the critical current density $j_c$ are expressed in terms of the disorder parameters $\gamma$ for $\delta T_c$ pinning and $\delta l$ pinning, Eq. (2.38). In the following we determine these disorder parameters from microscopic considerations and show that oxygen point defects are indeed an important source of pinning. Using independent experimental data on the dependence of $T_c$ on hole concentration and on the normal-state resistivity, we reproduce the experimentally observed magnitude of the critical current density in the oxide superconductors as well as the typical values of the other characteristic quantities determined by the weak collective pinning model.

In the following we first relate the GL parameters to microscopic quantities in order to relate disorder in $\alpha$ and in $m$ to disorder in $T_c$ and $l$, respectively. Since no microscopic theory of high-temperature superconductivity is available as yet, we have to base our analysis on the BCS theory. This simplification will probably have only a minor influence on the case of $\delta T_c$ pinning, whereas the consequences for the case of $\delta l$ pinning are less clear. We then investigate, first, the pinning strength produced by disorder in the transition temperature $T_c$, and, second, pinning due to disorder in the mean free path $l$. The latter case has been studied by van der Beek and Kes (1991) using the results of the microscopic calculation of the pinning force by Thuneberg, Kurkijärvi, and Rainer

(1984; see also Thuneberg, 1989). Here we follow a different approach, using GL theory with coefficients determined by the expansion of the Gor'kov equations near $T_c$ for the clean-limit case. Our results essentially agree with those obtained by van der Beek and Kes (1991). Numerical examples are discussed for the case of $YBa_2Cu_3O_{7-y}$.

In order to relate the GL parameters to microscopic quantities, we use the result of the microscopic derivation of the GL equations by Gor'kov (1959). A consistent set of GL coefficients that is particularly useful for the discussion of the pinning problem is

$$\alpha = -\frac{12\pi^2}{7\zeta(3)}\frac{T_c}{\varepsilon_F}(T_c - T) \,, \tag{3.64a}$$

$$\beta = \frac{18\pi^2}{7\zeta(3)}\frac{1}{N(\varepsilon_F)}\left[\frac{T_c}{\varepsilon_F}\right]^2 \,, \tag{3.64b}$$

$$m = \frac{m_e}{\chi(\rho)} \,. \tag{3.64c}$$

Here $N(\varepsilon_F)$ denotes the density of states [$N(\varepsilon_F)$ $= 3n/4\varepsilon_F$, $n =$ carrier density, $\varepsilon_F =$ Fermi energy] and $T_c$ is the transition temperature. The Gor'kov function $\chi(\rho)$ is given by

$$\chi(\rho) = \frac{8}{7\zeta(3)}\sum_{n=0}^{\infty}\frac{1}{(2n+1)^2(2n+1+\rho)} \,, \tag{3.65}$$

with the disorder parameter

$$\rho = \frac{\hbar v_F}{2\pi T_c l} \,, \tag{3.66}$$

$l$ being the mean free path. The numerical value of the zeta function is $\zeta(3) = 1.202$. In the clean limit (to which the new oxide superconductors seem to belong), the Gor'kov function becomes

$$\chi(\rho \to 0) \simeq 1 - \frac{\pi^4}{84\zeta(3)}\rho, \quad \text{clean limit} \,, \tag{3.67}$$

whereas the dirty limit is characterized by

$$\chi(\rho \to \infty) \simeq \frac{\pi^2}{7\zeta(3)}\frac{1}{\rho}, \quad \text{dirty limit} \,. \tag{3.68}$$

Using Eqs. (3.64a) to (3.64c) we can express the GL length scales $\xi$ and $\lambda$ by the zero-temperature BCS coherence length $\xi_{BCS} = \hbar v_F/\pi\Delta_{BCS}$ and the zero-temperature London penetration depth $\lambda_L = (mc^2/4\pi ne^2)^{1/2}$,

$$\xi^2(T) = \frac{7\zeta(3)}{48}\left[\frac{\pi}{e^C}\right]^2\xi_{BCS}^2\chi(\rho)\left[1 - \frac{T}{T_c}\right]^{-1}$$

$$= 0.54\xi_{BCS}^2\chi(\rho)\left[1 - \frac{T}{T_c}\right]^{-1} \,, \tag{3.69}$$

$$\lambda^2(T) = \frac{1}{2}\lambda_L^2\frac{1}{\chi(\rho)}\left[1 - \frac{T}{T_c}\right]^{-1} \,, \tag{3.70}$$

with $C = 0.577$ the Euler constant. Here $v_F$ is the Fermi

velocity and $\Delta_{BCS}$ denotes the (zero-temperature) BCS gap parameter. We have also used the equality $\Delta_{BCS}/T_c = \pi e^{-C}$. Similarly, the GL order parameter becomes $|\Psi_0(T)|^2 = n(1 - T/T_c)/2$. The BCS zero-temperature thermodynamic critical field $H_{c\,BCS} = \Phi_0/\sqrt{2/3}\pi^2\xi_{BCS}\lambda_L$ differs from the corresponding zero-temperature extrapolated value from GL theory, $H_c(T=0) = 1.74H_{c\,BCS}$.

Let us return to the problem of pinning and determine the disorder coefficients $\gamma$ for $\delta T_c$ and $\delta l$ pinning [see Eq. (2.38)]. First, we define the dimensionless pinning parameters

$$\delta_\alpha = \frac{1}{2\pi}\frac{\gamma_\alpha}{\alpha^2\xi^3} \tag{3.71}$$

and

$$\delta_m = \frac{7}{30\pi}\frac{\gamma_m}{m^2\xi^3} \tag{3.72}$$

for $\delta T_c$ and $\delta l$ pinning, respectively. In terms of the new dimensionless pinning parameter $\delta$ ($=\delta_\alpha$ or $\delta_m$), the characteristic quantities $L_c$, $U_c$, $S_E^{eff}$, and $j_c$ become

$$L_c = \xi\delta^{-1/3}, \quad U_c = H_c^2\xi^3\delta^{1/3} \,,$$

$$\frac{S_E^{eff}}{\hbar} = \frac{\hbar}{e^2}\frac{\xi}{\rho_n}\delta^{-1/3}, \quad j_c = j_0\delta^{2/3} \,, \tag{3.73}$$

and the corresponding quantities in the anisotropic superconductor for the case of a magnetic field aligned along the $c$ axis are

$$L_c^c = \varepsilon\xi\left[\frac{\delta}{\varepsilon}\right]^{-1/3}, \quad U_c^c = H_c^2\varepsilon\xi^3\left[\frac{\delta}{\varepsilon}\right]^{1/3} \,,$$

$$\frac{S_E^{eff,c}}{\hbar} = \frac{\hbar}{e^2}\frac{\varepsilon\xi}{\rho_n}\left[\frac{\delta}{\varepsilon}\right]^{-1/3}, \quad j_c^c = j_0\left[\frac{\delta}{\varepsilon}\right]^{2/3} \,. \tag{3.74}$$

It remains to determine the dimensionless pinning parameters, and we begin our discussion with the case of $\delta T_c$ pinning. Using Eqs. (3.64a) and (3.71) and the definition $\langle\delta T_c(\mathbf{r})\delta T_c(\mathbf{r}')\rangle = \gamma_T T_c^2\delta(\mathbf{r} - \mathbf{r}')$, we obtain

$$\delta_\alpha = \frac{1}{2\pi}\left[\frac{48}{7\zeta(3)}\right]^{3/2}\left[\frac{e^C}{\pi}\right]^3\frac{\gamma_T}{\xi_{BCS}^3}\frac{1}{(1-t)^{1/2}} \,, \tag{3.75}$$

where we have introduced the reduced temperature $t = T/T_c$. The transition temperature $T_c$ is determined by the mean hole concentration within the coherence volume $V_\xi = \pi\xi_{BCS}^2 d$, $d$ being the interlayer distance. Due to the quenched disorder produced by (charged) oxygen defects, the hole concentration also exhibits spatial fluctuations. For example, assuming the oxygen defects to be mainly concentrated within the CuO chains, the metallic planes will tend to screen the charged defects within a distance $\simeq d/2 < \xi_{BCS}$. The additional holes involved in the screening process then set up a fluctuating hole density $\delta n$, which is correlated with the oxygen disorder $\delta n_i$, where we denote the oxygen impurity density

by $n_i$. We can thus write the spatial fluctuations of $T_c$

$$T_c(\mathbf{r}) \simeq T_c + \frac{dT_c}{dn_i}\bigg|_{n_i} \overline{\delta n_i(\mathbf{r})} + \frac{1}{2}\frac{d^2T_c}{dn_i^2}\bigg|_{n_i} \overline{\delta n_i(\mathbf{r})^2} , \quad (3.76)$$

$$\overline{\delta n_i(\mathbf{r})} = \int d^3u \, \phi(\mathbf{r}-\mathbf{u})\delta n_i(\mathbf{u}) .$$

Here $\phi(\mathbf{r}-\mathbf{u})$ is a normalized test function, which is nonzero within the coherence volume $V_\xi$. Good material is usually conditioned so as to maximize the transition temperature $T_c$, hence $\partial_{n_i}T_c|_{n_i} \simeq 0$. For $\mathrm{YBa_2Cu_3O_{7-y}}$ the corresponding doping concentration typically is $y \lesssim 0.1$ or $n_i = y/V_{\mathrm{u.c.}} \simeq 5\times10^{20}$ cm$^{-3}$, with $V_{\mathrm{u.c.}}$ the unit cell volume, whereas for $\mathrm{Bi_2Sr_2CaCu_2O_{8+y}}$, $y \simeq 0.15$. The quadratic term in Eq. (3.76) then produces the disorder strength in $\delta T_c/T_c$,

$$\gamma_T = \frac{1}{2}\left[\frac{n_i}{T_c}\frac{d^2T_c}{dn_i^2}\right]^2 \frac{1}{V_\xi} , \quad (3.77)$$

where we assume short-scale disorder in the impurity distribution, $\langle \delta n_i(\mathbf{r})\delta n_i(\mathbf{r}')\rangle = n_i\delta(\mathbf{r}-\mathbf{r}')$. In particular, we have used here the decomposition rule for the fourth-order moment,

$$\langle \delta n_i(\mathbf{r}_1)\delta n_i(\mathbf{r}_2)\delta n_i(\mathbf{r}_3)\delta n_i(\mathbf{r}_4)\rangle$$

$$= \sum_{\mathrm{pairs}}\langle \delta n_i(\mathbf{r}_i)\delta n_i(\mathbf{r}_j)\rangle\langle \delta n_i(\mathbf{r}_m)\delta n_i(\mathbf{r}_n)\rangle$$

characteristic of Gaussian white noise. In addition, we have made the approximations

$$\Phi(\mathbf{r}) = \int d^3u \, \phi(\mathbf{u})\phi(\mathbf{r}-\mathbf{u}) \simeq \delta(\mathbf{r}) ,$$

$$\Phi^2(\mathbf{r}) \simeq \frac{1}{V_\xi}\delta(\mathbf{r}) .$$

Combining Eqs. (3.75) and (3.77), we obtain the final expression for the pinning parameter

$$\delta_\alpha = \frac{1}{4\pi^2}\left[\frac{48}{7\zeta(3)}\right]^{3/2}\left[\frac{e^C}{\pi}\right]^3\left[\frac{n_i}{T_c}\frac{d^2T_c}{dn_i^2}\right]^2$$

$$\times \frac{1}{\xi_{\mathrm{BCS}}^5 d}\frac{1}{(1-t)^{1/2}}$$

$$= 0.063\left[\frac{n_i}{T_c}\frac{d^2T_c}{dn_i^2}\right]^2\frac{1}{\xi_{\mathrm{BCS}}^5 d}\frac{1}{(1-t)^{1/2}} . \quad (3.78)$$

For anisotropic materials, this result is increased by a factor $1/\varepsilon$, $\delta_\alpha \to \delta_\alpha/\varepsilon$. Typically, a variation in the oxygen concentration $\delta y \simeq 0.15$ produces a change in $T_c$ of the order of $\delta T_c \simeq 10$ K (Cava, Batlogg, Chen, *et al.*, 1987). Thus $(n_i/T_c)(d^2T_c/dn_i^2) \simeq (2y/\delta y^2)(\delta T_c/T_c)V_{\mathrm{u.c.}} \simeq V_{\mathrm{u.c.}}$, where we have used $n_i = y/V_{\mathrm{u.c.}}$ and we have assumed a mean doping concentration $y \simeq 0.1$. The mean number of oxygen defects within the coherence volume $V_\xi$ is of the order of $n_iV_\xi \simeq 5$, hence fluctuations are indeed important. The final numerical estimate for the dimensionless pinning parameter due to $\delta T_c$ pinning then becomes

$$\frac{\delta_\alpha}{\varepsilon} \simeq \frac{1}{1000}\frac{1}{(1-t)^{1/2}} . \quad (3.79)$$

It is interesting to consider the case of nonoptimal doping, where the term linear in $\delta n_i$ essentially determines the fluctuations in $T_c$ due to oxygen disorder [see Eq. (3.76)]. In this case, which has been considered also by Fisher, Fisher, and Huse (1991), the calculation simplifies considerably and the disorder strength in $\delta T_c/T_c$ is immediately found to be

$$\gamma_T = \left[\frac{n_i}{T_c}\frac{dT_c}{dn_i}\right]^2\frac{1}{n_i} . \quad (3.80)$$

The final result for the pinning parameter $\delta_\alpha$ is then

$$\delta_\alpha = 0.4\left[\frac{n_i}{T_c}\frac{dT_c}{dn_i}\right]^2\frac{1}{\xi_{\mathrm{BCS}}^3 n_i}\frac{1}{(1-t)^{1/2}} , \quad (3.81)$$

and using typical values for YBCO (Cava, Batlogg, Chen, *et al.*, 1987), assuming an oxygen defect concentration $y \simeq 0.2$, around which a fluctuation of $\delta y = 0.1$ produces a variation in $T_c$ of the order of $\delta T_c \simeq 10$ K, we obtain a numerical value

$$\frac{\delta_\alpha}{\varepsilon} \simeq \frac{1}{100}\frac{1}{(1-t)^{1/2}} . \quad (3.82)$$

As expected, the linear variation of $T_c$ with doping concentration, relevant in materials with nonoptimal doping with respect to a maximal transition temperature, is able to produce stronger pinning. A systematic experimental study of the correlation between oxygen defect concentration $n_i$ and the critical current density $j_c$ would be highly desirable.

Next we discuss pinning due to disorder in the mean free path $l$. In a clean-limit superconductor, $\delta m \approx m_e[\pi^4/84\zeta(3)]\delta\rho$, where $\delta\rho \propto \delta(1/l)$; see Eq. (3.66). The mean free path $l$ is related to the impurity density $n_i$ and the scattering cross section $\sigma_i$, $l = 1/n_i\sigma_i$. Assuming again short-scale disorder in the impurity distribution, $\langle \delta n_i(\mathbf{r})\delta n_i(\mathbf{r}')\rangle = n_i\delta(\mathbf{r}-\mathbf{r}')$, we obtain the following expression for $\delta_m$:

$$\delta_m = \frac{7}{30\sqrt{3}}\left[\frac{\pi}{\sqrt{7\zeta(3)}}\right]^7\frac{e^C}{\pi}\frac{(1-t)^{3/2}}{\xi_{\mathrm{BCS}}l^2n_i} ,$$

$$= 0.13\frac{(1-t)^{3/2}}{\xi_{\mathrm{BCS}}l^2n_i} . \quad (3.83)$$

Combining Eqs. (2.40) and (3.83), we obtain $\langle \mathcal{E}_{\mathrm{pin}}^2(L)\rangle \propto \varepsilon_0^2(\xi_{\mathrm{BCS}}/\xi)^2(L/n_il^2)$, which agrees with the result of van der Beek and Kes (1991). Whereas the latter authors base their analysis on the microscopic calculation of the pinning force by Thuneberg, Kurkijärvi, and Rainer (1984), in our case the connection to the microscopic theory has been made by Gor'kov's (1959) derivation of the GL equations. It is important to realize that the analysis of Thuneberg *et al.* corresponds to the case of a *clean*-limit superconductor, where different de-

fects do not interfere. The agreement between the two approaches shows that the analysis of Gor'kov is indeed complete, as it accounts correctly for the results of Thuneberg *et al.* (the same conclusion has also been found by Thuneberg, 1984).

Let us continue with the numerical estimate of the pinning parameter $\delta_m$. The mean free path $l$ can be related to the residual resistivity $\rho_n$ and the hole density $n$, $l = (\hbar/e^2)(3\pi^2/n^2)^{1/3}/\rho_n$; using typical values for the normal-state resistivity extrapolated to zero temperature, $\rho_n(T \to 0) \simeq 10 \ \mu\Omega$ cm, and for the hole density, $n \simeq 2.5 \times 10^{21}$ cm$^{-3}$, we find a mean free path $l \simeq 700$ Å, placing the oxides definitely in the clean-limit regime. Note that in our discussion of pinning we are interested in the quenched disorder potential producing residual resistivity, and therefore we should not use the high-temperature normal-state resistivity, which also contains contributions from inelastic processes.

Finally, we have to estimate the active defect density $n_i$. An upper limit for $n_i$ is given by the doping concentration $n_i^{\max} = y/V_{\text{u.c.}}$ (note that in general $n_i \neq n$). The upper limit of $n_i$ is physically realized in Eq. (3.83) if all scattering centers are equivalent, i.e., all oxygen defects are concentrated either in the CuO plane or in the CuO chains. Using $y \simeq 0.1$ as a typical value for the defect concentration, we find an active defect density $n_i^{\max} \simeq 5 \times 10^{20}$ cm$^{-3}$. On the other hand, the scattering defects may be distributed among the planes and the intermediate layers, thus reducing the value of $n_i$ below the doping concentration $n_i^{\max}$. A lower bound for $n_i$ is then given by the expression $n_i^{\min} = 1/l\sigma_i^{\max}$ with $\sigma_i^{\max}$ an upper limit for the scattering cross section. Using $\sigma_i^{\max} = 2\pi R_{\text{ion}}^2$, $R_{\text{ion}} \simeq 1.4$ Å ($\simeq$ half the oxygen spacing), we obtain an estimated lower bound $n_i^{\min} \simeq 10^{20}$ cm$^{-3}$ for the active defect density. For the coherence length we use a value $\xi_{\text{BCS}} \simeq 16$ Å. We then find typical numerical values for the dimensionless pinning parameter $\delta_m/\varepsilon$ of the order of

$$\frac{\delta_m}{\varepsilon} \simeq (0.2-1)\frac{(1-t)^{3/2}}{1000} \ . \tag{3.84}$$

Let us compare the results (3.79) and (3.84) for $\delta T_c$ and $\delta l$ pinning. In both cases we have obtained a low-temperature pinning parameter $\delta/\varepsilon$ of the order of $10^{-3}$, for both $\delta T_c$ and $\delta l$ pinning. In spite of our rather careful analysis, in which we have tried to keep track of all the important numerical factors, we had to introduce estimates in order to make connection to experimentally observable quantities. We thus are unable to decide with certainty which of the two pinning mechanisms is really the more important one. The only statement that can be made is that $\delta T_c$ pinning becomes dominant at high enough temperature due to the different temperature dependencies of the two mechanisms; see Eqs. (3.79) and (3.84).

Finally, let us return to collective pinning theory and estimate the (low-temperature) collective pinning length

$L_c^c$, the pinning potential $U_c^c$, the effective action $S_E^{\text{eff},c}$, and the critical current density $j_c^c$. From the above discussion we have seen that the value $\delta/\varepsilon \simeq 10^{-3}$ is a reasonable estimate for the dimensionless pinning parameter; using Eqs. (3.74) we obtain

$$L_c^c \simeq 10\varepsilon\xi \ , \tag{3.85a}$$

$$U_c^c \simeq 50 \text{ K} \ , \tag{3.85b}$$

$$S_E^{\text{eff},c} \simeq 10^2\hbar \ , \tag{3.85c}$$

$$j_c^c \simeq 10^{-2}j_\circ \ . \tag{3.85d}$$

Here the following estimates have been used: for the thermodynamic critical field, $H_c \simeq 10^4$ G, for the residual resistivity $\rho_n$, $\rho_n \simeq 10 \ \mu\Omega$ cm, and for the depairing current density at low temperatures, $j_\circ \simeq 3 \times 10^8$ A cm$^{-2}$. Note that we have used the residual resistivity $\rho_n(T \to 0)$ because of the low temperatures needed for the observation of the quantum creep phenomenon. For the case of Hall tunneling in a super-clean material, the estimate for the action is $S_E^{H,c} \simeq 10\hbar$, one order of magnitude smaller than the result for the dissipative dynamics.

In the analysis of pinning and creep presented in Sec. II.A above we did not distinguish between the minimum and the saddle-point solution of the free-energy functional (2.44). This is consistent with our convention of dropping all the numerical factors and with the fact that there is only one transverse/longitudinal length ($\xi$ and $L_c$, respectively) and one energy scale ($U_c$) in the problem. However, a more careful analysis shows that the minimum solution of Eq. (2.44), which determines the critical current density $j_c$, differs from the saddle-point solution, determining the activation energy for creep, by a numerical factor in their amplitude $u$ which is not of order unity. As a consequence, the intravalley energy $U_c^c$, which determines quantities such as $j_c^c$ or $\tilde{T}_{\text{dp}}^s$, differs by a numerical factor from the activation energy determining the rate of creep near $j_c^c$. One way of obtaining an estimate for this numerical factor is discussed in Sec. III.E.3 below, where we consider the activation energy for creep of a string pinned by a periodic potential. From this analysis we obtain a numerical factor of the order of 10, such that the activation energy for creep near criticality is of the order of 500 K. The same discussion also applies to the effective action for the tunneling process. The obtained values for $U_c^c$, $S_E^{\text{eff},c}$, and $j_c^c$ then compare quite favorably with experimental results on the YBCO compound (for $U_c^c$, see Yeshurun *et al.*, 1988, 1989; for $S_E^{\text{eff},c}$, see Griessen *et al.*, 1991 and Mota *et al.*, 1991; for $j_c^c$, see Dinger *et al.*, 1987, Worthington *et al.*, 1987, Krusin-Elbaum *et al.*, 1992, and Tamegai *et al.*, 1992).

The above results have been obtained using GL equations with coefficients determined by the BCS theory. However, the basic mechanism of superconductivity in the high-$T_c$ materials is still unknown at present, and the question may be asked how strongly our results depend on the underlying microscopic theory. Regarding the

case of $\delta T_c$ pinning, we are confident that our results are quite generally valid. Every basic mechanism generating a GL-type phenomenological theory will produce pinning due to spatial fluctuations in the transition temperature $T_c$, on which the GL parameter $\alpha$ depends explicitly. Since we are using experimental data for the $T_c$ dependence on carrier density $n$, we circumvent the problem of calculating the fluctuations of $T_c$ from first principles— the basic mechanism of superconductivity is taken care of in the dependence $T_c(n)$ as obtained from experiment. The situation for the case of $\delta l$ pinning is much less clear. The coefficient of the gradient term [$1/m$ in Eq. (2.1)] depends on the effect of (nonmagnetic) impurity scattering on the pairing of the carriers, so an exotic type of pairing mechanism may lead to a dependence of the coherence length on impurity scattering that differs from Gor'kov's (1959) result. However, the above analysis shows that at least one pinning mechanism (and seemingly the more important and robust one produced by $\delta T_c$ fluctuations) is strong enough to account for the experimentally observed critical current densities in the oxides, putting the assumption of weak collective pinning by point defects on firm ground.

### D. Dynamic approach

In this section we introduce the dynamic approach to the problem of flux pinning in superconductors. This technique was introduced by Schmid and Hauger (1973) and by Larkin and Ovchinnikov (1973), who also applied it to the calculation of the critical current density and the current-voltage characteristic (CVC) of an inhomogeneous superconductor in the mixed state. Feigel'man and Vinokur (1990) then improved this approach to include thermal fluctuations of the flux lines. Here we follow the paper of Vinokur *et al.* (1991), where this method has been generalized to describe the situation in the vortex-liquid state. In order to treat the pinning problem in a (viscous) vortex liquid, we need a formalism that accounts for the time evolution of the liquid structure. Indeed, the dynamic approach can be formulated in a very general way that can be used for all the different thermodynamic vortex phases. The dynamic approach is also more reliable than the method of dimensional estimates discussed above. In fact, the first calculation of the critical current density in the presence of a weak-pinning potential (Larkin and Ovchinnikov, 1973; Schmid and Hauger, 1973) was carried out within the framework of the dynamic approach rather than using the method of dimensional estimates. A perturbative approach is also very useful for determining the properties of the vortex structure itself. In this case the behavior of the corrections gives information about the relevance of the random pinning potential within the different thermodynamic vortex phases. For example, Nelson and Le Doussal (1990) used perturbation theory in their calculation of the structure factor for the vortex-liquid state and found a "Lorentzian-squared" correction due to the presence of

weak quenched disorder. Note that all results concerning the relevance of disorder in the different thermodynamic vortex phases are equivalent and independent of which quantity is actually calculated from the perturbation theory.

Within the dynamic approach we investigate the motion of the entire vortex structure under the action of the constant Lorentz force $j \wedge \mathbf{B}/c$ produced by an applied current density $j > j_c$ in the presence of a weak random potential. The latter is treated as a small perturbation; thus the approach is a perturbative one. At large current densities, $j \gg j_c$, the random potential is not important, and the vortices move with a velocity

$$v_0 = \frac{jB}{c\eta} ,$$  (3.86)

where $\eta$ is the viscous drag coefficient (Bardeen and Stephen, 1965) for the vortex lattice, $\eta = \eta_l/a_0^2 \simeq BH_{c_2}/\rho_n c^2$. The current-voltage curve is linear and can be characterized by the flux flow resistivity

$$\rho_{\text{flow}} \simeq \rho_n \frac{B}{H_{c_2}} .$$  (3.87)

The presence of quenched disorder will lead to a correction $\delta v$ to the velocity $v_0$, which we can determine using a perturbative approach. The key question then is how this correction will depend on the velocity $v_0$ or on the driving current density $j$. Let us start out at large velocities $v_0$, where these corrections are small, and monitor the size of the perturbation $\delta v$ as we reduce the velocity. If the correction $\delta v$ remains small compared to the velocity $v_0$ itself for arbitrarily small velocity $v_0$, $\delta v(v_0 \rightarrow 0) \ll v_0$, the current-voltage characteristic remains linear with a constant resistivity $\rho_{\text{flow}}$, and the effect of pinning is unobservable. A more complicated scenario is encountered in the vortex solid: Here the corrections $\delta v$ always diverge as $v_0 \rightarrow 0$. Pinning then becomes relevant as the correction to the velocity becomes of the order of the velocity itself, $\delta v(v_c) \sim v_c$, and the condition $\delta v(v_c) = v_c$ can be used to determine the critical current density,

$$j_c = \frac{c\eta}{B} v_c .$$  (3.88)

This actually corresponds to a definition of the critical current density $j_c$ as marking the onset of nonlinearity in the current-voltage characteristic, $\delta \rho(j_c) \simeq \rho_{\text{flow}}$. For current densities $j < j_c$ the random potential cannot be treated as a small perturbation any longer, and the dynamic approach breaks down in this regime.

The interaction energy (per unit volume) of the moving vortex structure with the random potential can be written as

$$E_{\text{pin}}(\mathbf{r}, \mathbf{u}) = \sum_{\nu} U_{\text{pin}}(\mathbf{r}) p[\mathbf{R} - \mathbf{R}_{\nu}(z, t) - \mathbf{v}t - \mathbf{u}_{\rho, \nu}(z, t)] ,$$

(3.89)

with $U_{pin}(\mathbf{r})$ the disorder potential and $p(\mathbf{R})$ the single-vortex form factors introduced above, Eqs. (2.33) and (2.34). The time dependence of the vortex positions due to thermal fluctuations has been included in the definition of $\mathbf{R}_\nu(z,t)$, $\mathbf{R}_\nu(z,t) = \mathbf{R}_\nu + \mathbf{u}_{th,\nu}(z,t)$, whereas the corrections due to the presence of the disorder potential are described by the displacement amplitude $\mathbf{u}_{p,\nu}(z,t)$. The velocity $\mathbf{v}$ of the moving vortex structure is given by

$$\mathbf{v} = \mathbf{v}_o - \delta\mathbf{v}$$

with

$$\mathbf{v}_o = \frac{\mathbf{j} \wedge \mathbf{B}}{\eta c} , \qquad (3.90)$$

the velocity of the unpinned structure generated by the Lorentz force, and $\delta\mathbf{v}$ denotes the small correction to the velocity caused by the disorder potential.

Let us consider the forces acting on a sample unit volume of the moving vortex structure: The Lorentz force density $\mathbf{F}_L = \mathbf{j} \wedge \mathbf{B}/c$ is counteracted by the viscous friction force density $\mathbf{F}_\eta = -\eta\mathbf{v}$, the pinning force density

$$\mathbf{F}_{pin}(\mathbf{r},\mathbf{u}) = -\sum_\nu U_{pin}(\mathbf{r}) \frac{\partial p[\mathbf{R} - \mathbf{R}_\nu(z,t) - \mathbf{v}t - \mathbf{u}_\nu(z,t)]}{\partial \mathbf{R}_\nu} , \qquad (3.91)$$

and internal forces due to intervortex interactions. Upon averaging over the disorder, we find that only the term nonlinear in $\mathbf{u}_{p,\nu}$ present in the pinning force $\mathbf{F}_{pin}$ will survive, whereas the term describing the intervortex interaction, which is linear in $\mathbf{u}_{p,\nu}$, will vanish. By Newton's third law the force equation then becomes

$$\langle\langle \mathbf{F}_L + \mathbf{F}_\eta + \mathbf{F}_{pin} \rangle\rangle = 0 , \qquad (3.92)$$

where $\langle\langle \cdots \rangle\rangle$ denotes average over both thermal and quenched disorder. Substituting in (3.92) the expressions for all the forces and using the definition (3.90) of the unperturbed velocity $\mathbf{v}_o$, we obtain the following equation determining the correction $\delta\mathbf{v}$ to the velocity $\mathbf{v}_o$:

$$\eta\delta\mathbf{v} = -\langle\langle \mathbf{F}_{pin} \rangle\rangle$$
$$= -\left\langle\left\langle \sum_\nu U_{pin}(\mathbf{r})\nabla_p(\mathbf{R} - \mathbf{R}_\nu - \mathbf{v}t - \mathbf{u}_{p,\nu}) \right\rangle\right\rangle . \qquad (3.93)$$

Here we consider weak pinning, in which the interaction of the vortices with the disorder potential is much smaller than the intervortex interaction. In this case the displacement field $\mathbf{u}_{p,\nu}$ due to pinning varies slowly on the scale of the intervortex distance, and we can drop the subscript $\nu$. Expanding $\mathbf{F}_{pin}$ in the displacement field $\mathbf{u}_p$, we obtain

$$\eta\delta\mathbf{v} = \left\langle\left\langle \sum_\nu U_{pin}(\mathbf{r})(\mathbf{u}_p \cdot \nabla)\nabla p(\mathbf{R} - \mathbf{R}_\nu - \mathbf{v}t) \right\rangle\right\rangle . \qquad (3.94)$$

Within a linear approximation the displacement field $\mathbf{u}_p$ due to the disorder potential is related to the pinning force $\mathbf{F}_{pin}$ by

$$u_{p,\alpha}(\mathbf{r},t) = \int d^3r' \, dt' \, G_{\alpha\beta}(\mathbf{r},\mathbf{r}';t,t') F_{pin,\beta}(\mathbf{r}',t') , \qquad (3.95)$$

where $G_{\alpha\beta}$ is the response function of the system. Substituting Eq. (3.95) into (3.94) and performing the average over the quenched disorder using $\langle U_{pin}(\mathbf{r})U_{pin}(\mathbf{r}')\rangle = \gamma_U\delta(\mathbf{r}-\mathbf{r}')$, we obtain

$$\eta\delta\mathbf{v} = \gamma_U \int dt' G(0,t-t') \sum_{\mu\nu} \langle (\nabla p[\mathbf{R} - \mathbf{R}_\mu(t') - \mathbf{v}t'] \cdot \nabla)\nabla p[\mathbf{R} - \mathbf{R}_\nu(t) - \mathbf{v}t] \rangle_{th} , \qquad (3.96)$$

where we have used $G_{\alpha\beta}(\mathbf{r},\mathbf{r};t,t') = \delta_{\alpha\beta}G(0,t-t')$. After Fourier transformation with respect to the planar coordinate $R$ we find

$$\eta\delta\mathbf{v} = -\gamma_U \int \frac{d^2K'}{(2\pi)^2} \frac{d^2K}{(2\pi)^2} dt' G(0,t-t')(\mathbf{K}' \cdot \mathbf{K})p(K')i\mathbf{K}p(K) \cdot \sum_{\mu\nu} \langle \exp[i\mathbf{K}' \cdot (\mathbf{R} - \mathbf{R}_\mu - \mathbf{v}t') + i\mathbf{K} \cdot (\mathbf{R} - \mathbf{R}_\nu - \mathbf{v}t)] \rangle_{th} . \qquad (3.97)$$

Finally, we have to take the average over the planar coordinate $\mathbf{R}$,

$$\frac{1}{V_L} \int dz \, d^2R \, e^{i(\mathbf{K}'+\mathbf{K})\cdot\mathbf{R}} \ldots = \frac{(2\pi)^2}{V_L}\delta(\mathbf{K}'+\mathbf{K})\int dz \ldots ,$$

with $V_L = Na_o^2L$ the volume of the sample with dimension $L$ along the $z$ axis, and obtain the result

$$\frac{\delta v}{v} = \frac{\gamma_U}{\eta a_o^2} \int \frac{d^2K}{(2\pi)^2} dt \, K^2K_v |p(K)|^2 G(0,t)S(\mathbf{K},t)\frac{\sin(K_v vt)}{v} . \qquad (3.98)$$

Here $a_o$ is the average distance (2.16) between the vortices and $K_v$ is the component of $\mathbf{K}$ along the flow direction $\mathbf{v}_o$ of the vortices. The structure factor $S(\mathbf{K},t)$ is given by the expression

$$S(\mathbf{K},t) = \frac{1}{NL} \int dz \sum_{\mu\nu} \langle \exp\{i\mathbf{K}\cdot[\mathbf{R}_\mu(z,0) - \mathbf{R}_\nu(z,t)]\} \rangle_{th} , \qquad (3.99)$$

where $N$ is the total number of vortices and $L$ is the length of the sample along the $z$ axis.

For the case of an individual vortex line, the same type of analysis can be carried through with the simple result that Eq. (3.98) for the relative velocity correction $\delta v/v$ is still valid if we replace $G(0,t)$ by the Green's function (2.114) for a single vortex $[G(0,t)=\Theta(t)(1/4\pi\varepsilon_0\eta_l t)^{1/2}]$ and use the expression $S(\mathbf{K},t)=\exp(-K^2\langle u^2(t)\rangle_{th}/2)$ with $\langle u^2(t)\rangle_{th}$ given by Eq. (2.116) for the structure factor. Note that $\eta a_o^2=\eta_l$, hence Eq. (3.98) can be rewritten to contain only single-vortex quantities.

Equation (3.98), which is the main result of this section, relates the behavior of the vortex system in a disordered potential to the intrinsic properties of the system described by the Green's function $G(0,t)$ and the structure factor $S(\mathbf{K},t)$. In the following sections we shall make use of this result in the study of the pinning properties of the vortex solid and the vortex-liquid phase.

### E. Elastic manifolds in periodic potentials

The main focus in this review is on the statistical mechanics and the dynamics of vortices in type-II superconductors subject to a disorder potential producing effects such as pinning and creep. A particularly interesting phenomenon in this respect is the "glassy" response of the system at low driving fields, which is characteristic of a true superconducting state with a vanishing resistivity at vanishing driving force. It is important to realize that the phenomenon of "glassy" response is *not* specific to the *randomness* of the pinning potential but is rather a consequence of the interplay between the pinning potential and the *elasticity* of the manifold considered. In particular, pinning, creep, and a "glassy" response of an elastic manifold can be realized as well if the potential is periodic. A typical example is given by the intrinsic pinning of the vortex lattice in layered superconductors for the case where the magnetic field is directed along the planes and the Lorentz force acts to push the vortices across the superconducting layers (Chakravarty, Ivlev, and Ovchinnikov, 1990a, 1990b).

In this section we investigate the phenomena of pinning and creep of an elastic manifold driven by an external force field and subject to a one-dimensional periodic potential (washboard potential). Our aim is threefold: First, we wish to investigate the dynamic behavior of the manifold in the limit of a vanishing driving force, as well as for driving forces near criticality. The response of the system under small driving forces crucially depends on the dimensionality $d$ of the manifold. We shall see that "glassy" behavior is not specific to random systems, but occurs in the present toy model as well for $d \geq 2$. This "glassy" response at small driving force is a consequence of the diverging radius of the critical nucleus placing the manifold into the neighboring pinning valley; see Fig. 13. Interestingly, the size of the critical nucleus diverges not only for low driving forces but also near criticality. Using dimensional estimates, we shall determine the ex-
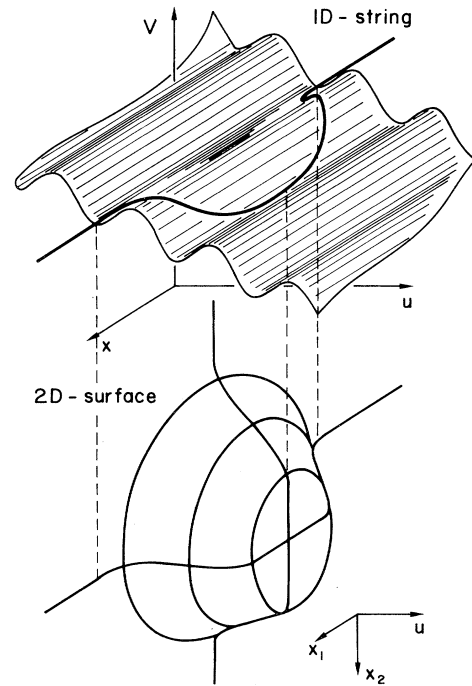


FIG. 13. Elastic manifold trapped in a (tilted) washboard potential. Top: One-dimensional elastic string with a finite segment (nucleus) activated to the next valley. The activation energy $2E_k$ involves the production of two kinks and remains always finite—the string is never in a "glassy" state. Bottom: Two-dimensional elastic surface with a finite nucleus activated to the next valley. The activation energy involves the creation of a one-dimensional (thin) wall, which costs an energy $2\pi rE_k$, where $r$ is the radius of the nucleus. If the nucleus is large enough, $r > r_c$, it expands and the elastic manifold moves on to the next valley. The critical radius $r_c$ increases with decreasing driving force $F$, $r_c=E_k/u_0 F$, and the manifold shows glassy behavior with a diverging activation energy at vanishing driving force, $U(F)=\pi E_k^2/u_0 F$.

ponents $\alpha$ and $\alpha_s$ describing the vanishing of the activation energy and the action near criticality [see Eq. (2.58)]. Second, we investigate the behavior of our system by means of the dynamic approach. We shall see that the dynamic approach is a very useful tool in determining the response of the system under an applied force. In spite of being a perturbative approach starting from the free limit at large forces, the dynamic approach clearly distinguishes between a glassy or a liquid phase, which is a thermodynamic property defined by the response under vanishing force. The experience gained with the dynamic approach in this well-defined situation will then be very helpful for the interpretation of the results obtained for the case of the vortex liquid subject to random disorder, as presented in Sec. VI below. Third, the periodic pinning potential allows for a quantitative determination of various quantities such as the critical force or the activation energy for creep. An analysis of the periodic pinning potential can therefore be used for obtaining an esti-

mate of the numerical factor quantifying the activation energy for creep.

## 1. Droplet model

Let us consider a $d$-dimensional elastic manifold (elasticity $C$) embedded in a $(d+1)$-dimensional space and subject to the tilted washboard potential $V(u)$,

$$V(u) = V_0(1 - \cos k_0 u) - Fu \ . \tag{3.100}$$

We call $u$ the transverse dimension. $V_0$ characterizes the strength of the pinning potential, and $k_0$ is related to the distance $u_0$ between neighboring minima via $k_0 = 2\pi/u_0$. Finally, $F$ is the applied force driving the manifold along the transverse direction $u$. The critical force $F_c$ is determined by the condition $\partial_u V(u) \leq 0$, i.e., $F_c = k_0 V_0$ is the maximal force for which metastable minima can exist.

Let us first consider creep near criticality, $F \lesssim F_c$, and determine the behavior of the activation energy $U(F)$ for classical creep as well as the action $S(F)$ for quantum creep. At criticality, both these quantities vanish, and the manifold depins:

$$U(F) \simeq U_c \left[ 1 - \frac{F}{F_c} \right]^\alpha \ , \tag{3.101}$$

$$S(F) \simeq S_c \left[ 1 - \frac{F}{F_c} \right]^{\alpha_S} \ . \tag{3.102}$$

The original theory of classical creep (Anderson, 1962; Anderson and Kim, 1964) assumes $\alpha = 1$ for the case of a three-dimensional vortex lattice pinned by a random potential. The actual values of the exponents $\alpha$ and $\alpha_S$ for a random pinning potential are not known. The present discussion of the periodic washboard potential may shed some light on this very nontrivial issue.

The dynamic behavior of the system is determined by the size of the critical nucleus (Langer, 1967), which we can determine by the method of dimensional estimates. With a free energy given by

$$\mathscr{F}[u] = \int d^d x \left[ \frac{C}{2} (\nabla u)^2 + V(u) \right] \ , \tag{3.103}$$

the energy of a distortion of the elastic manifold by $u$ on a scale $L$ is estimated to be

$$\mathscr{E}(u, L) \simeq \left[ \frac{C}{2} \left[ \frac{u}{L} \right]^2 + V(u) \right] L^d \ . \tag{3.104}$$

Close to the critical force $F_c$ we can expand the potential $V(u)$,

$$V(u) = \frac{45}{4} V_F \left[ \left[ \frac{u}{u_F} \right]^2 - \left[ \frac{u}{u_F} \right]^3 \right] \ , \tag{3.105}$$

with

$$V_F = V_0 \left[ 1 - \frac{F}{F_c} \right]^{3/2} \quad \text{and} \quad u_F = \frac{3u_0}{2\pi} \left[ 1 - \frac{F}{F_c} \right]^{1/2} \ . \tag{3.106}$$

The critical displacement $u_F$, which depins the manifold, scales with the applied force $F$ according to $(1 - F/F_c)^{1/2}$. The barrier $V_F$ to be overcome (potential-energy density) scales with $u^3 \propto (1 - F/F_c)^{3/2}$ and competes with the elastic-energy density $C(u/L)^2$. This competition determines the length scale $L$ of the saddle-point configuration, which becomes

$$L \simeq u_0 \left[ \frac{C}{V_0} \right]^{1/2} \left[ 1 - \frac{F}{F_c} \right]^{-1/4} \ . \tag{3.107}$$

Finally, the energy barrier for thermal activation of the manifold out of the pinning potential is

$$U(F) \simeq u_0^d V_0 \left[ \frac{C}{V_0} \right]^{d/2} \left[ 1 - \frac{F}{F_c} \right]^\alpha \ , \tag{3.108}$$

with

$$\alpha = \frac{6-d}{4} \ . \tag{3.109}$$

In order to obtain the exponent $\alpha_s$ governing quantum creep near criticality, we have to determine the time evolution of the critical nucleus, and hence we have to consider the (Euclidean) action for the process, which for the massive manifold is given by

$$\mathscr{S}_E(u) = \int dt \left\{ \int d^d x \frac{M}{2} \left[ \frac{du}{dt} \right]^2 + \mathscr{F}[u] \right\} \ . \tag{3.110}$$

Equation (3.110) is a $(d+1)$-dimensional uniaxially anisotropic generalization of Eq. (3.103), and simple rescaling of the (imaginary) time axis $t \rightarrow (C/M)^{1/2} t$ renders the problem isotropic again. Substitution of $d \rightarrow d+1$ in Eq. (3.108) and multiplication with the scaling factor $(M/C)^{1/2}$ leads to the result

$$S_E(F) \simeq u_0^{d+1} V_0 \left[ \frac{C}{V_0} \right]^{d/2} \left[ \frac{M}{V_0} \right]^{1/2} \left[ 1 - \frac{F}{F_c} \right]^{\alpha_S} \ , \tag{3.111}$$

with

$$\alpha_S = \frac{5-d}{4}, \quad \text{massive manifold} \ . \tag{3.112}$$

Note that the tunneling time $t$ also diverges at criticality,

$$t \simeq u_0 \left[ \frac{M}{V_0} \right]^{1/2} \left[ 1 - \frac{F}{F_c} \right]^{-1/4} \ . \tag{3.113}$$

For the overdamped situation we have to replace the kinetic energy in Eq. (3.110) by a term (Caldeira and Leggett, 1981, 1983)

$$\frac{M}{2} \left[ \frac{du}{dt} \right]^2 \rightarrow \frac{\eta}{4\pi} \int dt' \left[ \frac{u(t) - u(t')}{t - t'} \right]^2 \tag{3.114}$$

leading to a tunneling time $t \propto L^2$, more precisely,

$$t \simeq u_0^2 \frac{\eta}{V_0} \left[ 1 - \frac{F}{F_c} \right]^{-1/2} . \tag{3.115}$$

The action for quantum creep is given by $S_E(F) \simeq t U(F)$, and we obtain

$$S_E^{\text{eff}}(F) \simeq u_0^{d+2} V_0 \left[ \frac{C}{V_0} \right]^{d/2} \frac{\eta}{V_0} \left[ 1 - \frac{F}{F_c} \right]^{\alpha_S} , \tag{3.116}$$

with

$$\alpha_S = \frac{4-d}{4}, \quad \text{overdamped manifold .} \tag{3.117}$$

Hence the exponent for quantum creep is reduced due to the appearance of the additional divergent time scale near criticality.

The Hall tunneling case is somewhat special. Here we additionally need the scaling behavior for the transverse distance $u_y$ traced out during the tunneling motion. For the model potential (2.102), this scaling behavior is easily obtained by comparing the transverse energy $f u_y^2 / 2$ with the height $V_0(F)$ of the potential; see Eq. (3.106). With $u_y \propto (1 - F/F_c)^{3/4}$ we obtain for a point vortex the result $S_E^H(j) \simeq S_E^H (1 - j/j_c)^{5/4}$ and for a vortex line $S_E^H(j) \simeq S_E^H (1 - j/j_c)$. Note that the result for a pointlike particle is identical with the result for a massive particle ($d = 0$) moving in a 1D potential. The scaling behavior of $u_y$ (as well as that of $u_x$) depends on the specific form of the potential close to the saddle.

The scaling analysis of the creep near criticality shows that the relevant spatial scales of the critical nucleus diverge at criticality. It would be very interesting to study whether this feature is specific to our model potential or is a general characteristic of the critical state and hence would also be present for the case of a random pinning potential.

Next, let us turn to small driving forces, $F \ll F_c$. As the driving force $F$ approaches zero, the energy gain of the manifold due to transverse motion decreases. On the other hand, the energy cost to throw a finite part of the manifold into the neighboring pinning valley (see Fig. 13) remains large, i.e., it is not reduced by a small parameter. However, the energy gain due to the driving force is a *volume* effect, whereas the energy cost to deform the manifold scales only with the *surface* of the nucleus. Hence, for a small driving force $F \to 0$, we expect that the critical nucleus will be large, and we can adopt the thin-wall approximation, which assumes that the distorted regime of the manifold (surface of the nucleus) is small as compared with the size of the nucleus itself. For the isotropic situation considered here, the nucleus is spherically symmetric and the energy $E_k$ of the wall is obtained by a simple integration of the Euler-Lagrange equations of (3.103),

$$E_k = \frac{8}{k_0} (C V_0)^{1/2} . \tag{3.118}$$

The total energy for formation of a nucleus of size $r$ is then

$$\mathscr{E}(r) \approx E_k S_d(r) - u_0 F V_d(r) , \tag{3.119}$$

where $V_d = \pi^{d/2} r^d / \Gamma(1 + d/2)$ [$\Gamma(x)$ denotes the gamma function] and $S_d = \partial_r V_d$ denote the volume and the surface of the $d$-dimensional nucleus, respectively. The second term in Eq. (3.119), favoring formation of the nucleus, is the energy gain due to the displacement of the manifold by a distance $u_0$ in the force field $F$. The saddle point is determined by the extremal condition $\partial_r \mathscr{E}(r) = 0$, from which we obtain

$$r_c = \frac{(d-1) E_k}{u_0 F} . \tag{3.120}$$

When we insert this result back into Eq. (3.119), the activation energy becomes

$$U(F) \approx \frac{\sqrt{\pi} E_k}{\Gamma(1 + d/2)} \left[ (d-1) \sqrt{\pi} \frac{E_k}{u_0 F} \right]^{d-1} . \tag{3.121}$$

The action for the tunneling of a massive manifold is easily obtained from the classical result (3.121) by going over to the corresponding $(d+1)$-dimensional problem with a proper scaling of the time axis, and we find

$$S(F) \approx \frac{\sqrt{\pi M / C} E_k}{\Gamma(3/2 + d/2)} \left[ d \sqrt{\pi} \frac{E_k}{u_0 F} \right]^d . \tag{3.122}$$

The result (3.122) shows an interesting feature: Expressing the action through the radius $r_c$ of the nucleus, we find that $S \propto r_c^d$. This result can be obtained by letting the manifold tunnel as a "solid" object, in which case the total mass $M r_c^d$ has to tunnel under the barrier $V_0 r_c^d$, resulting in the action $u_0 (M r_c^d V_0 r_c^d)^{1/2} \propto r_c^d$. Alternatively, the manifold can exploit its elastic properties and create a thin-wall nucleus of mass $M r^{d-1}$, the mass of the wall, which tunnels under the potential $V_0 r^{d-1}$. The wall then has to move a distance $\propto r_c$, and hence the total action is again $\int dr (M r^{d-1} V_0 r^{d-1})^{1/2} \propto r_c^d$. This result is very different from the thermal case, where we have to pay an energy $\sim V_0 r_c^d$ if we lift the manifold as a "solid" object over the barrier; the motion via creation of a thin-wall nucleus involves only an activation energy $\propto r_c^{d-1}$. The reason behind this difference is that time is irrelevant in classical motion, but relevant in quantum motion. Hence an elastic manifold can take more advantage of its elasticity in classical creep than in the quantum creep case.

Let us return to the classical case (3.121) and consider dimensions $d > 2$: For vanishing driving force, $F \to 0$, the activation energy for creep diverges, $U(F) \propto F^{-(d-1)}$, and the manifold is in a "glassy" state, i.e., its low-field dynamic response is highly sublinear. This result is not changed by thermal fluctuations, as in dimensions $d > 2$ the correlator $\langle [u(\mathbf{r}, t) - u(0, 0)]^2 \rangle_{\text{th}}$ never diverges. On the other hand, in one dimension (the string problem) the surface of the nucleus consists of two kinks, which are

pointlike objects, and therefore the activation energy is always finite. As a result, the string is in a "liquid" state, where the term "liquid" here is used to describe a system with a characteristic linear response under small driving forces. The two-dimensional case is marginal. Here thermal fluctuations lead to a roughening transition (Burton, Cabrera, and Frank, 1951; Chui and Weeks, 1976) at a finite temperature $T_R$. This transition is of the Berezinskii-Kosterlitz-Thouless type (Berezinskii, 1971; Kosterlitz and Thouless, 1973; Pokrovskii and Uimin, 1973; Kosterlitz, 1974; José *et al.*, 1977) and can be characterized by a change in the long-distance behavior of the correlator $\langle [u(\mathbf{r},t)-u(0,0)]^2 \rangle_{\mathrm{th}}$. At small temperatures this correlator remains finite, whereas for $T > T_R$ the periodic potential $V_{\mathrm{o}} \cos k_{\mathrm{o}} u$ becomes irrelevant, and the correlator diverges logarithmically. As a consequence, the manifold is in a "glassy" state at low temperatures, $T < T_R$ [with diverging barriers; see Eq. (3.121)], and undergoes a finite-temperature phase transition to a liquid at $T = T_R$. In summary, we conclude that "dynamic glassiness" is *not* specific to randomness but rather a consequence of the competition between the elasticity of the manifold and the pinning potential.

### 2. Dynamic approach

In this section we investigate the dynamic approach as applied to the problem of pinning in a periodic potential. In particular, we are interested in understanding how far the dynamic approach is able to reproduce the results obtained above, where we followed a more conventional line of thought. This will provide us with an understanding of the predictive power of the dynamic approach, which will be very helpful in the analysis of the liquid-vortex phase in Sec. VI below.

Let us start by writing down the expression for the perturbative correction $\delta v$ to the velocity $v$. Following the analysis in Sec. D above, we obtain

$$\eta \delta v = \frac{\partial}{\partial u_p} V[vt + u_{\mathrm{th}}(\mathbf{x},t) + u_p(\mathbf{x},t)] , \qquad (3.123)$$

with $u_p$ the correction to the displacement field $u$ due to the presence of the pinning potential, to lowest order,

$$u_p(\mathbf{x},t) = -\int d^d x' \, dt' \, G(\mathbf{x},\mathbf{x}';t,t')$$

$$\times \partial_u V[vt' + u_{\mathrm{th}}(\mathbf{x}',t')] . \qquad (3.124)$$

Here $G(\mathbf{x},\mathbf{x}';t,t')$ denotes the (real-space) Green's function of the $d$-dimensional elastic manifold. Expanding Eq. (3.123) to lowest order in $u_p$ and using the Fourier representation

$$V_p(k) = \pi V_{\mathrm{o}} [2\delta(k) + \delta(k + k_{\mathrm{o}}) + \delta(k - k_{\mathrm{o}})] \qquad (3.125)$$

for the pinning potential $V_p$, we arrive at

$$\frac{\delta v}{v} = \frac{V_{\mathrm{o}}^2 k_{\mathrm{o}}^3}{2\eta} \int d^d x \, dt \, G(\mathbf{x},t)$$

$$\times \frac{\sin v k_{\mathrm{o}} t}{v} \exp[-\tfrac{1}{2} k_{\mathrm{o}}^2 \langle u_{\mathrm{th}}^2(\mathbf{x},t)\rangle] , $$

$$(3.126)$$

with $\langle u_{\mathrm{th}}^2(\mathbf{x},t)\rangle = \langle [u_{\mathrm{th}}(\mathbf{x},t) - u_{\mathrm{th}}(0,0)]^2 \rangle$.

Consider first the zero-temperature limit, where $\langle u_{\mathrm{th}}^2(\mathbf{x},t)\rangle = 0$. Using the elastic Green's function $G(\mathbf{q},\omega) = 1/(-i\eta\omega + Cq^2)$, we obtain, after integration over space and time, the final result

$$\frac{\delta v}{v} = \frac{V_{\mathrm{o}}^2 k_{\mathrm{o}}^2}{2\eta^2 v^2} . \qquad (3.127)$$

The condition

$$\frac{\delta v}{v} = \frac{1}{2} , \qquad (3.128)$$

then results in a critical force $\eta v_c = V_{\mathrm{o}} k_{\mathrm{o}}$, which agrees with the value $F_c = V_{\mathrm{o}} k_{\mathrm{o}}$ as obtained from the usual condition $\partial_u V(u)|_{F=F_c} \leq 0$ for criticality.

Next let us discuss the effects of finite temperature. Using the fluctuation-dissipation theorem (Landau and Lifshitz, 1958b), we find that the thermal displacement correlator $\langle u_{\mathrm{th}}^2(\mathbf{r},t)\rangle$ becomes

$$\langle u_{\mathrm{th}}^2(\mathbf{x},t)\rangle = 4T \int \frac{d^d q}{(2\pi)^d} \frac{d\omega}{2\pi} [1 - \cos(\mathbf{q}\mathbf{x} - \omega t)]$$

$$\times \frac{1}{\omega} \mathrm{Im} G(\mathbf{q},\omega) , \qquad (3.129)$$

which, after integration over frequency, reduces to

$$\langle u_{\mathrm{th}}^2(\mathbf{x},t)\rangle = \frac{2T}{C} \int \frac{d^d q}{(2\pi)^d} \frac{1}{q^2} \mathrm{Re}[1 - e^{i\mathbf{q}\mathbf{x}} e^{-(C/\eta)q^2 t}] .$$

$$(3.130)$$

Integration over $\mathbf{q}$ then leads to the result

$$\langle u_{\mathrm{th}}^2(\mathbf{x},t)\rangle \approx \frac{T}{\pi C x_{\mathrm{o}}^d} x_{\mathrm{o}}^2 \begin{cases} s(x,t), & d=1 , \\ \ln[s(x,t)], & d=2 , \\ \left[1 - \dfrac{1}{s(x,t)}\right], & d=3 , \end{cases}$$

$$(3.131)$$

where $s$ can be approximated by

$$s(x,t) \approx \left[ \frac{x^2 + (C/\eta)t}{x_{\mathrm{o}}^2} \right]^{1/2} . \qquad (3.132)$$

An exact result for the interpolation formula (3.132) has been given by Koshelev and Vinokur (1993) for the case $d = 1$. Here $x_{\mathrm{o}}$ denotes a short-distance cutoff given by the internal structure of the manifold. The simplest case to analyze is that of three dimensions and higher, where the displacement correlator $\langle u_{\mathrm{th}}^2(\mathbf{r},t)\rangle$ converges to a

finite value. The relative correlation $\delta v/v$ is then merely reduced by the Debye-Waller factor, $\exp(-Tk_o^2 x_o^2/2\pi C x_o^d)$, and hence still diverges as the driving force is reduced to zero; see Fig. 14. Let us compare this result with the analysis in Sec. III.E.1. There we found [see Eq. (3.121)] that the activation energy $U(F)$ of the critical nucleus for motion across the pinning barrier diverges as the driving force $F$ vanishes, and hence the manifold is in a glassy state. Thus we conclude that a velocity ratio $\delta v/v$, as obtained from the dynamic approach, which diverges at small velocities, $v \to 0$, is indeed characteristic of a glassy state. If this is true, then in one dimension the dynamic approach should produce a finite correction $\delta v/v$ at vanishing driving force, since the critical nucleus involves only a finite energy $U(F) \simeq 2E_k$ in this case. At any nonzero temperature this nucleus can be thermally activated at a finite rate, and the string will move with a velocity proportional to the driving force. The one-dimensional string in a periodic pinning potential then is not in a glassy state, in
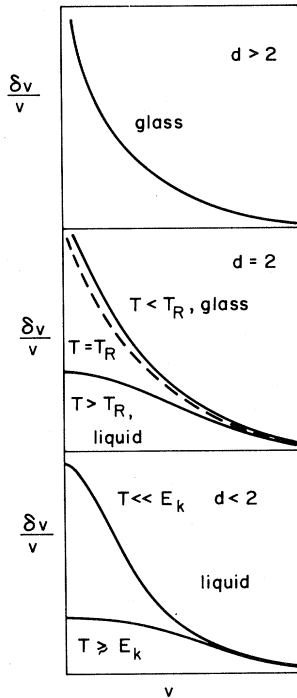


FIG. 14. Relative velocity correction $\delta v/v$ vs velocity $v$ of a driven elastic manifold as calculated via the dynamic approach. In the one-dimensional situation, the relative correction $\delta v/v$ remains finite, which is consistent with the finite activation barrier $2E_k$ against creep. For a three-dimensional manifold, the ratio $\delta v/v$ diverges at vanishing driving force ($v \to 0$), signalling the divergence of the corresponding activation barrier against creep. The two-dimensional case is intermediate between the two extreme cases discussed above. Below the roughening transition ($T < T_R$), the response $\delta v/v$ diverges and the system is in a glassy state, whereas above the roughening transition ($T > T_R$) the relative correction $\delta v/v$ remains finite and hence the surface shows the response of a liquid.

contrast to the string subject to *random* disorder. In fact, the dynamic approach provides a result fully consistent with this scenario. The relative correction to the velocity is given by

$$\frac{\delta v}{v} = \frac{V_o^2 k_o^3}{2\eta} \int dx\, dt\, \Theta(t) \frac{\exp(-\eta x^2/4Ct)}{\sqrt{4\pi C\eta t}} \frac{\sin v k_o t}{v}$$
$$\times \exp\left[-\frac{2\pi T}{u_o^2 C}[x^2+(C/\eta)t]^{1/2}\right]. \quad (3.133)$$

As the velocity $v$ approaches zero, the cutoff in the time integral is provided by the last factor, allowing for expansion of the velocity-dependent factor $\sin(vk_o t)/v \simeq k_o t$. The (finite) result of the integration is independent of velocity, and thus $\delta v/v$ is finite for all velocities, which is the characteristic feature of a nonglassy or liquid state. For small temperatures, $\delta v/v \gg 1$ as $v$ vanishes, indicating a strongly suppressed linear response to the driving force, whereas at high temperatures $\delta v/v$ is always small and the string is essentially free; see Fig. 14. The results of the dynamic approach can be understood in the following way: For the one-dimensional case, the activation barrier for motion is finite, and hence for temperatures $T > 2E_k$ the pinning potential is irrelevant. On the other hand, for the three-dimensional situation, the barrier diverges with vanishing force, and pinning is relevant at all temperatures.

Finally, let us consider the two-dimensional marginal case. The relative correction to the velocity is given by

$$\frac{\delta v}{v} = \frac{V_o^2 k_o^3}{2\eta} \int d^2x\, dt\, \Theta(t) \frac{\exp(-\eta x^2/4Ct)}{4\pi Ct}$$
$$\times \frac{\sin v k_o t}{v} \left[\frac{x_o^2}{x^2+(C/\eta)t}\right]^\beta, \quad (3.134)$$

with $\beta = Tk_o^2/4\pi C$. Integration over the space coordinate provides an additional factor $t$ such that the decisive final integration over time becomes

$$\int dt\, \Theta(t) t^{1-\beta} \to \begin{cases} \infty, & \beta < 2, \\ < \infty, & \beta > 2, \end{cases} \quad (3.135)$$

where we have again expanded the factor $\sin v k_o t \simeq v k_o t$ for $v \to 0$. At low temperatures, $T < T_R = 8C\pi/k_o^2$, the manifold is in a glassy state, whereas at high temperatures the manifold will exhibit nonglassy creep; see Fig. 14. The finite transition temperature $T_R$ for depinning is nothing but an estimate for the roughening transition temperature of a two-dimensional interface trapped in a cosine potential (Chui and Weeks, 1976).[5] Hence, in the two-dimensional case, the dynamic approach exactly

---

[5]Note that during the mapping of the roughening problem to the Coulomb gas problem of Kosterlitz and Thouless (1973), the temperature is inverted; hence the low-temperature Coulomb gas phase (Berezinskii phase) corresponds to the high-temperature rough phase in the roughening problem.

reproduces our knowledge about the dynamic behavior of an elastic manifold in a periodic potential as derived via the conventional approach.

We obtain the following consistent picture (Fig. 14): The thermodynamic state of the manifold can be found by determining the relative velocity correction $\delta v / v$ under infinitesimal driving force $(v \rightarrow 0)$. If this ratio diverges, the manifold is in a glassy state characterized by infinite barriers against motion under vanishing applied driving forces. This is the result found in three and higher dimensions. A finite ratio $\delta v / v$, on the other hand, is the characteristic of a liquid state, where the response under an external force field is linear at small fields. The string in a periodic potential therefore is always in a liquid state, in strong contrast to the situation in a random pinning potential, where the single string is characterized by a "glassy" response (Feigel'man, 1983). Finally, in two dimensions, the manifold is in a glassy state at low temperatures, $T < T_R$ (nonlinear, i.e., glassy response), and performs a transition to a liquid state (with a linear response) at a finite temperature $T_R$. The transition from the "glassy" to the "liquid" state is nothing but the roughening transition.

### 3. Intervalley and intravalley energy scales

As has already been mentioned in Sec. C above, we have to distinguish between two different types of "pinning energies" $U_c$. Let us concentrate on a single vortex. If we are interested in the behavior of the vortex within its pinning valley, the relevant transverse length scale we should consider is the typical extent of the valley, which is given by the core radius $\sqrt{2}\xi$. Quantities involving this *intravalley* pinning energy are the critical current density $j_c$ and the depinning energy $\tilde{T}^s_{\mathrm{dp}}$. On the other hand, the process of creep involves thermal activation of the vortex to the neighboring valley, which is further away than $\sqrt{2}\xi$ and therefore involves larger distances and thus larger elastic energies. The creep process then involves the *intervalley* pinning energy which we expect to be larger than its intravalley counterpart by a numerical factor. Here we shall use the well defined situation of a vortex trapped within a periodic pinning potential in order to obtain an estimate for this numerical factor, which enhances the intervalley pinning energy relevant for creep over the intravalley energy relevant for $j_c$.

The activation energy $U(F)$ for thermal creep of an elastic string in a washboard potential has been discussed in detail in the work of Büttiker and Landauer (1981). At small driving forces, $F \rightarrow 0$, the saddle-point solution to the free energy is given by two well separated kinks of energy $E_k = 8(CV_0)^{1/2}/k_0$, interacting only weakly, hence $U(F) \simeq 2E_k$, which is a special case of the above result (3.121). Near the critical force $F_c$, the thin-wall approximation breaks down and the activation energy $U(F)$ has to be calculated by integration of the differential equation determining the saddle-point configuration. The result is

$$U(F) = U_c \left[ 1 - \frac{F}{F_c} \right]^{5/4}, \qquad (3.136)$$

with

$$U_c = \frac{6}{5}2^{1/4}E_k = \frac{24}{5\pi}2^{1/4}\left[ \frac{\varepsilon_0 j_c \Phi_0 u_0^3}{2\pi c} \right]^{1/2}. \qquad (3.137)$$

Here we have replaced $C$ by the elasticity $\varepsilon_0$ of the vortex and expressed the amplitude $V_0$ of the periodic pinning potential via the critical force $F_c = k_0 V_0 = j_c \Phi_0 / c$, where the last equation relates the critical force $F_c$ to the depinning current density $j_c$. The final step is to relate the length scales $u_0$ and $\xi$ of the periodic and the random pinning potentials. This is done by requiring that the length scales defined by the mean energy-to-force ratio be the same for both potentials,

$$\frac{\langle (\partial_u V)^2 \rangle}{\langle V^2 \rangle} = \frac{\langle (\partial_u \mathscr{E}_{\mathrm{pin}})^2 \rangle}{\langle \mathscr{E}_{\mathrm{pin}}^2 \rangle}. \qquad (3.138)$$

The forces generated by the two potentials are easily found to be $\langle (\partial_u V)^2 \rangle = \langle V^2 \rangle k_0^2$ and $\langle (\partial_u \mathscr{E}_{\mathrm{pin}})^2 \rangle = \langle \mathscr{E}_{\mathrm{pin}}^2 \rangle / 6\xi^2$, hence

$$u_0 = 2\sqrt{6}\pi\xi. \qquad (3.139)$$

Inserting Eq. (3.139) into (3.137), we obtain for the intervalley energy scale of the random potential the result

$$U_c \approx 20 H_c^2 \xi^3 \left[ \frac{j_c}{j_0} \right]^{1/2}. \qquad (3.140)$$

Hence the energy scale for creep (saddle point of the free-energy functional) differs from the energy scale for pinning (minimum of the free-energy functional) by a numerical factor of the order of 10. In comparing our theoretical results with experiments, we always have to analyze which energy scale is involved in the quantity measured. For example, the critical current density $j_c$ and the depinning energy $\tilde{T}^s_{\mathrm{dp}}$ are determined by the intravalley energy scale, $U_c \simeq H_c^2 \xi^3 (j_c / j_0)^{1/2}$, whereas the logarithmic decay rate of the magnetization involves the intervalley energy scale, $\sim 10 U_c$.

### F. Elastic manifolds in quenched random media

During the past decade a great variety of physical systems has emerged that can be subsumed under the title of elastic manifolds in quenched random media. A first straightforward classification of these systems is given by the dimensionalities $d$ and $n$ of the elastic manifold itself and of its motional degrees of freedom, respectively. The most prominent examples are the "domain-wall problems" (DW, $n = 1$), where a $d$-dimensional elastic interface is roughened in a nontrivial manner due to the presence of randomness, and the "directed-polymer problems" (DP, $d = 1$), where a one-dimensional elastic string

performs large transverse excursions induced by an underlying random potential. Typical physical realizations are domain walls in Ising systems (Huse and Henley, 1985), limiting interfaces in flow problems (Huse and Guyer, 1979; Rhyner and Blatter, 1989), growth of directed polymers (Kardar and Zhang, 1987), the motion of dislocations in disordered media (Ioffe and Vinokur, 1987), the pinning of individual vortex lines in inhomogeneous superconductors (Nattermann and Lipowsky, 1988), or, via mapping to the Burgers equation (Kardar, Parisi, and Zhang, 1986; Medina *et al.*, 1989), the growth of Eden clusters (Wolf and Kertész, 1987) and ballistic deposition (Kim and Kosterlitz, 1989). In $D=2$ space dimensions, DW and DP problems become equivalent. Other systems combining features of DW with $d \geq 1$ and DP with $n \geq 1$ are pinned charge-density waves ($d=D$, $n=1$; Nattermann, 1990) and vortex lattices in bulk superconductors ($d=D$, $n=2$, Feigel'man *et al.*, 1989; Nattermann, 1990). All these systems can be described by a generic Hamiltonian

$$\mathcal{H} = \int d^d x \left\{ \frac{C}{2}(\nabla u)^2 + E_d(\mathbf{x}, \mathbf{u}) \right\} , \qquad (3.141)$$

where $\mathbf{u}(\mathbf{x})$ denotes the $n$-component displacement field of the elastic manifold. The manifold itself is characterized by an elasticity modulus $C$ and subject to the disorder potential $E_d$. The latter is usually characterized by correlated randomness of the Gaussian type, with mean zero and a variance

$$\langle E_d(\mathbf{x}, \mathbf{u}) E_d(\mathbf{x}', \mathbf{u}') \rangle = \Delta \delta^d(\mathbf{x} - \mathbf{x}') R^n(\mathbf{u} - \mathbf{u}') . \qquad (3.142)$$

The disorder correlator $R^n(u)$ is assumed to show an asymptotic power-law behavior, $R^n(u) \sim u^{-\beta(n)}$.

For the special case of short-range correlated disorder, $R^n$ becomes a $\delta$ function, $R^n(\mathbf{u} - \mathbf{u}') = \delta^n(\mathbf{u} - \mathbf{u}')$, i.e., $\beta(n) = n$ from scaling arguments. A prototype example for this case is the Ising model with random-bond disorder; see, for example, Huse and Henley (1985).

On the other hand, $R^n(u)$ can be long ranged, as is the case in the random-field disordered Ising model, where $\beta(n) = -n$ (Grinstein and Ma, 1983). For the single-vortex problem, $d=1$, $n=2$, $C=\varepsilon_l$, $E_d = \varepsilon_{\text{pin}}$, $\beta(2) = 2$, and Eq. (3.141) is equivalent to (2.31) with $\mathbf{f}_L = 0$. Similarly, for a vortex lattice, $d=3$, $n=2$, and $E_d$ is given by the random pinning potential $E_{\text{pin}}$ with $\mathbf{v} = 0$ [see Eq. (3.89)], whereas the elastic term is slightly more complicated [see Eq. (3.29) or (3.37)].

Here we shall concentrate on two main aspects of elastic manifolds. First we discuss the statistical mechanics of elastic interfaces subject to quenched random disorder. We shall see that the statistical mechanics of these objects is strongly affected by the competition between many metastable minima, which leads to a nontrivial scaling behavior of the low-energy states of the manifold regarding fluctuations in their displacement field and in their energy. In subsection III.F.2 we focus on the dynamic behavior of these manifolds. Here we follow the

ideas of Ioffe and Vinokur (1987; see also Nattermann, Shapir, and Vilfan, 1990), who describe the creep-type dynamics of the manifold as a nucleation process, in which a finite cell of the manifold (nucleus) has to be activated across the pinning barrier to the next low-lying metastable state. This approach is very similar in spirit to that used in the problem of metastability in a first-order phase transition, as studied by Langer (1967; see also Langer and Fisher, 1976; Lifshitz and Pitaevskii, 1981). Langer found that, to exponential accuracy, the transition rate is determined by a single generalized coordinate of the system, which is the size of the critical nucleus. This idea is also at the basis of our discussion of the dynamic behavior of elastic manifolds in a periodic potential, as presented in Sec. III.E above. However, for a random pinning potential it is crucial to account for the nontrivial scaling results characterizing the statistical mechanics properties of the manifold. In particular, our analysis of the dynamics will rely on the very basic assumption that an elastic manifold in a random potential develops only a single scale describing all the energy fluctuations at large distances, and therefore the barriers separating low-lying metastable states scale in the same manner as the fluctuations in energy between the low-lying states themselves (Ioffe and Vinokur, 1987).

### 1. Statistical mechanics

One of the major issues in the field of elastic manifolds in random media concerns the (large-distance, $L > L_c$) scaling behavior of the transverse fluctuations of the manifold (see Fig. 15),

$$\langle\langle [\delta u(L)]^2 \rangle\rangle^{1/2} \equiv \langle\langle [\mathbf{u}(\mathbf{L}) - \mathbf{u}(0)]^2 \rangle\rangle^{1/2} \propto L^{\zeta_{d,n}} .$$

$$(3.143)$$

as well as the scaling of the fluctuations in free energy $\mathcal{F}(L)$,
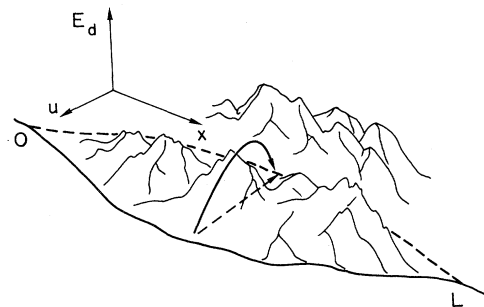


FIG. 15. Elastic string in a quenched random environment. Two low-lying metastable states differing from one another on a length $L$ are shown. The crucial quantities to be found are the transverse distance $u(L)$ between the two states and the energy barrier $\mathcal{E}^b$ separating them. Of particular relevance is the nontrivial scaling behavior $u \propto L^\zeta$ and $\mathcal{E}^b \propto L^\chi$ of these two quantities.

$$\langle\langle\, [\delta\mathcal{F}(L)]^2\,\rangle\rangle^{1/2} \equiv \langle\langle\, [\mathcal{F}(L) - \langle\langle\,\mathcal{F}(L)\,\rangle\rangle]^2\,\rangle\rangle^{1/2}$$

$$\propto L^{\chi_{d,n}} \; . \tag{3.144}$$

Here $\langle\langle\,\cdots\,\rangle\rangle$ denotes an average taken over both dynamic and quenched variables,

$$\langle\langle\, A\,\rangle\rangle = \left\langle \frac{\int \mathcal{D}[\mathbf{u}(\mathbf{x})]\, A\, e^{-\mathcal{H}[\mathbf{u}(\mathbf{x})]/T}}{\int \mathcal{D}[\mathbf{u}(\mathbf{x})]\, e^{-\mathcal{H}[\mathbf{u}(\mathbf{x})]/T}} \right\rangle_{\text{disorder}} \; . \tag{3.145}$$

At low temperatures, the main contribution to the average $\langle\langle\,\cdots\,\rangle\rangle$ is due to the low-lying metastable states in the system. Therefore the behavior of the manifold is affected in a nontrivial manner by the presence of disorder. In particular, for the case $d = n = 1$, the interface or string subject to a short-range correlated disorder potential fluctuates strongly with an exponent $\zeta_{1,1} = \frac{2}{3}$ (Huse and Henley, 1985; see also Kardar, 1985), which is bigger than the (thermal) random-walk value $\zeta^{\text{RW}} = \frac{1}{2}$ expected in the absence of disorder. The determination of the exponents $\zeta_{d,n}$ is far from trivial, the only exact result to date being the above random-bond example for $n = d = 1$ (Huse, Henley, and Fisher, 1985; see also Forster, Nelson, and Stephen, 1977; Kardar and Nelson, 1985; Kardar, 1987a). Once the wandering exponent $\zeta_{d,n}$ is known, simple scaling arguments can be used to determine the value of the second exponent $\chi_{d,n}$. Assuming that the fluctuations in the disorder energy $\delta\mathcal{E}_d$ [short notation for $\langle\langle\, [\delta\mathcal{E}_d]^2\,\rangle\rangle^{1/2}$] scale in the same way as the fluctuations in the elastic energy $\delta\mathcal{E}_{\text{el}} \propto \langle\langle\, [\delta u]^2\,\rangle\rangle L^{d-2}$, the exponent $\chi_{d,n}$ takes the value

$$\chi_{d,n} = 2\zeta_{d,n} + d - 2 \; . \tag{3.146}$$

An additional complication arises at finite temperatures, where fluctuations due to quenched randomness compete with those induced thermally. In the following we first consider the zero-temperature case and then comment on finite-temperature effects.

Various analytical and numerical methods have been devised for tackling the problem of disorder-roughened elastic manifolds. For the random-bond directed-polymer problem, a very successful approach is mapping to a particle problem, where the string $\mathbf{u}(x)$ corresponds to the world line of a particle in a $D = (n+1)$-dimensional space. The path integral

$$\mathcal{W}(x_0, \mathbf{u}_0) = \int_{(0,0)}^{(x_0, \mathbf{u}_0)} \mathcal{D}[\mathbf{u}(x)]\, e^{-\mathcal{H}[\mathbf{u}(x)]} \tag{3.147}$$

then obeys the dynamic equation

$$\partial_x \mathcal{W} = \left[ \frac{1}{2C}\nabla^2 + E_d(x, \mathbf{u}) \right] \mathcal{W} \; , \tag{3.148}$$

which is identical to the imaginary-time Schrödinger equation for a particle moving in $(n+1)$-dimensional space and subject to a random potential fluctuating in both space and time. When we define the velocity field $\mathbf{v} = -(1/C)\nabla\ln\mathcal{W}$, the dynamic equation (3.148) can be mapped to the Burgers equation for a randomly stirred

vorticity-free $(\nabla\wedge\mathbf{v} = 0)$ fluid (Huse, Henley, and Fisher, 1985),

$$\partial_x \mathbf{v} = \frac{1}{2C}\nabla^2\mathbf{v} - (\mathbf{v}\cdot\nabla)\mathbf{v} - \frac{1}{C}\nabla E_d \; . \tag{3.149}$$

In one dimension, an invariant distribution for $v$ is known, as a consequence of which a second scaling relation, $2\chi_{1,1} = \zeta_{1,1}$, can be obtained, implying the (exact) results $\zeta_{1,1} = \frac{2}{3}$ and $\chi_{1,1} = \frac{1}{3}$. Unfortunately, no invariant distribution is known in higher dimensions.

Again starting from Eq. (3.141), an alternative approach was taken by Kardar (1987a; see also Kardar and Zhang, 1987; Mézard, 1990) by using the replica method in dealing with the problem of disorder. The averaging over randomness produces an interaction $V_{\text{int}}(\mathbf{u} - \mathbf{u}') = \Delta R^n(\mathbf{u} - \mathbf{u}')$ between particles belonging to the $N$ different replicas, which is attractive for the case of a short-range correlated disorder potential. Such an attractive interaction in the random-bond problem leads to a clustering of the particles into an $N$-body bound state, which is the signature of the relevance of disorder in the particle formulation (for the long-ranged random-field case the interaction between the replicas is repulsive). For $n < 2$ space dimensions, an arbitrarily weak attraction leads to a bound state; thus disorder is always relevant. On the other hand, for $n > 2$, only strong attraction is able to produce a bound state, implying that only strong disorder is relevant for dimensions $n > 2$. The case $n = 2$ is marginal: Since any attractive interaction still produces a bound state (though it may be exponentially weak), disorder is always (marginally) relevant. Again, the one-dimensional case can be solved exactly: A short-range correlated disorder potential produces a $\delta$-function-type interaction between the replicated particles, and the problem can be solved exactly by means of the Bethe ansatz technique (Bethe, 1931). The quantity to be determined is the ground-state energy of the $N$-particle system, which takes the form $E_0(N) = E_1 N + E_3 N^3 + \ldots$, $E_3 < 0$. The mapping to the original directed-polymer problem is then established by the relation

$$\langle Z^N \rangle = e^{-E_0(N)L} \; , \tag{3.150}$$

with the partition function $Z = \mathcal{W}(L, 0)$ equivalent to the propagator (3.147). As usual, the brackets $\langle\,\cdots\,\rangle$ denote the average over disorder. With respect to the latter, $\mathcal{F} = -\ln Z$ can be viewed as a random variable. Introducing the probability distribution function $P(\mathcal{F})$ for the random variable $\mathcal{F}$, we can rewrite Eq. (3.150) in the form

$$\langle Z^N \rangle = \langle e^{-N\mathcal{F}} \rangle = \int d\mathcal{F}\, P(\mathcal{F}) e^{-N\mathcal{F}}$$

$$= e^{-E_0(N)L} \; . \tag{3.151}$$

Obviously, the expression $\exp[-E_0(N)L]$ is nothing but the Laplace transform of the distribution function $P(\mathcal{F})$ which, once the ground-state energy $E_0(N)$ of the $N$-

particle system is known, can be obtained by simple inversion (Zhang, 1990). The linear term $E_1 L$ in the ground-state energy $E_0(N)$ provides us with the free energy $\langle \mathcal{F}(L) \rangle$ of the string,

$$\langle \mathcal{F}(L) \rangle = -\frac{d}{dN} \langle e^{-N\mathcal{F}} \rangle |_{N=0} = E_1 L \ . \qquad (3.152)$$

Note that, due to the presence of the disorder potential $E_d$, the line energy $E_1$ of the string is lowered as compared with the homogeneous situation, since the string accommodates to the random potential by choosing favorable regions where $E_d < 0$.

Next, let us concentrate on the cubic term $E_3 N^3$ which determines the fluctuations of the free energy $\mathcal{F}$. In order to simplify the analysis we can assume, without loss of generality, that the line energy $E_1$ vanishes. The inverse Laplace transform of $\exp(aN^\alpha L^\gamma)$ takes the form (Kolomeisky, 1992)

$$P(\mathcal{F} > 0) \propto \exp\left[ -\left[ \frac{\mathcal{F}^\alpha}{aL^\gamma} \right]^{1/(\alpha - 1)} \right] , \qquad (3.153)$$

from which one easily obtains the scaling behavior for the fluctuations in the free energy $\mathcal{F}$ of the string,

$$\delta\mathcal{F}(L) = \delta\mathcal{E}_d(L) \propto L^{\gamma/\alpha} \ . \qquad (3.154)$$

For a string $(d=1)$ moving in one dimension $(n=1)$ we have $\gamma = 1$ and $\alpha = 3$, hence $\delta\mathcal{E}_d(L) \propto L^{1/3}$, and we obtain the desired exponent $\chi_{1,1} = \frac{1}{3}$ (Kardar, 1987a). Generalizing this scheme to higher dimensions $n$, one would again expect the $N$-body ground-state energy to be of the form $E_0(N) = E_1 N + E_{k_n} N^{k_n}$, with some positive integer $k_n$, implying that the exponent describing the fluctuations in the energy of the string subject to short-ranged disorder should have the form $\chi_{d,n} = 1/k_n$. The latter furnishes a simple check on which analytical expressions for the exponents $\zeta_{d,n}$ and $\chi_{d,n}$ can be tested.

The result (3.152) implies that the correction in the line energy of the string due to the presence of the disorder potential does not vanish. At first sight this seems to be in contradiction with the statement made in Sec. II.A.2 that the energy contribution linear in the disorder potential $E_d$ vanishes. However, in Sec. II above, our analysis was concerned with a *stiff* vortex, and the finite elasticity was only introduced in a second step in order to provide the necessary cutoff producing a finite pinning force density. Here we consider only elastic strings.

Let us analyze more carefully the relation between the two approaches. Consider a (straight) string in a homogeneous medium and choose the energy of its ground-state configuration as our zero-energy reference point. When we turn on a disorder potential $E_d$ [notably with $\langle E_d \rangle = 0$], the elastic string will relax to the new environment by choosing favorable regions where $E_d < 0$; thus the new ground-state configuration is characterized by a *finite* correction to the line energy. On the other hand, a stiff vortex cannot accommodate to the disorder potential, and its correction to the line energy due to disorder

remains zero. Consider, then, fluctuations in this (correction to the) line energy. To be precise we have to distinguish between two types of fluctuations. Taking the fluctuations over all states, we obtain a fluctuation amplitude growing linearly with the length $L$, $\langle [\mathcal{E}(L) - \langle \mathcal{E}^{\min}(L) \rangle]^2 \rangle^{1/2} \propto L$. In fact, these fluctuations are of the same order as the correction to the line energy of the elastic string itself. This type of fluctuation then leads to the *finite pinning force density* which determines the critical current density $j_c$ in Sec. II.A.2 above. For small scales, $L \simeq L_c$, the elasticity is not important, and we can calculate the amplitude of these fluctuations perturbatively with the result $\langle [\mathcal{E}(L_c) - \langle \mathcal{E}^{\min}(L_c) \rangle]^2 \rangle^{1/2} \simeq \langle [\mathcal{E}(L_c)]^2 \rangle^{1/2} \simeq U_c$. The calculation presented in Sec. II.A.2 was nothing but the determination of this type of fluctuation in the line energy of the string, leading to the phenomenon of *pinning*. On the other hand, we can consider the fluctuations in the *minima* of the line energies, $\delta\mathcal{E}(L) \equiv \langle [\mathcal{E}^{\min}(L) - \langle \mathcal{E}^{\min}(L) \rangle]^2 \rangle^{1/2}$. According to the above results these fluctuations grow much more slowly with distance, i.e., $\delta\mathcal{E}(L) \propto L^{1/3}$ in $1+1$ dimensions. The physical relevance of this latter type of fluctuation comes into play when we are interested in the phenomenon of *creep*, which is related to the *barriers* separating two low-lying states on long scales, $L \gg L_c$: We can make the reasonable assumption (Ioffe and Vinokur, 1987) that there is only one relevant scale for fluctuations in energy in the system, and therefore we expect that the typical barriers $\langle \mathcal{E}^b(L) \rangle$ separating two low-lying metastable states scale in the same manner as the typical energy differences between the two states, hence $\langle \mathcal{E}^b(L) \rangle \propto L^{1/3}$. These barriers become relevant in the discussion of the disorder-dominated dynamics of elastic manifolds, and we shall come back to this question in the next section.

One of the most successful analytic tools for dealing with the present problem is the scaling technique, with investigations ranging from simple Flory-type scaling estimates to very sophisticated (functional) renormalization-group analyses. Let us rewrite the Hamiltonian (3.141) in the new rescaled variables

$$x' = \frac{x}{b} \quad \text{and} \quad u' = \frac{u}{b^\zeta} \ , \qquad (3.155)$$

where $\zeta$ is an abbreviation for $\zeta_{d,n}$. The (coupling) parameters in (3.141) then scale according to

$$C' = C b^{y_C} \quad \text{and} \quad \Delta' = \Delta b^{y_\Delta} \ , \qquad (3.156)$$

with

$$y_C = 2\zeta + d - 2 \quad \text{and} \quad y_\Delta = d - \zeta\beta(n) \ . \qquad (3.157)$$

In the absence of any disorder, a scale-invariant theory necessitates $y_C = 0$ and hence $\zeta_0 = (2-d)/2$, the thermal exponent in the absence of disorder. Disorder is perturbatively relevant if $y_\Delta > 0$ at this free fixed point, implying that $d > d_c = 2\beta(n)/[2+\beta(n)]$ or $\beta(n) < \beta(n_c) = 2d/(2-d)$, $2-d > 0$. For the random-bond domain-

wall problem, $d_c = \frac{2}{3}$ (Huse and Henley, 1985; Kardar, 1987b), whereas for directed polymers with $d = 1$ and short-range correlated disorder we obtain $n_c = 2$. The simplest Flory-type result for the desired wandering exponent $\zeta$ is then obtained by requiring both terms in Eq. (3.141) to scale in the same way, $2y_C = y_\Delta$, resulting in the Flory exponent

$$\zeta_{d,n}^F = \frac{4-d}{4+\beta(n)} . \tag{3.158}$$

A quick comparison with the exact result $\zeta_{1,1} = \frac{2}{3}$ shows that this simple argument is too naive in general, since $\zeta_{1,1}^F = \frac{3}{5}$, where we have used $\beta(1) = 1$, the value for short-range correlated disorder. The reason for the failure lies in our implicit assumption that the disorder correlator $R^n(u)$ remains unchanged under rescaling. This is not the case in general, as can be shown explicitly by studying the scaling behavior of $R^n(u)$ in a functional renormalization-group (FRG) analysis. Within the replicated particle picture described above, the FRG analysis corresponds to determining the behavior of the interaction potential between the particles under rescaling. This is done by calculating the free energy of the system to one-loop order, followed by a rescaling of the lengths $x$ and $u$ with $b = 1 + \delta b$. The result is a nonlinear partial differential equation describing the behavior of the correlator (interaction) $R^n(u)$ under rescaling (see, for example, Halpin-Healy, 1990),

$$\partial_b R^n(u) = f(d, n, \zeta, R^n, \partial_u R^n, \partial_u^2 R^n) . \tag{3.159}$$

To one-loop order, $f$ takes the form

$$f = (4 - d - 4\zeta)R + \zeta u \partial_u R - \partial_u^2 R(0) \partial_u^2 R + \frac{1}{2}(\partial_u^2 R)^2$$
$$- (n-1)\partial_u^2 R(0)\frac{\partial_u R}{u} + \frac{n-1}{2}\left[\frac{\partial_u R}{u}\right]^2 , \tag{3.160}$$

where we have written $R$ for $R^n(u)$. The task then is to find the fixed-point function $R^*(u)$, $\partial_b R^*(u) = 0$, from which we can obtain the correct scaling behavior of the correlator at large distances and hence the relevant value of $\beta^*(n)$ to be used in the Flory formula (3.158). Unfortunately, the FRG equation (3.159) cannot be solved analytically, and approximate methods have to be used. The first analysis of Eq. (3.159) for the case $n = 1$ goes back to Fisher (1986), who interpreted the fixed-point condition $f(d, \zeta, R, \partial_u R, \partial_u^2 R) = 0$ as an eigenvalue problem, the solution of which depends on the boundary conditions at infinity. For the random-bond problem a short-ranged fixed-point function $R_{SR}^*(u)$ is expected to exist. In fact, it can be shown that (for general $n$) the fixed-point condition allows for a solution that behaves asymptotically like a Gaussian damped power law,

$$R_{SR}^*(u) \sim u^{-(4+n-(4-d)/\zeta)}\exp\left[-\frac{\zeta u^2}{2(4-d)}\right] . \tag{3.161}$$

The numerical result for $\zeta$ found by Fisher is $\zeta_{d,1} = 0.2083(4-d)$, which produces a value $\zeta_{1,1} = 0.625$,

quite close to the exact value $\frac{2}{3}$. On the other hand, as pointed out by Fisher (1986), for the random-field problem with $\beta(1) = -1$, Eq. (3.159) also allows for a long-ranged fixed-point function $R_{LR}^*(u) \sim u$ growing linearly at large distances and producing the eigenvalue $\zeta_{d,1} = (4-d)/3$, in agreement with the Flory result (3.158). In fact, the FRG analysis contributed substantially to a better understanding of how and why field-theoretic perturbative methods (Aharony *et al.*, 1976; Grinstein, 1976; Efetov and Larkin, 1977; Parisi and Sourlas, 1979), which produce a wandering exponent $\zeta_{d,1} = (4-d)/2$, fail to give the correct solution to the random-field domain-wall problem, while simple Imry-Ma or Flory-type arguments are better suited to capture the essential physics of the problem (Imry and Ma, 1975; Imbrie, 1984). However, recently, Mézard and Parisi (1991) have been able to take into account the existence of the many metastable states for the manifold by using the replica method in combination with a variational approach and a hierarchical breaking of the replica symmetry. This improved field-theoretic analysis is able to reproduce the Flory exponent (3.158).

The following general scenario for the behavior of the fixed-point solutions of Eq. (3.159) has been proposed by Halpin-Healy (1989): For the case of long-range interactions with $\beta(n)$ smaller than some critical value $\beta_c(n)$, a fixed-point function $R_{LR}^*(u) \sim u^{-\beta(n)}$ exists and produces an eigenvalue $\zeta$ consistent with the Flory result (3.158). We can conclude that for long-range disorder correlations, the correlator $R^n(u)$ remains asymptotically unchanged under rescaling and mean-field-like Flory-type arguments leading to the result (3.158) are correct. Let us then decrease the range of interactions by increasing the exponent $\beta(n)$. According to Halpin-Healy (1989), the system will change its behavior as we cross the critical value $\beta_c$. For $\beta(n) > \beta_c$, the FRG equation will rescale the initial correlator $R^n(u)$ to a new short-ranged and universal [i.e., independent of $\beta(n) > \beta_c(n)$] fixed-point function $R_{SR}^*(u)$ with an asymptotic Gaussian damped power-law behavior of the form (3.161). Interpreting this asymptotic behavior as a Gaussian damping of the *critical* power law $u^{-\beta_c}$ with

$$\beta_c = 4 + n - \frac{4-d}{\zeta} , \tag{3.162}$$

we now have obtained an expression for the relevant exponent $\beta$ to be inserted into the Flory formula (3.158). In fact, the Flory result is expected to be correct as we approach the critical value $\beta_c$ from below. Combining Eqs. (3.158) and (3.162), we obtain the results

$$\beta_c(n) = \frac{n}{2} \tag{3.163}$$

for the critical exponent $\beta_c$ and

$$\zeta_{d,n}^{SR} = \frac{2(4-d)}{8+n}, \quad \beta > \beta_c , \tag{3.164}$$

for the short-range wandering exponent $\zeta_{d,n}^{SR}$. In sum-

mary, for the case of long-range disorder correlations characterized by the condition $\beta(n) < n/2$, the simple Flory result (3.158) is exact, whereas for short-range correlations in the disorder potential with $\beta(n) \geq n/2$, the wandering exponent sticks to the value (3.164). This remarkable analysis due to Halpin-Healy (1989) thus produces the exact result $\zeta_{1,1}^{SR} = \frac{2}{3}$ for the random-bond problem in $1+1$ dimensions.

The two approaches of Fisher and of Halpin-Healy described above use the basic FRG equation (3.159) in quite a different manner. Fisher's numerical search for the eigenfunction implies an integration of the fixed-point condition $f(d, \zeta, R, \partial_u R, \partial_u^2 R) = 0$ from the origin $u = 0$ to some asymptotic value where $R^*(u) \to 0$ for the correct eigenvalue $\zeta$. Since the variation of the initial value $R^*(0)$ corresponds to a variation in the (guessed) eigenvalue $\zeta$, one has to rely on the correctness of the FRG equation (3.159) close to the origin. This reliance has been criticized by Halpin-Healy (1989, 1990), who pointed out that higher-order terms in the expansion leading to Eq. (3.160) are expected to be important close to the origin and can be neglected only in the asymptotic regime. On the other hand, since Eq. (3.160) is expected to be asymptotically exact, we can hope that the above derivation of the wandering exponent $\zeta$ will be exact if the important information determining the value of $\zeta$ is indeed contained only in the asymptotic behavior of the fixed-point function $R_{SR}^*(u)$.

An intermediate point of view has been taken by Nattermann and Leschhorn (1991), who use the moments of the FRG equation (3.159) in their three-parameter renormalization-group analysis of the problem, thereby basing their results on the *global* behavior of the fixed-point function $R_{SR}^*(u)$. In their analysis of the domain-wall problem, Nattermann and Leschhorn use a two-parameter ansatz for the correlator $R^1(u)$,

$$R^1(u) = \frac{\Delta}{\xi} r\left[\frac{u}{\xi}\right], \tag{3.165}$$

with $r(z)$ a normalized smooth function with a peak at the origin [note that here we have included the disorder parameter $\Delta$ in the definition of the correlator $R^1(u)$]. By an integration over small-wavelength fluctuations, renormalization-group (RG) equations for the parameters $\Delta(b)$ and $\xi(b)$ [and for the temperature $T(b)$] are obtained, which have a stable fixed-point solution if we choose the (domain-wall) wandering exponent $\zeta$ to take the form $\zeta_{d,1} = (4-d)/(5 - c_\Delta/c_\xi)$. The two unknown coefficients $c_\Delta$ and $c_\xi$ entering the RG equations for $\Delta(b)$ and $\xi(b)$, respectively, then are determined by use of the FRG equation (3.159). In fact, inserting the ansatz (3.165) for the correlator $R^1(u)$ and the RG equations for $\Delta(b)$ and $\xi(b)$ into Eq. (3.159), we obtain a functional relation that involves the two unknown parameters $c_\Delta$ and $c_\xi$. When we use a model function $r(z) = \exp(-z^2/2)$, each pair of moments of this functional relation provides us with a solution for $c_\Delta$ and $c_\xi$ and thence with a value

for the wandering exponent $\zeta_{d,1}$. It turns out that the solution is very stable with respect to the particular choice of moments, and the final result $\zeta_{d,1} = 0.2078(4-d)$ is obtained from the second and fourth moment of Eq. (3.159), a value close to Fisher's previous result.

A very interesting approach combining the ideas of replica-analysis and scaling analysis (replica-scaling analysis) has recently been proposed by Zhang (1990) and further elaborated by Kolomeisky (1992). In this approach the ground-state energy $E_0(N)$ of the replicated system, instead of being determined exactly, as is possible for the case $n = d = 1$ (Kardar, 1987a), is estimated with the help of scaling concepts. The method reproduces the exact result $\zeta_{1,1} = \frac{2}{3}$ for the $n = 1$ directed-polymer (or $d = 1$ domain-wall) problem. However, other findings are in contradiction to traditional experience. To summarize, for an attractive interaction between the replicated manifolds (the random-bond situation), Kolomeisky (1992) finds that at zero temperature $\zeta_{d,n} = (4-d)/4$ independent of $n$. This expression coincides with the Imry-Ma-type result obtained by Nattermann (1985) for the random-bond problem. For finite temperatures and small internal dimensions, $0 < d < 2n/(2+n)$, of the manifold, the Gaussian result $\zeta_{d,n} = \zeta_0 = (2-d)/2$ is recovered (note that the critical dimension $d_c$ above which disorder is perturbatively relevant is $d_c = \frac{2}{3}$ for the $d = n = 1$ random-bond problem, in agreement with Kolomeisky's result). For $d > 2n/(2+n)$, the wandering exponent turns out to be $\zeta_{d,n} = 2/(n+1)$ independent of the internal dimension $d$. The latter result implies a super-universal wandering exponent $\zeta_{d,1} = \frac{2}{3}$ for the domain-wall problem. For large $d$ the zero-temperature exponent $\zeta_{d,n} = (4-d)/4$ drops below the finite $T$ result $\zeta_{d,n} = 2/(2+n)$, in disagreement with common expectations. Finally, within the replica-scaling approach, the critical exponent $\beta_c$ separating long-range (random-field) and short-range (random bond) disorder turns out to be $\beta_c = 0$ independent of $n$: at $\beta = \beta_c$ the interaction between replicas changes from attractive (random-bond) to repulsive (random-field), giving a physically very appealing interpretation of the fundamental difference between short- and long-range disorder.

Scaling analysis of the problem, then, leaves us in a somewhat undetermined situation: we have a remarkably consistent scenario proposed by Halpin-Healy and an interesting replica-scaling analysis by Zhang and by Kolomeisky, which both reproduce the only known exact result in $1+1$ dimensions. Then there are the two calculations of Fisher and of Nattermann and Leschhorn, which, however, produce somewhat different results from those of Halpin-Healy. It is instructive to consider the analysis of Feigel'man *et al.* (1989), based on scaling arguments and purely physical considerations, which produces results in full agreement with those of Halpin-Healy without relying on the FRG equation (3.159).

The analysis of Feigel'man *et al.* is also based on

Flory-type arguments, assuming that the wandering exponent $\zeta$ is determined by the equal-scaling condition for fluctuations in the elastic energy $\delta\mathscr{E}_{el}(L)$ and the disorder energy $\delta\mathscr{E}_d(L)$. We then have to set up the corresponding scaling expressions for the two types of energy fluctuations $\delta\mathscr{E}_{el}$ and $\delta\mathscr{E}_d$. First, we make the assumption that, due to their different physical origins, we can independently set up the scaling laws for the two energies $\delta\mathscr{E}_{el}$ and $\delta\mathscr{E}_d$. The elastic energy involves only intrinsic properties of the manifold itself, which are its dimensionality $d$ and the elastic modulus $C$. The usual scaling ansatz $\delta\mathscr{E}_{el}\simeq C(u/L)^2L^d\propto L^{y_C}$, with $y_C=2\zeta+d-2$, is entirely consistent with the above requirement. Similarly, we expect $\delta\mathscr{E}_d$ to depend only on quantities describing the interaction of the manifold with the disorder potential. Thus $\delta\mathscr{E}_d$ should depend on the dimensionalities $d$ and $n$ and on the disorder strength $\Delta$, but not on the elasticity $C$ of the manifold. Following Feigel'man *et al.*, we then make the following scaling ansatz for fluctuations in the disorder energy,

$$\delta\mathscr{E}_d(L)\simeq U_c\left[\frac{V}{V_c}\right]^\delta\left[\frac{\xi}{u}\right]^{\tilde{\beta}(n)/2}. \quad (3.166)$$

Here $U_c$, $V_c$, and $\xi$ are the relevant scales of energy, volume, and length in the problem. In particular, $\xi$ describes the relevant length scale of the disorder potential, i.e., of the correlator $R^n(u)$ discussed above. Our second step is to combine the two expressions for $\delta\mathscr{E}_{el}$ and $\delta\mathscr{E}_d$ and require them to scale in the same way, from which we will obtain the desired wandering exponent $\zeta$. Note that here $\delta$ and $\tilde{\beta}(n)$ are unknown exponents to be determined below.

The ansatz (3.166), which is the main result of this subsection, provides a basis for determination of the wandering exponent $\zeta$. Its main message is that energy fluctuations due to disorder can be factorized into a pure volume factor $(V/V_c)^\delta$, which contains all the information about the dimensionality of the elastic manifold, and a linear factor $(\xi/u)^{\tilde{\beta}(n)/2}$, which describes the influence of the $n$ transverse motional degrees of freedom of the elastic manifold and does not depend on its dimensionality $d$. Physically, this second factor describes the reduction of fluctuations in $\delta\mathscr{E}_d$ as the manifold can choose between a large number of metastable states in the $n$ transverse dimensions describing its motional degrees of freedom. The ansatz (3.166) thus separates the dependence of the wandering exponent $\zeta_{d,n}$ on $d$ from its dependence on $n$. Once the exponent $\zeta_{\bar{d},\bar{n}}$ for a pair $\bar{d}$ and $\bar{n}$ is known, the exponents $\zeta_{d,\bar{n}}$ for arbitrary dimensions $d$ follow immediately. From our ansatz (3.166) we obtain the scaling behavior for the disorder energy, $\delta\mathscr{E}_d\propto L^{y_\Delta/2}$, with $y_\Delta=2d\delta-\zeta\tilde{\beta}(n)$. Requiring the elastic and the disorder energy fluctuations to scale in the same way, we find the wandering exponent

$$\zeta_{d,n}=\frac{4-2d(1-\delta)}{4+\tilde{\beta}(n)}. \quad (3.167)$$

Our remaining task is then the determination of the exponents $\delta$ and $\tilde{\beta}(n)$. The volume exponent $\delta$ is determined by the condition that the disorder energy (3.166) should not depend on the elasticity modulus $C$ of the manifold. Thus we have to determine the scales $U_c$ and $V_c$ and their dependence on $C$. For $u\leq\xi$, simple perturbation theory is appropriate, and our method of dimensional estimates can be applied straightforwardly: The elastic energy within the volume $V=L^d$, $\mathscr{E}_{el}\simeq Cu^2L^{d-2}$, competes with the disorder energy for a *stiff* manifold, $\mathscr{E}_d\simeq[\Delta L^dR^n(0)]^{1/2}$, where we have used Eq. (3.142). Note that, for the vortex problem, $n=2$, and $\Delta R^n(0)/\xi^2\simeq\Delta\xi^4$ is the mean squared random force density $W$ acting on a single vortex $(\Delta\simeq\gamma\xi^4)$ or on a vortex lattice $(\Delta\simeq\gamma\xi^4/a_0^2)$. For an *elastic* manifold, we have to cut off the above dependencies on $L$ when the displacement $u$ becomes of the order of the characteristic length $\xi$ of the disorder potential $E_d$. The length scale $L_c$ is then obtained by equating $\mathscr{E}_{el}$ and $\mathscr{E}_d$ at the maximal displacement $u\simeq\xi$, and we obtain

$$L_c\simeq\left[\frac{C^2\xi^4}{\Delta R^n(0)}\right]^{1/(4-d)}. \quad (3.168)$$

Inserting this result back into the expression for $\mathscr{E}_d$, we find for the energy scale $U_c$ the result

$$U_c\simeq(C\xi^2)^{d/(4-d)}[\Delta R^n(0)]^{(4-2d)/[2(4-d)]}. \quad (3.169)$$

Finally, inserting $U_c$ and $V_c\simeq L_c^d$ back into our ansatz (3.166), we obtain the dependence $\delta\mathscr{E}_d\propto C^{d(1-2\delta)/(4-d)}$, and therefore the exponent $\delta$ becomes $\delta=\frac{1}{2}$.

Second, we have to find the exponent $\tilde{\beta}(n)$ describing the influence of the transverse motional degrees of freedom on the disorder energy $\delta\mathscr{E}_d$. Within the simplest Flory-type analysis introduced at the beginning of this section, the exponent $\tilde{\beta}(n)$ is given by the asymptotic behavior of the disorder correlator $R^n(u)\sim u^{-\beta(n)}$, i.e., $\tilde{\beta}(n)=\beta(n)$. Here we are interested in short-range correlated disorder, where the correlator is expected to be renormalized at large distances, hence $\tilde{\beta}(n)$ is not known *a priori*. For a rigid manifold, the dependence of the disorder energy on the length $L$ is entirely due to the random addition of forces, which produces the simple square-root dependence on volume, $\delta\mathscr{E}_d\propto L^{d/2}$. Therefore a stiff manifold is characterized by an exponent $\tilde{\beta}(n)=0$. The finite elasticity allows the medium to wander in the transverse dimensions and to explore all the metastable states within the transverse volume $V_\perp=u^n$. The number of available low-lying metastable states should scale with the transverse volume $V_\perp$, hence $\tilde{\beta}(n)=\tilde{\beta}_0 n$, with $\tilde{\beta}_0$ a fixed constant independent of $d$ and $n$. Using the exact result $\zeta_{1,1}=\frac{2}{3}$, we obtain $\tilde{\beta}_0=\beta_c=\frac{1}{2}$, hence $\tilde{\beta}(n)=\beta_c(n)=n/2$, and the expression (3.167) becomes identical with the wandering exponent $\zeta_{d,n}^{SR}$ as obtained by Halpin-Healy. Without relying on the approximations necessary in dealing with the functional renormalization-group approach, the very general ideas of Feigel'man *et al.*, based only on physical arguments,

then lead to the same final answer for the wandering exponent $\zeta$ as obtained by Halpin-Healy and therefore strongly support the result (3.164).

Considerable effort has been invested in numerical investigations of the behavior of elastic manifolds subject to a quenched disorder potential. In their pioneering work on the domain-wall problem in the $(1+1)$-dimensional random-bond Ising model, Huse and Henley (1985; see also Kardar, 1985) numerically obtained the wandering exponent $\zeta_{1,1} = 0.66 \pm 0.02$, which agrees very accurately with the exact result $\zeta_{1,1} = \frac{2}{3}$ found later. Kardar and Zhang (1987) then investigated the directed-polymer problem in higher dimensions, $n \leq 3$. Their results, $\zeta_{1,2} = 0.62 \pm 0.04$ and $\zeta_{1,3} = 0.64 \pm 0.07$, led them to suggest that $\zeta_{1,n}$ might be a super-universal exponent, taking the value $\zeta_{1,n} = \frac{2}{3}$ independent of $n$. More precise simulations on Eden growth by Wolf and Kertész (1987) produced the values $\alpha_2 = 0.33 \pm 0.01$ and $\alpha_3 = 0.24 \pm 0.02$ for the scaling exponent $\alpha$ of the surface width, which is related to the directed-polymer wandering exponent via $\zeta_{1,n} = 1/(2 - \alpha_n)$. From their numerical results on $\alpha_n$, Wolf and Kertész conjectured that $\alpha_n = 1/(n+1)$, which transforms to a wandering exponent

$$\zeta_{1,n}^{WK} = \frac{n+1}{2n+1} , \qquad (3.170)$$

in disagreement with superuniversality. Similarly, a numerical study of ballistic deposition by Kim and Kosterlitz (1989) produced the values $\gamma_1 = 0.332 \pm 0.005$, $\gamma_2 = 0.250 \pm 0.005$, and $\gamma_3 = 0.20 \pm 0.01$ for the dynamic exponent $\gamma$ characterizing the time evolution of the surface width at short times. From their conjecture $\gamma_n = 1/(n+2)$ and using the relation $\zeta_{1,n} = (1 + \gamma_n)/2$ to the directed-polymer wandering exponent, they obtain for the latter the general result

$$\zeta_{1,n}^{KK} = \frac{n+3}{2n+4} . \qquad (3.171)$$

Recently, Forrest and Tang (1990), however, found the somewhat smaller exponents $\gamma_2 = 0.240 \pm 0.001$ and $\gamma_3 = 0.180 \pm 0.005$, indicating that Eq. (3.171) overestimates the true value of the line-wandering exponent $\zeta_{1,n}$.

We have to conclude that the numerical results unfortunately add to our confusion about the true value of the directed-polymer wandering exponent $\zeta_{1,n}$ rather than resolve it. Moreover, the following argument fails to improve the situation: As discussed above, the true energy fluctuation exponent $\chi_{1,n}$ in the directed-polymer problem is expected to be of the form $\chi_{1,n} = 1/k_n$, with $k_n$ a positive integer. Surprisingly, all three results, (3.164), (3.170), and (3.171), for the line-wandering exponent $\zeta_{1,n}$ do in fact produce an energy fluctuation exponent $\chi_{1,n}$ consistent with this requirement, and thus none of the above results can be rejected on the basis of this simple test. On the other hand, in the analysis of the behavior of vortices subject to a disorder potential, we need the two exponents $\zeta_{1,2}$ (single-vortex pinning) and $\zeta_{3,2}$ (pinning of

vortex bundles). At least for the single-vortex problem, we can rely on the rather consistent numerical value $\zeta_{1,2} = \frac{3}{5}$, since $\zeta_{1,2}^{SR} = \zeta_{1,2}^{WK} = \frac{3}{5}$ and $\zeta_{1,2}^{KK} = 0.625$ close to the other results.

Let us turn finally to the problem of competing thermally by induced and disorder-induced fluctuations at finite temperature. From the scaling behavior of the elastic energy in Eq. (3.141) we immediately see that temperature is relevant for small dimensions $d$ where $y_C = 2\zeta_{d,n} + d - 2 < 0$. In fact, the RG equation for the temperature is (Fisher, 1986)

$$\partial_b T = -y_C T , \qquad (3.172)$$

hence $T$ scales to zero for $y_C > 0$. The only interesting case, then, is $d = 1$, i.e., the directed-polymer problem. In this case the thermal wandering exponent obtained from the condition $y_C = 0$, $\zeta_0 = (d-2)/2 = \frac{1}{2}$, competes with the disorder exponent $\zeta_{1,n}$. Let us start at small $n$ values, where the Harris criterion (Harris, 1974) can be used to show that the infinite-temperature fixed point is unstable to disorder for $n < 2$ (Halpin-Healy, 1990), and hence the elastic string is always in a "glassy," i.e., disorder-dominated state. From the analysis of the Burgers equation (Forster, Nelson, and Stephen, 1977; Kardar, Parisi, and Zhang, 1986) it is known that $n = 2$ is the marginal dimension, with arbitrarily weak disorder still relevant asymptotically. For $n > 2$, a phase transition is known to exist (Imbrie and Spencer, 1988) separating disorder- and temperature-dominated phases at low and high temperatures, respectively. The question then is, does there exist an upper critical dimension $n_c^u < \infty$ of the directed-polymer problem, where the temperature is always dominant, i.e., $y_C < 0$? Taking the results (3.170) and (3.171) due to Wolf and Kertész (1987) and Kim and Kosterlitz (1989), we obtain $\zeta_{1,n} > \zeta_0 = \frac{1}{2}$ in all dimensions $n$. Thus there exists no finite upper critical dimension for these two results. On the other hand, using Eq. (3.164) for the short-range line-wandering exponent as obtained by Halpin-Healy (1989) and by Feigel'man *et al.* (1989), we find $\zeta_0 = \zeta_{1,4}$ and thus $n_c^u = 4$. The existence of a finite upper critical dimension to the directed-polymer problem is also consistent with the results of $1/D$ expansions performed by Cook and Derrida (1990). To summarize, a consistent picture has emerged for the dimensions $n \leq 3$, which has also been confirmed by numerical work (Renz and Nattermann, 1990). On the other hand, the physics for $n > 3$, in particular the existence of a finite upper critical dimension to the directed-polymer problem, remains unclear.

In the following, we shall use Eq. (3.164) for the wandering exponent $\zeta_{d,n}$ as proposed by Halpin-Healy and by Feigel'man *et al.* and for which we believe we have presented quite a number of supporting arguments. We also wish to point out that the precise numerical value of the wandering exponent affects the specific form of the results but does not change the basic physical concepts discussed below.

## 2. Dynamics

In this last subsection of Sec. III we wish to investigate the dynamic behavior of a "pinned" manifold subject to an external force field $F$ (force per unit volume $L^d$ of the manifold). If a *large* force field is applied to the manifold, the dynamic response will be determined by what we call its intrinsic properties, such as the mass density $M$ or the friction coefficient $\eta$. The latter is due to coupling to the environment and is therefore, strictly speaking, an extrinsic property. However, here we wish to distinguish between effects arising from the quenched disorder potential (extrinsic) and those also present in the absence of disorder (intrinsic); hence we call friction that is independent of disorder an intrinsic property of the manifold. For a mass-dominated dynamic response, the manifold will be accelerated to higher velocities, whereas in the friction-dominated regime the velocity saturates and we obtain a flow-type motion of the manifold. On the other hand, in a *small* force field $F$, the manifold, which originally is trapped in some low-lying metastable state, will start to move either due to thermal activation or, depending on the intrinsic dynamic behavior of the manifold, by quantum tunneling. Due to the presence of many metastable states generated by the disorder potential, the dynamic response of the manifold will be determined mainly by extrinsic properties (the disorder potential) and only to a lesser degree by intrinsic ones (mass density, friction). In fact, the motion will be of the creep type and proceed in terms of elementary jumps, where a finite and optimal cell (nucleus) of the manifold will hop into a neighboring favorable metastable state. The volume $V_{opt}$ of the optimal cell, the optimal hopping distance $u_{opt}$, and, in the quantum case, the optimal hopping time $t_{opt}$, depend strongly on the size of the external driving force density $F$. As a consequence, the activation barrier and the action, the quantities determining the probability for the hop and therefore the creep rate, also depend strongly on the applied force $F$, and the motion becomes highly nonlinear in character.

Let us, then, qualitatively determine the characteristic creep-type motion of the manifold at small driving forces $F$, where the motion is determined by the disorder potential. The free-energy functional we have to study is

$$\mathcal{F} = \int d^d x \left\{ \frac{C}{2} (\nabla \mathbf{u})^2 + E_d(\mathbf{x}, \mathbf{u}) - \mathbf{F} \cdot \mathbf{u} \right\} . \tag{3.173}$$

We shall again use scaling methods in order to obtain an estimate for the saddle point. First, we have to find the critical force density $F_c$, below which disorder becomes relevant. Above, we have determined the elementary energy and volume scales $U_c$ and $V_c = L_c^d$ produced by the disorder potential; see Eqs. (3.168) and (3.169). The critical force density $F_c$ is then obtained by balancing $F_c$ against the pinning force density $F_p \simeq U_c / V_c \xi$ produced by the disorder potential,

$$F_c \simeq F_p \simeq \frac{U_c}{V_c \xi} . \tag{3.174}$$

As the driving force $F$ drops below $F_c$, the character of the motion changes from a flow to a creep-type behavior (Dong, Marchetti, Middleton, and Vinokur, 1993).

We first concentrate on classical creep. For $F \lesssim F_c$ the saddle point for the motion to the next metastable state, which is a minimal distance $\xi$ away, is given by a cell of volume $L_c^d$ and involves an activation energy

$$U(F) \simeq U_c \left[ 1 - \frac{F}{F_c} \right]^\alpha . \tag{3.175}$$

The exponent $\alpha$ is not known for the case of a random pinning potential. For a smooth periodic pinning potential, this exponent has been derived in Sec. III.E above [see Eq. (3.109)], but it is still unclear how far this result can be transferred to the random situation discussed here. Let us turn to small driving forces $F \ll F_c$. The next favorable low-lying state has now moved farther away, and we should find the new spatial dimensions for the critical nucleus, i.e., we have to determine the saddle point of the effective free-energy functional. According to the above analysis, the distance $u$ to the next favorable low-lying state scales like $u(L) \simeq \xi(L/L_c)^{\zeta_{d,n}}$, whereas the energy barrier $E_d^b$ separating the two low-lying states scales with $E_d^b(L) \simeq U_c(L/L_c)^{\chi_{d,n}}$. Here we have made the assumption that the disorder potential produces only one relevant scale of fluctuations in the energy at large distance, $\delta E_d(L)$, and hence the height of the energy barriers should scale accordingly (Ioffe and Vinokur, 1987). We can then write for the effective free-energy functional the expression

$$\mathcal{F}(L) \simeq U_c \left[ \left[ \frac{L}{L_c} \right]^{\chi_{d,n}} - \frac{F}{F_c} \left[ \frac{L}{L_c} \right]^{d + \zeta_{d,n}} \right] . \tag{3.176}$$

Whereas small nuclei are bound to decay, all cells with dimension $L > L_{opt}(F)$ will be overcritical and remain stable (due to pinning) after activation, thus producing a finite motion of the manifold. The critical nucleus is found by determining the extremum of (3.176) (the saddle point). We obtain the characteristic size and hopping distance

$$L_{opt}(F) \simeq L_c \left[ \frac{F_c}{F} \right]^{1/(2 - \zeta_{d,n})} \tag{3.177}$$

and

$$u_{opt}(F) \simeq \xi \left[ \frac{F_c}{F} \right]^{\zeta_{d,n}/(2 - \zeta_{d,n})} . \tag{3.178}$$

Combining the above results, we find for the activation energy describing classical creep close to a vanishing driving force $F \ll F_c$

$$U(F) \simeq U_c \left[ \frac{F_c}{F} \right]^\mu , \quad \mu = \frac{2\zeta_{d,n} + d - 2}{2 - \zeta_{d,n}} . \tag{3.179}$$

For quantum motion we have to determine the saddle point of the (Euclidean) action. Consider a massive manifold trapped within a favorable state. The energy of the manifold is then lowered by the pinning energy density $-U_c/V_c$, which we choose as our zero-energy reference [see also the discussion in Sec. II.A.5, Eq. (2.107)]. The action then takes the form

$$S = \int d^d x \, dt \left\{ \frac{M}{2}(\partial_t \mathbf{u})^2 + \frac{C}{2}(\nabla \mathbf{u})^2 \right.$$
$$\left. + \left[ E_d(\mathbf{x},\mathbf{u}) + \frac{U_c}{V_c} \right] - \mathbf{F} \cdot \mathbf{u} \right\} . \quad (3.180)$$

Equation (3.180) can be understood as a $(d+1)$-dimensional anisotropic generalization of the $d$-dimensional free-energy functional (3.173), where the additional dimension is given by the time axis and the anisotropy is determined by the ratio $C/M$. Note, however, that the random potential does not depend on time; therefore simple rescaling of the time axis and substitution of $d$ for $d+1$ in the above results is not appropriate. First we determine the basic time scale $t_c$ in the problem (the tunneling time to the neighboring state), which can be obtained by equating the kinetic-energy density $M(\xi/t_c)^2$ to the elastic one, $C(\xi/L_c)^2$, resulting in

$$t_c \simeq \left[ \frac{M}{C} \right]^{1/2} L_c . \quad (3.181)$$

The action for quantum motion close to the critical force $F \lesssim F_c$ is

$$S(F) \simeq S_c \left[ 1 - \frac{F}{F_c} \right]^{\alpha_S} , \quad (3.182)$$

with $S_c \simeq t_c U_c$. The critical exponent $\alpha_S$ close to the depinning threshold is not known for the present situation involving a random potential [for the periodic pinning potential, see Eq. (3.117)].

At small driving forces, $F \ll F_c$, we follow the ideas outlined in Sec. II.A.5 above and replace the time integral by an integration over the displacement $u$,

$$S \gtrsim \left[ \frac{MV_c}{U_c} \right]^{1/2} \int d^d x \, du \left\{ \frac{M}{2}(\partial_t \mathbf{u})^2 + \frac{C}{2}(\nabla \mathbf{u})^2 \right.$$
$$\left. + \left[ E_d(\mathbf{x},\mathbf{u}) + \frac{U_c}{V_c} \right] \right\} , \quad (3.183)$$

where we used the short-wavelength limit for the velocity $|\partial_t u|_{\max} \simeq \sqrt{U_c/MV_c}$. The integration over $u$ then averages the random potential $E_d(\mathbf{x},\mathbf{u})$ to zero, and using $U_c \simeq C\xi^2 L_c^{d-2}$ we obtain the estimate for the action

$$S \gtrsim S_c \left[ \frac{L}{L_c} \right]^d \frac{u}{\xi} . \quad (3.184)$$

Finally, the hopping distance is related to the bundle size

$L$ via the relation $u(L) \simeq \xi(L/L_c)^{\zeta_{d,n}}$ characterizing optimal metastable states. The connection to the driving force (providing for the elastic energy $Cu^2 L^{d-2}$) is further described by (3.177), resulting in the following expression for the Euclidean action governing quantum creep at small driving forces:

$$S(F) \simeq S_c \left[ \frac{F_c}{F} \right]^{\mu_S} , \quad (3.185)$$

with the exponent

$$\mu_S = \frac{d + \zeta_{d,n}}{2 - \zeta_{d,n}} . \quad (3.186)$$

For an overdamped manifold, we have to replace the kinetic energy in Eq. (3.180) by a term describing damping, which for the case of Ohmic dissipation is given by (3.114) above. The elementary tunneling time $t_c$ becomes

$$t_c \simeq \frac{\eta}{C} L_c^2, \quad \text{overdamped motion} . \quad (3.187)$$

The effective action close to criticality is again of the form (3.182) with an unknown exponent $\alpha_S$. Similarly, the effective action at small driving force takes the form (3.185) with the same exponent (3.186), the different dynamics entering only in the prefactor $S_c$ within the present approximation (it seems that replacing massive by dissipative dynamics introduces logarithmic corrections to the above results; see Sec. VIII.C.2). A similar analysis provides results for the case of Hall motion [$\eta \rightarrow \alpha$ in (3.187)].

Finally, we discuss the dynamic evolution of the force field $F$ itself. Consider a manifold prepared in a non-equilibrium (e.g., critical) state and relaxing back to equilibrium. The dynamic equation determining the evolution of the system is given by

$$\partial_t F \simeq -\frac{F_c}{\tau_0} e^{-U(F)/T} . \quad (3.188)$$

For the quantum case we have to substitute $S(F)/\hbar$ for $U(F)/T$. To exponential accuracy, the solution of Eq. (3.188) is given by

$$U(F) = T \ln \left[ 1 + \frac{t}{t_0} \right] , \quad (3.189)$$

with the normalization time $t_0 = \tau_0 T/F_c |\partial_F U|$ (Geshkenbein and Larkin, 1989; see also Sec. X). An equivalent expression is valid for the quantum case. Using the results (3.179) and (3.185) and inverting the solution (3.189), we find that the trapped force field $F$ relaxes only on a logarithmic time scale,

$$F(t) \simeq \begin{cases} F(t=0) \left[ \dfrac{U_c}{T} \dfrac{1}{\ln(t/t_0)} \right]^{1/\mu} , & \text{classical creep} , \\[3ex] F(t=0) \left[ \dfrac{S_c}{\hbar} \dfrac{1}{\ln(t/t_0)} \right]^{1/\mu_S} , & \text{quantum creep} . \end{cases}$$
$$(3.190)$$

The above results for the disorder-dominated creep-type dynamics of elastic manifolds apply to various physical systems, among which we cite the motion of domain walls in disordered Ising models (Huse and Henley, 1985; Fisher, 1986), the motion of dislocations in solids (Ioffe and Vinokur, 1987), the motion of pinned charge-density waves (Nattermann, 1990), and, of course, the creep of vortices in type-II superconductors (Feigel'man *et al.*, 1989; Feigel'man and Vinokur, 1990; Nattermann, 1990; Fisher, Fisher, and Huse, 1991; Fischer and Nattermann, 1991).

## IV. PINNING OF VORTEX BUNDLES

Collective pinning and creep of the vortex lattice in a type-II superconductor presents quite a formidable problem if studied in its full complexity. The basic reason for this is found in the large number of length scales that are relevant for an accurate description of the physics. Interestingly, these different length scales are properties of the vortex lattice, i.e., of the *elastic manifold* itself, and are not related to the disorder potential producing the pinning.

The smallest length scale involved is the coherence length $\xi$, which describes the extent of the vortex cores responsible for the coupling of the manifold to the pinning potential. $\xi$ therefore also defines the basic scale $r_p$ of the disorder potential for the case of weak pinning by point defects.

Next, the intervortex distance $a_0$ sets the scale for interaction between the vortices, which leads to the formation of collectively pinned vortex bundles. This scale also determines the *internal structure* of the elastic manifold formed by the discrete flux lines. This internal structure becomes relevant for creep involving large transverse displacements, $u > a_0$, of the lattice and opens up the possibility of an internal phase transition (melting), which changes drastically the elastic properties of the manifold itself (vanishing shear modulus).

Third, the penetration depth $\lambda$ defines the *range* of the interaction between the vortices: For distances $R < \lambda$ the interaction is logarithmic, whereas for large distances, $R > \lambda$, the interaction between the vortices becomes exponentially small. The range $\lambda$ of the interaction enters the theory in the specific form of the *dispersive* elastic moduli $c_{11}(\mathbf{k})$ and $c_{44}(\mathbf{k})$, with a strong suppression of these moduli for large wave numbers, $k > 1/\lambda$. With respect to the problem of pinning and creep, the scale $\lambda$ plays an important role in the determination of the *size* of the vortex bundles, which in turn affects quantities such as the critical current density $j_c$ and the barrier $U_c^b$ against creep.

At elevated temperatures, a fourth intermediate length scale (between $\xi$ and $a_0$) comes into play when thermal fluctuations in the vortex lattice lead to an effective smearing of the vortex cores over distances $\langle u^2 \rangle_{\text{th}}^{1/2} > \xi$, where $\langle u^2 \rangle_{\text{th}}^{1/2}$ denotes the mean thermal displacement of the individual vortices. These thermal fluctuations in-

teract with the disorder potential, leading to a smoothing corresponding to an increase in the basic length $r_p$ of the disorder potential from its low-temperature value $r_p(0) \simeq \xi$ to $r_p(T) \simeq \langle u^2 \rangle_{\text{th}}^{1/2}$. Note that the vortex lattice will melt when the mean displacement due to thermal fluctuations becomes of the order of the lattice constant $a_0$, hence $\xi \leq r_p(T) \leq a_0$. Simplifying theories based on a single (universal) length scale (Nattermann, 1990; Fisher, Fisher, and Huse, 1991) are then very useful in explaining the basic features of the system and are also physically relevant in the vicinity of the melting transition, where many of these length scales merge into the single scale $a_0 (\simeq r_p \simeq \xi$; the latter estimate applies for the case in which the melting transition is close to the mean-field transition line $H_{c_2}$). However, within a large portion of the phase diagram away from this transition, the full complexity of the system should be taken into account.

Here, we concentrate on the theory of weak collective pinning and creep as formulated by Larkin (1970) and by Larkin and Ovchinnikov (1973, 1979), and refined later by Feigel'man *et al.* (1989) and Nattermann (1990) (extensions to small current densities), by Feigel'man and Vinokur (1990, thermal fluctuations), and by Blatter *et al.* (1991, quantum creep; 1992, anisotropy). Following closely the ideas presented in Sec. III.F above, we first concentrate on the statistical mechanics of the vortex lattice subject to a quenched random potential (Sec. IV.A). We shall see that, due to the existence of the various internal length scales of the manifold, the statistical mechanics of the vortex lattice becomes much richer. Equipped with this knowledge we then turn to the dynamic behavior of the vortex lattice (Sec. IV.B); we determine the critical current density as a function of the applied magnetic field and discuss creep, classical and quantum, near criticality and near vanishing driving force, where we shall find the "glassy" behavior typical of an elastic manifold subject to a quenched disorder potential. In Sec. IV.C we generalize the discussion to include the effects of thermal fluctuations. Section IV.D is devoted to the problem of anisotropy. Finally, we briefly discuss the issue of long-range order in Sec. IV.E.

### A. Statistical mechanics

We begin with the investigation of the spatial fluctuations $\langle u^2(\mathbf{r}) \rangle^{1/2} \equiv \langle [\mathbf{u}(\mathbf{r}) - \mathbf{u}(0)]^2 \rangle^{1/2}$ of the vortex lattice subject to a quenched random potential. Let us follow the evolution of the displacement field from the smallest to the largest length scales. First, consider a weak-pinning situation where $\xi < L_c < a_0$. The latter condition guarantees that the system starts out in the single-vortex pinning regime at weak enough magnetic fields. As shown above (Sec. II.D), for lengths $L < a_0$ we can neglect interaction with the other vortices, and the displacement field is determined by the competition between the disorder potential and the elasticity of the individual vortices. We then summarize the results obtained

in Sec. II above: At the smallest scale, $L < L_c$, the perturbative approach of Larkin and Ovchinnikov is correct, and we obtain

$$\langle u^2(L)\rangle^{1/2} \simeq \xi \left[\frac{L}{L_c}\right]^{3/2}, \quad u < \xi, \quad L < L_c . \quad (4.1)$$

The result (4.1) can be obtained via dimensional estimates by comparing the elastic energy $\varepsilon_0 u^2/L$ with the pinning energy $(\gamma L \xi^2)^{1/2}(u/\xi)$ due to the restoring force $(\gamma L)^{1/2}$. Going beyond $L_c$, the displacement $u$ becomes larger than the extent of the individual pinning valley, and the string can choose between many metastable states. Therefore, following the general ideas of Sec. III.F, the fluctuations of the string grow much more slowly,

$$\langle u^2(L)\rangle^{1/2} \simeq \xi \left[\frac{L}{L_c}\right]^{3/5}, \quad \xi < u < \xi \left[\frac{a_0}{L_c}\right]^{3/5},$$

$$L_c < L < a_0 . \quad (4.2)$$

As $L$ becomes larger than the lattice constant $a_0$, interactions between the vortices become relevant and we have to investigate the full three-dimensional problem. Within weak collective pinning theory we adopt a continuum elastic description of the flux-line lattice, with a free energy given by the combination of the elastic energy (3.37), the pinning energy (3.89) with $\mathbf{v}=0$, and the action of the Lorentz force,

$$\mathcal{F}[\mathbf{u}] = \int d^3r \left[\frac{c_{11}}{2}(\nabla\cdot\mathbf{u})^2 + \frac{c_{66}}{2}(\nabla_\perp\cdot\mathbf{u})^2 \right.$$

$$\left. + \frac{c_{44}}{2}(\partial_z\mathbf{u})^2 + E_{pin}(\mathbf{r},\mathbf{u}) - \mathbf{F}_L\cdot\mathbf{u}\right] . \quad (4.3)$$

For small displacements, $u(\mathbf{r}) < a_0$, the disorder potential $E_{pin}$ can be taken to be short-scale correlated,

$$\langle E_{pin}(\mathbf{r},\mathbf{u})E_{pin}(\mathbf{r}',\mathbf{u}')\rangle = \gamma \frac{\xi^4}{a_0^2}\delta(\mathbf{r}-\mathbf{r}')k(\mathbf{u}-\mathbf{u}') , \quad (4.4)$$

with the disorder parameter $\gamma(=\Delta a_0^2/\xi^4)$ and the correlator $k(\mathbf{u})$ given by Eqs. (2.38) and (2.39), respectively. In the following we express the correlator (4.4) via the parameter $\Delta$ [see Eq. (3.142)], which determines the amplitude of the energy fluctuations in the disorder potential and is not related to the spatial fluctuations of the potential. In particular, a change in the basic length scale of the disorder potential will affect the pinning force, but not the fluctuations in the energy as described by $\Delta$.

The above description in terms of the continuum elastic theory of the vortex lattice is valid within a regime characterized by the condition $u < a_0$, where the lattice structure is only weakly perturbed by the disorder potential $E_{pin}$. Below we present estimates for the transverse and longitudinal lattice correlation lengths $R_a$ and $L_a$ defined by the conditions $u(R_a) \simeq u(L_a) \simeq a_0$, which turn out to be quite large for typical parameters appropriate for the oxide superconductors. For large displacements, $u \gtrsim a_0$, we have to take the internal structure of the periodic flux-line lattice into account, and we shall come back to this point later in this section. Also, despite our writing the simple local expression for the elastic energy of the vortex lattice in Eq. (4.3), we shall take the nonlocality of the elastic moduli $c_{11}(\mathbf{k})$ and $c_{44}(\mathbf{k})$ properly into account.

Again, we wish to start out with the smallest possible scale, $u < \xi$. In order to make sure that the lattice description is valid we have to consider larger fields such that $a_0 < L_c$. For small displacements, $u < \xi$, the perturbative approach of Larkin and Ovchinnikov is valid, and we can rigorously calculate the displacement field $\langle u^2(\mathbf{r})\rangle^{1/2}$: Using the (static) elastic Green's function (3.21), we can relate the displacement field $\mathbf{u}(\mathbf{r})$ to the force field $\mathbf{F}_{pin}(\mathbf{r})$ due to the disorder potential, in Fourier representation,

$$u_\alpha(\mathbf{k}) = G_{\alpha\beta}(\mathbf{k},\omega=0)F_{pin,\beta}(\mathbf{k}) . \quad (4.5)$$

The pinning force density $\mathbf{F}_{pin}(\mathbf{r})$ is given by Eq. (3.91) with $\mathbf{v}=0$ and, again using short-range disorder in $U_{pin}$ [see Eq. (2.36)], we find

$$\langle F_{pin,\alpha}(\mathbf{k})F_{pin,\beta}(\mathbf{k}')\rangle = 2\pi\gamma_U\delta(k_z+k_z')\sum_{\mu,\nu}\int d^2R e^{-i(\mathbf{K}+\mathbf{K}')\mathbf{R}}\partial_\alpha p(\mathbf{R}-\mathbf{R}_\mu)\partial_\beta p(\mathbf{R}-\mathbf{R}_\nu) . \quad (4.6)$$

Going over to Fourier representation of the form factors $p$ and evaluating the lattice sums over $\mu$ and $\nu$, we arrive at

$$\langle F_{pin,\alpha}(\mathbf{k})F_{pin,\beta}(\mathbf{k}')\rangle = -2\pi\gamma_U\delta(k_z+k_z')\frac{1}{a_0^4}\sum_{\mu,\nu}\int d^2R e^{-i(\mathbf{K}+\mathbf{K}')\mathbf{R}}e^{-i(\mathbf{K}_\mu+\mathbf{K}_\nu)\mathbf{R}}K_{\mu,\alpha}p_{K_\mu}K_{\nu,\beta}p_{K_\nu} . \quad (4.7)$$

We average the rapidly oscillating factor $\exp[-i(\mathbf{K}_\mu+\mathbf{K}_\nu)\mathbf{R}]$ over the unit cell and obtain the final result

$$\langle F_{pin,\alpha}(\mathbf{k})F_{pin,\beta}(\mathbf{k}')\rangle = (2\pi)^3\delta_{\alpha\beta}\delta(\mathbf{k}+\mathbf{k}')W , \quad (4.8)$$

with the mean-squared force density

$$W \simeq \gamma_U \frac{1}{2a_0^4}\sum_\mu \mathbf{K}_\mu^2|p_{K_\mu}|^2 \simeq \frac{\gamma_U}{a_0^2} . \quad (4.9)$$

The displacement correlation function $\langle u^2(\mathbf{r})\rangle \equiv \langle [\mathbf{u}(\mathbf{r})-\mathbf{u}(0)]^2\rangle$ can then be written in the form

$$\langle u^2(\mathbf{r})\rangle = 2W \int \frac{d^3k}{(2\pi)^3}(1-\cos\mathbf{k}\mathbf{r})$$

$$\times G_{\alpha\beta}(\mathbf{k})G_{\alpha\beta}(-\mathbf{k}) , \quad (4.10)$$

where we have used Eq. (4.5) as well as the result (4.8) for the force-force correlator. The main contribution to the

displacement field is due to the transverse part in the Green's function (3.30), and we have to evaluate the expression

$$\langle u^2(\mathbf{r}) \rangle \simeq 2W \int \frac{d^3k}{(2\pi)^3} \frac{(1-\cos \mathbf{k}\mathbf{r})}{[c_{66}K^2 + c_{44}(\mathbf{k})k_z^2]^2} \ . \qquad (4.11)$$

The largest contribution to the integral originates from the long-wavelength regime $\mathbf{k} \rightarrow 0$, where the denominator vanishes. The resulting divergence is then cut off on

the scale $k \sim 1/r$ by the numerator. Depending on the distance $\mathbf{r} = (\mathbf{R}, L > 0)$, the dispersion in $c_{44}(\mathbf{k})$ [see Eq. (3.31)] will be relevant $(a_o < R < \lambda, \ a_o < L < \lambda^2/a_o)$ or can be neglected $(R > \lambda, L > \lambda^2/a_o)$.

Let us consider first the case of large distances, where we can approximate the tilt modulus by the expression for uniform tilt, $c_{44}(k \rightarrow 0) = \hat{c}_{44}$, within the relevant regime. After performing the average over angles in the plane and rescaling the $k_z$ axis according to $(\hat{c}_{44}/c_{66})k_z^2 \rightarrow k_z^2$, we arrive at

$$\langle u^2(\mathbf{r}) \rangle \simeq \frac{2W}{c_{66}\sqrt{\hat{c}_{44}c_{66}}} \int \frac{d^3k}{(2\pi)^3} \frac{1}{k^4} \left\{ 1 - J_0(KR)\cos\left[ \left[ \frac{c_{66}}{\hat{c}_{44}} \right]^{1/2} k_z L \right] \right\} \ . \qquad (4.12)$$

The combination of the Bessel function $J_0(KR)$ and the factor $\cos[(c_{66}/\hat{c}_{44})^{1/2}k_z L]$ provides the cutoff $k_o \simeq 2[R^2 + (a_o L/\lambda)^2]^{-1/2}$ for the divergence at small wave vectors, and we obtain the final result

$$\langle u^2(\mathbf{r}) \rangle \simeq \frac{W\lambda}{2\pi^2 c_{66}\sqrt{\hat{c}_{44}c_{66}}} \left[ \frac{R^2}{\lambda^2} + \frac{a_o^2 L^2}{\lambda^4} \right]^{1/2} \ . \qquad (4.13)$$

Second, we concentrate on the dispersive regime, where we have to keep the factor $(1+\lambda^2 k^2)^{-1}$ in the tilt

modulus $c_{44}(\mathbf{k})$. Again, the main contribution arises from the small-wave-vector regime around the cutoff $K_o \simeq (R^2 + a_o L)^{-1/2}$, where the relevant values of $k_z \sim (c_{66}/\hat{c}_{44})^{1/2}\lambda K^2 \sim [a_o/(R^2 + a_o L)^{1/2}]K$ are small compared to $K$ itself. Hence we can approximate $1 + \lambda^2 k^2 \simeq \lambda^2 K^2$, and the integral in Eq. (4.11) simplifies to

$$\langle u^2(\mathbf{r}) \rangle \simeq 2W \int \frac{d^3k}{(2\pi)^3} \frac{(1-\cos \mathbf{k}\mathbf{r})\lambda^4 K^4}{[c_{66}\lambda^2 K^4 + \hat{c}_{44}k_z^2]^2} \ . \qquad (4.14)$$

Performing the (contour) integration over $k_z$ and the angular integration in the plane, we arrive at

$$\langle u^2(\mathbf{r}) \rangle \simeq - \frac{W\lambda}{4\pi} \frac{\partial}{\partial c_{66}} \int_0^{K_{BZ}^2} dK^2 \frac{1 - J_0(KR)e^{-(c_{66}/\hat{c}_{44})^{1/2}K^2\lambda L}}{\sqrt{\hat{c}_{44}c_{66}}K^2} \ . \qquad (4.15)$$

The logarithmic divergence is cut off by the numerator at $K_o^2 \simeq (R^2 + a_o L)^{-1}$, and we obtain the final result for the dispersive regime

$$\langle u^2(\mathbf{r}) \rangle \simeq \frac{W\lambda}{4\pi c_{66}\sqrt{\hat{c}_{44}c_{66}}} \frac{1}{2} \ln\left[ \frac{R^2}{a_o^2} + \frac{L}{a_o} \right] \ . \qquad (4.16)$$

The results (4.13) and (4.16) then can be combined into the general expression

$$\langle u^2(\mathbf{r}) \rangle \simeq \xi^2 \left[ \frac{a_o}{L_c} \right]^3 \left[ \left[ \frac{R^2}{\lambda^2} + \frac{a_o^2 L^2}{\lambda^4} \right]^{1/2} + \ln\left[ 1 + \frac{R^2}{a_o^2} + \frac{L}{a_o} \right] \right], \ u < \xi \ ,$$

$$a_o < L_c \ , \qquad (4.17)$$

first obtained by Larkin and Ovchinnikov [1979; a mistake in the last term of Eq. (4.17) in the original paper was later corrected by Brandt, 1986]. This result was generalized to films of finite thickness by Brandt (1986) and by Wördenweber and Kes (1987). In Eq. (4.17) we

have expressed the prefactor in terms of the more familiar length scales $\xi$, $a_o$, and the *single-vortex* collective pinning length $L_c$, using Eqs. (3.31), (3.32), and (2.45). Within the context of pinning of vortex bundles, the single-vortex collective pinning length $L_c$ does not have the meaning of a physical length scale but is used as a convenient measure for the strength of the pinning potential.

The result (4.17) is applicable within a regime bounded by the conditions

$$\langle u^2(R_c) \rangle \simeq \xi^2, \quad \langle u^2(L_c^b) \rangle \simeq \xi^2 \ . \qquad (4.18)$$

The two length scales $R_c$ and $L_c^b$ determine the real-space boundaries for the region of small spatial fluctuations $u \leq \xi$. They are usually called elastic or collective pinning lengths and are quantities corresponding to the collective pinning length $L_c$ in the single-vortex pinning regime. Note that we explicitly distinguish between the single-vortex collective pinning length $L_c$ and the longitudinal elastic length $L_c^b$ in the vortex lattice. Inverting the condition (4.18), we can easily determine the depen-

dence of the elastic lengths $R_c$ and $L_c^b$ on magnetic field and on the disorder strength. Within the dispersive regime (small length scales), we obtain an exponential dependence of the elastic lengths on the size of the magnetic field ($\tilde{c}$ is a constant of order unity),

$$R_c \simeq a_0 \exp\left[\tilde{c}\left[\frac{L_c}{a_0}\right]^3\right] \quad a_0 < R_c < \lambda \,, \tag{4.19}$$

and

$$L_c^b \simeq \frac{R_c}{a_0}R_c, \quad a_0 < L_c^b < \frac{\lambda}{a_0}\lambda \,. \tag{4.20}$$

Note that the strength of the disorder potential is parametrized by the single-vortex collective pinning length $L_c$, whereas the magnetic field enters through the lattice constant $a_0$. Within the nondispersive regime, inverting Eq. (4.18) with the help of (4.13) leads to

$$R_c \simeq \lambda\left[\frac{L_c}{a_0}\right]^3, \quad \lambda < R_c \,, \tag{4.21}$$

and

$$L_c^b \simeq \frac{\lambda}{a_0}R_c, \quad \frac{\lambda}{a_0}\lambda < L_c^b \,. \tag{4.22}$$

The crossover between the dispersive and the nondispersive regime takes place when $R_c \simeq \lambda$, and using the result (4.19) we obtain the condition

$$a_0 \simeq L_c\left[\frac{1}{\tilde{c}}\ln\frac{\lambda}{L_c}\right]^{-1/3} < L_c \,, \tag{4.23}$$

which differs only by a small logarithmic factor from the condition $a_0 \simeq L_c$ defining the boundary of the single-vortex pinning regime. Hence, in general, the dispersive regime is quite narrow. In order to obtain the explicit dependence on the magnetic-field strength $B$, we can use Eq. (2.45) above and express the ratio $L_c/a_0$ via the magnetic field $B$ and the single-vortex depinning critical current density $j_c$,

$$\frac{L_c}{a_0} \simeq \left[\frac{j_0}{j_c}\frac{B}{\beta_{sb}H_{c_2}}\right]^{1/2} \,. \tag{4.24}$$

The length scales $R_c$ and $L_c^b$ define a characteristic volume, which is elongated along the field direction and grows with increasing magnetic field. Within this volume, a maximal displacement $u \simeq \xi$ is accumulated due to elastic deformation produced by the pinning potential, and thus the vortex lattice is collectively pinned within a single metastable state. Outside of this volume the mean displacement $u$ grows beyond the elementary scale $\xi$ and the lattice is subject to competing metastable states. We call such a collectively pinned object a *small vortex bundle* if its transverse size is $R_c < \lambda$, and a *large vortex bundle* if $R_c > \lambda$; see Fig. 16. At the crossover between the single-vortex pinning regime and the lattice pinning regime all length scales are equal,
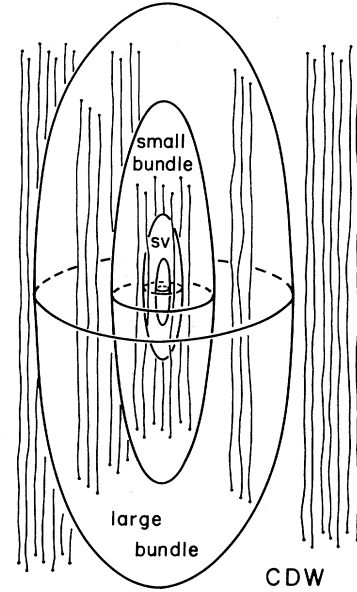


FIG. 16. Different pinning regimes appearing in a realistic description of a vortex lattice subject to quenched disorder. The innermost ellipsoid symbolizes the perturbative region where $L < L_c, u < \xi$, and where the transverse displacement field is growing according to $u \propto L^{3/2}$. Next follows the single-vortex pinning regime $L_c < L < a_0$, $u > \xi$, where $u \propto L^{3/5}$. As $L$ grows beyond the lattice constant $a_0$, the system enters the small-bundle pinning regime, where dispersion in the elastic moduli is relevant. The transverse dimension is limited by $a_0 < R < \lambda$ and the displacement correlator grows only logarithmically, $u \propto \ln R$. Within the large-bundle pinning regime ($\lambda < R < R_a$), the dispersion is irrelevant and $u$ scales according to $u \propto L^{1/5}$, which is the behavior of a conventional elastic manifold with $n = 2$, $d = 3$. At large distances, $R > R_a$, the effect of the disorder becomes weak with $u \propto \ln R$ (CDW-type pinning regime).

$L_c \simeq a_0 \simeq R_c \simeq L_c^b$, and hence the small bundles grow continuously out of the collectively pinned single-vortex segments at the crossover point.

For large distances, $R > R_c$ and $L > L_c^b$, the displacement field $\langle u^2(\mathbf{r})\rangle^{1/2}$ will grow beyond the elementary scale $\xi$ of the disorder potential, and we should take the existence of many metastable states into account. To be specific, in the above derivation we made two approximations that break down at large distances: First, the random potential was replaced by a random force independent of the displacement $\mathbf{u}$ in Eq. (4.5), which is correct in an expansion near the equilibrium position but breaks down when the displacement $u$ grows beyond the typical length scale $\xi$ of the random potential. Second, in the derivation of Eq. (4.10) we performed only an average over disorder but dropped the thermal average over all possible configurations for $\mathbf{u}$; see Eq. (3.145). Again, this approximation is correct in the vicinity of the equilibrium state, since only one minimal state is important. For large distances, however, the above procedure performs an average over all extremal states with the same weight,

which is inappropriate, since the main contribution should originate from the low-lying metastable states only. According to the results of Sec. III.F.1, the large-distance behavior of $\langle u^2(\mathbf{r}) \rangle$ should follow a power law with an exponent $\zeta_{3,2} \simeq \frac{1}{5}$. Assuming a general large-distance scaling behavior described by

$$\langle u^2(\mathbf{r}) \rangle \simeq \xi^2 \left\{ \left[ \frac{a_\circ}{L_c} \right]^3 \left[ \left[ \frac{R^2}{\lambda^2} + \frac{a_\circ^2 L^2}{\lambda^4} \right]^{1/2} \right. \right.$$
$$\left. \left. + \ln \left[ 1 + \frac{R^2}{a_\circ^2} + \frac{L}{a_\circ} \right] \right] \right\}^{2\zeta_{3,2}},$$
$$\xi < u < a_\circ, \quad (4.25)$$

then allows us to interpolate smoothly between the various expressions for the displacement correlation function. In particular, note that at large distances, where we can neglect effects due to dispersion, we correctly obtain $\langle u^2(\mathbf{r}) \rangle \propto r^{2\zeta_{3,2}}$. The interpolation formula (4.25) allows us to take the effect of dispersion in the elastic moduli into account. The weak logarithmic growth of the displacement field $\langle u^2(\mathbf{r}) \rangle^{1/2}$ within the dispersive regime changes the effective wandering exponent of the vortex lattice to the new value, $\zeta = 0$. We remark also that no condition on the magnetic-field strength has been associated with (4.25). For the case of weak fields, $a_\circ > L_c$, Eq. (4.25) describes the growth of the displacement field at large distances, following Eq. (4.2). For higher fields with $a_\circ < L_c$, the result (4.25) simply provides the continuation of the Larkin-Ovchinnikov result (4.17) for $u > \xi$.

At this point one may ask whether the above rather involved determination of the displacement field could not be obtained in a much simpler way by using dimensional estimates. The answer is "yes" and "no." In fact, the result for the nondispersive regime involving large distances, $R > \lambda$ and $L > \lambda^2/a_\circ$, can be obtained via simple estimates; however, the logarithmic growth of $\langle u^2(\mathbf{r}) \rangle^{1/2}$ within the dispersive regime cannot. The following rederivation of the result (4.13) by means of dimensional estimates serves as an illustration of the above statement and provides a better understanding of the result (4.17).

In the absence of an external force field, the vortex lattice adjusts itself to the underlying disorder potential via shear and tilt deformations alone. Due to the anisotropic elastic properties of the vortex lattice, the displacement field $\langle u^2(\mathbf{r}) \rangle^{1/2}$ grows faster along the transverse dimension: the surfaces of constant amplitude $\langle u^2(\mathbf{r}) \rangle^{1/2} = $ const are cigar shaped, with axis $L$ (longitudinal dimension, along the field) and $R$ (transverse dimension, perpendicular to the field) related via

$$L \simeq \left[ \frac{c_{44}}{c_{66}} \right]^{1/2} R > R. \quad (4.26)$$

Equation (4.26) is a consequence of the competition between the shear and tilt deformations of the lattice involving energy densities $c_{44}(u/L)^2$ and $c_{66}(u/R)^2$, re-

spectively. The ratio $c_{44}/c_{66}$ determining the aspect ratio $L/R$ depends on the length scale considered. For small distances involving deformations on a transverse length $R < \lambda$, the modulus $c_{44}(k \approx 0) = \hat{c}_{44}$ for uniform tilt will be reduced by a factor $1/(1 + \lambda^2/R^2) \simeq R^2/\lambda^2$, whereas at large distances we can approximate the tilt modulus by its uniform limit $\hat{c}_{44}$. Inserting this result back into Eq. (4.26), we find

$$L \simeq \begin{cases} \dfrac{R}{a_\circ} R, & a_\circ < R < \lambda, \\[2ex] \dfrac{\lambda}{a_\circ} R, & \lambda < R, \end{cases} \quad (4.27)$$

which is consistent with the result (4.17). Note that the aspect ratio $L/R$ grows rapidly within the dispersive regime. In addition, the shear and tilt energies have to compete with the pinning energy. Again, only fluctuations will lead to a finite pinning energy, and we have to determine

$$\langle \mathscr{E}_{\text{pin}}^2(V) \rangle = \int d^3r \, d^3r' \langle E_{\text{pin}}(\mathbf{r},0) E_{\text{pin}}(\mathbf{r}',0) \rangle. \quad (4.28)$$

For a deformation with amplitude $u < \xi$ we obtain the estimate

$$\mathscr{E}_{\text{pin}} \simeq \frac{\sqrt{\Delta V}}{\xi} \frac{u}{\xi}, \quad (4.29)$$

with $V = R^2 L$ and $\Delta$ the disorder parameter describing energy fluctuations in the disorder potential; see Eq. (3.142). Balancing the pinning energy against the elastic (shear) energy within the volume $V$, we obtain

$$u \simeq \frac{\sqrt{\Delta L}}{c_{66}\xi^2} \frac{R}{L}, \quad (4.30)$$

and inserting the result (4.27) we find for the nondispersive regime

$$u^2 \simeq \xi^2 \left[ \frac{a_\circ}{L_c} \right]^3 \frac{R}{\lambda}, \quad (4.31)$$

in agreement with the Larkin-Ovchinnikov formula (4.17). Note that the exponents $\frac{3}{2}$ and $\frac{1}{2}$ in Eqs. (4.1) and (4.31), characterizing the small-distance fluctuations in the displacement field $u$, are in agreement with the Flory result (3.158) with a random-field exponent $\beta(2) = -2$. Within the dispersive regime the distance $R$ drops out of the equation, and we obtain $\langle u^2(\mathbf{r}) \rangle \simeq$ const; instead of a weak logarithmic growth the method of dimensional estimates produces a constant value for $\langle u^2(\mathbf{r}) \rangle$. In fact, the situation is quite similar to that encountered in Sec. II.B above, where dimensional estimates failed to produce the temperature-dependent collective pinning length $L_c(T)$ for a vortex embedded in three-dimensional space. Calculating the displacement $\langle\langle u_p^2(L) \rangle\rangle$ from perturbation theory produced a *logarithmic* dependence on the length $L$, and thus we could trace back the failure of simple dimensional estimates to the marginality of the disorder for

a single vortex in three dimensions.

The above results are applicable within a regime where the typical displacement $u$ is less than the lattice constant $a_0$ of the flux-line lattice. On the other hand, the spatial fluctuations of the vortex lattice can grow well beyond this value, implying quite a drastic change in the nature of its interaction with the disorder potential. In order to understand this change, we should realize that in our analysis above we made two very basic assumptions that we have to abandon when the displacement $u$ increases beyond $a_0$: (i) adopting a continuum elastic description, we actually treat the lattice as a homogeneous, structureless medium, and (ii) the pinning of this structureless medium was achieved by assuming that a shifted vortex lattice is exposed to a *different* disorder potential, i.e., uncorrelated with the disorder potential at the initial position. Very briefly, above we studied a five-dimensional problem, where the three-dimensional vortex lattice moves within the additional two transverse dimensions uncorrelated with the original space. For displacements larger than the lattice constant, we cannot ignore the fact that the two transverse dimensions belong to our original three-dimensional space, and we have to return to the three-dimensional problem. With this point of view, for $u > a_0$ the displacement becomes "longitudinal," and therefore we should expect that the importance of the disorder potential will be drastically reduced. To be more specific, consider Eq. (4.28) describing fluctuations in the pinning energy within a volume $V$. The basic definition of the pinning energy implies the calculation of

$$\{(\mathscr{E}_{\rm pin}[\mathbf{u}_0(\mathbf{r})+\delta\mathbf{u}(\mathbf{r})]-\mathscr{E}_{\rm pin}[\mathbf{u}_0(\mathbf{r})])^2\} \ ,$$

with $\mathbf{u}_0(\mathbf{r})$ a displacement field describing some low-lying metastable state and $\delta\mathbf{u}(\mathbf{r})$ a typical excursion from $\mathbf{u}_0(\mathbf{r})$ within the volume $V$. The average $\{\cdots\}$ then has to be

taken over different metastable states with the *same* underlying disorder potential. Equation (4.28) is equivalent to the above definition if, after a displacement by a distance $\delta\mathbf{u}(\mathbf{r})$, the vortex lattice is subject to a different random environment, i.e., the disorder potential is uncorrelated over the distance $\delta\mathbf{u}(\mathbf{r})$. This assumption of uncorrelated disorder is indeed legitimate as long as the displacement of the lattice is small, $u < a_0$, but breaks down when $u$ increases beyond $a_0$, as the flux-line lattice will roughly feel the *same* disorder potential after the displacement. As a consequence, the vortex lattice cannot be pinned within the homogeneous continuum approximation for the vortex lattice. On the other hand, taking the periodically modulated internal structure of the vortex lattice into account, we again recover a finite pinning effect, which we should expect to be different from pinning due to uncorrelated disorder involving small transverse displacements $u < a_0$. In fact, Nattermann (1990) has shown that the pinning of the flux-line lattice for displacements on the scale of the lattice constant $a_0$ is in the universality class of the charge-density-wave (CDW) problem, with a wandering exponent $\zeta = 0$.

Let us follow Nattermann and consider the pinning energy

$$\mathscr{E}_{\rm pin}[\mathbf{u}(\mathbf{r})] = \int d^3r \, E_{\rm pin}(\mathbf{r},\mathbf{u})$$

$$= \int d^3r \, U_{\rm pin}(\mathbf{r}) \sum_{\nu} p\,[\mathbf{R}-\mathbf{R}_\nu-\mathbf{u}(\mathbf{R}_\nu,z)] \ .$$

(4.32)

Using the identity

$$\sum_{\nu} \delta(\boldsymbol{\rho}-\mathbf{R}_\nu) = \frac{1}{a_0^2} \sum_{\nu} e^{i\mathbf{K}_\nu \boldsymbol{\rho}}$$

we can transform Eq. (4.32) to

$$\mathscr{E}_{\rm pin}[\mathbf{u}(\mathbf{r})] = \int d^2R \, dz \, U_{\rm pin}(\mathbf{R},z) \int \frac{d^2\rho}{a_0^2} p\,[\mathbf{R}-\boldsymbol{\rho}-\mathbf{u}(\boldsymbol{\rho},z)] \left\{1+2\sum_{\nu>0}\cos\mathbf{K}_\nu\boldsymbol{\rho}\right\} \ . \qquad (4.33)$$

Performing the transformation of variables $\boldsymbol{\rho}+\mathbf{u}(\boldsymbol{\rho},z)\to\boldsymbol{\rho}$ and approximating the sharply peaked form function $p(\mathbf{R})$ by a delta function $p(\mathbf{R})\simeq\xi^2\delta(\mathbf{R})$, we arrive at

$$\mathscr{E}_{\rm pin}[\mathbf{u}(\mathbf{r})] \simeq \frac{\xi^2}{a_0^2} \int d^2R \, dz \, U_{\rm pin}(\mathbf{R},z)(1-\nabla\mathbf{u}) \left\{1+2\sum_{\nu>0}\cos\mathbf{K}_\nu[\mathbf{R}-\mathbf{u}(\mathbf{R},z)]\right\} \ . \qquad (4.34)$$

Since the displacement field $\mathbf{u}(\mathbf{r})$ is a smoothly varying function, $\nabla\mathbf{u}$ is small and the first term in the curly brackets produces only a weak dependence of $\mathscr{E}_{\rm pin}$ on the displacement field $\mathbf{u}$, hence we drop it. This is tantamount to saying that, within the homogeneous continuum approximation, the vortex lattice cannot be pinned. Restricting the sum over $\nu$ in the second term to the two primitive reciprocal-lattice vectors and assuming for simplicity a square lattice, we obtain an effective pinning energy density of the form

$$E_{\rm pin}(\mathbf{r},\mathbf{u}) \simeq \frac{2\xi^2}{a_0^2} U_{\rm pin}(\mathbf{r}) \left\{\cos\left[\frac{2\pi}{a_0}[x-u_x(\mathbf{r})]\right] \right.$$

$$\left. +\cos\left[\frac{2\pi}{a_0}[y-u_y(\mathbf{r})]\right]\right\} \ ,$$

(4.35)

which is roughly equivalent to the pinning potential in the CDW problem. Next, consider the fluctuations

$\delta \mathcal{E}_{\text{pin}}(V)$ in the pinning energy, for which we take as a reasonable measure the quantity

$$\langle \mathcal{E}_{\text{pin}}^2(V) \rangle \sim \int d^3r \, d^3r' \langle E_{\text{pin}}(\mathbf{r}, \mathbf{u}) \overline{E}_{\text{pin}}(\mathbf{r}', \overline{\mathbf{u}}) \rangle \, , \tag{4.36}$$

where $\mathbf{u}$ ($\overline{\mathbf{u}}$) denotes the *minimal* solution corresponding to the realization $E_{\text{pin}}$ ($\overline{E}_{\text{pin}}$). Inserting the result (4.35), we obtain

$$\langle \mathcal{E}_{\text{pin}}^2(V) \rangle \sim \gamma \left[ \frac{\xi}{a_0} \right]^4 \int d^3r \left\langle \cos \left[ \frac{2\pi}{a_0}(\overline{u}_x(\mathbf{r}) - u_x(\mathbf{r})) \right] + \cdots \right\rangle$$

$$\sim \gamma \left[ \frac{\xi}{a_0} \right]^4 V \exp \left[ -\frac{1}{2} \left[ \frac{2\pi}{a_0} \right]^2 \langle [\delta u]^2 \rangle \right] \, , \tag{4.37}$$

where we have assumed Gaussian fluctuations in order to evaluate the average over the displacement fields. Using Flory-type arguments, we equate the fluctuations in the elastic and the pinning energies in order to find the wandering exponent $\zeta_{\text{CDW}}$. Note that on these large length scales one should take into account the possible existence of dislocations, which can destroy the elastic properties of the lattice. Later (see Sec. VII.C) we shall argue that, due to the presence of finite dislocation loops, the shear modulus will be renormalized but remain finite at large distances, so that elastic theory is still applicable. Within this elastic approach we then obtain a logarithmic behavior for the displacement correlator at large distances,

$$\langle u^2(R) \rangle^{1/2} \simeq \frac{a_0}{\sqrt{2}\pi} \ln \frac{R}{R_{\text{CDW}}} \, , \tag{4.38}$$

with $R_{\text{CDW}} \simeq \lambda (L_c/\xi)^3 (a_0/\xi)^3$, implying a wandering exponent $\zeta_{\text{CDW}} = 0$. The weak logarithmic growth of the displacement correlator indicates that the effect of the disorder potential becomes very weak at large distances, where displacements on the scale of the lattice constant $a_0$ become relevant. This is in agreement with the above remark that pinning at large distances takes on a "longitudinal" character and should therefore be weak. The wandering of the manifold is the result of the competition between the energy gain from the disorder potential and the energy cost due to elastic distortion. At large distances, $u > a_0$, the cost in elastic energy remains the same, but the possible gain in the pinning energy is strongly restricted, as the vortex lattice experiences the same disorder potential after a shift by the lattice constant $a_0$. We also draw attention to the recent work of Bouchaud, Mézard, and Yedidia (1991, 1992), who arrive at somewhat different conclusions: Within their variational theory of the disordered vortex lattice they obtain a Flory exponent $\zeta = \frac{1}{6}$ at small displacements, $u < a_0$, and a larger value $\zeta = \frac{1}{4}$ for large displacements, $u > a_0$, hence their results produce larger fluctuations at large distances. Two very recent studies by Korshunov (1993) and by Giamarchi and Le Doussal (1994) based on the variational approach of Bouchaud *et al.* report finding the logarithmic large-distance behavior (4.38) for the displacement correlator.

The crossover to a charge-density-wave (CDW)-type

pinning regime takes place at length scales $R_a$ and $L_a$, where the conditions

$$\langle u^2(R_a) \rangle \simeq a_0^2 \quad \text{and} \quad \langle u^2(L_a) \rangle \simeq a_0^2 \tag{4.39}$$

are fulfilled. Approaching these lengths from below, it is easy to see that within the framework of weak collective pinning theory this condition is always encountered within the lattice pinning regime. Within the single-vortex pinning regime the transverse fluctuations of the string scale with distance according to

$$\langle u^2(L) \rangle^{1/2} \simeq \xi \left[ \frac{L}{L_c} \right]^{3/5} , \quad \xi < L_c < L < a_0 \, , \tag{4.40}$$

and hence the boundary in $u$-space terminating the single-vortex pinning regime, is given by the relation

$$u_{\text{sv}} \sim \xi \left[ \frac{a_0}{L_c} \right]^{3/5} < \xi^{2/5} a_0^{3/5} < a_0 \, . \tag{4.41}$$

For the case of rather strong disorder with $L_c < \xi(\xi/a_0)^{2/3} [\ln(\lambda/a_0)]^{1/3}$, the condition (4.39) is met within the dispersive regime, so that $a_0 < R_a < \lambda$. More precisely,

$$R_a \simeq a_0 \exp \left[ \overline{c} \left[ \frac{L_c}{\xi} \right]^3 \left[ \frac{a_0}{\xi} \right]^2 \right], \quad a_0 < R_a < \lambda \, , \tag{4.42}$$

where we have used Eq. (4.25), as is appropriate for the large displacement $u \simeq a_0 > \xi$. The dispersive regime is very narrow in $u$ space [$u$ grows only by a factor $\ln(\lambda/a_0)$], so that the condition (4.39) is usually fulfilled within the nondispersive regime at very large distances. In such a weak-pinning situation $R_a > \lambda$ and, inverting Eq. (4.39) with the help of (4.25), we obtain

$$R_a \simeq \lambda \left[ \frac{L_c}{\xi} \right]^3 \left[ \frac{a_0}{\xi} \right]^2 , \quad \lambda < R_a \, . \tag{4.43}$$

The longitudinal length $L_a$ is trivially determined with the help of Eq. (4.27). The length $R_a$ differs from $R_{\text{CDW}}$, the cutoff parameter obtained when approaching the boundary to the lattice pinning regime from above. However, we cannot hope to find the correct result when starting from the CDW regime, where $u$ depends only logarithmically on distance, and we should modify the result (4.38) to read

$$\langle u^2(r)\rangle^{1/2} \simeq \frac{a_\circ}{2\sqrt{2\pi}}\ln\left[1+\frac{R^2}{R_a^2}+\frac{a_\circ^2 L^2}{\lambda^2 R_a^2}\right] . \quad (4.44)$$

This completes our discussion of disorder-induced spatial fluctuations in the vortex lattice. The various regimes of single-vortex, small-bundle, large-bundle, and CDW-type relaxation of the vortex lattice to the disorder potential are illustrated in Fig. 16.

In the remainder of this section, let us turn to the fluctuations in energy. Having found all the important length scales in the problem, as well as the relevant wandering exponents we are able to calculate these quite simply. First we have to determine the basic energy scale in the problem, which is called the elastic or collective pinning energy. For the single-vortex pinning regime this energy ($U_{sv} = U_c$) was found in Sec. II.A, and the result is [Eq. (2.46)]

$$U_{sv} \simeq H_c^2 \xi^3 \frac{\xi}{L_c}, \quad L_c < a_\circ .$$

Within the lattice pinning regime, this quantity is determined in an analogous way: For a relaxed vortex lattice the tilt, shear, and pinning energies are all equal, and we use the shear energy $c_{66}(u/R)^2 V$ for expressing the basic energy scale in the problem. The latter is obtained by considering an elementary elastic domain characterized by a displacement $u \simeq \xi$ on a scale $R_c$ within the collective pinning volume $V_c \simeq R_c^2 L_c^b$,

$$U_c \simeq c_{66}\left[\frac{\xi}{R_c}\right]^2 V_c . \quad (4.45)$$

Inserting the results (4.19) and (4.20) (dispersive regime) and (4.21), (4.22) (nondispersive regime) into the expression for the shear energy, we obtain

$$U_c \simeq \begin{cases} U_{sv} \simeq H_c^2 \xi^3 \dfrac{\xi}{L_c}, & L_c < a_\circ , \\[2ex] U_{sv}\dfrac{L_c}{a_\circ}e^{2\tilde{c}(L_c/a_\circ)^3}, & L_c[\ln(\lambda/L_c)/\tilde{c}]^{-1/3} < a_\circ < L_c , \\[2ex] U_{sv}\left[\dfrac{\lambda}{a_\circ}\right]^2\left[\dfrac{L_c}{a_\circ}\right]^4, & a_\circ < L_c[\ln(\lambda/L_c)/\tilde{c}]^{-1/3} . \end{cases}$$

$$(4.46)$$

$U_c(a_\circ)$ is called the collective pinning energy. Within the small-bundle pinning regime at intermediate field strengths the pinning energy $U_c \propto \exp(B^{3/2})$ grows exponentially with field, whereas the further increase of $U_c$ in the large-bundle pinning regime turns algebraic, $U_c \propto B^3$; see Fig. 17.

Our next step is to write down the long-distance scaling behavior of the energy fluctuations of competing low-lying metastable states. We believe that these scaling laws also describe the energy barriers separating different metastable states. Assuming a weak-pinning situation
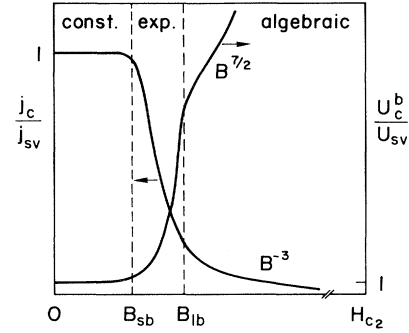


FIG. 17. Magnetic-field dependence of the critical current density $j_c$ and of the activation energy $U_c^b$ against creep. For low fields, $B < B_{sb}$, the interaction between the vortices is irrelevant and neither $j_c$ nor $U_c^b$ depends on the magnetic field. Within the small-bundle pinning regime, $B_{sb} < B < B_{lb}$, where dispersion in the elastic moduli is relevant, the critical current density decreases exponentially, whereas the activation energy shows an exponential growth. Finally, in the large-bundle pinning regime, $B > B_{lb}$, the field dependence of $j_c$ and of $U_c^b$ turns algebraic, with $j_c \propto B^{-3}$ and $U_c^b \propto B^{7/2}$.

($L_c < a_\circ$), the fluctuations in energy evolve with increasing size according to

$$U(R) \simeq U_{sv}\begin{cases} \left[\dfrac{L}{L_c}\right]^{1/5}, & L_c < L < a_\circ , \\[2ex] \left[\dfrac{a_\circ}{L_c}\right]^{1/5}\left[\dfrac{R}{a_\circ}\right]^2, & a_\circ < R < \lambda , \\[2ex] \left[\dfrac{a_\circ}{L_c}\right]^{1/5}\left[\dfrac{\lambda}{a_\circ}\right]^2\left[\dfrac{R}{\lambda}\right]^{7/5}, & \lambda < R < R_a , \\[2ex] \left[\dfrac{a_\circ}{L_c}\right]^{1/5}\left[\dfrac{\lambda}{a_\circ}\right]^2\left[\dfrac{R_a}{\lambda}\right]^{7/5}\dfrac{R}{R_a}, & R_a < R , \end{cases}$$

$$(4.47)$$

where we have used relation (3.146) between the exponents $\chi_{d,n}$ and $\zeta_{d,n}$ and have enforced continuity across the various boundaries. Note that within the dispersive regime the exponent $\chi_{d,n}$ differs from Eq. (3.146), since the longitudinal length $L$ of the small bundle scales with $R^2$; see Eq. (4.27) above. Starting out at higher fields such that $a_\circ < L_c$, we find that the elementary scale $U_c$ becomes field dependent [see Eq. (4.46)] and the scaling behavior begins within the lattice pinning regime itself. In particular, for $L_c[\ln(\lambda/L_c)]^{-1/3} < a_\circ < L_c$ the result is

$$U(R) \simeq U_c\begin{cases} \left[\dfrac{R}{a_\circ}\right]^2, & R_c < R < \lambda , \\[2ex] \left[\dfrac{\lambda}{a_\circ}\right]^2\left[\dfrac{R}{\lambda}\right]^{7/5}, & \lambda < R < R_a , \\[2ex] \left[\dfrac{\lambda}{a_\circ}\right]^2\left[\dfrac{R_a}{\lambda}\right]^{7/5}\dfrac{R}{R_a}, & R_a < R , \end{cases} \quad (4.48)$$

with $U_c \simeq U_{sv}(L_c/a_o) \exp[2\tilde{c}(L_c/a_o)^3]$, and the remaining cases are treated in an analogous fashion.

Within the present section we have presented a detailed discussion of the statistical mechanics of a flux-line lattice subject to quenched random disorder. Due to its nontrivial internal structure (length scales $\xi$ and $a_o$) and the long-range interaction between the individual vortex lines (length scales $a_o$ and $\lambda$), the statistical mechanics of a vortex lattice is much richer than that of a simple elastic manifold. This richness presents itself in a large number of different regimes, across which the interaction of the lattice with the quenched random potential changes in nature. The single-vortex pinning regime, which is relevant for low fields, $a_o > L_c$, and small distances, $L < L_c$, gives way to the small-bundle pinning regime, where dispersion in the elastic moduli renders the effect of the pinning potential marginal ($\zeta = 0$). The small bundles grow rapidly (exponentially) with increasing field strength, and the system enters the nondispersive regime as the lattice constant $a_o$ drops below $L_c[\ln(\lambda/L_c)/\tilde{c}]^{-1/3}$ or if transverse distances $R > \lambda$ are considered. Within the large-bundle pinning regime, the vortex lattice behaves like a conventional anisotropic three-dimensional elastic manifold with a wandering exponent $\zeta_{3,2} = \frac{1}{5}$. When we go to large distances, $R > R_a$ (note that the lattice correlation length $R_a$ can be smaller than $\lambda$ if the disorder is strong enough), the internal structure of the vortex lattice becomes important and we enter the CDW-type pinning regime. Here pinning is again marginally relevant ($\zeta = 0$), which we believe is a consequence of the "longitudinal" character of the transverse displacement $u > a_o$ at these large distances.

## B. Dynamics

In analogy to Sec. III.F.2 above, we shall now investigate the dynamic behavior of the vortex lattice under an applied force field. The field can be imposed by a transport current density $j_t$ flowing through the sample and generating a Lorentz force density $j_t B/c$ acting on the flux-line lattice. An alternative way to expose the manifold to a driving force field is by turning on a magnetic field and thereby forcing the sample into a critical state.

The resulting density gradient in the flux-line lattice is, via Maxwell's equations, equivalent to a screening current density $j_s$, generating again a Lorentz force density $j_s B/c$ acting on the lattice. Below, we follow the general discussion in Sec. III.F.2, but the rich structure present in the statistical mechanics of a vortex lattice, as outlined above, will also strongly influence its dynamic behavior. This can be understood by noting that the elementary scales of length ($R_c$ and $L_c^b$) and of energy ($U_c$) in the problem strongly depend on the strength of the magnetic field, i.e., on the internal length scale $a_o$ of the elastic manifold. These field-dependent elastic lengths then determine the critical force or current density. Second, a driving force field $F \simeq jB/c$ defines an additional length scale $R_{opt} \geq R_c$ in the system, which is the size of the critical nucleus determining the rate of creep. Depending on the relative position of this length with respect to the other length scales in the problem, the nature of creep will change. Let us, then, first determine the relevant scale of the driving force, i.e., the critical force or critical current density.

### 1. Critical current density

The critical force $F_c$ leading to the depinning of the manifold is given by Eq. (3.174). Each vortex bundle of volume $V_c \simeq R_c^2 L_c^b$ is collectively pinned with an energy $U_c$ given by Eq. (4.46), and the relevant length scale for pinning is the core diameter $\xi$. Therefore the pinning force is $F_p \simeq U_c/\xi$. In order to obtain the critical current density $j_c$, we have to balance the pinning force $F_p$ against the Lorentz force $F_L \simeq j_c B V_c/c$, and we obtain

$$j_c \simeq \frac{c}{B} \frac{U_c}{V_c \xi} \simeq \frac{\xi^2}{R_c^2} j_o \;, \tag{4.49}$$

where we have used the definition of $U_c$ in terms of the elastic shear energy; see Eq. (4.45). The result has been expressed via the depairing current density $j_o$ given by Eq. (2.30). Inserting Eqs. (4.19) and (4.21) for the small-bundle and large-bundle transverse dimension $R_c$, we obtain the field-dependent critical current density (see Fig. 17),

$$j_c \simeq \begin{cases} j_{sv} \simeq \dfrac{\xi^2}{L_c^2} j_o, & L_c < a_o \;, \\[3mm] j_{sv} \left[\dfrac{L_c}{a_o}\right]^2 \exp\left[-2\tilde{c}\left[\dfrac{L_c}{a_o}\right]^3\right], & L_c[\ln(\lambda/L_c)/\tilde{c}]^{-1/3} < a_o < L_c \;, \\[3mm] j_{sv}\left[\dfrac{a_o}{\lambda}\right]^2 \left[\dfrac{a_o}{L_c}\right]^4, & a_o < L_c[\ln(\lambda/L_c)/\tilde{c}]^{-1/3} \;. \end{cases} \tag{4.50}$$

As discussed above in detail, the bundle volume increases with magnetic-field strength. Since the individual pinning centers add up only randomly within the collective pinning volume, we then obtain a *decrease* in the critical

current density with increasing field. The decrease in the critical current density with increasing field strength shows an exponential dependence, $j_c \propto \exp[-B^{3/2}]$, within the small-bundle pinning regime and turns alge-

braic ($j_c \propto 1/B^3$) in the regime of large-bundle pinning; see Fig. 17. The crossover from the single-vortex pinning regime to the small-bundle pinning region takes place at a current density $j_c \sim (\xi/a_0)^2 j_0$, whereas the crossover to the large-bundle regime is given by the estimate $j_c \sim j_0/\kappa^2$. In an anisotropic superconductor the latter result remains unchanged, whereas the former one takes the form $j_c \sim (\xi/\varepsilon a_0)^2 j_0$.

Let us also remind ourselves that, in order to express the above results via the magnetic-field strength $B$, we simply have to make the substitution

$$\frac{L_c}{a_0} \simeq \left[\frac{B}{B_{sb}}\right]^{1/2}$$

in the above formulas. In particular, the crossover field from small-bundle to large-bundle pinning is given by

$$B_{lb} \simeq \beta_{lb} H_{c_2} \frac{j_{sv}}{j_0} \left[\ln\left[\kappa^2 \frac{j_{sv}}{j_0}\right]\right]^{2/3} \qquad (4.51)$$

and differs from the field $B_{sb} = \beta_{sb}(j_{sv}/j_0)H_{c_2}$, $\beta_{sb} \approx 5$, limiting the single-vortex pinning regime only by a logarithmic factor. The prefactor $\beta_{lb}$ can be estimated using the dynamic approach, and the result is $\beta_{lb} \approx 2$ (see Sec. VI.A.3 below). The arrangement of the various crossover fields is illustrated in Fig. 18.
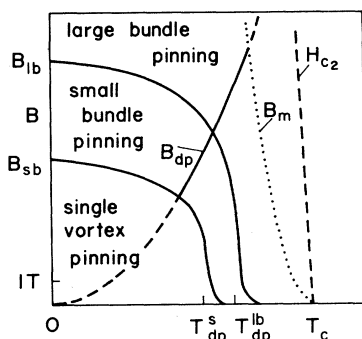


FIG. 18. Various pinning regimes and their relative position within the $B$-$T$ plane. The single-vortex pinning regime at small fields and temperatures is bounded by $B_{sb}$ and by the single-vortex depinning temperature $T_{dp}^s$. All quantities within this regime are independent of field. Within the small-bundle pinning regime, limited by $B_{lb}$ and by $T_{dp}^{lb}$, the field and temperature dependence is exponential, a consequence of dispersion in the elastic moduli. At large temperatures and fields, the system enters the large-bundle pinning regime, where dispersion is irrelevant and the dependence on $T$ and on $B$ is algebraic. With increasing temperature $T$, the crossover lines $B_{sb}(T)$ and $B_{lb}(T)$ drop rapidly after crossing the depinning line $B_{dp}(T)$ for the vortex lattice. For weak enough pinning, the melting line $B_m(T)$ is within the large-bundle pinning region and hence the melting of the vortex lattice is only weakly perturbed by the disorder. Parameters chosen apply to YBCO with $B_{sb} \approx 6$ T, $B_{lb} \approx 10$ T, $T_{dp}^s \approx 60$ K, and $T_{dp}^{lb} \approx 70$ K.

## 2. Creep near criticality

In the above discussion of the behavior of the vortex lattice in the presence of a disorder potential, we considered only tilt and shear deformations. For large magnetic fields, the compression modulus is much larger than the shear modulus, and the accommodation of the manifold to the random potential is due to the softer shear mode and does not involve compression. In the present section, we are interested in the process of creep at current densities $j \lesssim j_c$, where a small portion of the vortex lattice, the vortex bundle, jumps into a neighboring favorable metastable state, while the remaining part of the lattice remains in place. In order to gain energy from the driving Lorentz force, the lattice then has to undergo a compression. Consider a displacement field $\mathbf{u}(\mathbf{r})$ restricted to the bundle volume $V$. The energy gain $\mathcal{E}_L(V)$ due to the Lorentz force is given by

$$\mathcal{E}_L(V) = \frac{1}{c} \int dV [\mathbf{j} \wedge \mathbf{B}] \cdot \mathbf{u} , \qquad (4.52)$$

which can be transformed to

$$\mathcal{E}_L(V) = \frac{1}{c} \int dV [\mathbf{j} \wedge \mathbf{B} \cdot \mathbf{r}](\nabla \cdot \mathbf{u}) , \qquad (4.53)$$

and the lattice indeed has to undergo a finite compression in order to gain energy out of its motion in the force field. For fields $B > B_{sb}$, the interaction among the vortices is essential, and the hop of a vortex bundle will involve considerable compression energy, which we should take into account in our determination of the activation energy. If we then allow a number of bundles to jump simultaneously, we can lower the compressional energy involved in the creep process. The idea is that an elongated (along the direction of the jump) bundle of bundles, a superbundle with dimensions $R_\parallel$ (parallel to the jump direction), $R_\perp \simeq R_c$ (transverse to the field and the jump direction), and $L^b$ (along the field direction), will constitute the elementary unit in the creep process; see Fig. 19. The dimensions of this superbundle have to be determined by minimizing the total elastic energy involved in the jump, including the compression energy as well. The following simple estimate works well in the nondispersive regime, where the vortex-vortex interaction is effectively short ranged. Comparing the compression and shear energy densities $c_{11}(u/R_\parallel)^2 \simeq c_{66}(u/R_\perp)^2$, the parallel dimension $R_\parallel$ can be expressed through the perpendicular size $R_\perp$,

$$R_\parallel \simeq \left[\frac{c_{11}}{c_{66}}\right]^{1/2} R_\perp \qquad (4.54a)$$

and one obtains the scaling relation

$$R_\parallel \simeq \frac{\lambda}{a_0} R_\perp \qquad (4.54b)$$

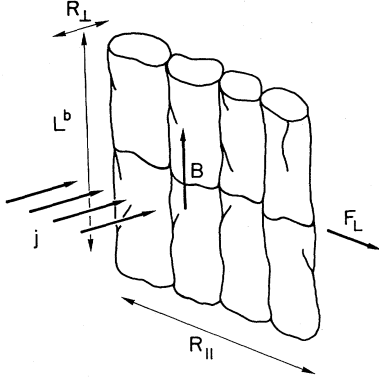between the parallel and perpendicular dimensions of the superbundle. In the original treatments of classical col-

FIG. 19. Superbundle made up of collectively pinned bundles. Due to the compression of the vortex lattice in the direction of the jump, the optimal configuration for creep involves an elongated superbundle with dimensions $R_\perp$ (perpendicular), $R_\parallel$ (parallel to the hop), and $L^b$ (parallel to the field). Close to criticality, the jump involves $(R_\parallel/R_c)(L^b/L_c^b)=(R_c/a_0)^3$ collectively pinned bundles.

lective creep by Feigel'man *et al.* (1989) and of quantum collective creep by Blatter *et al.* (1991) the same approach has been used in the nonlocal regime by accounting for the dispersive nature of the compression modulus via the substitution $c_{11} \rightarrow c_{11}(1/R_\perp)$ in (4.54a), producing the scaling $R_\parallel \simeq R_\perp^2/a_0$. It has been pointed out by Koshelev (1994) that this simple treatment cannot be applied in the region where the two planar scales $R_\perp$ and $R_\parallel$ become different and that a more careful analysis produces the different scaling behavior $R_\parallel \simeq R_\perp^3/a_0^2$ within the (fully) dispersive regime. In the following we adopt the approach by Koshelev (1994) and present a derivation of the superbundle dimensions valid for any size and form of the superbundle.

For small bundles we have to account for the long-range nature of the vortex-vortex interaction (dispersion in the elastic moduli) and we obtain the following estimates for the tilt and compression energies

$$\mathcal{E}_{\text{tilt}} = \frac{B^2}{32\pi^2\lambda^2} \int d^3r\, d^3r' \frac{e^{-|\mathbf{r}-\mathbf{r}'|/\lambda}}{|\mathbf{r}-\mathbf{r}'|} \partial_z \mathbf{u}\, \partial_{z'}\mathbf{u}$$

$$\sim \frac{B^2}{\lambda^2} \frac{R_\perp^2 R_\parallel^2}{R_\parallel} u^2 \,, \qquad (4.55\text{a})$$

where we have assumed that $R_\parallel$ is the largest dimension of the bundle. Similarly, we obtain for the compression energy

$$\mathcal{E}_{\text{comp}} = \frac{B^2}{32\pi^2\lambda^2} \int d^3r\, d^3r' \frac{e^{-|\mathbf{r}-\mathbf{r}'|/\lambda}}{|\mathbf{r}-\mathbf{r}'|} (\nabla \mathbf{u})(\nabla'\mathbf{u})$$

$$\sim \frac{B^2}{\lambda^2} \frac{R_\perp^2(L^b)^2}{R_\parallel} u^2 \,. \qquad (4.55\text{b})$$

Equating tilt and compression energy we find $L^b \simeq R_\parallel$

and the comparison with the shear energy

$$E_{\text{shear}} = \frac{B^2 a_0^2}{64\pi^2\lambda^2} \int d^3r\, d^3r' \delta(\mathbf{r}-\mathbf{r}')(\nabla_\perp \mathbf{u})(\nabla'_\perp \mathbf{u})$$

$$\sim \frac{B^2 a_0^2}{\lambda^2} \frac{R_\perp R_\parallel L^b}{R_\perp^2} u^2 \,, \qquad (4.55\text{c})$$

provides the estimates

$$R_\parallel \simeq L^b \simeq \frac{R_\perp^3}{a_0^2}, \quad R_\perp < R_\parallel \simeq L^b < \lambda \,, \qquad (4.56\text{a})$$

for the superbundle dimensions in the fully dispersive regime (small superbundle). Note, that the scaling (4.56a) differs from the previous result (4.27), $L \simeq R^2/a_0$, which applies to the elementary bundle where no compression is involved and hence $R_\parallel \simeq R_\perp = R_c$. The corresponding result can be obtained from a comparison of (4.55a) with (4.55c), taking into account that in this case the largest dimension is $L^b$ rather than $R_\parallel$.

As the largest dimensions $L^b$ and $R_\parallel$ increase beyond the screening length $\lambda$ we should cut the corresponding lengths in (4.55a) and (4.55b) on the scale $\lambda$ and find $\mathcal{E}_{\text{tilt}} \simeq (B^2/\lambda^2)(R_\perp^2 \lambda R_\parallel /L^b)u^2$ and the same result with $R_\parallel$ and $L^b$ interchanged for $\mathcal{E}_{\text{comp}}$. The size of the superbundle in this semidispersive regime (intermediate superbundle) is then given by

$$R_\parallel \simeq L^b \simeq \left[\frac{R_\perp^3 \lambda}{a_0^2}\right]^{1/2}, \quad R_\perp < \lambda < R_\parallel \simeq L^b \,. \qquad (4.56\text{b})$$

Finally, as the smallest length scale $R_\perp$ crosses the screening length $\lambda$ as well, we enter the nondispersive regime where the vortex interaction is effectively short ranged and we find the (large) superbundle dimensions [see also the result (4.54b) above]

$$R_\parallel \simeq L^b \simeq \frac{\lambda}{a_0} R_\perp, \quad \lambda < R_\perp < R_\parallel \simeq L^b \,. \qquad (4.56\text{c})$$

The activation energy of a superbundle in the creep process near $j_c$ is given by

$$U_c^b \simeq c_{66} \frac{u^2}{R_\perp^2} R_\perp R_\parallel L^b \simeq \frac{R_\parallel}{R_c} \frac{L^b}{L_c^b} U_c \,. \qquad (4.57)$$

The important point to note here is that the individual subbundles are formed independently via the competition between the elastic tilt and shear energies and the disorder potential (the transverse size $R_\perp \simeq R_c$ follows from this optimization of the *sub*bundles). For the creep process, the large value of the compression modulus, $c_{11} \gg c_{66}$, prohibits the hopping of individual subbundles and therefore the latter are coupled together, leading to the hop of a large superbundle. The activation energy $U_c^b$ for such a correlated hop is then roughly given by the sum of the activation energies for the subbundles.

Inserting in (4.57) the above results for the (super)bundle dimensions we obtain the following final result for the activation energy $U_c^b$ of a vortex bundle near $j_c$:

$$U_c^b \simeq \begin{cases} U_{sv} \simeq H_c^2 \xi^3 \left[ \dfrac{j_{sv}}{j_0} \right]^{1/2} \simeq \dfrac{T_c \sqrt{1-t}}{\sqrt{Gi}} \left[ \dfrac{j_{sv}}{j_0} \right]^{1/2}, \quad L_c < a_0, \\[4mm] U_{sv} \dfrac{L_c}{a_0} e^{5\tilde{c}(L_c/a_0)^3}, \quad L_c[\ln(\lambda/L_c)/3\tilde{c}]^{-1/3} < a_0 < L_c, \\[4mm] U_{sv} \dfrac{L_c \lambda}{a_0^2} e^{2\tilde{c}(L_c/a_0)^3}, \quad L_c[\ln(\lambda/L_c)/\tilde{c}]^{-1/3} < a_0 < L_c[\ln(\lambda/L_c)/3\tilde{c}]^{-1/3} \\[4mm] U_{sv} \left[ \dfrac{\lambda}{a_0} \right]^3 \left[ \dfrac{L_c}{a_0} \right]^4, \quad a_0 < L_c[\ln(\lambda/L_c)/\tilde{c}]^{-1/3}. \end{cases} \tag{4.58}$$

The case of quantum creep can be handled in an analogous fashion. The additional quantity to be determined is the duration of the hop, the collective tunneling time $t_c$. The dynamic behavior of a vortex lattice is usually dominated by dissipation; hence we can estimate the energy density stored in the damped motion to be $\eta \xi^2 / t_c$. Equating this result to the (shear) elastic energy density,

we obtain a tunneling time $t_c \simeq (\eta/c_{66})R_c^2$, and the action for quantum creep becomes

$$S_c^b \simeq t_c U_c^b \simeq \eta \xi^2 R_\perp R_\parallel L^b. \tag{4.59}$$

Making use of Eqs. (4.19), (4.21), and (4.56a)–(4.56c), and using the Bardeen-Stephen result (2.26) for the friction coefficient, we obtain the final results

$$S_c^b \simeq \begin{cases} S_{sv} \simeq \dfrac{\hbar^2}{e^2} \dfrac{\xi}{\rho_n} \left[ \dfrac{j_0}{j_{sv}} \right]^{1/2} \simeq \dfrac{\hbar}{Qu} \left[ \dfrac{j_0}{j_{sv}} \right]^{1/2}, \quad L_c < a_0, \\[4mm] S_{sv} \dfrac{a_0}{L_c} e^{7\tilde{c}(L_c/a_0)^3}, \quad L_c[\ln(\lambda/L_c)/3\tilde{c}]^{-1/3} < a_0 < L_c, \\[4mm] S_{sv} \dfrac{\lambda}{L_c} e^{4\tilde{c}(L_c/a_0)^3}, \quad L_c[\ln(\lambda/L_c)/\tilde{c}]^{-1/3} < a_0 < L_c[\ln(\lambda/L_c)/3\tilde{c}]^{-1/3}, \\[4mm] S_{sv} \left[ \dfrac{\lambda}{a_0} \right]^5 \left[ \dfrac{L_c}{a_0} \right]^8, \quad a_0 < L_c[\ln(\lambda/L_c)/\tilde{c}]^{-1/3}. \end{cases} \tag{4.60}$$

At criticality the activation energy for classical creep and the action for quantum creep vanish according to

$$U(j) \simeq U_c^b \left[ 1 - \dfrac{j}{j_c} \right]^\alpha \tag{4.61}$$

and

$$S(j) \simeq S_c^b \left[ 1 - \dfrac{j}{j_c} \right]^{\alpha_S}. \tag{4.62}$$

Unfortunately, the exponents $\alpha$ and $\alpha_S$ are not known for the random pinning potential. For the periodic pinning potential the exponents were found in Sec. III.E above; see Eqs. (3.109) and (3.117). For the periodic potential the dimensions of the critical nucleus diverge near criticality. If this divergence were also present for the random pinning potential, the system would show a very interesting behavior by exploring all the different pinning regimes as the critical nucleus expands to infinity on approaching $j_c$.

### 3. Creep at small driving forces

Next we want to investigate the dynamic response of the system at small current densities, $j \ll j_c(a_0)$, where

the hopping distance $u$ for optimal jumps grows beyond the elementary length scale $r_p \simeq \xi$ of the disorder potential. The original discussion of pinning and creep by Larkin (1970) and by Larkin and Ovchinnikov (1973, 1979) was based on the perturbative approach, which is valid for displacements $u$ smaller than the characteristic length scale $r_p$ of the pinning potential. As the displacements grow beyond this limit, the perturbative approach breaks down in two respects: First of all, due to the presence of many metastable minima, the elastic medium can choose among many low-lying states, which then leads to a different scaling behavior of the mean displacement field and of the energy fluctuations, as discussed in detail in Sec. III.E. Second, pinning is due to the presence of a random potential rather than a random force field. For small distances, $u < r_p$, this distinction is not important, as the random pinning potential can be expanded and becomes equivalent to a random force field. However, this expansion breaks down for displacements going beyond the scale $r_p$ of the pinning potential. As shown above in Sec. III.F, the scaling behavior of an elastic manifold subject to a random field differs quite appreciably from the scaling behavior induced by a short-range correlated random potential. Instead of a random pinning force we

then have to consider a random pinning potential in our discussion of creep at small current densities. In the following we shall analyze collective creep in a vortex lattice as outlined in the work of Feigel'man *et al.* (1989).

As pointed out in Sec. III.F.2 above, the present case of vortex creep can be considered as a special application of the general theory of disorder-dominated creep-type motion of elastic manifolds subject to an external force field $F$. Therefore all the results obtained in Sec. III.F.2 above can be adapted to the vortex lattice with only minor modifications. These modifications are due to the long-range nature of the interaction among the vortices and also due to the internal structure of the vortex lattice itself. We should expect deviations from the standard results within the small- (and intermediate-)bundle regime at distances, $a_o < R, L < \lambda$ (where the long-range interaction leads to dispersive elastic moduli $c_{11}$ and $c_{44}$) and again within the CDW-type pinning regime at large distances, $R > R_a$ (where the displacement field takes on a "longitudinal" character and only the internal structure of the lattice produces pinning).

To begin with, consider a sample prepared in a critical state at low temperature and magnetic-field values, $T < T_{dp}^s \ln[(j_{sv}/j_o)(\beta_{sb}H_{c_2}/B)]^{1/3}$, $B < B_{sb}$, where we can apply the results of the single-vortex collective pinning theory. According to Eqs. (2.71) and (2.78), the current density $j$ will decay with a nonlinear logarithmic time law

$$j(t) \sim j_{sv} \left[ \frac{T}{U_{sv}} \ln \frac{t}{t_o} \right]^{-7} \tag{4.63}$$

until the current density $j_{sb} \simeq j_{sv}[(B/\beta_{sb}H_{c_2})(j_o/j_{sv})]^{7/10}$ has been reached, where the interaction between the vortices becomes important. These results, of course, are in agreement with the more general results of Sec. III.F.2 if we identify $F = f_L = j\Phi_o/c$, $F_c = j_{sv}\Phi_o/c$, and use the value $\zeta_{1,2} = \frac{3}{5}$ for the line-wandering exponent. As the current drops below $j_{sb}$, we enter the lattice pinning regime, and the critical nucleus for creep will be a small vortex bundle elongated along the direction both of the

field and of the motion. The general results (3.179), (3.185), and (3.190), with the appropriate values for the exponents $\mu$ and $\mu_S$, then have to be modified due to the dispersive nature of the elastic moduli.

Within the small-bundle pinning regime, the bundle dimensions along the field as well as along the direction of the hop grow very fast, $L^b \simeq R_\parallel \simeq R_\perp^3/a_o^2$. Using the scaling behavior of $R_\perp$ with current density $j$, Eq. (3.177), $R_\perp(j) \propto (j_o/j)^{1/(2-\zeta)}$, we find the scaling laws $L^b \sim R_\parallel \propto (j_o/j)^{3/(2-\zeta)}$ for the bundle dimensions in the field/force plane. For intermediate size bundles we have $L^b \simeq R_\parallel \simeq (R_\perp^3\lambda/a_o^2)^{1/2}$ and hence $L^b \sim R_\parallel \propto (j_o/j)^{3/2(2-\zeta)}$. Finally, for large bundles, $L^b \simeq R_\parallel \simeq (\lambda/a_o)R_\perp$, and no additional scaling factors arise. To summarize, we have to modify the results of Sec. III.F within the small- (and intermediate-)bundle pinning regime by changing the exponents $\mu$ and $\mu_S$,

$$\mu \to \mu + \frac{4}{2-\zeta} ,$$

$$\mu_S \to \mu_S + \frac{4}{2-\zeta}, \quad \text{small bundles} . \tag{4.64a}$$

$$\mu \to \mu + \frac{1}{2-\zeta} ,$$

$$\mu_S \to \mu_S + \frac{1}{2-\zeta}, \quad \text{intermediate bundles} . \tag{4.64b}$$

A second complication concerns the wandering exponent $\zeta$: Within the small-bundle pinning regime, the generalized Larkin-Ovchinnikov result (4.25) for the displacement correlation function $\langle u^2(r) \rangle$ depends only logarithmically on the distances $R$ and $L$, and hence the wandering exponent changes to the new value $\zeta = 0$ within the small-bundle creep regime. This reduced exponent remains also valid within the intermediate-bundle creep regime where the transverse length $R_\perp$ due to the shear relaxation in the subbundles is still smaller than the screening length $\lambda$. Combining the results of Sec. III.F.2 with the above considerations, we obtain the following exponents $\mu$ and $\mu_S$ (overdamped motion) characterizing creep of vortex bundles within the lattice pinning regime:

$$\mu, \mu_S = \begin{cases} \frac{5}{2}, \frac{7}{2} & \text{small bundles}, \ a_o < R_\perp, \ R_\parallel \simeq L^b < \lambda , \\ 1, 2 & \text{intermediate bundles}, \ a_o < R_\perp < \lambda < R_\parallel \simeq L^b , \\ \frac{7}{9}, \frac{16}{9} & \text{large bundles}, \ \lambda < R_\perp, \ R_\parallel \simeq L^b . \end{cases} \tag{4.65}$$

The above results are applicable within a lattice pinning regime where the typical hopping distance $u$ is less than the lattice constant $a_o$ of the flux-line lattice. On the other hand, the relevant hopping distance $u$ can grow well beyond this value, e.g., when the current density $j$ is decreased or when relaxation is simply considered on very large scales (see Sec. IV.E), implying a crossover to CDW-type pinning as discussed in Sec. IV.A above. Within this regime, the line-wandering exponent $\zeta$ is again reduced to zero, so that the exponents $\mu$ and $\mu_S$ be-

come

$$\mu, \mu_S = \frac{1}{2}, \frac{3}{2}, \quad \text{CDW-type pinning}, \ R_a < R . \tag{4.66}$$

We are now ready to collect the results describing creep at small driving forces, $j \ll j_c$. Let us assume that our sample initially was prepared in a critical state belonging to the single-vortex pinning regime, that is, $L_c < a_o$. As the current $j$ decays due to creep, the activation barrier $U(j)$, the action $S(j)$, and the current $j$ itself, evolve according to the following scheme:

$$U(j) \simeq \begin{cases} U_{sv}\left[\dfrac{j_{sv}}{j}\right]^{1/7}, & j_{sb} < j \ll j_{sv}, \\[2ex] U_{sb}\left[\dfrac{j_{sb}}{j}\right]^{5/2}, & j_{sb}(a_o/\lambda)^{2/3} < j < j_{sb}, \\[2ex] U_{sb}\dfrac{\lambda}{a_o}\dfrac{j_{sb}}{j}, & j_{lb} < j < j_{sb}(a_o/\lambda)^{2/3}, \\[2ex] U_{lb}\left[\dfrac{j_{lb}}{j}\right]^{7/9}, & j_{CDW} < j < j_{lb}, \\[2ex] U_{CDW}\left[\dfrac{j_{CDW}}{j}\right]^{1/2}, & 0 < j < j_{CDW}, \end{cases} \qquad (4.67)$$

$$S(j) \simeq \begin{cases} S_{sv}\left[\dfrac{j_{sv}}{j}\right]^{8/7}, & j_{sb} < j \ll j_{sv}, \\[2ex] S_{sb}\left[\dfrac{j_{sb}}{j}\right]^{7/2}, & j_{sb}(a_o/\lambda)^{2/3} < j < j_{sb}, \\[2ex] S_{sb}\dfrac{\lambda}{a_o}\left[\dfrac{j_{sb}}{j}\right]^{2}, & j_{lb} < j < j_{sb}(a_o/\lambda)^{2/3}, \\[2ex] S_{lb}\left[\dfrac{j_{lb}}{j}\right]^{16/9}, & j_{CDW} < j < j_{lb}, \\[2ex] S_{CDW}\left[\dfrac{j_{CDW}}{j}\right]^{3/2}, & 0 < j < j_{CDW}, \end{cases} \qquad (4.68)$$

$$j(t) \simeq \begin{cases} j_{sv}\left[\dfrac{T}{U_c}\ln\dfrac{t}{t_0}\right]^{-7}, & j_{sb} < j \ll j_{sv}, \\[2ex] j_{sb}\left[\dfrac{T}{U_{sb}}\ln\dfrac{t}{t_o}\right]^{-2/5}, & j_{sb}(a_o/\lambda)^{2/3} < j < j_{sb}, \\[2ex] j_{sb}\dfrac{\lambda}{a_o}\left[\dfrac{T}{U_{sb}}\ln\dfrac{t}{t_o}\right]^{-1}, & j_{lb} < j < j_{sb}(a_o/\lambda)^{2/3}, \\[2ex] j_{lb}\left[\dfrac{T}{U_{lb}}\ln\dfrac{t}{t_o}\right]^{-9/7}, & j_{CDW} < j < j_{lb}, \\[2ex] j_{CDW}\left[\dfrac{T}{U_{CDW}}\ln\dfrac{t}{t_o}\right]^{-2}, & 0 < j < j_{CDW}. \end{cases}$$

$$(4.69)$$

The parameters

$$U_{sb} \simeq U_{sv}\left[\dfrac{a_o}{L_c}\right]^{1/5}, \qquad S_{sb} \simeq S_{sv}\left[\dfrac{a_o}{L_c}\right]^{8/5},$$

$$j_{sb} \simeq j_{sv}\left[\dfrac{L_c}{a_o}\right]^{7/5}, \qquad U_{lb} \simeq U_{sb}\left[\dfrac{\lambda}{a_o}\right]^{3},$$

$$S_{lb} \simeq S_{sb}\left[\dfrac{\lambda}{a_o}\right]^{5}, \qquad j_{lb} \simeq j_{sb}\left[\dfrac{a_o}{\lambda}\right]^{2}, \qquad (4.70)$$

$$U_{CDW} \simeq U_{lb}\left[\dfrac{a_o^2 L_c^3}{\xi^5}\right]^{7/5}, \qquad S_{CDW} \simeq S_{lb}\left[\dfrac{a_o^2 L_c^3}{\xi^5}\right]^{16/5},$$
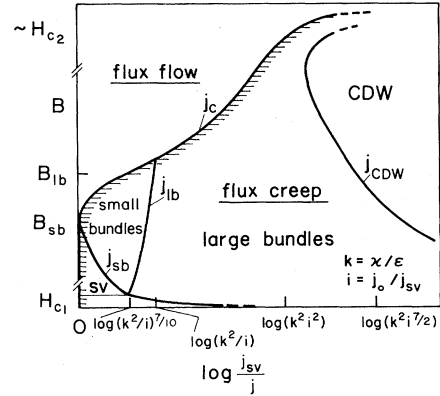


FIG. 20. Various creep regimes and their relative position within the $B$-$j$ plane. The $B$-$j$ plane is divided up into a large-field/large-current part, where the disorder is irrelevant (flux-flow regime), and a low-field/low-current portion below the critical current density $j_c(B)$, where the vortex system moves only via creep. The flux-creep regime is divided up into a single-vortex creep regime at large current densities (creep via activation of individual vortex segments) followed by the small to intermediate and large-bundle creep regimes at lower current densities (larger fields), where the nucleus for creep consists of a three-dimensional vortex bundle. At very low current densities the system enters the CDW creep regime. Note that the CDW regime cannot be reached by increasing the field, but only by decreasing the current density, i.e., by approaching equilibrium ($j \to 0$).

$$j_{CDW} \simeq j_{lb}\left[\dfrac{\xi^5}{a_o^2 L_c^3}\right]^{9/5}$$

are determined by the condition of continuity at the crossover between the various regimes. The dependencies $j_c(B)$, $j_{sb}(B)$, $j_{lb}(B)$, and $j_{CDW}(B)$ and the resulting partition of the $B$-$j$ plane into the various dynamic regimes is illustrated in Fig. 20. The time evolution of the screening current density $j$ for the case of quantum creep is obtained by simple inversion of the relation $S(j) = \hbar \ln(t/t_o)$ and use of Eq. (4.68).

The glass exponents $\mu$ derived above differ from those obtained by Feigel'man *et al.* (1989) within the nonlocal regime: The exponent $\mu = \frac{3}{2}$ characterizing the small-bundle regime has to be substituted by $\mu = \frac{5}{2}$. Furthermore, an additional intermediate regime appears which is characterized by the exponent $\mu = 1$. The mistake in the original derivation is due to the oversimplified derivation of the superbundle dimensions based on (4.54a), a fact pointed out by Koshelev (1994). The same mistake has been done in a preprint version of this work with consequences for the results on both the classical as well as on the quantum collective creep.

## C. Thermal depinning

In close analogy to the case of single-vortex pinning, thermal fluctuations will also lead to a smoothing of the disorder potential for a pinned three-dimensional vortex

lattice. Hence we expect an increase in the collective pinning volume $V_c$ with temperature and, consequently, an increase in the activation energy $U_c^b$ and a decrease in the critical current density $j_c$.

The first discussion of thermal smoothing of the disorder potential was that of Feigel'man and Vinokur (1990), who based their calculation on the dynamic approach.

Later, Koshelev (1990) used the method of dimensional estimates in his analysis of the interplay between thermal fluctuations and pinning in a two-dimensional vortex lattice. Here we shall concentrate on the simpler approach using dimensional estimates. Let us follow the discussion in Sec. II.B and determine the time-averaged pinning energy to lowest order in the disorder parameter $\gamma_U$,

$$\langle\langle\mathscr{E}_{\text{pin}}(V)\rangle_t^2\rangle=\int\frac{dt}{t_o}d^3r\int\frac{dt'}{t_o}d^3r'\langle E_{\text{pin}}[\mathbf{r},\mathbf{u}(\mathbf{r},t)]E_{\text{pin}}[\mathbf{r}',\mathbf{u}(\mathbf{r}',t')]\rangle\ ,\qquad(4.71)$$

with the pinning energy density $E_{\text{pin}}$ given by Eq. (3.89) with $\mathbf{v}=0$ and $\mathbf{u}_p=0$. Assuming a short-scale correlated disorder potential and going over to Fourier representation for the form factors $p$, we obtain

$$\langle\langle\mathscr{E}_{\text{pin}}(V)\rangle_t^2\rangle=\gamma_U L\sum_{\mu,\nu}\int\frac{dt}{t_o}\frac{dt'}{t_o}\int\frac{d^2K}{(2\pi)^2}|p_\mathbf{K}|^2e^{i\mathbf{K}(\mathbf{R}_\mu-\mathbf{R}_\nu)}e^{i\mathbf{K}[\mathbf{u}_\mu(t)-\mathbf{u}_\nu(t')]}\ .\qquad(4.72)$$

The largest contribution is obtained from the terms with $\mu=\nu$. Assuming Gaussian thermal fluctuations, we arrive at

$$\langle\langle\mathscr{E}_{\text{pin}}(V)\rangle_t^2\rangle\simeq\frac{\gamma_U}{a_o^2}V\int\frac{d^2K}{(2\pi)^2}|p_K|^2e^{-(1/2)K^2\langle u^2(t)\rangle_{\text{th}}}\ .\qquad(4.73)$$

Compared with the one-dimensional case studied in Sec. II.B above, the discussion of thermal fluctuations in the vortex lattice is considerably simplified by the finiteness of the mean-squared thermal displacement $\langle u^2(t\to\infty)\rangle_{\text{th}}=2\langle u^2\rangle_{\text{th}}$, with $\langle u^2\rangle_{\text{th}}=\langle u^2(\mathbf{r},t)\rangle_{\text{th}}$, independent of position and time. At small temperatures, where $\langle u^2\rangle_{\text{th}}<\xi^2$, the $K$ integral in Eq. (4.73) is cut off by the factor $|p_\mathbf{K}|^2$ at a wave vector $K\sim1/\xi$,

$$\langle\langle\mathscr{E}_{\text{pin}}(L)\rangle_t^2\rangle\simeq\gamma_U\frac{\xi^2}{a_o^2}V\simeq\frac{\Delta}{\xi^2}V,\quad T\to0\ .\qquad(4.74)$$

At higher temperatures, where $\langle u^2\rangle_{\text{th}}>\xi^2$, the Debye-Waller factor $\exp[-K^2\langle u^2\rangle_{\text{th}}]$ provides the cutoff at $K\sim1/\langle u^2\rangle_{\text{th}}^{1/2}$ and

$$\langle\langle\mathscr{E}_{\text{pin}}(L)\rangle_t^2\rangle\simeq\gamma_U\frac{\xi^4}{a_o^2\langle u^2\rangle_{\text{th}}}V\simeq\frac{\Delta}{\langle u^2\rangle_{\text{th}}}V\ ,$$

$$T>T_{\text{dp}}\ .\qquad(4.75)$$

Here we have introduced the depinning temperature $T_{\text{dp}}$ for a vortex lattice defined by the crossover condition

$$\langle u^2(T_{\text{dp}})\rangle_{\text{th}}\simeq\xi^2\ .\qquad(4.76)$$

Next, let us determine the mean-square amplitude of thermal fluctuations $\langle u^2\rangle_{\text{th}}$. We first relate the correlator $\langle u^2\rangle_{\text{th}}$ to the static elastic Green's function $G(\omega=0)$: Expressing the Green's function $G(\omega)$ in the fluctuation-dissipation theorem (2.113) by its Fourier transform

$G(t)$, we obtain

$$\langle u^2(t)\rangle_{\text{th}}=4T\int\frac{d\omega}{2\pi}$$
$$\times\int dt'\frac{\sin\omega t'}{\omega}[1-\cos(\omega t)]G(\mathbf{r}=0,t')\ ,$$

$$(4.77)$$

which can be further simplified to

$$\langle u^2(t)\rangle_{\text{th}}=2T\int dt'G(t')\int\frac{d\omega}{\pi}\frac{1}{\omega}[\sin\omega t'-\tfrac{1}{2}\sin\omega(t'+t)$$
$$-\tfrac{1}{2}\sin\omega(t'-t)]\ .$$

$$(4.78)$$

The integral over frequencies produces the cutoff function

$$\text{sign}t'-\tfrac{1}{2}\text{sign}(t'+t)-\tfrac{1}{2}\text{sign}(t'-t)\qquad(4.79)$$

and we obtain

$$\langle u^2(t)\rangle_{\text{th}}=2T\int_o^t dt'\,G(t')\ .\qquad(4.80)$$

Going back to Fourier space and taking the limit $t\to\infty$, we immediately find [note that $G(t<0)=0$]

$$\langle u^2(t)\rangle_{\text{th}}=2TG(\mathbf{r}=0,\omega=0)\qquad(4.81)$$

and hence

$$\langle u^2\rangle_{\text{th}}=\langle u_x^2+u_y^2\rangle_{\text{th}}=T\int\frac{d^3k}{(2\pi)^3}\sum_\alpha G_{\alpha\alpha}(\mathbf{k},\omega=0)=T\int\frac{d^3k}{(2\pi)^3}\left[\frac{1}{c_{11}(\mathbf{k})K^2+c_{44}(\mathbf{k})k_z^2}+\frac{1}{c_{66}K^2+c_{44}(\mathbf{k})k_z^2}\right]\ ,$$

$$(4.82)$$

where we have used the Green's function (3.30) for the vortex lattice. A very accurate calculation of the correlator $\langle u^2 \rangle_{\text{th}}$ has been given by Houghton, Pelcovits, and Sudbø (1989). Here we present only a rough estimate for illustrative purposes. The main contribution to the integral originates from the second term and is concentrated in the region $K \sim K_{\text{BZ}}$, $k_z \sim (c_{66}/\hat{c}_{44})^{1/2} \lambda K^2 \lesssim K/2$. Hence we can drop the $k_z^2$ term in comparison with $K^2$ [we remind reader that $\hat{c}_{44} = c_{44}(\mathbf{k} = 0)$ is the elastic modulus for a uniform tilt ]. The integral then simplifies to

$$\langle u^2 \rangle_{\text{th}} \approx T \int \frac{dK^2}{4\pi} \frac{dk_z}{2\pi} \frac{\lambda^2 K^2}{c_{66}\lambda^2 K^4 + \hat{c}_{44}k_z^2} . \qquad (4.83)$$

The integration over $k_z$ leads to

$$\langle u^2 \rangle_{\text{th}} \approx \frac{\lambda T}{8\pi\sqrt{c_{66}\hat{c}_{44}}} \int_0^{K_{\text{BZ}}^2} dK^2 , \qquad (4.84)$$

which indeed is dominated by the large-$K$ wave vectors near the Brillouin-zone boundary. The final result can be written in a particularly simple form,

$$\langle u^2 \rangle_{\text{th}} \approx \frac{1}{8\sqrt{\pi}} \frac{T}{c_{66}a_o^3} a_o^2 \approx \frac{1}{2\sqrt{\pi}} \frac{T}{\varepsilon_o a_o} a_o^2 . \qquad (4.85)$$

This result can be interpreted in the following way: Consider a large-amplitude deformation of the vortex lattice with $\delta u \simeq a_o$ on a length $a_o$. Such a deformation costs a typical energy $c_{66}a_o^3 \approx \varepsilon_o a_o /4$. As $T$ reaches this characteristic energy, the thermal amplitude of fluctuations becomes of the order of the lattice constant $a_o$.

Combining the result (4.85) with the definition (4.76), we obtain the depinning temperature

$$T_{\text{dp}} \simeq 2\sqrt{\pi} \varepsilon_o \xi^2 \left[ \frac{B}{\Phi_o} \right]^{1/2} . \qquad (4.86)$$

Note that right-hand side of (4.86) does not depend on temperature. Moreover, Eq. (4.86) for the depinning temperature of the vortex lattice crosses over to the result (2.130) for the single-vortex depinning temperature as the field $B$ drops below $B_{\text{sb}}$; see Fig. 18. It is convenient to express the depinning temperature in terms of the ratio of the two parameters characterizing the strength of thermal fluctuations $Gi$ and of the disorder potential $j_{\text{sv}}/j_o$. Using the definition (4.86) for the depinning temperature and Eq. (2.47) for the Ginzburg number $Gi$, we obtain

$$T_{\text{dp}} \approx \frac{T_c}{\sqrt{Gi}} \left[ \frac{B}{\beta_{\text{dp}}H_{c_2}(0)} \right]^{1/2} \approx \left[ \frac{B}{B_{\text{sb}}} \right]^{1/2} \tilde{T}_{\text{dp}}^s$$

$$\simeq \left[ \frac{1}{Gi} \frac{j_{\text{sv}}(0)}{j_o(0)} \right]^{1/2} \left[ \frac{B}{B_{\text{sb}}(0)} \right]^{1/2} T_c , \qquad (4.87)$$

where we have made use of the definition (2.79) of the crossover field $B_{\text{sb}}$ in the last relation. The ratio $j_{\text{sv}}(0)/(j_o(0)Gi)$ is of the order of unity in YBCO and is

smaller than 0.1 for the Bi- and Tl- based compounds where $Gi \sim 0.1 - 1$. In conventional superconductors, the corresponding quality is much larger due to the smallness of $Gi$. Hence we obtain the important result that the depinning line in the $H$-$T$ phase diagram

$$B_{\text{dp}} = \beta_{\text{dp}}Gi \, H_{c_2}(0) \left[ \frac{T}{T_c} \right]^2$$

$$\simeq Gi \frac{j_o(0)}{j_{\text{sv}}(0)} B_{\text{sb}}(0) \left[ \frac{T}{T_c} \right]^2 , \qquad (4.88)$$

rises much more steeply with temperature than in conventional superconductors, emphasizing the important role of thermal fluctuations. Using the results of Houghton, Pelcovits, and Sudbø (1989) for the thermal displacement amplitude $\langle u^2 \rangle_{\text{th}}$, we obtain the prefactor

$$\beta_{\text{dp}} \approx 8 . \qquad (4.89)$$

The shape of the depinning line is illustrated in Fig. 18.

Let us return to the pinning problem and discuss the effect of thermal fluctuations on the smoothing of the disorder potential. Comparison between the low- and high-temperature results (4.74) and (4.75) shows that, if we first express the disorder strength by the parameter $\Delta$, then the high-temperature result (4.75) can be obtained from the low-temperature equation (4.74) by a simple substitution of $\langle u^2 \rangle_{\text{th}}$ for $\xi^2$. Here we should remember that the disorder parameter $\Delta$ describes fluctuations in energy [see Eq. (3.142)] and therefore is not rescaled due to thermal smoothing, which affects only the pinning forces via the change in the basic length scale $r_p$ of the disorder potential and leaves the basic energy scale unchanged. Second, in all the expressions for the shear, tilt, and compression energy densities, as well as in the energy gain due to the Lorentz force, we have to substitute for the length scale $r_p(T \to 0) \simeq \xi$ of the disorder potential the thermal length $r_p(T > T_{\text{dp}}) \simeq \langle u^2 \rangle_{\text{th}}^{1/2}$, as the latter represents the new minimal length scale that can be resolved by the individual vortices. This recipe of substituting $\langle u^2 \rangle_{\text{th}}$ for $\xi^2$ then allows us to generalize the results of Secs. IV.A and B in a simple way so as to include the effects of thermal fluctuations. In particular, we can combine the low- and high-temperature results into one expression by defining the temperature-dependent effective length scale $r_p(T)$ of the disorder potential,

$$r_p^2(T) \simeq \xi^2 \left[ 1 + \frac{\langle u^2 \rangle_{\text{th}}}{\xi^2} \right] \simeq \xi^2 \left[ 1 + \frac{T}{T_{\text{dp}}} \right] . \qquad (4.90)$$

Let us concentrate first on the collective pinning length $R_c$. Substituting $\Delta/\xi^4$ for the mean-squared force density $W$ in the Larkin-Ovchinnikov result (4.17), we obtain the new prefactor

$$\frac{W}{4\pi} \frac{1}{c_{66}\sqrt{\hat{c}_{44}c_{66}}} \to r_p^2(T) \left[ \frac{\xi^2}{r_p^2(T)} \frac{a_o}{L_c} \right]^3 ; \qquad (4.91)$$

hence the transverse pinning length $R_c$ determined by the condition $\langle u^2(\mathbf{r}) \rangle \simeq r_p^2(T)$ becomes

$$R_c \simeq \begin{cases} a_\circ, & L_c(T) < a_\circ, \\[2ex] a_\circ \exp\left\{ \tilde{c} \left[ \dfrac{L_c}{a_\circ} \dfrac{r_p^2(T)}{\xi^2} \right]^3 \right\}, & L_c[r_p^2(T)/\xi^2]\{\ln[\lambda\xi^2/L_c r_p^2(T)]\}^{-1/3} < a_\circ < L_c(T), \\[2ex] \lambda \left[ \dfrac{L_c}{a_\circ} \dfrac{r_p^2(T)}{\xi^2} \right]^3, & a_\circ < L_c[r_p^2(T)/\xi^2]\{\ln[\lambda\xi^2/L_c r_p^2(T)]\}^{-1/3}. \end{cases} \qquad (4.92)$$

In order to obtain the explicit dependence on the magnetic field $B$ and on temperature, we have to substitute

$$\frac{L_c}{a_\circ} \frac{r_p^2(T)}{\xi^2} \rightarrow \left[ \frac{B}{B_{\mathrm{sb}}} \left[ 1 + \frac{T}{T_{\mathrm{dp}}} \right]^2 \right]^{1/2} \qquad (4.93)$$

in the above formulas. In particular, the temperature-dependent crossover fields $B_{\mathrm{sb}}(T)$ and $B_{\mathrm{lb}}(T)$ are given by

$$B_{\mathrm{sb}}(T) \approx \beta_{\mathrm{sb}} \frac{j_{\mathrm{sv}}}{j_\circ} H_{c_2} \left[ 1 + \frac{T}{\tilde{T}_{\mathrm{dp}}^s} \right]^2 \exp\left[ -2c \left[ \alpha + \frac{T}{\tilde{T}_{\mathrm{dp}}^s} \right]^3 \right] \qquad (4.94)$$

[see Eq. (2.178)] and

$$B_{\mathrm{lb}}(T) \approx \beta_{\mathrm{lb}} \frac{j_{\mathrm{sv}}}{j_\circ} H_{c_2} \left[ \frac{T_{\mathrm{dp}}}{T_{\mathrm{dp}} + T} \right]^2$$
$$\times \left\{ \ln\left[ \kappa^2 \frac{j_{\mathrm{sv}}}{j_\circ} \left[ \frac{T_{\mathrm{dp}}}{T_{\mathrm{dp}} + T} \right]^2 \right] \right\}^{2/3}, \qquad (4.95)$$

and decrease with increasing temperature $T$; see Fig. 18.

Next, let us determine the complete temperature and field dependence of the critical current density $j_c(B, T)$ and of the activation energy $U_c^b(B, T)$ for creep. The generalization of Eq. (4.49) to arbitrary temperatures reads

$$j_c(B, T) \simeq \frac{\xi r_p(T)}{R_c^2} j_\circ. \qquad (4.96)$$

Note that the product $\xi j_\circ$ is independent of $\xi$ in the above expression. The final result for the critical current density is

$$j_c(B, T) \simeq \begin{cases} j_\circ \dfrac{B_{\mathrm{sb}}}{\beta_{\mathrm{sb}} H_{c_2}} \left[ 1 + \dfrac{T}{\tilde{T}_{\mathrm{dp}}^s} \right]^2 \exp\left\{ -\dfrac{3c}{2} \left[ \alpha + \dfrac{T}{\tilde{T}_{\mathrm{dp}}^s} \right]^3 \right\}, & B < B_{\mathrm{sb}}(T), \\[3ex] j_\circ \dfrac{B}{\beta_{\mathrm{sb}} H_{c_2}} \left[ 1 + \dfrac{T}{T_{\mathrm{dp}}} \right]^{1/2 + 2\tilde{c}/c} \exp\left\{ -2\tilde{c} \left[ \dfrac{B}{B_{\mathrm{sb}}} \left[ 1 + \dfrac{T}{T_{\mathrm{dp}}} \right]^2 \right]^{3/2} \right\}, & B_{\mathrm{sb}}(T) < B < B_{\mathrm{lb}}(T), \\[3ex] j_\circ \dfrac{1}{\kappa^2} \left[ \dfrac{B_{\mathrm{sb}}}{B} \right]^3 \left[ \dfrac{T_{\mathrm{dp}}}{T_{\mathrm{dp}} + T} \right]^{11/2}, & B_{\mathrm{lb}}(T) < B, \end{cases} \qquad (4.97)$$

where we have already substituted the scaled temperature, field, and disorder variables $T/T_{\mathrm{dp}}$, $B/B_{\mathrm{sb}}$, and $j_{\mathrm{sv}}/j_\circ$ for the corresponding length scales $r_p(T)$, $a_\circ$, and $L_c$. Care has been taken to smoothly connect the single-vortex and small-bundle pinning regimes. The results (4.97) are in agreement with those obtained by Feigel'man and Vinokur (1990) based on the dynamic approach. The parameter $\alpha$ (of order unity) has been introduced in order to interpolate properly between the $T = 0$ and the $T > T_{\mathrm{dp}}^s$ results. In particular, as follows from the dynamic approach (see Sec. VI.A.1), finite-

temperature corrections enter the formalism via a Debye-Waller factor $\exp(-K^2 \langle u^2 \rangle_{\mathrm{th}}/2)$. Expanding this factor, we find that the lowest-order correction, $K^2 \langle u^2 \rangle_{\mathrm{th}} \propto T$, is linear in the temperature.

Similarly, we obtain the basic expression for the pinning energy $U_c(B, T)$ of an elementary bundle in the form

$$U_c(B, T) \simeq c_{66} \frac{r_p^2(T)}{R_c^2} V_c, \qquad (4.98)$$

and the activation energy for creep becomes

$$U_c^b(B) \simeq U_{sv} \begin{cases} \left[1+\dfrac{T}{\tilde{T}_{dp}^s}\right], & B < B_{sb}(T) , \\[4mm] \left[\dfrac{B}{B_{sb}}\left[1+\dfrac{T}{T_{dp}}\right]^2\right]^{1/2} \exp\left\{3\tilde{c}\left[\dfrac{B}{B_{sb}}\left[1+\dfrac{T}{T_{dp}}\right]^2\right]^{3/2}\right\}, & B_{sb}(T) < B < B_{lb}(T) , \\[4mm] \kappa^3\left[\dfrac{B}{H_{c_2}}\right]^{3/2}\left[\dfrac{B}{B_{sb}}\left[1+\dfrac{T}{T_{dp}}\right]^2\right]^2, & B_{lb}(T) < B . \end{cases} \qquad (4.99)$$

Note that the ratio of current densities $j_{sv}/j_o$ entering the right-hand side of Eqs. (4.92), (4.97), and (4.99) via $L_c$ or $B_{sb}$ describes the disorder strength and can be replaced by the dimensionless disorder parameter $\delta$ introduced in Sec. III.C, $j_{sv}/j_o = \delta^{2/3}$.

The high-temperature limit $T > T_{dp}$ of the results (4.92), (4.97), and (4.99) can be simplified considerably by noting that

$$\left[\frac{B}{B_{sb}}\left[1+\frac{T}{T_{dp}}\right]^2\right]^{1/2} \simeq \frac{L_c}{a_o}\frac{r_p^2(T)}{\xi^2} \simeq \frac{T}{\tilde{T}_{dp}^s} + \left[\frac{B}{B_{sb}}\right]^{1/2} . \tag{4.100}$$

For $T > T_{dp}$, the first term on the right-hand side of Eq. (4.100), which does not depend on the magnetic field, is dominant. However, the residual dependence on the magnetic field described by the second term is not necessarily small, and we must be careful in dropping this term. With this proviso we can obtain a very simple result for the relevant length scale of a collectively pinned object at high temperatures, to leading order,

$$L_c(T) \simeq L_c e^{(T/\tilde{T}_{dp}^s)^3}, \quad L_c(T) < a_o ,$$

$$R_c(T) \simeq \begin{cases} L_c \exp\left[\dfrac{T}{\tilde{T}_{dp}^s} + \cdots\right]^3, & a_o < R_c(T) < \lambda , \\[4mm] \lambda\left[\dfrac{T}{\tilde{T}_{dp}^s} + \cdots\right]^3, & \lambda < R_c(T) , \end{cases} \tag{4.101}$$

where we have substituted $L_c$ for the prefactor $a_o$ in the expression for the radius $R_c(T)$ within the small-bundle pinning regime in order to guarantee continuity. Most interestingly, to leading order in the parameter $T/\tilde{T}_{dp}^s$, all these lengths become independent of the magnetic field $B$ at high temperatures. The corresponding expressions for the critical current density $j_c$ and for the activation energy $U_c^b$ in the high-temperature limit can be obtained straightforwardly. Note that we have to take the additional temperature dependence of the microscopic parameters $\xi(T)$ and $\lambda(T)$ as well as the temperature dependence of the disorder parameter $\delta$ into account as we approach the transition temperature $T_c$. For the case of $\delta T_c$ pinning, the latter is given by Eq. (3.78), $\delta(T) \propto (1-T/T_c)^{-1/2}$. The temperature dependence of the single-vortex depinning energy $\tilde{T}_{dp}^s$ (which is the relevant parameter at high temperatures) then becomes $\tilde{T}_{dp}^s = \tilde{T}_{dp}^s(0)(1-T/T_c)^{1/3}$, whereas the depinning tem-

perature $T_{dp}$ does not depend on $T/T_c$.

At smaller temperatures, $T < T_{dp}$, we have to expand the temperature-dependent factor $(1+T/T_{dp})^n \simeq 1+nT/T_{dp}$, and the leading temperature dependence is determined by the ratio $T/T_o$ with

$$T_o \simeq T_{dp}\left[\frac{B_{sb}}{B}\right]^{3/2}$$

$$\simeq T_c\left[\frac{1}{Gi}\frac{j_{sv}(0)}{j_o(0)}\right]^{1/2}\frac{B_{sb}(0)}{B}\left[1-\frac{T}{T_c}\right] , \tag{4.102}$$

where we have used the definition (2.79) for the field $B_{sb}$ limiting the single-vortex pinning regime and we have expressed the depinning temperature via the ratio $j_{sv}/j_o$ $Gi$ measuring the relative strengths of quenched and thermal disorder; see Eq. (4.87). In the high-temperature superconductors, typical values for the combination $j_{sv}(0)/j_o(0)Gi$ are of the order of unity (for conventional superconductors, the corresponding quantity is much larger due to the smallness of the Ginzburg number), and hence for large enough fields, $B \gg B_{sb}$, we shall obtain an appreciable temperature dependence of the various characteristic scales $(R_c, j_c, U_c^b)$ even at low temperatures $T \ll T_c$. In particular, within the small-bundle pinning regime the critical current density will decay exponentially with

$$j_c(B,T) \propto e^{-T/T_o(B)}, \quad B_{sb} < B < B_{lb} . \tag{4.103}$$

Close to the transition temperature (but still above the depinning line), the temperature dependence of the critical density will be dominated by the leading term in the expansion of $(1+T/T_{dp})^3$ (i.e., 1) and hence

$$j_c(B,T) \propto e^{-(B/B_{sb}(0))^{3/2}[T_c/(T_c-T)]}, \quad B_{sb} < B < B_{lb} . \tag{4.103'}$$

Finally, let us briefly discuss how the various pinning regimes fit into the $H$-$T$ phase diagram. Here we should offer a word of warning: The boundaries $B_{sb}(T)$ and $B_{lb}(T)$ are quantities relevant at critical current densities $j \simeq j_c$ and therefore *do not* belong to the equilibrium phase diagram, which is characterized by a vanishing current density $j=0$. In order to describe the relevant physics of the vortex lattice, we therefore should consider a three-dimensional diagram $H$-$T$-$j^{-1}$ as shown in Fig. 21. The numerical estimates for the various characteristic quantities as they typically apply to the new high-temperature superconductors will be presented at the end

of Sec. IV.D below, after the discussion of effects due to anisotropy. Let us first concentrate on the equilibrium phase diagram at $j=0$. Here the important lines are the mean-field transition line $H_{c_2}(T)$, separating regions with zero and finite local order parameter, and the line marking the lower critical field $H_{c_1}$, separating the Meissner-Ochsenfeld regime from the mixed state. As we shall discuss in more detail in Sec. V, thermal fluctuations can lead to melting of the vortex lattice at temperatures still well below the mean-field transition line $H_{c_2}(T)$, thus defining a melting line $B_m(T)$ which separates the vortex solid from the vortex liquid phase. The latter can be estimated by the Lindemann criterion (Lindemann, 1910), which predicts a melting transition as the thermal fluctuations $\langle u^2 \rangle_{th}^{1/2}$ in the vortex lattice grow to a substantial fraction of the lattice constant $a_0$,

$$\langle u^2(T_m) \rangle_{th} \approx c_L^2 a_0^2 , \qquad (4.104)$$

with the Lindemann number $c_L \sim 0.1 - 0.2$. Making use of the result (4.85), we obtain a melting temperature $T_m(B)$

$$T_m(B) \approx 2\sqrt{\pi} \varepsilon_0 c_L^2 \left[ \frac{\Phi_0}{B} \right]^{1/2}$$

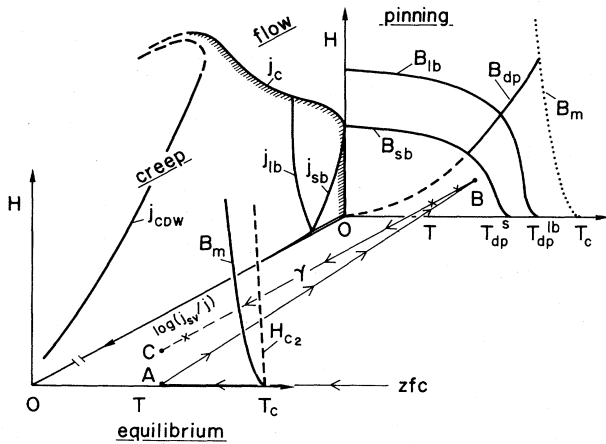$$\approx \left[ \frac{\beta_m}{Gi} \right]^{1/2} c_L^2 \left[ \frac{H_{c_2}}{B} \right]^{1/2} T_c , \qquad (4.105)$$



FIG. 21. Three-dimensional phenomenological phase diagram $H$-$T$-$j$ for an anisotropic high-temperature superconductor. Parameters for YBCO have been chosen. The different regimes of pinning, creep, and flow divide the phase space into separate regions. The various pinning regimes relevant at $j \simeq j_c$ are shown in the back; see also Fig. 18. When the current density $j$ is decreased, the system probes the various creep regimes on approaching equilibrium; see also Fig. 20. Under equilibrium conditions (front) the currents in the system vanish. The current axis also can be understood as a time axis via the relation $j(t) \propto [\ln(t/t_0)]^{-1/\mu}$. The path of a typical magnetic relaxation experiment is illustrated, in which a sample is cooled under zero-field conditions to the point $A$. When a magnetic field is switched on, a critical state is formed ($B$), which subsequently decays via creep ($\gamma$) to the equilibrium vortex-glass state ($C$).

with

$$\beta_m \approx \pi^2 . \qquad (4.106)$$

Inverting Eq. (4.105), we obtain the melting line in the $H$-$T$ diagram (for a more detailed discussion, see Sec. V, below)

$$B_m(T) \approx \beta_m \frac{c_L^4}{Gi} H_{c_2}(0) \left[ 1 - \frac{T}{T_c} \right]^2 , \qquad (4.107)$$

where $H_{c_2}(0)$ again denotes the upper critical field extrapolated *linearly* to zero. Using the more accurate results of Houghton, Pelcovits, and Sudbø (1989), we see that the coefficient $\beta_m$ takes the value

$$\beta_m \approx 5.6 . \qquad (4.108)$$

For the oxide superconductors, the main part of the phase diagram is covered by the mixed phase with an extremely steep $H_{c_2}$ line and a correspondingly flat $H_{c_1}$ boundary. For anisotropic (as opposed to strongly layered) superconductors, the melting temperature $T_m$ is still close to the transition temperature $T_c$.

On the opposite side at $j \simeq j_c$ we first concentrate on the depinning line. Typically, the melting temperature is close to $T_c$ and the intersection of the depinning line with the melting line takes place at a temperature $T^* \approx T_c$ and a field $H^* \approx \beta_{dp} Gi\, H_{c_2}(0) \approx 8Gi\, H_{c_2}(0)$; see Eq. (4.88) above. Next let us insert the various pinning regimes into the diagram. Consider a case in which the pinning is very weak so that

$$T_{dp}^s \approx \alpha_{dp}^s \left[ \frac{1}{Gi} \frac{j_{sv}}{j_0} \right]^{1/2} T_c \ll T_c , \qquad (4.109)$$

with $\alpha_{dp}^s \approx 0.7$ if we base the determination of $T_{dp}^s$ on the more reliable dynamic approach (see Sec. VI.A.3 below). Note that the condition (4.109) clearly distinguishes the new high-temperature superconductors, which are characterized by a rather large Ginzburg number, from the conventional superconductors with a small value for $Gi$. The weak-pinning condition (4.109) is usually satisfied by the Bi- and Tl-based compounds with $Gi \sim 0.1 - 1$ and is on the borderline for YBCO; however, it is very difficult to fulfill in conventional materials. The single-vortex pinning regime is always located below the melting line $B_m(T)$. Note that the two boundaries limiting the single-vortex pinning regime in temperature $(T < T_{dp}^s)$ and in field $(B < B_{sb})$ always intersect on the depinning line; see Fig. 18. The same is true for the boundaries limiting the small-bundle pinning regime. Evaluating $B_{lb}(T)$ for $T < T_{dp}$, we obtain $B_{lb}(T) \approx \beta_{lb}(j_{sv}/j_0)\{\ln[\kappa^2(j_{sv}/j_0)]\}^{2/3} H_{c_2}$, hence $B_{lb}$ follows the shape of the upper critical field until it intersects with the depinning line. The logarithmic correction factor is usually small, so that $B_{lb}$ closely follows the boundary $B_{sb}$ of the single-vortex pinning regime. The extent of the dispersive regime is rather narrow. When we expand $B_{lb}(T)$ for temperatures $T > T_{dp}$, the field drops out of the equation, and hence the small-bundle regime

is bounded by a straight line at $T_{dp}^{lb}$ $\simeq \{\ln[\kappa^2(j_{sv}/j_{\circ})]\}^{1/3} T_{dp}^s$; see Figs. 18 and 21.

As we move away from the critical current density towards thermodynamic equilibrium (where $j = 0$), we cross the various regimes of single-vortex creep, small-bundle creep, and the large-bundle creep regime. Finally, at very small current densities the system enters the CDW-type creep regime; see Fig. 21. The three-dimensional diagram is very useful for the understanding of the time evolution of the system. Consider for example a typical magnetic relaxation experiment, where a sample is first cooled in zero field to a point $A = (j = 0, H = 0, T < T_c)$ within the phase diagram. Upon switching on a field $H_a$, a critical state is established within the sample, and the system jumps to the point $B = (j = j_c, H = H_a, T)$. After this, the critical state decays slowly in time and the system evolves gradually through the various creep regimes as indicated by the line $\gamma$ until it reaches equilibrium $(C)$. Note that by the time the system reaches the CDW-type creep regime a "glassy" order, as discussed in Sec. A, above has been established within the sample.

If the pinning is rather "strong," so that $T_{dp}^s$ approaches the transition temperature $T_c$, we have to account for the various temperature dependencies appearing in the expression for $\tilde{T}_{dp}^s$ [see Eq. (2.128)]. Let us first concentrate on the limit of vanishing field. Using Eqs. (3.73) and (3.79) we obtain an implicit equation for the depinning temperature $T_{dp}^s$,

$$\frac{T_{dp}^s}{T_c} \simeq \left[ \frac{1}{Gi} \frac{j_{sv}(0)}{j_{\circ}(0)} \right]^{1/2} \left[ 1 - \frac{T_{dp}^s}{T_c} \right]^{1/3}, \qquad (4.110)$$

which can be trivially solved near $T_c$ to give

$$T_{dp}^s \simeq T_c \left\{ 1 - \left[ Gi \frac{j_{\circ}(0)}{j_{sv}(0)} \right]^{3/2} \right\} \simeq T_c . \qquad (4.111)$$

The condition for $T_{dp}^s$ to lie outside of the critical regime of fluctuations is $1 - T_{dp}^s/T_c > Gi$ and thus we obtain the weak-pinning condition

$$\left[ \frac{j_{sv}(0)}{j_{\circ}(0)} \right]^3 < Gi . \qquad (4.112)$$

Since $(j_{sv}/j_{\circ})^3 \ll j_{sv}/j_{\circ}$, we then find that if pinning in the high-temperature superconductors is relatively large, so that $T_{dp}^s$ is driven close to $T_c$, the weaker condition (4.112) is usually easy to fulfill and hence, due to the largeness of $Gi$, we expect $T_{dp}^s$ to lie outside of the critical regime. On the other hand, in conventional superconductors with a rather small Ginzburg number, the condition (4.112) may not be fulfilled and therefore the pinning can be strong.

Let us consider such a strong-pinning situation where the depinning temperature $T_{dp}^s$ is driven into the critical regime. Again using Eqs. (3.73) and (3.79), we can determine the temperature $T_d$, where disorder becomes strong in the sense that $j_{sv}(T_d) \simeq j_{\circ}(T_d)$. For the present situation of strong disorder with $[j_{sv}(0)/j_{\circ}(0)]^3 > Gi$, the tem-

perature $T_d \simeq 1 - [j_{sv}(0)/j_{\circ}(0)]^3$ then comes to lie *outside* the critical regime as defined by $T/T_c > 1 - Gi$. Therefore fluctuations induced by the quenched disorder potential are larger than those induced by thermal disorder within the entire critical regime. As a consequence, the transition itself will change its nature from a homogeneous transition dominated by thermal fluctuations to an inhomogeneous, percolation-type transition dominated by the strong disorder potential (Ioffe and Larkin, 1981).

Let us turn now to finite values of the magnetic field and determine the condition which guarantees that the entire single-vortex pinning regime is located below the melting line. The latter is a necessary requirement for the melting transition itself not to be strongly influenced by disorder. The depinning line crosses the melting line at the field value $H^* \approx \beta_{dp} Gi \, H_{c_2}(0) \approx 8 Gi \, H_{c_2}(0)$, and in order for the single-vortex pinning regime not to touch the melting line the condition $B_m(T_{dp}^s) > H^*$ has to be fulfilled. The melting line $B_m(T)$ depends quadratically on $1 - T/T_c$ [see Eq. (4.107) above]. Evaluating the melting field at the depinning temperature,

$$B_m(T_{dp}^s) \approx \beta_m \frac{c_L^4}{Gi} H_{c_2}(0) \left[ 1 - \frac{T_{dp}^s}{T_c} \right]^2 , \qquad (4.113)$$

and using the result (4.111) for the single-vortex depinning temperature near $T_c$ (for the case where $T_{dp}^s$ is far below $T_c$ the single-vortex pinning regime terminates far below the melting line), we obtain the condition

$$\left[ \frac{j_{sv}(0)}{j_{\circ}(0)} \right]^3 < Gi \, c_L^4 \frac{\beta_m}{\beta_{dp}} \approx \frac{5.6}{8} Gi \, c_L^4 . \qquad (4.114)$$

Again, in the high-temperature superconductors this condition is still easy to fulfill due to the largeness of the Ginzburg number $Gi$, and thus we expect that the melting line is not strongly influenced by the quenched disorder potential.

## D. Anisotropy

Since the oxide superconductors are all highly anisotropic, there is an obvious need to generalize our results to anisotropic materials. We have a choice between two alternative methods, the traditional approach used in Sec. II.C for the regime of single-vortex pinning and the scaling approach introduced in Sec. III.A. Pinning of vortex bundles is concerned with length scales that can grow beyond the London penetration depth; therefore we cannot hope to obtain all the desired results from the scaling approach. On the other hand, the scaling approach provides simpler and more direct access to the desired results. We shall therefore split the discussion of anisotropy into two parts: In Sec. IV.D.1 we use the scaling approach in order to find the results within the dispersive regime involving length scales $R < \lambda$. Since the dispersive moduli also contain the larger penetration

depth $\lambda/\varepsilon$, the above condition does not enclose all of the dispersive regime, let alone the nondispersive one. In Sec. IV.D.2, we then demonstrate how to obtain the results for all length scales for the special case in which the magnetic field is pointing along the high-symmetry axis of the crystal. It turns out that the analysis of even this simple situation is already very tedious, and we therefore refrain from presenting the most general results here. Neither of the two regimes discussed below covers the small but interesting regime of small fields, $H < H_{c_1}^c/\varepsilon_\vartheta$, away from the $c$ axis, where very interesting phenomena such as lattice instabilities (formation of vortex chains) have been observed (Bolle *et al.*, 1991; Gammel *et al.*, 1992; see the discussion in Sec. III.B).

### 1. Scaling results

For the regime of single-vortex pinning the generalization of the results to anisotropic materials has been discussed in Secs. II.C, II.D, and III.A. Here we concentrate on the lattice pinning regime where we can use our scaling approach in the small but important regime of small-bundle pinning. Let us first determine the boundary restricting the applicability of the scaling method. Unfortunately, the scaling approach is not able to cover all of the dispersive regime limited by the condition $R_\perp \simeq \lambda/\varepsilon$, but has to be restricted to length scales $R_c = R_\perp < \lambda$ for the case of pinning and to $R_\parallel < \lambda$ for creep. Here, $R_\parallel$ denotes the dimension of the superbundle along the direction of the hop. In fact, we will see that the scaling results are valid even in the larger regime characterized by the condition $R_\parallel < \lambda/\varepsilon = \lambda_c$. First concentrate on pinning: Inserting for $R_\perp$ the collective pinning length $R_c \simeq a_0 \exp[\tilde{c}(L_c/a_0)^3]$ and rescaling the condition $R_\perp \simeq \lambda$ with the help of Eq. (3.12), we find that the scaling results are restricted to fields $B < B_{sc}$, with

$$B_{sc} \simeq H_{c_2}(\vartheta)\frac{J_{sv}^c}{j_0}\left[\frac{1}{2\tilde{c}}\ln\left[\kappa^2\frac{j_{sv}^c}{j_0}\right]\right]^{2/3} . \qquad (4.115)$$

Here, $j_{sv}^c$ is the planar critical current density in the single-vortex pinning regime for the case $\mathbf{H}\|c$, $j_{sv}^c \simeq \varepsilon^{-2/3}j_{sv}^{iso}$, and $H_{c_2}(\vartheta)$ is the angle-dependent upper critical field, $H_{c_2}(\vartheta) = \Phi_0/2\pi\varepsilon_\vartheta\xi^2$. For creep the condition $R_\parallel \simeq \lambda/\varepsilon$ translates to $(R_\perp/a_0)^3 \simeq \lambda/\varepsilon a_0$ (see below; we assume here that $\mathbf{B}\|c$) and we have to replace the coefficient $2\tilde{c}$ in (4.115) by $6\tilde{c}$. The in-plane critical current density $j_c^\parallel(\vartheta)$ ($\mathbf{j}\perp\mathbf{H}$) and the activation energy and action for creep near criticality are obtained by applying the scaling rule (3.12) to the results (4.50), (4.58), and (4.60), and we find

$$j_c^\parallel(\vartheta) \simeq j_{sv}^c\left[\frac{\sqrt{\varepsilon_\vartheta}}{\varepsilon}\frac{L_c^c}{a_0}\right]^2\exp\left[-2\tilde{c}\left[\frac{\sqrt{\varepsilon_\vartheta}}{\varepsilon}\frac{L_c^c}{a_0}\right]^3\right] ,$$
$$(4.116a)$$

$$U_c^b(\vartheta) \simeq U_{sv}^c\frac{\sqrt{\varepsilon_\vartheta}}{\varepsilon}\frac{L_c^c}{a_0}\exp\left[5\tilde{c}\left[\frac{\sqrt{\varepsilon_\vartheta}}{\varepsilon}\frac{L_c^c}{a_0}\right]^3\right] , \qquad (4.116b)$$

$$S_c^b(\vartheta) \simeq S_{sv}^c\frac{\varepsilon}{\sqrt{\varepsilon_\vartheta}}\frac{a_0}{L_c^c}\exp\left[7\tilde{c}\left[\frac{\sqrt{\varepsilon_\vartheta}}{\varepsilon}\frac{L_c^c}{a_0}\right]^3\right] , \qquad (4.116c)$$

with $L_c^c = \varepsilon^{4/3}L_c^{iso}$, $U_{sv}^c = \varepsilon^{2/3}U_{sv}^{iso}$, and $S_{sv}^c = \varepsilon^{4/3}S_{sv}^{iso}$. The out-of-plane critical current density $J_c^\perp(\vartheta)$ has to be scaled with the scaling factor for transverse lengths and thus becomes $j_c^\perp(\vartheta) \simeq \varepsilon_\vartheta j_c^\parallel(\vartheta)$. All these results are trivially obtained out of the isotropic results by the substitutions $j_{sv} \to j_{sv}^c$, $U_{sv} \to U_{sv}^c$, $S_{sv} \to S_{sv}^c$, and

$$\frac{L_c}{a_0} \to \frac{\sqrt{\varepsilon_\vartheta}}{\varepsilon}\frac{L_c^c}{a_0} \simeq \left[\frac{B}{B_{sb}(\vartheta)}\right]^{1/2} . \qquad (4.117)$$

In order to include the effects of thermal fluctuations, we should also have an expression for the depinning temperature, in particular, its angular dependence. The relevant length scale for depinning is $r_p(T) < a_0 < \lambda$, and thus our scaling method can be applied. Using the scaling rule (3.12) and the isotropic results (2.128) and (4.86) for the single-vortex depinning energy and the lattice depinning temperature, we obtain

$$\tilde{T}_{dp}^s(\vartheta) \simeq \varepsilon^2\varepsilon_0\frac{\xi^2}{L_c^c} \simeq U_{sv}^c \qquad (4.118a)$$

and

$$T_{dp}(\vartheta) \simeq 2\sqrt{\pi}\varepsilon\varepsilon_0\xi^2\left[\frac{\varepsilon_\vartheta B}{\Phi_0}\right]^{1/2} . \qquad (4.118b)$$

The temperature-dependent results (4.97) and (4.99) then are generalized to the anisotropic situation by the substitution rules

$$j_{sv} \to j_{sv}^c ,$$
$$U_{sv} \to U_{sv}^c ,$$
$$H_{c_2} \to H_{c_2}(\vartheta) = \frac{\Phi_0}{2\pi\varepsilon_\vartheta\xi^2} , \qquad (4.119)$$
$$T_{dp} \to T_{dp}(\vartheta) .$$

Let us turn to collective creep at small driving forces, $j \ll j_{sv}^c$, with $j$ directed along the planes, $\mathbf{j}\perp\mathbf{H}$. Here we assume that the system has started out in the single-vortex pinning regime, so that $L_c^c < \varepsilon a_0/\sqrt{\varepsilon_\vartheta}$. We briefly repeat the results of the single-vortex pinning regime: with decreasing current density $j$, the relevant length $L_{opt}(j)$ increases according to $L_{opt}(j) \simeq L_c(\vartheta)(j_{sv}^c/j)^{5/7}$, with $L_c(\vartheta) \simeq L_c^c/\varepsilon_\vartheta$, and so does the activation barrier for creep, $U(j) \simeq U_{sv}^c(j_{sv}^c/j)^{1/7}$, and the action for quantum creep, $S(j) \simeq S_{sv}^c(j_{sv}^c/j)^{8/7}$. As the current density $j$ drops below $j_{sb}(\vartheta,B) \simeq j_{sv}^c(\sqrt{\varepsilon_\vartheta}L_c^c/\varepsilon a_0)^{7/5}$, we enter the lattice pinning regime where the activation barrier increases rapidly, $U(\vartheta,j,B) \simeq U_{sb}(\vartheta,B)[j_{sb}(\vartheta,B)/j]^{5/2}$, with $U_{sb}(\vartheta,B) \simeq U_{sv}^c(\varepsilon a_0/\sqrt{\varepsilon_\vartheta}L_c^c)^{1/5}$, obtained by requiring

continuity across the boundary between the single-vortex and the lattice pinning regimes. Similarly, the action for quantum creep increases according to $S(\vartheta,j,B) \simeq S_{sb}(\vartheta,B)[j_{sb}(\vartheta,B)/j]^{7/2}$, with $S_{sb}(\vartheta,B) \simeq S_{sv}^c(\varepsilon a_o/\sqrt{\varepsilon_\vartheta}L_c^c)^{8/5}$. The boundary $j_{sc}(\vartheta,B)$, within which our scaling theory can be applied, is found by rescaling the condition $R_\parallel(j_{sc}) \simeq a_o(j_{sb}/j_{sc})^{3/2} \simeq \lambda/\varepsilon$, and we obtain $j_{sc}(\vartheta,B) \simeq j_{sb}(\vartheta,B)(\varepsilon a_o/\sqrt{\varepsilon_\vartheta}\lambda)^{2/3}$. Note that $j_{sc}$ is larger than the current density $j_{lb}$ limiting the small/intermediate-bundle pinning regime. For a current density $j$ directed along the $y'$ axis (out-of-plane current), the creep motion is directed along the superconducting planes, and we have to replace the in-plane current-density ratios $j_{sv}^c/j$ and $j_{sb}/j$ by their out-of-plane counterparts $\varepsilon_\vartheta j_{sv}^c/j$ and $\varepsilon_\vartheta j_{sb}/j$ in the above formulas.

## 2. High symmetry: H∥c

Now let us consider pinning and creep in a uniaxially anisotropic superconductor with the magnetic field applied along the high-symmetry direction. Our analysis will proceed along the traditional path, using dimensional estimates in order to obtain the desired results. The most simple quantities to calculate are the collective pinning energy $U_c$ and the critical current density $j_c$, as these quantities are determined by the tilt and shear relaxation alone. The collective pinning radius $R_c$ can be obtained from the Larkin-Ovchinnikov result for the displacement correlator

$$\langle u^2(\mathbf{r}) \rangle \simeq \xi^2 \left[ \frac{a_o\varepsilon}{L_c^c} \right]^3 \left[ \varepsilon \left[ \frac{R^2}{\lambda^2} + \frac{a_o^2 L^2}{\lambda^4} \right]^{1/2} \right.$$
$$\left. + \ln \left[ 1 + \frac{R^2}{a_o^2} + \frac{L}{\varepsilon a_o} \right] \right] , \quad (4.120)$$

which can be easily obtained by repeating the derivation of (4.17) above with the appropriate expression (3.42) for the tilt modulus. The bundle dimensions $R_c$ and $L_c^b$ are found to be

$$R_c \simeq \begin{cases} a_o \exp \left[ \tilde{c} \left[ \frac{L_c^c}{\varepsilon a_o} \right]^3 \right] , & a_o < R_c < \frac{\lambda}{\varepsilon} , \\ \frac{\lambda}{\varepsilon} \left[ \frac{L_c^c}{\varepsilon a_o} \right]^3 , & \frac{\lambda}{\varepsilon} < R_c , \end{cases} \quad (4.121)$$

and

$$L_c^b \simeq \begin{cases} \frac{\varepsilon}{a_o} R_c^2, & a_o < R_c < \frac{\lambda}{\varepsilon} , \\ \frac{\lambda}{a_o} R_c, & \frac{\lambda}{\varepsilon} < R_c , \end{cases} \quad (4.122)$$

allowing us to determine the pinning energy $U_c$ of an elementary bundle and the planar critical current density $j_c$,

$$j_c \simeq \begin{cases} j_o \left[ \dfrac{\varepsilon\xi}{L_c^c} \right]^2 , & L_c^c < \varepsilon a_o , \\[2ex] j_{sv}^c \left[ \dfrac{L_c^c}{\varepsilon a_o} \right]^2 \exp \left[ -2\tilde{c} \left[ \dfrac{L_c^c}{\varepsilon a_o} \right]^3 \right] , & a_o < R_c < \dfrac{\lambda}{\varepsilon} , \\[2ex] j_{sv}^c \left[ \dfrac{\varepsilon a_o}{\lambda} \right]^2 \left[ \dfrac{\varepsilon a_o}{L_c^c} \right]^4 , & \dfrac{\lambda}{\varepsilon} < R_c . \end{cases}$$

$$(4.123)$$

Next we wish to calculate the creep rate in an anisotropic superconductor. Since creep involves also compression of the bundle, we have to determine the bundle dimensions by minimizing simultaneously the compression, tilt, and shear energies involved in the hop. Our first concern then is the calculation of the length scales $R_\perp$, $R_\parallel$, and $L^b$ determining the (super)bundle dimensions. The major complication arises from the nontrivial dispersive behavior of the elastic moduli $c_{44}(\mathbf{k})$ and $c_{11}(\mathbf{k})$, which renders the calculation of the compression and tilt energies a bit cumbersome. For the case H∥c studied here, the tilt and compression moduli take the form (see Sec. III.B.2)

$$c_{44}(\mathbf{k}) = \frac{B^2}{4\pi} \frac{1}{1+(\lambda^2/\varepsilon^2)K^2+\lambda^2 k_z^2} , \quad (4.124a)$$

$$c_{11}(\mathbf{k}) = \alpha(k)c_{44}(\mathbf{k}) , \quad (4.124b)$$

$$\alpha(k) = \frac{1+(\lambda^2/\varepsilon^2)k^2}{1+\lambda^2 k^2} . \quad (4.124c)$$

The shear modulus is not dispersive and remains unchanged with respect to the isotropic result (3.32). The dispersive regime now extends to the larger scale, $R < \lambda/\varepsilon = \lambda_c$. Again, we follow the technique proposed by Koshelev (1994) for the determination of the superbundle dimensions in the dispersive regime.

Modeling the superbundle by a Gaussian of widths $R_\parallel$ and $R_\perp$ along and transverse to the jump and $L^b$ along the field direction, we have to estimate the following expressions for the compression and tilt energies (for the isotropic situation discussed in Sec. B.2 above, a real space analysis is more convenient; in the present anisotropic situation it is advantageous to go over to Fourier space)

$$\mathcal{E}_{comp} \simeq V^2 \int \frac{d^3k}{(2\pi)^3} \frac{c_{11}(\mathbf{k})}{2} K_\parallel^2 u^2 e^{-K_\perp^2 R_\perp^2 - K_\parallel^2 R_\parallel^2 - k_z^2 L^{b^2}} , \quad (4.125)$$

and

$$\mathcal{E}_{tilt} \simeq V^2 \int \frac{d^3k}{(2\pi)^3} \frac{c_{44}(\mathbf{k})}{2} k_z^2 u^2 e^{-K_\perp^2 R_\perp^2 - K_\parallel^2 R_\parallel^2 - k_z^2 L^{b^2}} , \quad (4.126)$$

where $V = R_\parallel R_\perp L^b$ denotes the superbundle volume. In

the following discussion it is helpful to use the ordering $R_\perp R_\parallel$, which follows from simple physical arguments and which can easily be checked at the end of the calculation.

$$\mathcal{E}_{\text{comp}} \sim \hat{c}_{11} \frac{u^2 V^2}{R_\parallel^3} \int dK_\perp dk_z \frac{[1+\lambda_c^2(R_\parallel^{-2}+K_\perp^2+k_z^2)]}{[1+\lambda^2(R_\parallel^{-2}+K_\perp^2+k_z^2)]} \frac{e^{-K_\perp^2 R_\perp^2 - k_z^2 L^{b2}}}{[1+\lambda_c^2(R_\parallel^{-2}+K_\perp^2)+\lambda^2 k_z^2]} . \tag{4.127}$$

In the regime $R_\parallel < \lambda_c$, $L^b < \lambda$ the first factor in the integral reduces to $1/\varepsilon^2$ and we can drop the term $1+\lambda_c^2/R_\parallel^2$ in the second factor. The remaining integration provides only a logarithmic dependence on the lengths $L^b$ and $R_\perp$ which we ignore, hence

$$\mathcal{E}_{\text{comp}} \sim \hat{c}_{11} \frac{u^2 V^2}{R_\parallel^3 \varepsilon \lambda^2}, \quad R_\parallel < \lambda_c, \quad L^b < \lambda . \tag{4.128}$$

In the regime $R_\parallel > \lambda_c$ we also have $L^b > \lambda$ [see Eqs. (4.135) and (4.136)] and we can drop all terms $K_\parallel \sim R_\parallel^{-2}$ and $k_z^2 \sim (L^b)^{-2}$ in (4.127). After integration over $k_z$ the remaining integral can be written as a sum of two terms,

$$\mathcal{E}_{\text{comp}} \sim \hat{c}_{11} \frac{u^2 V^2}{R_\parallel^3 L^b} \int dK_\perp \frac{e^{-K_\perp^2 R_\perp^2}}{[1+\lambda^2 K_\perp^2]}$$
$$+ \frac{\lambda_c^2 e^{-K_\perp^2 R_\perp^2}}{L^{b2}[1+\lambda_c^2 K_\perp^2][1+\lambda^2 K_\perp^2]}$$
$$\sim \hat{c}_{11} \frac{u^2 V^2}{R_\parallel^3 L^b} \left[ \frac{1}{R_\parallel + \lambda} + \frac{\lambda_c^2}{L^{b2}(R_\perp + \lambda_c)} \right] . \tag{4.129}$$

$$\mathcal{E}_{\text{tilt}} \sim \hat{c}_{44} \frac{u^2 V^2}{L^{b3}} \int dK_\perp dK_\parallel \frac{e^{-K_\perp^2 R_\perp^2 - K_\parallel^2 R_\parallel^2}}{[1+\lambda_c^2(K_\parallel^2+K_\perp^2)+\lambda^2(L^b)^{-2}]} , \tag{4.131}$$

and for $R_\parallel < \lambda_c$ (note that $\lambda/L^b < \lambda_c/R_\perp$) we find up to logarithmic corrections

$$\mathcal{E}_{\text{tilt}} \sim \hat{c}_{44} \frac{u^2 V^2}{L^{b3} \lambda_c^2}, \quad R_\parallel < \lambda_c, \quad L^b < \lambda . \tag{4.132}$$

In the regime $R_\parallel > \lambda_c$ we can drop the term $\lambda_c^2 R_\parallel^{-2}$ and perform the integral over $K_\parallel$,

$$\mathcal{E}_{\text{tilt}} \sim \hat{c}_{44} \frac{u^2 V^2}{L^{b3} R_\parallel} \int dK_\perp \frac{e^{-K_\perp^2 R_\perp^2}}{[1+\lambda_c^2 K_\perp^2+\lambda^2(L^b)^{-2}]} . \tag{4.133a}$$

The final integration over $K_\perp$ provides the result

$$\mathcal{E}_{\text{tilt}} \sim \hat{c}_{44} \frac{u^2 V^2}{L^{b3} R_\parallel} \begin{cases} \dfrac{1}{\lambda_c}, & R_\perp < \lambda_c < R_\parallel , \\[2ex] \dfrac{1}{R_\perp}, & \lambda_c < R_\perp < R_\parallel . \end{cases} \tag{4.133b}$$

Let us then first concentrate on the compression energy. The integration over $K_\parallel$ is dominated by the large wave vector $K_\parallel \sim 1/R_\parallel$ and using the abbreviation $\hat{c}_{11} = c_{11}(\mathbf{k}=0)$ we obtain

The final result for the compression energy then depends on the relative ordering of the lengths $R_\perp$ and $L^b$ with respect to the various screening lengths:

$$\mathcal{E}_{\text{comp}} \sim \hat{c}_{11} \frac{u^2 V^2}{R_\parallel^3 L^b} \begin{cases} \dfrac{\lambda_c}{L^{b2}}, & R_\perp < \lambda < L^b < \sqrt{\lambda \lambda_c} , \\[2ex] \dfrac{1}{\lambda}, & R_\perp < \lambda < \sqrt{\lambda \lambda_c} < L^b , \\[2ex] \dfrac{\lambda_c}{L^{b2}}, & \lambda < R_\perp < L^b < \sqrt{\lambda_c R_\perp} < \lambda_c , \\[2ex] \dfrac{1}{R_\perp}, & \lambda < R_\perp < \sqrt{\lambda_c R_\perp} < L^b , \\[2ex] \dfrac{1}{R_\perp}, & \lambda_c < R_\perp < L^b . \end{cases} \tag{4.130}$$

The last result in (4.130) is identical to the nondispersive limit $E_{\text{comp}} \sim \hat{c}_{11}(u/R_\parallel)^2 V$.

Along the same lines the tilt energy can be determined for the various regimes. The integration over $k_z$ contributes a factor $1/L^{b3}$,

Again, the last result is the nondispersive limit $\mathcal{E}_{\text{tilt}} \sim \hat{c}_{44}(u/L^b)^2 V$. Finally, the calculation of the shear energy is trivial as the shear modulus $c_{66}$ is nondispersive,

$$\mathcal{E}_{\text{shear}} \sim c_{66} \left[ \frac{u}{R_\perp} \right]^2 V . \tag{4.134}$$

Note that $\hat{c}_{11} = \hat{c}_{44} \sim c_{66}(\lambda/a_\circ)^2$.

The scaling of the bundle dimensions can now be obtained from the comparison of the three elastic energies $\mathcal{E}_{\text{comp}} \simeq \mathcal{E}_{\text{tilt}} \simeq \mathcal{E}_{\text{shear}}$. Here we quote only the final result expressing $R_\parallel$ and $L^b$ in terms of the transverse length $R_\perp$. For the longitudinal length $L^b$ we find

$$L^b \simeq \begin{cases} \varepsilon R_\parallel \simeq \varepsilon \dfrac{R_\perp^3}{a_o^2}, & a_o < R_\perp < \left[\dfrac{a_o^2 \lambda}{\varepsilon}\right]^{1/3}, \\[2ex] \left[\dfrac{R_\perp^3 \lambda \varepsilon}{a_o^2}\right]^{1/2}, \quad \left[\dfrac{a_o^2 \lambda}{\varepsilon}\right]^{1/3} < R_\perp < \lambda_c, \\[2ex] \dfrac{\lambda}{a_o} R_\perp, & \lambda_c < R_\perp. \end{cases} \quad (4.135)$$

For the parallel dimension $R_\parallel$ we have to distinguish between two field regimes:

$a_o < \varepsilon\lambda$:

$$R_\parallel \simeq \begin{cases} \dfrac{R_\perp^3}{a_o^2}, & a_o < R_\perp < \left[\dfrac{a_o^2 \lambda}{\varepsilon}\right]^{1/3}, \\[2ex] \lambda_c, \quad \left[\dfrac{a_o^2 \lambda}{\varepsilon}\right]^{1/3} < R_\perp < \left[\dfrac{a_o^2 \lambda}{\varepsilon^2}\right]^{1/3}, \\[2ex] \dfrac{L^b}{\sqrt{\varepsilon}} \simeq \left[\dfrac{R_\perp^3 \lambda}{a_o^2}\right]^{1/2}, \quad \left[\dfrac{a_o^2 \lambda}{\varepsilon^2}\right]^{1/3} < R_\perp < \lambda, \\[2ex] \dfrac{\lambda}{a_o} R_\perp, & \lambda < R_\perp. \end{cases} \quad (4.136a)$$

$\varepsilon\lambda < a_o$:

$$R_\parallel \simeq \begin{cases} \dfrac{R_\perp^3}{a_o^2}, & a_o < R_\perp < \left[\dfrac{a_o^2 \lambda}{\varepsilon}\right]^{1/3}, \\[2ex] \lambda_c, \quad \left[\dfrac{a_o^2 \lambda}{\varepsilon}\right]^{1/3} < R_\perp < \dfrac{a_o}{\varepsilon}, \\[2ex] \dfrac{\lambda}{a_o} R_\perp, & \lambda < \dfrac{a_o}{\varepsilon} < R_\perp. \end{cases} \quad (4.136b)$$

We are now in a position to calculate the activation energy $U_c^b$ for the creep motion. Close to criticality $(j \lesssim j_c)$ the activation energy can be obtained from the general expression

$$U_c^b \simeq c_{66} \left[\frac{u}{R_c}\right]^2 V \simeq U_{sv}^c \frac{L_c^c}{\varepsilon a_o} \frac{V}{\varepsilon a_o R_c^2}, \quad (4.137)$$

where $R_\perp = R_c$ is given by Eq. (4.121) above. However, contrary to the determination of the pinning energy $U_c$, the activation energy $U_c^b$ for creep involves the dimensions of the superbundle which takes the compression of the flux lattice into account and hence the volume $V$ is given by $V = R_\perp R_\parallel L^b$, with $R_\parallel$ and $L^b$ given by Eqs. (4.135) and (4.136) above. Consider first the strong field case with $a_o < \varepsilon\lambda$. The activation energy $U_c^b$ then takes the form

$$U_c^b \simeq \begin{cases} U_{sv}^c \simeq H_c^2 \varepsilon \xi^3 \dfrac{\varepsilon\xi}{L_c^c}, & L_c^c < \varepsilon a_o, \\[2ex] U_{sv}^c \dfrac{L_c^c}{\varepsilon a_o} \exp\left[5\tilde{c}\left[\dfrac{L_c^c}{\varepsilon a_o}\right]^3\right], & a_o < R_c < \left[\dfrac{a_o^2 \lambda}{\varepsilon}\right]^{1/3}, \\[2ex] U_{sv}^c \dfrac{L_c^c}{\varepsilon a_o} \left[\dfrac{\lambda}{\varepsilon a_o}\right]^{3/2} \exp\left[\dfrac{\tilde{c}}{2}\left[\dfrac{L_c^c}{\varepsilon a_o}\right]^3\right], & \left[\dfrac{a_o^2 \lambda}{\varepsilon}\right]^{1/3} < R_c < \left[\dfrac{a_o^2 \lambda}{\varepsilon^2}\right]^{1/3}, \\[2ex] U_{sv}^c \dfrac{L_c^c}{\varepsilon a_o} \dfrac{\lambda}{\sqrt{\varepsilon a_o}} \exp\left[2\tilde{c}\left[\dfrac{L_c^c}{\varepsilon a_o}\right]^3\right], & \left[\dfrac{a_o^2 \lambda}{\varepsilon^2}\right]^{1/3} < R_c < \lambda, \\[2ex] U_{sv}^c \dfrac{L_c^c}{a_o} \left[\dfrac{\lambda}{\varepsilon a_o}\right]^{3/2} \exp\left[\dfrac{3\tilde{c}}{2}\left[\dfrac{L_c^c}{\varepsilon a_o}\right]^3\right], & \lambda < R_c < \dfrac{\lambda}{\varepsilon}, \\[2ex] U_{sv}^c \varepsilon \left[\dfrac{\lambda}{\varepsilon a_o}\right]^3 \left[\dfrac{L_c^c}{\varepsilon a_o}\right]^4, & \dfrac{\lambda}{\varepsilon} < R_c. \end{cases} \quad (4.138)$$

For the opposite case of weak magnetic field with $a_o > \varepsilon\lambda$ we should use the expressions (4.136b) for the parallel dimension $R_\parallel$ and obtain the following changes for the activation energy $U_c^b$ within the region $a_o < R_c < \lambda/\varepsilon$:

$$U_c^b \simeq \begin{cases} U_{sv}^c \dfrac{L_c^c}{\varepsilon a_o} \exp\left[5\tilde{c}\left[\dfrac{L_c^c}{\varepsilon a_o}\right]^3\right], & a_o < R_c < \left[\dfrac{a_o^2 \lambda}{\varepsilon}\right]^{1/3}, \\[2ex] U_{sv}^c \dfrac{L_c^c}{\varepsilon a_o} \left[\dfrac{\lambda}{\varepsilon a_o}\right]^{3/2} \exp\left[\dfrac{\tilde{c}}{2}\left[\dfrac{L_c^c}{\varepsilon a_o}\right]^3\right], & \left[\dfrac{a_o^2 \lambda}{\varepsilon}\right]^{1/3} < R_c < \dfrac{a_o}{\varepsilon}, \\[2ex] U_{sv}^c \dfrac{L_c^c}{a_o} \left[\dfrac{\lambda}{\varepsilon a_o}\right]^{3/2} \exp\left[\dfrac{3\tilde{c}}{2}\left[\dfrac{L_c^c}{\varepsilon a_o}\right]^3\right], & \dfrac{a_o}{\varepsilon} < R_c < \dfrac{\lambda}{\varepsilon}. \end{cases} \quad (4.139)$$

Within the regime $a_o < R_{\parallel} < \lambda/\varepsilon$ the above results agree with those found previously via the scaling approach. Note that the results for the nondispersive regime $R_{\perp} > \lambda/\varepsilon$ are independent of the parameter $\varepsilon$, as has to be expected. Given the disorder strength, e.g., through the parameter $L_c^c$, and the magnetic field, the appropriate expression for the activation energy can be obtained from the above results (4.138) and (4.139).

For completeness, we also present the results for the action determining quantum creep, concentrating on the more relevant overdamped situation. The result can be most easily derived from the general expression $S_c^b \simeq S_{sv}^c (\varepsilon a_o / L_c^c)(V/\varepsilon a_o^3)$. For large magnetic fields with $a_o < \varepsilon\lambda$ we obtain

$$
S_c^b \simeq
\begin{cases}
S_{sv}^c \simeq \dfrac{\hbar^2}{e^2}\dfrac{\varepsilon\xi}{\rho_n}\left[\dfrac{j_o}{j_{sv}^c}\right]^{1/2}, & L_c^c < \varepsilon a_o \ , \\[2ex]
S_{sv}^c \dfrac{\varepsilon a_o}{L_c^c}\exp\left[7\widetilde{c}\left[\dfrac{L_c^c}{\varepsilon a_o}\right]^3\right], & a_o < R_c < \left[\dfrac{a_o^2\lambda}{\varepsilon}\right]^{1/3} \ , \\[2ex]
S_{sv}^c \dfrac{\varepsilon a_o}{L_c^c}\left[\dfrac{\lambda}{\varepsilon a_o}\right]^{3/2}\exp\left[\dfrac{5\widetilde{c}}{2}\left[\dfrac{L_c^c}{\varepsilon a_o}\right]^3\right], & \left[\dfrac{a_o^2\lambda}{\varepsilon}\right]^{1/3} < R_c < \left[\dfrac{a_o^2\lambda}{\varepsilon^2}\right]^{1/3} \ , \\[2ex]
S_{sv}^c \dfrac{\varepsilon a_o}{L_c^c}\dfrac{\lambda}{\sqrt{\varepsilon a_o}}\exp\left[4\widetilde{c}\left[\dfrac{L_c^c}{\varepsilon a_o}\right]^3\right], & \left[\dfrac{a_o^2\lambda}{\varepsilon^2}\right]^{1/3} < R_c < \lambda \ , \\[2ex]
S_{sv}^c \dfrac{\varepsilon^2 a_o}{L_c^c}\left[\dfrac{\lambda}{\varepsilon a_o}\right]^{3/2}\exp\left[\dfrac{7\widetilde{c}}{2}\left[\dfrac{L_c^c}{\varepsilon a_o}\right]^3\right], & \lambda < R_c < \dfrac{\lambda}{\varepsilon} \ , \\[2ex]
S_{sv}^c\,\varepsilon\left[\dfrac{\lambda}{\varepsilon a_o}\right]^5\left[\dfrac{L_c^c}{\varepsilon a_o}\right]^8, & \dfrac{\lambda}{\varepsilon} < R_c \ ,
\end{cases}
\tag{4.140}
$$

whereas for the weak field case $a_o > \varepsilon\lambda$ the results are modified within the intermediate regime $a_o < R_c < \lambda/\varepsilon$,

$$
S_c^b \simeq S_{sv}^c
\begin{cases}
\dfrac{\varepsilon a_o}{L_c^c}\exp\left[7\widetilde{c}\left[\dfrac{L_c^c}{\varepsilon a_o}\right]^3\right], & a_o < R_c < \left[\dfrac{a_o^2\lambda}{\varepsilon}\right]^{1/3} \ , \\[2ex]
\dfrac{\varepsilon a_o}{L_c^c}\left[\dfrac{\lambda}{\varepsilon a_o}\right]^{3/2}\exp\left[\dfrac{5\widetilde{c}}{2}\left[\dfrac{L_c^c}{\varepsilon a_o}\right]^3\right], & \left[\dfrac{a_o^2\lambda}{\varepsilon}\right]^{1/3} < R_c < \dfrac{a_o}{\varepsilon} \ , \\[2ex]
\dfrac{\varepsilon^2 a_o}{L_c^c}\left[\dfrac{\lambda}{\varepsilon a_o}\right]^{3/2}\exp\left[\dfrac{7\widetilde{c}}{2}\left[\dfrac{L_c^c}{\varepsilon a_o}\right]^3\right], & \dfrac{a_o}{\varepsilon} < R_c < \dfrac{\lambda}{\varepsilon} \ .
\end{cases}
\tag{4.141}
$$

Next we discuss the evolution of collective creep as we decrease the current density $j$. Since the displacement $u$ now grows beyond the scale $\xi$ of the disorder potential, the Larkin-Ovchinnikov result (4.120) has to be replaced by

$$
u \simeq \xi\left[\dfrac{a_o\varepsilon}{L_c^c}\right]^{3/5}\left[\varepsilon\left[\dfrac{R^2}{\lambda^2}+\dfrac{a_o^2 L^2}{\lambda^4}\right]^{1/2}\right.
$$

$$
\left.+\ln\left[1+\dfrac{R^2}{a_o^2}+\dfrac{L}{\varepsilon a_o}\right]\right]^{1/5}, \tag{4.142}
$$

hence $u \propto R^\zeta$ with $\zeta = 0$ within the dispersive regime, where $a_o < R < \lambda/\varepsilon$, and $\zeta \simeq 1/5$ within the nondispersive region $R > \lambda/\varepsilon$. The dependence of the bundle size $R_{\perp}$ on the current density $j$ is given by Eq. (3.177), $R_{\perp}(j) \simeq R_o(j_o/j)^{1/(2-\zeta)}$, with $R_o$ and $j_o$ determined by continuity across the various regimes. The length scales $L^b$ and $R_{\parallel}$ are related to $R_{\perp}(j)$ via Eqs. (4.135) and (4.136). Let us consider again a situation in which the system starts out within the single-vortex pinning regime ($L_c^c < \varepsilon a_o$) and follow the evolution of the main scale parameter $L(j)$ or $R_{\perp}(j)$ as the current decreases below $j_{sv}^c$. Within the single-vortex pinning regime,

$$
L(j) \simeq L_c^c\left[\dfrac{j_{sv}^c}{j}\right]^{5/7}, \quad j_{sb} < j \ll j_{sv}^c \ , \tag{4.143}
$$

with $j_{sb} \simeq j_{sv}^c(L_c^c/\varepsilon a_o)^{7/5}$ obtained from the condition $L(j_{sb}) \simeq \varepsilon a_o$. As $j$ drops below $j_{sb}$ we go over to the bundle pinning regime and the relevant scale is $R_{\perp}(j)$,

$$
R_\perp(j) \simeq \begin{cases}
a_0 \left[ \dfrac{j_{\text{sb}}}{j} \right]^{1/2} , & j_{\text{lb}} < j < j_{\text{sb}} , \\[3ex]
\dfrac{\lambda}{\varepsilon} \left[ \dfrac{j_{\text{lb}}}{j} \right]^{5/9} , & j_{\text{CDW}} < j < j_{\text{lb}} , \\[3ex]
R_a \left[ \dfrac{j_{\text{CDW}}}{j} \right]^{1/2} , & j < j_{\text{CDW}} ,
\end{cases}
\tag{4.144}
$$

with $j_{\text{lb}} \simeq (\varepsilon a_0 / \lambda)^2 j_{\text{sb}}$ and $j_{\text{CDW}} \simeq (\varepsilon^3 \xi^5 / a_0^2 L_c^{c3})^{9/5} j_{\text{lb}}$ obtained from the conditions of continuity $R_\perp(j_{\text{lb}}) \simeq \lambda/\varepsilon$ and $R_\perp(j_{\text{CDW}}) \simeq R_a$. For weak enough pinning, the lat-

tice correlation length $R_a$ is larger than $\lambda/\varepsilon$,

$$
R_a \simeq \frac{\lambda}{\varepsilon} \left[ \frac{L_c^c}{\varepsilon \xi} \right]^3 \left[ \frac{a_0}{\xi} \right]^2 ,
\tag{4.145}
$$

which in fact is independent of $\varepsilon$ and therefore equivalent to the isotropic expression (4.43) upon substitution of $\varepsilon^{4/3} L_c$ for $L_c^c$. The growth of the activation barrier $U(j)$ with decreasing current density $j$ is complicated by the dispersive nature of the compression and tilt moduli. Consider first the case of large fields with $a_0 < \varepsilon \lambda$. The activation barrier $U(j) \simeq c_{66}(u/R_\perp)^2 V \simeq U_{\text{sb}}^c (V/\varepsilon a_0 R_\perp^2)$ evolves according to

$$
U(j) \simeq \begin{cases}
U_{\text{sv}}^c \left[ \dfrac{j_{\text{sv}}^c}{j} \right]^{1/7} , & j_{\text{sb}} < j \ll j_{\text{sv}}^c , \\[3ex]
U_{\text{sb}}^c \left[ \dfrac{j_{\text{sb}}}{j} \right]^{5/2} , & \left[ \dfrac{\varepsilon a_0}{\lambda} \right]^{2/3} j_{\text{sb}} < j < j_{\text{sb}} , \\[3ex]
U_{\text{sb}}^c \left[ \dfrac{\lambda}{\varepsilon a_0} \right]^{3/2} \left[ \dfrac{j_{\text{sb}}}{j} \right]^{1/4} , & \left[ \dfrac{\varepsilon^2 a_0}{\lambda} \right]^{2/3} < j < \left[ \dfrac{\varepsilon a_0}{\lambda} \right]^{2/3} j_{\text{sb}} , \\[3ex]
U_{\text{sb}}^c \dfrac{\lambda}{\sqrt{\varepsilon a_0}} \dfrac{j_{\text{sb}}}{j} , & \left[ \dfrac{a_0}{\lambda} \right]^2 j_{\text{sb}} < j < \left[ \dfrac{\varepsilon^2 a_0}{\lambda} \right]^{2/3} , \\[3ex]
U_{\text{sb}}^c \varepsilon \left[ \dfrac{\lambda}{\varepsilon a_0} \right]^{3/2} \left[ \dfrac{j_{\text{sb}}}{j} \right]^{3/4} , & j_{\text{lb}} < j < \left[ \dfrac{a_0}{\lambda} \right]^2 j_{\text{sb}} , \\[3ex]
U_{\text{lb}}^c \left[ \dfrac{j_{\text{lb}}}{j} \right]^{7/9} , & j_{\text{CDW}} < j < j_{\text{lb}} , \\[3ex]
U_{\text{CDW}}^c \left[ \dfrac{j_{\text{CDW}}}{j} \right]^{1/2} , & 0 < j < j_{\text{CDW}} ,
\end{cases}
\tag{4.146}
$$

with $U_{\text{sb}}^c \simeq U_{\text{sv}}^c (\varepsilon a_0 / L_c^c)^{1/5}$, $U_{\text{lb}}^c \simeq U_{\text{sb}}^c \varepsilon (\lambda/\varepsilon a_0)^3$, and $U_{\text{CDW}}^c \simeq U_{\text{lb}}^c (a_0^2 L_c^{c3} / \varepsilon^3 \xi^5)^{7/5}$. For small fields with $a_0 > \varepsilon \lambda$, $R_\parallel$ is given by Eq. (4.136b), and we obtain for the current range $j_{\text{lb}} < j < j_{\text{sb}}$ the behavior

$$
U(j) \simeq \begin{cases}
U_{\text{sb}}^c \left[ \dfrac{j_{\text{sb}}}{j} \right]^{5/2} , & \left[ \dfrac{\varepsilon a_0}{\lambda} \right]^{2/3} j_{\text{sb}} < j < j_{\text{sb}} , \\[3ex]
U_{\text{sb}}^c \left[ \dfrac{\lambda}{\varepsilon a_0} \right]^{3/2} \left[ \dfrac{j_{\text{sb}}}{j} \right]^{1/4} , & \varepsilon^2 j_{\text{sb}} < j < \left[ \dfrac{\varepsilon a_0}{\lambda} \right]^{2/3} j_{\text{sb}} , \\[3ex]
U_{\text{sb}}^c \varepsilon \left[ \dfrac{\lambda}{\varepsilon a_0} \right]^{3/2} \left[ \dfrac{j_{\text{sb}}}{j} \right]^{3/4} , & j_{\text{lb}} < j < \varepsilon^2 j_{\text{sb}} .
\end{cases}
\tag{4.147}
$$

The results for the high $(j > j_{\text{sb}})$ and for the low current-density regimes $(j < j_{\text{lb}})$ remain unchanged. The same analysis can be carried through for the action, and we quote the results for the more relevant overdamped situation here: For large fields

$a_0 < \varepsilon\lambda,$

$$S(j) \simeq \begin{cases} S^c_{sv} \left[\dfrac{j^c_{sv}}{j}\right]^{8/7}, & j_{sb} < j \ll j^c_{sv}, \\[2ex] S^c_{sb} \left[\dfrac{j_{sb}}{j}\right]^{7/2}, & \left[\dfrac{\varepsilon a_0}{\lambda}\right]^{2/3} j_{sb} < j < j_{sb}, \\[2ex] S^c_{sb} \left[\dfrac{\lambda}{\varepsilon a_0}\right]^{3/2} \left[\dfrac{j_{sb}}{j}\right]^{5/4}, & \left[\dfrac{\varepsilon^2 a_0}{\lambda}\right]^{2/3} < j < \left[\dfrac{\varepsilon a_0}{\lambda}\right]^{2/3} j_{sb}, \\[2ex] S^c_{sb} \dfrac{\lambda}{\sqrt{\varepsilon a_0}} \left[\dfrac{j_{sb}}{j}\right]^{2}, & \left[\dfrac{a_0}{\lambda}\right]^{2} j_{sb} < j < \left[\dfrac{\varepsilon^2 a_0}{\lambda}\right]^{2/3}, \\[2ex] S^c_{sb} \varepsilon \left[\dfrac{\lambda}{\varepsilon a_0}\right]^{3/2} \left[\dfrac{j_{sb}}{j}\right]^{7/4}, & j_{lb} < j < \left[\dfrac{a_0}{\lambda}\right]^{2} j_{sb}, \\[2ex] S^c_{lb} \left[\dfrac{j_{lb}}{j}\right]^{16/9}, & j_{CDW} < j < j_{lb}, \\[2ex] S^c_{CDW} \left[\dfrac{j_{CDW}}{j}\right]^{3/2}, & 0 < j < j_{CDW}, \end{cases} \qquad (4.148)$$

with $S^c_{sb} \simeq S^c_{sv}(\varepsilon a_0/L^c_c)^{8/5}$, $S^c_{lb} \simeq S^c_{sb}\varepsilon(\lambda/\varepsilon a_0)^5$, and $S^c_{CDW} \simeq S^c_{lb}(a^2_0 L^{c3}_c/\varepsilon^3\xi^5)^{16/5}$. For small fields with $a_0 > \varepsilon\lambda$, the intermediate current range $j_{lb} < j < j_{sb}$ is described by

$$S(j) \simeq \begin{cases} S^c_{sb} \left[\dfrac{j_{sb}}{j}\right]^{7/2}, & \left[\dfrac{\varepsilon a_0}{\lambda}\right]^{2/3} j_{sb} < j < j_{sb}, \\[2ex] S^c_{sb} \left[\dfrac{\lambda}{\varepsilon a_0}\right]^{3/2} \left[\dfrac{j_{sb}}{j}\right]^{5/4}, & \varepsilon^2 j_{sb} < j < \left[\dfrac{\varepsilon a_0}{\lambda}\right]^{2/3} j_{sb}, \\[2ex] S^c_{sb} \varepsilon \left[\dfrac{\lambda}{\varepsilon a_0}\right]^{3/2} \left[\dfrac{j_{sb}}{j}\right]^{7/4}, & j_{lb} < j < \varepsilon^2 j_{sb}. \end{cases} \qquad (4.149)$$

The time decay of the screening current $j$ due to classical creep is straightforwardly obtained using the relation $U(j) = T\ln(t/t_0)$ in combination with Eqs. (4.146) and (4.147), and accordingly the results for the quantum case can be obtained.

Let us finally discuss more quantitatively the $H - T - j^{-1}$ phase diagram for the prototype anisotropic oxide superconductor YBCO for the case $H\|c$; see Fig. 21. The main parameters determining the position of the various crossover lines in the phase diagram are the critical current-density ratio $j^c_{sv}/j_0$, which measures the strength of the disorder and typically is of the order of $10^{-2}$, and the Ginzburg number $Gi$, which determines the importance of thermal fluctuations and takes values of the order of $10^{-2}$. The single-vortex pinning regime then is bounded by $T^s_{dp} = \alpha^s_{dp}(j^c_{sv}/j_0 Gi)^{1/2}T_c \approx 60$ K and by $B_{sb} \approx \beta_{sb}(j^c_{sv}/j_0)H_{c_2} \approx 6$ T. This large value for the single-vortex pinning boundary, below which the critical current density $j_c$ is expected to be independent of the magnetic field, is in good agreement with the experimental findings of Dinger *et al.* (1987) and of Tamegai *et al.* (1992). The logarithmic correction factor $\ln(\kappa^2 j^c_{sv}/\varepsilon^2 j_0)$

determining the width of the small-bundle pinning regime is $\sim 8$, so that $B_{lb} \approx 4(\beta_{lb}/\beta_{sb})B_{sb} \approx 10$ T [see Eqs. (4.94) and (4.95)] and $T^{lb}_{dp} \approx T_{dp}(B_{lb}) \approx 0.8T_c \approx 70$ K. The melting temperature is still close to the transition temperature and the intersection of the melting line with the depinning line is located at $(T^*, H^*) \approx [T_c, B_{dp}(T_c)] \approx (T_c, 10$ T$)$. A first attempt to map out the various regimes in the weak collective pinning theory has been undertaken by Krusin-Elbaum *et al.* (1992) based on the analysis of magnetic hysteresis data $M(H, T)$ taken on a single crystal of YBCO.

Using the above set of parameters, we find that on approaching the melting line the vortex lattice ends up in the large-bundle pinning regime. Hence close to the melting transition the interaction between vortices dominates over the interaction of vortices with the pinning potential, so that the melting transition itself is only weakly affected by the presence of disorder. However, it is important to realize that the character of the phase diagram depends strongly on the basic material parameters $j^c_{sv}/j_0$ and $Gi$, which are not very accurately known and also depend on sample preparation. In particular, $Gi \propto \kappa^4$

and typical uncertainties in $\kappa$ of the order of 2 can drastically change the character of the phase diagram. An accurate determination of the basic material parameters is therefore a prerequisite for the construction of the overall phase diagram.

## E. Loss of long-range order

In real type-II superconductors the Abrikosov vortex lattice is subject to disorder, both thermal and quenched. Both types of disorder will tend to destroy the long-range order (LRO) of the ideal flux-line lattice, and it is the aim of the present section to discuss these effects in more detail. In doing so, we have to distinguish between two types of LRO, the translational (TLRO), which is usually characterized by the correlator

$$g^t(\mathbf{K}_\nu, \mathbf{r}) = \langle\langle e^{i\mathbf{K}_\nu \cdot [\mathbf{u}(\mathbf{r}) - \mathbf{u}(0)]} \rangle\rangle , \qquad (4.150)$$

and the orientational long-range order (OLRO), which, in a hexagonal symmetry, is characterized by (Halperin and Nelson, 1978; Nelson and Halperin, 1979)

$$g^o(6, \mathbf{r}) = \langle\langle e^{i6[\theta(\mathbf{r}) - \theta(0)]} \rangle\rangle . \qquad (4.151)$$

Here $\theta(\mathbf{r})$ is the (hexatic) bond-angle field describing the local orientation of the vortex lattice in the position $\mathbf{r}$ relative to some reference orientation. Within a continuum approximation of the vortex lattice, $\theta(\mathbf{r})$ can be expressed by the displacement field $\mathbf{u}(\mathbf{r})$ via

$$\theta(\mathbf{r}) = \frac{1}{2}\left[\frac{\partial u_y}{\partial x} - \frac{\partial u_x}{\partial y}\right] . \qquad (4.152)$$

The correlator (4.150) is closely related to the structure factor of the lattice.

Loss of long-range order in the Abrikosov lattice of the oxide superconductors has attracted a good deal of interest, both from the experimental and from the theoretical side. The most obvious way of losing LRO is, of course, via melting of the flux-line lattice due to thermal fluctuations (Nelson, 1988), a phenomenon which we shall discuss in detail in Sec. V below. Here we wish to concentrate on the solid phase, where, by definition, thermal fluctuations lead only to a damping of the Bragg peaks in the structure factor but do not destroy LRO. The main question we wish to address, then, is the competition between LRO and the quenched random potential.

Larkin (1970) was the first to show that arbitrarily weak disorder is sufficient to destroy the translational LRO of the Abrikosov lattice. Later, Larkin and Ovchinnikov (1979) improved upon the original discussion by taking the nonlocal character of the elastic medium into account. The perturbative treatment of Larkin (1970) and of Larkin and Ovchinnikov (1979), however, is not appropriate for the discussion of long-range order if the displacements grow beyond the characteristic scale $r_p \simeq \xi$ of the pinning potential. Feigel'man *et al.* (1989) generalized the older perturbative results, valid at small

distances, to arbitrary distances by determining the relevant exponents describing the large-scale behavior of the system. Recently, Chudnovsky (1989, 1990) discussed the loss of LRO in the oxide superconductors, again based on the perturbative approach of Larkin and Ovchinnikov. In particular, he suggested that the low-temperature phase of disordered type-II superconductors is a hexatic vortex glass, which is characterized by the absence of translational LRO but has finite orientational LRO (Chudnovsky, 1989). By including the presence of disorder-induced dislocations (which were neglected in Chudnovsky's 1989 analysis), Toner (1991a) showed that arbitrarily weak disorder will also destroy orientational LRO in $d < 4$ space dimensions. On the other hand, orientational LRO can be restored by the interaction of the flux-line lattice with the underlying crystal lattice (Toner, 1991a). Experimental evidence for the existence of a hexatic vortex glass in the oxides has been obtained by the Bitter decoration technique (Murray *et al.*, 1990; Grier *et al.*, 1991), which allows a direct imaging of the flux-line lattice over large spatial regions, at least for small enough magnetic fields, $B \lesssim 100$ G. Such Bitter decoration patterns also provide an alternative (to $j_c$ measurements) approach to measuring the strength of the disorder potential in a type-II superconductor (Dolan *et al.*, 1989; Chudnovsky, 1990; Murray *et al.*, 1990; Grier *et al.*, 1991). Recently, Houghton, Pelcovits, and Sudbø (1992) improved the analysis of Chudnovsky (1990) by taking into account both the effects of nonlocality and the important effects of anisotropy.

After this introductory overview we present a more detailed discussion of the loss of long-range order in the Abrikosov flux-line lattice. We shall concentrate first on translational LRO and defer the discussion of orientational LRO to Sec. IV.E.2. Two of the main messages we wish to convey here are that (i) loss of LRO should not be treated perturbatively, i.e., the existence of many competing low-lying metastable states for the vortex lattice has to be taken into account in the relaxation to the disorder potential, and (ii) in comparing theoretical predictions, in particular line shapes, with experiments, the dynamic aspects of the relaxation cannot be ignored.

## 1. Translational LRO

The discussion of translational LRO is synonymous with a discussion of the correlator $g^t(\mathbf{K}_\nu, \mathbf{r})$ given by Eq. (4.150). We divide the displacement field $\mathbf{u}$ into a thermal part $\mathbf{u}_{th}$ and a disorder-induced contribution $\mathbf{u}_p$. Note that the intravalley internal fluctuations will lead to a smoothing of the disorder potential, and it is this effective pinning potential which determines the long-distance behavior of $\mathbf{u}_p$ and, due to the finiteness of $\langle u^2 \rangle_{th}$, also of $\mathbf{u}$. The correlator $g^t$ then factorizes into a thermal part (Debye-Waller factor) $g^t_{th}$ and a disorder-induced part $g^t_p$, $g^t = g^t_{th} g^t_p$. Assuming Gaussian fluctuations, these two factors take the form

$$g_{\mathrm{th}}^t(\mathbf{K}_v,\mathbf{r})=e^{-(1/2)K_v^2\langle[\mathbf{u}_{\mathrm{th}}(\mathbf{r})-\mathbf{u}_{\mathrm{th}}(0)]^2\rangle} \qquad (4.153)$$

and

$$g_p^t(\mathbf{K}_v,\mathbf{r})=e^{-(1/2)K_v^2\langle[\mathbf{u}_p(\mathbf{r})-\mathbf{u}_p(0)]^2\rangle} \ . \qquad (4.154)$$

Within the solid phase, the mean-squared thermal displacement amplitude remains finite asymptotically [see Eq. (4.85)] and thus merely introduces a damping of the Bragg peaks in the structure factor. Let us, then, concentrate on the disorder-induced factor $g_p^t(\mathbf{K}_v,\mathbf{r})$. The decisive quantity here is the displacement correlator $\langle u_p^2(\mathbf{r})\rangle$, which was studied in detail in Sec. IV.A above

in the low-temperature limit. Due to the long-range interaction between the vortices and the internal structure of the vortex lattice, the correlator $\langle u_p^2(\mathbf{r})\rangle$ exhibits a quite nontrivial behavior as a function of distance r. Let us briefly summarize the evolution of the correlator $\langle u_p^2(\mathbf{r})\rangle$ as it grows with increasing distance r from the Larkin-Ovchinnikov single-vortex pinning regime through various stages up to the regime of CDW-type pinning at large distances; see Fig. 16. We consider a case in which the magnetic field is small or the disorder strong enough that the condition $L_c<a_0$ is fulfilled; for arbitrary temperature we obtain $[\mathbf{r}=(\mathbf{R},L)]$

$$\langle u_p^2(\mathbf{r})\rangle^{1/2}\simeq\begin{cases}\xi\left[\dfrac{L}{L_c}\right]^{3/2}, & L<L_c,\quad T\ll T_{\mathrm{dp}}^s,\\[2ex] r_p^s\left[\dfrac{L}{L_c(0)}\right]^{1/2}, & L<L_c(T),\quad T>T_{\mathrm{dp}}^s,\\[2ex] r_p^s\left[\dfrac{L_c(T)}{L_c(0)}\right]^{1/2}\left[\dfrac{L}{L_c(T)}\right]^{3/5}, & L_c(T)<L<a_0,\\[2ex] r_p\left[\dfrac{\xi^2}{r_p^2(T)}\dfrac{a_0}{L_c}\right]^{3/5}\ln\left[1+\dfrac{R^2}{a_0^2}+\dfrac{L}{a_0}\right], & \begin{matrix}a_0<R<\lambda,\\ a_0<L<\lambda^2/a_0,\end{matrix}\\[2ex] r_p\left[\dfrac{\xi^2}{r_p^2(T)}\dfrac{a_0}{L_c}\right]^{3/5}\left[\dfrac{R^2}{\lambda^2}+\dfrac{a_0^2L^2}{\lambda^4}\right]^{1/10}, & \begin{matrix}\lambda<R<R_a(T),\\ \lambda<a_0L/\lambda<R_a(T),\end{matrix}\\[2ex] a_0\ln\left[1+\dfrac{R^2}{R_a^2(T)}+\dfrac{a_0^2L^2}{\lambda^2R_a^2(T)}\right], & \begin{matrix}R_a(T)<R,\\ \lambda R_a(T)/a_0<L.\end{matrix}\end{cases} \qquad (4.155)$$

Here we have introduced the relevant length scale of the disorder potential for the single-vortex pinning regime, $r_p^{s2}\simeq\xi^2(1+T/\tilde{T}_{\mathrm{dp}}^s)$, which is obtained from $r_p$ via the substitution $T_{\mathrm{dp}}\to\tilde{T}_{\mathrm{dp}}^s$. The temperature-dependent crossover lengths are given by

$$L_c(T)\simeq L_c(0)\exp\left[\left[\dfrac{T}{\tilde{T}_{\mathrm{dp}}^s}\right]^3\right], \qquad (4.156)$$

$$R_a(T)\simeq\begin{cases}a_0\exp\left[\tilde{c}\left[\dfrac{L_c}{\xi}\right]^3\left[\dfrac{a_0}{\xi}\right]^2\dfrac{r_p}{\xi}\right], & a_0<R_a(T)<\lambda,\\[2ex] \lambda\left[\dfrac{L_c}{\xi}\right]^3\left[\dfrac{a_0}{\xi}\right]^2\dfrac{r_p}{\xi}, & \lambda<R_a(T).\end{cases} \qquad (4.157)$$

Note that the regime of pinning of small bundles is very narrow regarding the change of the displacement amplitude but is in general quite wide with respect to the distances R and L.

The relevant scale for the loss of crystalline order is the length $R_a(T)$ marking the borderline to the CDW-type creep regime and defined by the condition $\langle u_p^2(R_a(T))\rangle\simeq a_0^2$. Beyond this distance, the displacement field $\langle u_p^2(\mathbf{r})\rangle^{1/2}$ grows beyond the lattice constant $a_0$, and dislocations may become relevant. Note that

typical displacement amplitudes produced by dislocations are of the order of $a_0$. Also, $R_a(T)$ defines the length scale on which the correlator $g_p^t(\mathbf{K}_v,\mathbf{r})$ starts to decay for the two primitive reciprocal-lattice vectors with lengths of the order of $1/a_0$. Our result (4.157) for the lattice correlation length shows a different field dependence than the one obtained by Chudnovsky (1990; he obtains $R_a\propto\sqrt{B}$ ), the reason being the modified scaling behavior of the displacement field $u_p$ within the nondispersive regime at long distances, Eq. (4.155), involving a power $\frac{1}{5}$ rather than the perturbative result $\frac{1}{2}$ [see the discussion about the breakdown of the perturbative approach given above Eq. (4.25)].

Let us discuss the result (4.157) for the lattice correlation length $R_a$ and concentrate first on high temperatures. For the case of weak collective pinning in the sense that $j_{\mathrm{sv}}/j_0<Gi$, thermal depinning of single vortices takes place before the melting line is reached, so that the melting line itself is limiting the lattice pinning regime throughout all of the phase diagram. The lattice correlation length $R_a(T)$ is always large as compared with the lattice constant $a_0$, since each of the three factors on the right-hand side of Eq. (4.157) is equal to or larger than unity. Near the melting transition ($T\simeq T_m$), the above result simplifies to

$$R_a(T_m) \simeq \begin{cases} a_0 e^{\tilde{c}(j_0/j_{sv})^{3/2}}, & a_0 < R_a(T_m) < \lambda, \\ \lambda \left[ \dfrac{j_0}{j_{sv}} \right]^{3/2}, & \lambda < R_a(T_m), \end{cases} \qquad (4.158)$$

where we have used $r_p(T_m) \simeq a_0 \simeq \xi$ and the latter estimate applies if the melting line is still close to the mean-field transition line $H_{c_2}(T)$. This is the case for large enough magnetic fields; see Sec. V.A. In these rough estimates we have dropped the Lindemann number in the relation $r_p(T_m) \simeq a_0$. Note that for small magnetic fields the above results are modified by the appearance of an additional factor $H_{c_2}(T_m)/B$. For $\delta T_c$ pinning, which we expect to be dominant at high temperatures, the result for the large-bundle regime, $R_a(T_m) \simeq \lambda (j_0/j_{sv})^{3/2}$, does not depend on $T/T_c$, since $j_0/j_{sv} \simeq \delta^{-2/3} \propto (1-T/T_c)^{1/3}$, and thus the result becomes universal, i.e., independent of field (as long as $H > H_{c_1}$) and temperature. For a quantitative estimate of the lattice correlation length near the melting transition, we should also take the anisotropy of the material into account, for $\mathbf{H} \| c$,

$$R_a(T_m) \simeq \begin{cases} a_0 e^{\tilde{c}(j_0/j_{sv}^c)^{3/2}}, & a_0 < R_a(T_m) < \lambda/\varepsilon, \\ \dfrac{\lambda}{\varepsilon} \left[ \dfrac{j_0}{j_{sv}^c} \right]^{3/2}, & \lambda/\varepsilon < R_a(T_m). \end{cases} \qquad (4.159)$$

Near the melting transition the lattice correlation radius $R_a(T_m)$ is larger than $\sim (\kappa/\varepsilon)(j_0/j_{sv}^c)^{3/2} a_0$, e.g., taking as an example the YBCO compound with a typical critical current ratio $j_0/j_{sv}^c \simeq 10^2$, we find the lattice order preserved over distances of the order of $10^3 \lambda(0)/\varepsilon$. Since the melting transition itself involves the scale $a_0 \ll R_a$, we have to conclude that disorder only weakly perturbs the melting transition itself.

The second important issue we wish to discuss is the dynamic evolution of the system into the glassy state. To be specific, consider a sample immersed in a magnetic field and cooled through the melting transition. Below the transition the vortex structure is frozen in by forming lattice-correlated bundles of size $R_c(T_m)$. The displacement field accumulated within the individual bundles is of the order of $u_p \simeq a_0$. As we investigate distances beyond the individual bundles, we expect the displacement field to grow randomly, that is, $u_p \simeq a_0 (R/R_c)^{1/2}$. The elastic length $R_c(T_m)$ and the lattice correlation length $R_a(T_m)$ are roughly equal, since $r_p(T_m) \simeq a_0$, and no further lattice order is established at this high temperature. When the sample is cooled down, $R_a$ starts to deviate from $R_c$, the lattice correlation length $R_a$ becoming increasingly large as compared with the elastic length $R_c$. This behavior confronts us with the problem of the dynamic evolution of the lattice towards the glass order

($\sim$ lattice order on scale $R_a$) as described by Eq. (4.155) above. The important question is whether the lattice order will be frozen in at low temperatures $T$ on the scale $R_a(T_m) \simeq R_c(T_m)$ or whether the relaxation to the glass order changes the lattice order to the scale $R_a(T)$. The relaxation is determined by the relation

$$U(R) \simeq T \ln \frac{t}{t_0}, \qquad (4.160)$$

saying that within a time $t$ the barriers $U(R)$ which can be overcome are of the order of $T \ln(t/t_0)$. We then need to know the dependence of the "glassy" barriers on distance $R$ as well as the available energy $T \ln(t/t_0)$. Let us consider the most favorable case (for relaxation) and evaluate the latter quantity at high temperatures. For typical experimental time scales we obtain $U_g \simeq T \ln(t/t_0) \sim 3000$ K. Second, let us estimate the glassy barriers at low temperatures, where they are smallest. The relevant barrier for uniform relaxation is $U(R)$ [not $U^b(R)$] as no compression is involved; it was obtained in Sec. A above, Eq. (4.47). With $U_{sv} \simeq 10^2$ K, $(a_0/L_c)^{1/5} \sim 1$, we find that the radius of glassy relaxation $R_g$ typically is located within the bundle pinning regime,

$$R_g \simeq \begin{cases} a_0 \left[ \dfrac{U_g}{U_{sv}} \right]^{1/2}, & R_g < \lambda, \\ a_0 \left[ \dfrac{U_g}{U_{sv}} \left[ \dfrac{a_0}{\lambda} \right]^{3/5} \right]^{5/7}, & \lambda < R_g < R_a, \end{cases} \qquad (4.161)$$

and thus is only a few lattice constants in size. Going over to an anisotropic material, the above result remains essentially unchanged,

$$R_g \simeq \begin{cases} a_0 \left[ \dfrac{U_g}{U_{sv}^c} \right]^{1/2}, & R_g < \dfrac{\lambda}{\varepsilon}, \\ a_0 \left[ \dfrac{U_g}{U_{sv}^c} \left[ \dfrac{\varepsilon a_0}{\lambda} \right]^{3/5} \right]^{5/7}, & \dfrac{\lambda}{\varepsilon} < R_g < R_a. \end{cases} \qquad (4.162)$$

Let us compare this result with the lattice correlation radius $R_a(T)$: at small temperatures and for weak pinning, $R_a \simeq \lambda (j_0/j_{sv})^{3/2}(H_{c_2}/B)$, which is much larger than the glassy radius $R_g$. Thus we find that even under these *optimized conditions* the relaxation to the glassy state is strongly limited by the slow dynamics of the relaxation process, and the system essentially exhibits lattice order as it has been frozen in near the melting transition.

### 2. Orientational LRO

Orientational long-range order is determined by the bond-angle correlator $\langle \theta^2(\mathbf{r}) \rangle = \langle [\theta(\mathbf{r}) - \theta(0)]^2 \rangle$, and a first straightforward way to tackle the problem is to calculate this quantity within the Larkin (1970) model. Expressing the bond-angle field via the displacement vector

u(r) [see Eq. (4.152)], and relating the latter via the lattice Green's function (3.30) to the random force density $F_{pin}$ [see Eq. (4.5)], we obtain

$$\langle \theta^2(\mathbf{r}) \rangle = \frac{1}{2} \int \frac{d^3k}{(2\pi)^3} (1 - \cos k r) K_{\perp,\alpha} K_{\perp,\beta} G_{\alpha,\gamma} G_{\beta,\gamma} W \; ,$$

(4.163)

where we have assumed a short-scale correlation for the random force density, Eq. (4.8). Only the transverse part of the Green's function, i.e., only shear relaxation, affects the bond-angle correlator, and we have to calculate

$$\langle \theta^2(\mathbf{r}) \rangle = \frac{W}{2} \int \frac{d^3k}{(2\pi)^3} \frac{(1 - \cos k r) K^2}{[c_{66} K^2 + c_{44}(\mathbf{k}) k_z^2]^2} \; .$$

(4.164)

Since the bond-angle field is given by the *derivative* of the displacement field, the singularity at small wave vectors is removed, and the above integral converges without the help of the factor $(1 - \cos k r)$ depending on distance. The main contribution to the integral in Eq. (4.164) originates from the Brillouin-zone boundary, so that we should use the dispersive limit for the tilt modulus $c_{44}(\mathbf{k}) \simeq \hat{c}_{44}/\lambda^2 K^2$. Repeating all the steps in the calculation of the displacement correlator above, we arrive at the result

$$\langle \theta^2(\mathbf{r}) \rangle \simeq \frac{W\lambda}{8 c_{66} \sqrt{\hat{c}_{44} c_{66}} a_o^2} \simeq \left[ \frac{\xi}{a_o} \right]^2 \left[ \frac{a_o}{L_c} \right]^3 \; .$$

(4.165)

Thus we see that, within the present model, orientational LRO is preserved for a vortex lattice subject to a disorder potential coupling to the displacement field u(r), a result first obtained by Chudnovsky (1989). Since at the same time the translational LRO is destroyed, the resulting phase is called a hexatic vortex glass. Note, that in two dimensions, orientational LRO decays algebraically (Nelson, Rubinstein, and Spaepen, 1982; Chudnovsky, 1986).

The above perturbative derivation (4.165) can be expected to be correct if disorder is not driving the bond-angle correlator $\langle \theta^2(\mathbf{r}) \rangle^{1/2}$ beyond an individual pinning valley, that is, $\langle \theta^2(\mathbf{r}) \rangle^{1/2} \lesssim \xi/a_o$, which is the case for small disorder and large enough fields, $a_o < L_c$. Otherwise, we should again substitute for the random force the more appropriate random pinning potential and determine the correct long-distance scaling behavior for the correlator. An additional difficulty arises if we want to prove the existence of orientational LRO rather than its destruction. While to demonstrate the *destruction* of LRO it is sufficient to come up with some particular type of fluctuation, to demonstrate the *preservation* of LRO it is necessary to show stability against all possible types of fluctuations. This has been pointed out by Toner (1991a), who showed that orientational LRO is destroyed in $d < 4$ space dimensions by a quenched random torque field which couples directly to the bond-angle field $\theta(\mathbf{r})$. The latter possibility has also been suggested by Marchetti and Nelson (1990a), who argued that such a torque field could be set up by randomly oriented pairs of closely

spaced impurities, singling out a preferred local orientational axis for the flux-line lattice. Obviously, the final answer whether orientational LRO is preserved or not crucially depends on our choice of Hamiltonian describing the fluctuations of the bond-angle field.

The simplest way to obtain Toner's result is to consider a Larkin-type formulation of the problem, modified to describe the bond angle rather than the displacement field. The elastic Hamiltonian for the bond-angle field $\theta(\mathbf{r})$ in the presence of a random torque field $\tau(\mathbf{r})$ takes the form (Toner, 1991a)

$$\mathcal{H} = \int d^d r \left[ \frac{K^{(2)}}{2} (\nabla^{(2)}\theta)^2 + \frac{K_z}{2} (\partial_z \theta)^2 + E_d(\mathbf{r},\theta) \right] \; ,$$

(4.166)

with

$$E_d(\mathbf{r},\theta) = \tau(\mathbf{r})\theta(\mathbf{r}) \; .$$

(4.167)

The random torque field in Eq. (4.167) is taken to be short-range correlated (on a scale $a_o$) with $\langle \tau(\mathbf{r})\tau(\mathbf{r}') \rangle = \gamma_\tau \delta(\mathbf{r} - \mathbf{r}')$. Such a random torque field has to be expected to occur due to correlations in the disorder potential on the scale $a_o$; it is reduced in strength compared with the original disorder potential due to the small parameter $\xi/a_o$ (see also Toner, 1991c; Chudnovsky, 1991). However, this Hamiltonian suffers from the same deficiencies as the usual Larkin model if we wish to investigate the large-distance behavior for the bond-angle field $\theta(\mathbf{r})$. First, the distortion of the lattice is produced by a random potential rather than by a random torque, and second, the perturbative approach breaks down at large length scales, where the bond orientation field has grown beyond the critical value $\xi/a_o$. In order to improve upon Eq. (4.166), a random potential should be substituted for the last term $E_d$. Taking the symmetries of the problem into account, the random potential

$$E_d^6(\mathbf{r},\theta) = E_6 \cos[6\theta(\mathbf{r}) - \alpha(\mathbf{r})] \; ,$$

(4.168)

with $\alpha(\mathbf{r})$ a short-range correlated random-phase field, is expected to give a more appropriate description of the problem. For small angles (small distances), $E_d^6(\mathbf{r},\theta)$ reduces to the random torque field used in Toner's approach. However, with the random potential $E_d^6$ substituted for the random torque field $E_d$, the Hamiltonian (4.166) is in the universality class of the charge-density-wave problem. As a consequence, we then expect the bond-angle correlator $\langle \theta^2(\mathbf{r}) \rangle^{1/2}$ to grow logarithmically with distance in $d < 4$ space dimensions and the orientational correlator $g^o(6,\mathbf{r})$ to decay algebraically. In fact, such behavior is also in better agreement with the experimental findings; see the discussion below.

While a random torque field coupling directly to the bond-angle field, as well as its large-scale generalization involving a random potential $E_d^6$, will ultimately lead to the destruction of orientational LRO, one would still expect orientational order to be preserved over large dis-

tances compared with the translational lattice order. Alternatively, orientational LRO can be restored rigorously by coupling the flux lattice to the underlying crystal lattice. As shown by Toner, any crystal/flux-lattice coupling of the form $V_p \cos p\theta$, with $p$ an even integer, will produce a finite correlator $g^o(p, \mathbf{r} \to \infty) > 0$. A particularly interesting situation occurs when the magnetic field is directed along a high-symmetry axis of the crystal, as is the case in the oxides when $\mathbf{H}$ is pointing along the $c$ axis. In this case the fourfold symmetry of the lattice cannot couple directly to the sixfold symmetry of the flux-line lattice, allowing for a hexatic *transition* at finite temperature, where $g^o(p, \mathbf{r} \to \infty)$ goes to zero (Toner, 1991a).

Of course, the issue of the dynamic evolution of the relaxation to the disorder potential is also relevant for the question of orientational LRO. In particular, the question arises whether the defect structure of the low-temperature solid phase is due to dislocations induced thermally at high temperatures and trapped in part by the disorder as the system goes through the melting transition, or whether the lattice defects are rather a true reflection of the disorder potential with the dislocations induced by the disorder itself. The case in which the dislocations are induced thermally has been discussed in detail by Marchetti and Nelson (1990a). In their theory of the vortex-liquid phase, they show that a finite density of thermally induced dislocations does destroy translational LRO but leaves the orientational LRO intact, resulting in a hexatic vortex-*liquid* phase. Upon cooling, this thermally induced defect structure may become partly frozen in by the quenched disorder or, alternatively, the vortex lattice may relax to the disorder potential and transform into a true hexatic vortex *glass*, where the defect structure is induced by the quenched disorder. From our estimates above we would expect glassy radii of the order of a few lattice constants, which indeed is much smaller than the observed regimes of orientational LRO extending over $\sim 10^2$ $\mu$m (Murray *et al.*, 1990; Grier *et al.*, 1991); hence one would conclude that the observed order is frozen in upon cooling rather than induced by the quenched disorder potential.

Finally, let us comment on the experimental findings (Murray *et al.*, 1990; Grier *et al.*, 1991) concerning the measurement of both translational and orientational long-range order. Bitter decoration analysis of the lattice structure requires the internal magnetic-field strength $B$ to be small, typically less than 100 G. Typical length scales measured for the lattice correlation length change from $R_a(10 \text{ G}) \simeq a_o$ to roughly $10^2 a_o$ at the maximal available field values of $\sim 100$ G (Grier *et al.*, 1991). From the above considerations, we can assume that the measured quantity is the frozen-in bundle correlation radius $R_a(T_m)$ rather than the relaxed low-temperature lattice correlation radius $R_a(T)$. However, we should not simply use the result (4.159) in a comparison with the experiments discussed here, as these experiments were performed at very small field values, $B < H_{c_1}$, whereas the result (4.159) applies to fields $B \gg H_{c_1}$, where Eq. (3.32)

for the shear modulus is valid. Below $H_{c_1}$, the shear modulus $c_{66}$ decays exponentially with decreasing field (Labusch, 1967, 1969; Larkin, 1970),

$$c_{66} = \left[ \frac{\pi}{6} \right]^{1/2} \frac{\varepsilon_o}{\lambda^2} \left[ \frac{\lambda}{a_o} \right]^{1/2} e^{-a_o/\lambda} , \qquad (3.36)$$

leading to a rapid decrease of the lattice correlation radius $R_a$ with decreasing field. Let us analyze this low-field situation in more detail for an anisotropic superconductor with $\mathbf{B} \| c$, which corresponds to the actual experimental situation. A comparison of the elastic tilt and shear energy densities shows that the interaction between the vortices becomes important on length scales

$$L > L_a \simeq \left[ \frac{c_{44}}{c_{66}} \right]^{1/2} a_o \simeq \varepsilon\lambda \left[ \frac{a_o}{\lambda} \right]^{1/4} e^{a_o/2\lambda} , \quad (4.169)$$

where we have used the single-vortex limit of the tilt modulus $c_{44} \simeq \varepsilon^2\varepsilon_o/a_o^2$. In the calculation of the displacement field $u_p$ we should note that for anisotropic superconductors the dispersive regime extends down to the region $K \gtrsim \varepsilon/\lambda$, so that dispersion is still relevant in the field regime defined by the condition $\lambda < a_o < \lambda/\varepsilon$, that is, $\varepsilon^2 < B/H_{c_1} < 1$. Since the displacement field is dominated by long-wavelength fluctuations, we then have to take into account the dispersion in the tilt modulus $c_{44}(\mathbf{k})$, and $c_{44} \simeq (B^2/4\pi)(\varepsilon^2/\lambda^2 K^2)$. Thus the displacement field $u_p$ grows with distance according to

$$u_p \simeq \begin{cases} \xi \left[ \dfrac{L}{L_c^c} \right]^{3/5} , & L_c^c < L < L_a , \\[3ex] \xi \left[ \dfrac{L_a}{L_c^c} \right]^{3/5} \ln \dfrac{R}{a_o}, & a_o < R < \dfrac{\lambda}{\varepsilon} , \\[3ex] \xi \left[ \dfrac{L_a}{L_c^c} \right]^{3/5} \left[ \dfrac{\varepsilon R}{\lambda} \right]^{1/5} , & \dfrac{\lambda}{\varepsilon} < R , \end{cases} \qquad (4.170)$$

and the longitudinal and transverse length scales are related by

$$L \simeq (c_{44}/c_{66})^{1/2} R \simeq \varepsilon(\lambda/a_o)^{3/4}(R/a_o K)\exp(a_o/2\lambda) ,$$

with $K \simeq 1/R$ in the dispersive regime and $K \simeq 1/a_o$ at large distances, $R > \lambda/\varepsilon$. Lattice order can only be established if the condition $u_p \sim a_o$ is met within the bundle pinning regime, which implies that [see Eq. (4.170)]

$$a_o < a_x \simeq \lambda \left[ \ln \frac{j_o}{j_{sv}^c} + \frac{4}{3}\ln\kappa + \frac{17}{6}\ln\frac{a_x}{\lambda} \right] . \qquad (4.171)$$

The crossover from single-vortex pinning to small-bundle pinning then takes place at fields corresponding to $a_o = a_x \sim 10\lambda$, i.e., a few Gauss. Above this crossover field, the lattice correlation length $R_a$ as obtained from Eq. (4.170) is

$$R_a \simeq \begin{cases} a_0 \exp\left[\tilde{c}\left[\frac{L_c^c}{L_a}\right]^3\left[\frac{a_0}{\xi}\right]^5\right], & a_0 < R_a < \frac{\lambda}{\varepsilon}, \\ \frac{\lambda}{\varepsilon}\left[\frac{L_c^c}{L_a}\right]^3\left[\frac{a_0}{\xi}\right]^5, & \frac{\lambda}{\varepsilon} < R_a. \end{cases} \quad (4.172)$$

Due to the exponential dependence of the shear modulus on the lattice constant, $c_{66} \propto \exp(-a_0/\lambda)$, the combination

$$\left[\frac{L_c^c}{L_a}\right]^3\left[\frac{a_0}{\xi}\right]^5 \simeq \left[\frac{a_0}{a_x}\right]^{17/4}\exp\left[-\frac{3}{2}\frac{a_0-a_x}{\lambda}\right] \quad (4.173)$$

increases rapidly with field, leading to a steep increase in the lattice correlation length $R_a$ above the crossover field $B_x \simeq \Phi_0/a_x^2$. In fact, due to the extremely sharp rise of $R_a$ just above the crossover field $B_x$, the extent of the dispersive regime is very narrow, and $R_a$ increases from $R_a/a_0 \simeq 1$ to $R_a/a_0 \simeq \lambda/\varepsilon a_x \simeq 1/10\varepsilon$ at crossover. Note that for $\lambda/\varepsilon < a_x$ the single-vortex pinning regime goes directly over into the large-bundle pinning regime, and the intermediate dispersive regime is absent.

In a next step we have to analyze the question of the relaxation towards the glassy state discussed above. When the sample is cooled down (at fixed induction $B$) through the melting line, lattice order is established on a scale $R_a(T_m)$ just below $T_m$. Since the melting line is located above the lower critical field $H_{c_1}(T)$, the interaction between the vortices is strong, and the lattice correlation length is large, $R_a(T_m) \simeq (\lambda/\varepsilon)(j_0/j_{sv}^c)^{3/2}(H_{c_2}/B)$ [we consider a weak-pinning situation here where $R_a(T_m) > \lambda/\varepsilon$]. Upon cooling, the radius $\lambda$ of the vortices drops below their mean separation $a_0$, and their mutual interaction, which produced the lattice at $T_m$, decreases exponentially. The crucial question again is whether the high-temperature lattice order is preserved upon cooling to below $H_{c_1}(T)$ or whether this lattice order will be destroyed by creep. We therefore have to determine the relaxation barriers for this weak-field situation,

$$U(R) \simeq U_{sv}^c \begin{cases} \left[\frac{L}{L_c^c}\right]^{1/5}, & L_c^c < L < L_a, \\ \left[\frac{L_a}{L_c^c}\right]^{1/5}\left[\frac{R}{a_0}\right]^2, & a_0 < R < \frac{\lambda}{\varepsilon}, \\ \left[\frac{L_a}{L_c^c}\right]^{1/5}\left[\frac{\lambda}{\varepsilon a_0}\right]^2\left[\frac{\varepsilon R}{\lambda}\right]^{7/5}, & \frac{\lambda}{\varepsilon} < R < R_a. \end{cases}$$

$$(4.174)$$

First, we estimate the barrier for creep at crossover, $U_x \simeq U_{sv}^c(L_a/L_c^c)^{1/5} \simeq U_{sv}^c(a_0/\xi)^{1/3} \simeq U_{sv}^c(10\kappa)^{1/3}$. For BiSCCO, we obtain $U_{sv}^c \simeq \varepsilon^{2/3}U_{sv}^{c,iso} \simeq 10$ K, hence $U_x \simeq 10^2$ K at crossover. (Note that, at crossover, $L_a \simeq L_c^c(a_x/\xi)^{5/3} \simeq L_c^c(10\kappa)^{5/3}$, hence $L_a$ is of the order of

the sample thickness, which typically is $\sim 10$–$100$ $\mu$m). Due to the smallness of these barriers as compared to the typical glassy barriers $U_g \simeq T \ln t/t_0 \simeq 3.10^3$ K, which can be overcome within experimental time scales $t$, we find that the lattice order will be destroyed due to creep at fields $B < B_x$.

Let us now turn to larger fields, $B > B_x$ (here we neglect the small-field regime where the dispersion is relevant). Low-temperature lattice order can be established if $U(R_a) \lesssim U_g$. Expressing the result (4.174) through the lattice correlation length $R_a$ itself, we obtain

$$U(R_a) \simeq U_{sv}^{c,iso}\left[\frac{\lambda\kappa}{a_0}\right]^{1/3}\left[\frac{R_a}{a_0}\right]^{4/3}. \quad (4.175)$$

Assuming typical parameters for $U_g$ and $U_{sv}^{c,iso}$, we find that the highly correlated initial state is relaxed to the low-temperature glassy state with a reduced lattice correlation length $R_a$ for $R_a/a_0 \lesssim 10$.

In summary, then, the following picture emerges: A highly correlated vortex lattice state is frozen in at $T_m$ upon cooling, the large lattice correlation length $R_a(T_m)$ being a consequence of the melting line's lying above $H_{c_1}(T)$. Cooling the sample to below the lower critical field $H_{c_1}(T)$ causes the interaction between the vortices to decrease exponentially, hence the natural tendency to produce a lattice is lost. Due to creep, the highly correlated state that was frozen in at $T_m$ then transforms to the less correlated low-temperature glassy state at small enough fields. For fields $B < B_x$, where the crossover field $B_x$ is of the order of a few Gauss, lattice order is completely lost. At higher fields, $B > B_x$, lattice order starts to increase and the system relaxes to a state with $R_a$ given by Eq. (4.172) for $R_a/a_0 \lesssim 10$. Finally, at even higher fields, complete relaxation to the low-temperature glassy phase is no longer possible due to the largeness of the creep barriers at large length scales, $R_a/a_0 > 10$, and the high-temperature highly correlated lattice phase is preserved. Hence we obtain a lattice correlation length $R_a$ that *increases* with field at small fields, in agreement with the experimental findings of Grier *et al.* (1991).

Regarding orientational LRO, the experimental situation can be summarized as follows: First observations of hexagonally correlated vortices in YBCO have been reported by Gammel *et al.* (1987). Quantitative analyses on the extent of both translational and orientational LRO in BiSCCO have been performed by Murray *et al.* (1990) and by Grier *et al.* (1991). It has been observed that the long-distance behavior of the orientational correlator can be fit by an algebraic decay law, $g^o(6, \mathbf{r}) \propto r^{-\eta_6}$, which is consistent with the result obtained for the random potential of the form (4.168). However, note that theories on 2D hexatics, liquids (Halperin and Nelson, 1978; Nelson and Halperin, 1979),[6] or glasses (Nelson,

---

[6]In the absence of a fast-relaxation dynamics the liquid order prevailing at high temperatures is frozen in at low temperatures.

Rubinstein, and Spaepen, 1982; Chudnovsky, 1986) also predict an algebraic decay of the correlator $g^o(6,r)$. Typical values for $\eta_6$ are around 0.05 ($B \simeq 30$–100 G), close to the experimental resolution, with a rather sharp increase to values around 1 below fields of the order of 10 G. The sharp rise in $\eta_6$ for small magnetic fields is accompanied by a sharp drop in the translational correlation length, a feature clearly observable at least for the more disordered sample in the report by Grier *et al.* (1991). This is consistent with the expected crossover to single-vortex pinning at very low fields, where $R_a$ drops below one lattice constant and the phase becomes dominated by disorder.

## V. THERMODYNAMIC PROPERTIES

Several basic parameters of the new high-temperature superconductors conspire to enhance dramatically the importance of thermal fluctuations. First of all, according to our scaling analysis in Sec. III.A, the large transition temperature $T_c$ combines with the anisotropy $\varepsilon$ to produce an *effective* fluctuation temperature of the order of $T_{\rm eff} \simeq T_c/\varepsilon \sim 10^3$ K–$10^4$ K. This energy scale then has to be compared with the relevant elastic energy scale $\varepsilon_0 a_0$ in the vortex lattice. The ratio of these two energies can be written in terms of the Ginzburg number, $T_{\rm eff}/\varepsilon_0 a_0 \simeq \{Gi/[H_{c_2}(T)/B](1 - T/T_c)\}^{1/2}$. Obviously, for fields $B$ close enough to the upper critical-field line $H_{c_2}(T)$ and temperatures $T$ near the critical temperature $T_c$, this ratio becomes of the order of unity. In the high-temperature superconductors the Ginzburg number is rather large, and therefore thermal fluctuations are able to melt the vortex lattice over a significant portion of the $B$-$T$ phase diagram. In this section we first discuss the *melting transition* of the vortex lattice and then analyze in some detail the resulting high-temperature *vortex-liquid phase*. The melting transition depends strongly on the value of the applied field $B$, and below we shall separately discuss the three cases of low, $B < H_{c_1}$, intermediate, $H_{c_1} \ll B \ll H_{c_2}$, and high $B \sim H_{c_2}$, fields. Regarding the thermodynamic nature of the vortex-liquid phase, we shall concentrate mainly on the question of whether the vortex liquid is a genuine new thermodynamic state that is *qualitatively* different from the normal metal. Alternatively, the vortex liquid could merely differ *quantitatively* from the normal state, in which case the upper critical-field line $H_{c_2}(T)$ would only mark a crossover from normal metal to a strongly fluctuating superconducting state, with no real phase transition taking place until the melting line is reached.

Within the present section we shall neglect the influence of the quenched disorder potential on the thermodynamic properties of the vortex system. As we always consider the case of weak disorder, this approximation does not seem to impose a severe restriction on the

generality of our discussion. In particular, we have shown above that we expect the relevant lattice correlation length $R_a(T_m)$ to be much larger than the mean vortex spacing $a_0$, and thus disorder will only weakly affect the melting transition itself. Moreover, we shall concentrate on the *continuous anisotropic* description of superconductivity here, so that the discussion is pertinent to $YBa_2Cu_3O_{7-y}$-like systems or to those regions of the phase diagram of the strongly layered Bi- and Tl-based materials where an anisotropic description is valid. Typical effects of layering will be discussed in Sec. VIII below.

### A. Vortex-lattice melting

#### 1. Moderate magnetic fields: $H_{c_1} \ll B \ll H_{c_2}$

Depending on the value of the magnetic field $B$ as compared with the lower and upper critical fields $H_{c_1}$ and $H_{c_2}$, the elastic properties of the vortex lattice and hence its stability with respect to thermal fluctuations are rather different (see, for example, Brandt, 1977a, 1977b; Larkin and Ovchinnikov, 1979). To begin with, we concentrate on the intermediate regime characterized by the conditions

$$H_{c_1} \ll B < 0.2 H_{c_2} \ . \tag{5.1}$$

For high-$\kappa$ materials, such as the high-temperature superconductors, the relation $H_{c_2} = 2\kappa^2 H_{c_1}/\ln\kappa$ shows that this regime is very large and covers most of the experimentally accessible field range. The first inequality in (5.1) guarantees that the mean vortex separation $a_0$ is small as compared with the London penetration depth $\lambda$; hence the interaction between the individual vortex lines is large and strongly nonlocal. The second inequality makes sure that the vortex cores do not overlap, and thus the London approximation can be used to determine the energy of the elastically deformed vortex lattice (Brandt, 1977b). Unfortunately, even for this well-defined situation, no consistent theory of vortex-lattice melting is known today. Various approaches have been used to tackle the problem of vortex-lattice melting. The two most prominent methods are based on the Lindemann criterion and on Monte Carlo simulations.

The semiquantitative approach based on the Lindemann criterion (Lindemann, 1910) assumes that a crystalline lattice becomes unstable with respect to thermal fluctuations of its constitutive elements (atoms, vortex lines, etc.) as the mean-squared amplitude of fluctuations $\langle u^2 \rangle_{\rm th}$ increases beyond a certain fraction $c_L$ of the lattice constant $a_0$,

$$\langle u^2(T_m) \rangle_{\rm th} \approx c_L^2 a_0^2 \ . \tag{5.2}$$

With a Lindemann number $c_L \approx 0.1$–0.2 depending only weakly on the specific material, the criterion (5.2) provides a reasonable estimate for the melting temperature

$T_m$ for a large variety of three-dimensional solid-liquid transitions. Moreover, it has been found that the same criterion holds approximately for the quantum melting of a two-dimensional solid at $T=0$ (Ceperley, 1978), with $c_L \approx 0.3$ (Xing and Tešanović, 1990) somewhat larger than for the conventional melting transition of a three-dimensional solid. For the present discussion of vortex-lattice melting, the use of the Lindemann criterion (5.2) is particularly fruitful, as it allows us to determine the shape of the melting line $T_m(B)$ over a broad range of magnetic-field values by assuming a constant value for $c_L$ over the entire range $H_{c_1} \ll B < 0.2H_{c_2}$. As both the type of lattice and the (long-range) nature of the interaction are unchanged throughout this regime, such an assumption seems to be quite reasonable: Indeed, since $a_0 \ll \lambda$ within the present regime of interest, we can neglect screening effects in the determination of the melting line, and the relevant free energy of the vortex system can be written in terms of an unscreened interaction potential $V^{int}(r) = 1/r$ in the energy functional (3.23),

$$\mathcal{F}[\mathbf{u}] = \frac{\varepsilon_0 a_0}{2} \sum_{\mu, \nu} \int \frac{d\mathbf{s}_\mu \cdot d\mathbf{s}_\mu}{|\mathbf{s}_\mu - \mathbf{s}_\nu|} , \qquad (5.3)$$

where the positions $\mathbf{s}_\mu$ are measured in units of $a_0$. The statistical mechanics of the vortex system then is completely determined by the parameter ratio $\varepsilon_0 a_0 / T$ containing all the dependencies on field $B$ and on the temperature $T$. Therefore the melting line will be determined by some universal constant related to the Lindemann number $c_L$. More elaborate theories of the melting transition are able to predict the numerical value of this universal constant, whereas the functional dependence of the melting line on the parameters $B$ and $T$ can already be read off the representation of the free energy (5.3).

Recently, the problem of the vortex-liquid/Abrikosov-lattice transition has been addressed by a variety of more basic approaches not relying on the Lindemann criterion Ma and Chui (1991) have presented a mechanism for the flux lattice melting in terms of a proliferation of edge dislocations. They find that the interaction of a dislocation with the thermal fluctuations of the flux lines produces a negative contribution to the energy of the dislocation, which grows in magnitude with increasing temperature, so that the overall energy of the dislocation vanishes at the melting transition. The effective Lindemann number that they find is approximately $c_L \approx 0.3$. Sengupta *et al.* (1991) find a first-order melting transition within their density-functional approach to the solid-liquid transition in the flux-line lattice, and their Lindemann number is $c_L \approx 0.2$. Further, the melting transition has been studied by means of Monte Carlo simulations by Li and Teitel (1991,1993) and by Ryu *et al.* (1992). Whereas Li and Teitel base their analysis on an anisotropic, uniformly frustrated $XY$ model, a Lawrence-Doniach model of stacked superconducting layers is studied in the simulations of Ryu *et al.* The Lindemann number obtained within the latter model

turned out to be different for very low ($c_L \approx 0.1$ for $B \sim 50$ G) and for high ($c_L \approx 0.4$ for $B \sim 50$ T) fields, with a large intermediate regime between $\sim 0.1$ and 10 T where $c_L \approx 0.2$ is roughly constant, in agreement with our discussion above. A very interesting result has been obtained by Hetzel, Sudbø, and Huse (1992), who find strong numerical evidence for the melting transition being first order. Their Monte Carlo analysis is also based on the anisotropic, uniformly frustrated $XY$ model. It shows a clear hysteretic behavior and thus a finite latent heat ($0.3T$ per vortex and layer) as the temperature is varied across the melting transition. Experimental evidence for a first-order melting transition has been reported by Safar, Gammel, Huse, *et al.* (1992b, 1993), by Charalambous (1992; see also Charalambous *et al.*, 1993), and by Kwok *et al.* (1994a, 1994b) based on the observation of a sharp transition combined with a hysteretic trace in the linear-response resistance as a function of temperature. In the following we shall concentrate on the analysis based on the Lindemann criterion and determine the shape of the melting line within the various field ranges.

In order to make use of the Lindemann criterion (5.2), we have to determine the mean-squared amplitude of fluctuations $\langle u^2(T) \rangle_{th}$ for the vortex lattice. This has been calculated by Houghton, Pelcovits, and Sudbø (1989) and by Brandt (1989), and a rough estimate has also been given in Sec. IV.C above. For an isotropic material or for the special case of an anisotropic superconductor with $\mathbf{H} \| c$, we have to solve the following implicit equation for the melting line (Houghton, Pelcovits, and Sudbø, 1989):

$$\frac{\sqrt{b_m(t)}}{1 - b_m(t)} \frac{t}{\sqrt{1-t}} \left[ \frac{4(\sqrt{2}-1)}{\sqrt{1 - b_m(t)}} + 1 \right] = \frac{2\pi c_L^2}{\sqrt{Gi}} , \qquad (5.4)$$

with $b_m(t) = B_m(T)/H_{c_2}(T)$, $t = T/T_c$, and $Gi$ the Ginzburg number introduced in Eq. (2.47) above, which determines the width of the fluctuational region close to the upper critical-field line $H_{c_2}(T)$; see Fig. 2. For temperatures close to $T_c$, the melting line is far below the upper critical field $H_{c_2}(T)$, $b_m(t) \ll 1$, and the implicit equation (5.4) can be simplified considerably to produce a melting line (see Fig. 2),

$$B_m(T) \approx \beta_m \frac{c_L^4}{Gi} H_{c_2}(0) \left[ 1 - \frac{T}{T_c} \right]^2 , \qquad (5.5)$$

with

$$\beta_m \approx 5.6 . \qquad (5.6)$$

Again, we denote by $H_{c_2}(0)$ the upper critical field extrapolated *linearly* to zero. Note that the Ginzburg number depends on the anisotropy parameter $\varepsilon$ in general. The results (5.5) and (4.107) differ slightly in their numerical prefactors, as we used our rough estimate (4.85) for the displacement field $\langle u^2 \rangle_{th}$ above, whereas here we have

based our analysis on the more accurate result of Houghton, Pelcovits, and Sudbø (1989). Note also that, since the main contribution to the displacement field $\langle u^2 \rangle_{th}^{1/2}$ originates from wave vectors close to the Brillouin zone, the strongly dispersive part of the tilt modulus $c_{44}^c$ competes with the single-vortex contribution $c_{44}^c$; see Sec. III.B, $c_{44}(K \simeq K_{BZ}) \simeq (\varepsilon^2 \varepsilon_0 / a_0^2)[1 + \ln(H_{c_2}/B)^{1/2}]$. As long as the melting line $B_m$ is not suppressed too far below the mean-field critical line $H_{c_2}$, we can safely ignore the single-vortex contribution. This is the case for YBCO within the intermediate-field regime $H_{c_1} \ll B \ll H_{c_2}$. However, at low fields, $B \lesssim H_{c_1}$, and for strongly layered superconductors where $B_m \ll H_{c_2}$, the single-vortex contribution becomes dominant (see Glazman and Koshelev, 1991a).

An important feature of the result (5.5) is the quadratic dependence of $B_m$ on $T_c - T$ upon approaching the transition temperature $T_c$, guaranteeing that the melting line $B_m(T)$ is indeed situated far below the mean-field transition line $H_{c_2}(T)$, in agreement with our original assumption (5.1). Using a very-high-precision low-frequency torsional-oscillator technique on an untwinned single crystal of YBa$_2$Cu$_3$O$_{7-y}$, Farrell, Rice, and Ginsberg (1991) have observed a sharp dissipation peak, whose position shows a $(T_c - T)^2$ dependence when plotted in the $H$-$T$ phase diagram. This dissipation peak has been interpreted as the signature of the melting transition of the vortex lattice, and the resulting transition line is in good agreement with the theoretical prediction for the shape of the flux-lattice melting line.

A word of caution is appropriate here: As will be shown in Sec. VI.B below, the resistivity within the thermally activated flux-flow regime $[T > T_m(B)]$ is determined by the plastic barriers $U_{pl} \propto (T_c - T)/\sqrt{B}$ and hence is expected to be constant along the lines $B \propto (T - T_c)^2$. As discussed in Sec. X, the dissipation peak in this type of measurement is most straightforwardly explained through a combination of the skin effect and the finite size effect, whereby the peak arises when the ac field exactly penetrates the entire sample cross section. In this sense, the observed $B \propto (T - T_c)^2$ behavior can also be interpreted as simply measuring a constant-resistivity curve *without the concomitant association with a melting transition*. We point out that the recent results found by Safar, Gammel, Huse et al. (1992b, 1993), by Charalambous (1992; see also Charalambous et al., 1993), and by Kwok et al. (1994a, 1994b) do give strong support for the melting scenario (see Geshkenbein, Ioffe, and Larkin, 1994, for a discussion of the hysteretic effects observed in connection with the melting transition).

Let us discuss the range of applicability of the result (5.5). First of all, we require the temperature $T$ to lie outside of the fluctuation regime, hence $1 - T/T_c \gtrsim Gi$. At the borderline of this region (marked by a superscript) the result (5.5) becomes

$$B_m' \approx 5 c_L^4 H_{c_2}' \ll H_{c_2}' \, , \qquad (5.7)$$

where we have used that $H_{c_2}(T) = H_{c_2}(0)(1 - T/T_c)$. Evidently, the suppression of the melting line $B_m(T)$ with respect to the $H_{c_2}(T)$ line upon leaving the critical regime is due to the smallness of the Lindemann number $c_L$ and does not depend on $Gi$. In other words, it is the smallness of $c_L$ which guarantees that the melting line comes to lie outside of the critical fluctuation regime; see Fig. 2.

Second, the regime of applicability of the result (5.5) from above, i.e., at small temperatures, is given by the condition $B_m \ll 0.2 H_{c_2}(T)$, leading to

$$1 - \frac{T}{T_c} \ll 0.2 \frac{Gi}{\beta_m c_L^4} \, . \qquad (5.8)$$

With typical values for $Gi \sim 10^{-2}$ (YBa$_2$Cu$_3$O$_{7-y}$) and a Lindemann number $c_L \approx 0.2$, we obtain a parameter $Gi/\beta_m c_L^4 \approx 1$, and our result (5.5) should be valid near $T_c$. Away from $T_c$, the melting line moves closer to the $H_{c_2}(T)$ line, and the suppression of the order parameter due to overlapping vortex cores becomes relevant. Hence the full equation (5.4) (Houghton, Pelcovits, and Sudbø, 1989) has to be used for the determination of the melting line. In fact, for YBa$_2$Cu$_3$O$_{7-y}$ the simple power-law result (5.5) is limited to a regime extending only a few Kelvin below $T_c$ (see, for example, Blatter and Ivlev, 1994). The main correction to the simple power-law result can be obtained by accounting for the suppression of the order parameter via the substitution $\lambda \to \lambda' = \lambda/[1 - b(t)]^{1/2}$ [see Sec. III.B.1; $b(t) = B/H_{c_2}(T)$ is the reduced field],

$$B_m(T) \approx \beta_m \frac{c_L^4}{Gi} H_{c_2}(0) \left[ \frac{T_c}{T} \right]^2 \left[ 1 - \frac{T}{T_c} - \frac{B_m}{H_{c_2}(0)} \right]^2 , \qquad (5.9)$$

[the factor $T_c^2/T^2$ accounts for the proportionality $\langle u^2 \rangle_{th} \propto T$]. Equation (5.9) can be easily solved for $B_m(T)$, and we find the improved result

$$B_m(T) \approx H_{c_2}(0) \frac{4\theta^2}{(1 + \sqrt{1 + 4\theta T_s/T})^2} , \qquad (5.10)$$

with the new temperature variable

$$\theta = c_L^2 \sqrt{(\beta_m/Gi)} \left[ \frac{T_c}{T} - 1 \right] \qquad (5.11)$$

and

$$T_s = T_c c_L^2 \sqrt{\beta_m/Gi} \, . \qquad (5.12)$$

The result (5.10) describes a melting line that is shifted towards smaller temperatures and fields and that can no longer be expressed in terms of a simple power law. In fact,

$$B_m \approx \begin{cases} H_{c_2}(0)\theta^2, & \theta \to 0 , \\ \dfrac{\theta T}{T_s}, & \theta > \dfrac{T_c}{T_s} , \end{cases} \qquad (5.13)$$

and with increasing field (decreasing temperature) the "effective" power decreases. This result is in agreement with various experimental determinations of the melting line. Whereas Farrell, Rice, and Ginzberg (1991) obtained an exponent 2 on a field range of the order of 2 T, the measurements of Krusin-Elbaum *et al.* (1991), Schilling, Ott, and Wolf (1992), and Safar *et al.* (1993) covering a field range between 6 and 10 T produce "effective" power-law exponents in the range 1.35–1.45. Hence the attribution of a power law to the melting line is a compact way of describing the data rather than a deep physical concept.

For the strongly layered Bi- and Tl-based compounds, the Ginzburg number is of the order of $Gi \sim 1$, so that $Gi/\beta_m c_L^4 \gg 1$ and the result (5.5) is valid over a very wide regime in temperatures below $T_c$; see Fig. 3. Its applicability is limited by the occurrence of specific effects of two-dimensionality at field strengths $B \gtrsim \Phi_o/\Lambda^2$ ($\sim 1$ T for BiSSCO), with $\Lambda \simeq d/\varepsilon$ ($d =$ interlayer spacing) the length scale characterizing the strength of the interlayer Josephson coupling. Note that, for the case of the strongly layered superconductors, the Ginzburg number (2.47) should not be understood as describing the width of the fluctuation regime (which rather is given by the two-dimensional analog of the Ginzburg number; see Sec. VIII.B.2), but simply as a useful combination of phenomenological parameters making sense in the description of properties that can be addressed within a 3D continuum anisotropic model.

In all the calculations of the mean displacement amplitude $\langle u^2 \rangle$ discussed so far we have neglected quantum effects. For example, in expressing $\langle u^2 \rangle$ via the fluctuation-dissipation theorem we have always substituted the factor $\mathrm{ctgh}(\hbar\omega/2T)$ via its high-temperature expansion $2T/\hbar\omega$ [see Eq. (2.113) above]. Such an expansion is appropriate if the energy scale of the fluctuations is small compared with the temperature, so that all modes behave classically. Comparison of the elastic energy scale $e_{\mathrm{elast}} \simeq (\varepsilon_o/a_o^2)K_{\mathrm{BZ}}^2 u^2$ with the typical dynamical energy $e_{\mathrm{dyn}} \simeq \eta|\omega|u^2$ gives us the typical frequency scale

$$\hbar\omega = \frac{4\pi\hbar\varepsilon_o}{\eta a_o^4} . \qquad (5.14)$$

[Equation (5.14) defines the thermal relaxation time in the vortex lattice; see Sec. VI.A.1]. Using a simple Bardeen-Stephen expression for the viscous drag coefficient, as well as the relations $\sigma_n = \omega_p^2 \tau_r/4\pi$, $\omega_p^2 = 4\pi n e^2/m$, and $\lambda^2 = c^2/\omega_p^2$, which seem to be well fulfilled for the YBCO material (Batlogg *et al.*, 1990), we obtain the dimensionless ratio

$$\frac{\hbar\omega}{T} \approx \frac{B}{H_{c_2}} \frac{\hbar/\tau_r}{T} . \qquad (5.15)$$

With the estimate $\hbar/\tau_r \simeq T_c$ we finally obtain

$$\frac{\hbar\omega}{T} \simeq \frac{B}{H_{c_2}} \frac{T_c}{T} . \qquad (5.16)$$

Quantum effects, then, should play a role at high enough fields and low enough temperatures (note that the relaxation time $\tau_r$ is itself also temperature dependent, $\hbar/\tau_r \simeq T$ at high temperatures, and a saturation is expected as $T \to 0$). The effects of quantum fluctuations on the melting line in YBCO have been investigated by Blatter and Ivlev (1993; the suppression of the order parameter close to $H_{c_2}$ was neglected in this work, which led the authors to overestimate the effect of quantum fluctuations) and by Blatter and Ivlev (1994). By taking into account the effects of the order-parameter suppression close to $H_{c_2}$ and of quantum fluctuations (Blatter and Ivlev, 1994) one can obtain a very good fit to the experimentally measured melting line. The experimentally accessible part of the melting line ($B \lesssim 15$ T, $T > 70$ K) is too narrow, however, to allow for an unambiguous determination of quantum statistical effects. Other systems (e.g., the vortex lattice in thin-film superconductors with high normal-state resistivity) may be more promising candidates for the observation of a quantum melting transition (Blatter *et al.*, 1994).

Finally, we generalize the above results to the situation in which the applied magnetic field $B$ encloses an arbitrary angle $\vartheta$ with the superconducting planes (here we concentrate on uniaxially anisotropic materials such as the oxide superconductors). Within the present regime, the melting line $B_m(T)$ always passes above the lower critical field $H_{c_1}(T)$, hence the relevant scale for melting, which is the lattice constant $a_o$, is smaller than the penetration depth $\lambda$, and our scaling approach (see Sec. III.A) can be applied. Using the scaling rule (3.12), we obtain (Blatter, Geshkenbein, and Larkin, 1992)

$$B_m(T,\vartheta) = \frac{1}{\varepsilon_\vartheta} B_m(T, \pi/2) . \qquad (5.17)$$

The prediction (5.17) for the angular dependence of the melting line is in excellent agreement with the experimental findings of Beck *et al.* (1992; see also Kwok *et al.*, 1992), who determined the melting line in an untwinned $YBa_2Cu_3O_{7-y}$ single crystal for arbitrary direction of the magnetic field.

### 2. Low magnetic fields: $B \lesssim H_{c_1}$

For low inductions $B \lesssim H_{c_1}$ the shape of the melting line $B_m(T)$ changes drastically and becomes an *increasing* function of $B$ (at least for small temperatures). As a consequence, the $B$-$T$ phase diagram will exhibit reentrance as a function of $B$. When the magnetic field is decreased, we will observe a sequence of phases: normal-

metal/vortex-liquid/vortex-lattice/vortex-liquid; see Figs. 2 and 3. The origin of this interesting behavior is found in the dependence of the interaction between the vortex lines on the field strength $B$. For $B \lesssim H_{c_1}$ the intervortex spacing increases beyond the penetration depth $\lambda$, and the vortex-vortex interaction decreases exponentially. The melting transition in this field regime and its analogy with the transition between a crystalline and a superfluid phase in a system of two-dimensional bosons has been discussed extensively by Nelson (1988) and by Nelson and Seung (1989). A mean-field-theory of such a transition has also been developed recently by Feigel'man and Ziegler (1992). Here we restrict ourselves to a discussion of the melting line in the low-field regime as obtained from a Lindemann criterion and defer detailed analysis of the resulting liquid phase to the next section.

Due to the exponential dependence of the interaction between the vortex lines in the present low-density regime, the applicability of the Lindemann criterion based on a density-independent Lindemann number $c_L$ is much less obvious. However, we expect that the approach is still useful for providing an order-of-magnitude estimate for the melting transition.

In order to estimate the mean-squared amplitude of thermal fluctuations $\langle u^2(T) \rangle_{\text{th}}$, we have to use the appropriate expressions for the elastic moduli valid in the low-density regime $B \lesssim H_{c_1}$. The relevant wave vectors $K$ and $k_z$ are then small, e.g., $K \lesssim 1/a_0 < 1/\lambda$, and for an isotropic situation the dispersion in the elastic moduli can be neglected and simple, nondispersive expressions (Labusch, 1967, 1969; Larkin and Ovchinnikov, 1973) can be used. However, the situation is more complicated in an anisotropic superconductor, where the dispersive regime for the tilt elastic modulus $c_{44}(\mathbf{k})$ extends down to very small wave vectors, $\varepsilon/\lambda \lesssim K \lesssim 1/a_0$ (Sudbø and Brandt, 1991a). Since $\langle u^2(T) \rangle_{\text{th}}$ is mainly determined by short-wavelength fluctuations with $K \simeq K_{\text{BZ}} \simeq \sqrt{4\pi}/a_0$, the reduction of the tilt modulus due to the dispersion in $c_{44}(\mathbf{k})$ can be neglected only for very small fields, $B \lesssim \varepsilon^2 H_{c_1}/\ln\kappa$. Within the interesting range of fields with $\lambda \lesssim a_0 \lesssim \lambda/\varepsilon$, we can use the single-vortex limit of the tilt modulus, $c_{44}(K_{\text{BZ}}) = \varepsilon^2 \varepsilon_0 \ln(H_{c_2}/B)/2a_0^2$ as determined by Sudbø and Brandt (1991a). The shear modulus as given by Eq. (3.36) is exponentially suppressed within this regime, and the compression modulus $c_{11} = 3c_{66}$ is nondispersive and unaffected by the anisotropy (Sudbø and Brandt, 1991b). Using this set of (nondispersive) elastic moduli and following the same steps as in the derivation of Eq. (4.85) above, we obtain the following result for the mean-squared displacement amplitude (Nattermann, Feigel'man, and Lyuksyutov, 1991):

$$\langle u^2 \rangle_{\text{th}} = \frac{T}{a_0 \sqrt{4\pi c_{44} c_{66}}} \left[ 1 + \frac{1}{\sqrt{2 + c_{11}/c_{66}}} \right]$$

$$\approx a_0^2 \frac{0.5}{\sqrt{\ln\kappa}} \frac{T}{\varepsilon\varepsilon_0\lambda} \left[ \frac{\lambda}{a_0} \right]^{7/4} e^{a_0/2\lambda} . \qquad (5.18)$$

Combining this result with the Lindemann criterion (5.2), we obtain the implicit equation determining the melting line $B_m(T)$ at low inductions,

$$\left[ \frac{\lambda}{a_0} \right]^{7/2} e^{a_0/\lambda} = \beta'_m \frac{c_L'^4 \kappa^2 \ln\kappa}{Gi} \left[ \frac{T_c}{T} \right]^2 \left[ 1 - \frac{T}{T_c} \right] , \qquad (5.19)$$

with

$$\beta'_m \approx 0.5 . \qquad (5.20)$$

Here we have introduced the Lindemann number $c_L'$ in order to emphasize the possibility of having different parameters $c_L$ for the three regimes of low, intermediate, and high inductions $B$. We have also used the approximation $\ln(H_{c_2}/B) \simeq 2\ln\kappa$. A comparison of Eq. (5.19) with its intermediate-field counterpart (5.5) shows that the role of thermal fluctuations parametrized by the Ginzburg number $Gi$ is significantly suppressed within the present weak-field regime, as indicated by the replacement of $Gi$ by the much smaller effective parameter $Gi/\kappa^2\ln\kappa$. Using parameters appropriate for $YBa_2Cu_3O_{7-y}$ and assuming a Lindemann number $c_L' \approx 0.2$, we obtain an estimate for $\tilde{\beta}'_m = \beta'_m c_L'^4 \kappa^2 \ln\kappa/Gi$ of $\tilde{\beta}'_m \approx 2.5 \times 10^3$.

Let us analyze the result (5.19) in more detail. Defining $x = \lambda(0)/a_0$, we have to solve the implicit equation

$$f(x,t) = x^{7/2} e^{\sqrt{1-t}/x} = \tilde{\beta}'_m \frac{(1-t)^{11/4}}{t^2} , \qquad (5.21)$$

which becomes trivial in the limit $t \to 0$. We then obtain a melting line $B_m(T \to 0) \simeq H_{c_1}(0)[\ln(T/T_c)]^{-2}$, which indeed increases with increasing temperature, producing a reentrant behavior, as discussed above; see Figs. 2 and 3. The solution of Eq. (5.21) for arbitrary values of $t$ is more complicated and can only be done numerically. Since $f(x,t)$ has a minimum at $x = (2/7)(1-t)^{1/2}$, Eq. (5.21) either has two solutions ($x_1 < x_2$) or no solution at all. The solution $x_2$ is above the $H_{c_1}(T)$ line and thus irrelevant. No solution is found for high temperatures where $(1-t)/t^2 < (1-t^*)/t^{*2} = (2/7)^{7/2}\exp(7/2)/\tilde{\beta}'_m \approx 0.41/\tilde{\beta}'_m$. At $t^*$ the right-hand side of Eq. (5.19) is of the order of unity, implying that $a_0^* \approx 4\lambda(T^*)$ at the turning point of the low-field melting line. A comparison of $B^* = \Phi_0/a_0^{*2}$ with the values of the lower critical field $H_{c_1}(T^*)$ and of the extrapolated melting point $B_m(T^*)$ as given by Eq. (5.5) produces the relations

$$B^* \approx \frac{\pi}{4\ln\kappa} H_{c_1}(T^*) \qquad (5.22)$$

$$\approx \frac{\ln\kappa}{10} \left[ \frac{c_L'}{c_L} \right]^4 \frac{1}{t^{*2}} B_m(T^*) . \qquad (5.23)$$

As a result, the intersection of the melting line (5.5) coming from above with the low-field melting line (5.19) is close to the turning point $(B^*, T^*)$ if we assume that $c_L' \approx c_L$ (see Fig. 22), and thus the intermediate-field melt-
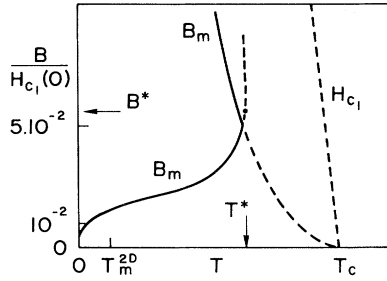
FIG. 22. Equilibrium phase diagram showing the low-field part of the melting lines $B_m(T)$ as well as the lower critical field $H_{c_1}(T)$. A set of parameters for BiSCCO as quoted by Kapitulnik [(1991; $\xi(0) \approx 15$ Å, $\lambda(0) \approx 2000$ Å, $\varepsilon^2 \approx 1/5000$, and $c_L' \approx 0.1$] has been chosen. The form of the melting line depends quite substantially on the numerical value of the chosen parameters, as a comparison with Fig. 3 clearly demonstrates. The drawing is to scale.

ing line smoothly crosses over to the low-field melting line at $H_{c_1}(T^*)$. The width of the low-density liquid regime is rather narrow; using parameters appropriate for YBCO or BiSCCO, the maximum of the low-field melting line is found to be of the order of a few Gauss; see Figs. 2, 3, and 22.

In order for the above analysis to be correct, we have to make sure that the melting line stays away from the fluctuation regime, which is the case if the condition $1-t^* > Gi$ is fulfilled. Interestingly, our ability to treat the entire melting transition within a mean-field description does not depend on the width of the fluctuation regime as given by $Gi$, but is determined by the relative sizes of the Ginzburg-Landau and Lindemann parameters $\kappa$ and $c_L$. The melting line passes outside of the fluctuation regime if

$$\kappa^2 \ln\kappa < c_L'^{-4} . \qquad (5.24)$$

With $c_L' \approx 0.2$, the largest possible value for $\kappa$ is around 20. For high-$\kappa$ materials such as the oxide superconductors, the melting lines obtained from Eqs. (5.5) and (5.19) enter the fluctuation regime *before* they intersect, and hence the reentrance point $T^*$ lies outside the regime where the mean-field-type approach is valid. Close to $T_c$, in addition to fluctuations in the phase of the order parameter (which are correctly treated in our approach), fluctuations in the amplitude of the order parameter become strong and can no longer be neglected.

The above discussion indicates that for the oxide superconductors the reentrant behavior of the melting line cannot be analyzed completely without exploring the properties of the vortex lattice within the fluctuation regime. This seems to be the case at least for the YBa$_2$Cu$_3$O$_{7-y}$ compound, for which the anisotropic three-dimensional description is valid. A discussion of the (scaling) behavior of the melting line within the fluc-

tuation regime has been given by Fisher, Fisher, and Huse (1991). On approaching $T_c$, the superconductor is expected to enter a regime where the fluctuations in the order parameter $\Psi$ are essentially those of an unchanged superfluid or $XY$ model. Within this regime, the two fundamental length scales $\tilde{\xi}$ and $\tilde{\lambda} \propto \rho_s^{-1/2r}$ (where $\rho_s$ is the superfluid density) are expected to scale according to $\tilde{\xi} \simeq \tilde{\xi}_0 (1-t)^{-2/3}$ and $\tilde{\lambda} \simeq \tilde{\lambda}_0 (1-t)^{-1/3}$, with $\tilde{\lambda}_0^2/\tilde{\xi}_0 = \gamma \lambda^2(0)/\xi(0)$ and $\gamma = 1/2\pi c_s \sqrt{2Gi} > 1$. Within the mean-field regime, the ratio $\lambda^2/\xi$ grows with $(1-t)^{-1/2}$ until it reaches the value $\tilde{\lambda}_0^2/\tilde{\xi}_0$ marking the borderline of the $XY$ critical region; hence $1-t_{XY} = 1/\gamma^2$. Using the estimates of Fisher, Fisher, and Huse (1991), we see that the fluctuation regime becomes very large (they used a parameter $c_s \approx 0.4$, whereas the conventional Ginzburg criterion would correspond to a value $c_s \approx 0.1$), of the order of 10 K. This value appears to be much larger than the broadening of the transition due to fluctuations under zero-field conditions, which is of the order of 1 K. We wish to point out that a width for the fluctuation regime of the order of 1 K in fact is in agreement with the predictions of the conventional Ginzburg criterion, and thus we prefer to use a value $\approx 0.1$ for the parameter $c_s$. Finally, it has been argued (Fisher, Fisher, and Huse, 1991) that, within the $XY$ critical regime, the melting line is expected to scale according to $\tilde{\xi}^{-2}$, hence $B_m(T) \propto (T_c - T)^{4/3}$. However, this result should be interpreted with some care, since the scaling behavior for the parameters $\tilde{\xi}$ and $\tilde{\lambda}$ was obtained for a *zero-field* phase transition. On the other hand, the melting transition under consideration here is intrinsically associated with a *finite* magnetic field, thus possibly leading to a different type of phase transition, and further investigations are required to resolve these subtle questions (see, for example, Brézin, Nelson, and Thiaville, 1985; Tešanović, 1991; Tešanović and Xing, 1991).

The situation is different for the strongly layered Bi- and Tl-based materials. Here the Ginzburg number $Gi$ (a quantity characterizing a three-dimensional superconductor) does not coincide with the actual width of the transition region, which appears to be much narrower than predicted from the rather large value $Gi \approx 0.1-1.0$. On the other hand, for weak enough fields, $B < \Phi_0/\Lambda^2$, the melting line can still be described by the above three-dimensional anisotropic theory, and hence the description of the reentrant melting line as outlined above should be fully applicable to these materials. Monte Carlo simulations of vortex-lattice melting in a layered superconductor have been presented by Kapitulnik (1991) and by Ryu *et al.* (1992). In their study, which covers a field range from 10 G to 50 T, they find a reentrant behavior at low fields with a turning point given by $T^* \approx 0.5 T_c$ and $B^* \approx \Phi_0/\lambda^2(T^*)$, i.e., the ratio of $a_0/\lambda$ is approximately unity at $(B^*, T^*)$. These Monte Carlo results for $(B^*, T^*)$ are in reasonable agreement with our estimates obtained from the matching of the low- and high-field branches of the melting line if we use the set of phenomenological parameters for BiSCCO quoted by

Kapitulnik [1991; $\xi(0)=15$ Å, $\lambda(0)=2000$ Å, $\varepsilon^2=1/5000$, $c_L' \approx 0.1$]; see Fig. 22. On the other hand, using a slightly different set of parameters [$\xi(0)=18$ Å, $\lambda(0)=1000$ Å, $\varepsilon^2=1/2500$, $c_L' \approx 0.2$; see Eq. (2.135)], we obtain a value for $T^*$ much closer to $T_c$; see Fig. 3. Hence the actual shape of the melting line depends strongly on the set of material parameters, even within the rather small family of the oxide superconductors. Alternatively, an accurate determination of the melting line makes it possible to obtain the phenomenological parameters of these materials with a higher accuracy.

## 3. Large magnetic fields: $B \sim H_{c_2}$

The melting transition of the vortex lattice under high-field conditions has been studied by Hikami, Fujita, and Larkin (1991), for both the two- and the three-dimensional situation (see also Tešanović and Xing, 1991). Their calculation was based on the lowest Landau-level approximation, which is valid for high magnetic fields, and makes use of an asymptotic high-temperature expansion for the free energy (up to 11th order for the two-dimensional case and up to 9th order for a three-dimensional bulk superconductor). This series expansion was then analyzed by means of Padé and Borel-Padé summation methods, and the Abrikosov ratio $\beta_A = \langle |\Psi|^4 \rangle / \langle |\Psi^2| \rangle^2$ was determined as a function of the reduced temperature $y = [T-T_{c_2}(B)]/Gi(B)$ for $T < T_{c_2}(B)$. Here, $T_{c_2}(B)$ denotes the inverse of the $H_{c_2}(T)$ function and $Gi(B)$ is the field-dependent width of the fluctuation region, $Gi(B) \simeq Gi^{1/3}[B/H_{c_2}(0)]^{2/3}$ $\gg Gi$ [$B \gg GiH_{c_2}(0)$ within the field regime considered here]. Extrapolating the Abrikosov ratio for the liquid high-temperature phase down to the low-temperature regime ($y \to -\infty$; we consider the three-dimensional case here), one arrives at an asymptotic value $\beta_A \approx 1.28$ at best, a value that is still considerably higher than the corresponding ratio for the Abrikosov lattice, which is $\beta_A \approx 1.16$. Since the lowest-energy state of the vortex system is realized by the configuration with the smallest Abrikosov ratio $\beta_A$ (Abrikosov, 1957), the above result indicates that the high-temperature liquid phase becomes unstable at low temperatures and will undergo a transition to a vortex-lattice phase. The melting temperature $T_m(B)$ was determined by a comparison between the free energies of the Abrikosov lattice as determined by Thouless (1975), and of the liquid phase as obtained from the Padé analysis of the high-temperature series expansion. The transition turns out to be first order (finite intersection angle at the transition) and occurs at a value $y \approx -7$, that is, an appreciable distance away from the critical fluctuation regime. Additional support for a first-order melting transition stems from Monte Carlo simulations (Hetzel *et al.* 1992). The first experimental results hint-

ing at a discontinuous transition have been reported by Safar, Gammel, Huse, *et al.* (1992b, 1993), by Charalambous (1992; see also Charalambous *et al.*, 1993), and by Kwok *et al.* (1994a). The comparison between the above high-field result and the high-field portion of the melting line obtained by Houghton, Pelcovits, and Sudbø (1989) produces an estimate $c_L \approx 0.14$ for the Lindemann number.

In the above analysis we have assumed that no intermediate vortex-liquid phase is present between the high-temperature (entangled) vortex liquid or metallic phase and the low-temperature Abrikosov-lattice phase. In the following section we present some arguments in favor of the existence of such an intermediate phase within the field regime $B < 0.2 H_{c_2}(T)$, where the melting line is far away from the upper critical-field line, $B_m(T) \ll H_{c_2}(T)$. The arguments in favor of such an intermediate state, however, cannot be applied to the high-field situation discussed here.

## B. Vortex-liquid phase: 2D bosons

In the previous section we saw that under certain conditions encountered in the high-temperature superconductors the vortex lattice can be melted due to thermal fluctuations over a significant portion of the $B$-$T$ phase diagram. Within this regime, crystalline long-range order is absent, but since the magnetic field $B$ is much lower than $H_{c_2}$ the superconducting order parameter is still preserved locally, i.e., on length scales less than the mean vortex spacing. The question that we wish to address in this section concerns the thermodynamic nature of the resulting vortex-liquid state: is the vortex-liquid a genuine new thermodynamic phase with macroscopic properties different from those of the normal metal? Is the transition to the vortex liquid a true thermodynamic phase transition or is there merely a crossover line, where the macroscopic properties of the normal metal are changed in a quantitative way only? Starting from the notion of symmetry breaking, the above questions can be formulated in a very transparent way: Consider the symmetries that are broken when passing from the high-temperature normal-metal phase at high fields and temperatures to the mixed state at low temperatures and fields. In fact, there are *two* symmetries that are broken. The longitudinal gauge symmetry is broken due to the appearance of a superfluid density, and the transverse translation symmetry is broken due to the appearance of the Abrikosov lattice (note that there is no transverse superconducting response in the mixed state in the absence of pinning, as a test current $j \perp B$ will induce vortex motion and hence dissipation). The question, then, is whether these two symmetries are broken simultaneously or sequentially. In the former case the superconductor turns normal upon melting of the vortex system, i.e., the

vortex liquid does not represent a genuine new thermodynamic phase and there is no phase transition in the system except the melting transition of the vortex lattice. By contrast, if the two symmetries are broken sequentially, we shall have a new intermediate vortex-liquid state with continuous translational symmetry but one that is still superconducting along the direction of the magnetic field. Only after a further phase transition in which the longitudinal superfluid density vanishes will we enter the well-known normal-metallic phase at high fields and temperatures.

In order to address these questions, we should analyze the partition function for a system of arbitrarily curved flux lines and determine the response of the system to the presence of an external electromagnetic field **A**. The first step in this program was carried out by Nelson (1988; see also Fisher and Lee, 1989; Nelson and Seung, 1989), who proposed to make use of the formal correspondence between the partition functions of a system of directed lines and the Feynman path representation of the partition function of a system of two-dimensional Bose particles. The basic ideas underlying this correspondence are that (i) the flux lines cannot terminate inside the sample, i.e., in each plane of constant $z$ ($z$ denotes the axis directed along the field) their number is a conserved quantity, a statement which maps to the particle conservation along the imaginary time axis $\tau$ in the Bose problem, and (ii) all configurations of the vortex system give a positive contribution to the partition function, so that the corresponding particles are indeed bosons, and not, say, fermions or anyons. With the $z$ axis identified with the (imaginary) time direction $\tau$ of the quantum system, we have to identify the physical temperature $T$ in the vortex system with the "Planck constant" $\hbar^B$ of the Bose system (to avoid confusion, note that the parameter $\hbar^B$ in the Bose system has no relation whatsoever to the usual Planck constant $\hbar$, and the latter will not appear throughout the present section. In particular, our $\hbar^B$ carries the dimension of energy here instead of that of an action). The thickness $L$ of the superconductor along the $z$ direction has to be identified with the imaginary time period, i.e., the inverse temperature $\hbar^B/T^B$, $T^B$ being the effective temperature of the Bose system (in units of energy/length). The last point, however, requires some care: the imaginary-time representation of the quantum statistics of bosons involves periodic boundary conditions along the imaginary-time axis (Abrikosov, Gor'kov, and Dzyaloshinski, 1975; Popov, 1987), implying that the vortex configurations in the planes $z=0$ and $z=L$ should be identical up to permutations. This condition is rather unnatural for the vortex system, where free boundary conditions are usually the relevant ones, whereas periodic boundary conditions would correspond to the somewhat artificial situation of a toroidal-shaped sample with the flux lines following the torus. As a consequence we should not use the flux-line/2D-boson analogy when the properties of the system substantially depend on the specific nature of the boundary conditions. On the other

hand, for infinitely long (bulk) samples, corresponding to the ground-state ($T^B=0$) configuration of the Bose system, the difference in the boundary conditions should play no role. In the thermodynamic limit ($L \to \infty$), the finite-temperature statistical mechanics problem of the vortex system then maps to the $T^B=0$ quantum-mechanical ground-state problem in the Bose system, where the role of thermal fluctuations in the vortex picture is played by the quantum fluctuations of the bosons. Being interested in the thermodynamic behavior of the vortex system, we shall concentrate on the limit $L \to \infty$ or $T^B=0$ in the following.

A further requirement to be fulfilled in order to exploit the flux-line/2D boson analogy is the finiteness of the energy barriers for vortex crossing. Since all trajectories contribute to the partition function in the Bose problem, the same must be true for the vortex system. However, infinite barriers for vortex line crossing would severely restrict the phase space in the vortex system, and our analogy would fail, whereas possibly high but finite barriers allow the vortex system to explore the entire phase space.

Below we discuss the mapping of the vortex system to an equivalent 2D liquid of (charged) bosons, concentrating first on the low-field regime, $B \ll H_{c_1}$ (Sec. V.B.1, "uncharged" bosons with instantaneous short-range repulsion) and second on the intermediate-field regime, $H_{c_1} \ll B \ll H_{c_2}$ (Sec. V.B.2), where the interaction between the bosons is long-ranged (but screened) and retarded ("charged" bosons). In Sec. V.B.3 we discuss the duality between the Bose liquid and the vortex liquid and show that a superfluid ground state in the Bose system produces a normal-metal behavior in the vortex system, whereas a normal ground state for the bosons results in a superconducting response in the direction parallel to the magnetic field for the vortex system. The question of whether there exists a genuine vortex-liquid phase that is different from the normal-metal phase and separated from the latter by a true phase transition then reduces to the question of whether the "charged" 2D Bose system does or does not develop a normal ground state. In Sec. V.B.4 we present some arguments supporting the idea of the existence of an intermediate normal ground state for the "charged" Bose system.

### 1. Low magnetic fields: $B < H_{c_1}$

After this introduction, let us be more specific and consider the energy of a system of vortex lines within the London approximation (which is valid due to the condition $B \ll H_{c_2}$). For an isotropic superconductor in a magnetic field $H$, we obtain

$$\mathcal{H}[\mathbf{s}_\mu] = \frac{\varepsilon_0}{2} \sum_{\mu,\nu} \int d\mathbf{s}_\mu \cdot d\mathbf{s}_\nu \frac{e^{-|\mathbf{s}-\mathbf{s}|/\lambda}}{|\mathbf{s}_\mu - \mathbf{s}_\nu|} - \int d^3r \frac{\mathbf{H} \cdot \mathbf{B}(\mathbf{r})}{4\pi} ,$$

$$(5.25)$$

where the sums runs over all flux lines and we have to cut off the integration at small distances $|s_\mu - s_\nu| \leq \xi$.

We first concentrate on the simplest case of a low vortex density, $B \ll H_{c_1}$, corresponding to a dilute 2D Bose gas. The terms $\mu = \nu$ in Eq. (5.25) provide the self-energies of the vortex lines,

$$\mathcal{H}_s[s_\mu] = \varepsilon_0 \ln\kappa \sum_\mu \int ds_\mu , \tag{5.26}$$

where $ds_\mu$ denotes the length of a line element of the $\mu$th vortex line. Here we have assumed only long-wavelength $\kappa < 1/\lambda$ distortions of the vortex line, which is a well justified approximation for the relevant configurations in the low-density limit [otherwise a dispersive line tension (2.18) has to be considered in Eq. (5.26)]. Expanding Eq. (5.26) in $\partial_z s_\mu$ and changing notation $z \to \tau$, $\varepsilon_0 \ln\kappa \to m^B$, we see that the self-energy part of the flux-line system transforms to the action (in imaginary-time representation) of a system of free nonrelativistic particles (bosons) of mass $m^B$ moving in two-dimensional space,

$$\mathcal{S}_0[s_\mu] = \int d\tau \sum_\mu \left[ \frac{m^B}{2} \left[ \frac{d\mathbf{R}_\mu(\tau)}{d\tau} \right]^2 - \mu^B \right] , \tag{5.27}$$

with $\mu^B = H\Phi_0/4\pi - \varepsilon_0 \ln\kappa$ the chemical potential of the Bose system. We have used the decomposition $s_\mu = (\mathbf{R}_\mu(\tau), \tau)$ with $\mathbf{R}_\mu(\tau)$ denoting the actual position of the vortex lines.

The remaining terms $\mu \neq \nu$ in Eq. (5.25) then provide the interactions between the Bose particles. Due to the low-density condition $n^B = B/\Phi_0 \ll \lambda^{-2}$, this interaction can be reduced to an instantaneous $[\delta(\tau - \tau')]$ short-range repulsion with an integrated strength

$$u_0 = 2\varepsilon_0 \int d^2R \, K_0 \left[ \frac{R}{\lambda} \right] = \frac{\Phi_0^2}{4\pi} , \tag{5.28}$$

with $K_0$ the zero-order modified Bessel function describing the interaction between two straight vortex lines. Thus we have mapped our original classical statistical mechanics problem (5.25) to the quantum ground-state problem of a dilute 2D Bose gas characterized by the action (Nelson, 1989; see also Nelson and Le Doussal, 1990),

$$\mathcal{S}[s_\mu] = \int d\tau \left\{ \sum_\mu \left[ \frac{m^B}{2} \left[ \frac{d\mathbf{R}_\mu(\tau)}{d\tau} \right]^2 - \mu^B \right] \right.$$
$$\left. + u_0 \sum_{\mu \neq \nu} \delta_\lambda[\mathbf{R}_\mu(\tau) - \mathbf{R}_\nu(\tau)] \right\} , \tag{5.29}$$

with $\delta_\lambda$ a two-dimensional $\delta$ function smeared over a scale $\lambda$.

The dilute Bose gas with short-range repulsion has been studied in detail by Popov (1972) and by Fisher and Hohenberg (1988). The main results of this analysis are (i) the ground state of the dilute Bose gas is superfluid, with a superfluid density $n_s^B$ equal to the total density of bosons $n^B$; (ii) the bare interaction strength $u_0$ is renor-

malized down to the effective value $u_{\text{ren}} = 4\pi\hbar^{B\,2} / [m^B \ln(\delta_l^{-1})] = u_0 \, 8Gi / [\kappa^2 \ln\kappa \ln(\delta_l^{-1})] \ll u_0$, where $\delta_l = n^B \lambda^2 \ll 1$ is a dimensionless density parameter; and (iii) the transition temperature to the superfluid state $T_c^B$ goes to zero with $\delta_l \to 0$,

$$T_c^B = \frac{2\pi\hbar^{B\,2} n^B}{m^B} \frac{1}{\ln\ln(\delta_l^{-1})} , \tag{5.30}$$

which is in agreement with the absence of superfluidity in an ideal $(\delta_l = 0)$ 2D Bose gas at finite temperatures, $T^B > 0$.

Going back to the original vortex problem, the above results led Nelson (1988; see also Nelson and Seung, 1989) to the conclusion that the transition from the Meissner state to the vortex-lattice state should go via an intermediate *vortex-liquid* phase corresponding to the superfluid ground state of the 2D bosons. This new vortex-liquid phase has been named an *entangled vortex liquid* (EVL). The superfluid phase in the boson problem is characterized by the presence of ($\sim$ equal-$\tau$) cooperative ring-exchange processes involving arbitrarily large numbers of bosons. In the original vortex problem, these quantum fluctuations correspond to ($\sim$ equal-$z$) vortex-loop excitations of arbitrarily large diameter. As a consequence, both the boson world lines and the vortex lines
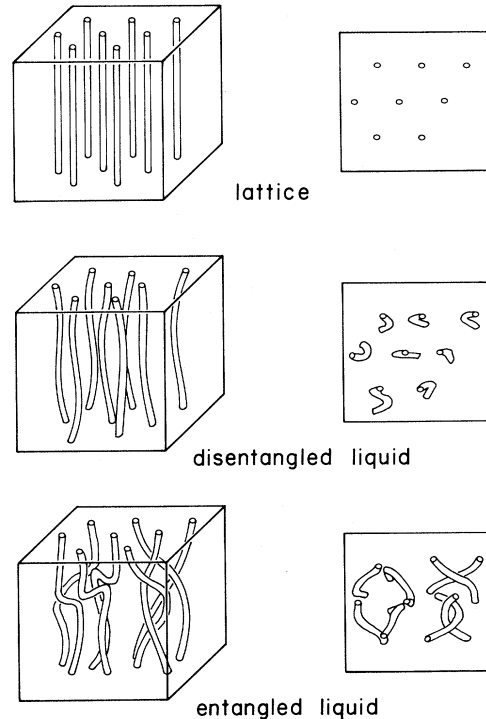


FIG. 23. Various equilibrium phases for a vortex system comprising a vortex-lattice phase (a "Wigner crystal" in the equivalent Bose system), a disentangled vortex-liquid phase (normal ground state), and an entangled vortex-liquid phase (superfluid groundstate) which is equivalent to the normal-metal phase. A vortex-loop excitation (cooperative ring-exchange process) is illustrated in the bottom picture.

are strongly entangled, hence the same "entangled vortex liquid." In analogy to the well-known solid-to-superfluid transition taking place in $^4$He when the density of particles is decreased (see, for example, Feynman, 1972), it is reasonable to assume that the vortex system transforms to an entangled-vortex-liquid phase below the melting line $B_m(T)$ as given by the low-induction formula (5.19) (Nelson, 1988). Two characteristic vortex configurations, for the solid and for the entangled-liquid phase, are illustrated in Fig. 23.

In order to gain a complete understanding of the phase diagram of a type-II superconductor, we have to address the following two questions (Feigel'man, Geshkenbein, and Vinokur, 1990): (i) How can we generalize the above analysis valid for small inductions, $B \ll H_{c_1}$, to the important regime of moderate fields, $H_{c_1} \ll B \ll H_{c_{22}}$, where the interaction between the vortices is long ranged? and (ii) what are the physical properties of the vortex-liquid phase? In particular, how does it compare with the normal-metal and vortex-lattice phases between which it interpolates? In order to answer these questions, we shall now consider the full nonlocal expression (5.25) for the energy of the vortex system and map it to the Lagrangian of a 2D "charged" Bose liquid.

## 2. Moderate magnetic fields: $H_{c_1} \ll B \ll H_{c_2}$

To begin with, let us neglect screening and consider the limit $\lambda \rightarrow \infty$ of the energy (5.25), while keeping $\varepsilon_0$ constant. We can map this problem to a system of 2D "charged" bosons by introducing the fictitious gauge field $\mathbf{a}(\mathbf{R}, \tau)$ (see also Popov, 1987, where this mapping was carried out for vortices in a two-dimensional Bose system),

$$\mathcal{S}_\infty[\mathbf{s}_\mu, \mathbf{a}] = \mathcal{S}_0 + \int d\tau \, d^2R \left\{ i \mathbf{j}^B \cdot \mathbf{a} + \frac{1}{2g^2}(\nabla \wedge \mathbf{a})^2 \right\},$$

$$(5.31)$$

with $\mathbf{j}^B = (\rho^B, \mathbf{J}^B)$,

$$\rho^B = \sum_\mu \delta[\mathbf{R} - \mathbf{R}_\mu(\tau)],$$

$$\mathbf{J}^B = \sum_\mu (\partial_\tau \mathbf{R}_\mu) \delta[\mathbf{R} - \mathbf{R}_\mu(\tau)],$$

$$(5.32)$$

the three-dimensional current produced by the Bose particles. Number conservation then implies $\nabla \mathbf{j}^B = 0$. The coupling constant $g$ is given by $g^2 = 4\pi\varepsilon_0$. The two systems, (5.25) with $\lambda = \infty$ and (5.31), are easily found to be equivalent by considering their partition functions $Z$ in a Feynman path representation over vortex/world lines and integrating out the fictitious gauge field $\mathbf{a}$,

$$Z = \int \mathcal{D}[\mathbf{s}_\mu(z)] e^{-\mathcal{H}[\mathbf{s}(z)]/T}$$

$$= \int \mathcal{D}[\mathbf{s}_\mu(\tau)] \mathcal{D}[\mathbf{a}] e^{-\mathcal{S}[\mathbf{s}(\tau), \mathbf{a}]/\hbar^B}.$$

$$(5.33)$$

Next we introduce screening by coupling the system to a true electromagnetic field. In the Bose picture, this is equivalent to giving a finite mass $(1/\lambda^2)$ to the fictitious gauge field $\mathbf{a}$, a task that can be accomplished by coupling the true electromagnetic vector potential $\mathbf{A}$ via a Chern-Simons-like term to the fictitious gauge field $\mathbf{a}$. When we include the self-energy $(\nabla \wedge \mathbf{A})^2/8\pi$ of the electromagnetic field, the full action for the Bose system then becomes

$$\mathcal{S}[\mathbf{s}_\mu, \mathbf{a}, \mathbf{A}] = \mathcal{S}_0 + \int d\tau \, d^2R \left\{ i \left[ \mathbf{j}^B - \frac{1}{\Phi_0} \nabla \wedge \mathbf{A} \right] \cdot \mathbf{a} + \frac{1}{2g^2}(\nabla \wedge \mathbf{a})^2 + \frac{1}{8\pi}(\nabla \wedge \mathbf{A})^2 \right\}.$$

$$(5.34)$$

Note that in $\mathcal{S}_0$ we should now use everywhere the bare mass $m_0 = \varepsilon_0$ instead of the dressed mass $m^B = \varepsilon_0 \ln\kappa$ (the corresponding terms in $S_0$ describe only the contribution from the vortex core). In the low-density limit, the retarded self-interaction between bosons and their self-generated gauge field then produces the "bosonic mass renormalization" $m_0 \rightarrow m^B$ (i.e., the enhancement of the vortex line energy and line tension due to the currents). The functional (5.25) can then be obtained from Eq. (5.34) by first integrating out the fluctuations of the electromagnetic field $\mathbf{A}$ in the partition function. As a result, an additional term $\mathbf{a}_\perp^2/2(g\lambda)^2$ will appear in the effective action, producing a gauge-invariant mass $1/\lambda^2$ for the mediating gauge field $\mathbf{a}$ [here $\mathbf{a}_\perp$ denotes the trans-

verse component of $\mathbf{a}$, in Fourier representation, $\mathbf{a}_\perp(\mathbf{k}) = (\mathbf{k} \wedge \mathbf{a}) \wedge \mathbf{k}/k^2$]. A second functional integration over the now massive gauge field $\mathbf{a}$ produces the original functional (5.25).

Finally, we go over to a coherent-state formulation of the boson problem (534) (see, for example, Popov, 1987, or Negele and Orland, 1988). Instead of an integration over world lines $\mathbf{s}_\mu(\tau)$ we then have to integrate over the complex Bose field $\phi$ in the partition function, with an action now given by

$$\mathcal{S}[\phi, \mathbf{a}, \mathbf{A}] = \int d\tau \, d^2R \left\{ \mathcal{L}_B[\phi, \mathbf{a}] + \mathcal{L}_g[\mathbf{a}, \mathbf{A}] \right\} \quad (5.35)$$

and the Lagrange densities

$$\mathcal{L}_B[\phi, \mathbf{a}] = \phi^* \left[ (\hbar^B \partial_\tau + i a_0) - \frac{1}{2m_0}(\hbar^B \nabla^{(2)} + i \mathbf{a}^{(2)})^2 - \mu^B \right] \phi + V_{sr}(\phi^* \phi) + \frac{1}{2g^2}(\nabla \wedge \mathbf{a})^2 \quad (5.36)$$

and

$$\mathcal{L}_g[\mathbf{a}, \mathbf{A}] = \frac{i}{2\sqrt{\pi}\lambda g}(\nabla \wedge \mathbf{a}) \cdot \mathbf{A} + \frac{1}{8\pi}(\nabla \wedge \mathbf{A})^2 . \qquad (5.37)$$

Here $\nabla^{(2)}$ and $\mathbf{a}^{(2)}$ denote the planar components of $\nabla$ and $\mathbf{a} = (a_0, \mathbf{a}^{(2)})$. The chemical potential $\mu^B$ has to be determined such that the boson density $n^B = B/\Phi_0$ reproduces the appropriate induction $B$ in a given external field $H$. The term $V_{sr}$ represents a short-range repulsion on the scale $\xi$ between the bosons, allowing for the possibility of a finite-temperature phase transition into the superfluid state. The free energy of the system takes the form

$$\mathcal{F} = -T \ln \left[ \int \mathcal{D}[\phi] \mathcal{D}[\phi^*] \mathcal{D}[\mathbf{a}] \mathcal{D}[\mathbf{A}] e^{-\mathcal{S}[\phi, \mathbf{a}, \mathbf{A}]/\hbar^B} \right] .$$

$$(5.38)$$

With the action (5.35) we have arrived at a field-theoretic representation of the original vortex problem (5.25). The action (5.35) takes the nonlocal nature of the interaction between the vortices fully into account. Its regime of validity is limited only by the requirement $B \ll H_{c_2}$ (so that the London approximation is valid), producing relevant space scales in the boson problem which are larger than the cutoff length $\xi$. The interaction in the 2D "charged" boson problem, to which the original problem has been mapped, is mediated by the fictitious gauge field $\mathbf{a}$, whose component $a_0$ produces the static (i.e., equal-time) interaction between the Bose particles (in analogy to the scalar electromagnetic potential), whereas $\mathbf{a}_\perp$ mediates the dynamic (i.e., nonlocal in $\tau$) part of the interaction. Finally, the coupling of the true electromagnetic field $\mathbf{A}$ to the fictitious field $\mathbf{a}$ leads to the screening of the interaction between the bosons on the scale $\lambda$. Thus we have generalized the mapping "vortices↔2D bosons" to the regime $H_{c_1} \ll B \ll H_{c_2}$.

In the following we concentrate on the second of the above questions: What is the correspondence between the physical properties of the different possible ground states in the Bose system and the corresponding thermodynamic phases in the vortex system?

### 3. Bose-liquid/vortex-liquid duality

In this subsection we shall show that the superfluid ground state of the Bose system, and hence the entangled vortex liquid (EVL), is equivalent to the normal-metal phase. More specifically, we shall show that the large-scale electromagnetic response of the EVL is that of a normal metal. On the other hand, we shall demonstrate that if the Bose system develops a *nonsuperfluid* ground state, then the corresponding *disentangled* vortex-liquid phase (DVL) is a new thermodynamic phase different both from the normal metal and from the vortex lattice. The characteristic features of this new phase are the absence of long-range translational order (no vortex lattice) combined with superconducting properties along the field

direction [i.e., a transverse external field is screened due to the dissipation-free flow of longitudinal screening currents $\mathbf{j} = (0, 0, j_z)$]. The (potential) ground states of the Bose system, with their analogs in the vortex picture, are illustrated in Fig. 23. The question of whether this new thermodynamic state can exist will be addressed in Sec. B.4 below.

Following Feigel'man, Geshkenbein, and Vinokur (1990), we consider the response of the system under a variation of an external electromagnetic vector potential $\mathbf{A}'$. In particular, we are interested in the response to the variation of a longitudinal field $A_z'$ producing a transverse field $\mathbf{H}' \perp \mathbf{H}$ and thus a screening current $\mathbf{j}' = (0, 0, j_z')$. Note that we expect the same qualitative response of the vortex system and of the normal-metal phase for a transverse test field $\mathbf{A}^{(2)'}$ in the absence of any pinning potential. The quantity of interest is the superfluid density $\rho_s^{zz}$ in the vortex system,

$$\rho_s^{zz}(\mathbf{q}) \equiv \frac{\partial^2 \mathcal{F}}{\partial A_z'(\mathbf{q}) \partial A_z'(-\mathbf{q})}$$

$$= \frac{1}{c^2 T} \langle j_z(\mathbf{q}) j_z(-\mathbf{q}) \rangle , \qquad (5.39)$$

where the second equality follows from coupling the test field $\mathbf{A}'$ via a term $\mathbf{j} \cdot \mathbf{A}'/c$ to the Hamiltonian of the electronic system, with $c$ denoting the speed of light. Note that in a diagrammatic representation of the current-current correlator no diagrams appear that can be disconnected by cutting a single photon propagator, which is due to the fact that $\mathbf{A}'$ is only a test field.

Going over to the Bose representation of the problem and taking the second derivative of the free energy $\mathcal{F}$ with respect to the test field $\mathbf{A}'$, we obtain for the superfluid density

$$\rho_s^{zz}(\mathbf{K}, \omega) = \frac{1}{\hbar^B} \frac{1}{4\pi g^2 \lambda^2} \langle h_0(\mathbf{K}, \omega) h_0(-\mathbf{K}, \omega) \rangle , \qquad (5.40)$$

with $h_0 = \partial_1 a_2 - \partial_2 a_1$ the two-dimensional "magnetic field" generated by the gauge field $\mathbf{a}$. We have also, decomposed the three-component vector $\mathbf{q}$ into a frequency $\omega$ and wave vector $\mathbf{K}$ part, $\mathbf{q} = (\mathbf{K}, \omega)$. Since we are interested in the long-wavelength static properties of the system, we shall concentrate on the limit $\mathbf{q} \to 0$. Note that in Eq. (5.40) the external vector potential $\mathbf{A}'$ is only a test field, which is not integrated over. With (5.40) we have established the correspondence between the response $\rho_s^{zz}(\mathbf{K}, \omega)$ of the superconducting system and the ground-state fluctuations of the two-dimensional "magnetic" field $h_0(\mathbf{K}, \omega)$ in the Bose system, the latter being strongly dependent on the nature (superfluid or normal) of the ground state.

Consider a first a superfluid ground state for the Bose liquid with some finite density $n_s^B$. Integration over the Bose field $\phi$ produces an additional polarization term $(1/2)\Pi^\phi \mathbf{a}_\perp^2$,

$$\Pi^\phi = \frac{n_s^B}{m_0} \qquad (5.41)$$

in the effective Lagrangian for the gauge field **a**. Combining this term with the field energy $(\nabla \wedge \mathbf{a})^2/2g^2$ and using $h_0(\mathbf{q}) = \mathbf{K} \wedge \mathbf{a}^{(2)}$, we obtain for the correlator of the $h_0$ field after integration over **a**

$$\langle h_0(\mathbf{K}, \omega) h_0(\mathbf{K}', \omega') \rangle = \hbar^B \delta(\mathbf{K} + \mathbf{K}')$$
$$\times \delta(\omega + \omega') \frac{K^2 g^2}{K^2 + \omega^2 + g^2 n_s^B / m_0} \; . \tag{5.42}$$

The static response of the superconductor then is given by

$$\rho_s^{zz}(\mathbf{K}, 0) = \chi_d K^2 \; , \tag{5.43}$$

with the diamagnetic susceptibility

$$\chi_d = \frac{1}{\nu_s} \frac{\Phi_0}{16\pi^2 \lambda^2 B} \; . \tag{5.44}$$

Here $\nu_s = n_s^B / n^B$ denotes the superfluid fraction in the Bose system, and we have returned to the superconductor notation in expressing $\chi_d$. The result (5.43) indicates that the vortex system does not show a superconducting response at large scales $K \to 0$; instead, the system possesses a finite diamagnetic susceptibility $\chi_d$. This can be rigorously seen by calculating the correlator $D_{zz}(\mathbf{K}) = \langle A_z(\mathbf{K}) A_z(-\mathbf{K}) \rangle$ of the electromagnetic vector potential **A**: Using the Dyson equation

$$D_{zz}(\mathbf{K}) = \frac{D_{zz}^0(\mathbf{K})}{1 + D_{zz}^0(\mathbf{K}) \Pi(\mathbf{K})} \; , \tag{5.45}$$

with $D_{zz}^0(\mathbf{K}) = 4\pi / K^2$ and $\Pi(\mathbf{K}) = \rho_s^{zz}(K)$, the polarization of the combined boson and gauge fields, we obtain the diamagnetic response

$$D_{zz}(\mathbf{K}) = \frac{4\pi}{K^2} \frac{1}{1 + 4\pi \chi_d} \; , \tag{5.46}$$

with the diamagnetic permeability of the medium given by $\mu_d = 1/(1 + 4\pi \chi_d)$. Hence the entangled vortex liquid qualitatively has the same properties as the normal-metal phase. In a dilute vortex liquid with $n^B \lambda^2 \ll 1$ the diamagnetism is very strong, $\mu_d \ll 1$, which is a natural consequence of the system's being nearly free of vortices with a correspondingly large superconducting screening. Nevertheless, the strong entanglement of the vortex lines will eventually make the system appear normal on large enough length scales. In the opposite case of a dense vortex liquid the diamagnetism is weak, $\chi_d \ll 1$, which can be understood as a result of superconducting fluctuations in the normal-metal phase.

Second, let us study the consequences of a *normal* ground state for the Bose system, that is, $n_s^B = 0$. In this case, integration over the boson field produces a polarization term $(1/2)\Pi^\phi \mathbf{a}_\perp^2$, with

$$\Pi^\phi(\mathbf{K} \to 0, \omega = 0) = \frac{4\pi}{g^2} \chi^B K^2 \; , \tag{5.47}$$

in the effective Lagrangian for the **a** field. Equation (5.47) for the polarization function $\Pi^\phi$ is the simplest expression taking the requirements of a vanishing superfluid density $n_s^B = 0$ and the analyticity in $K$ into account. The factor $4\pi/g^2$ has been chosen in order to obtain the definition of the diamagnetic susceptibility $\chi^B$ of the Bose system in its usual form; see below. Integration over the gauge field provides us with the *finite* (in the limit $\mathbf{K} \to 0$) result

$$\rho_s^{zz}(\mathbf{K}, 0) = \frac{\mu^B}{4\pi \lambda^2} \tag{5.48}$$

for the superfluid density along $z$ in the original vortex problem. Here $\mu^B$ is the magnetic permeability of the Bose system,

$$\mu^B = \frac{1}{1 + 4\pi \chi^B} \; . \tag{5.49}$$

The key result is the finite superfluid density $\rho_s^{zz}$, which allows supercurrents to flow along the $z$ axis. In fact, the electromagnetic response function now reads

$$D_{zz}(\mathbf{K}) = \frac{4\pi}{K^2 + \lambda_{\mathrm{eff}}^{-2}} \; , \tag{5.50}$$

that is, the vector potential $A_z$ has become massive with an effective penetration depth $\lambda_{\mathrm{eff}}^2 = \lambda^2 / \mu^B$. Hence the disentangled vortex liquid, which corresponds to the normal ground state in the Bose system, exhibits fluctuations of the vector potential $A_z$ like those in the Meissner state with a renormalized penetration depth $\lambda_{\mathrm{eff}}$.

In summary, we have obtained the following duality between the physical properties of a vortex liquid and those of a dual Bose system: The vortices (i.e., the bosons) are topological defects of the superconductor. Off-diagonal long-range *order*, i.e., superfluidity, in the Bose system then introduces *disorder* in the original vortex system, which therefore is in an entangled phase. Quantitatively, the order in the superfluid is measured by its superfluid density $n_s^B$, which polarizes the gauge potential **a**, $\Pi^\phi \propto n_s^B = \mathrm{const}$. In turn, this polarization of the gauge potential produces a diamagnetic polarization $\Pi = \rho_s^{zz} = \chi_d K^2$ of the electromagnetic potential $A_z$, such that the final response of the vortex system is diamagnetic, with $\chi_d \propto 1/\Pi^\phi$; see Eqs. (5.41), (5.43), and (5.46). On the other hand, a finite diamagnetic susceptibility $\chi^B$ of the Bose liquid (i.e., a normal ground state) produces a polarization $\Pi^\phi \propto \chi^B K^2$ in the gauge field **a**, which in turn leads to a finite superfluid density in the superconductor, $\Pi = \rho_s^{zz} \propto \mu^B$, with $\mu^B = (1 + 4\pi \chi^B)^{-1}$. The electromagnetic vector potential $A_z$ therefore becomes massive, $\lambda_{\mathrm{eff}}^{-2} \propto \mu^B$, and transverse magnetic-field fluctuations are screened (Meissner effect); see Eqs. (5.47), (5.48), and (5.50).

Let us finally discuss the above rather formal results for the vortex-boson duality in more phenomenological terms. We should remind ourselves that the main difference between the superfluid and the normal ground

state of the Bose system is the existence (in the superfluid) of cooperative ring-exchange processes involving an arbitrarily large number of bosons (see Pollock and Ceperley, 1987, and Ceperley and Pollock, 1989, who discuss the superfluid properties of the Bose system in terms of particle trajectories). Within the vortex system, these cooperative ring-exchange processes correspond to planar closed vortex loops of arbitrary size, which represent the characteristic feature of the entangled-vortex-liquid phase; see Fig. 23. On the other hand, only simple two-particle exchange processes are present in the normal ground state of the Bose system, which then maps to the disentangled-vortex-liquid phase exhibiting only a low density of small loops. Note that the crucial difference between the entangled and the disentangled phases is not the presence or absence of vortex loops but the existence of arbitrarily large loops in the entangled phase (thus the disentangled vortex liquid is also entangled in some weak sense due to neighboring vortices' interchanging positions; however, such a "mechanical" entanglement is also present in the vortex-lattice phase).

Let us consider the effect of the presence or absence of arbitrarily large (transverse) vortex loops on the resistivity $\rho^{zz}$ of the mixed state. The energy dissipated by a current flow $j_z$ along the field direction $z$ is due to the creation and subsequent expansion of transverse vortex loops. In the entangled liquid, such loops of arbitrary size *are already present in thermal equilibrium,* hence the current $j_z$ will merely shift the thermodynamic equilibrium between loops of positive and negative circulation and thereby produce a finite electric field $E_z \propto j_z$. Thus the linear resistivity is nonzero, $\rho^{zz}(j_{zz} \to 0) = dE_z/dj_z|_{j_z=0} \neq 0$. On the other hand, within the disentangled phase, the formation of large loops with characteristic radii $R \gg a_0$ costs a free energy $\mathcal{F}(R) \propto R$, which has to be provided by the current density $j_z$. The free energy of a vortex-loop excitation in the presence of an external driving current $j_z$ is

$$\mathcal{F}(R, j_z) \simeq 2\pi R \varepsilon_0 - \frac{1}{c} j_z \Phi_0 \pi R^2 , \qquad (5.51)$$

and hence the critical radius for the nucleation of such a loop is $R_c \simeq c \varepsilon_0 /(\Phi_0 j_z)$. As a result the electric field due to thermally activated vortex loops is

$$E_z \propto e^{-\mathcal{F}(R_c, j_z)/T} \simeq e^{-j_T/j_z} , \qquad (5.52)$$

with $j_T \simeq j_0 (\varepsilon_0 \xi /T)$. Therefore $\rho^{zz}(j_z \to 0) = 0$, and the disentangled phase shows true superconductivity in the longitudinal direction (i.e., parallel to the field $B$) in agreement with the above conclusion about the existence of superconducting screening of fluctuations in $A_z$.

Thus we have shown that if a nonsuperfluid ground state of the Bose system really exists, then the corresponding phase in the vortex system would introduce an additional true thermodynamic vortex-liquid phase intermediate between the normal-metal and the vortex-lattice

phases at high and low temperatures, respectively; see Fig. 23. The transition from the normal-metal to the vortex-lattice phase would then proceed via two separate generic phase transitions, where first longitudinal superconductivity and second (transverse) long-range order would be established.

On the other hand, if such a normal ground state does not exist in the Bose system, then there is only one phase transition, where both longitudinal superconductivity and transverse long-range order appear simultaneously. In this case a *crossover* from a disentangled vortex liquid to an entangled liquid is expected to occur in a sample of *finite thickness* (see Nelson, 1991). This crossover occurs when the entanglement length $L_E \simeq \varepsilon^2 \varepsilon_0 a_0^2 /T$ (the length a vortex line diffuses along the $z$ axis before colliding with its nearest neighbors, $\varepsilon_l a_0^2 /L_E \simeq T$) is of the order of the sample thickness $L$; hence we obtain a crossover line to an entangled-vortex phase of the form

$$B_E(T) \simeq \frac{\varepsilon \xi(0)}{L} \frac{1}{\sqrt{Gi}} H_{c_2}(0) \frac{T_c}{T} \left[ 1 - \frac{T}{T_c} \right] . \qquad (5.53)$$

At low enough fields a disentangled liquid may be realized within an intermediate regime, based on geometrical reasons. At high fields the entanglement field $B_E(T)$ crosses the melting line $B_m(T)$ [at $T_c/T - 1 \simeq (\varepsilon \xi(0)/L)(\sqrt{Gi} /c_L^4)$] and the vortex liquid is always entangled. In the limit $L \to \infty$ the disentangled phase vanishes altogether from the phase diagram.

Let us investigate in more detail the possibility of the existence of a nonsuperfluid ground state in the Bose system.

### 4. Possible existence of a nonsuperfluid ground state in the Bose liquid

A system of interacting bosons at $T^B = 0$ is known to be either a crystal or a superfluid, with a well-known example found in $^4$He, which shows a first-order phase transition between a crystalline and a superfluid phase as a function of pressure (which acts to change the strength of quantum fluctuations). It has been speculated (Andreev and Lifshitz, 1969; Kirzhnits and Nepomnyashii, 1970; Liu and Fisher, 1973) that under certain circumstances there exists a kind of mixed phase, in which both crystalline and superfluid order are present simultaneously. Here we wish to consider another alternative, which in our opinion, is relevant for a 2D Bose system with long-range interactions. Following Feigel'man, Geshkenbein, Ioffe, and Larkin (1993), we shall argue that in such a system there exists an intermediate regime of densities, where both the crystalline and the superfluid order are unstable with respect to quantum fluctuations, so that a new *normal* ground state is established for the Bose liquid. Since the long-range nature of the interaction is at the heart of the argument, we expect the following discussion to be relevant for a dense vortex liquid with $n^B \lambda^2 \gg 1$. We then can adopt the approximation $\lambda \to \infty$ while keeping the coupling $g$ constant, i.e., we

shall neglect the screening of the gauge field **a** mediating the interaction between the bosons. Such an approximation seems to be reasonable at high densities, $n^B\lambda^2 \gg 1$, where the basic properties of the ground state can hardly

be changed by a modification of the interaction between the particles on scales much larger than the interparticle distance. Thus, in the following, we concentrate on the reduced Lagrangian

$$\mathcal{L}_B[\phi,\mathbf{a}] = \phi^* \left[ (\hbar^B \partial_\tau + ia_0) - \frac{1}{2m_o}(\hbar^B \nabla^{(2)} + i\mathbf{a}^{(2)})^2 - \mu^B \right] \phi + V_{sr}(\phi^*\phi) + \frac{1}{2g^2}(e_1^2 + e_2^2) + \frac{c_B^2}{2g^2}h_0^2 \,, \tag{5.54}$$

with $e_\alpha = \partial_0 a_\alpha - \partial_\alpha a_0$ and $h_0 = \partial_1 a_2 - \partial_2 a_1$. The functional (5.54) reduces to $\mathcal{L}_B[\phi,\mathbf{a}]$ as given by Eq. (5.36) in the limit $c_B = 1$. With $c_B$ an additional parameter, we are free to study a more general situation, where the strength of the scalar interaction differs from the transverse one. The case $c_B \neq 1$ is also physically relevant in the discussion of the microscopic origin of high-temperature superconductivity based on the gauge-field approach to the Mott insulator (see Anderson, 1987; Baskaran and Anderson, 1988; Ioffe, Kalmeyer, and Wiegmann, 1991; Ioffe and Kalmeyer, 1991).

The system defined by Eq. (5.54) can be characterized by two dimensionless coupling constants,

$$\alpha_t = \frac{g^2}{8\pi m_o c_B^2}, \quad \alpha_C = \frac{m_o g^2}{16\pi^2 \hbar^{B2} n^B} \,, \tag{5.55}$$

where the numerical factors have been introduced for later convenience. In terms of the original parameters

characterizing the vortex liquid, these coupling constants take the values $\alpha_t = \frac{1}{2}$ and $\alpha_C = (\varepsilon_o a_o /2\sqrt{\pi}T)^2$.

In the following we present arguments supporting the idea that, in the presence of both Coulomb and transverse interactions, an intermediate density range exists where the Bose system is neither crystalline nor superfluid, since both these phases are destroyed by quantum fluctuations. Let us look first at the case of a pure *static scalar Coulomb interaction*. Consider the limit $c_B \to \infty$ in Eq. (5.55) and assume that a superfluid ground state is realized for the Bose liquid at high densities $n^B$ (note that in a system with long-range Coulomb interactions a crystalline phase is expected to exist at *low* densities, as is well known for the Wigner crystal). The important degrees of freedom of the superfluid system are given by the (quantum) fluctuations in the phase $\theta(\mathbf{R},\tau)$ and in the density $\pi(\mathbf{R},\tau) = n(\mathbf{R},\tau) - n^B$, where $\theta$ and $\pi$ are conjugated variables. The effective action for these fluctuations can be written in the form

$$\mathcal{S}[\pi,\theta] = \int d\tau \sum_{\mathbf{K}} \left\{ \frac{g^2}{2K^2}\pi(\mathbf{K},\tau)\pi(-\mathbf{K},\tau) + \frac{i\hbar^B}{2}[\pi(\mathbf{K},\tau)\dot\theta(-\mathbf{K},\tau) + \text{H.c.}] + \frac{\hbar^{B2}n^B}{2m_o}K^2\theta(\mathbf{K},\tau)\theta(-\mathbf{K},\tau) \right\} \,, \tag{5.56}$$

where $\dot\theta$ denotes the derivative of $\theta$ with respect to time $\tau$ and where a wave-vector representation has been introduced. The long-wavelength fluctuations in the density $\pi$ are suppressed due to the long-range Coulomb interaction [producing the $1/K^2$ singularity in the first term of Eq. (5.56)] and hence the fluctuations in the phase $\theta$ are enhanced. Indeed, integrating out the density fluctuations and determining the correlation function for the phase fluctuations, we obtain

$$\langle \theta(\mathbf{K},\omega)\theta(\mathbf{K}',\omega') \rangle = \frac{1}{\hbar^B}\delta(\omega+\omega')\delta(\mathbf{K}+\mathbf{K}')[1/K^2(n^B/m_o + \omega^2/g^2)] \,.$$

$$\tag{5.57}$$

The Coulomb interaction thus produces a $1/K^2$ singularity in the phase correlator $\langle \theta\theta \rangle$, which remains effective at finite frequencies $\omega$ [contrary to the usual situation, where $\langle \theta\theta \rangle \propto (\omega^2 + c^2K^2)^{-1}$]. As a result, the ground-state correlation function of the superfluid will exhibit a power-law behavior asymptotically (Ioffe and Larkin, 1990),

$$\langle \phi(0)\phi^*(\mathbf{R}) \rangle \propto \langle e^{i[\theta(0)-\theta(\mathbf{R})]} \rangle \propto R^{-\sqrt{\alpha_C}} \,. \tag{5.58}$$

Such a result is well known for superfluidity in 2D, where thermal fluctuations tend to reduce the order at finite temperatures $T^B$—the peculiarity of the Coulomb interaction then is to extend this result even down to zero

temperature, $T^B = 0$. Thus we can see that superfluid long-range order is absent in the ground state of a "charged" Bose liquid. For a small enough exponent, $\alpha_C \ll 1$, we still expect the presence of superfluidity in the system, but, as $\alpha_C$ becomes large with decreasing density $n^B$ [see Eq. (5.55)], we expect that superfluidity will be destroyed, in analogy to the finite-temperature Berezinsky-Kosterlitz-Thouless transition in an "uncharged" Bose system. In fact, it is possible to show that an upper bound for the possible existence of superfluidity in a "charged" Bose liquid is given by

$$\alpha_C^{max} < 4 \,. \tag{5.59}$$

Hence a phase transition to a normal state is expected (at least) at small densities,

$$n^B < \frac{m_0 g^2}{64\pi^2 \hbar^{B^2}} \ . \tag{5.60}$$

The condition (5.59) can be understood in a simple way: for large couplings, $\alpha_C > 2$, the Fourier transform $N(\mathbf{K}) = G(\mathbf{K}, t=0)$, where $G(\mathbf{K}, t)$ denotes the Green's function of the interacting Bose system, becomes nonsingular as $\mathbf{K} \to 0$. Such a result seems to be inconsistent with the existence of a finite superfluid density [note that $N(\mathbf{K})$ is nothing but the quasiparticle momentum distribution, which has a $\delta$-function singularity at $\mathbf{K}=0$ in the usual Bose condensed state with off-diagonal long-range order].

Next, let us include the effects of *transverse interactions* on the superfluid ground state of a "charged' Bose liquid. As an immediate consequence of this nonlocal (in time) interaction, one can no longer argue that at $T=0$ the superfluid density $n_s^B$ should coincide with the total density $n^B$ of the bosons (the relation $n_s^B = n^B$ is a consequence of Galilei invariance, which is broken explicitly by the coupling to the gauge field). Let us then estimate the perturbative correction to the superfluid density $n_s^B$ due to the finite transverse interaction (coupling constant $\alpha_t$) in the Bose system. We start from the "bare" system's ground state, which includes the effects of the instantaneous Coulomb interaction in the high-density regime, $\alpha_C \ll 1$, and determine the Green's functions. These Green's functions can be constructed in a manner similar to the usual Bogoliubov solution for a low-density Bose gas (e.g., Popov, 1983). The condition $\alpha_C \ll 1$ ensures that the number of particles within the Debye length is large, and thus a mean-field approximation is reasonable [note that the high-density regime of a "charged" Bose system is similar to the low-density region of a Bose system with short-range interaction; see Eq. (5.59)]. The result for the normal and the anomalous Green's functions is conveniently expressed in a $(\mathbf{K}, t)$ representation and reads

$$G(\mathbf{K}, t) = \left[ \frac{1}{2\varepsilon(K)} \left[ \frac{\hbar^{B^2} K^2}{2m_0} + \frac{g^2 n^B}{K^2} \right] + \frac{1}{2} \mathrm{sgn} t \right] e^{-i\varepsilon(K)|t|} \ , \tag{5.61}$$

$$F(\mathbf{K}, t) = -\frac{1}{2\varepsilon(K)} \frac{g^2 n^B}{K^2} e^{-i\varepsilon(K)|t|} \ , \tag{5.62}$$

where $\varepsilon^2(K) = (\hbar^{B^2} K^2 / 2m_0)^2 + g^2 n^B / m_0$ [note that the result (5.58) for the equal-time Green's function goes beyond the mean-field result (5.61)]. The main correction $\Pi_1^\phi$ to the bare transverse polarization function $\Pi_0^\phi = n^B / m_0$ is given by

$$\Pi_1^\phi = -\frac{2n^B}{m_0^2} \int \frac{d^2 q}{(2\pi)^2} dt \, D(\mathbf{K}, t) [G(\mathbf{K}, t) + F(\mathbf{K}, t)] \ , \tag{5.63}$$

where

$$\begin{aligned} D_{\mu\nu} &= D(\mathbf{K}, t)(\delta_{\mu\nu} - K_\mu K_\nu / K^2) \ , \\ D(\mathbf{K}, t) &= \frac{g^2}{2\omega(K)} e^{-i\omega(K)|t|} \ , \end{aligned} \tag{5.64}$$

is the gauge-field propagator with $\omega^2(K) = c_B^2 K^2 + g^2 n^B / m_0$. Note that within the present perturbative approach one has to take into account the gap in the photon spectrum produced by the finite superfluid density. The expression for the relative correction $\Pi_1^\phi / \Pi_0^\phi$ can be recast in the form

$$\frac{\Pi_1^\phi}{\Pi_0^\phi} = -2\alpha_t u J(u) \ , \tag{5.65}$$

where $u = \sqrt{\alpha_C} / \alpha_t$ measures the relative strength of the transverse and the Coulomb interaction, and

$$\begin{aligned} J(u) &= \int_0^\infty \frac{x \, dx}{\sqrt{1+x^2}\sqrt{1+ux} \, (\sqrt{1+x^2} + \sqrt{1+ux})} \\ &\sim \begin{cases} \ln\dfrac{2}{u}, & u \ll 1 \ , \\ \dfrac{1}{2u} \ln(2u^2), & 1 \ll u \ . \end{cases} \end{aligned} \tag{5.66}$$

With decreasing density $n^B$ (increasing scalar coupling $\alpha_C$), the corrections become large. For a moderately small parameter $\alpha_t$ (note that $\alpha_t$ is fixed to the value $\alpha_t = \frac{1}{2}$ in the vortex liquid), the relative correction (5.65) to the superfluid density becomes substantial, even for small parameters, $\alpha_C \ll 1$, where our perturbative approach is still valid. In order to estimate the density $n^B$ or the coupling strength $\alpha_C \propto 1/n^B$ [see Eq. (5.55)] where fluctuations completely suppress the superfluidity in the sense $\Pi^\phi \approx \Pi_0^\phi + \Pi_1^\phi = 0$, we have to solve the implicit equation $2\alpha_t u^* J(u^*) = 1$ for $u^*$. The critical coupling strength $\alpha_C^*$ is given by $\alpha_C^* = (u^* \alpha_t)^2$, and for the case $\alpha_t = \frac{1}{2}$ relevant for the vortex liquid we obtain the result $\alpha_C^* \approx 0.1$. This value of the critical coupling strength is considerably smaller than the purely Coulombic estimate (5.59) found above and thus indicates that transverse gauge-field fluctuations assist the scalar interaction in suppressing superfluidity in the Bose system. Clearly the above estimate cannot serve as a proof of the destruction of superfluidity at $\alpha_C \gtrsim 0.1$, but at least it provides a strong argument for the loss of superfluidity within the regime $\alpha_C < 1$.

Let us discuss the deeper physical reason for the destruction of superfluidity by the coupling to a gauge field. We refer to the work of Halperin, Lubensky, and Ma (1974), who have shown that the phase transition between a normal metal and a type-I superconductor is driven first-order by the fluctuations of the electromagnetic field. The long-wavelength fluctuations in the electromagnetic field are suppressed in the presence of a finite superfluid density $\rho_s \sim |\Psi|^2$ as compared with the normal state. This suppression leads to the appearance

of two additional terms in the free-energy functional describing the transition: The first is a cubic term $\propto |\Psi|^3$, which drives the transition first order. The second one is $\propto |\Psi|^2$ and leads to a *reduction* of the transition temperature. It is this latter effect in which we are interested here. The idea is that, for strong enough coupling of the bosons to the gauge field **a**, and for not too high density $n^B$, the energy gain due to Bose condensation can become smaller than the energy loss due to suppression of the gauge-field fluctuations produced by a finite $n_s^B$. Therefore we consider the large perturbative corrections to the polarization function $\Pi^\phi$ calculated above as a signature of a complete suppression of superfluidity in the density regime characterized by the condition $\alpha_C > \alpha_C^*$ with $\alpha_C^* \lesssim 1$. For densities $n^B$ corresponding to $\alpha_C > \alpha_C^*$, the Bose liquid is in a "normal" (i.e., nonsuperfluid) state even at $T^B = 0$.

On the other hand, upon further decreasing the density $n^B$, we expect a second instability to occur in the "charged" Bose system, in which the normal liquid transforms into a Wigner crystal. In order to obtain the relevant value for the parameter $\alpha_C$, we can rewrite this coupling constant in terms of the original parameters of the vortex system,

$$\alpha_C = \left[ \frac{\varepsilon_0 a_0}{2\sqrt{\pi}T} \right]^2 , \qquad (5.67)$$

and then substitute the melting temperature $T_m$ [see Eq. (5.5)] for the temperature $T$. As a result we obtain a melting or solidification transition at a critical value $\alpha_C^m \approx (3c_L)^{-4}$. Rewriting both conditions, $\alpha_C > \alpha_C^*$ where $\alpha_C^* \lesssim 1$ (condition for nonsuperfluid state) and $\alpha_C < \alpha_C^m$ where $\alpha_C^m > 1$ (condition for liquid state) in terms of the original parameters of the vortex system, we find that an intermediate disentangled vortex liquid can exist within the regime

$$B_m(T) < B < \frac{1}{\alpha_C^*} \left[ \frac{1}{3c_L} \right]^4 B_m(T) . \qquad (5.68)$$

The resulting phase diagram is illustrated in Fig. 24. Recently, Li and Teitel (1993) have found evidence for the existence of an intermediate disentangled-vortex-liquid phase in their Monte Carlo simulation of the vortex system. Experimental results by Steel, White, and Graybeal (1993) and by Safar *et al.* (1994) also point to the existence of an intermediate vortex-liquid phase within an artificially grown layered material.

## VI. PINNING IN VORTEX LIQUIDS

In this section we discuss the influence of disorder on the properties of the vortex-liquid phase. We shall base our discussion on the dynamic approach introduced in Sec. III.D above. Since it is very instructive to understand in greater depth the crucial difference between a vortex solid and a vortex liquid, we shall discuss both
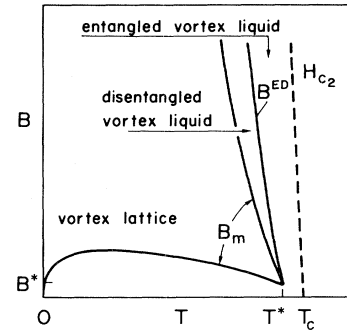


FIG. 24. Equilibrium phase diagram for a vortex system for the case in which an intermediate disentangled vortex-liquid phase does exist. In decreasing the temperature, we cross the crossover line $H_{c_2}(T)$ (the entangled vortex liquid has the same symmetries as the normal-metal phase) and subsequently the first phase-transition line $B^{ED}(T)$ to the disentangled vortex liquid, which exhibits a longitudinal (parallel to the magnetic field) superconducting response. A second phase transition at $B_m(T)$ transforms the liquid into a solid, where continuous translation symmetry is now also broken.

these cases and point out where the main differences have to be located (Sec. VI.A). In particular, we shall show that the dynamic approach distinguishes between the solid and the liquid vortex phase via the presence or the absence of a divergence in the relative velocity correction factor $\delta v / v|_{v \to 0}$. The presence or absence of such a divergence gives additional support to the existence or absence of infinite barriers in the thermodynamic equilibrium phases of the solid and the liquid, respectively. Therefore, when disorder is introduced into the system, the vortex solid turns into a glass, whereas the liquid remains a liquid. In Sec. VI.B we concentrate on the characteristic feature of a pinned liquid, which is the existence of two Ohmic regimes, one at high current densities (flux flow) and the other at low current densities, where the resistivity is exponentially suppressed due to pinning (thermally assisted flux flow, or TAFF). We determine the resistivity in the TAFF regime and the crossover current density where the Ohmic flux-flow behavior at high current densities becomes strongly modified due to the presence of disorder. Finally, in Sec. VI.C we consider the influence of quenched disorder on the dilute vortex liquid which is present in the vicinity of the lower critical field $H_{c_1}$.

### A. Role of disorder in the solid and liquid states

In Secs. II.B and IV.C above we have discussed the influence of thermal fluctuations on the pinning properties of a single vortex line (II.B) and of a vortex lattice (IV.B). We have demonstrated that, for both cases, thermal fluctuations lead to a partial smearing of the ran-

dom potential and thus to *a decrease* in the critical current density. However, the basic feature of the pinned state, the *divergence* of the energy barriers $U(j)$ determining the rate of flux creep at small current densities $j \to 0$, has been found to persist in the presence of thermal fluctuations, and thus the current-voltage characteristic (CVC) remains strongly nonlinear for vanishing $j$. Here we present some general arguments showing that this result is a generic feature of a vortex solid interacting with weak disorder. By contrast, we show that a very different result is obtained in a vortex-liquid phase: whereas the presence of a random potential can lead to a substantial *decrease* of the linear resistivity $\rho_{\text{lin}} = dE/dj|_{j \to 0}$ with respect to its flux-flow value, it will still *remain finite*, $\rho_{\text{lin}} > 0$, throughout all of the liquid phase. Note that here we do not consider the influence of disorder on the overall thermodynamic properties of the vortex system, e.g., we neglect a possible shift of the melting line due to the presence of disorder. Such an approximation is appropriate for the case of weak disorder if the melting transition is of first order in the pure system. Otherwise our approach should not be used close to the melting line. Theoretical support for the existence of a first-order melting transition has been found in numerical simulations by Hetzel, Sudbø, and Huse (1992), and experimental evidence has been obtained by Safar, Gammel, Huse, *et al.* (1992), Charalambous (1992), and Kwok *et al.* (1994a). For a more detailed discussion of the influence of strong disorder on the transition into the superconducting state, see Sec. VII.A.3 below.

Let us point out that the existence of a substantial pinning effect in a vortex-liquid state is not at all obvious. Indeed, in a dense liquid the interaction between the vortex lines and the random potential is much weaker than the interaction between the vortex lines themselves, the latter also being relatively weak compared with the temperature, since the pure system is considered to be a liquid. Therefore a naive guess would be that a weak random potential is always irrelevant for a vortex liquid. On the other hand, for a single vortex line, disorder is always relevant (cf. Sec. II.B), hence the ineffectiveness of the random potential in pinning a vortex liquid is a nontrivial issue.

In order to clarify the situation, let us start with some qualitative considerations concerning the influence of thermal fluctuations on the pinning of a vortex solid (Vinokur *et al.*, 1990, 1991). Above the depinning temperature $T_{\text{dp}}$, the mean-squared value of the thermal displacement $\langle u^2 \rangle_{\text{th}}$ becomes larger than the core size $\xi^2$, and the thermal motion of the vortices averages the pinning potential over the area $\langle u^2 \rangle_{\text{th}}$. The characteristic averaged range of the random potential can be approximated by $r_p \simeq (\xi^2 + \langle u^2 \rangle_{\text{th}})^{1/2}$, and the critical current decreases rapidly with increasing temperature. In deriving an expression for $j_c$, the averaging process was initially carried out over the thermal fluctuations and only afterwards performed over the random potential; see Secs. II.B and IV.C. Such an approach can only be used if the charac-

teristic time $t_{\text{th}}$ of the thermal fluctuations is much smaller than the characteristic time scale for pinning $t_{\text{pin}}$. We determine these time scales below and will show that

$$\frac{t_{\text{pin}}}{t_{\text{th}}} \propto \frac{j_{\circ}}{j_c} . \tag{6.1}$$

Hence, for the case of weak pinning, $j_c \ll j_{\circ}$, we obtain $t_{\text{pin}} \gg t_{\text{th}}$ and, consequently, the procedure employed in Secs. II.B and IV.C is justified.

Pinning occurs as a direct result of the inhomogeneous vortex structure. The point to be noted here is that, although the thermal fluctuations lead to a considerable smearing of the vortex cores, the vortex lattice preserves its periodicity, and the interaction of this periodic, i.e., inhomogeneous, structure with the disorder potential provides pinning at all temperatures lower than the melting temperature $T_m$.

Let us turn to the vortex-liquid state. In a "conventional" liquid, all the characteristic times are of the same order as $t_{\text{th}}$, and thus after averaging over thermal fluctuations during the time $t_{\text{pin}} \gg t_{\text{th}}$ one obtains a completely smoothed homogeneous vortex structure, which cannot be pinned. Such a consideration does not hold for a *very viscous liquid*, which is characterized by *two* time scales, $t_{\text{th}}$ and $t_{\text{pl}} \gg t_{\text{th}}$, where $t_{\text{pl}}$ denotes the time scale of plastic deformations. The crucial point is that, in a *viscous* liquid, an inhomogeneous structure is preserved over time scales $t < t_{\text{pl}}$. If this characteristic smoothing time of the structure is large compared with the pinning time $t_{\text{pin}}$, $t_{\text{pl}} \gg t_{\text{pin}}$, the thermal averaging over the pinning time is not complete, and the vortex liquid retains its homogeneous structure, which then can be pinned by the random potential. As a result, depending on the relative size of the plastic time $t_{\text{pl}}$ and of the pinning time $t_{\text{pin}}$, the vortex liquid either can be pinned or unpinned; see Fig. 25.

A possible origin of the exponentially large smoothing time $t_{\text{pl}}$ in the vortex liquid is the presence of the energy barriers $U_{\text{pl}}$ associated with the thermally activated plastic motion of the vortex structure, in which case we obtain $t_{\text{pl}} \sim t_{\text{th}} \exp(U_{\text{pl}}/T)$. The size of the characteristic plastic barriers has been estimated by Geshkenbein *et al.* (1989) and by Vinokur *et al.* (1990, 1991). The basic idea in estimating these barriers is that the relevant excitations all involve deformations of the vortex lines on a scale $a_{\circ}$. The elastic moduli describing such short-wavelength deformations all are of the same order and produce the plastic deformation energy

$$U_{\text{pl}} \sim \varepsilon \varepsilon_{\circ} a_{\circ} \propto \frac{T_c - T}{\sqrt{H}} . \tag{6.2}$$

Note that the same basic energy scale appears in the free-energy functional (5.3) relevant in the description of the vortex-lattice melting transition; see Sec. V.A. In fact, the melting temperature $T_m$ as obtained from the Lindemann criterion can be expressed via the plastic energy barrier $U_{\text{pl}}$,

$$T_m \simeq 2c_L^2 U_{\text{pl}} ,\qquad (6.3)$$

which demonstrates that the large barriers against (plastic) vortex motion are retained in the liquid phase due to the smallness of the Lindemann number $c_L$, $U_{\text{pl}}(T_m) \gg T_m$.

Typical vortex configurations involving the barrier (6.2) occur in connection with the dynamic behavior of the entangled vortex liquid. Different mechanisms have been proposed to be relevant for the vortex motion in such a liquid. The relative motion of the vortices can take place either by reptation (Nelson and Seung, 1989; Obukhov and Rubinstein, 1990) or via cutting and reconnection of the vortex lines. The latter mechanism seems to be preferable, since the characteristic relaxation time for reptation grows very rapidly with the dimension $L$ of the sample, $t_{\text{rep}} \propto L^3$ according to Nelson and Seung (1989) and even $t_{\text{rep}} \propto \exp[(TL/\varepsilon_0 a_0^2)^3]$ according to Obukhov and Rubinstein (1990). On the other hand, the reconnection barriers for fields $H \gg H_{c_1}$ are given by Eq. (6.2), since $U_{\text{pl}}$ corresponds to the energy needed to distort two vortex lines on a scale $a_0$. Hence $T_{\text{rec}} \sim t_{\text{pl}}$, which usually is much smaller than $t_{\text{rep}}$. Note that the energy (6.2) relevant for the vortex cutting process
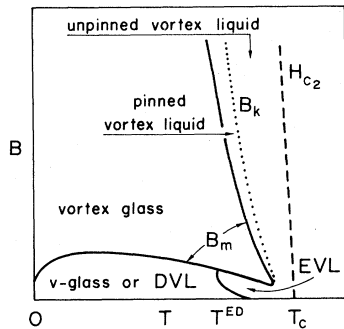


FIG. 25. Equilibrium phase diagram for a vortex system including the effects of thermal fluctuations and of quenched disorder. Disorder is always relevant in the vortex-lattice phase (finite shear modulus), which is transformed to a vortex-glass phase with $\rho(j \to 0) \to 0$. Disorder is irrelevant in the vortex-liquid phase above the melting line $B_m(T)$, which remains a liquid with a linear-response characteristic $\rho(j \to 0) > 0$. Close to the melting line the liquid is still very viscous, with a plastic relaxation time $t_{\text{pl}}$ exceeding the pinning time $t_{\text{pin}}$; hence the liquid can be pinned and $\rho(j \to 0) \approx \rho_0 \exp(-U_{\text{pl}}/T) \ll \rho_{\text{flow}}$ (TAFF regime). As the plastic time approaches the pinning time with increasing temperature, $t_{\text{pl}}(T_k) \simeq t_{\text{pin}}(T_k)$, the system crosses over to an unpinned liquid with $\rho(j \to 0) \approx \rho_{\text{flow}}$ (FF regime). The crossover line $B_k$ appears as a kink in the resistive transition. Recent experiments (Kwok *et al.*, 1994a and 1994b) suggest that this kink develops into a sharp first-order transition in very clean samples. Within the dilute vortex-liquid phase at low fields, the role of thermal fluctuations is suppressed and disorder can strongly alter the behavior of the pure system. At low temperatures, disorder is expected to transform the entangled vortex-liquid phase into a (pinned) disentangled liquid or even into a glass phase. The entangled liquid survives only close to the transition temperature $T_c$. Drawing is not to scale.

roughly corresponds to the energy of a vortex segment of length $a_0$ rather than $\xi$, the value suggested by Nelson and Seung (1989) and by Obukhov and Rubinstein (1990), since, in order for the vortices to reconnect, they have to bend, and the characteristic length scale along $c$ for bending is of the order of the lattice constant $a_0$ (in the anisotropic case $\sim \varepsilon a_0$). Therefore the core interaction energy is only a small part (a fraction $\sim \xi/a_0$) of the total energy (6.2). In fact, as has been pointed out by Brandt and Sudbø (1991b; see also Obukhov and Rubinstein, 1991) and by Sudbø and Brandt (1991c), the core contribution can be even smaller if the vortices will cross each other under a small angle.

The inhomogeneities in the vortex liquid are relevant as long as $t_{\text{pin}} < t_{\text{pl}}$ holds. With increasing temperature the size of the characteristic plastic barriers decreases, and a crossover from a pinned to an unpinned regime takes place at a temperature $T_k$, where

$$t_{\text{pin}}(T_k) \approx t_{\text{pl}}(T_k) \sim t_{\text{th}}(T_k) e^{U_{\text{pl}}(T_k)/T_k} \qquad (6.4)$$

(see Fig. 25). This crossover can manifest itself as a "kink" or "shoulder" in the resistive curve $\rho(T)$ (Iye *et al.*, 1987; Malozemoff *et al.*, 1989; Kwok *et al.*, 1990; Worthington *et al.*, 1990). Note that, due to the weakness of the pinning, $t_{\text{pin}} \gg t_{\text{th}}$ and therefore the plastic barriers present in the system at $T_k$ are still large compared to temperature, $U_{\text{pl}}(T_k) \gg T_k$, in agreement with experimental findings (Liu *et al.*, 1989; Palstra *et al.*, 1989, 1990; Worthington, Holtzberg, and Feild, 1990; Chien *et al.*, 1991; Iye, Terashima, and Bando). After the above heuristic introduction, let us turn to a quantitative analysis—based on the dynamic approach—of the disorder-induced effects in the vortex system. We start with the simplest case of a vortex solid.

### 1. Vortex solid subject to disorder—the dynamic approach

In order to calculate the effect of the underlying disorder potential on the dynamic properties of the mixed state, we shall follow the general approach presented in Sec. III.D above. In this approach we consider a vortex system driven by a high current density $j$ and calculate the correction $\delta v$ to the flow velocity $v$ of the vortex system due to the presence of a random potential. Within this perturbative approach, we can express this correction in terms of the intrinsic properties of the vortex system *in the absence of pinning*, as expressed by the Green's function $G(0,t)$ and the structure factor $S(\mathbf{K}, t)$,

$$\frac{\delta v}{v} = \frac{\gamma v}{\eta a_0^2} \int \frac{d^2 K}{(2\pi)^2} dt\, K^2 K_v |p(K)|^2$$

$$\times G(0,t) S(\mathbf{K}, t) \frac{\sin(K_v vt)}{v} . \qquad (6.5)$$

As the current density $j$ decreases, the relative correction $\delta v / v$ to the velocity grows, and eventually becomes of

the order of unity for some value of $j$ which we identify with the critical current density $j_c$. Let us calculate the relative velocity correction (6.5) for a vortex lattice. Of course, the results obtained via this method are in agreement with those derived in Sec. IV above based on dimensional estimates.

In the vortex-lattice state the structure factor $S(\mathbf{K}, t)$ as defined in Eq. (3.99) is given by a sum of $\delta$ functions reflecting the presence of crystalline long-range order,

$$S(\mathbf{K}, t) = \left[\frac{2\pi}{a_0}\right]^2 \sum_{\mathbf{K}} \delta(\mathbf{K} - \mathbf{K}_\mu) e^{-(1/2)K^2 \langle u^2 \rangle_{\mathrm{th}}}, \qquad (6.6)$$

where the $\mathbf{K}_\mu$ are the reciprocal vectors of the vortex lattice and the exponential factor in Eq. (6.6) is the Debye-Waller factor. The Green's function $G(0,t)$ can be obtained from its Fourier representation, Eq. (3.21) [below we neglect a term in $G(0,t)$ corresponding to bulk compression modes, since this term is usually much smaller than the term involving shear modes],

$$G(0,t) = \int \frac{d^3k}{(2\pi)^3} \frac{d\omega}{2\pi} G_{\alpha\alpha}(\mathbf{k}, \omega) e^{-i\omega t}$$

$$= \frac{\Theta(t)}{\eta} \int \frac{d^3k}{(2\pi)^3} e^{-[c_{66}K^2 + c_{44}(\mathbf{k})k_z^2]t/\eta}. \qquad (6.7)$$

The remaining integration over the Brillouin zone is complicated due to the dispersive nature of the tilt modulus $c_{44}(\mathbf{k})$, and we shall do it separately for the two asymptotic time regions where the dispersion can be neglected and where it is relevant. For large time scales the spatial dispersion of the tilt modulus can be neglected, $c_{44}(\mathbf{k}) \simeq B^2/4\pi$, and with $c_{66}$ given by Eq. (3.32) we obtain

$$G(0,t) = \frac{\Theta(t)}{4\sqrt{\pi}\eta\lambda a_0^2} \left[\frac{t_{\mathrm{th}}}{t}\right]^{3/2},$$

$$\left[\frac{\lambda}{a_0}\right]^2 t_{\mathrm{th}} \ll t, \qquad (6.8)$$

where we have defined

$$t_{\mathrm{th}} = \frac{\eta}{c_{66}K_{\mathrm{BZ}}^2} = \frac{8\kappa^2 a_0^2}{c^2 \rho_n} \qquad (6.9)$$

as the characteristic time for short-scale elastic deformations. At times $t \ll t_{\mathrm{th}}(\lambda/a_0)^2$ (but still much longer than $t_{\mathrm{th}}$), the spatial dispersion of the tilt modulus has to be taken into account, $c_{44} \simeq B^2/4\pi\lambda^2 K^2$, and the result is

$$G(0,t) = \frac{\sqrt{\pi}}{4} \frac{\Theta(t)}{\eta a_0^3} \left[\frac{t_{\mathrm{th}}}{t}\right]^2,$$

$$t_{\mathrm{th}} \ll t \ll \left[\frac{\lambda}{a_0}\right]^2 t_{\mathrm{th}}. \qquad (6.10)$$

Finally, for very short times, $t < t_{\mathrm{th}}$, the $\mathbf{K}$ integration in Eq. (6.7) is not cut off by the exponential function but by the finiteness of the Brillouin zone. For this case the

shear mode in (6.7) becomes irrelevant, and the lattice tilt mode goes over into the single-vortex tilt mode—at very small times, the lattice structure is irrelevant, and the response of the system is determined by the individual vortex lines (see Sec. III.D). The Green's function then takes the form

$$G(0,t) = \frac{\Theta(t)}{2\eta a_0^3} \left[\frac{t_{\mathrm{th}}}{t}\right]^{1/2}, \quad t < t_{\mathrm{th}}. \qquad (6.11)$$

With the expressions for the structure factor (6.6) and for the Green's function (6.8), (6.10), and (6.11), we can determine the relative correction to the velocity $\delta v/v$ as given by Eq. (6.5). In the limit of small driving forces, the velocity $v$ drops to zero, and we can replace the sine function in (6.5) by its argument. The integral over $d^2\mathbf{K}$ is replaced by the sum over reciprocal lattice vectors $\mathbf{K}_\mu$, which is dominated by the wave vectors $\mathbf{K}_\mu \approx 1/\xi$ at low temperatures [cutoff provided by the single-vortex form factor $p(K)$] and by $1/\langle u^2 \rangle_{\mathrm{th}}^{1/2}$ at high temperatures, $T \gg T_{\mathrm{dp}}$ [cf. Eq. (4.86)]. For both cases, the structure factor does not depend on time $t$, and the remaining integral over time reduces to

$$\left.\frac{\delta v}{v}\right|_{v \to 0} \propto \int dt \, t G(0,t). \qquad (6.12)$$

Using Eq. (6.8) for the long-time asymptotics of the Green's function, we find that the right-hand side of Eq. (6.12) and hence the relative velocity correction $\delta v/v$ diverges in the limit $v \to 0$; see Fig. 26. On the other hand, for finite values of $v$, this divergence will be cut off by the factor $\sin(K_v vt)$ at $t \sim r_p/v$, with $r_p \simeq (\xi^2 + \langle u^2 \rangle_{\mathrm{th}})^{1/2}$. For small enough velocities $v$, this cutoff is realized deep within the nondispersive regime (large $t$), and using Eq. (6.8) we obtain
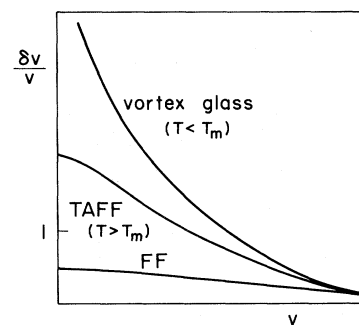


FIG. 26. Relative velocity correction $\delta v/v$ vs velocity $v$, as calculated via the dynamic approach. Whereas for the vortex lattice the response $\delta v/v$ diverges with vanishing driving force, signalling the appearance of infinite barriers in the system, the relative velocity correction $\delta v/v$ remains always finite within the vortex-liquid phase. The crucial difference between the solid and the liquid phases leading to this different behavior is not the presence or absence of translational long-range order but their different dynamic properties, as manifested in the time dependence of the structure factor $S(\mathbf{K}, t)$.

$$\frac{\delta v}{v} \propto \frac{1}{\sqrt{v}}, \quad v \ll \frac{r_p}{t_{\text{th}}} \left[\frac{a_\circ}{\lambda}\right]^2 . \tag{6.13}$$

For higher velocities the time integral is cut off within the dispersive regime, so that the Green's function is given by Eq. (6.10), and we obtain a logarithmic dependence for the relative velocity correction,

$$\frac{\delta v}{v} \propto \ln\frac{1}{v}, \quad \frac{r_p}{t_{\text{th}}} \left[\frac{a_\circ}{\lambda}\right]^2 \ll v \ll \frac{r_p}{t_{\text{th}}} . \tag{6.14}$$

For even higher velocities $v > r_p/t_{\text{th}}$, the cutoff in the time integral drops below the thermal time $t_{\text{th}}$, and the response is determined by the individual vortex lines,

$$\frac{\delta v}{v} \propto \begin{cases} \dfrac{1}{v^{3/2}}, & T < T_{\text{dp}}^s, \quad \dfrac{r_p}{t_{\text{th}}} \ll v , \\[3mm] \dfrac{1}{T^3}\ln\dfrac{1}{v}, & T_{\text{dp}}^s < T, \quad \dfrac{r_p}{t_{\text{th}}} \ll v . \end{cases} \tag{6.15}$$

The above results show that, with decreasing velocity $v$, the relative correction $\delta v$ increases and eventually becomes of the order of unity; hence disorder cannot be treated perturbatively for $v \to 0$. It is possible to show (Larkin and Ovchinnikov, 1973) that higher-order corrections to the velocity also become of order unity, within the same velocity range as does the lowest-order correction. Therefore one can identify the value of the velocity determined by the condition

$$\left.\frac{\delta v}{v}\right|_{v=v_c} = 1 \tag{6.16}$$

with the critical velocity $v_c$, and the corresponding value of the current density

$$j_c = \frac{c\eta}{B} v_c \tag{3.88}$$

with the critical value. The values of $j_c$ as obtained via the present dynamic approach then agree (up to factors of the order of unity) with those obtained previously within the static approach (cf. Secs. II.A, II.B, IV.B, and IV.C). Note that due to the weak pinning condition, $j_c \ll j_\circ$, the characteristic pinning time $t_{\text{pin}} = r_p/v_c$, which corresponds to the cutoff time at $v = v_c$ and gives the main contribution to the integral (6.5), turns out to be much longer than the thermal time $t_{\text{th}}$,

$$t_{\text{pin}} \simeq \frac{j_\circ}{j_c} \frac{r_p}{a_\circ} \left[\frac{T}{U_{\text{pl}}}\right]^{1/2} t_{\text{th}}, \quad T_{\text{dp}} < T , \tag{6.17}$$

thus verifying *a posteriori* the correctness of taking a sequential average first over thermal fluctuations and second over the disorder potential in our determination of the dynamical behavior of the vortex lattice. The same analysis carried out for the single-vortex pinning regime gives $t_{\text{pin}}/t_{\text{th}} \simeq 1$, $T_{\text{dp}}^s < T$. Note that the single-vortex thermal time $t_{\text{th}} \simeq (\eta_l/\varepsilon_l)L_c^2$ differs from the

thermal time in the vortex lattice.

Let us discuss the physical meaning of the critical current density $j_c$ as obtained within the present dynamic approach. Obviously, $j_c$ provides an estimate for the current density below which the current-voltage characteristic of the superconductor deviates strongly from Ohmic flux-flow behavior. At zero temperatures and neglecting the possibility of quantum motion, one could conclude (as was done by Larkin and Ovchinnikov, 1973) that as $j$ decreases below $j_c$ the motion of the vortex lines is stopped, $v = 0$, and hence the electric field along the current direction vanishes, $E = 0$. This is obviously not the case at finite temperatures, $T > 0$, where the vortices can jump over the energy barriers due to thermal activation. In Sec. IV above we have shown that the free-energy barriers $U(j)$ relevant for creep driven by a current density $j$ grow indefinitely as $j$ decreases, implying that the pinning equilibrium state with $j = 0$ is characterized by the presence of arbitrarily high barriers. The dynamic approach then provides us with an independent and more general argument in favor of the existence of arbitrarily high free-energy barriers in the vortex system and thus gives additional support for the existence of a true vortex-glass phase. Suppose, by contrast, that the pinning energy barriers are high but finite, such that there are no barriers higher than some value $U_{\text{max}}$. At high enough temperatures, $T \gg U_{\text{max}}$, these barriers become ineffective and the current-voltage characteristic turns Ohmic in the limit $j \to 0$. However, this cannot be the case for a vortex lattice whose current-voltage characteristic shows strong deviations from linearity at $j \lesssim j_c(T)$, with $j_c(T)$ remaining finite at any value of $T$ (though decreasing with increasing $T$). Thus we have to conclude that to assume the existence of an upper cutoff $U_{\text{max}}$ for the barrier energy distribution is wrong, and the height of the barriers grows indefinitely as the driving force goes to zero. Note also that, for the solvable model of an elastic manifold in a periodic potential (Sec. III.E), the above "dynamic" criterion for the existence of arbitrarily high barriers has been shown to be valid. The important implicit point in the above argument is the existence of the vortex lattice itself—which is clearly not fulfilled for arbitrarily high temperatures. Therefore the above conclusion has to be interpreted in the following way: a vortex lattice subject to a weak random potential is pinned due to the presence of arbitrarily high barriers between metastable states *until* the lattice itself becomes unstable with respect to thermal fluctuations and melts.

Let us generalize the above arguments. First of all, they apply equally well for the case of a single-vortex line. At high temperatures, $T \gg T_{\text{dp}}^s$ [see Eq. (2.130)] the relative correction to the velocity behaves as $\delta v/v \propto T^{-3}\ln(1/v)$ (Feigel'man and Vinokur, 1990), and the result (2.132) for $j_c(T)$ as well as the conclusion about the existence of arbitrarily high-energy barriers follows. Note that the latter result is quite nontrivial, as it holds for $d \leq 3$ dimensions only; in higher dimensions, $d > 3$, the relative correction $\delta v/v$ remains finite at $v \to 0$, and

we conclude that the barriers should be finite for this case. Returning to the discussion of the vortex solid, the important point to note here is that the existence of crystalline long-range order has in no way been crucial to our arguments. Indeed, if we consider instead a kind of vortex glass characterized by a structure factor $S(\mathbf{K},t)$, with the Bragg-peaks replaced by a smooth maximum at $K \approx K_0 = 2\pi/a_0$, the above analysis would go through without any changes apart from a numerical constant of the order of unity in our estimate for the velocity ratio $\delta v/v$. The only important point in our derivation is that we are dealing with a vortex solid that possesses a finite $t \to \infty$ limit for the structure factor $S(\mathbf{K},t)$. Therefore the possible existence of some low density of disorder-induced dislocations in the vortex solid would not affect our conclusion about the existence of infinitely high pinning barriers, since the dislocations themselves would be pinned by the random potential. On the other hand, the

properties of the vortex-liquid phase are quite different, as we shall now show.

## 2. Vortex liquid subject to quenched disorder

Consider a vortex liquid at a temperature close to the melting line $T_m(B)$. For the very viscous liquid considered above, the liquid nature reveals itself only on rather long time scales, $t_{\mathrm{pl}} \gg t_{\mathrm{th}}$, whereas on intermediate time scales between $t_{\mathrm{th}}$ and $t_{\mathrm{pl}}$ the vortex system looks more like a solid. In particular, the large viscosity implies that the structure factor $S(\mathbf{K},t)$ is almost time independent for $t \ll t_{\mathrm{pl}}$ and possesses a smooth maximum at $K \approx K_0 = 2\pi/a_0$, whereas for long times, $t \gtrsim t_{\mathrm{pl}}$, the amplitude of that maximum vanishes rapidly, $S(K_0, t \gg t_{\mathrm{pl}}) \to 0$. Let us use these assumptions and estimate the relative correction $\delta v/v$ to the velocity in the limit $v \to 0$. From Eq. (6.5) we obtain

$$\left. \frac{\delta v}{v} \right|_{v \to 0} = \frac{\gamma_U}{\eta a_0^2} \int \frac{d^2K}{(2\pi)^2} K^2 K_v^2 |p_K|^2 \int dt \, t G(0,t) S(\mathbf{K},t) \ . \tag{6.18}$$

For a simple order-of-magnitude estimate of the integrals in Eq. (6.18) we can assume that the main contribution comes from the region $K \sim K_0$ (we shall verify this assumption later on) and $t \sim t_{\mathrm{pl}}$. Then we can approximate (6.18) by

$$\left. \frac{\delta v}{v} \right|_{v \to 0} \approx \frac{\gamma_U}{\eta a_0^2} \int \frac{d^2K}{(2\pi)^2} K^2 K_v^2 |p_K|^2 S(\mathbf{K},0) t_{\mathrm{pl}} \int_0^{t_{\mathrm{pl}}} dt \, G(0,t)$$

$$\approx \frac{\gamma_U \xi^4}{\eta a_0^2} \frac{K_0^6}{4\pi} \frac{\langle u^2(t_{\mathrm{pl}}) \rangle_{\mathrm{th}}}{T} t_{\mathrm{pl}} \ , \tag{6.19}$$

where the last line was obtained by making use of the fluctuation-dissipation theorem in the form [see Eq. (4.80)]

$$\langle u^2(t) \rangle_{\mathrm{th}} = 2T \int_0^t dt' G(0,t') \ .$$

Finally, assuming that $\langle u^2(t_{\mathrm{pl}}) \rangle_{\mathrm{th}} \sim a_0^2$, we obtain

$$\left. \frac{\delta v}{v} \right|_{v \to 0} \sim \frac{\gamma_U \xi^4}{\eta T} \frac{K_0^6}{4\pi} t_{\mathrm{pl}} \ . \tag{6.20}$$

The most important feature of the result (6.20) is that the relative correction to the velocity is *finite* in the limit $v \to 0$ and proportional to $t_{\mathrm{pl}}$—the time necessary to discriminate between the viscous liquid and the solid phase; see Fig. 26. For weak disorder and a not too large plastic time $t_{\mathrm{pl}}$, the correction (6.20) is small, and disorder has no significant effect on the vortex liquid. For this case the current-voltage characteristic essentially follows its flux-flow behavior down to vanishing current densities $j \to 0$; see Fig. 26. In the opposite case of a very long plastic relaxation time $t_{\mathrm{pl}}$ and/or sufficiently strong pinning strength $\gamma_U$, the correction (6.20) is much larger than unity (see Fig. 26). The low current-density part of the current-voltage characteristic is then strongly affected by the presence of disorder, and the linear resis-

tivity $\rho_{\mathrm{lin}}$ is strongly suppressed as compared with the flux-flow value $\rho_{\mathrm{flow}} \simeq \rho_n H/H_{c_2}$. However, contrary to the case of a vortex solid, we do not expect the existence of arbitrarily high pinning barriers in the liquid phase, which would lead to a vanishing linear resistivity in the limit $j \to 0$, the reason simply being the finiteness of the correction (6.20) (an analogous situation was discussed in Sec. III.E in connection with the pinning of a one-dimensional string in a periodic potential at finite temperatures). Below we shall argue that $\rho_{\mathrm{lin}}$ follows the behavior of the thermal activation rate $1/t_{\mathrm{pl}}$ for plastic deformations, with a characteristic energy barrier that depends only weakly on the disorder strength.

Before proceeding further, let us verify that the region of small wave vectors $\mathbf{K}$ is indeed irrelevant in the evaluation of the integral (6.18). For $K \ll K_0$ we can use a hydrodynamic approximation for the structure factor $S(\mathbf{K},t)$. The hydrodynamic theory of the vortex liquid has been developed by Nelson and Le Doussal (1990), Marchetti and Nelson (1990b, 1991), and Marchetti (1991). They have shown that the static structure factor $S(\mathbf{k},0)$ at small $\mathbf{k}$ can be expressed via the correlation function $\langle \delta n(\mathbf{k}) \delta n(-\mathbf{k}) \rangle$ for the density fluctuation $\delta n(\mathbf{k}) = n_0 \mathbf{K} \cdot \mathbf{u}(\mathbf{k})$, where $n_0 = B/\Phi_0$ denotes the aver-

age vortex density in the system. The liquid state differs from the solid in its response under shear involving transverse displacements with $\mathbf{K} \cdot \mathbf{u}(\mathbf{k}) = 0$. The structure factor, however, is determined by longitudinal modes involving compression, which do not differ essentially for the solid and liquid phases. Therefore we can relate the static structure factor to the correlator of the longitudinal component of the displacement field in the solid and obtain [see Eq. (3.21)]

$$S(\mathbf{k}, 0) = \frac{TK^2 n_0^2}{c_{11}(\mathbf{k})K^2 + c_{44}(\mathbf{k})k_z^2} . \tag{6.21}$$

The time dependence of the structure factor in the hydrodynamic region can be inferred from the relaxation rate $\gamma(\mathbf{k})$ of the long-wavelength density fluctuations (Marchetti and Nelson, 1991)

$$\gamma(\mathbf{k}) = \frac{1}{\eta}[c_{11}(\mathbf{k})K^2 + c_{44}(\mathbf{k})k_z^2] . \tag{6.22}$$

Combining Eq. (6.21) with (6.22), we obtain the dynamic structure factor $S(\mathbf{k}, t) = S(\mathbf{k}, 0)\exp[-\gamma(\mathbf{k})t]$. Note that the structure factor $S(\mathbf{K}, t)$ appearing in Eq. (6.5) correlates equal $z$ values, and hence it involves an additional integration over $k_z$,

$$S(\mathbf{K}, t) = \int dk_z S(\mathbf{k}, 0) e^{-\gamma(\mathbf{k})t} . \tag{6.23}$$

Using the result (6.23) and neglecting the time dependence of the Green's function $G(0, t)$, we can obtain an upper estimate for the hydrodynamic contribution to the integral (6.18),

$$\left. \frac{\delta v}{v} \right|_{\text{hydr}} \propto T \int d^2K \, dk_z K^6 [c_{11}(\mathbf{k})K^2 + c_{44}(\mathbf{k})k_z^2]^{-3} . \tag{6.24}$$

The integral in (6.24) is rapidly converging at small $\mathbf{k}$, and the contribution of that region is indeed small.

### 3. Numerical factors

In this short section we briefly sketch the derivation of the prefactors $\beta_{\text{sb}}$ [see Eqs. (2.79) and (2.155)], $\beta_{\text{lb}}$ [see Eq. (4.51)], and $\alpha_{\text{dp}}^s$ [see Eq. (4.109)] used in Secs. II and IV above. The following analysis is based on the dynamic approach. Concentrating first on $\beta_{\text{sb}}$ and $\beta_{\text{lb}}$, the basic idea is to compare the time scale for pinning, $t_{\text{pin}} \simeq \xi/v_c$, with the crossover times $t_{\text{th}}$ and $(\lambda/a_0)^2 t_{\text{th}}$, where the Green's function changes from the single-vortex propagator (6.11) at small times, $t < t_{\text{th}}$, to the small-bundle propagator (6.10) at intermediate times, $t_{\text{th}} < t < (\lambda/a_0)^2 t_{\text{th}}$, and finally to the large-bundle propagator (6.8) for large times, $t_{\text{th}}(\lambda/a_0)^2 < t$. Single-vortex pinning is realized if the time cutoff $t_{\text{pin}}$ provided by the factor $\sin(K_v vt)$ in Eq. (6.5) is smaller than $t_{\text{th}}$, so that the time integration involves only the single-vortex Green's function. If $t_{\text{pin}}$ becomes larger than $t_{\text{th}}$ the integration involves the

small-bundle Green's function, and we enter the small-bundle pinning regime. Similarly, as $t_{\text{pin}}$ increases beyond $(\lambda/a_0)^2 t_{\text{th}}$, large bundles are collectively pinned.

First, we have to find the relevant $K$ vector entering the expression for the pinning time $t_{\text{pin}}$. The $K$ integration in Eq. (6.5) involves the form factor $p(K)$, which can be easily calculated for the case of $\delta T_c$ pinning. Using Eq. (2.34) and Clem's (1975) variational wave function to model the vortex core, we obtain

$$p(K) = 4\pi\xi^2 K_0(\sqrt{2}\xi K) . \tag{6.25}$$

The $K$ integration involves the function $f(K) = K^5[K_0(\sqrt{2}\xi K)]^2$, which has a maximum at $K_{\max} = \sqrt{2}/\xi$. The relevant $K$ vector in the cutoff factor $\sin(K_v vt)$ is then chosen to be $K = K_{\max}$. In a second step we have to find a precise criterion for the crossover between the single-vortex and the small-bundle pinning regime. We therefore consider the time integral in Eq. (6.5) which involves the expression

$$\int dt \, \sin(K_{\max}vt)G(0, t)$$

$$\propto \int_0^{t_{\text{th}}} dt \sqrt{t_{\text{th}}t} + \frac{\sqrt{\pi}}{4} \int_{t_{\text{th}}}^{1/K_{\max}v} dt \frac{t_{\text{th}}^2}{t} ,$$

where we have split the integral into a contribution containing the single-vortex Green's function and a second term involving the small-bundle propagator. As we enter the small-bundle pinning regime, the second term becomes dominant, and we obtain the criterion

$$\ln\frac{1}{K_{\max}v_c t_{\text{th}}} \approx \frac{4}{3\sqrt{\pi}} . \tag{6.26}$$

Here we have made use of the fact that the relevant velocity where pinning starts to become important is the critical velocity $v_c$. Using $v_c = j_c B/\eta c$ as well as Eq. (6.9) for the thermal fluctuation time, we obtain the following final form for the crossover criterion:

$$\frac{a_0^2}{c_{66}K_{\text{BZ}}^2} \approx \frac{c\xi}{2\sqrt{2}j_c B_{\text{sb}}} , \tag{6.27}$$

from which we can extract the limiting field $B_{\text{sb}}$ for single-vortex pinning,

$$B_{\text{sb}} \approx 5\frac{j_c}{j_0}H_{c_2} , \tag{6.28}$$

and hence $\beta_{\text{sb}} \approx 5$. A similar analysis can be carried out in order to find the crossover field $B_{\text{lb}}$ to the large-bundle pinning regime. The criterion now reads

$$K_{\max}v_c t_{\text{th}} \approx \frac{1}{\pi^2}\left[\frac{a_0}{\lambda \ln(\lambda/a_0)}\right]^2 . \tag{6.29}$$

Using the result for the critical current density as obtained from the dynamic approach (Feigel'man and Vinokur, 1990), we can estimate the factor $\beta_{\text{lb}} \approx 2$.

Finally, the $\alpha_{\text{dp}}^s$ determining the value of the single-vortex depinning temperature $T_{\text{dp}}^s$ [see Eq. (4.109)] can be

extracted from the result of the dynamic approach as obtained by Feigel'man and Vinokur (1990). Relating the disorder parameter $\gamma$ (note that $\gamma_{FV}$ corresponds to $\gamma\xi^4 = \gamma_{FV}$ in the present notation) to the single-vortex critical current density $j_c$, we obtain $T_{dp}^s \approx 0.7(j_c/j_0\, Gi)^{1/2}T_c$ if we use a critical current-density ratio of the order of $j_c/j_0 \simeq 10^{-2}$ and hence $\alpha_{dp}^s \approx 0.7$.

## B. Resistivity and critical current densities

Equation (6.20) is the result of a perturbative analysis and is correct in the limit $\delta v \ll v$, which holds at high enough temperatures where $t_{pl}$ is not very large. Within this region the disorder leads only to small corrections to the resistivity and hence $\rho \simeq \rho_{flow} \simeq \rho_n H/H_{c_2}$; see Figs. 5 and 27. From the smallness of the relative velocity correction $\delta v/v$ at high temperatures, we have drawn the conclusion that the barriers suppressing vortex motion in the low-temperature pinned liquid (where the corrections $\delta v/v$ become large and our perturbative approach cannot be used any longer) remain finite at all current densities, and hence vortex motion is characterized by thermally assisted flux flow (TAFF; Kes *et al.*, 1989; see Figs. 5 and 27). The characteristic time which controls the vortex motion in the liquid phase is the plastic relaxation time $t_{pl} \simeq t_{th}\exp(U_{pl}/T)$, and thus it seems natural to
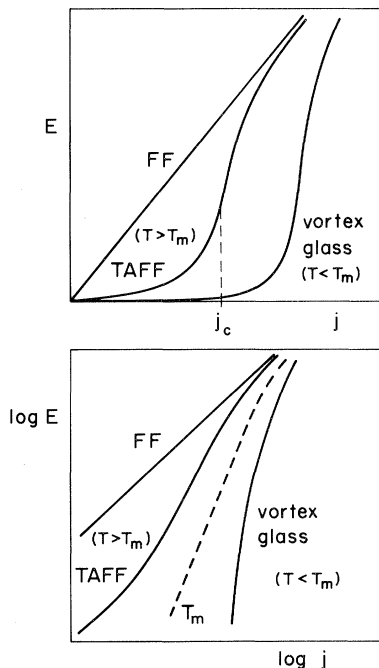


FIG. 27. Current-voltage characteristic in a lin-lin and in a log-log plot for the three different dynamic regimes of flux flow (FF), thermally assisted flux flow (TAFF), and glassy response. The different response is due to the different types of barriers appearing in the vortex system, with small ($U_{pl} \sim T$) and large but finite ($T \ll U_{pl} < \infty$) plastic barriers in the FF and in the TAFF regimes and diverging elastic barriers [$U(j \to 0) \to \infty$] in the glass phase.

identify the activation barriers relevant for TAFF with $U_{pl}$. The resistivity within the TAFF regime can be written in the form

$$\rho \simeq \rho_0 e^{-U_{pl}/T} \propto \frac{1}{t_{pl}} . \qquad (6.30)$$

The preexponential factor $\rho_0$ in Eq. (6.30) can be estimated by making use of the result (6.20) and noting that the crossover from flux flow to TAFF behavior takes place when the correction (6.20) becomes of order unity. Assuming that the behavior of $\rho$ follows the behavior of $1/t_{pl}$, a simple interpolation gives

$$\rho \simeq \rho_{flow} \bigg/ \left[ 1 + \frac{\gamma_U \xi^4}{\eta T} \frac{K_0^6}{4\pi} t_{pl} \right] ,$$

$$\simeq \frac{\rho_{flow}}{1 + Ae^{U_{pl}/T}} , \qquad (6.31)$$

with the coefficient $A$ [note that $\gamma_U = \gamma/2\pi$ for the case of $\delta T_c$ pinning; see Eq. (2.38)],

$$A \simeq 4(2\pi)^6 \frac{\gamma_U \xi^4}{\Phi_0^2 T} \left[ \frac{\lambda}{a_0} \right]^2$$

$$\simeq \sqrt{2}\pi^2 Gi \left[ \frac{j_c(0)}{j_0(0)Gi} \right]^{3/2} \frac{B}{H_{c_2}(T)} . \qquad (6.32)$$

The preexponential $\rho_0$ to the resistivity in the TAFF regime then is given by

$$\rho_0 \simeq \frac{\rho_{flow}}{A} \simeq \frac{1}{\pi^2\sqrt{2Gi}} \left[ \frac{j_0(0)Gi}{j_c(0)} \right]^{3/2} \rho_n . \qquad (6.33)$$

The exact determination of the resistivity in the TAFF regime would involve a summation over higher-order terms in the perturbation series, since the correction $\delta v/v$ becomes large. The summation of this series is a difficult problem and has not yet been done. On the other hand, the following simple analysis gives additional support for the correctness of the interpolation formula (6.31). The equation of motion for a pinned vortex liquid can be written in the simple form (we neglect a possible finite Hall angle here)

$$\eta\mathbf{v} = \mathbf{f}_L + \mathbf{f}_{pin} . \qquad (6.34)$$

Symmetry arguments require the pinning force to be directed along $\mathbf{v}$, and hence we can write $\mathbf{f}_{pin} = -\eta_{pin}(v)\mathbf{v}$. The coefficient $\eta_{pin}(v)$ can be expressed through the relative velocity correction $\delta v/v$, $\eta_{pin} = \eta(\delta v/v)$ and should be determined via summation of the perturbation series. The pinning force $\mathbf{f}_{pin}$ in (6.34) renormalizes the friction coefficient to become $\bar{\eta}(v) = \eta + \eta_{pin}(v)$. Making use of the relation $E = (v/c)B$ between the electric field $E$ and the velocity $v$, we immediately obtain for the resistivity

$$\rho = \frac{\rho_{flow}}{1 + \delta v/v} , \qquad (6.35)$$

which is our interpolation formula (6.31). Instead of having to deal with a series expansion of the pinning force in Eq. (6.34), we have now arrived at an expression in which the relative velocity correction $\delta v / v$ appears in the denominator, and hence the result (6.35) makes sense even in the regime where $\delta v / v > 1$. Finally, as an approximation to the true value of the relative velocity correction $\delta v / v$, we use the lowest-order result (6.20).

Equation (6.31) shows that a regime of thermally assisted flux-flow behavior at weak current densities $j$ actually can exist if the condition

$$A \frac{t_{\text{pl}}}{t_{\text{th}}} \gg 1 \qquad (6.36)$$

is fulfilled. Below we show that this condition coincides with the criterion $t_{\text{pl}} \gg t_{\text{pin}}$, which we discussed in our qualitative analysis of the pinning problem at the beginning of Sec. VI.A. If this condition holds, the current-voltage characteristic of the pinned liquid will exhibit two ohmic regimes at low and at high current densities, with the resistivities $\rho(j \to 0) \simeq \rho_0 \exp(-U_{\text{pl}}/T) \propto 1/t_{\text{pl}}$ and $\rho(j > j_{\text{cr}}) \simeq \rho_{\text{flow}}$; see Figs. 5 and 27. The value of the crossover current density $j_{\text{cr}}$ can be estimated in the same manner as the critical current density for a pinned vortex lattice. From the above arguments we know that the correction $\delta v / v|_{v \to 0}$ is large in the TAFF regime. Therefore, if we are to obtain a correction of the order of

unity, the sine factor present in our basic equation (6.5) has to cut off the time integral at times $t \sim 1/K_0 v \ll t_{\text{pl}}$, and we can neglect the time dependence of the structure factor $S(\mathbf{K}, t)$,

$$\frac{\delta v}{v} \approx \frac{\gamma v}{\eta a_0^2} \int \frac{d^2 K}{(2\pi)^2} K^2 K_v |p(K)|^2 S(\mathbf{K}, t = 0)$$

$$\times \frac{1}{v} \text{Im} G(0, \omega = v K_v), \qquad (6.37)$$

with $G(0, \omega)$ the Fourier transform of the response function $G(0, t)$. In order to estimate the integral (6.37), we need an explicit form for the Green's function $G(\omega)$ of a viscous liquid. Here we make use of the Maxwell model (Landau-Lifshitz, 1959a), i.e., we assume that the transition from an elastic to a viscous behavior can be described by replacing the shear modulus of the medium by an interpolating expression of the type

$$\bar{c}_{66}(\omega) = \frac{c_{66}}{1 + i/\omega t_{\text{pl}}} . \qquad (6.38)$$

For high frequencies, $\omega t_{\text{pl}} \gg 1$, Eq. (6.38) reduces to the ordinary shear modulus $c_{66}$ of the vortex lattice, whereas (6.38) describes a liquid with a shear viscosity $v = t_{\text{pl}} c_{66}$ in the opposite limit of low frequencies. The Green's function for this viscoelastic medium is given by

$$G(\omega) = \int \frac{d^2 K}{(2\pi)^2} \frac{dk_z}{2\pi} \frac{1}{-i\omega\eta + \bar{c}_{66}(\omega)K^2 + c_{44}(\mathbf{k})k_z^2}$$

$$= \frac{\sqrt{\eta}}{4\pi c_{66}} \left\{ \left[ \frac{1}{c_{44}(K_0)t_{\text{th}}} \right]^{1/2} - \left[ \frac{-i\omega}{c_{44}(0)} \right]^{1/2} \right\} \left[ 1 + \frac{i}{\omega t_{\text{pl}}} \right]^{1/2} . \qquad (6.39)$$

Within the frequency range $t_{\text{pl}}^{-1} \ll \omega \ll t_{\text{th}}^{-1}$ of interest here, the imaginary part $\text{Im} G$ of the Green's function (6.39) shows two main competing contributions,

$$\text{Im} G(\omega) = \frac{1}{8\pi c_{66}} \left[ \frac{\eta}{t_{\text{th}}} \right]^{1/2} \left[ \frac{1}{\omega t_{\text{pl}} \sqrt{c_{44}(K_0)}} + \left[ \frac{2\omega t_{\text{th}}}{c_{44}(0)} \right]^{1/2} \right] , \qquad (6.40)$$

where the second term $\propto \omega^{1/2}$ describes the lattice properties of the medium at high frequencies, while the first term $\propto \omega^{-1}$ reflects the breakdown of the crystalline order over large time scales (note that for large times, $t > t_{\text{pl}}$, thermal fluctuations produce a diffusive motion of the liquid, $\langle u^2(t) \rangle_{\text{th}} \simeq \langle u^2 \rangle_{\text{th}} (t/t_{\text{pl}})^{1/2}$). The crossover from elastic to liquid behavior takes place at frequencies $\omega_x \simeq t_{\text{pl}}^{-1} (\lambda/a_0)^{2/3} (t_{\text{pl}}/t_{\text{th}})^{1/3}$. Evaluating Eq. (6.37) within the liquid regime ($\omega < \omega_x$), we obtain

$$\frac{\delta v}{v} \approx \frac{\gamma \xi^4}{8\pi c_{66} a_0^2} \left[ \frac{1}{\eta t_{\text{th}} c_{44}(K_0)} \right]^{1/2} \frac{1}{t_{\text{pl}} v^2} \int \frac{d^2 K}{(2\pi)^2} K^2 S(\mathbf{K}, t = 0)$$

$$\approx A \frac{T}{T_m} \frac{1}{t_{\text{pl}} t_{\text{th}}} \frac{1}{K_0^2 v^2}, \quad \frac{a_0}{t_{\text{pl}}} \ll v \ll \frac{a_0}{t_{\text{pl}}} \left[ \frac{\lambda}{a_0} \right]^{2/3} \left[ \frac{t_{\text{pl}}}{t_{\text{th}}} \right]^{1/3} . \qquad (6.41)$$

The high current-density part of the current-voltage characteristic of the weakly pinned flux liquid then takes the form

$$E = \rho_{\text{flow}} j \left[ 1 - \frac{j_{\text{cr}}^2}{j^2} \right] , \qquad (6.42)$$

with the characteristic crossover current density $j_{\text{cr}}$ marking the onset of nonlinear behavior given by

$$j_{\text{cr}} \approx j_0 \sqrt{Gi} \left[ \frac{j_c(0)}{j_0(0)Gi} \right]^{3/4} \left[ \frac{T}{T_m} \frac{t_{\text{th}}}{t_{\text{pl}}} \right]^{1/2} \frac{B}{H_{c_2}} . \qquad (6.43)$$

Note that $j_{cr}$ *grows* with decreasing plastic time $t_{pl}$—a smaller plastic relaxation time allows the vortices to adapt themselves more easily to the pinning potential, and hence pinning is improved.

From the above derivation it becomes clear that the crossover current density $j_{cr}$ describes the deviation of the linear current-voltage characteristic in the TAFF regime when coming from above, i.e., from high current densities. On the other hand, within the TAFF regime a second Ohmic regime with an exponentially suppressed resistivity exists at low current densities. The determination of the crossover current density $j_T < j_{cr}$, where the linear current-voltage characteristic turns nonlinear from below (see Fig. 27), is a difficult task, as it requires a detailed analysis of the flux-flow mechanism within the TAFF regime, and we shall not go into this any further here.

In summary, then, it seems that the concept of collective pinning of a very viscous liquid by weak disorder is able to explain the temperature dependence of the linear resistivity $\rho(T)$ in the presence of a strong magnetic field, as found in the new high-temperature superconductors. The main experimentally observed features of this broadened resistive transition involve a sharp crossover from a flux-flow regime to a thermally assisted flux-flow regime at a temperature $T_k > T_m$ (see Fig. 25), where the latter regime is characterized by an activated behavior for the resistivity, $\rho(T) = \rho_0 \exp(-U_{pl}/T)$, $T_m < T < T_k$. The crossover temperature $T_k$ is determined by the equation

$$A \frac{t_{pl}}{t_{th}} = A \exp\left[\frac{U_{pl}(T_k)}{T_k}\right] \simeq 1 , \qquad (6.44)$$

with the coefficient $A$ given by Eq. (6.32). The condition (6.44) coincides with the condition $t_{pin}(T_k) \simeq t_{pl}(T_k)$ obtained above [see Eq. (6.4)] on the basis of qualitative arguments if we determine the pinning time $t_{pin}$ via the relation $t_{pin} \simeq a_0/v_c$, with $v_c$ the critical velocity obtained from setting the relative velocity correction (6.41) equal to unity. The sharpness of the crossover at $T_k$ is predicted by the inequality $A \ll 1$, which is attributed to the weakness of the pinning. Note that Eq. (6.44) predicts a weak (logarithmic) increase of $T_k$ with increasing strength of the disorder. The preexponential factor $\rho_0 = \rho_{flow}/A \gg \rho_{flow}$ to the resistivity in the TAFF regime is large, which again is a consequence of the weak pinning condition. Such a large preexponential factor has indeed been observed experimentally (Palstra *et al.*, 1988a, 1989, 1990; Liu *et al.*, 1989; Malozemoff *et al.*, 1989).

An interesting alternative model describing the resistive transition in the oxides and addressing the origin of the "kink" in the resistivity curve $\rho(T)$ at $T_k$ has been proposed by Marchetti and Nelson (1990b). Again, the vortex fluid is modeled as a very viscous liquid, which then is *strongly* pinned by the presence of twin boundaries in YBCO. The problem of the vortex motion in the superconductor in the presence of twin boundaries is reduced to the hydrodynamic flow problem of a viscous liquid enclosed between parallel plates (of mean distance $d$), providing the boundary conditions for the flow (for strong pinning a boundary condition $\mathbf{v}=0$ is chosen). For a high enough viscosity $\nu$, $\nu \gg d^2\eta$, the vortices move with a velocity $v \propto 1/\nu = 1/t_{pl}c_{66}$, and hence a resistivity proportional to the inverse plastic time $t_{pl}$ is obtained. In this model the large value of the preexponential factor to the activated resistivity is related to the large separation between the twin boundaries.

Very recently, the sample quality has been strongly improved (e.g., twin free YBCO single crystals), and very sharp (and hysteretic) first-order-type transitions from a resistive vortex-liquid state to a pinned vortex solid characterized by a nonlinear response have been observed (Charalambous, 1992; Safar, Gammel, Huse, *et al.*, 1992, 1993; Charalambous *et al.*, 1993; Kwok *et al.*, 1994a, 1994b). From these observations it appears that the "kink" at $T_k$ develops into the transition temperature for the first-order melting transition of the vortex lattice. Artificially increasing the disorder via electron irradiation, producing point defects, smears this transition and leads to the appearance of "kink" or "shoulder" in the resistive transition. Subsequent annealing restores the sharp transition. Hence the appearance of the pinned liquid phase can be directly influenced by the amount of disorder in the sample.

## C. Diluted vortex liquids subject to disorder

In this section we discuss the influence of quenched disorder on a dilute (that is, $a_0 \gg \lambda$) vortex-liquid phase. In a pure system, such a liquid phase has been shown to exist below the low-field branch of the melting line; see Sec. V.A.2 above and Figs. 2, 3, and 24. Most probably this liquid is in an entangled phase, as first proposed by Nelson (1988) and discussed in more detail by Nelson and Seung (1989) and Nelson and Le Doussal (1990). The large-scale thermodynamic properties of the entangled vortex-liquid state coincide with those of the normal metal (see the discussion in Sec. V.B.3). However, the presence of even weak disorder can considerably modify the properties of this phase or even lead to a qualitative change of the $B$-$T$ phase diagram in its low-field regime. The important point to note is that the effective strength of thermal fluctuations is considerably reduced in the low-field branch of the melting line, as the relevant parameter describing the strength of thermal fluctuations is $Gi/\kappa^2\ln\kappa$ rather than the usual value $Gi$, which is appropriate for the upper part of the melting line. Therefore condition (4.114) guarantees neither the stability of the low-density part of the melting line nor that of the resulting dilute liquid phase under the influence of disorder.

In order to investigate the significance of disorder for an entangled vortex liquid, we start from a comparison of the two relevant length scales, $L_E(T)$ and $L_c(T)$, corre-

sponding to the length over which the vortices entangle in a pure phase and to the single-vortex collective pinning length (we consider either an isotropic or an anisotropic situation with $\mathbf{B} \| c$ axis here). In order to obtain the entanglement length $L_E(T)$, we can remind ourselves that the entangled vortex liquid corresponds to the superfluid ground state of a system of 2D bosons with a transition temperature given by $T_c^B \approx 2\pi n^B \hbar^{B^2}/m^B$, with $\hbar^B = T$, $m^B = \varepsilon^2 \varepsilon_0 \ln\kappa$, and $n^B = B/\Phi_o = a_o^{-2}$. Since the length along $z$ in the vortex system maps to the temperature in the Bose formulation, $L = \hbar^B/T^B$, the critical temperature $T_c^B$ for the superfluidity of the bosons maps to the entanglement length in the original vortex picture, and hence

$$L_E(T) = \frac{\hbar^B}{T_C^B} \approx \frac{\varepsilon^2 \varepsilon_0 \ln\kappa}{2\pi T} a_o^2 \ . \tag{6.45}$$

Thus the large-scale properties of the pure entangled-vortex-liquid phase develop on scales $L > L_E(T)$ (along the $c$ axis) and $R > a_o$ (within the superconducting planes). On the other hand, the interaction of a single vortex line with the disorder potential becomes strong on a scale $L_c(T)$, which is given by [see Eq. (2.127)]

$$L_c(T) \approx L_c(0) \frac{\tilde{T}_{\text{dp}}^s}{T} \exp\left[ c \left( \alpha + \frac{T}{\tilde{T}_{\text{dp}}^s} \right)^3 \right] \ . \tag{6.46}$$

The relative importance of the random potential for the entangled-vortex-liquid phase can be inferred from a comparison between the two lengths $L_c$ and $L_E$. When $L_E \ll L_c$, the macroscopic properties of the entangled liquid are developed *before* the random potential becomes relevant for a single-vortex line. Since the entangled vortex liquid is simply a normal-metal phase on scales $L \gg L_E$, the random potential never becomes relevant for the weak-pinning case in which $L_E \ll L_c$. These qualitative arguments are supported by renormalization-group calculations (Nelson and Le Doussal, 1990) showing that the effective coupling to the random potential is always weak as long as $L_E \ll L_c$. On the other hand, for strong disorder in the sense that $L_E \gg L_c$, the effect of disorder becomes strong before the collective properties of the multivortex system can develop, i.e., the dominant effect to be considered first is the pinning of the individual vortex lines by the disorder potential. An interesting reformulation of the above arguments is obtained within the Bose picture: The isotropic random potential maps to a white-noise disorder potential fluctuating in both space and time. These fluctuations tend to destroy the phase coherence of the boson wave function, with the length $L_c$ now playing the role of a dephasing time. If this "phase-breaking" time is larger than the time $L_E = \hbar^B/T_c^B$ needed to establish superfluidity, phase-breaking effects are irrelevant, and superfluidity survives. On the other hand, if $L_E \ll L_c$, the phase coherence between the bosons is strongly suppressed, and the existence of superfluidity is rather improbable.

At present it is unclear what type of thermodynamic state is formed when disorder is relevant ($L_c \ll L_E$). In the most natural scenario, the Bose system adopts a nonsuperfluid ground state, which then would map to a disentangled vortex-liquid phase in the original vortex picture. However, the formation of a vortex-glass phase is also a viable alternative, and even the survival of some (strongly suppressed) superfluidity cannot be ruled out, though it seems quite improbable. A few words of additional explanation are in order here. At first glance the isotropic random potential enhances the transverse wandering of the vortex lines and thus seems to assist the thermal fluctuations in their tendency to entangle the vortex lines. However, we should distinguish between entanglement as a synonym for superfluidity in the equivalent Bose system and the simple "mechanical" entanglement of the vortex lines, which does not establish a new thermodynamic phase (see the discussion at the end of Sec. V.B.3). The difference between these two types of entanglement is that, in the first case, many topologically different configurations (connected via vortex line cutting and reconnection processes) contribute substantially to the partition function, whereas in the second case such cutting and reconnection processes are ineffective and the system is trapped within a small subspace of all the possible configurations. Such a configuration can turn out to be quite heavily entangled in the mechanical sense, but this entanglement has nothing in common with the superfluidity of the equivalent Bose system. Correspondingly, such a mechanically entangled phase does not imply the presence of a normal-metal phase.

The above discussion serves as a motivation to use the condition $L_E \simeq L_c$ to define a characteristic line in the $B$-$B$ phase diagram marking the transition between a low-density entangled-vortex-liquid phase and some other phase, probably a disentangled liquid or a vortex glass. In the following we discuss the shape of this transition line as it arises from a comparison of $L_E$ and $L_c$ as given by Eqs. (6.45) and (6.46). To begin with, suppose that the temperature $T$ is below the single-vortex depinning temperature $T_{\text{dp}}^s$, as given by Eq. (2.130). Expressing $L_c$ through the critical current density $j_c$, (2.51a), we obtain the ratio

$$\frac{L_E}{L_c} \approx \frac{\pi}{\sqrt{2}} \kappa^2 \ln\kappa \left[ \frac{a_o}{2\pi\lambda(0)} \right]^2$$

$$\times \left[ \frac{j_c(0)}{Gi\, j_o(0)} \right]^{1/2} \frac{(1-t)^{4/3}}{t} \ . \tag{6.47}$$

Let us remind ourselves that here we discuss the low-density vortex liquid with the field $B$ lying below the melting line, as given by Eq. (5.19); see Figs. 2, 3, and 24. Using typical parameter values for YBCO, we find that the ratio $L_E/L_c$ as given by Eq. (6.47) is always much larger than unity. In other words, we find that the entangled-vortex-liquid phase is unstable everywhere below the single-vortex depinning temperature $T_{\text{dp}}^s$, and

pinning is dominant. When the temperature is increased beyond $T_{dp}^s$, the thermal fluctuations smooth out the pinning potential considerably, and $L_c(T)$ increases exponentially. Substituting the full temperature dependence of $L_c(T)$, as given by Eq. (2.127), into our equation for the transition line, we obtain the implicit equation

$$\left[\frac{t}{t_{dp}^s}\right]^3 \approx \ln\kappa^2 + \frac{1}{2}\ln\frac{j_c(0)}{j_\circ(0)Gi}$$
$$+\ln\frac{H_{c_1}(T)}{B} + \ln\frac{(1-t)^{1/3}}{t_{dp}^s} . \qquad (6.48)$$

Note that here we adopt the simplified model introduced in Sec. V.B above, which describes the interaction between the vortex lines in the dilute liquid via a hard-core repulsive potential on the scale $\lambda$. Hence we always remain in the single-vortex pinning regime within the present model. For a rough estimate of the form of the phase diagram, we can assume a typical thermal versus quenched disorder ratio $j_c(0)/j_\circ(0)Gi \sim 1$. The lowest temperature (highest field $B \sim H_{c_1}$) where Eq. (6.48) can be fulfilled is then given by the condition $t^3 \sim (t_{dp}^s)^3[\ln\kappa^2 + \ln(1-t)^{1/3}]$, from which we obtain a transition temperature $T^{ED}$ very close to $T_c$. Above $T^{ED}$ the transition line drops very fast towards small values for the magnetic field as the temperature increases towards $T_c$. The corresponding shape of the phase diagram is sketched in Fig. 25.

# VII. VORTEX GLASS

## A. Zoology of glasses

Probably the most straightforward association with the notion "glass" is the ordinary *window glass* encountered in everyday life. Due to its characteristic property of undergoing a transition or crossover from a high-temperature liquid to a low-temperature "solid" phase without an apparent breaking of any symmetry, (window) glass has lent its name to a whole class of materials exhibiting an equivalent behavior. Over the past two decades, much effort, both experimental and theoretical, has been devoted to investigating and understanding the physics of glassy systems, the nature of the transition, and the properties of the glass state itself. Interestingly, the most carefully studied system is not the ancestor of all glassy materials, window glass, but rather a system known as *spin glass*. This is due mainly to the lack of a simple model able to capture the essential physics of window glass. On the other hand, spin glasses, such as those obtained by a dilute solution of magnetic transition-metal impurities in noble-metal hosts (e.g., Mn in Cu, Ag, or Au), can be described by a simple model Hamiltonian (Edwards and Anderson, 1975),

$$\mathcal{H} = -\frac{1}{2}\sum_{i,j}J_{ij}\mathbf{S}_i\cdot\mathbf{S}_j , \qquad (7.1)$$

of the Heisenberg form. Here the spins $\mathbf{S}_i$ are constrained to lie on a regular translationally invariant lattice, and the crucial element of randomness responsible for the glassy behavior is introduced via the random couplings $J_{ij}$, which are characterized by a distribution function $\mathcal{P}(J_{ij})$, for example, of Gaussian shape,

$$\mathcal{P}(J_{ij}) = \frac{1}{\sqrt{2\pi\Delta_{ij}}}e^{-J_{ij}^2/2\Delta_{ij}} , \qquad (7.2)$$

with the variance $\Delta_{ij}$ depending on distance in general. In nature, such random couplings between spins can be realized by positional disorder in the magnetic impurities combined with the RKKY exchange interaction between the spins mediated via the conduction electrons of the host material. An even simpler variant of this model system is the Ising model with spin variables restricted to $S_i \in \{-1,1\}$. Other systems closely related to the spin glasses are the so-called *dipolar glasses,* such as mixtures of $RbH_2PO_4$ and $NH_4H_2PO_4$, or *quadrupolar glasses,* e.g., $(KCN)_x(KBr)_{1-x}$.

An alternative system exhibiting glassy behavior is *polymer glass.* In this system the constitutive objects are *lines* as opposed to the *pointlike objects* relevant in a spin glass. Quite naturally, then, the idea arises that a system of vortices subject to quenched disorder can exhibit glassy behavior, too. In fact, glassy features exhibited by various experiments on high-temperature superconductors, as well as fundamental considerations regarding loss of long-range order in a vortex "lattice" subject to quenched disorder, have led to the suggestion that the vortices in a superconductor find themselves in a glass state at low temperatures (Fisher, 1989), thus adding the *vortex glass* to the list of systems exhibiting glassy character.

What is the characteristic property of a vortex glass? Let us define here the thermodynamic equilibrium state of the superconductor via its (dynamic) response properties. Extrapolating the Kim-Anderson result for thermally activated creep down to vanishing driving forces with $j \rightarrow 0$, we are confronted with the fact that transport in type-II superconductors is always associated with dissipation. Hence "true" superconductivity in the sense of dissipation-free transport of charge is never realized. A "true" superconductor, on the other hand, is required to approach zero resistivity at vanishing driving force; see Figs. 5 and 27 (since we are discussing the existence of a thermodynamic equilibrium phase, we are interested in a system response under the application of a vanishing force that does not drive the system out of its equilibrium state). Within this context the "true" superconductor is realized by the vortex-glass state, as proposed by Fisher (1989).

An alternative approach to glassiness in a superconductor starts from the notion of the phase $\varphi_i$ of the order parameter. Consider a granular superconductor in the presence of a magnetic field $\mathbf{H}$ (Shih, Ebner, and Stroud,

1984). For small enough grains,[7] the modulus of the order parameter can be taken to be a constant, leaving only the phases $\varphi_i$ of the individual grains as dynamical degrees of freedom. A model Hamiltonian describing this system is then given by

$$\mathcal{H} = \sum_{\langle ij \rangle} J_{ij} \cos(\varphi_i - \varphi_j - A_{ij}) ,\qquad (7.3)$$

with

$$A_{ij} = \frac{2\pi}{\Phi_o} \int_i^j \mathbf{A} \cdot d\mathbf{l} \qquad (7.4)$$

denoting the line integral of the vector potential $\mathbf{A}$ between sites $i$ and $j$, where $J_{ij}$ is the Josephson coupling energy between neighboring grains. Usually, screening is weak and fluctuations in the vector potential can be neglected. Disorder can be introduced into the model via randomness in the (nearest-neighbor) couplings $J_{ij}$. However, since the coupling constants do not change sign, they cannot produce the necessary frustration crucial for obtaining spin-glass behavior. In this sense the couplings $J_{ij}$ are usually taken to be uniformly equal to $J$. Another way to introduce randomness and frustration into the system is via the vector potential $A_{ij}$, for example, through positional disorder of the individual grains. For high enough fields, $A_{ij}$ will vary over the entire interval $[0, 2\pi]$, leading to sign changes in the effective coupling between neighboring grains and thus to strong frustration between the phases $\varphi_i$. The model system described by Eq. (7.3) is known as a *gauge glass*. Glassy behavior in a type-II superconductor, then, can be associated with the phase degree of freedom or with the zeros of the order parameter (vortices), and it is an interesting and important question whether these two points of view are equivalent or different.

The characteristic properties of the above systems associating them with glassiness is the existence of a finite-temperature freezing transition, in which the distribution of relaxation times extends to macroscopic time scales. Furthermore, the resulting low-temperature phase shows specific dynamic signatures such as (slowly decaying) remanence and irreversibility. Dynamic response functions such as the magnetic ac susceptibility in spin glasses also show a cusp at the freezing transition. Identifying this cusp with the freezing temperature $T_g$ we are immediately confronted with two problems. First, the position of the cusp depends on frequency, hence $T_g = T_g(\omega)$, and second, the cusp is not completely sharp. This brings us to the most fundamental question in the theory of glasses: Is the glass state a true thermodynamic equilibrium phase set apart from the high-temperature "liquid" phase by a generic thermodynamic phase transition, or, is the glassy phase merely a frozen "liquid" with

---

[7] For very small grains charging effects become relevant and the phase becomes a dynamic variable. We do not consider this limit here.

$T_g$ marking only a crossover to a very high viscosity. Probably the answer to this question will depend on the particular system under consideration. For example, it seems likely that window glass itself is not a thermodynamic state, but is unstable to decay into the lower-energy crystalline state at very long but finite time scales. On the other hand, depending on dimensionality and symmetry, the spin-glass system is generally believed to undergo a finite-temperature thermodynamic phase transition into a true glass phase. It has been suggested that vortex glass also is a generic thermodynamic phase and thus is fundamentally different from the high-temperature liquid state (Fisher, 1989). In the following we concentrate on three systems: spin glass, gauge glass, and the vortex glass. As spin glass is the most carefully studied system, we briefly summarize and discuss the basic questions and concepts by means of this simple model system. A finite-temperature glass transition in the gauge glass is usually interpreted as supporting evidence for the existence of the vortex-glass phase, and thus we shall discuss this system in some detail. Finally, our ultimate interest is of course the existence of a true thermodynamic vortex-glass phase, and we shall summarize the various aspects in the current discussion of this interesting proposal.

### 1. Spin glasses

To set the stage for the later discussion of the gauge glass and of the vortex glass we summarize in some detail the theory of spin glasses, the best understood model system for a glass today. We shall concentrate on two aspects of the theory, the mean-field picture and the scaling approach. For a more detailed discussion of the physics of spin glasses we refer the reader to the reviews of Binder and Young (1986), Mézard, Parisi, and Virasoro (1987), Dotsenko, Feigel'man, and Ioffe (1990), and Fischer and Hertz (1991).

The most basic concept in the theory of phase transitions is the concept of broken symmetry. The simplest example is the Ising ferromagnet described by a model Hamiltonian of the form (7.1) with spin variables $S_i \in \{-1, 1\}$ and uniform couplings $J_{ij} = J > 0$ restricted to nearest neighbors. In the high-temperature (paramagnetic) phase the (inversion) symmetry of the Hamiltonian is preserved, whereas the low-temperature (ferromagnetic) phase breaks this symmetry. Since a symmetry has been broken, we need an additional variable in order to describe the low-temperature phase, the order parameter, which for the above example of an Ising ferromagnet is the spontaneous magnetization $m(T) = N^{-1} \sum_i \langle S_i \rangle$, with $N$ the number of spins in the system and $\langle \cdots \rangle$ denoting thermodynamic average. Let us analyze in more detail the precise meaning we associate with this description. If we took the definition of averaging over the entire phase space in $\langle \cdots \rangle$ literally, the resulting order parameter $m(T)$ would always be zero, since the weights in the statistical sum for the two inversion-

symmetric phases with $m > 0$ and $m < 0$ are equal. Thus the broken symmetry has to be introduced by hand, e.g., via application of an infinitesimal symmetry-breaking field $H^+$, adding a term $\sum_i H^+ S_i$ to the system Hamiltonian. For $H^+ > 0$, the phase with $m < 0$ is favored over the "down" phase by a factor $\exp(2NH^+m)$. Taking the two limits $\lim_{H^+ \to 0} \lim_{N \to \infty}$ in this sequence, we obtain the desired finite order parameter describing the low-temperature phase. Essentially what we did was to break the *ergodicity* of the system as a consequence of breaking its *symmetry*. In the low-temperature phase, the two phases with spins "up" and "down" are separated from each other by infinite barriers ($N \to \infty$), and the phase space splits into two (energetically) disjoint parts. Therefore a system finding itself in one valley at some time will never find itself in the opposite valley at a later time, and hence we can replace time averages (the relevant quantity in an experiment) by a statistical average $\langle \cdots \rangle$ if we first break the symmetry of the system by hand, leading to the desired breaking of ergodicity. In a (spin) glass the symmetry of the Hamiltonian is never broken. Both the high- and the low-temperature phase are paramagnetic phases from the point of view of symmetry. However, ergodicity is broken in the low-temperature phase of a spin glass. Spin glasses, then, show broken ergodicity *without* an accompanying broken symmetry. Broken ergodicity implies the existence of a low-temperature phase described by a restricted phase space, separated from other parts of phase space by infinite barriers. The *order parameter* describing this phase therefore will not be the signature of a broken symmetry, but only testify to the presence of broken ergodicity. Such a spin-glass order parameter has been introduced by Edwards and Anderson (1975),

$$q_{\text{EA}} = \lim_{t \to \infty} q(t) , \tag{7.5}$$

with the time correlator $q(t)$ defined by

$$q(t) = \lim_{N \to \infty} \langle\langle S_i(t_\circ) S_i(t_\circ + t) \rangle_{\text{th}} \rangle_{\text{dis}} . \tag{7.6}$$

Here we denote the disorder average by the bracket $\langle \cdots \rangle_{\text{dis}}$ in order to express the appropriate sequence of taking the averages over statistical ($\langle \cdots \rangle_{\text{th}}$) and quenched ($\langle \cdots \rangle_{\text{dis}}$) variables.

Spin-glass order implies the development of *local* spontaneous magnetization in the system, for which the order parameter (7.5) gives a quantitative measure. If the system develops many equivalent phases $a$ (corresponding to the two phases "up" and "down" in the Ising ferromagnet), we can write

$$q_{\text{EA}} = \left\langle \sum_a P_a (m_i^a)^2 \right\rangle_{\text{dis}} , \tag{7.7}$$

where $P_a = \exp(-F_a/T)$ denotes the statistical weight of the phase $a$ with free energy $F_a$, and where $m_i^a$ is the local moment in phase $a$, $\langle S_i \rangle = \sum_a P_a m_i^a$. The Edwards-Anderson order parameter, which describes the mean-

square *single-valley* local spontaneous magnetization, in general is different from the equilibrium or statistical mechanics order parameter $q$ for a spin glass, which is given by

$$q = \langle\langle S_i \rangle_{\text{th}}^2 \rangle_{\text{dis}} = \left\langle \sum_{ab} P_a P_b m_i^a m_i^b \right\rangle_{\text{dis}} . \tag{7.8}$$

The statistical mechanics order parameter $q$ differs from $q_{\text{EA}}$ in having additional "intervalley" contributions, so that the difference $\delta q \equiv q_{\text{EA}} - q \geq 0$ is a measure of the degree of broken ergodicity, with $\delta q = 0$ if the system develops a unique low-temperature phase, $P_a = \delta_{a0}$. In general, however, one has to expect a more complicated structure of the phase space, with many valleys present describing different phases. The correlation between these phases is measured by the "overlap" distribution function

$$P(q) = \left\langle \sum_{ab} P_a P_b \delta(q - q^{ab}) \right\rangle_{\text{dis}} , \tag{7.9}$$

with

$$q^{ab} = \frac{1}{N} \sum_i m_i^a m_i^b .$$

Clearly, the statistical mechanics order parameter is simply the first moment of $P(q)$. As the correlations between the phases cannot exceed the mean-square magnetization of a single phase, we can identify the Edwards-Anderson order parameter with the maximal $q$ for which $P(q)$ is finite.

The experimentally measured uniform susceptibility $\chi$ showing a cusp at the freezing temperature $T_g$ is related to the order parameter $q$ via $\chi = (1 - q)/T$ (for symmetrically distributed interactions between different spins; Fischer, 1976). More precisely, in a "short-time" experiment in which the system finds itself in a single valley, we measure a susceptibility $\chi = (1 - q_{\text{EA}})/T$, whereas if the barriers separating different valleys are finite (e.g., due to the finite sample dimensions) and the experimental time scale is large enough, the equilibrium value $\chi = (1 - q)/T$ is measured. A very useful quantity is the spin-glass susceptibility $\chi_{\text{SG}}$, which corresponds to the ordinary susceptibility in a ferromagnet. Turning on a random field $h_i$, we can induce a nonzero order parameter $q$ even above the glass transition, $q = \chi_{\text{SG}} h^2$, with $h^2$ the variance of the random field $h_i$. The spin-glass susceptibility can be calculated from the correlator $C_{ij}$,

$$C_{ij} = \langle S_i S_j \rangle_{\text{th}} - \langle S_i \rangle_{\text{th}} \langle S_j \rangle_{\text{th}} , \tag{7.10}$$

$$\chi_{\text{SG}} = \frac{1}{N} \sum_{ij} \langle C_{ij}^2 \rangle_{\text{dis}} , \tag{7.11}$$

and diverges as the glass transition is approached from above. The analytical or numerical determination of $\chi_{\text{SG}}$ then allows for a simple determination of the glass transition temperature.

How can we determine the size of the order parameter of the system? The simplest standard method in the

theory of phase transitions consists in breaking the symmetry by hand and calculating the order parameter in mean-field theory. In spin glasses, both of these steps are far from trivial. First of all, since there is no broken symmetry in the spin-glass phase, we do not know the spatial form of the magnetic field $h_i^+$ singling out a particular valley. However, although this field is not known to us, it is known to the system itself (Blandin, 1978). Hence by introducing a second replica of the system (with identical quenched variables) and coupling the two systems by a term $-H^+ \sum_i S_i^\alpha S_j^\beta$, we can evaluate the order parameter from

$$q^{\alpha\beta} = \lim_{H^+ \to 0} \lim_{N \to \infty} \langle\langle (S_i^\alpha S_j^\beta)_{\text{th}} \rangle_{\text{dis}} , \qquad (7.12)$$

where the superscripts $\alpha$ and $\beta$ refer to different replicas. Furthermore, introducing replicas is also the standard tool for dealing with the average over the quenched variables. Evaluation of the thermodynamic potential $F = -T \langle \ln Z \rangle_{\text{dis}}$ is elegantly done by use of the replica trick, consisting in calculating the averaged partition function $\langle Z^n \rangle_{\text{dis}}$ for an $n$-fold replicated system and performing the limit

$$\langle \ln Z \rangle_{\text{dis}} = \lim_{n \to 0} \frac{\langle Z^n \rangle_{\text{dis}} - 1}{n} \qquad (7.13)$$

afterwards. Application of this replica idea allows us to arrive at a consistent mean-field solution for the Ising spin glass. One expects the mean-field theory for the transition to become exact in the infinite range limit for the interaction, a circumstance which motivated Sherrington and Kirkpatrick (1975) to study the Ising limit of Eq. (7.1) with $\Delta_{ij} = \langle J_{ij}^2 \rangle_{\text{dis}} = J^2/N$ independent of distance. Using the replica trick one arrives at a self-consistency condition for the order parameter $q^{\alpha\beta}$. Assuming a replica-symmetric solution $q = q^{\alpha\beta}$, $\alpha \neq \beta$, this equation takes the form

$$q = \int \frac{dx}{\sqrt{2\pi}} e^{-x^2/2} \tanh^2 \frac{J\sqrt{q}\,x}{T} , \qquad (7.14)$$

with a solution $q = 0$ at high temperatures, $T > T_g = J$, approaching unity for zero temperature, and vanishing at $T_g$ according to $\sqrt{q} \propto (T_g - T)^{1/2}$. Unfortunately, this solution turned out to be unstable below $T_g$ (negative eigenvalues in the fluctuation spectrum, negative entropy), more generally, below a line $H_{\text{AT}}$ in the $H$-$T$ phase diagram if a finite magnetic field $H$ is present. The line $H_{\text{AT}}(T)$ is called the de Almeida-Thouless line (de Almeida and Thouless, 1978) and is associated with the occurrence of irreversibility and remanence for temperatures and magnetic fields below this line. It was Parisi (1979, 1980) who first presented a consistent solution of the Sherrington-Kirkpatrick model which breaks the replica symmetry. The order parameter of the system is described by a monotonically increasing *order-parameter function* $q(x, T, H)$, $0 \leq x \leq 1$. The susceptibility $\chi$ is given by

$$\chi = \frac{1}{T} \left[ 1 - \int_0^1 dx\, q(x) \right] , \qquad (7.15)$$

and the Edwards-Anderson order parameter can be obtained from the maximum value of $q(x)$, due to monotonicity,

$$q_{\text{EA}} = q(1) . \qquad (7.16)$$

In fact, $q(x)$ describes the temporal evolution of the order parameter $q(t)$ as given by Eq. (7.6) on different time scales, which all diverge in the thermodynamic limit, with $t_{x=1}$ the shortest and $t_{x=0}$ the largest diverging time (Sompolinsky, 1981). For zero magnetic field, $q(x=0) = 0$ and hence $q(t_{x=0}) = 0$, that is, $q(t)$ is finite for the smallest, but zero for the largest diverging time scale in the system.

The second important quantity in the Parisi solution is the overlap distribution function (7.9), which is related to the order parameter function $q(x)$ via

$$P(q) = \int_0^1 dx\, \delta[q - q(x)] = \frac{dx}{dq} . \qquad (7.17)$$

The Parisi solution for $P(q)$ consists in a sharp $\delta$ peak at $q_{\text{EA}}(T)$, with a smooth continuation extending down to $q = 0$ at zero applied field. This solution is interpreted in the following way: As a finite fraction of the total weight is in the $\delta$ peak at $q_{\text{EA}}$, the statistical mechanics of the system is dominated by a single phase. The remaining finite weight extending to smaller $q$ values indicates the presence of many valleys with configurations resembling each other to all possible degrees. For finite fields $H$ the weight in the continuous part decreases and is shifted to the peak at $q_{\text{EA}}$ until all of the weight has been accumulated in the peak as we cross the de Almeida-Thouless line. This scenario naturally explains the occurrence of effects such as remanence and irreversibility as the consequence of the splitting of the phase space into distinct valleys below the de Almeida-Thouless line.

The mean-field picture of the spin glass describes the glass transition as a generic thermodynamic phase transition into a phase with a nontrivial broken ergodicity characterized by the existence of many competing ground states separated by infinite barriers. We cannot go deeper into the analysis of the structure of the phase space here, which would lead us to the notions of hierarchical structures and ultrametricity (Mézard *et al.*, 1984a, 1984b; Rammal *et al.*, 1986). Instead, we turn to an alternative approach to describing the physics of spin glasses, based on scaling ideas, an approach that goes back to McMillan (1984a, 1984b, 1984c), Bray and Moore (1984, 1985), and Fisher and Huse (1986; see also 1988a, 1988b). Let us make clear from the beginning that the scaling approach differs from the exact mean-field treatment discussed above by its essentially phenomenological character. To date, no first-principles microscopic justification for the scaling approach to the spin-glass problem has been presented.

Real spin glasses are characterized by short-range in-

teractions, and their physical realization involves $d=2$ or $d=3$ space dimensions. On the other hand, the mean-field approach is expected to become exact for infinite-range interactions or in higher dimensions (in fact, the upper critical dimensionality for spin glasses is $d_u=6$). Hence typical experimental realizations are quite far away from the region where mean-field theory is a good guide. A very helpful tool for dealing with this situation is found in the renormalization or scaling approach, and we briefly discuss the main achievements of this method.

The basic idea of the scaling approach is to investigate the flow of the coupling constants in the Hamiltonian under iterative integration over short-wavelength degrees of freedom. This idea suggests that we study the effective coupling $J(L)$ across the sample as the basic quantity describing the phase of the system. Consider a short-range (nearest-neighbor) coupled Ising spin glass of size $L^d$ in $d$ space dimensions. The free energy under free boundary conditions is denoted by $F(L)$. Reversing the $L^{d-1}$ spins on one end of the block while keeping those on the opposite side fixed, and denoting the corresponding free energy by $F_r(L)$, we obtain the effective coupling $J(L)$ across the sample from

$$J(L)=F(L)-F_r(L) \ . \tag{7.18}$$

The above procedure introduces a domain wall into the sample. For an ordered system (e.g., an Ising ferromagnet), $J(L)$ scales with system size according to $J(L) \propto L^{\theta}$, $\theta=d-1$, producing a lower critical dimension $d_l=1$. In a disordered sample, the domain wall adjusts to the energy landscape in a nontrivial way (see Sec. IV.F above), leading to a reduction of the exponent $\theta < d-1$ and hence to an increase in the lower critical dimensionality of the system. The task then is to determine the scaling exponent $\theta$ for the effective coupling constant $J(L)$; for $\theta < 0$ the coupling decreases with increasing length $L$, and the system is in a disordered (paramagnetic, high-temperature) phase, while a positive exponent $\theta > 0$ is the signature of an ordered (rigid) low-temperature phase. In a disordered system the situation is somewhat more complicated, as the couplings $J(L)$ are random objects, and the decisive quantity to study is the distribution function $P[J(L)]$. For large $L$ this distribution function takes the scaling form

$$P[J(L)]=\frac{1}{L^{\theta}}f\left[\frac{J(L)}{L^{\theta}}\right] \ . \tag{7.19}$$

As the critical point, $\theta=0$ and thus $P(J)=f(J)$ independent of $L$. The exponent $\theta$ and the scaling function $f$ can be determined by numerical simulations or by some renormalization procedure. Numerical results for the Ising model (Bray and Moore, 1984) indicate that the lower critical dimensionality of this system is between $d=2$ and $d=3$. Bray and Moore find for the exponent $\theta$ the values $\theta \approx -0.291 \pm 0.002$ for $d=2$ and $\theta \approx 0.19 \pm 0.01$ for $d=3$. Furthermore, the scaling function $f(x)$ turns out to be continuous with a finite weight as $x \to 0$. A

renormalization-group calculation produces similar results (Southern and Young, 1977), with $\theta=[d-1+\log_2(1-2/\pi)]/2$, resulting in $\theta(d=2) \approx -0.23$ and $\theta(d=3) \approx 0.26$. As argued by Fisher and Huse (1986), the expression $(d-1)/2$ in fact provides an upper bound for the exponent $\theta$, $\theta \le (d-1)/2$. For vector spins ($XY$ model, Heisenberg model), numerical results indicate that the lower critical dimension is $d_l=4$ (Morris et al., 1986).

Following Fisher and Huse (1986; see also 1988a, 1988b), we can describe the spin-glass phase by studying the low-lying excitations in the system. Fisher and Huse hypothesize that these excitations consist in compact droplets of size $L$, with of the order of $L^d$ spins flipped relative to the ground state, which is assumed to be uniquely defined (up to the trivial inversion symmetry $S_i \to -S_i$), in contrast to the mean-field solution put forward by Parisi. The surface of these droplets is presumably fractal, with a dimension $d-1 \le d_s \le d$. The excitation energy of the droplets scales in the same manner as the domain wall introduced above, $F_d(L) \sim JL^{\theta}$, whereas the barriers to be surpassed in order to create such a droplet scale with a different exponent $\psi$, $U_d(L) \sim L^{\psi}$. The probability distribution for droplets of energy $F_d(L)$ finally has the scaling form (7.19). The finite weight of the scaling function $f(x)$ for small $x$ then implies a nonzero density of states at arbitrarily low energies. Of all the available low-energy droplets of size $L$ with energies distributed according to Eq. (7.19), only a fraction $T/JL^{\theta}$ (those with energies less than, or of the order of, $T$) are thermally active at low temperatures. It is these droplets which determine the spatial and temporal evolution of the spin-glass phase at low temperatures. In particular, the spin-glass correlation function $\langle C_{ij}^2 \rangle_{\text{dis}}$, with $C_{ij}$ given by Eq. (7.10), vanishes algebraically in the spin-glass phase. The finite contributions to $C_{ij}$ are provided by those droplets which contain both spins $i$ and $j$, hence

$$\langle C_{ij}^2 \rangle_{\text{dis}} \sim \frac{T}{J|i-j|^{\theta}} \ . \tag{7.20}$$

The stiffness of the spin-glass phase producing barriers $U_d(L) \sim JL^{\psi}$ against droplet excitations leads to a very slow, i.e., logarithmic, dynamics. At time $t$, the relevant barriers in the system are of size $T \ln(t/t_0)$, allowing rearrangement of spatial regions of size

$$L(t) \propto \left[\frac{T}{J}\ln\frac{t}{t_0}\right]^{1/\psi} \ . \tag{7.21}$$

Again, the fraction of active droplets scales according to $L^{-\theta}$, and hence the temporal correlation function $C(t)=\langle\langle S_i(0)S_i(t)\rangle_{\text{th}}-\langle S_i \rangle_{\text{th}}^2\rangle_{\text{dis}}$ decays on a logarithmic time scale,

$$C(t) \propto \left[\frac{J}{T}\frac{1}{\ln(t/t_0)}\right]^{\theta/\psi} \ . \tag{7.22}$$

The Fourier transform of Eq. (7.22), i.e., the noise spectrum of spin fluctuations, then exhibits $1/f$ behavior up to logarithmic corrections,

$$C(\omega) \propto |\omega \ln\omega|^{-(1+\theta/\psi)} . \qquad (7.23)$$

The trivially broken ergodicity in the droplet model leads to quite different predictions for the physics of the spin-glass phase than does the mean-field theory. For example, there is no de Almeida-Thouless line within the scaling theory of spin glasses; the spin-glass phase transition gives way to a simple crossover at finite magnetic fields. However, a fundamental feature of the mean-field theory, the extreme sensitivity of the energy landscape in phase space to changes of external variables such as temperature or magnetic field, is also present in the scaling theory of spin glasses. Consider a perturbation changing the bond strength by an amount of order $\delta J$. This perturbation will then change the wall energy of the droplet by an amount of the order of $\delta J L^{d_s/2}$. For $\theta < d_s/2$ this perturbation will always dominate the original wall energy $J L^\theta$ at large length scales, implying that on scales

$$L > L^* \propto \left[ \frac{J}{\delta J} \right]^{1/(d_s/2 - \theta)} \qquad (7.24)$$

the ground state of the spin glass and its low-lying excitations will be completely changed. Since $\theta \leq (d-1)/2$ (Fisher and Huse, 1986) this sensitivity to external fields always has to be expected in spin glasses.

A few remarks about the (continuous) glass transition itself. Within the scaling approach, the static and dynamic features of the transition are described by a spin-glass correlation length $\xi_{SG}(T)$ and a relaxation time $\tau_{SG}(T)$, which both diverge as the glass transition $T_g$ is approached,

$$\xi_{SG}(T) \propto |T - T_g|^{-\nu} , \qquad (7.25)$$

$$\tau_{SG}(T) \propto [\xi_{SG}(T)]^z \propto |T - T_g|^{-\nu z} , \qquad (7.26)$$

while the order parameter $q$ and its associated susceptibility $\chi_{SG}$ behave according to

$$q(T) \propto (T_g - T)^{-\beta} , \qquad (7.27)$$

$$\chi_{SG}(T) \propto |T - T_g|^{-\gamma} . \qquad (7.28)$$

Within mean-field theory the exponents take the values $\nu = 1/2$, $z = 4$, $\beta = 1$, and $\gamma = 1$. Corrections to these mean-field results have been calculated within $\varepsilon = d_u - d$ expansion. Due to the appearance of a cubic term in the effective Hamiltonian, the upper critical dimensionality $d_u$ of the system is shifted to $d_u = 6$. As $d$ drops below $d_u$, the exponents $\nu$ and $z$ both increase. However, extrapolation down to $d = 3$ seems of little use. Numerical work for the $d = 3$ Ising model consistently produces values $\nu \approx 1.2 - 1.4$, $z \approx 5 - 6$, $\beta \approx 0.5$, and $\gamma \approx 3$ (Young, 1984; Bhatt and Young, 1985; Ogielski, 1985; Ogielski and Morgenstern, 1985). The last two exponents were obtained from the scaling relations $\gamma = \nu(2 - \eta)$ and

$\beta = \nu(d - 2 + \eta)/2$, with $\eta \approx -0.25$ the exponent for the spin correlator $\langle S(0)S(r) \rangle \propto r^{-(d-2+\eta)}$.

Above, we have reviewed two quite different approaches to spin-glass theory, the mean-field theory, which is an *exact* description for a model with an infinite range of interactions or in high dimensions, and the droplet model, which, it is hoped, describes the situation in real three-dimensional spin glasses with short-range interactions, but which is based on rather strong assumptions and cannot be derived from some microscopic Hamiltonian. A natural question to ask, then, is, which of the two approaches is more appropriate for an accurate description of real spin glasses? The different organization of the phase space obtained/assumed in these two models makes this a very interesting question. At present, there is no clear answer, but most probably both approaches capture some essential features of the relevant physics of real spin glasses. Neither of the two models is fully consistent with the experimental data, and hence an appropriate synthesis of them remains to be found. In the following, we briefly describe one possible approach to this synthesis by concentrating on the *critical* behavior of spin glasses. This synthesis will comprise features from both the mean-field solution (hierarchical organization of relaxation times) and the droplet model (superspins).

Let us first recall some well established features of the glass transition in real spin glasses. Above $T_g$, this transition has been explored experimentally both by static magnetization experiments [in which case the relevant quantity is the nonlinear magnetic susceptibility $\chi_{nl} = \partial^3 M / \partial h^3 |_{h \to 0} = [\chi_{SG} - 2/(3T^2)]/T \propto (T - T_g)^{-\gamma}$] and by ac magnetic susceptibility measurements, from which the exponent $\nu z$ of the spin-glass relaxation time $\tau_{SG} \propto (T - T_g)^{-\nu z}$ (critical slowing down) can be determined. The results from both kinds of experiment are fairly consistent with the heuristically proposed scaling behavior (7.28) and (7.26), and the values for the exponents $\gamma$ and $\nu z$ drawn from experiments agree fairly well with those obtained from Monte Carlo simulations (see, for example, the review of Binder and Young, 1986). Whereas mean-field theory at least does make a prediction for such a scaling behavior, the results for the exponents differ considerably from the data. A natural way to improve upon the mean-field values is by means of $\varepsilon = d_u - d$ expansion around $d_u = 6$; however, extrapolation down to $d = 3$ cannot be hoped to be even qualitatively reliable. On the other hand, the droplet model does not make any prediction concerning these exponents, since it concentrates on the glass phase itself rather than on the critical regime.

A semiquantitative analytical approach for the calculation of the critical exponents in real, three-dimensional spin glasses has been developed by Ioffe and Feigel'man (1985) and further improved by Dotsenko, Feigel'man, and Ioffe (1990). The basic idea of this approach is to consider an Edwards-Anderson model with a large number of nearest neighbors $z$ (so that it goes over to a

Sherrington-Kirkpatrick model in the limit $z \rightarrow \infty$), and to construct a renormalization-group procedure. The starting point is an expansion of the slowly decaying components $m_i = \langle S_i \rangle_{\text{fast}}$ of the magnetization field in terms of the eigenmodes $\sigma_\lambda(i)$ of the coupling matrix $J_{ij}$,

$$\sum_j J_{ij}\sigma_\lambda(j) = J_\lambda \sigma_\lambda(i) , \tag{7.29}$$

$$m_i = \sum_\lambda m_\lambda \sigma_\lambda(i) . \tag{7.30}$$

Here, $\langle \cdots \rangle_{\text{fast}}$ denotes the average over the fast, i.e., noncritical, modes. The most relevant eigenmodes with large $m_\lambda$ near the transition $T_g$ correspond to *localized* eigenfunctions $\sigma_\lambda(i)$, with eigenvalues $J_\lambda$ close to the mobility edge $J_c$. At a moderate distance $(T - T_g)/T_g$ away from the transition point, the system behaves like a superparamagnet, with superspins corresponding to the spin clusters as defined by the relevant localized modes $\sigma_\lambda(i)$. The crucial difference between the present situation and a conventional superparamagnet is that the extent of the superspins, as given by the localization lengths of the wave functions $\sigma_\lambda(i)$, is much larger than that of the rigid spin clusters relevant in the conventional case. As a consequence, these superspins are strongly overlapping in real space, and the value of the local magnetization $m_i$ is determined by a large number of such fractal clusters. Upon decreasing the temperature, we find that the interaction between these clusters becomes strong and random in sign, so that they can be described again by an Edwards-Anderson model, and the renormalization step is completed. Hence we have constructed a discrete renormalization-group transformation from the original spins $S_i$ to the new "superspins" $S_\lambda^{(1)} = \text{sgn}(m_\lambda)$. Further decrease of the temperature $T$ then introduces new generations of superspins. The sequence of temperatures $T_n$ marking the appearance of a new generation of superspins converges to a finite value, which is identified with the glass transition temperature, $\lim_{n \rightarrow \infty} T_n = T_g$, since both the spin-glass susceptibility $\chi_{\text{SG}}(T)$ and the relaxation time $\tau_{\text{SG}}(T)$ diverge at this point. Within the present analysis, the critical exponents $\gamma$ and $\nu z$ are related to exponents characterizing the singular behavior of the eigenfunctions $\sigma_\lambda(i)$ close to the mobility edge, $J_\lambda \approx J_c$. By determining these "localization" exponents from a numerical diagonalization of a large $(20^3)$ random matrix $J_{ij}$ (nearest-neighbor coupling; see Dotsenko, Feigel'man, and Ioffe, 1990), Dotsenko *et al.* have found spin-glass critical exponents for the Ising model with results that are in reasonable agreement with the experimental and with the Monte Carlo values.

The most interesting feature emerging from the above analysis, however, is the hierarchical nature of the slowly relaxing magnetization modes relevant for the critical behavior near $T_g$. At some intermediate temperature $T_{n+1} < T < T_n$, the long-time decay of the magnetization $S_i(t)$ in some site $i$ is governed by all those modes $S_\lambda^{(1)}$ having a considerable amplitude at this site. In turn, the

long-time relaxation of the superspin $S_\lambda^{(1)}(t)$ is governed by a large number of modes on the next hierarchy level $S_\lambda^{(2)}(t)$, and so on. The longest relaxation time $\tau_{\text{SG}}(T)$ in the system is then given by the effective dynamic time scale of the $n$th-level superspin $S_\lambda^{(n)}(t)$. The crucial difference between the picture presented here and the simplest droplet approach is the hierarchical organization of the relaxation. Within the droplet model, droplets of different sizes $L$ [and correspondingly different relaxation times $\tau_L \propto \exp(JL^\psi/T)$] do not overlap and hence flip independently of each other. By contrast, the hierarchical organization of the modes implies that fast modes are strongly coupled to slow ones as the former are "embedded" into the latter. The origin of the critical hierarchy as developed by Ioffe and Feigel'man (1985) seems to be rather generic for a strongly frustrated system in the absence of any apparent spatially regular structure, i.e., when the breaking of ergodicity is not accompanied by a breaking of symmetry (see also Palmer *et al.*, 1984, where the appearance of a hierarchically constrained dynamics is discussed from a very general point of view). It seems very reasonable that the same kind of hierarchical organization should also survive at low temperatures, $T < T_g$, within the glass phase itself (at least for the case of a sufficiently large coordination number $z$). However, a quantitative theory corresponding to the renormalization-group approach discussed above and extending these ideas to $T < T_g$ still has to be developed. Qualitatively, a first step in this direction has been taken by Villain (1986), who noticed that within a generalized droplet-like approach one can assume that droplets are not just simple compact objects but rather are organized in a hierarchical way, with smaller droplets embedded within bigger ones. Based on some rather plausible assumptions, he showed that in such a generalized droplet model a de Almeida-Thouless line is recovered, i.e., the model shows a true spin-glass transition in a finite magnetic field, in contrast to the simplest droplet model proposed by Fisher and Huse (1986).

Let us remember that the hierarchical organization of phase space into valleys is an intrinsic feature of the mean-field solution with replica symmetry breaking, which, combined with the above discussion, gives some credit to the idea that a kind of hierarchical organization might indeed be relevant in the low-temperature phase of a real three-dimensional spin glass. Moreover, this point of view is also supported by recent experiments on insulating spin glasses by Lefloch, Hamman, Ocio, and Vincent (1992, ac magnetic susceptibility) and in mesoscopic samples of metallic spin glasses by Israeloff, Alers, and Weissman (1991; second spectrum of the magnetic noise, i.e., spectrum of calculation in the noise power; see also Weissman *et al.*, 1992). In both cases it has been shown that the data are in much better agreement with a hierarchical model of relaxation than with a parallel dynamics as produced by the simplest droplet model of Fisher and Huse (1986). However, it should be noted that on a general level both the simple droplet picture

and the hierarchical model produce roughly similar answers. In this sense, the above-mentioned experiments, which are able to distinguish between the two approaches, are highly nontrivial.

The main challenge in this field then is to develop a consistent theory of the spin-glass phase for a realistic three-dimensional spin-glass model, which reproduces the hierarchical organization of states. Still, in the absence of such a theory, important insights can be gained from the mean-field theory if one accepts the idea that the hierarchical organization of valleys is relevant for a real spin-glass system.

## 2. Gauge glass

It seems that the interest in gauge glasses is an outgrowth of studies of spin glasses, particularly the $XY$ spin glass, in connection with the problem of "trivial" disorder, i.e., disorder that can be removed by a gauge transformation (Fradkin *et al.*, 1978). Here we are interested in the gauge glass as a model system for granular superconductors and as a simplified model for studying glassiness in bulk superconductors. Within this context, the first (numerical) study of three-dimensional granular superconductors in a magnetic field was that of Shih, Ebner, and Stroud (1984, see also Ebner and Stroud, 1985). Upon an increase of the magnetic field **H**, they found a transition from a "ferromagnetic" to a "spinglass"-type phase. The crossover between these two phases took place at field values $H_g$ producing of the order of one flux quantum per plaquette, leading to a large frustration between the phases $\varphi_i$. The transition temperature $T_g(H)$ into the superconducting state, as obtained from a calculation of the stiffness of the phase under a change of boundary conditions (helicity modulus), dropped rapidly with increasing field and saturated above the critical field $H_g$. Below the freezing temperature $T_g(H > H_g)$, typical glassy effects such as remanence and irreversibility appeared. However, no definite conclusion about the existence of a generic thermodynamic phase transition could be given.

The mean-field phase diagram for a disordered granular superconductor near percolation was worked out by John and Lubensky (1985, 1986). In addition to the usual Meissner phase at very low field and an Abrikosov phase at intermediate field values, they found a glass phase for fields exceeding the critical value $H_g \simeq \Phi_o/\xi_p^2$, with $\xi_p$ the percolation coherence length. This glass phase was characterized by a vanishing averaged condensate wave function $\langle\langle \Psi \rangle_{th} \rangle_{dis} = 0$, but a finite Edwards-Anderson order parameter $\langle |\langle \Psi \rangle_{th}|^2 \rangle_{dis}$. The applied magnetic field penetrated completely, with fluctuations due to frozen Josephson current loops decaying only as a power law with distance. A glass phase was also present locally within the cores of the individual vortices in the Abrikosov phase. Qualitatively, the transition to the glass at $H \simeq H_g$ can be understood as being due to the overlap of the individual vortex cores, with $H_g$ adopting the role of the upper critical field $H_{c_2}$ in the mean-field phase diagram of the homogeneous bulk superconductor. The calculation was carried out in a replica field-theoretic language, with a solution that did not break the replica symmetry. The upper critical dimension above which these mean-field results are expected to become exact is $d_u = 6$.

The use of the (unstable) replica-symmetric solution leads to the disappearance of superconductivity in the gauge glass in terms of a vanishing of the superfluid density $\rho_s$, as defined by the relation $\delta \mathbf{j} = -\rho_s \delta \mathbf{A}$. A connection between the absence of replica symmetry breaking and the vanishing superfluid density can be concluded from a comparison of the present problem with a study of the $XY$ spin glass by Sompolinsky, Kotliar, and Zippelius (1984), who find a finite transverse stiffness (the analog of $\rho_s$) in the glass phase within a replica symmetry-breaking approach. A consistent mean-field theory of the gauge glass exhibiting superconductivity has been developed by Vinokur, Ioffe, Larkin, and Feigel'man (1987). Instead of using the replica formalism, they developed an alternative method capable of handling a nontrivially broken ergodicity. Within this approach, an actual state [characterized by the point $(H_1, T_1)$ in the phase diagram] of the system is considered to be a functional of the path in the $(H, T)$ plane along which this point has been reached. The common view that a state within the glass phase depends on its detailed history is borne out quite naturally within this approach. The simplest example of such a history dependence is the difference between the field-cooled (FC) and zero-field-cooled (ZFC) magnetic susceptibilities, as obtained within a replica symmetry-breaking mean-field solution for the spin glass, $\chi_{FC} - \chi_{ZFC} \propto (T_g - T)^2$. The method developed by Vinokur *et al.* allows one to study this kind of phenomenon within a very general context, i.e., without the limitation of having to remain within the linear-response regime. The basic quantities to be determined are the correlation function $q(t,t') = \langle\langle S_i \rangle^t \langle S_i^* \rangle^{t'} \rangle_{dis}$, where $S_i = \exp(i\varphi_i)$ and the average $\langle \cdots \rangle^t$ denotes a thermal average taken with fixed external parameters $(H(t), T(t))$, and the long-time response function $\Delta(t,t') = \langle \partial \langle S_i \rangle^t/\partial h_i^{t'} \rangle_{dis}$. Here $h_i$ is not a real magnetic field that couples via the gauge potential to the phases $\varphi_i$, but is a fictitious external field, which is linearly coupled to the spins, $\mathcal{H}_h = -\sum_i h_i(S_i + S_i^*)$. The order parameter $q(t,t')$ then measures the overlap between frozen spin configurations at different times $t$ and $t'$. The very existence of the response function $\Delta(t,t')$, which does not decay to zero in the long-time limit $t - t' \to \infty$, reflects the presence of a nontrivially broken ergodicity in the system, and hence the approach is indeed qualitatively equivalent to a replica symmetry-breaking solution. Given a cooling path $(H(t), T(t))$, the task then consists in solving the pair of coupled nonlinear integral equations for the two functions $q(t,t')$ and $\Delta(t,t')$ and there-

by obtaining a complete description of the history-dependent final state. The same method can be used, as well, in the spin-glass problem (Ioffe, 1988; Freixa-Pascual and Horner, 1990). In fact, as has been shown by Freixa-Pascual and Horner (1990), the corresponding equations in the spin-glass problem can be reduced to the Parisi equations if one assumes that both $q$ and $\Delta$ depend only on the time difference $t - t'$, which implies an additional thermodynamic averaging over all possible valleys. The basic difference between the "path-dependent" mean-field approach and the Parisi solution is that, in the former case, the system is considered to be trapped in some specific valley in phase space and follows the evolution of this valley as the external parameters $H$ and $T$ are changed, whereas in the latter case a complete equilibration is considered to have occurred.

An explicit calculation of the solutions $q$ and $\Delta$ has been carried out for the two simplest cooling paths shown in Fig. 28. Along path $\alpha$, the sample is cooled down to $T_1$ at fixed field $H_1$, whereas along $\beta$, cooling to $T_1$ is done in a field $H_1 - \Delta H$ with a subsequent increase $\Delta H$ in field at $T_1$. The final magnetization $M_\alpha$ as obtained along $\alpha$ turns out to be zero, hence there is *no Meissner effect* in the gauge glass. On the other hand, a finite magnetization $M_\beta$ is found when following path $\beta$, with

$$\Delta M = M_\beta - M_\alpha \propto -\Delta H (T_g - T)^3 \ . \tag{7.31}$$

Hence there is *diamagnetic screening* in the system. The result (7.31) then implies a finite value $\rho_s \propto (T_g - T)^3$ for the superfluid density, in agreement with the result of Sompolinsky, Kotliar, and Zippelius (1984) obtained via a replica symmetry-breaking approach. Note that the present method allows us to go beyond the linear-response regime and explore the full nonlinear dependence of $M_{\mathrm{irr}}$. The general expression for the irreversible magnetic response is (Vinokur *et al.*, 1987)

$$-M_{\mathrm{irr}}(t) \propto \int_0^t dt' q(t,t') \Delta(t,t') [H(t) - H(t)'] \ , \tag{7.32}$$
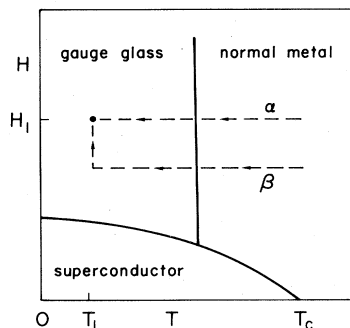


FIG. 28. Two cooling paths leading to a different response in the gauge glass. The final magnetization along path $\alpha$ is zero, whereas a finite diamagnetic moment appears along $\beta$. Hence the gauge glass shows no Meissner effect but finite diamagnetic screening, i.e., the superfluid density is nonzero.

where the functions $q(t,t')$ and $\Delta(t,t')$ have to be determined for the given cooling path $[H(t),T(t)]$. In the limit $\Delta H \to 0$, the result (7.32) reduces to the linear-response formula (7.31). As shown by Dotsenko, Feigel'man, and Ioffe (1990), the linear-response regime extends up to fields $\Delta H \simeq H_{nl} \propto T_g - T$, whereas for $\Delta H \gg H_{nl}$ the irreversible magnetization approaches a maximum value $\Delta M_c \propto (T_g - T)^4$, which is the analog of the critical current density.

The history dependence of the magnetic response is the main qualitative feature of glassy superconductivity. The first observation of this kind of behavior in the new high-temperature superconductors is due to Müller, Takashige, and Bednorz (1987). In their investigations on ceramic samples of $La_{2-x}Ba_x CuO_{4-y}$, they observed that the result $M_{FC}(H,T)$ of a field-cooled magnetization differs from the zero-field-cooled value $M_{ZFC}(H,T)$ for a final state $(H,T)$ below some characteristic line $H_g(T) \propto (T_g - T)^{3/2}$, which therefore was identified with a transition line separating ergodic from nonergodic (glassy) behavior. Note that the two values $M_{FC}(H,T)$ and $M_{ZFC}(H,T)$ are just the magnetization values for the two paths $\alpha$ and $\beta$ discussed above, with $\Delta H = H$, and the nonergodic response $M_{\mathrm{irr}} = M_\beta - M_\alpha$ is expected to be a nonlinear one.

The general status of the mean-field theory of gauge glass is analogous to that for the spin-glass problem: The mean-field analysis applies to the case of high dimensions $d > d_u = 6$ or to a model with an infinite interaction range. Again, a droplet-like model can also be formulated for the gauge glass, and again it will differ quite appreciably in its predictions regarding the behavior of the system below the irreversibility line. In particular, within a droplet approach the irreversible magnetization $M_{\mathrm{irr}}$ will not remain stationary, but will decay on a logarithmic time scale according to

$$M_{\mathrm{irr}}(t) \propto \left[ \ln \frac{t}{t_o} \right]^{-1/\mu} , \tag{7.33}$$

thus reflecting one of the crucial differences between the two approaches—the presence or absence of a nontrivially broken ergodicity. At the moment it is unclear whether a hierarchically organized droplet model, like that discussed for the spin-glass problem above, will show an irreversible magnetic moment that decays asymptotically to zero. Hence the description of real gauge glasses as realized by a three-dimensional superconducting network in a magnetic field suffers from the same problems as does the description of the spin-glass systems. In addition, the very existence of a three-dimensional gauge-glass phase can be questioned. An analytical treatment of this problem along the lines of the renormalization-group approach described in Sec. VII.A.1 above shows that the gauge-glass transition in 3D is very similar to the Ising spin-glass transition (Dotsenko, Feigel'man, and Ioffe, 1990). The main difference between the two models consists in the replacement of the real symmetric cou-

pling matrix $J_{ij}$ in the spin-glass case by a Hermitian random matrix for the gauge glass. Accordingly, the eigenmodes $\sigma_\lambda(i)$ constituting an orthogonal ensemble in the spin-glass model are then replaced by a unitary ensemble in the gauge glass. Remarkably enough, the same kind of analysis carried out for an $XY$ (or any other $n$-vector) spin glass turns out to be significantly different from the Ising case. Thus analysis of the 3D gauge glass and of the $XY$ spin glass shows that the two models belong to different universality classes, in spite of their close similarity within a mean-field theory.

Very recently, much effort has been invested in the determination of the lower critical dimension of the gauge glass, with a strong emphasis on numerical methods. The first numerical study addressing the *existence* of a true phase transition in the gauge glass is that of Huse and Seung (1990), who concentrate on the (possible) divergence of the gauge-glass susceptibility $\chi_{GG} = \sum_j \langle |C_{ij}|^2 \rangle_{dis}$ on approaching the phase transition, where in correspondence to Eq. (7.10),

$$C_{ij} = \langle e^{i(\varphi_i - \varphi_j)} \rangle_{th} . \qquad (7.34)$$

In their comparative study of the Ising spin glass ($\varphi_i \in \{0, \pi\}$, $A_{ij} \in \{0, \pi\}$), the $XY$ spin glass ($A_{ij} \in \{0, \pi\}$), and the gauge glass, Huse and Seung find that gauge glass is more similar to the Ising than to the $XY$ model, in agreement with the analytical results of Dotsenko, Feigel'man, and Ioffe (1990). Since the Ising model seems to have a finite-temperature glass transition in 3D, whereas the $XY$ model does not (see the discussion in Sec. VII.A.1 above), this result provides some evidence for the existence of a generic thermodynamic glass phase in the $d = 3$ gauge-glass model. As pointed out by Huse and Seung, this result is actually rather unexpected, since at first sight the gauge glass looks much more like the $XY$ than the Ising model. The $XY$ spin-glass Hamiltonian is invariant under global proper and improper rotations in spin space, whereas the gauge glass has a smaller symmetry group, restricted to global proper rotations (due to the presence of the magnetic field, the time-reversal symmetry or reflection symmetry $\varphi_i \rightarrow -\varphi_i$ is broken). The Ising spin-glass Hamiltonian, on the other hand, is only symmetric under global inversion of the spins, corresponding to a proper rotation $\varphi_i \rightarrow \varphi_i + \pi$, which is again a subgroup of the symmetry group of the gauge glass. Hence the absence or presence of *continuous* rotational symmetry seems to be of less importance than the breaking of time-reversal symmetry in the gauge glass.

A different approach was taken by Reger *et al.* (1991; see also Fisher, Tokuyasu, and Young, 1991), who concentrate on the gauge glass and base their analysis on the determination of the scaling behavior of the domain-wall energy $J(L) \propto L^\theta$. A zero-temperature calculation provides results consistent with $\theta(d = 3) \simeq 0$, indicating that the 3D gauge glass is more marginal than the Ising spin glass, which is characterized by an exponent $\theta(d = 3) \simeq 0.2$. Second, a finite-temperature Monte Carlo

simulation was carried out in order to investigate the scaling behavior of the current $I = \partial J / \partial \Theta$ and the stiffness $Y = \partial^2 J / \partial \Theta^2$ under an infinitesimal rotation $\Theta$ of the boundary conditions [in this terminology the domain-wall energy $J(L)$ involves a finite rotation $\Theta = \pi$]. Near the glass transition temperature one expects a scaling behavior $I(L, T) = i[L / \xi_{GG}(T)]$, with $\xi_{GG}(T) \propto (T - T_g)^{-\nu}$ the gauge-glass correlation length. The current $I(L, T)$ then is expected to become independent of $L$ at $T_g$ and to "splay out" for different $L$ at temperatures below and above the transition temperature $T_g$. Such behavior indeed could be observed in the analysis of Reger *et al.*, with $T_g \approx 0.45 \pm 0.05$ (in units of the elementary coupling $J$ between the grains). A scaling plot of $I(L, T)$ produces an exponent $\nu \approx 1.3 \pm 0.4$ for the glass correlation length, close to the Ising value. From a scaling analysis of the time needed to reach equilibrium at $T_g$, a dynamic exponent $z \approx 4.7 \pm 0.7$ is obtained.

It is well known that the universality class of spin (glass) systems depends on the spatial as well as the spin dimensionality of the model. That *symmetry* also is a relevant issue in the search for a true thermodynamic glass phase has become clear in comparative studies involving different types of spin glasses by Cieplak *et al.* (1991, 1992) and by Gingras (1992). The models studied within the present context are of the $XY$ or Ising type and involve the Ising and $XY$ spin glasses themselves ($I$ and $XY$), the gauge glass with random gauge field $A_{ij}(GG)$, the gauge glass with site disorder in a large magnetic field ($SGG$; note that this model has the correct spatial symmetry, which is broken by the presence of the magnetic field), and the $XY$ spin glass with Dzyaloshinsky-Moriya interaction and Gaussian randomness ($XYDMG$) and with bimodal randomness ($XYDMB$). These five models can be classified according to their symmetry properties: the models $I$, $GG$, $SGG$, and $XYDMG$ all show local gauge invariance, whereas the models $XY$ and $XYDMB$ do not. Second, the models $GG$, $SGG$, $XYDMG$, and $XYDMB$ break time-reversal (or reflection) symmetry, whereas $I$ and $XY$ do not. Both studies concentrate on the scaling behavior of the effective coupling $J(L)$ and involve a Migdal-Kadanoff renormalization scheme (Cieplak *et al.*, 1992) as well as a zero-temperature finite size scaling analysis (Cieplak *et al.*, 1991; Gingras, 1992). Cieplak *et al.* (1991, studying the models $XY$, $SGG$, and $GG$; 1992, studying $XY$, $XYDMG$, $GG$) then propose that the decisive feature for the existence of a finite-temperature glass transition is the presence of local gauge invariance in the model, as they find that all models showing gauge invariance are characterized by a common exponent $\theta \approx 0.26 > 0$, whereas the $XY$ model does not show spin-glass order in $d = 3$. On the other hand, Gingras (1992, studying the models $GG$, $SGG$, $XYDMG$, and $XYDMB$) concludes that the important difference between the various $XY$-type spin-glass models is the breaking of time-reversal symmetry (see also Gingras, 1991b): The results for the two-dimensional case consistently give $\theta \approx -0.45$ for all four

models studied, hence $d_l > 2$. The numerical analysis in 3D is limited to two relevant sizes, $L=3$ and $L=4$; however, the results again consistently produce an exponent $\theta \approx 0.05$ for the four models, indicating a lower critical dimension $d_l$ below but close to three. In addition, real-space Migdal-Kadanoff renormalization-group analysis (for the gauge glass and for an $XY$ spin-glass model with random Dzyaloshinsky-Moriya interaction; see Gingras, 1991a), as well as numerical studies on Ising (Bray and Moore, 1984) and on vector spin-glass models (Morris et al., 1986), indicate that $\theta(d=3) \approx \theta(d=2)+0.5$, lending additional support for the results found by Gingras. Note that this "gauge-glass" universality class is different both from the Ising spin glass with $\theta(d=3) \simeq 0.2$ and from the $XY$ spin glass with $\theta(d=3) \simeq -0.5$. Hence one is tempted to conclude that the gauge-glass model does indeed show a finite-temperature glass transition in three dimensions and that the important difference from the $XY$ spin glass is the breaking of time-reversal invariance. An additional interesting and important result provided by the studies of Cieplak et al. (1991) and of Gingras (1992) is that the breaking of spatial symmetry by the magnetic field in a realistic gauge glass does not appear to be crucial, since the two models $SGG$ and $GG$ produce nearly identical results.

The early experiments on the history dependence of the magnetization (e.g., Müller, Takashige, and Bednorz, 1987) were interpreted in terms of the gauge-glass (or superconductive glass) model (Morgenstern, Müller, and Bednorz, 1987). Later, the concept of pinning and (giant) creep of vortices was invoked in order to analyze the magnetic behavior of the new oxide superconductors (Yeshurun and Malozemoff, 1988), which finally led to the notion of the vortex glass (Fisher, 1989). Arguments favoring the vortex picture over the superconductive glass picture has been presented by Malozemoff, Krusin-Elboum, et al. (1988) based on a careful analysis of experimental data in terms of the two models.

### 3. Vortex glass

Disorder plays a crucial role in the Abrikosov phase of type-II superconductors. First of all, disorder destroys the long-range order of the vortex lattice, and thus there is no conventional off-diagonal long-range order in this phase. Second, disorder leads to pinning of the vortex lines and thereby produces a highly nonlinear dynamic response of the system with a current-voltage characteristic exhibiting a critical current density below which dissipation is strongly reduced. Within the Kim-Anderson theory, however, dissipation remains finite down to vanishing driving forces. Hence the resulting phase has the dynamic properties of a highly viscous *liquid*. Alternatively, following the seminal work of Fisher (1989), the low-temperature phase of a bulk disordered superconductor is a *vortex glass*, which is a true thermodynamic phase, characterized statically by the existence of a nonvanishing Edwards-Anderson order parameter

$$q_{EA} = \langle |\langle \tilde{\Psi}(\mathbf{r}) \rangle_{th}|^2 \rangle_{dis}, \qquad (7.35)$$

with the gauge-invariant order parameter $\tilde{\Psi}(\mathbf{r})$ $= \Psi(\mathbf{r}) \exp[i(2\pi/\Phi_0) \int^{\mathbf{r}} \mathbf{A} \cdot d\mathbf{l}]$. Dynamically this phase is characterized by a zero resistivity $\rho$ at vanishing driving force, $\rho(j \to 0) \to 0$. These two requirements can be understood as a consequence of the development of *infinite barriers* in the system, which lock the vortices into a specific state.

One of the most important questions then is whether the vortex-glass exists in a bulk three-dimensional superconductor. In one attempt to answer this question it is assumed that vortex glass and gauge glass belong to the same universality class, since both models possess the same kind of Edwards-Anderson order parameter. If this is true, the results obtained for gauge glass could be transferred to the vortex-glass problem and vice versa, and numerical results indicating the existence of a gauge-glass phase in 3D could be interpreted as giving evidence for the existence of a vortex-glass phase in 3D. However, in spite of being closely related, the two models need not to be identical, as the following discussion shows.

First, in studying the vortex-glass problem we should start from a system with vortices, i.e., a system of line objects, directed along the external magnetic field on average. Hence there is no obvious reason for such a system to be isotropic (even without the anisotropy of the oxide superconductors taken into account). In the absence of disorder, both the vortex lattice and the disentangled vortex liquid discussed in Sec. V.B above are clearly anisotropic phases, within a finite superconducting response $j_z = -\rho_s^{zz} A_z$ present along the direction of the magnetic field, but with a metallic behavior in response to a transverse current density $\mathbf{j} \perp \mathbf{H}$. On the other hand, isotropy is restored in an entangled vortex liquid, which has the same large-scale properties as a normal metal; see Sec. V.B. Second, let us introduce disorder into the system and characterize its strength by the zero-temperature critical current density ratio $j_c/j_0 \ll 1$. When the disorder is weak with respect to the strength of thermal fluctuations,[8] $j_c/j_0 \ll Gi^{1/3}$, the melting line is not strongly affected by the presence of disorder, and therefore the vortex-glass phase should continuously grow out of the vortex lattice, which is anisotropic. Moreover, the non-linear vortex-glass current-voltage characteristic at low current densities is clearly anisotropic. The energy barriers $U(j_\perp)$ for a transverse current density $j_\perp$ scale as $U(j_\perp) \propto j_\perp^{-\mu}$ with $\mu < 1$, whereas the barriers for a longitudinal current $j_\parallel$ scale as $U(j_\parallel) \propto j_\parallel^{-1}$ even in the absence of pinning. Therefore it is quite natural to suspect that the vortex-glass phase itself, as well as its critical behavior near the transition (assuming that the latter is

---

[8]Here we are not addressing the stability of the low-field part of the melting line (see Sec. V.A.2 above) with respect to disorder. See Sec. VI.C for a discussion of this point.

continuous), should be anisotropic. On the other hand, if the disorder is sufficiently strong, with $Gi_d = (j_c/j_0)^3 \gg Gi$ (which is definitely not the case in the high-temperature superconductors but which can be realized quite naturally in conventional type-II superconductors), the vortex-glass transition can arise directly out of the isotropic entangled-vortex-liquid (i.e., normal) phase, in which case there is no reason for the vortex-glass transition to be anisotropic, and thus it should indeed be equivalent to the gauge-glass transition. Such a strongly disordered situation has been considered by Fujita, Hikami, and Larkin (1991), who obtained a gauge-glass transition of the percolation type for a three-dimensional dirty superconductor in fields $H \gtrsim Gi_d H_{c_2}(0)$ [the ratio $W/\Delta$ in the paper of Fujita *et al.* is equivalent to $(Gi_d/Gi)^{1/2}$ in our notation].

Let us mention an additional argument why the low-disorder vortex glass could be different from the strongly disordered gauge glass. In spite of the absence of positional long-range order in the vortex-glass phase, there is still a considerable amount of short-range crystalline order present (see Sec. IV.F). This feature, which seems to be irrelevant in the droplet approach, does make a difference within a mean-field theory involving replica symmetry breaking, such as the one developed by Bouchaud, Mézard, and Yedidia (1991). In fact, their variational mean-field-like approach to describing the pinned vortex lattice looks rather different from the approach of Parisi (1980) and Mézard *et al.* (1984) for the spin-glass problem, whereas the corresponding approach to the gauge glass is equivalent to the spin-glass problem. Finally, one should also keep in mind that the effect of screening has been neglected in all of the gauge-glass models considered so far (i.e., the magnetic field inside the sample is considered to be uniform and equal to its external value), whereas in a system of vortices the penetration depth $\lambda$ is finite. On approaching the transition, this finite penetration length clearly becomes shorter than the vortex-glass correlation length $\xi_{VG}$, and hence screening will change the nature of the interaction on scales smaller than $\xi_{VG}$. To summarize, it therefore seems quite possible that the vortex glass in a weakly disordered superconductor is not in the same universality class as the gauge glass.

Another way of providing evidence for the existence of a true vortex-glass phase has been proposed by Fisher (1989). His attempt is based on a dimensional reduction of the problem to two dimensions and consideration of a toy model of vortices confined within a plane. Physically, such a model corresponds roughly to an extended Josephson junction with the magnetic field applied parallel to the junction plane. Once the existence of a glass phase in the 2D toy model has been shown, one could then argue that a corresponding phase should also exist in three dimensions, where the effect of (thermal) fluctuations is reduced. Let us give a brief summary of the main steps involved in this approach. First, the three-dimensional vortex problem is mapped to a system of in-

teracting bosons in 2D at $T=0$ (corresponding to a *bulk* superconductor with $L \to \infty$), where the boson world lines $\mathbf{R}_\nu(t)$ play the role of the vortex position $\mathbf{R}_\nu(z)$; see also Sec. V.B. The 3D disorder potential in the vortex problem then maps to a random potential in the boson problem, fluctuating both in space and in time. Calculating the ensemble average of the free energy by introducing $n$ replicas (Kardar, 1987), one arrives at an effective replicated boson Hamiltonian which, due to the presence of the disorder potential, contains an attractive interaction $\Delta_B$ between bosons belonging to different replicas (see Sec. IV.F above). In 2D the bosons are expected to bind into $n$-molecules. At $T^B=0$ the system will undergo a Bose condensation, and it is argued that disorder is relevant if the $n$-molecules survive this transition. Such a scenario of course is very difficult to prove. However, as pointed out by Fisher (1989), when reducing the model to $1+1$ dimensions (corresponding to vortices confined to a plane), the problem can be mapped to the two-dimensional random-field $XY$ model without vortices, which has been studied by Cardy and Ostlund (1982). A renormalization analysis shows that, depending on temperature, the disorder parameter $\Delta_B$ will scale either to zero (high temperatures, $T > T_g$) or to infinity ($T < T_g$). In his analysis, Fisher (1989) obtains a finite $T_g$ and correspondingly a finite-temperature glass transition in the original flux-line model. On the other hand, Nattermann, Lyuksyutov, and Schwartz (1991) have shown that, at least in the weak-field limit with $a_0 \gg \lambda$, the system always scales to a disorder-dominated phase, and therefore the two-dimensional system is always in a glassy phase (i.e., $T_g = \infty$). Thus the question whether the $1+1$ vortex model exhibits a finite-temperature glass transition or whether it remains within the glass phase at all temperatures has not been settled at present. This question is closely related to the possible decoupling transition of a layered superconductor in a parallel-field configuration; see Sec. VIII.B.5: A finite-temperature decoupling transition is equivalent to a finite-temperature glass transition in the disordered $1+1$ model. According to Nelson (1993), both scenarios might actually be realized at different field values, with a finite-temperature transition $T_g < \infty$ taking place at high field values and $T_g \to \infty$ as the vortex density goes to zero (see Sec. VIII.B.5 for more details).

The resulting glassy order in the $1+1$ model turns out to be marginal, with energy barriers scaling with $\ln L$ [Nattermann, Lyuksyutov, and Schwartz, 1991; Tsai and Shapir, 1992; see also Toner, 1991b, who obtains a scaling behavior $(\ln L)^{1/2}$ for this model, and the discussion between Toner, 1992, and Nattermann and Lyuksyutov, 1992]. Since the vortex-glass phase is stable in 2D, one would expect on general arguments that such a phase should also exist in a three-dimensional system. However, for the present problem this conclusion seems to be rather dangerous: First of all, the two- and three-dimensional systems differ quite appreciably in that the three-dimensional vortex lattice can suffer from disloca-

tions and can even melt, whereas neither of these two features is present in the two-dimensional toy model (see also the discussion in Sec. VIII.B.5 below concerning the absence of a melting transition in this system). Second, the usual argument that thermal disorder is less important in higher dimensions and therefore a thermodynamic phase should be more stable does not trivially apply to the present glass problem. Since the vortex glass is *created* by a quenched disorder potential, it is important that the effects of randomness remain strong as we go to higher dimensions. However, as shown by Larkin (1970), disorder becomes irrelevant in dimensions $d > 4$, hence it is unclear whether the quenched or the thermal disorder is more strongly reduced as we go to higher dimensions.

We have discussed two approaches to the existence of the vortex-glass phase in a 3D bulk superconductor— one based on the similarity of the vortex-glass problem and the gauge-glass model and a second based on a dimensional reduction scheme. Neither of these approaches seems to be able to provide convincing evidence for the existence of the 3D vortex-glass phase and, even worse, the results of the two approaches are in some sense contradictory if they are not treated with the necessary care. Let us discuss the problem in more detail.

Consider the approach based on dimensional reduction. The original 3D vortex problem can be viewed as a problem in $(2+1)$-dimensional space, where we have split the original three-dimensional space into a two-dimensional planar component perpendicular to the field direction and a timelike axis along the field itself. This notation naturally bears out the anisotropy in the vortex problem. When dimensionally reducing the problem, we obviously can do it in two very different ways, $2+1 \rightarrow 2+0$ or $2+1 \rightarrow 1+1$. The $2+0$ problem corresponds to an assembly of vortices in a film with the external field directed perpendicular to the film plane. This system is known *never* to be in a glassy state, i.e., $T_g = 0$ (see Sec. VIII.D.3 for details), hence the lower critical dimension is $d_l > 2$. Note that this $2+0$ problem is *isotropic* on large scales and probably equivalent to the gauge-glass model in 2D. The $1+1$ problem is completely different: this system corresponds to the toy model described above with the vortex lines confined to a plane. The system is *always* in a glassy state, since $T_g = \infty$, hence $d_l \leq 2$ (in fact $D = 2$ is just the marginal dimension for this problem, hence $d_l = 2$; see the above discussion). Regarding symmetry, the system is obviously *anisotropic*. Now, let us to back to 3D. The $2+0$ problem can be extended to 3D in two ways: Using $2+0 \rightarrow 3+0$, we produce an isotropic three-dimensional model corresponding to the gauge glass in 3D. This scenario is consistent with a lower critical dimension larger than 2 for the gauge glass, as shown in various numerical studies. The alternative way to go over to a three-dimensional model is via $2+0 \rightarrow 2+1$, producing an anisotropic model which we associate with the vortex glass. The same model is obtained when extending the $1+1$ model to three dimensions, $1+1 \rightarrow 2+1$. The lower critical dimension for this

model then seems to be $d_l = 2$. Hence again we obtain strong indications that the vortex-glass model and the gauge-glass model are not necessarily equivalent.

Finally, the existence of a true thermodynamic vortex-glass phase in three-dimensional bulk superconductors seems to be clearer for the situation where the pinning potential consists of columnar defects, as they can be created by irradiation with heavy ions (Civale *et al.*, 1991; Gerhäuser *et al.*, 1992; see Sec. IX.B). For the case of vortices lined up with such columnar defects, the disorder potential is mapped to a *static* random potential in the boson problem (Nelson and Vinokur, 1992). Strong arguments have been presented (Fisher *et al.*, 1989b) that a glassy phase exists in the two-dimensional disordered Bose system, thus indicating the existence of a true thermodynamic vortex-glass phase for this special defect structure.

After this discussion about the possible *existence* of a true thermodynamic glass phase in bulk 3D superconductors, let us study the *physical consequences* of such a state. Following Fisher (1989), the existence of a glass phase has very interesting consequences for the (dynamic) response properties of the system. Consider again the 2D toy model with vortices confined to a plane. The positions of the individual vortex lines can be specified by the condition $A(x,z) = 2\pi l$, $l = $ integer, with $A$ the vector potential, $\partial_x A = B(x,z)$. Within the vortex-glass phase the symmetry $A \rightarrow A + 2\pi N$, $N = $ integer, producing a shift of the vortex system by $N$ lines, is broken. Hence neighboring phases with $N$ differing by unity are separated from each other by infinite barriers. For a finite current density $j$ producing a Lorentz force $jB/c$ acting on the vortices in phase $N$, droplets of phase $N+1$ can be created by thermal activation over barriers $U_d(L)$ which diverge as the droplet size $L$ goes to infinity. Creation of such droplets can conveniently be interpreted as the formation of a vortex loop. Assuming the vortex-loop area $S$ to scale with an exponent $\kappa > 1$, $S \propto L^{\kappa}$, the energy of the loop scales with $L^{\theta}$, where $0 \leq \theta \leq \kappa/2$. The largest exponent $\theta = \kappa/2$ is realized for a loop with nonzero line tension and no relaxation of the other vortices. Expansion of this loop finally requires overcoming barriers scaling according to $L^{\psi}$, $\theta \leq \psi \leq \kappa/2$. Under the action of the Lorentz force $\propto jL^{\kappa}$, the saddle point for the loop expansion has a size $L_{opt} \propto j^{-1/(\kappa-\theta)}$, and hence the barriers against droplet expansion (i.e., vortex motion) scale according to $U_d(j) \propto j^{-\mu}$, with $\mu = \psi/(\kappa-\theta)$ (Fisher, 1989; Fisher, Fisher, and Huse, 1991). Finally, droplet or loop expansion produces a finite creep velocity of the vortices and hence an electric field $E$ that decreases dramatically with vanishing driving force $j$,

$$E \propto e^{-c(j_c/j)^{\mu}} . \tag{7.36}$$

Equation (7.36) indicates that the dc resistance vanishes in the vortex-glass phase and hence the latter can be called a true superconductor; see Figs. 5 and 27. Second, the result (7.36) immediately leads to the slow

logarithmic-in-time relaxation typical of a glassy phase, e.g., the diamagnetic screening current $j$ itself decays according to $j(t) \propto [\ln(t/t_o)]^{-1/\mu}$ as $t \to \infty$ (Fisher, 1989).

Assuming the existence of a true thermodynamic vortex-glass phase in a disordered bulk type-II superconductor, the next question to be addressed is the nature of the transition into this phase itself. At present, the order of this transition seems rather unclear. Although the transition to the Abrikosov lattice is continuous in mean-field theory, according to Brézin, Nelson, and Thiaville (1985; see also Affleck and Brézin, 1985), fluctuations drive this transition first order in dimensions $d < 6$. Similarly, a dislocation-mediated melting transition of the Abrikosov lattice is also expected to be first order (Marchetti and Nelson, 1990). Numerical evidence for a first-order melting transition has been given by Hetzel, Sudbø, and Huse (1992), while recent experiments by Charalambous (1992), by Safar, Gammel, Huse, *et al.* (1992b), and by Kwok *et al.* (1994a) support the presence of a first-order transition. When a 6 T magnetic field is applied to a clean untwinned YBCO single crystal, a hysteretic behavior is found in the linear-response resistance measured as a function of temperature. Whereas weak disorder is not expected to change the nature of the transition (Imry and Wortis, 1979; Pentegov and Feigel'man, 1988), the presence of strong disorder may turn the first-order melting transition between the vortex lattice and the vortex liquid into a continuous glass transition. If this is the case, one can use a scaling analysis to describe the static and dynamic behavior of the system within the critical region around the transition (Koch *et al.*, 1989; Fisher, Fisher, and Huse, 1991).

## B. Vortex-glass scaling near $T_g$

In the following we discuss the transition into the vortex-glass state as presented by Fisher, Fisher, and Huse (1991). Following these authors, we assume a continuous glass transition at $T_g$, where the vortex-glass correlation length $\xi_{VG}(T) \propto |T - T_g|^{-\nu}$ and the characteristic relaxation time $\tau_{VG}(T) \propto \xi_{VG}^z(T)$ both diverge [cf. Eqs. (7.25) and (7.26)]. Furthermore, we assume that the scaling behavior of the system is isotropic. Hence instead of having two exponents $\nu_{\parallel}$ and $\nu_{\perp}$, describing separately the divergence of the correlation length $\xi_{VG}(T \to T_g)$ for directions parallel and orthogonal to the magnetic field, the following analysis will consider only one exponent $\nu = \nu_{\parallel} = \nu_{\perp}$. Therefore the present discussion does not contain any feature reminiscent of vortex lines, and we believe that the results described below apply rather to the isotropic gauge glass, while their application to the anisotropic vortex glass seems less evident. The glass correlation length $\xi_{VG}$ determines the long-distance behavior of the vortex-glass correlation function

$$\chi_{VG}(\mathbf{r} - \mathbf{r}') = \langle |\langle \Psi(\mathbf{r})\Psi(\mathbf{r}') \rangle_{th}|^2 \rangle_{dis} . \tag{7.37}$$

A mean-field analysis of this transition has been carried out by Dorsey, Huang, and Fisher (1992). They find a glass transition that is isotropic and characterized by the mean-field exponents $\nu = \frac{1}{2}$ and $z = 4$. The upper critical dimension above which these results are expected to become exact is $d_u = 6$. In terms of these characteristic parameters, then, the vortex glass is very similar to the Ising spin and to the gauge glass. In the approach of Dorsey *et al.*, no short-range structures such as vortex lines are present, explaining why their glass transition appears to be isotropic. Moreover, the glass transition temperature $T_g(H)$ obtained by Dorsey, Huang, and Fisher approaches zero in the limit of small disorder and not the melting line $T_m(H)$, which again can be attributed to the absence of any short-range structure. However, some caution is in order here. Since their analysis is based on the first Landau-level-approximation, it is unclear whether the extrapolation to zero temperatures can be carried out, as this approximation usually works best close to the upper critical-field line.

The assumption of a continuous transition characterized by the diverging length and time scales $\xi_{VG}$ and $\tau_{VG}$ allows us to predict the response of the system in the vicinity of the critical regime. Let us first concentrate on the transition itself. The following scaling analysis predicts an algebraic current-voltage characteristic at the transition. Since the vector potential $A$ scales as an inverse length, the electric field $E \propto \partial_t A$ is expected to scale like $1/\xi_{VG}\tau_{VG}$; hence $E\xi_{VG}^{1+z}$ is an appropriate scaling combination. On the other hand, since $j \propto \partial_A f$, with $f$ denoting the free-energy density, the scaling combination for the current density is $j\xi_{VG}^{d-1}$. Hence we obtain the scaling ansatz

$$E \propto \xi_{VG}^{-(z+1)} e_{\pm}(j\xi_{VG}^{d-1}) . \tag{7.38}$$

The ansatz (7.38) is consistent with that obtained for the complex conductivity $\sigma(\omega) \simeq \rho_s/(-i\omega + \varepsilon)$. Since the superfluid density $\rho_s$ scales with length according to $\rho_s \propto \xi^{2-d}$ (Fisher, Barber, and Jasnow, 1973), we expect a scaling law for the complex conductivity of the form

$$\sigma(\omega) \propto \xi_{VG}^{2+z-d} s_{\pm}(\omega\xi_{VG}^z) . \tag{7.39}$$

Let us first concentrate on the current-voltage characteristic (7.38). Above $T_g$, we expect the response to be ohmic at large scales, $L > \xi_{VG}$. Large distances, $L > \xi_{VG}$, are probed with small current densities, $j < j_x^+ \propto \xi_{VG}^{1-d}$. Hence the scaling function $e_+(x)$ vanishes linearly in $x$, $e_+(x \to 0) \sim x$. Below $T_g$, the system shows a glassy response at large scales, $L > \xi_{VG}$ (i.e., small current densities $j < j_x^- \propto \xi_{VG}^{1-d}$), and the scaling function $e_-$ takes the form $e_-(x \to 0) \sim \exp(-a/x^\mu)$. Approaching the transition, the diverging length scale in Eq. (7.38) has to cancel out, and hence $e_{\pm}(x \to \infty) \sim x^\alpha$ with $\alpha = (z+1)/(d-1)$. We then obtain the following general behavior for the current-voltage characteristic in the vicinity of the glass transition: Right at the transition the current-voltage characteristic shows power-law behavior, with

$$E \propto j^{(z+1)/(d-1)}. \tag{7.40}$$

Since we expect $z > 4$ in $d = 3$, an exponent $\alpha > 2.5$ is predicted. Above the transition, the characteristic should change from ohmic behavior, with

$$\rho(T) \propto (T - T_g)^{\nu(z+2-d)} \tag{7.41}$$

at small current densities, $j < j_x^+$, to power-law behavior at large current densities, $j > j_x^+$. The crossover current density $j_x^+$ vanishes on approaching the transition temperature according to

$$j_x^+ \propto (T - T_g)^{\nu(d-1)} . \tag{7.42}$$

Below the transition, the crossover between the small and large current density regimes separated by $j_x^-$ changes the characteristic from glassy

$$E \propto e^{-c(j_c/j)^\mu} \tag{7.43}$$

at low current densities to (critical) power-law behavior at large current densities. Again, the crossover current density $j_x^-$ scales according to

$$j_x^- \propto (T_g - T)^{\nu(d-1)} . \tag{7.44}$$

An (experimental) analysis of the current-voltage characteristic in the vicinity of the transition into the glass phase can then be used to extract the scaling exponents $z$ and $\nu$ (see Fig. 29). The slope of the power-law characteristic at $T_g$ in a log-log plot provides a measure of the dynamic exponent $z$. Determining the crossover current densities $j_x^+$ and $j_x^-$ makes possible an estimate of the static exponent $\nu$. Finally, a measurement of the resistivity $\rho(T)$ above $T_g$ provides a consistency check for the two exponents $z$ and $\nu$. The vortex-glass exponent $\mu$ determining the response below $T_g$ is usually difficult to measure.

The first analysis of this type providing experimental evidence for a continuous transition into a vortex-glass phase was performed by Koch *et al.* (1989). The experiments were carried out on epitaxial thin films of $YBa_2Cu_3O_{7-y}$ deposited by laser ablation onto $SrTiO_3$ substrates. The large critical current densities, $j_c(T=77$ K, $H=0) > 10^6$ A cm$^{-2}$, indicate the presence of rather strong pinning (large disorder) in these samples. Magnetic-field values ranging from 0.5 T to 4 T were studied. The exponents $z$ and $\nu$, as determined from the power-law characteristic at $T_g$ and the crossover current densities $j_x^+$ and $j_x^-$ above and below the transition, are $z \approx 4.8 \pm 0.2$, $\nu^+ \approx 1.7 \pm 0.4$, and $\nu^- \approx 1.5 - 2.0$. The consistency check on $\rho(T)$ provides $z \approx 4.8$, $\nu \approx 1.7$, in good agreement with the previous independent measurements of $z$ and $\nu$. The vortex-glass exponent $\mu$, obtained by fitting the characteristic to a form (7.43) takes the value $\mu \approx 0.4 \pm 0.2$. One should remark that a large dynamic range is needed in order to distinguish vortex-glass behavior (7.43) from a simple power-law characteristic. As pointed out by Coppersmith, Inui, and Littlewood (1990), the evidence for a vortex-glass transition provided
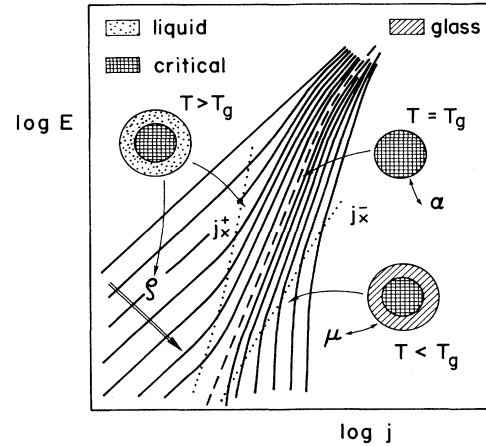


FIG. 29. Current-voltage characteristic of a superconductor in the mixed state, taking thermal as well as quenched disorder into account. The plot contains all the relevant information on the dynamic response of the vortex system, allowing us to extract from it the vortex-glass scaling laws for $E(j)$, $\rho(T)$, and $j_x^\pm(T)$, as well as the glass exponent $\mu$. At the glass transition $T_g$ the characteristic is algebraic, $E \propto j^\alpha$, with $\alpha = (z+1)/(d-1)$. Above $T_g$ the system is a liquid over large distances, with $\rho \propto (T - T_g)^{\nu(z+2-d)}$, and critical at small distances. Below $T_g$ we have a glassy response at large distances, $E \propto \exp[-c(j_c/j)^\mu]$, and again a critical behavior at small scales. The crossover current densities $j_x^\pm$ separating the critical behavior at small scales (probed by large current densities) from the liquid/glassy response at large distances (probed by small current densities) scale as $j_x^\pm \propto |T - T_g|^{\nu(d-1)}$. Typical values for the correlation length exponent $\nu[\xi_{VG} \propto |T - T_g|^{-\nu}]$ and the dynamic exponent $z[\tau_{VG} \propto \xi_{VG}^z]$ are $\nu = 1/2$, $z = 4$ in the mean-field approximation and $\nu \approx 1-2$, $z \approx 4-5$ as extracted from various experiments.

by the experiment of Koch *et al.* (1989) is not conclusive, as their data can be reinterpreted in terms of a standard Anderson-Kim flux-creep model. However, according to Koch, Foglietti, and Fisher (1990), the analysis based on the flux-creep model relies on a rather strong temperature dependence of the activation barrier $U(T) \propto (T_c - T)^{2.5}$ and also produces a systematic smearing in a scaling plot near criticality, a feature that is not present in the experimental data. The data of Koch *et al.* have also been reanalyzed by Jensen and Minnhagen (1991) in terms of a vortex-unbinding transition with a surprisingly good agreement between theory and experiment.

Additional support for the existence of a vortex-glass transition has been provided by Gammel, Schneemeyer, and Bishop (1991). Their experiments were carried out on microtwinned crystals of $YBa_2Cu_3O_{7-y}$ using SQUID picovoltometry, allowing for an extension of the dynamic range of the experiment by about four orders of magnitude in current density and about six orders of magnitude in electric field as compared with the original experiment by Koch *et al.* (1989). Magnetic-field values in the range 1-6 T were analyzed. The exponents $z$ and $\nu$, obtained from the current-voltage characteristic at $T_g$ and the

crossover current density $j_x^+$, were $z \approx 3.4 \pm 1.5$ and $v^+ \approx 2.0 \pm 1.0$. The consistency check based on the scaling behavior of the resistivity (7.41) gave $v \approx 2.0 \pm 1.0$ and $z \approx 4.3 \pm 1.5$. Transforming the crossover current $j_x^+$ to a length scale for thermally active droplets $\xi_d \simeq (cT/\Phi_0 j_x^+)^{1/2}$, Gammel *et al.* found typical scales $\xi_d \sim 15~\mu m$, which is about 50 times larger than the length scales probed in the experiment of Koch *et al.* (1989). Finally, a scaling plot of the data,

$$\frac{E}{j\rho} \sim f\left[\frac{j}{j_x}\right] , \tag{7.45}$$

provides evidence that the experiment cannot be interpreted in terms of thermally assisted flux flow. Unfortunately, a plot of the data by Koch *et al.* within the same graph shows considerable disagreement with the data of Gammel *et al.*, which can be interpreted as a lack of universality. More recent data by Yeh *et al.* (1992) carried out on YBCO single crystals produce somewhat smaller values for the critical exponents $v$ and $z$. Based on dc and (low-frequency) ac transport measurements, Yeh *et al.* find the values $v \approx 0.9 \pm 0.2$ and $z \approx 2.0 \pm 0.2$. Given the rather large error bars in the result of Gammel *et al.*, the two sets of exponents are not inconsistent.

SQUID piocvoltometry has also been used to investigate the glass transition in a strongly layered BiSCCO single crystal (Safar, Gammel, Bishop, *et al.*, 1992), with results compatible with those obtained in the YBCO single crystal. The analysis of the resistance above $T_g$ yields the product $v(z-1) \approx 7 \pm 1$, which is close to the value $6.5 \pm 1.5$ observed in the microtwinned YBCO single crystal. Finally, a scaling analysis of the glass transition performed on a polycrystalline (i.e., ceramic) YBCO sample by Worthington *et al.* (1991) yields a set of exponents consistent with those obtained by Koch *et al.* (1989) for the thin film: $z \approx 4.6 \pm 0.2$ and $v \approx 1.1 \pm 0.2$.

Let us turn to the dynamic behavior of the system near the transition. Analysis of Eq. (7.39) above, below, and at the transition suggests the following behavior for the scaling functions $s_+$ and $s_-$ (Dorsey, 1991; Fisher, Fisher, and Huse 1991): Above the transition, $\sigma(\omega \to 0) \sim \text{const}$ and hence $s_+(x \to 0) \sim \text{const}$. Below the transition, $\sigma(\omega \to 0) \propto 1/\omega$ and thus $s_-(x \to 0) \propto 1/(-ix)$. At the transition, $\xi_{VG} \to \infty$ and hence $s_+(x \to \infty) \propto x^\alpha$ with $\alpha = (d-z-2)/z$. In addition, causality requires the phase angle $\varphi_\sigma$ of $\sigma = |\sigma| \exp(i\varphi_\sigma)$ to scale as

$$\varphi_\sigma(T,\omega) = p_\pm(\omega \xi_{VG}^z) , \tag{7.46}$$

with $p_\pm(x \to 0) \to 0$ and $p_\pm(x \to \infty) \to \pi(2-d+z)/2z$ (Dorsey, 1991), so that at the transition,

$$\sigma(\omega) \propto (-i\omega)^{(d-z-2)/z} . \tag{7.47}$$

Above the glass transition temperature $T_g$, a crossover from a frequency-independent to a frequency-dependent response is expected for $\omega > \Omega(T)$, with

$$\Omega(T) \sim \frac{1}{\tau_{VG}} \propto (T-T_g)^{vz} . \tag{7.48}$$

The dynamical analysis of the current-voltage characteristic at $T_g$ produces a crossover current density $j_x \propto \omega^{2/z}$. Following Olsson *et al.* (1991), we recall that the current-voltage characteristic at $T_g$ is expected to obey the scaling law

$$E \propto j^{(z+1)/(d-1)} e(j\xi_{VG}^{d-1}, \omega\tau_{VG}) . \tag{7.49}$$

In order to obtain a finite result at $T_g$, the scaling function $e(x,y)$ should depend only on the combination $xy^{(1-d)/z}$, so that

$$E \propto j^{(z+1)/(d-1)} e(j\omega^{(1-d)/z}) , \tag{7.50}$$

with $e(x \to 0) \sim x^\alpha$, $\alpha = (d-2-z)/(d-1)$, and $e(x \to \infty) \sim \text{const}$. We then expect the following dynamic behavior characteristic of a vortex-glass transition: Above the transition temperature $T_g$, we expect a finite complex impedance $Z(\omega) = 1/\sigma(\omega)$ at small current densities, which becomes frequency dependent for $\omega > \Omega(T)$. At the transition, $Z(w)$ shows power-law behavior in frequency, with $Z(\omega) \propto \omega^{(z-1)/z}$, and the phase angle takes the universal value $(\pi/2)(z-1)/z$. Finally, mapping out the current-voltage characteristic at $T_g$ for finite frequencies, one expects a power-law behavior at large current densities, $j > j_x \propto \omega^{2/z}$, turning linear for current densities dropping below the crossover density $j_x$.

This scenario for the dynamic response of the system in the critical regime has been experimentally analyzed by Olsson *et al.* (1991). Again, the experiments were carried out on a thin film characterized by a high critical current density of the order of $j_c(77~K) \gtrsim 10^6~A~cm^{-2}$ in a magnetic field $H = 0.55$ T. The current-voltage characteristic at $T_g$ produced a dynamic exponent $z \approx 5.2$, and from an analysis of the crossover current density $j_x^+$ an exponent $v \approx 1.1$ was extracted. The power-law dependence of the impedance $Z(\omega) \propto \omega^{(z-1)/z}$ at $T_g$ led to an exponent $z \approx 5.9$, whereas the determination of the phase angle $\varphi_\sigma$ gave a result $z \approx 5.6$. A consistency check based on the crossover frequency $\Omega(T)$ produced the exponents $v \approx 1.1$ and $z \approx 5.2$, and from the scaling of the crossover current density $j_x$ with frequency at $T_g$, an exponent $z \approx 5.2$ was found. To summarize, analysis of the dynamic behavior near $T_g$ provides scaling exponents $z \approx 5.2 \pm 0.6$ and $v \approx 1.1 \pm 0.4$, which are consistent with those obtained from static measurements.

To complete the discussion we also mention the numerical work of Lee and Stroud (1991), who study the current-voltage characteristic within a gauge-glass model. Performing a scaling analysis according to Eq. (7.45), they find that their data collapse to a universal scaling function if they use the parameter set $T_g \approx 0.4$–$0.5$, $z \approx 4$, and $v \approx 0.5$. These exponents coincide with the mean-field values and are somewhat smaller than those found experimentally.

The above experiments lending support to the ex-

istence of a continuous phase transition into the glass phase were all carried out on (strongly) disordered samples, either thin epitaxial films with high critical current densities or heavily twinned crystals or polycrystalline material. Also, one should note that, in spite of the very high sensitivity achieved in the experiment of Gammel *et al.* (1991), the vortex-glass transition in the current-voltage characteristic is rather difficult to observe in a single crystal as compared with the thin-film data presented by Koch *et al.* (1989). The idea of relating the continuous glass transition with strong disorder finds additional support from the experiments of Worthington, Holtzberg, and Feild (1990). In their experiments on a single crystal characterized by a smaller critical current density (i.e., weaker pinning) than that for thin films, they find no indication of vortex-glass scaling whatsoever.

## C. Vortex-glass dynamics—collective creep

The fundamental feature of the vortex-glass phase is the existence of diverging barriers which lead to the quenching of the dynamical degrees of freedom into a specific state. As a consequence, the vortices become immobile and the resistivity at vanishing driving force is zero. Hence the glass phase describes a true superconductor. Since the vortices are frozen into their positions, the topological part of the phase of the wave functions is also quenched, and only the nontopological component can produce (Gaussian) fluctuations. However, the latter are not expected to lead to dissipation, as they do not contribute to the reduction of the overall phase gradient set up by a macroscopic transport current.

Barriers diverging for vanishing driving forces have been predicted by several authors (Feigel'man, Geshkenbein, Larkin, and Vinokur, 1989; Fisher, 1989; Nattermann, 1990; Fisher, Fisher, and Huse, 1991). Here one should distinguish between the phenomenological scaling approach of Fisher (1989) and of Fisher, Fisher, and Huse (1991), which is based on the droplet model, and the analysis of Feigel'man *et al.* (1989) and of Nattermann (1990), who develop their theory starting from an elastic Hamiltonian, which is perturbed by the presence of a quenched disorder potential. The droplet model of Fisher, Fisher, and Huse (1991) provides a very general approach to the problem. The only starting assumption to be made is the rigidity of the vortex-glass phase, producing a positive scaling exponent $\theta$ for the wall or droplet energy $E_d(L) \propto L^\theta$ (we express all the scaling laws through the longitudinal length $L$). Introducing two more scaling exponents, one of the droplet volume (loop area) $S_d \propto L^\kappa$ and a third describing the scaling behavior of the energy barriers $U_d(L) \propto L^\psi$, allows for the determination of the barrier dependence on the driving current density $j$. Balancing the Lorentz force energy $\propto jL^\kappa$ against the droplet energy $\propto L^\theta$, one arrives at an optimal droplet (loop) size $L_{\rm opt} \propto j^{-1/(\kappa-\theta)}$, and inserting this result back into the expression for the barrier $U_d$, one arrives at

$$U_d(j) \propto j^{-\mu}, \quad \mu = \frac{\psi}{\kappa-\theta}. \tag{7.51}$$

The allowed values for the exponents $\kappa$, $\theta$, and $\psi$ are constrained by the conditions $\kappa > 1$ (loop area), $\theta > 0$ (rigidity), $\theta \le \kappa/2$ (maximal energy cost of a loop excitation with no relaxation), and $\theta \le \psi \le \kappa/2$ (barriers between metastable states), hence $0 < \mu \le 1$. It has been argued (e.g., Dekker, Eidelloth, and Koch, 1992) that a small exponent, $\mu \ll 1$, is obtained if the vortex glass is close to its lower critical dimensionality, where by definition $\theta$ vanishes. However, in order to reach this conclusion one has to assume that $\psi = \theta$, which is exactly the assumption made by Ioffe and Vinokur (1987), saying that at a given length scale the system develops only one relevant scale in energy. Furthermore, the closeness of the vortex-glass problem in three dimensions to its lower critical dimension is usually concluded from numerical studies of gauge glass, and it seems rather unclear at this stage if and under which circumstances (e.g., strong disorder) the above results can be applied to the vortex-glass problem.

The starting point of weak collective pinning theory is the elastic free energy [Eq. (4.3)]. The approach is perturbative, as one starts with an elastic property for the vortex lattice which then is assumed to be preserved in the presence of weak disorder. Viewing the vortex lattice in its pinning potential as an elastic manifold subject to a quenched disorder potential, one can draw from the many results obtained in this field concerning the wandering exponent $\zeta_{d,n}$ and the stiffness exponent $\chi_{d,n} = 2\zeta_{d,n} + d - 2$. Following Ioffe and Vinokur (1987), we make the additional assumption that at a given length scale there is a unique energy scale in the system, hence the barriers between metastable states are expected to scale in the same manner as the fluctuations in the energy of the metastable states themselves, that is, $\psi = \theta$ in the notation of the droplet model. Thus no additional exponent occurs, but the barriers, too, are expected to scale with the stiffness exponent $\chi_{d,n}$. Determining the dimensions of the saddle point and their dependence on the driving current density $j$ by the usual dimensional estimates, and inserting the result back into the scaling expression for the energy barriers, one arrives at (nondispersive regime)

$$U(j) \propto j^{-\mu}, \quad \mu = \frac{2\zeta_{d,n} + d - 2}{2 - \zeta_{d,n}}, \tag{7.52}$$

depending on only *one* exponent $\zeta_{d,n}$ as compared to *three* in the droplet model. Furthermore, this exponent is at least approximately known through general considerations regarding the statistical mechanics of elastic manifolds subject to quenched disorder; see Sec. III.F. The price to be payed for this very specific result lies in the assumptions to be made about the elasticity of the lattice and the existence of a unique energy scale in the problem. Here, one should point out that the result (7.52) is not the primary consequence of randomness in the problem, but rather is due to the elasticity of the manifold. Randomness plays an important role in the determination of the

numerical value for the exponent $\zeta_{d,n}$, but, it is not crucial for the existence of diverging barriers in the system (see Sec. IV.E). The numerical values for the glassy exponent $\mu$, obtained within the elastic theory, are $\mu = \frac{1}{7}, \frac{3}{2}, \frac{7}{9}$, and $\frac{1}{2}$, depending on the length scale probed by the current $j$. This dependence on external parameters such as magnetic field, temperature, and current density is due to the rich internal structure of the vortex lattice, as discussed in Sec. IV.B. The smallness of the exponent $\frac{1}{7}$ within the single-vortex pinning regime is a consequence of the closeness to marginality of the string problem in 3D. The value $\mu = \frac{1}{2}$ seems to be a lower bound for the elastic manifold in 3D. The elastic energy $C(u/L)^2 L^3$ scales at least with $L$. From the competition with the Lorentz force one obtains the minimal scaling $L_{\text{opt}} \propto j^{-1/2}$, hence $U(j) \propto j^{-1/2}$. The largeness of the exponent $\mu = \frac{3}{2}$ for the small-bundle regime is mainly a consequence of the rapid growth of the bundle with decreasing current density, due to dispersion in the elastic moduli. Finally, $\mu = \frac{7}{9}$ is the result for a homogeneous, elastic manifold. A variation of the glass exponent $\mu$ with temperature, current, and field in rough agreement with the predictions of collective creep theory, has been observed by Thompson *et al.* (1991 and unpublished work).

One should note that both the collective creep model and the phenomenological scaling approach proposed by Fisher, Fisher, and Huse (1991) belong to some kind of droplet model, with the consequences (e.g., regarding the structure of the phase space) known from our discussion of the spin-glass and gauge-glass problems above. In particular, we can ask ourselves what predictions will be made by a mean-field theory of vortex glass and how these predictions compare with experiment. A very interesting approach to a mean-field-like theory for the vortex-glass phase has been developed by Bouchaud, Mézard, and Yedidia (1991, 1992). In order to solve the statistical mechanics problem of a system of vortices subject to a weak random potential, they apply the replica formalism and use a self-consistent variational technique to find the best quadratic approximation to the resulting Hamiltonian in the replicated system. The solution that preserves the replica symmetry essentially reproduces the perturbative results of the Larkin model. More importantly, they present a replica symmetry-breaking solution that produces results in qualitative agreement with those of the collective creep theory as developed by Feigel'man *et al.* (1989), at least within the intermediate regime, where a simple continuum elastic theory can be applied. In particular, they obtain the Flory exponent $\zeta_{3,2} = \frac{1}{6}$ producing a glassy exponent $\mu = \frac{8}{11}$, whereas the corresponding results of the collective creep theory in the nondispersive regime are $\zeta_{3,2} = \frac{1}{5}$ and $\mu = \frac{7}{9}$. At larger length scales, however, there is a qualitative disagreement between the results obtained by Bouchaud, Mézard, and Yedidia and those of Nattermann (1990). The mean-field theory produces $\zeta_{3,2} = \frac{1}{4}$ and $\mu = \frac{6}{7}$, whereas Nattermann

finds $\zeta_{3,2} = 0$ and $\mu = \frac{1}{2}$. The results $\zeta_{3,2} = \frac{1}{4}$ and $\mu = \frac{6}{7}$ describing the large-scale asymptotics of the system appear to be rather strange, since the natural expectation is to find *smaller* exponents as the disorder becomes less relevant, when the fluctuations in the displacement field $\langle u_p^2(\mathbf{r}) \rangle$ grow beyond the lattice constant $a_0$ at large distances. We suspect that the above unexpected result could be due to an incorrect treatment of the lattice periodicity in the mean-field approach. In fact, most recently, Giamarchi and Le Doussal (1993) and Korshunov (1993), using the method of Bouchaud, Mézard, and Yedidia, have obtained results in agreement with those of Nattermann (1990). The analytical approach developed by Bouchaud, Mézard, and Yedidia seems to be very useful and promising, as it actually allows us to *derive* the important relations between the relevant space and energy scales of the fluctuations in the system. Moreover, it produces the first derivation of the hierarchical structure of valleys in a system with well developed local order (as opposed to models with complete randomness, such as spin glass and gauge glass).

Experimental investigations on the properties of the vortex-glass phase have been carried out by Dekker, Eidelloth, and Koch (1992). The experiments involve three different films characterized by a high critical current density of $j_c(77\ \text{K}) \sim 10^6\ \text{A cm}^{-2}$, and thus the films are expected to be highly disordered. A scaling analysis of the glass transition provides the exponents $\nu \approx 1.8 \pm 0.2$ and $z \approx 6 \pm 2$. An analysis of the current-voltage characteristic at low temperature leads to a glass exponent $\mu$ that depends on current density $j$ and that decreases from a value $\mu \approx 1$ at high current density to $\mu \approx 0.2$ at low $j$. Elastic theory predicts first an increase in the glass exponent from $\frac{1}{7}$ to $\frac{3}{2}$, followed by a decrease in $\mu$ via $\frac{7}{9}$ to $\frac{1}{2}$ with decreasing current density $j$. For fields $H > B_{\text{sb}} \approx 6$ T, the initial rise in $\mu$ is cut off. Whereas the decrease of $\mu$ with decreasing current density seems consistent with elastic theory, the numerical values found in the experiment clearly lie below expectations. Under certain conditions (assuming $\theta = \psi$ as well as equivalence between gauge glass and vortex glass), one might argue that the droplet model, which allows for arbitrarily small values of $\mu$ (restricted only by the closeness of the system to its lower critical dimension), fits the experiment better. On the other hand, smaller glass exponents are obtained within collective pinning theory if one allows for a decay of the shear modulus on large length scales. Let us assume that at very large length scales, $R > R_a$, the shear modulus is renormalized to $c_{66}(K) \propto K^{2\beta}$, say, by the presence of dislocations. At large length scales, $R > \lambda$, the elastic moduli are nondispersive and we obtain

$$R_\perp \simeq \left[ \frac{c_{66}(K)}{c_{44}} \right]^{1/2} L \propto R_\perp^{-\beta} L \ ,$$

$$R_\parallel \simeq \left[ \frac{c_{11}}{c_{44}} \right]^{1/2} L \simeq L \ . \tag{7.53}$$

Using Nattermann's result for the scaling behavior of the pinning energy, $\mathscr{E}_{\text{pin}} \propto \sqrt{V} \exp[-(\delta u/a_0)^2]$ at large distances, $R > R_a$, we obtain a wandering exponent $\zeta = 0$. From a comparison of the compression energy $c_{11}(u/R_{\parallel})^2 V$ with the energy gain due to the Lorentz force, we find the scaling behavior $R_{\parallel}(j) \propto j^{-1/2}$; hence the activation energy $c_{11}(u/R_{\parallel})^2 R_{\parallel} R_{\perp} L$ depends on the driving current density $j$ according to $U(j) \propto j^{-\mu}$ with $\mu = 1/2(1+\beta)$. Thus we see that a renormalization of the shear modulus at large distances does lead to a reduction of the glass exponent $\mu$. However, it is important to realize that the exponent $\beta$ cannot be arbitrarily large. In fact, there exists an upper bound on $\beta$ beyond which the structure factor will vanish rapidly enough at large time scales to transform the glass phase into a liquid. The precise value of this upper bound is not known at the moment, but it seems that it should be less than 2, hence $\mu \geq \frac{1}{4}$ at very low current densities.

Let us return to the elastic theory of the vortex-glass phase and ask ourselves if this theory is consistent. Does disorder destroy the elasticity of the manifold and turn it into a liquid or are the elastic properties also preserved in the disordered glass phase? It has been argued (Fisher, Fisher, and Huse, 1991) that disorder leads to the appearance of dislocations in the lattice at scales $R > R_a$ [=lattice correlation length, $\langle u^2(R_a) \rangle \simeq a_0^2$], so that the system may turn into liquid at large length scales. We then have to distinguish between dislocation loops and infinite dislocation lines. The presence of dislocation *loops,* (which are thermodynamic objects, in that they can be excited by thermal fluctuations) will renormalize the shear modulus at large distances to a smaller but finite value. Hence one expects the elastic properties of the lattice to be preserved. Note that dislocation loops in the vortex lattice do not carry magnetic flux, since the two edge dislocations (directed along the field) are bound to lie within the same sliding plane for topological reasons (no magnetic monopoles). To drive the shear modulus all the way to zero requires a finite density of *infinite* dislocation loops. We then have to address two problems: First, we should ask ourselves whether infinite dislocation loops are thermodynamic objects, i.e., is the energy necessary to create such an object finite or infinite? In order to obtain a finite energy of creation, the energy gain due to a favorable accommodation of the vortices to the disorder potential has to match the elastic energy to be paid for the creation of the dislocation line. It seems to us that for weak disorder the total line energy (energy per unit length) is nonzero, and therefore infinite dislocation lines are not thermodynamic objects. A proof of this statement seems to be possible within the approach developed by Bouchaud, Mézard, and Yedidia (1991). Second, if contrary to our expectations, disorder is indeed able to generate infinite dislocations in the system, or if such infinite dislocations have been frozen in upon cooling the system from the high-temperature vortex-liquid phase through the melting transition, these objects will appear in definite places where the vortices can ac-

commodate favorably to the disorder potential. However, this is tantamount to saying that the dislocation lines will be pinned by the disorder potential. Pinned dislocation lines are unable to drive the shear modulus to zero, and hence we expect that the elastic properties of the original vortex lattice are not destroyed by weak disorder.

Additional support for the correctness of the above arguments can be drawn from an analysis of the results provided by the dynamic approach, results which provide information about the perturbative relevance of disorder. Starting out with a liquid phase, we find that the relative velocity correction $\delta v/v$ remains finite (see Sec. VI.A), hence disorder is perturbatively irrelevant, and the system remains a (pinned) liquid. This has to be contrasted with the situation in which we start out with a vortex lattice. Here the correction $\delta v/v$ diverges, which signals that disorder, however weak, will drive the static vortex lattice into a glass. One could then argue that extrapolation down to zero driving force $v$ is dangerous and that the resulting phase is not a solid glass but again a liquid. However, it seems that such an argumentation is incorrect and that it fails to capture the essential physical difference between the two starting points, the liquid and the lattice. Let us discuss this important difference in more detail.

It is generally believed that a single vortex in three-dimensional space is in a glassy state. Going over to a vortex lattice, the interactions between the vortices suppress the effect of thermal fluctuations, and hence one would expect the instability to be stronger for a lattice than for a single line. The question to be asked then is "why is there a liquid?" The basic reason for the existence of a liquid phase is found in its *dynamical* properties. In a vortex liquid the vortex lines fluctuate in such a way as to completely average out the effect of the disorder potential; hence the liquid cannot be pinned. By contrast, a vortex lattice develops a spatially inhomogeneous structure that can be pinned by the disorder potential. Accordingly the translational symmetry properties of the lattice play no role whatsoever. Any spatially inhomogeneous static structure will do. Therefore the crucial difference between the lattice and the liquid is not the existence of LRO but their different dynamical properties. This can be nicely understood by a closer inspection of the dynamic approach. A careful analysis of the origin of the divergence in $\delta v/v$ shows that it is the *dynamic* behavior of the structure factor that is decisive for the result. We then should ask ourselves what effect the (static) disorder potential can have on the dynamic properties of the flux-line lattice. It seems rather unlikely that static disorder *enhances* the dynamic fluctuations. On the contrary, it seems that disorder tends to *suppress* the dynamical degrees of freedom of the vortex lattice. At least, this is obviously the case for the diffusive behavior of a single string in a disordered potential, which is reduced from an algebraic $\langle u^2 \rangle_{\text{th}} \propto t^{1/2}$ to a logarithmic $\langle\langle u^2 \rangle\rangle \propto [\ln t]^{2\zeta/(2\zeta-1)}$ behavior in the presence of disor-

der. This result follows trivially from rewriting the relevant barriers for creep motion as a function of displacement, $U(u) \simeq \varepsilon_0 u^2/L$ with $L \propto u^{1/\zeta_{d,n}}$, and using the connection between the relevant barriers for different times scales, $U(u) \simeq T \ln(t/t_0)$. Since we do not expect that static disorder will change the dynamic properties of the vortex lattice, we argue that the divergence in the response as obtained within the dynamical approach indeed signals the transition of the lattice into the glass phase. In summary, then, we believe that the perturbative approach to the vortex-glass phase based on elastic theory is internally consistent and that elasticity, which is the crucial requirement in this theory, is preserved in the glass phase.

## VIII. LAYERED SUPERCONDUCTORS

From the materials point of view, the new oxide superconductors are layered compounds with building blocks made out of conducting (metallic) CuO planes separated by buffer layers which serve as a charge reservoir. The transport properties are roughly uniaxial, with a large anisotropy between the $c$ axis and the $ab$ planes due to the layered structure and essentially isotropic behavior within the CuO planes. For not too large anisotropy, a description in terms of a *continuous* anisotropic Ginzburg-Landau or London theory is applicable. On the other hand, for very large anisotropy the discreteness of the structure becomes relevant, and a description in terms of a set of weakly coupled superconducting layers is more appropriate. Such a description is provided by the *discrete* Lawrence-Doniach (1971) model, which will provide the basis for the discussion of the physics of layered superconductors presented in this section.

The criterion usually adopted to go from a continuous anisotropic to a discrete layered description is the smallness of the coherence length $\xi_c$ along the $c$ axis with respect to the layer separation $d$ as expressed by the dimensionless ratio $\tau_{cr} = 2\xi_c^2(0)/d^2$. The ratio $\tau_{cr}$ characterizes the crossover from quasi-2D layered to continuous 3D anisotropic behavior: For a large coherence length $\xi_c(0)$, i.e., $\tau_{cr} \gg 1$, the continuous description is always appropriate. On the other hand, for small $\tau_{cr} \ll 1$, a crossover will take place at a temperature $T_{cr} = (1 - \tau_{cr})T_c < T_c$, where the system behaves in a quasi-two-dimensional manner at low temperatures, $T < T_{cr}$, and exhibits 3D anisotropic behavior above $T_{cr}$ (Farrell *et al.*, 1990). In general, a continuous anisotropic description is applicable to YBCO over a large temperature regime, whereas the more strongly layered Bi and Tl compounds belong to the class of materials with $\tau_{cr} \ll 1$, and hence the Lawrence-Doniach model applies. The layered organic superconductors of the BEDT-TTF family are other candidates requiring a discrete description, and the most extreme members of this class of materials are the artificially grown multilayer structures of $PrBa_2Cu_3O_{7-y}$ and $YBa_2Cu_3O_{7-y}$ (Triscone *et al.*, 1989,

1990; Li *et al.*, 1990; Lowndes *et al.*, 1990; Brunner *et al.*, 1991; Jakob *et al.*, 1992) and the $Mo_xGe_{1-x}/Ge$ system (White, Kapitulnik, and Beasley, 1991; Urbach *et al.*, 1992).

It should be pointed out that the continuous anisotropic Ginzburg-Landau or London-based analysis often can provide a rather good description of the physics of layered materials. For example, this is the case for the discussion of the elastic properties of the vortex lattice within a wide angular regime, the reason being that the nonlinear term in the Lawrence-Doniach model depending on the gauge-invariant phase difference between the layers can be linearized in many situations (Brandt, 1992c). Other properties, e.g., the thermodynamic properties of the superfluid or of the vortex lattice, can more closely resemble those of a 2D superconducting film (with a Berezinskii-Kosterlitz-Thouless-type behavior) than those of a 3D bulk material. The question of continuous anisotropic description versus discrete layered description therefore not only has to be decided by the smallness of the coherence length $\xi_c$ with respect to the layer spacing $d$, but depends strongly on the specific physical question at hand.

In the following, we attempt to present the most prominent additional features of the phenomenology of superconductivity that confront us when dealing with layered materials. We start (Sec. VIII.A) with a description of the vortex structure, which can differ quite appreciably from the continuous Abrikosov vortex system. We then proceed to the analysis of the thermodynamic properties of layered superconductors in Sec. VIII.B. Section VIII.C is devoted to the question of *intrinsic* pinning and creep as originating from the layered structure, whereas we concentrate on pinning by pointlike defects in Sec. VIII.D.

### A. Vortex structure

In a layered superconductor, the structure of the individual vortices as well as that of the vortex lattice can be
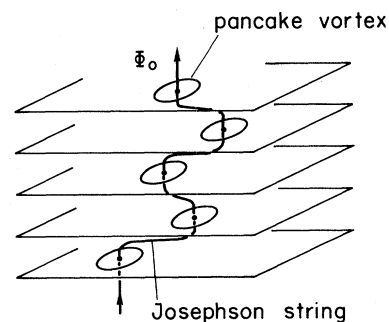


FIG. 30. Single flux-line structure in a strongly layered superconductor. The vortex line can be viewed as an array of pancake vortices threading the individual superconducting layers and interconnected by Josephson strings.

strongly modified. In what follows, we first concentrate on an individual vortex line which, unlike the continuous Abrikosov vortex, is not a rectilinear object, but rather is composed of so-called pancake vortices directed along the $c$ axis and joined by Josephson vortices whose axes thread through the junctions between the superconducting layers [see Fig. 30 and Doniach (1989)]. After discussing the nature of Josephson and pancake vortices, we shall concentrate on the lock-in transition. For magnetic fields **H** nearly aligned with the superconducting planes (but still a finite angle $\vartheta_H > 0$ away from the planar direc-

tion), the vortices prefer to match up with the layered structure so that the internal field is perfectly aligned, $\vartheta = 0$. Finally, we briefly discuss the modifications of the vortex-lattice structure in layered superconductors.

The basis for the phenomenological description of layered superconductors is given by the Lawrence-Doniach model (1971; see also Bulaevskii, 1973; Klemm, Luther, and Beasley, 1975; Efetov, 1979). The (Gibbs) free-energy functional describes a discrete set of superconducting layers with order parameter $\Psi_n$ separated by a distance $d$ and coupled together by a Josephson term,

$$\mathcal{G}[\Psi_n, \mathbf{A}] = \int d^2R \left\{ d \sum_n \left[ \alpha |\Psi_n|^2 + \frac{\beta}{2} |\Psi_n|^4 + \frac{\hbar^2}{2m} \left| \left( \frac{\nabla^{(2)}}{i} + \frac{2\pi}{\Phi_\circ} \mathbf{A}^{(2)} \right) \Psi_n \right|^2 \right] \right.$$
$$\left. + \frac{\hbar^2}{2Md^2} \left| \Psi_{n+1} \exp\left[ \frac{2\pi i}{\Phi_\circ} \int_{nd}^{(n+1)d} dz\, A_z \right] - \Psi_n \right|^2 \right\} + \int dz \left[ \frac{B^2}{8\pi} - \frac{\mathbf{B} \cdot \mathbf{H}}{4\pi} \right] \right\} . \tag{8.1}$$

The above formulation allows us to make direct contact with the continuous anisotropic Ginzburg-Landau functional (2.1) upon approximation of the discrete coupling term as a derivative along $z$; $M$ denotes the effective mass along $z$, $m$ is the corresponding planar parameter, and $\varepsilon^2 = m/M$ is the usual anisotropy parameter. The full functional (8.1) can be treated in a London-type approximation by assuming a constant modulus $\Psi_n$ within the planes and allowing only for phase degrees of freedom (currents),

$$\mathcal{G}[\varphi_n, \mathbf{A}] = \int d^2R \frac{\varepsilon_\circ d}{2\pi} \left\{ \sum_n \left[ \nabla^{(2)}\varphi_n + \frac{2\pi}{\Phi_\circ} \mathbf{A}^{(2)} \right]^2 + \frac{2m}{Md^2} \left[ 1 - \cos\left[ \varphi_{n+1} - \varphi_n + \frac{2\pi}{\Phi_0} \int_{nd}^{(n+1)d} dZ\, A_z \right] \right] \right\}$$
$$+ \int d^3r \left[ \frac{B^2}{8\pi} - \frac{\mathbf{B} \cdot \mathbf{H}}{4\pi} \right] , \tag{8.2}$$

where we use

$$\frac{\hbar^2 |\Psi_n|^2}{2m} = \frac{\varepsilon_\circ}{2\pi} . \tag{8.3}$$

With Eq. (8.3) we have adopted a particularly simple description of the layered structure, in which we express the (superconducting) properties of the CuO layers by the period $d$ of the layer structure and the planar bulk penetration depth $\lambda$. An alternative description is based on the thickness $d_s$ of the superconducting layers themselves combined with the actual penetration depth $\lambda_s$ of the layer material. The two descriptions are related through the equality $d/\lambda^2 = d_s/\lambda_s^2$ starting that the superfluid sheet density has to be equal in the two approaches. For layered superconductors, the two quanti-

ties $d$ and $\lambda$ are well known, and it is appropriate to use the first description in this case. On the other hand, for artificially grown superstructures (such as the $Mo_xGe_{1-x}/Ge$ system), the experimentally known parameters are $d_s$ and $\lambda_s$, and the second approach may be more straightforward. The present description (in terms of $d$ and $\lambda$) is appropriate as long as we are not interested in variations (e.g., of the magnetic field) on a scale $z < d$. Furthermore, a splitting of the distance $d$ into a layer thickness $d_s$ and a layer separation $d - d_s$ would require a more precise knowledge of the behavior of the order parameter along the $z$ axis, a subject that requires microscopic considerations.

Variation of Eq. (8.2) with respect to the vector potential **A** and the phases $\varphi_n$ provides us with the fundamental differential equations for **A** and $\varphi_n$:

$$\frac{\partial \mathcal{G}}{\delta \mathbf{A}^{(2)}} = 0: \quad \lambda^2 \Delta \mathbf{A}^{(2)} = d \sum_n \delta(z - nd) \left[ \mathbf{A}^{(2)} + \frac{\Phi_\circ}{2\pi} \nabla^{(2)}\varphi_n \right] , \tag{8.4}$$

$$\frac{\delta \mathcal{G}}{\delta A_z} = 0: \quad \Delta A_z = \frac{4\pi}{c} j_J \sin\Phi_{n+1,n} , \tag{8.5}$$

$$\frac{\delta \mathcal{G}}{\delta \varphi_n} = 0: \quad \Lambda^2 \left[ \Delta^{(2)} \varphi_n + \frac{2\pi}{\Phi_o} \nabla^{(2)} \mathbf{A}^{(2)} \right] = \sin\Phi_{n,n-1} - \sin\Phi_{n+1,n} \ . \tag{8.6}$$

Here, $\Phi_{n+1,n}$ is the gauge-invariant phase difference between the layers $n$ and $n+1$,

$$\Phi_{n+1,n} = \varphi_{n+1} - \varphi_n + \frac{2\pi}{\Phi_o} \int_{nd}^{(n+1)d} dz\, A_z \ ; \tag{8.7}$$

$j_J$ is the Josephson-coupling current density between the layers,

$$j_J = \frac{c\Phi_o \varepsilon}{8\pi^2 \lambda^2 \Lambda} \simeq j_o \frac{\varepsilon\xi}{\Lambda} \ ; \tag{8.8}$$

$\Lambda$ is the relevant phase screening length where nonlinearities in the coupling between the layers are important,

$$\Lambda = d \left[ \frac{M}{m} \right]^{1/2} = \frac{d}{\varepsilon} \ ; \tag{8.9}$$

and we have used a gauge with $\nabla \mathbf{A} = 0$. Note that $\nabla^{(2)}$, $\Delta^{(2)}$, and $\mathbf{A}^{(2)}$ denote the planar components of $\nabla$, $\Delta$, and $\mathbf{A}$. Equation (8.6) is equivalent to the current conservation law $\nabla \mathbf{j} = 0$. We now concentrate on (8.6) and study in more detail the structure of a Josephson vortex.

### 1. Josephson vortices

We consider a magnetic field in the $ab$ plane pointing along the $y$ direction and investigate the structure of an individual Josephson vortex aligned with the $y$ axis (Bulaevskii, 1973; Efetov, 1979; Clem and Coffey, 1990; Carton, 1991). We choose a gauge with $A_y = 0$ and $A_x, A_z$ depending only on $x$ and $z$. Subtracting the phase equations (8.6) for $n+1$ and for $n$ from each other and rewriting

$$\partial_x^2 (\varphi_{n+1} - \varphi_n) + \frac{2\pi}{\Phi_o} [\partial_x A_x(nd+d) - \partial_x A_x(nd)] = \partial_x^2 \Phi_{n+1,n} - \frac{e^2}{\lambda^2} \sin\Phi_{n+1,n} \ ,$$

we obtain a coupled set of equations for the gauge-invariant phase differences $\Phi_{n+1,n}$ (Bulaevskii and Clem, 1991),

$$\partial_x^2 \Phi_{n+1,n} = \frac{1}{\Lambda^2} [2 \sin\Phi_{n+1,n} - \sin\Phi_{n+2,n+1} - \sin\Phi_{n,n-1}] + \frac{\varepsilon^2}{\lambda^2} \sin\Phi_{n+1,n} \ . \tag{8.10}$$

Outside a core region with dimensions $\Lambda$ and $d$, the nonlinearities in the above equations and their discreteness become irrelevant, and (8.10) can be approximated by the continuum differential equation

$$\left[ \partial_x^2 + \varepsilon^2 \partial_z^2 - \frac{\varepsilon^2}{\lambda^2} \right] \Phi(\mathbf{r}) = 0 \ . \tag{8.11}$$

Indeed, it is easy to see that the screening current density along the $z$ axis in the continuum anisotropic description,

$$j_z = -(2e\hbar/m)|\Psi|^2 \varepsilon \partial_z \tilde{\varphi} \simeq (c\Phi_o \varepsilon/8\pi\lambda^2 x) \ ,$$

becomes equal to the Josephson current density $j_J$ at $x \simeq \Lambda$; hence, for distances $x > \Lambda$, the linearized continu-

um approximation provides a good description of the situation. On the other hand, for small distances, $x < \Lambda$, a further increase in the current density $j_z$ is cut off by the condition $|j_{zj}| < j_J$, and the discreteness of the problem becomes relevant. The second critical dimension $d$ along the $z$ axis follows trivially from the scaling of $z$, $z = \varepsilon\Lambda = d$.

Equation (8.11) tells us that the driving (gauge-invariant) phase differences vanish due to screening on a length scale $\lambda/\varepsilon$ along the $x$ axis and on a scale $\lambda$ along the $z$ direction. Since the phase difference is the quantity driving the currents, we obtain a magnetic extent, $\lambda/\varepsilon$ (along $x$) and $\lambda$ (along $z$), for the Josephson vortex (see Fig. 31). On these magnetic length scales the Josephson

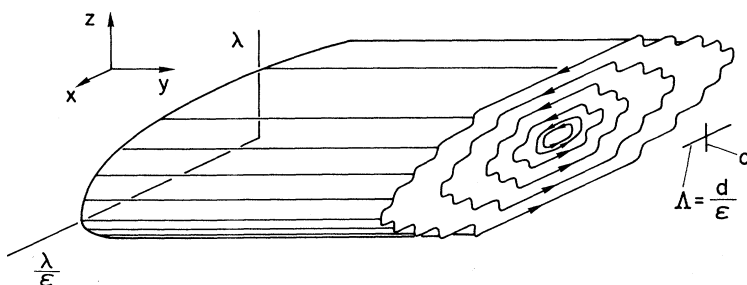FIG. 31. Josephson vortex in a strongly layered superconductor. The usual normal core of the Abrikosov vortex (dimensions $\varepsilon\xi$ and $\xi$ along $z$ and $x$, respectively) is replaced by the phase core (dimensions $d$ and $\Lambda = d/\varepsilon$ along $z$ and $x$, respectively) within which the nonlinearity and the discreteness of the situation are relevant. The region outside the phase core is roughly equivalent to the corresponding regime in an Abrikosov vortex with screening currents extending a distance $\lambda$ along $z$ and $\lambda/\varepsilon$ along $x$.

and Abrikosov vortices in an anisotropic superconductor are roughly equivalent (Bulaevskii, 1973; Efetov, 1979), apart from tiny corrections in the current flow and the magnetic-field pattern due to the layered structure (see, for example, Coffey and Clem, 1990). Within the distances $\Lambda$ (along $x$) and $d$ (along $z$), we have to take into account the nonlinearity and the discreteness of Eq. (8.10). On these scales the phase is changing rapidly and the current density $j_z$ reaches its maximum value $j_J$ at a distance $\approx 0.88\Lambda$ away from the axis of the vortex (Clem and Coffey, 1990). Furthermore, within this region the order parameter is weakly suppressed in the layers adjacent to the axis of the Josephson vortex. We can determine this suppression perturbatively (Blatter and Geshkenbein, 1992). The Ginzburg-Landau equation for the order parameter $\Psi_n$ ($\Psi_n^\infty = 1$) in the $n$th layer reads

$$\xi^2 e^{-i\varphi_n}\nabla^2(|\Psi_n|e^{i\varphi_n})+|\Psi_n|-|\Psi_n|^3=0 , \qquad (8.12)$$

where we ignore the coupling to the other layers for the time being. Separating Eq. (8.12) into real and imaginary parts, we obtain for the real part

$$\{\xi^2[\Delta^2-(\nabla^{(2)}\varphi_n)^2]+1-|\Psi_n|^2\}|\Psi_n|=0 . \qquad (8.13)$$

If a Josephson vortex directed along the $y$ axis is present between the $n$th and the $(n+1)$th layers, the phase $\varphi_n(x)$ will rapidly change on the scale $\Lambda$ and we can approximate the derivative of the phase $\partial_x\varphi_n \simeq 1/\Lambda$. Combining this estimate with (8.13), we obtain a suppression of the order parameter $\Psi_n$ of the order of

$$\delta|\Psi_n| \simeq \left[\frac{\xi}{\Lambda}\right]^2 \qquad (8.14)$$

at the center ($x=0$) of the Josephson vortex. Thus, in contrast to the Abrikosov vortex, where the large current flow near the core leads to complete suppression of the order parameter, the suppression of the order parameter in the superconducting layers is only weak when a Josephson vortex is present.

In summary, within the core region $\Lambda$, $d$, the full non-linearity and discreteness of the problem are relevant; the gauge-invariant phase difference is large and changes rapidly; the current density reaches its maximum value $j_J$; and the order parameter in the adjacent layers is (weakly) suppressed. We call this region the *phase core* of the Josephson vortex (see Fig. 31). We point out that this core region differs substantially from the core of an Abrikosov vortex, where the order parameter goes to zero on the scales $\xi$ and $\varepsilon\xi$ (note the equivalent ratio of length scales $d/\Lambda=\varepsilon\xi/\xi=\varepsilon$).

One should point out that the set of equations (8.10) for the gauge-invariant phase differences is not specific to the situation in which a field is applied parallel to the layers, but can be written in a more general form (Bulaevskii, Ledvij, and Kogan, 1992) if we replace the derivative $\partial_x^2$ in (8.10) by the planar Laplacian $\partial_x^2+\partial_y^2$. The resulting equations have to be supplemented by boundary conditions that describe the singularities in the phase field produced by the vortices,

$$\nabla^{(2)}\wedge(\nabla^{(2)}\Phi_{n+1,n})\equiv\partial_x\partial_y\Phi_{n+1,n}-\partial_y\partial_x\Phi_{n+1,n}$$

$$=2\pi\sum_\nu[\delta(\mathbf{r}-\mathbf{s}_{n+1,\nu})-\delta(\mathbf{r}-\mathbf{s}_{n,\nu})] ,$$

$$(8.15)$$

where $\mathbf{s}_{n,\nu}$ denotes the position of the singularity in the phase $\varphi_n$ corresponding to the $\nu$th vortex in the $n$th layer. Note that a straight vortex with $\mathbf{s}_{n,\nu}=\mathbf{s}_{n+1,\nu}$ produces no driving singularity for the phase differences $\Phi_{n+1,n}$; i.e., no screening currents crossing the layers are set up. It is quite remarkable that such a closed set of equations involving only the gauge-invariant phase differences $\Phi_{n+1,n}$ can be found.

It is interesting to note that the Josephson vortex in a layered superconductor is characterized by *two* length scales, $\Lambda=d/\varepsilon$ and $\lambda_c=\lambda/\varepsilon$, along the $x$ axis. This has to be contrasted with the case of a Josephson vortex placed in the junction between two weakly coupled bulk superconductors, for which there is only one characteristic length scale, $\lambda_J=[c\Phi_o/16\pi^2\lambda j_J]^{1/2}$, with $\lambda$ being the penetration depth of the bulk superconductors and $j_J$ the coupling current density of the junction. The difference between these two cases can be understood in the following way: Consider two bulk superconductors joined via a junction characterized by its coupling current density $j_J$. Let us place a vortex line in the junction and analyze its evolution from an Abrikosov vortex at strong coupling ($j_J \approx j_o$) to a Josephson vortex at weak coupling, $j_J \ll j_o$ (Gurevich, 1992; see also Likharev, 1979). For $j_J$ very close to the bulk depairing current density $j_o$, the Abrikosov vortex survives with a weakly distorted normal core elongated along the plane of the junction. The presence of a normal core is due to the large screening currents, $j \approx j_o$, flowing within the region $R < \xi$ around the vortex center. As $j_J$ drops below $\alpha j_J$, with the prefactor $\alpha \lesssim 1$ still of the order of unity, the large screening currents are cut off by $j_J$ and the normal core disappears. Instead, a phase core appears of size $\xi_J \simeq \xi(j_o/j_J)$ along the junction, inside of which the screening currents are large, of the order of $j_J$. As long as the core remains smaller than $\lambda$, the screening currents are only weakly modified, and we still have two length scales along the junction, with $\xi_J$ characterizing the width of the core and the scale $\lambda$ describing the flow of the screening currents. With a decrease in $j_J$, the phase core expands until it becomes larger than the magnetic screening length $\lambda$ by the time the coupling current density has reached a value $j_J \simeq j_o/\kappa$. As $j_J$ drops below this critical value, the transformation to the Josephson vortex, with only one length scale $\lambda_J$ describing the phase, the currents, and the field across the junction, has been completed. The analogous discussion for a layered superconductor produces quite a different result. In a layered material, the screening currents flowing perpendicular to the planes not only have to cross a single junction, but

have to overcome the large number of $\lambda/d$ junctions. When the coupling strength between the layers is decreased, the screening current density along the $c$ axis is also reduced so that the current pattern of the original Abrikosov vortex immediately starts to expand along the junction. As a result, the ratio between the magnetic extent of the vortex and the size of its phase core remains always the same, $\Lambda/\lambda_c = d/\lambda = \text{const}$, independent of the coupling strength, and we always keep the two length scales describing the core and the magnetic size of the Josephson vortex.

From this discussion we can understand that a Josephson vortex is very similar to an Abrikosov vortex, but with a different core size and structure. This conclusion is also confirmed by the calculation of the Josephson vortex line energy by Bulaevskii (1973) and by Efetov (1979). The line energy of a vortex can be obtained from an integration of the kinetic energy of the currents. Making use of the analogy between the Abrikosov vortex and the Josephson vortex, we obtain the line energy

$$e_J \approx \varepsilon \varepsilon_0 \ln \frac{\lambda}{d} \,, \tag{8.16}$$

where the inner and outer cutoff lengths in the logarithm are provided by the magnetic $(\lambda_c, \lambda)$ and phase core $(\Lambda, d)$ extent of the Josephson vortex. The calculation of Clem, Coffey, and Hao (1991) gives the more accurate result

$$e_J = \varepsilon \varepsilon_0 \left[ \ln \frac{\lambda}{d} + 1.12 \right] \,. \tag{8.17}$$

The corresponding result for an Abrikosov vortex in an anisotropic superconductor and directed along the planes is (Hu, 1972)

$$e_l = \varepsilon \varepsilon_0 \left[ \ln \frac{\lambda}{\varepsilon \xi} + 0.50 \right] \,. \tag{8.18}$$

Note the different temperature dependence for the two results (8.17) and (8.18), arising from the replacement of $\xi_c(T) = \varepsilon \xi(T)$ by the layer distance $d$ under the logarithm. With result (8.17) for the line energy, the equation for the lower critical field along the planes follows trivially, $H_{c_1}(\vartheta = 0) = 4\pi e_J/\Phi_0$. The elastic tension of a Josephson vortex is equal to its line energy, due to the isotropy within the planar dimension.

A quantity depending on the core structure rather than on the current flow outside the core is the viscous drag coefficient. This coefficient has been calculated by Clem and Coffey (1990), and they find a result that differs only by a numerical factor from the corresponding (Bardeen-Stephen) expression for an Abrikosov vortex in which the appropriate dimensions for the phase core has been substituted,

$$\eta_J = 2.226 \frac{\Phi_0^2}{2\pi \rho_n^c c^2 \varepsilon \Lambda^2} \,, \tag{8.19}$$

where $\rho_n^c$ is the normal-state resistivity along the $c$ axis. The corresponding Bardeen-Stephen result for an Abrikosov vortex under equivalent conditions is

$$\eta_l = \frac{\Phi_0^2}{2\pi \rho_n^c c^2 \varepsilon \xi^2} \,. \tag{8.20}$$

It appears that the Josephson vortex is very similar to the corresponding Abrikosov vortex, if we carefully take into account the modifications due to the different core sizes and core structures.

### 2. Pancake vortices

Here we discuss the structure of a vortex and its constituents (pancake vortices) for the case when the field is aligned with the $c$ axis of the material. It is very interesting to understand the similarities and differences between the three cases of an isolated thin film (Pearl, 1964), an uncoupled stack of parallel films, i.e., a layered material with $j_J = 0$ (Efetov, 1979; Artemenko and Kruglov, 1990; Buzdin and Feinberg, 1990; Feigel'man, Geshkenbein, and Larkin, 1990; Clem, 1991; Fischer, 1991), and a layered superconductor with $j_J > 0$ (Artemenko and Kruglov, 1990; Chakravarty, Ivlev, and Ovchinnikov, 1990a; Feigel'man, Geshkenbein, and Larkin, 1990; Bulaevskii, Ledvij, and Kogan, 1992). We therefore start with the simplest case of a 2D thin film of thickness $d$. Again we choose $\lambda$ to denote the penetration depth of the corresponding bulk material such that the effective penetration depth of the film becomes $\lambda_{\text{eff}} = 2\lambda^2/d$. The solution for a vortex positioned at the origin of the coordinate system is given by the Pearl solution (Pearl, 1964; see also de Gennes, 1966 and Abrikosov, 1988). The magnetic field follows from the vector potential

$$A_\varphi(R,z) = \Phi_0 \int_0^\infty \frac{dq}{2\pi} \frac{J_1(qR)e^{-q|z|}}{1+\lambda_{\text{eff}}q} \tag{8.21}$$

$[J_1(x)$ is a Bessel function of integer order] by taking derivatives, and its asymptotic behavior resembles that of a magnetic monopole generating a magnetic flux $\Phi_0$ within the upper half-space,

$$\mathbf{B}(r \gg \lambda_{\text{eff}}) \approx \frac{\Phi_0}{2\pi} \frac{z}{|z|} \frac{\mathbf{r}}{r^3} \,; \tag{8.22}$$

see Fig. 32. The magnetic flux crossing the film within a circle of radius $R$ is

$$\Phi(R) \approx \Phi_0 \begin{cases} \dfrac{R}{\lambda_{\text{eff}}}, & R \ll \lambda_{\text{eff}} \,, \\[2mm] 1 - \dfrac{\lambda_{\text{eff}}}{R}, & \lambda_{\text{eff}} \ll R \,, \end{cases} \tag{8.23}$$

and approaches the unit flux quantum $\Phi_0$ at large distances. The current density in the film is given by
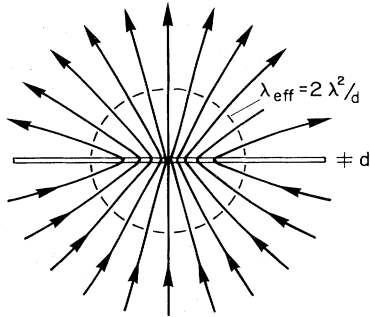
FIG. 32. Pearl solution for a vortex in a superconducting film taking the form of a magnetic monopole asymptotically.

$$J_\varphi(R) \approx \frac{\Phi_o c}{4\pi^2 \lambda_{eff}^2} \begin{cases} \frac{\lambda_{eff}}{R}, & R \ll \lambda_{eff}, \\ \left[\frac{\lambda_{eff}}{R}\right]^2, & \lambda_{eff} \ll R. \end{cases} \qquad (8.24)$$

(We denote a current per unit length by $J$ in order to distinguish it from the usual current density $j$.) In terms of the depairing current density $j_o$ of the bulk material, the current scale in (8.24) is given by $\Phi_o c/4\pi^2 \lambda_{eff}^2 = dj_o (3\sqrt{3}/4)(\xi d/\lambda^2)$.

Finally, the Lorentz force $F_L(R) = J_\varphi(R)\Phi_o/c$ acting on a second vortex with the same vorticity a distance $R$ away generates the interaction potential

$$V^{int}(R) \approx 2d\varepsilon_o \begin{cases} \ln\frac{\lambda_{eff}}{R}, & R \ll \lambda_{eff}, \\ \frac{\lambda_{eff}}{R}, & \lambda_{eff} \ll R. \end{cases} \qquad (8.25)$$

The logarithmic interaction potential for distances $R \ll \lambda_{eff}$ generates a Berezinskii-Kosterlitz-Thouless transition, which is cut off due to screening on a scale $\lambda_{eff}$. For very thin films, $\lambda_{eff} \propto 1/d$ can become larger than the size of the film, and the sharp transition is cut off (rounded) due only to the finiteness of the sample.

Next, let us consider the case of an array of parallel thin films where the coupling is of pure electromagnetic origin, $j_J = 0$ (Artemenko and Kruglov, 1990; Buzdin and Feinberg, 1990; Feigel'man, Geshkenbein, and Larkin, 1990; Clem, 1991; Fischer, 1991). The basic equation describing this situation is (8.4). Ignoring the small variations on the scale $d$, we can rewrite (8.4) in the form

$$\lambda^2 \Delta \mathbf{A}^{(2)} - \mathbf{A}^{(2)} = \frac{d\Phi_o}{2\pi} \sum_n \delta(z - nd)\nabla^{(2)}\varphi_n . \qquad (8.26)$$

An individual vortex line threading the stack is characterized by the positions $\mathbf{R}_n$ of the vortex cores within each layer. Each core generates a driving phase field

$$\nabla^{(2)}\varphi_n(\mathbf{R}) = -\frac{\mathbf{n} \wedge (\mathbf{R} - \mathbf{R}_n)}{|\mathbf{R} - \mathbf{R}_n|^2} , \qquad (8.27)$$

in response to which a screening current starts to flow in this layer. Equation (8.26) couples the $n$th layer electromagnetically to all the other layers; hence screening currents in response to a vortex core in the $n$th layer will also be set up within the other layers of the stack. Since (8.26) is a set of linear equations, we can easily determine the building blocks of the vortex line. Consider a single-vortex core $\nabla^{(2)}\varphi_n(\mathbf{R}) = -\mathbf{e}_\varphi/R$ placed at the origin of the $n$th layer (positioned at $z=0$), with all the other driving terms vanishing. Such a building block is called a pancake vortex (Clem, 1991) and furnishes the Green's function of the problem. The solution of (8.26) is easily obtained by going over to Fourier space, and we find

$$\mathbf{A}^{(2)}(\mathbf{K}, k_z) = \frac{id\Phi_o \mathbf{K} \wedge \mathbf{n}}{K^2(1 + \lambda^2 k^2)} . \qquad (8.28)$$

The magnetic field then follows from Fourier-transforming the expression $\mathbf{k} \wedge \mathbf{A}^{(2)}$, and the result is (Artemenko and Kruglov, 1990; Feigel'man et al., 1990; Clem, 1991)

$$B_z(\mathbf{r}) = \frac{\Phi_o}{4\pi\lambda^2} \frac{d}{r} e^{-r/\lambda} ,$$

$$\mathbf{B}^{(2)}(\mathbf{r}) = \frac{\Phi_o}{4\pi\lambda^2} \frac{d\mathbf{R}}{R^2} \text{sgn}z \left[ e^{-|z|/\lambda} - \frac{|z|}{r} e^{-r/\lambda} \right] . \qquad (8.29)$$

The shape of the magnetic-field distribution differs quite drastically from the monopole-like Pearl solution (see Fig. 33). The screening effect due to the other layers in the stack squeezes the field into a narrow strip of size $\lambda$ along the $z$ axis, and the magnetic field has to escape parallel to the layers rather than spreading out uniformly over the entire solid angle. This field redistribution due to screening has important consequences. First, the squeezing of the field reduces the flux threading the central layer $n$ to
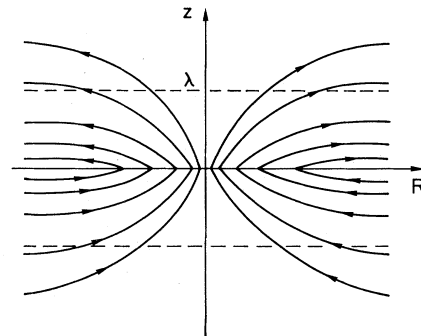


FIG. 33. Pancake vortex in a layered superconductor with vanishing interlayer Josephson coupling. The screening currents present in the neighboring layers squeeze the magnetic field into the planar direction. The screening current density in the central layer decays like $j \propto 1/R$ to all length scales, resulting in a true Berezinskii-Kosterlitz-Thouless behavior at all scales.

$$\Phi(R) = \Phi_0 \frac{d}{2\lambda}(1 - e^{-R/\lambda}) \; ; \tag{8.30}$$

hence the current flow is never able to screen the driving phase field in the central layer. Indeed, the current density of the central layer decays like $1/R$ to all length scales,

$$J_\varphi(R, z = 0) = \frac{\Phi_0 c}{4\pi^2 \lambda_{eff}^2} \frac{\lambda_{eff}}{R} \left[ 1 - \frac{d}{2\lambda}(1 - e^{-R/\lambda}) \right] , \tag{8.31}$$

and therefore the logarithmic dependence of the interaction potential $V^{int}$ between two vortices placed in the same layer persists to infinity,

$$V_{em}^{int}(R, z = 0) = 2d\varepsilon_0 \left[ \ln\frac{\xi}{R} + O(d/\lambda) \right] ,$$

$$\xi < R < \infty \; . \tag{8.32}$$

Here we have used the planar coherence length $\xi$ of the bulk layered material as a short-distance cutoff. As a result, the system of parallel decoupled superconducting layers is expected to develop a true Berezinskii-Kosterlitz-Thouless transition at $T_{BKT} = \varepsilon_0 d/2$ on all length scales.

Instead of placing the second pancake vortex in the same layer, we can equally well probe the field generated by a vortex at the origin $r = 0$ in a different layer with $z \neq 0$. The interaction between two vortices of the same vorticity is then attractive and reduced by the small factor $d/\lambda \ll 1$,

$$V_{em}^{int}(R, z \neq 0) \approx \frac{1}{2} d\varepsilon_0 \frac{d}{\lambda} \begin{cases} \dfrac{R}{\lambda}, & |z| \ll R \ll \lambda , \\[2mm] e^{-|z|/\lambda} \ln\dfrac{R}{\lambda}, & \lambda \ll R . \end{cases} \tag{8.33}$$

Let us return to the full vortex line where a phase singularity is present in each layer. The calculation of the field distribution, the line energy, and the lower critical field $H_{c_1}^c$ (Clem, 1991) gives results that are in complete agreement with the continuous anisotropic description,

$$B_z = \frac{\Phi_0}{2\pi\lambda^2} K_0 \left[ \frac{R}{\lambda} \right] ,$$

$$e_l = \frac{\Phi_0}{4\pi} H_{c_1}^c = \varepsilon_0 \ln\kappa \tag{8.34}$$

Similarly, the line energy $e_l(\vartheta)$ for a vortex tilted an angle $\theta = \pi/2 - \vartheta$ away from the $c$ axis agrees (to logarithmic accuracy) with the continuous anisotropic result (2.141) in the limit $\varepsilon \to 0$,

$$e_l(\vartheta) = \varepsilon_0 \sin\vartheta \ln \left| \frac{\kappa}{\sin\vartheta} \frac{1 + \sin\vartheta}{2} \right| . \tag{8.35}$$

Note that $\varepsilon_\vartheta = \sin\vartheta$ for the present case of perfectly

decoupled layers with $\varepsilon = 0$.

An interesting property of the vortex line in a decoupled layered system is its finite "evaporation" temperature $T_e$. As the temperature rises beyond $T_e$, the vortex line disintegrates into a gas of free pancake vortices. It turns out that an individual pancake vortex is harmonically bound to the vortex line at small distances, $R < \lambda$, but only logarithmically attracted to the line at large distances, $R > \lambda$ (Clem, 1991; Fischer, 1991). The weak (logarithmic) binding of an individual pancake vortex to the vortex line, then, leads to a divergence of the mean-squared thermal displacement of an individual pancake vortex at a temperature $T_e = T_{BKT}$. This result can be understood in a simple way: A vortex line with one pancake moved a distance $R$ away is equivalent to a vortex line plus a vortex-antivortex pair of separation $R$. At $T_{BKT}$, the pair becomes free (unbinding transition, see Sec. VIII.B); hence the vortex line evaporates.

Finally, let us turn on the Josephson coupling between the superconducting layers and study the consequences (Artemenko and Kruglov, 1990; Chakravarty *et al.*, 1990; Feigel'man *et al.*, 1990; Bulaevskii *et al.*, 1992). It now becomes impossible to introduce a single pancake vortex into the system. In addition to the electromagnetic interaction between the layers, we now have a contribution

$$\mathcal{I}_J = \frac{d\varepsilon_0}{\pi} \int \frac{d^2R}{\Lambda^2} [1 - \cos\Phi_{n+1,n}(\mathbf{R})] , \tag{8.36}$$

from the Josephson coupling to the total energy of the system. Introducing an individual pancake vortex into the system leads to a phase difference $\Phi_{n+1,n} \neq 0$ between the plane containing the vortex and its two neighbors, and the coupling energy to these two layers becomes infinite. Ignoring a possible relaxation of the phase pattern, we find that Eq. (8.36) would predict an energy of an individual pancake vortex that grows with the area of the sample. However, the phase pattern due to a single pancake vortex can relax to a state with an energy growing only linearly in the same size, with the linear energy arising from the Josephson strings that take the flux to and away from the pancake vortex. Let us therefore introduce a pair of oppositely "charged" vortices into the same plane. The energy contribution from the Josephson coupling is then (2 vortices, layers $n \pm 1$)

$$\mathcal{I}_J = 2d\varepsilon_0 \int \frac{d^2R'}{\pi\Lambda^2} [1 - \cos\Phi_{n+1,n}(\mathbf{R}')] . \tag{8.37}$$

The phase differences $\Phi_{n+1,n}(\mathbf{R}')$ are determined by the coupled set of equations (8.6). In order to truncate this system of equations, we assume the phases $\varphi_{n\pm1}$ to be undisturbed; only the phase $\varphi_n$ is distorted due to the presence of the pair in layer $n$. The phase difference $\Phi = \varphi_{n+1} - \varphi_n = \varphi_{n-1} - \varphi_n$, then, is a solution of

$$\Lambda^2 \Delta^{(2)}\Phi = -2\sin\Phi , \tag{8.38}$$

where we have neglected the additional screening term

due to the vector potential, which becomes relevant on large scales, $R > \lambda/\varepsilon$, only. For small phase differences $\Phi$, we can expand the sine in (8.38) and obtain the natural length scale (screening length) $\Lambda = d/\varepsilon$ of the problem. On scales $R < \Lambda$, the Josephson currents cannot build up, and the system essentially behaves like an uncoupled layered material with its ideal 2D behavior. On the other hand, for distances $R > \Lambda$, the currents along $z$ are no longer hampered by the discreteness of the material, and a continuous anisotropic 3D behavior results.

Let us first study the case of two pancake vortices close to each other with a separation $R \ll \Lambda$. The solution of (8.38) then behaves as

$$\Phi(R') \simeq \begin{cases} \mathbf{R} \cdot \nabla^{(2)} \varphi = \dfrac{R \cos\varphi}{R'}, & R \ll R' \ll \Lambda , \\ \sim e^{-R'/\Lambda}, & \Lambda \ll R' , \end{cases}$$

where $\varphi = \arctan(y/x)$ is the azimuthal angle in the plane. For small phase differences $\Phi$, we can expand the cosine in Eq. (8.37), and a trivial integration supplies us with the Josephson interaction energy of the pair,

$$V_J^{\text{int}}(R) = d\varepsilon_0 \left[ \frac{R}{\Lambda} \right]^2 \ln\frac{\Lambda}{R}, \quad R \ll \Lambda . \tag{8.39}$$

For large separations $R \gg \Lambda$, two Josephson strings connecting the pair are created between the layers $n$ and $n \pm 1$. The interaction between the two pancake vortices is dominated by the energies of the two strings and takes the form [see Eq. (8.17)]

$$V_J^{\text{int}}(R) = 2 d\varepsilon_0 \left[ \alpha \frac{R}{\Lambda} - \frac{\Lambda}{4R} \right], \quad \Lambda \ll R \ll \lambda/\varepsilon , \tag{8.40}$$

with $\alpha$ a factor of order unity arising from cutting off the logarithm in Eq. (8.17) at a distance of the order of the separation $d$ between the Josephson strings (Cataudella and Minnhagen, 1990; Glazman and Koshelev, 1990). The last term in Eq. (8.39) is a higher-order correction to the leading string term arising from the Josephson coupling. It was obtained by Chakravarty, Ivlev, and Ovchinnikov (1990a) within the London approximation for kinked vortices, which describes well the situation for distances $|z| > d$ and $R > \Lambda$ away from the core region. The correction term decays like a power law $\propto 1/R$ for distances $R < \lambda/\varepsilon$ and exponentially fast for distances $R > \lambda/\varepsilon$; hence at very large distances, $R > \lambda/\varepsilon$, only the linear string term remains and

$$V_J^{\text{int}}(R) = 2 d\varepsilon_0 \alpha \frac{R}{\Lambda}, \quad \lambda/\varepsilon \ll R . \tag{8.41}$$

The comparison of the Josephson interaction energies (8.39) and (8.40) with the electromagnetic energy (8.30) of the pair shows that the electromagnetic contribution is larger at small distances, $R < \Lambda$, and that the Josephson term becomes dominant for large distances, $R > \Lambda$.

In summary, we obtain the following picture for the interaction between two pancake vortices placed in the same layer of a Josephson-coupled system: At small distances, $R < \Lambda$, the Josephson currents have not yet built up, the electromagnetic energy is dominant, and we obtain a logarithmic interaction. As $R$ grows beyond $\Lambda$, the Josephson currents have been established, the magnetic field between the two vortices has been redirected into two Josephson strings, and the interaction grows linearly; i.e., the pair becomes confined,

$$V^{\text{int}}(R,z=0) \approx 2 d\varepsilon_0 \begin{cases} \ln\dfrac{R}{\xi}, & \xi < R < \Lambda , \\[2mm] \dfrac{R}{\Lambda} - \dfrac{\Lambda}{4R}, & \Lambda < R < \lambda/\varepsilon , \\[2mm] \dfrac{R}{\Lambda}, & \lambda/\varepsilon < R . \end{cases} \tag{8.42}$$

As a result, the Berezinskii-Kosterlitz-Thouless transition is cut off at the length scale $\Lambda$ introduced into the system due to the finite Josephson coupling.

For completeness, let us also present the results for a double-kink structure in a vortex line directed parallel to the layers (see Fig. 34). For two oppositely charged vortices (the vortex line remains in the same plane asymptotically), we obtain, following Chakravarty, Ivlev, and Ovchinnikov (1990a),

$$V_{K,-K}^{\text{int}} \simeq 2 d\varepsilon_0 \begin{cases} \ln\dfrac{R}{\xi}, & \xi < R < \Lambda , \\[2mm] \ln\dfrac{\Lambda}{\xi} - \dfrac{\Lambda}{4R}, & \Lambda < R < \lambda/\varepsilon , \\[2mm] \ln\dfrac{\Lambda}{\xi}, & \lambda/\varepsilon < R . \end{cases} \tag{8.43}$$

This configuration corresponds to the nucleus for creep motion along the $c$ axis (see Sec. III.E.1). The leading term for $R < \Lambda$ is due to the currents flowing within the plane containing the two kinks, and we have ignored the additional contribution arising from the Josephson coupling to the neighboring planes [Eq. (8.38)]. The long-distance behavior at $\Lambda < R$ can be calculated using the
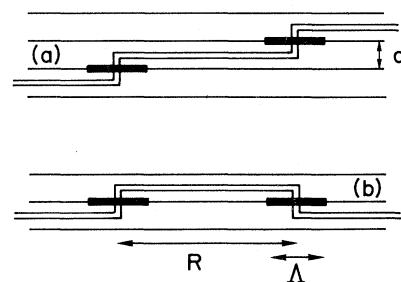


FIG. 34. Kinked vortex configurations in a strongly layered superconductor: (a) Double-kink configuration representing the building block of a vortex line tilted at a small angle $\vartheta < \varepsilon$ with respect to the planes. (b) Kink-antikink configuration representing the nucleus for vortex motion across the superconducting layers.

London approximation for kinked vortices and consists of the (in-plane current) core contributions of the two kinks plus the correction term due to Josephson coupling to the neighboring layers. Since the string connecting the two kinks is only shifted by a distance $d$ and not newly created, there is no linear confinement term in Eq. (8.43).

Two equally charged kinks lead to a shift of the vortex line by a distance $2d$ along the $c$ axis (see Fig. 34). This configuration can be considered as providing the building block of a tilted vortex. The interaction between the two kinks is (Artemenko and Kruglov, 1990)

$$V_{K,K}^{int} \simeq d\varepsilon_0 \begin{cases} \dfrac{d}{2\lambda}\dfrac{R}{\lambda} + \dfrac{1}{2}\left[\dfrac{R}{\Lambda}\right]^2 \ln\dfrac{\Lambda}{R}, & \xi < R < \Lambda , \\[2ex] \dfrac{\Lambda}{2R}, & \Lambda < R < \lambda/\varepsilon , \end{cases}$$
(8.44)

with the two terms at short distances, $R < \Lambda$, arising from the electromagnetic and the Josephson coupling between the vortices.

The above discussion allows us to study arbitrary single-vortex configurations in layered superconductors and their configurational energies in terms of sets of pointlike particles interacting via their interaction potential. As an example, we calculate below the elastic line tensions (to logarithmic accuracy only) for the in-plane and for the out-of-plane tilt modes of a single-vortex line in a layered material.

The line energy of a vortex enclosing an angle $\vartheta$ with the superconducting layers is obtained by summing up the energies of the individual pancake vortices, including their interactions as given by Eq. (8.44) and the contributions from the Josephson strings [Eq. (8.16)]. The interaction term contains contributions from both the magnetic and the Josephson couplings, and we concentrate on the leading contribution arising here from the Josephson coupling between the layers. For large angles $\vartheta > \varepsilon$, the separation between neighboring pancake vortices is less than $\Lambda$, and the line energy becomes (Blatter and Geshkenbein, 1992; Bulaevskii, Ledvij, and Kogan, 1992)

$$\varepsilon_l(\vartheta > \varepsilon) = \varepsilon_0 \sin\vartheta \left[ \ln\dfrac{\alpha\lambda}{\xi\sin\vartheta} + \dfrac{\varepsilon^2}{2\tan^2\vartheta}\ln\dfrac{\alpha'\lambda\tan\vartheta}{d} \right] ,$$
(8.45)

where $\alpha$ and $\alpha'$ are prefactors of order unity. Within this angular regime the Josephson strings have not yet developed, and the interlayer coupling produces the term (8.39) only. For small angles $0 < \vartheta < \varepsilon$, the Josephson string gives a large contribution to the energy, and the combination of Eq. (8.40) with (8.44) results in

$$\varepsilon_l(0 < \vartheta < \varepsilon) = \varepsilon_0 \sin\vartheta \left[ \ln\dfrac{\Lambda}{\xi} + \dfrac{\varepsilon}{\tan\vartheta}\ln\dfrac{\lambda}{d} + \dfrac{1}{2\varepsilon}\tan\vartheta \right] .$$
(8.46)

Using again definitions (2.143) and (2.145) for $\varepsilon_l^{\perp}(\vartheta)$ and

for $\varepsilon_l^{\|}(\vartheta)$ above, we well as the expressions for the change in length $\delta L$ and angle $\delta\vartheta$, we obtain the following results (to logarithmic accuracy) for the out-of-plane and the in-plane line tensions in a layered material:

$$\varepsilon_l^{\perp}(\vartheta) \simeq \dfrac{\varepsilon_0}{\varepsilon} \begin{cases} \dfrac{1}{\cos^3\vartheta}, & 0 < \vartheta < \varepsilon , \\[2ex] \left[\dfrac{\varepsilon}{\sin\vartheta}\right]^3, & \varepsilon < \vartheta < \dfrac{\pi}{2} , \end{cases}$$
(8.47)

and

$$\varepsilon_l^{\|}(\vartheta) \simeq \varepsilon\varepsilon_0 \begin{cases} \cos\vartheta, & 0 < \vartheta < \varepsilon , \\[2ex] \dfrac{\varepsilon}{\sin\vartheta}, & \varepsilon < \vartheta < \dfrac{\pi}{2} . \end{cases}$$
(8.48)

Note that, due to the intrinsic pinning (lock-in transition, see below), the out-of-plane tilt modulus diverges as the angle $\vartheta$ goes to zero. In the above calculation of the tilt modulus, we have ignored this effect, which, however, becomes relevant when the vortex segment to be tilted is locked to the plane along its entire length. On the other hand, in the presence of kinks, the tilt modulus becomes finite due to the mobility of the pancake vortices along the planes. Using $\varepsilon_\vartheta^2 = \varepsilon^2\cos^2\vartheta + \sin^2\vartheta$, we find that the elasticities for an anisotropic and for a layered superconductor are roughly identical. This can be understood from the fact that the line tension is dominated by the current flow in the vortex, which is equal for discrete and continuous cases outside the (rather small) core region. The different sizes of the core regions would produce deviations in the logarithmic factors, which we have ignored in the above analysis.

### 3. Vortex lattice and lock-in transition

In this section we turn our attention to the behavior of the vortex *lattice* in layered superconductors. In general, the continuous anisotropic description provides a rather good first approximation of the properties of the vortices and their lattice in a layered superconductor. The discreteness of the material and the weak Josephson-type coupling, however, introduce two important modifications into the free energy of the system, which lead to very interesting effects. These two corrections introduced by the layering consist of *logarithmic corrections* due to the different core structure of the kinked vortices from those of the rectilinear Abrikosov vortices and the appearance of a *linear term* $\propto \vartheta$ due to the trapping of the vortex line in the region between the superconducting layers. To illustrate, let us consider an individual vortex line and compare the line energies of a rectilinear Abrikosov vortex (described by a continuous anisotropic model) with that of a kinked vortex (based on a Lawrence-Doniach description). Including, as well, the contributions from the core condensation energies, we obtain ($\vartheta < \varepsilon$)

$$e_l^r = \varepsilon_0 \varepsilon_\vartheta \left[ \ln \frac{\lambda}{\varepsilon_\vartheta \xi} + 0.5 \right] , \qquad (8.49)$$

$$e_l^k = \varepsilon_0 \left[ \varepsilon \cos\vartheta \ln \frac{\lambda}{d} + |\sin\vartheta| \left( \ln \frac{\Lambda}{\xi} + 0.5 \right) \right] . \qquad (8.50)$$

The line energy of the Abrikosov vortex comprises a contribution from the screening currents (of extent $\lambda$) and a second term due to the loss of condensation energy in the core region. The various terms in Eq. (8.50) arise from the Josephson and pancake vortex segments (see Fig. 35). The Josephson vortex contributes only a part arising from the screening currents, since there is no normal core. The pancake vortices contribute a term due to the 2D core region of size $\Lambda$, where the Josephson currents have not yet fully developed, and a second term due to the normal core of size $\xi$. Note that Eq. (8.50) is valid at small angles, $\vartheta < \varepsilon$. For large angles with $d/\xi < \tan\vartheta$, the screening currents mainly flow in the planes, the contribution from the pancake vortices changes to $\varepsilon_0 \sin\vartheta [\ln(\lambda/\xi) + 0.5]$, and no Josephson vortex segment is present. As a result, the continuous description applies well to this large-angle regime, and no new phenomena due to the layered structure are expected here. Within the intermediate regime, $\varepsilon < \tan\vartheta < d/\xi$, a crossover takes place where the kinked structure is developed and the screening currents shift from predominantly planar to Josephson. Within this region, both the 2D pancake core and the Josephson segments are built up and the planar screening currents disappear.

Let us expand the line energies $e_l^r$ and $e_l^k$ for small angles,

$$e_l^r \approx \varepsilon_0 \left[ \varepsilon + \frac{\vartheta^2}{2\varepsilon} \right] \left[ \ln \frac{\lambda}{\varepsilon \xi} + 0.5 \right] , \qquad (8.51)$$

$$e_l^k \approx \varepsilon_0 \left[ \varepsilon \ln \frac{\lambda}{d} + |\vartheta| \left( \ln \frac{\Lambda}{\xi} + 0.5 \right) \right] . \qquad (8.52)$$

Equations (8.51) and (8.52) exhibit the two features mentioned previously: The terms order $(\vartheta)^0$ have different logarithmic arguments, which is the result of the different cutoff lengths $d$ and $\varepsilon\xi$ introduced by the different core structures. In addition, a normal core is
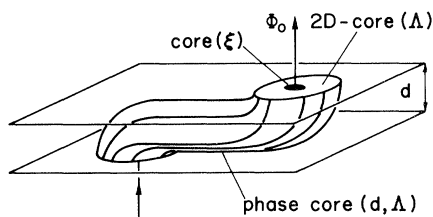


FIG. 35. Building block of a vortex line tilted at a small angle $\vartheta < \varepsilon$ with respect to the layers. The 2D core region of the pancake vortex as well as the phase core of the Josephson string are fully developed.

present in the Abrikosov vortex, whereas the corresponding object is absent in the Josephson vortex. The logarithmic corrections to the free energy of the vortex lattice thus may lead to new physical effects such as the transition from the tilted, kinked vortex lattice to a combined lattice of independent Josephson and Abrikosov vortices running parallel and orthogonal to the planes (see Kes *et al.*, 1990; Theodorakis, 1990; Bulaevskii, Ledvij, and Kogan, 1992). Second, a term linear in the angle $\propto |\vartheta|$ appears as a result of the kinked structure of the vortex. The linear term in the energy is a typical characteristic of the trapping of the vortex in a more favorable direction and leads to the lock-in transition (Feinberg and Villard, 1990; Bulaevskii, 1991; Ivlev, Ovchinnikov, and Pokrovsky, 1991; Maslov and Pokrovsky, 1991). Such a linear term is not peculiar to the present situation, but appears elsewhere, i.e., when one considers the trapping of vortex lines within the attractive potential wells of extended defects such as twin boundaries or columnar defects (see Sec. IX). No such term is present for the Abrikosov vortex [see Eq. (8.51)], where the corrections are of order $(\vartheta)^2$; hence no lock-in transition can be obtained within an approximate continuous anisotropic description of the layered material.

The appearance of the three angular regimes—a large-angle region $(d/\xi < \tan\vartheta)$ where the normal cores of the pancake vortices still overlap (line core) and the physics of the vortex system is well described by a continuum description; an intermediate regime $(\varepsilon < \tan\vartheta < d/\xi)$ where the screening currents change from planar to Josephson; and a small-angle region $(\vartheta < \varepsilon)$ where the kinked vortex structure is fully developed—is not specific to the single-vortex situation described in detail above but also applies to the discussion of the vortex lattice in layered superconductors. In addition, a fourth, very interesting angular "regime" appears in the discussion of the vortex lattice in layered material, which is given by the condition $\vartheta = 0$, i.e., for a perfectly aligned vortex system. In this situation the vortices are pinned by the discrete structure. While they are still free to arrange themselves via intraplanar motion, relaxations involving a crossing of layers (motion along $z$) is strongly suppressed. This phenomenon of intrinsic pinning leads to interesting effects based on a shear instability developed in the vortex lattice (Ivlev, Kopnin, and Pokrovsky, 1990; Levitov, 1991; Ivlev and Campbell, 1993). In the following we present a more detailed discussion of the lock-in transition and the appearance of a combined vortex lattice at small angles, $\vartheta < \varepsilon$. We also briefly describe the origin and consequences of shear instability in a perfectly aligned vortex lattice.

Much attention has been devoted to the new phenomenon of the lock-in transition (Feinberg and Villard, 1990; Ivlev, Ovchinnikov, and Pokrovsky, 1990; Bulaevskii, 1991; Maslov and Pokrovsky, 1991). At small angles, $\vartheta_{H_a} < \vartheta_L$, of the external field $\mathbf{H}_a$, the vortex lattice can gain energy by aligning itself with the $ab$ planes, thereby creating a pure lattice of Josephson vortices and

avoiding strong perturbations of the superconductor in the layers. In the following we present a quantitative determination of the lock-in angle $\vartheta_L$. We first study the continuous anisotropic situation and determine the misalignment between the internal magnetic field **H** and the magnetic induction **B**. We then proceed to the layered case where this misalignment is modified due to the presence of an additional linear term in the free energy of the vortex system. Third, we determine the lock-in angle in layered superconductors, taking demagnetization effects properly into account.

Within an anisotropic superconductor, the magnetic induction **B** (enclosing an angle $\vartheta$ with the planes) and the magnetic field **H** directed along $\vartheta_H$ are generally not parallel, $\vartheta < \vartheta_H$. Under equilibrium conditions (no pinning), both the magnitude $H$ and the direction $\vartheta_H$ of the magnetic field are determined by the free-energy density $F(\mathbf{B})$ of the system via

$$\mathbf{H} = 4\pi \frac{\partial F}{\partial \mathbf{B}} \ . \tag{8.53}$$

For magnetic fields $H_{c_1} \ll H \ll H_{c_2}$, the free-energy density takes the form (Campbell, Doria, and Kogan, 1988; Kogan, 1988)

$$F = \frac{B^2}{8\pi} + \frac{\Phi_0 B \varepsilon_\vartheta}{2(4\pi\lambda)^2} \ln\left[\frac{\alpha H_{c_2}^c}{\varepsilon_\vartheta B}\right] \ , \tag{8.54}$$

where $\alpha$ is a factor of order unity. The first term in Eq. (8.54) is the usual magnetic energy contribution, whereas the second term arises from the line energies of the vortices with a large-distance cutoff under the logarithm provided by the mean vortex separation $a_0 / \sqrt{\varepsilon_\vartheta}$ rather than the screening length $\lambda$ relevant for fields $H_{c_1} \ll H$. Neglecting the angular dependence under the logarithm, we obtain the misfit angle $\vartheta_H - \vartheta$ as a solution to [use $\sin(\vartheta_H - \vartheta) = (\mathbf{H} \wedge \mathbf{B})/BH$]

$$\sin(\vartheta_H - \vartheta) = \frac{H_{c_1}^c}{H} \frac{(1-\varepsilon^2)\sin\vartheta\cos\vartheta}{\varepsilon_\vartheta}$$
$$\times \frac{\ln(\alpha H_{c_2}^c / \varepsilon_\vartheta B)}{2\ln\kappa} \tag{8.55}$$

(Balatskii, Burlachkov, and Gor'kov, 1986; Kogan, 1988; Bulaevskii, 1991). Obviously, the vortex lattice has a tendency to align itself with the superconducting planes, but is restricted by the directing action of the magnetic field **H** to tilt far away from $\vartheta_H$. The misfit is of order $\vartheta_H - \vartheta \propto H_{c_1}^c / H$ and vanishes smoothly for both $\vartheta = 0$ and $\vartheta = \pi/2$.

Now let us move to the discrete layered case. A detailed calculation of the free-energy density was carried out by Ivlev, Ovchinnikov, and Pokrovsky (1991) and by Bulaevskii, Ledvij, and Kogan (1992). The result for small angles, $\vartheta < \varepsilon$, and intermediate fields, $H_{c_1} \ll H \ll H_{c_2}$, takes the form

$$F = \frac{B^2}{8\pi} + \frac{\Phi_0 B \varepsilon \cos\vartheta}{2(4\pi\lambda)^2} \left[\ln\left[\frac{\alpha' H_\Lambda}{\varepsilon B}\right] + \frac{2|\tan\vartheta|}{\varepsilon}\ln\frac{\alpha'' \Lambda}{\xi}\right] \ , \tag{8.56}$$

where we define the magnetic field $H_\Lambda$ by

$$H_\Lambda = \frac{\Phi_0}{\Lambda^2} \ . \tag{8.57}$$

The first two terms (with the modifications $\varepsilon_\vartheta \leftrightarrow \varepsilon \cos\vartheta$, $H_{c_2}^c / \varepsilon_\vartheta B \leftrightarrow H_\Lambda / \varepsilon B$) are also present in the continuous anisotropic description (8.54). An additional feature arising due to the layering is the term *linear* in the angle $|\vartheta|$ accounting for the energies $\varepsilon_0 d \ln(\alpha'' \Lambda / \xi)$ of the 2D pancake (current) cores. Determining the magnetic field **H** from Eq. (8.56), we obtain a new behavior for the misfit angle $\vartheta_H - \vartheta$ between the magnetic field **H** and the magnetic induction **B** when the fields are closely aligned with the planes,

$$\vartheta = \begin{cases} 0, & \vartheta_H < \vartheta^* \ , \\ \vartheta_H - \vartheta^* + o(\vartheta), & \vartheta^* < \vartheta_H \ , \end{cases} \tag{8.58}$$

with the critical angle $\vartheta^*$ given by

$$\vartheta^* \simeq \frac{H_{c_1}^c}{H} \frac{\ln(\alpha'' \Lambda / \xi)}{\ln(\lambda / \xi)} \ . \tag{8.59}$$

Hence we understand that in an anisotropy or layered superconductor the magnetic field **H** and the magnetic induction **B** are not aligned under general conditions. The lock-in transition is related to the above phenomenon, but involves the *external* magnetic field $\mathbf{H}_a$ as a driving force. For a correct description of the lock-in transition, it is therefore necessary to take into account the demagnetization fields (Maslov and Pokrovsky, 1991). We consider a sample in the form of a rotational ellipsoid with demagnetization factors $v_x = v_y = v \simeq L_z / L_y \ll 1$ and $v_z = 1 - 2v$. The appropriate thermodynamic potential depends on the external applied field $H_a$ and is given by

$$G = F(\mathbf{B}) - \frac{B^2}{8\pi} + \frac{(\mathbf{B} - \mathbf{H}_a)\mathbf{M}}{2} \ . \tag{8.60}$$

The magnetization **M**, the inductance **B**, and the applied field $\mathbf{H}_a$ are related by

$$\mathbf{H}_a = \mathbf{B} - 4\pi(1-v)\mathbf{M} \ , \tag{8.61}$$

where $v$ is the tensor of demagnetization factors. Combining Eqs. (8.56), (8.60), and (8.61) requires us to minimize

$$G = \frac{\Phi_0 B_y \varepsilon}{2(4\pi\lambda)^2} \ln\frac{\alpha' H_\Lambda}{\varepsilon B} + \frac{\Phi_0 B_z}{(4\pi\lambda)^2} \ln\frac{\alpha'' \Lambda}{\xi}$$
$$+ \frac{(B_y - H_{ay})^2}{8\pi(1-v)} + \frac{(B_z - H_{az})^2}{16\pi v} \tag{8.62}$$

with respect to $B_y$ and $B_z$, and we obtain $B_y \simeq H_{ay}$, $B_z = H_{az} - 2v(\Phi_0/4\pi\lambda^2)\ln(\alpha'' \Lambda / \xi)$. Below the lock-in

transition the component $B_z$ vanishes, and we find the locking angle

$$\vartheta_L \simeq 2\nu \frac{H_{c_1}^c}{H_a} \frac{\ln(\alpha''\Lambda/\xi)}{\ln(\lambda/\xi)} \ . \tag{8.63}$$

For angles $\vartheta_{H_a} < \vartheta_L$, the vortex lattice is locked to the planes of the layered material, $\vartheta = 0$. Note that $\vartheta_H = \vartheta^*$ when $\vartheta_{H_a} = \vartheta_L$. The transition corresponds to a second-order phase transition, with the external angle $\vartheta_{H_a}$ playing the role of the driving parameter and the internal angle $\vartheta$ corresponding to the order parameter going continuously from $\vartheta = 0$ for $\vartheta_{H_a} < \vartheta_L$ to finite values $\vartheta = \vartheta_{H_a} - \vartheta_L$ for $\vartheta_{H_a} > \vartheta_L$. With typical ratios $L_z/L_y \sim 10^{-2} - 10^{-1}$, and $H_{c_1}^c/H_a \lesssim 10^{-1}$, lock-in angles of the order of $0.1° - 1°$ can be expected (Kwok *et al.*, 1991).

Another more traditional effect arising from the misalignment of the external magnetic field $\mathbf{H}_a$ and the induction $\mathbf{B}$ is the appearance of a finite torque, $\mathbf{T} = \mathbf{M} \wedge \mathbf{H}_a$, acting on the sample. Within the regime $H_a \gg H_{c_1}$ which we are interested in here, the magnetization $M \propto H_{c_1}$ is always small as compared with the applied magnetic field, and demagnetization effects are not important in the calculation of the torque. For an anisotropic superconductor, we obtain

$$T = \frac{H_a H_{c_1}^c}{4\pi} \frac{(1-\varepsilon^2)\sin\vartheta\cos\vartheta}{\varepsilon_\vartheta} \frac{\ln(\alpha H_{c_2}^c/\varepsilon_\vartheta B)}{2\ln\kappa} \ . \tag{8.64}$$

The torque shows a maximum as a function of angle $\vartheta$,

$$\vartheta_{\max} \simeq \begin{cases} \varepsilon^{1/2}, & 1 \ll \varepsilon \ln\dfrac{\alpha H_{c_2}^c}{\varepsilon B} \ , \\[2ex] \varepsilon \left[\ln\dfrac{\alpha H_{c_2}^c}{\varepsilon B}\right]^{1/2}, & \varepsilon \ln\dfrac{\alpha H_{c_2}^c}{\varepsilon B} \ll 1 \ , \end{cases}$$

and thus provides an excellent tool for the determination of the anisotropy parameter $\varepsilon$ of the material (Farrell *et al.*, 1989, 1990; Tuominen *et al.*, 1990; Martínez *et al.*, 1992). In layered superconductors the torque is modified at small angles,

$$T = \frac{H_a H_{c_1}^c}{4\pi} \begin{cases} \dfrac{\vartheta_{H_a} H_a}{2\nu H_{c_1}^c}, & \vartheta_{H_a} < \vartheta_L \ , \\[2ex] \dfrac{\vartheta_L H_a}{2\nu H_{c_1}^c} + O(\vartheta) \simeq \dfrac{\ln(\alpha''\Lambda/\xi)}{\ln\kappa}, & \vartheta_L < \vartheta_{H_a} \ . \end{cases} \tag{8.65}$$

Compared with the anisotropic case, the torque in a layered superconductor is shifted upward at small angles and drops rapidly to zero within the narrow angular interval below the lock-in angle $\vartheta_L$.

Let us turn to the structure of the vortex lattice at small angles $\tan\vartheta < d/\xi$. Away from the lock-in transition, we expect to find a kinked vortex lattice, which has

to be characterized by three unit vectors instead of only two as for the continuous anisotropic description. The reason for the appearance of a third lattice vector is found in the structure of an individual vortex line, which is no longer a simple rectilinear object. The London free energy of the kinked vortex lattice as a function of the lattice parameters was determined by Ivlev, Ovchinnikov, and Pokrovsky (1991). However, the explicit equilibrium configuration is still unknown. An interesting proposal regarding a complete rearrangement of the vortex lattice was offered by Kes *et al.* (1990) and Theodorakis (1990) and has recently been studied in more detail by Bulaevski, Ledvij, and Kogan (1992): It was proposed that in layered superconductors the field components parallel and perpendicular to the planes can penetrate independently from one another and set up a combined vortex lattice, made up of coexisting Abrikosov ($\perp ab$ planes) and Josephson ($\parallel ab$ planes) vortices. As the two lattices are mutually orthogonal, they do not interact with each other; thus they correspond to separate degrees of freedom of the vortex system. As shown by Bulaevskii *et al.* (1992), such a new vortex-lattice phase is expected to occur within the intermediate-field range $H_{c_1} < H_a < H_J = \Phi_0/d\Lambda$ for small enough coupling, $\varepsilon < d/\lambda$; i.e., the 2D screening scale $\Lambda$ has to become larger than the 3D screening length $\lambda$, $\Lambda > \lambda$. Under these extreme conditions the critical field $H_{c_t}^c$ drops below $(\Phi_0/4\pi\lambda^2)\ln(\Lambda/\xi)$ and the lock-in angle becomes equal to $\vartheta_L = 2\nu H_{c_1}^c/H_a$. With an increase in $\vartheta_{H_a}$ beyond $\vartheta_L$, the parallel lattice evolves into a combined lattice via a second-order transition. The transition between the combined and the conventional tilted lattice is of first order and takes places at an angle below $\vartheta = \arctan(d/\xi)$. It has been argued (Bulaevskii *et al.*, 1992) that for high fields, $H_a > H_J$, and small angles, $\vartheta < \varepsilon$, the Josephson cores in neighboring layers start to overlap, and the combined lattice should always be favored irrespective of the ratio $\Lambda/\lambda$. In order to test the correctness of these ideas and to find the positions of the phase boundaries, one needs to determine the free energies of the various phases *beyond* logarithmic accuracy. In addition, one should note that it is not sufficient to show that a specific vortex arrangement is a solution of the Euler-Lagrange equations derived from the free-energy functional as done by Theodorakis (1990). As a simple example, consider two Abrikosov vortices arranged in an orthogonal configuration, which is a solution of the London equation; however, the configuration is not force-free, as the vortices will arrange themselves into an antiparallel state with lower energy. Similarly, it appears that the configuration comprising two pancake vortices placed above and below a Josephson vortex is unstable (see Fig. 36): The Lorentz force exerted by the screening currents of the Josephson vortex drives the pancake vortices apart, and a kinked structure appears.

Let us finally turn to the case of a strictly parallel field where the vortices are intrinsically pinned by the layered
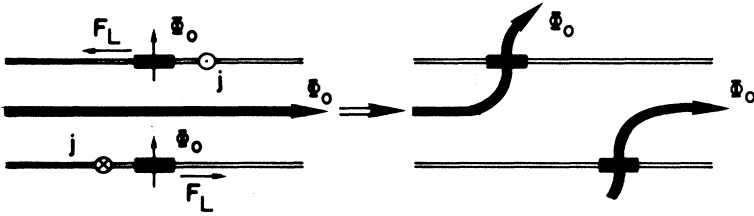
FIG. 36. Configuration with two pancake vortices enclosing a Josephson vortex. This configuration is unstable, so that the combined configuration decays into a kinked one.

structure. To be explicit, we consider a situation in which the superconductor is cooled in the presence of a parallel magnetic field. At low enough temperatures, the vortex lattice will adjust itself to the periodic potential produced by the layered structure with a lattice constant $z_0 = \mathrm{Int}(\sqrt{\varepsilon}a_\Delta/d)d$, an integer multiple of the layer spacing $d$ along the $z$ axis. Here $\mathrm{Int}(x)$ denotes the integer part of $x$, and we neglect additional effects arising from the commensuration problem. The remaining degrees of freedom (including variations of the field strength) are changes in the lattice constant $x_0$ along the $x$ axis and the in-plane shear distortion $qx_0$ of the vortex lattice (see Fig. 37). Experimentally, a change of $x_0$ can be realized by lowering the external field, which leads to an increase in the lattice constant $x_0$. We are interested in the equilibrium configuration and the stability of the vortex lattice and therefore have to determine the free energy of the vortex configuration as a function of $x_0$ and $q$. Within the intermediate-field regime $H_{c_1} \ll H \ll H_{c_2}$, we can use the London approximation; the result is (Ivlev, Kopnin, and Pokrovsky, 1990; see also Ivlev, Kopnin, and Salomaa, 1991)

$$F = \frac{B^2}{8\pi} + \frac{\Phi_0 B \varepsilon}{2(4\pi\lambda)^2} \left[ \ln\left[ \frac{\alpha H_\Lambda}{\varepsilon B} \right] + \gamma(p,q) \right], \quad (8.66)$$
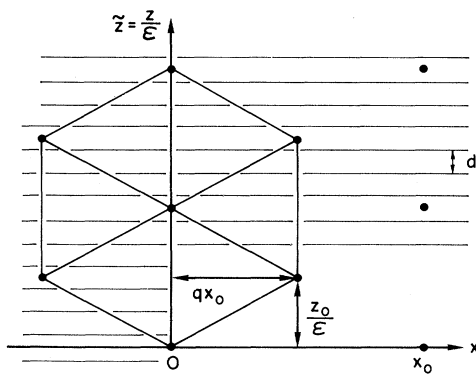
with



FIG. 37. Parallel-field vortex configuration in a strongly layered superconductor. The $z$ axis has been rescaled according to $\tilde{z} = z/\varepsilon$ (expansion along $z$). The configuration can be described by the coordinates $x_0, z_0$ and the geometry parameter $q$. Shown is the stable equilibrium configuration with $q = 1/2$ and $p = 2\pi z_0/\varepsilon x_0 = \sqrt{3}\pi$.

$$\gamma(p,q) = \sum_{n=1}^{\infty} \frac{2}{n} \left[ \frac{\sinh pn}{\cosh pn - \cos 2\pi qn} - 1 \right] - \ln p + \frac{p}{6}$$

and

$$p = 2\pi \frac{z_0}{x_0 \varepsilon}, \quad x_0 z_0 B = \Phi_0 .$$

Equation (8.66) for the free-energy density applies, provided that $\varepsilon x_0, z_0 \ll \lambda$. Note that the parameters $p$ and $q$ are pure geometrical quantities determining the form of the vortex lattice; i.e., simultaneous scaling of $x_0$ and $z_0$ leaves $p$ and $q$ invariant but changes the magnetic field $B$. For a rescaled $(z \to \tilde{z} = z/\varepsilon)$ equilateral triangular Abrikosov lattice, $q = 1/2$ and $p = \sqrt{3}\pi$ or $p = \pi/\sqrt{3}$, where the latter lattice is rotated by 30° with respect to the former when drawn in the isotropized system with $z \to \tilde{z} = z/\varepsilon$. The stability of the lattice under shear distortions is obtained by calculating the shear modulus $c_{66}^\parallel$,

$$c_{66}^\parallel = 2c_{66}\varepsilon^3 \left[ \frac{z_0}{\varepsilon x_0} \right]^2 \frac{\partial^2 \gamma}{\partial q^2} , \quad (8.67)$$

where $c_{66} = \Phi_0 B/(8\pi\lambda)^2$ and we have used $\partial_z u_x = (x_0/z_0)\delta q$. It turns out that $\partial_q^2 \gamma$ is always negative for $q = 0$; hence the rectangular lattice is always unstable. The other candidate for a stable lattice is the rhombic configuration with $q = 1/2$. For this case the shear modulus becomes (Ivlev *et al.*, 1990)

$$c_{66}^\parallel = c_{66}\varepsilon^3 \begin{cases} -\dfrac{2\pi^2}{3}\dfrac{1}{p}, & p \ll 1 , \\[2mm] 2(2p)^2 e^{-p}, & 1 \ll p , \end{cases} \quad (8.68)$$

with $c_{66}^\parallel$ becoming negative for $p < p_c \approx 1.51$. Hence lattices that are dense along the $x$ axis $(x_0 < 4.16 z_0/\varepsilon)$ are stable under shear distortions, whereas lattices diluted along the $x$ axis become unstable.

The next question, then, is which rhombic lattices are equilibrium configurations. A plot of $\gamma(p, q = 1/2)$ shows two minima, at $p = \sqrt{3}\pi$ and at $p = \pi/\sqrt{3}$, and a maximum at $p = \pi$ in between; hence the (rescaled) equilateral triangular Abrikosov lattices indeed are stable configurations. Note that the true equilibrium state is unique and corresponds to a configuration with $p = \sqrt{3}\pi$; i.e., the hexagons of the triangular lattice point along the $z$ axis (Campbell, Doria, and Kogan, 1988). The maximum at $p = \pi$ corresponds to a square lattice in the isotropized system, which has a slightly higher energy than

the triangular lattice.

Now imagine decreasing the external magnetic field $B$. As vortices start to leave the sample, the lattice constant $x_0$ increases while $z_0$ remains constant; hence $p$ decreases. As $p$ drops below $p_c$, the shear instability drives the vortex lattice into new states, thereby avoiding all configurations with a finite lattice constant along the $z$ axis, an effect which is due to the dominance of the repulsion between the vortices along the $z$ axis. In fact, as shown by Levitov (1991), the parameter $q > \frac{1}{2}$ continuously evolves towards the golden mean $\tau = (\sqrt{5} - 1)/2 \approx 0.618$, thereby avoiding all the fractions $q = F_n/F_{n+1}$ made from Fibonacci numbers ($F_{n+1} = F_n + F_{n-1}, F_0 = 0, F_1 = 1$) which correspond to lattices with a short lattice constant along the $z$ axis.

On the other hand, for the case $B > H_J = \Phi_0/d\Lambda$, the initial lattice constant $2z_0$ along the $z$ axis is already minimal, $z_0 = d$, and it is possible to squeeze the lattice by further increasing the external field (note that increasing the field starting from smaller fields, $B < H_J$, introduces vortices into different layers, and our original assumptions regarding the structure of the vortex lattice break down). Result (8.68) shows that such a squeezed lattice has an exponentially small shear modulus, $c_{66}^{\parallel} \propto \exp(-2\pi B/H_J)$. In addition, as shown by Bulaevskii and Clem (1991), the magnetization of this squeezed state vanishes more rapidly, $M(H) \propto \varepsilon H_{c_1}^c (H_J/H)^3$, than the usual logarithmic behavior $M(H) \propto \varepsilon H_{c_1}^c \ln(H_{c_2}^c/\varepsilon H)$ obtained within the London model for the intermediate-field region $H_{c_1} \ll H \ll H_{c_2}$. Note that the upper critical field $H_{c_2}$ in the present situation is determined by the paramagnetic effect, $H_{c_2} \sim \Phi_0/\xi\lambda_F$, with $\lambda_F \ll \xi$ the Fermi wavelength; hence $H_{c_2} \gg H_J$. At smaller fields, $H < H_J$, interesting commensuration effects are expected to appear (Bulaevskii and Clem, 1991; Burkov, 1991), but we shall not go into this here. Instead we mention another interesting application of the shear instability of the vortex lattice, which has been used to explain (Ivlev and Campbell, 1993) the flux chain buckling found by Dolan *et al.* (1989) in decoration experiments with the field applied parallel to the layers (see also Sec. III.B).

## B. Thermodynamic properties

The thermodynamic properties of layered superconductors can be quite strongly influenced by the weakness of the interlayer coupling and the resulting quasi-two-dimensionality of the system. For very weak interlayer coupling, as it is realized in the Bi- and Tl-based compounds, a good starting point is to consider the thermodynamic properties of an individual layer first and then to study the influence of the finite coupling perturbatively. We have to study the thermodynamics of two-dimensional systems first, with their enhanced fluctuations preventing a true phase transition from taking place

in the system. Instead, the phase transitions we are interested in (superconducting coherence, vortex-lattice melting) are topological ones and of the Berezinskii-Kosterlitz-Thouless (BKT) type. In the following we shall first briefly review the main elements of the BKT theory. In Sec. VIII.B.2 we apply the results of the general theory to the case of charged superfluids ($H = 0$), first to the individual 2D layers and second to the coupled system. We then study the behavior of the system in a finite field ($\mathbf{H} \| c$), where we again concentrate first on the 2D situation and second on the melting transition of the vortex lattice in a layered system, which can be predominantly 3D (small fields) as well as 2D (large fields) in nature. In Sec. VIII.B.3 we discuss the possibility of the existence of a decoupling transition along the field direction with the field applied parallel to the $c$ axis of the material. This section is more speculative in nature, and the final answers to this very interesting body of problems are not yet clear. Finally, In Sec. VIII.B.4, we concentrate on the parallel-field case ($\mathbf{H} \| ab$ plane), where the intrinsic pinning provided by the layered structure leads to new physical effects, such as the absence of melting of the Josephson vortex lattice due to a dimensional reduction of the fluctuations.

### 1. BKT transition in planar degenerate systems

It is well known that in two dimensions a degenerate system, i.e., a system described by a multicomponent "order parameter" $\Psi = \{\psi_\alpha(\mathbf{R})|\alpha = 1, \ldots, n\}$ and thus possessing a continuous symmetry, does not exhibit conventional long-range order (Mermin and Wagner, 1966; Hohenberg, 1967), meaning that the expectation value of the putative "order parameter"

$$\langle \Psi \rangle = 0 \tag{8.69}$$

vanishes at all finite temperatures. On the other hand, such systems still develop a finite-temperature phase transition where the resulting low-temperature phase is characterized by a finite transverse stiffness $v_s > 0$. Examples of such systems are the $XY$ Heisenberg model ($\Psi \leftrightarrow \mathbf{S}$, $v_s \propto$ helicity modulus $\Upsilon$); the neutral and, with some provisos, the charged superfluid [$\Psi \leftrightarrow |\Psi| \exp(i\varphi)$, $v_s \propto$ superfluid density $\rho_s$]; and the crystal ($\Psi \leftrightarrow \mathbf{u}$, $v_s \propto$ shear modulus $c_{66}$). Restricting ourselves to two-component "order parameters" of the form $\Psi = |\Psi| \exp(i\varphi)$, we find that the generic Hamiltonian describing the phenomena we are interested in is (we chose $|\Psi| = 1$ in the following)

$$\mathcal{J} = -\mathcal{J} \sum_{\langle \mu, \nu \rangle} \Psi^*(\mathbf{R}_\mu)\Psi(\mathbf{R}_\nu)$$

$$= -\mathcal{J} \sum_{\langle \mu, \nu \rangle} \cos[\varphi(\mathbf{R}_\mu) - \varphi(\mathbf{R}_\nu)], \tag{8.70}$$

with $\langle \mu, \nu \rangle$ denoting the summation over nearest neighbors and $\mathcal{J} > 0$. The low-energy excitations of the system are characterized by smoothly varying phase fields $\varphi(\mathbf{R})$, and we can pass to a continuum description,

$$\mathcal{H} = \frac{\mathcal{J}}{2} \int d^2R \, (\nabla\varphi)^2 \ . \tag{8.71}$$

With Eq. (8.71) we have actually established the relation to the problem we are interested in here. Comparing Eq. (8.71) with (8.2), we see that (8.71) describes a thin-film superconductor if we set

$$\mathcal{J} = \frac{\varepsilon_0 d}{\pi} \tag{8.72}$$

and take the limit $e \to 0$, with the latter condition allowing us to neglect screening effects so that we can replace the gauge-invariant phase difference $\tilde{\varphi}$ in (8.2) by the phase $\varphi$ of the superconductor (uncharged superconductor). The phase field $\varphi$ can be split into a regular $(\varphi_r)$

and a singular $(\varphi_s)$ component with

$$\oint \nabla\varphi_r . dl = 0 \quad \text{and} \quad \oint \nabla\varphi_s . dl = 2n\pi \ , \tag{8.73}$$

where the contour is taken to be a small circle of the size of the cutoff radius $R_0$ in the problem. The singular part of the phase field is most conveniently expressed by the vortex distribution function $n_v(\mathbf{R})$, which is related to $\varphi_s$ via Poisson's equation,

$$\Delta v_s(\mathbf{R}) = 2\pi n_v(\mathbf{R}), \quad \text{where} \quad \nabla \wedge n v_s = \nabla\varphi_s \ . \tag{8.74}$$

The total energy of a configuration $\varphi(\mathbf{R})$ can then be written as

$$\mathcal{H} = \frac{\mathcal{J}}{2} \int d^2R \, (\nabla\varphi_r)^2 - \pi\mathcal{J} \int d^2R \, d^2R' n_v(\mathbf{R}) \left[ \ln\frac{|\mathbf{R}-\mathbf{R}'|}{R_0} - \ln\frac{L}{R_0} \right] n_v(\mathbf{R}') \ , \tag{8.75}$$

where $L$ denotes the system dimension. The first term in Eq. (8.75) describes the energy content of (nonsingular) Gaussian fluctuations in the system (note that the range of $\varphi_r$ is $-\infty < \varphi_r < \infty$; see Berezinskii, 1970), whereas the second term describes the energy of the topological excitations (vortices; note that $\pi\mathcal{J} = \varepsilon_0 d$ for the superconductor). The term $\ln(L/R_0)$ requires that the vortex system remain "uncharged" (in the thermodynamic limit), i.e.,

$$\int d^2R \, n_v(\mathbf{R}) = 0 \ . \tag{8.76}$$

The main physics going on in degenerate 2D systems can be conveniently described in terms of the generic Hamiltonian (8.75), and the following interesting picture has emerged as the result of many investigations (Berezinskii, 1970, 1971; Kosterlitz and Thouless, 1973; Kosterlitz, 1974; Pokrovskii and Uimin, 1974; José *et al.*, 1977; Nelson and Kosterlitz, 1977; Wiegmann, 1978):

The system develops a low-temperature phase exhibiting topological order. This low-temperature phase can be described by the Gaussian part of (8.75) with a renormalized coupling $v_s(T)\mathcal{J}$,

$$\mathcal{H} = \frac{v_s\mathcal{J}}{2} \int d^2R \, (\nabla\varphi)^2, \quad 0 < v_s \leq 1 \ , \tag{8.77}$$

with the role of the vortex excitations being to suppress the coupling $\mathcal{J}$ to the renormalized value $v_s\mathcal{J}$ [José *et al.*, 1977; a similar result is obtained within a self-consistent harmonic approximation (see Pokrovskii and Uimin, 1974]. The topological order expresses itself in the correlator of the order parameter,

$$\langle \Psi^*(\mathbf{R})\Psi(0) \rangle = e^{-\langle[\varphi(\mathbf{R})-\varphi(0)]^2\rangle/2} \ . \tag{8.78}$$

Evaluating the phase correlator $\langle[\varphi(\mathbf{R})-\varphi(0)]^2\rangle$ in the usual path-integral formulation, we obtain the logarithmic dependence

$$\langle[\varphi(\mathbf{R})-\varphi(0)]^2\rangle = \frac{2T}{v_s\mathcal{J}} \int \frac{d^2K}{(2\pi)^2} \frac{1-\cos\mathbf{K}\mathbf{R}}{K^2}$$

$$= \frac{T}{\pi v_s\mathcal{J}} \ln\frac{R}{R_0} \ , \tag{8.79}$$

which implies an algebraic decay of the order-parameter correlator,

$$\langle \Psi^*(\mathbf{R})\Psi(0) \rangle = \left[\frac{R_0}{R}\right]^{\eta}, \quad \eta = \frac{T}{2\pi v_s\mathcal{J}} \ ; \tag{8.80}$$

hence the system appears to be scale invariant (critical) at all temperatures where (8.80) is valid. Result (8.80) has to be contrasted with the behavior of an analogous system in three dimensions, which develops a finite order parameter $\langle\Psi\rangle \neq 0$ in the low-temperature phase and where the correlator (8.80) decays exponentially with distance in the high-temperature phase; the power-law dependence for the correlator is restricted to the critical point.

If we could restrict ourselves to Gaussian fluctuations, the topologically ordered phase would persist throughout the entire regime of temperatures. However, it turns out that vortex excitations renormalize the stiffness $v_s$ to zero above a temperature $T_{\text{BKT}}$,

$$T_{\text{BKT}} = \frac{\pi}{2} v_s^\infty \mathcal{J}, \quad v_s^\infty = v_s(T_{\text{BKT}}) > 0 \ , \tag{8.81}$$

and the topological order is lost, meaning that the order-parameter correlator decays exponentially for $T > T_{\text{BKT}}$,

$$\langle \Psi^*(\mathbf{R})\Psi(0) \rangle = e^{-R/\xi_{\text{BKT}}(T)} \ , \tag{8.82}$$

with the coherence length

$$\xi_{\text{BKT}}(T) \propto \exp\left[\left[b\frac{T_{\text{BKT}}}{T-T_{\text{BKT}}}\right]^{1/2}\right] \tag{8.83}$$

diverging on approaching $T_{BKT}$ from above (and remaining infinite throughout the entire low-temperature phase). The parameter $b$ is nonuniversal, and typical values obtained in thin superconducting films are in the range 2–16 (Fiory, Hebard, and Glaberson, 1983; Kadin, Epstein, and Goldman, 1983).

Whereas the low-temperature phase is, with renormalized coupling, well described by the Gaussian part of Hamiltonian (8.75), it is the vortex part in (8.75) that drives the transition into the high-temperature disordered phase. The vortex part in Hamiltonian (8.75) is nothing but the Hamiltonian of a Coulomb gas in two dimensions, which thus provides a prototype system for the Berezinskii-Kosterlitz-Thouless transition itself (see Kosterlitz and Thouless, 1973; Minnhagen, 1987). The origin of this analogy lies in the fact that the singular phase field $\varphi_s(\mathbf{R})$ as well as the potential $V(\mathbf{R})$ in the Coulomb gas problem are solutions of the Poisson equation (8.74) with the vortex or charge density acting as a source term. The transition is due to an unbinding of vortex pair excitations and can be understood in a simple heuristic picture (Kosterlitz and Thouless, 1973) as being driven by the entropic part of the free energy of the system. In fact, the free energy of an individual vortex excitation is

$$\mathcal{F} = \pi \mathcal{J} \ln \frac{L}{R_o} - T \ln \left[ \frac{L}{R_o} \right]^2$$

$$= 2 \left[ \frac{\pi}{2} \mathcal{J} - T \right] \ln \frac{L}{R_o} \qquad (8.84)$$

and changes sign when $T$ crosses the transition point at $\pi \mathcal{J}/2$. It is quite surprising that this simple result survives throughout all the more elaborate theories (involving renormalization-group analysis of the transition), if we replace the coupling $\mathcal{J}$ by the renormalized coupling $v_s^\infty \mathcal{J}$ in the above equation for the transition point, leading to result (8.81).

The following general picture emerges: Below the Berezinski-Kosterlitz-Thouless transition, $T < T_{BKT}$, the system is in a topologically ordered state with algebraically decaying correlations, $\langle \Psi(\mathbf{R})\Psi(0) \rangle \propto (R_o/R)^\eta$, where $\eta = T/2\pi v_s(T)\mathcal{J}$ depends on temperature and adopts the universal value $\eta = \frac{1}{4}$ at $T_{BKT}$. In this phase, the vortex excitations are bound into pairs interacting logarithmically like Coulomb charges in two dimensions. These vortex excitations can be polarized, and the concomitant screening effect leads to a downward renormalization of the coupling constant $\mathcal{J}$ to $v_s(T)\mathcal{J}$. The phase is scale invariant and well described by the Gaussian part of (8.75) with renormalized coupling $v_s\mathcal{J}$. At $T = T_{BKT}$ the logarithmically bound pairs dissociate and the transverse stiffness of the low-temperature phase $v_s\mathcal{J}$ is lost as $v_s(T)$ jumps to zero. This jump at $T_{BKT}$ is universal in the sense $v_s^\infty \mathcal{J}/T_{BKT} = 2/\pi$, which, upon use of Eqs. (8.3) and (8.72), transforms to the famous universal jump in the superfluid density $\rho_s = dv_s^\infty |\Psi|^2$ at $T_{BKT}$ (Nelson and Kosterlitz, 1977),

$$\frac{\rho_s(T_{BKT})}{T_{BKT}} = \frac{2m}{\hbar^2 \pi} . \qquad (8.85)$$

The transition itself is continuous with a singular part in the free energy $\mathcal{F}_{\text{sing}}(T \to T_{BKT}^+) \propto \xi_{BKT}^{-2}$, and thus all derivatives are continuous. Note that the jump in the transverse stiffness does not correspond to a first-order transition, since $v_s$ is not an order parameter. Within the high-temperature phase $T > T_{BKT}$, the correlations decay exponentially with $\langle \Psi(\mathbf{R})\Psi(0) \rangle \propto \exp[-R/\xi_{BKT}(T)]$ and a correlation length $\xi_{BKT}(T) \propto \exp[\sqrt{b/(1 - T/T_{BKT})}]$ diverging rapidly on approaching $T_{BKT}$ from above. On scales $R < \xi_{BKT}(T)$, the vortex pairs are still bound, whereas the individual vortices become free on scales $R > \xi_{BKT}(T)$; hence the density of free vortices is

$$n_v \sim \xi_{BKT}^{-2}(T) . \qquad (8.86)$$

The presence of free vortices in the system leads to the screening of the transverse stiffness $v_s\mathcal{J}$ on the scale $\xi_{BKT}$; hence $\mathcal{J}v_s(K) \propto 1/[1 + (K\xi_{BKT})^{-2}]$ and $\mathcal{J}v_s(K = 0) = 0$.

### 2. BKT behavior in charged superfluids ($H = 0$)

The first important caveat to be made when discussing the relation between BKT behavior and charged superfluids is the problem of screening: As follows from the Pearl solution for a vortex in a finite-thickness 2D film (see Sec. VIII.A.2), the logarithmic interaction between the vortices is cut off on the scale $\lambda_{\text{eff}} = 2\lambda^2/d$ where screening becomes important [see Eq. (8.25)]. Due to this cutoff, the creation energy of a free vortex becomes finite, $\mathcal{E}_c \simeq \varepsilon_o d \ln(\lambda_{\text{eff}}/\xi)$; hence we shall have a *finite* density of free vortices present at any nonzero temperature. This statement also applies to any finite system in the absence of screening ($XY$ model or uncharged superfluid), since the logarithmic growth of the self-energy of a topological excitation is cut off at the sample size, $\mathcal{E}_c \simeq \pi \mathcal{J} \ln(L/R_o)$. In both cases, the (sharp) phase transition expected for an unscreened and infinite system is transformed into a (smooth) crossover as the divergence of the correlation length $\xi_{BKT}(T \to T_{BKT}^+)$ is cut off at the screening length $\lambda_{\text{eff}}$ or at the sample size $L$. Since any sample has finite dimensions, it is interesting to know if the transition in a charged superconductor is cut off by the screening length $\lambda_{\text{eff}}$ or by the sample size $L$. Making use of the universality of the jump in the superfluid density $\rho_s = v_s d|\Psi|^2 = T_{BKT} 2m/\hbar^2\pi$, one obtains (Beasley, Mooij, and Orlando, 1979)

$$\lambda_{\text{eff}}(T_{BKT}) = \frac{\Phi_o^2}{16\pi^2 T_{BKT}} \approx \frac{2 \text{ cm}}{T_{BKT} \text{ (in K)}} , \qquad (8.87)$$

demonstrating that finite sample dimensions usually provide the more stringent condition for the sharpness of the transition.

The second important aspect to be taken into account in the discussion of superfluids is the strong temperature dependence of the superfluid density due to the vicinity of $T_{BKT}$ to the mean-field transition temperature $T_{c_0}$ below which a finite superfluid density $\rho = \langle |\Psi|^2 \rangle > 0$ is established *locally* [note that we distinguish between the superfluid density $\rho_s = v_s \rho$ describing the transverse stiffness of the low-temperature phase and the local density of the condensate $\rho$: Whereas $\rho \propto (T_{c_0} - T)$ within mean-field theory, $\rho_s$ remains zero until $T_{BKT}$ is reached from above, where it jumps to $(2m/\hbar^2\pi)T_{BKT}$]. As a consequence, the transition temperature $T_{BKT}$ has to be found from a self-consistent solution of

$$\frac{v_s^\infty}{2}d\varepsilon_0(T_{BKT}) = T_{BKT} \; , \tag{8.88}$$

resulting in the approximate expression

$$T_{BKT} \approx T_{c_0} \left[ 1 - \frac{2T_{c_0}}{v_s^\infty d\varepsilon_0(0)} \right] \; . \tag{8.89}$$

Note that the suppression of $T_{BKT}$ due to the renormalization $v_s^\infty < 1$ is usually small, as typical values of $v_s^\infty$ are $\approx 0.5$–$0.9$ for the systems considered here (Nelson and Kosterlitz, 1977; Fiory, Hebard, and Glaberson, 1983; Kadin, Epstein, and Goldman, 1983). Similarly, care must be taken in the discussion of the temperature dependence of the coherence length $\xi_{BKT}(T)$ due to the underlying presence of the Ginzburg-Landau coherence length $\xi(T)$, which itself diverges algebraically as $T$ approaches $T_{c_0}$ from below. A useful interpolation formula for the superfluid is (Minnhagen, 1981)

$$\xi_{BKT}(T) \simeq \xi(T)\exp\left[ \left[ b\frac{T_{c_0} - T}{T - T_{BKT}} \right]^{1/2} \right] \; . \tag{8.90}$$

Another interesting feature of charged superfluids is the interplay between the BKT behavior of the system and its dynamic response (see, for example, Halperin and Nelson, 1979 and Minnhagen, 1987).[9] At low temperatures the bound vortex pairs can dissociate in the presence of an applied current density $J$ ($= jd$). The free energy of a vortex pair separated by a distance $R$ and directed perpendicular to the current flow is

$$\mathcal{F}(R) = 2v_s\varepsilon_0 d \left[ \ln\frac{R}{\xi} - \frac{J}{J_0}\frac{R}{\xi} \right] \; , \tag{8.91}$$

with the current $J_0 = (v_s 3\sqrt{3}/2)j_0 d$ being of the order of the depairing critical current. The saddle point determining the activation energy for the current-assisted thermal unbinding is given by the critical distance

_____

[9]See Ambegaokar *et al.* (1978, 1980) for a description of dissipation in uncharged superfluids.

$$R_c \simeq \xi\frac{J_0}{J} \tag{8.92}$$

and the activation energy

$$U_c \simeq 2v_s\varepsilon_0 d \ln\frac{J_0}{J} \; . \tag{8.93}$$

The rate of production of free vortices is $\Gamma \propto \exp(-U_c/T)$, and their mutual annihilation is determined by the rate equation

$$\partial_t n_v = \Gamma - \frac{\xi^2}{\tau_{rec}}n_v^2 \; , \tag{8.94}$$

with $\xi^2/\tau_{rec}$ denoting the recombination parameter. Under steady-state conditions, we obtain $n_v \propto \Gamma^{1/2}$. Using the Bardeen-Stephen formula for the flux-flow resistivity, we find a resistance

$$\rho = 2\pi\xi^2\rho_n n_v \propto \left[ \frac{J}{J_0} \right]^{v_s\varepsilon_0 d/T} \; , \tag{8.95}$$

where $\rho_n$ is the normal-state resistivity (=resistance) of the film. The resulting current-voltage characteristic is algebraic,

$$V = \rho I \propto \left[ \frac{J}{J_0} \right]^\alpha \; , \tag{8.96}$$

with a temperature-dependent exponent

$$\alpha(T) = 1 + \frac{v_s\varepsilon_0 d}{T} \tag{8.97}$$

adopting the universal value $\alpha(T_{BKT}) = 3$ at the transition $T_{BKT}$. The finite density of free vortices $n_v \simeq \xi_{BKT}^{-2}$ above the transition induces Ohmic behavior at small current densities, $J < J_x$,

$$\frac{\rho(T)}{\rho_n} \simeq 2\pi \left[ \frac{\xi}{\xi_{BKT}} \right]^2 \simeq 2\pi \exp\left[ -2 \left[ b\frac{T_{c_0} - T}{T - T_{BKT}} \right]^{1/2} \right] \; , \tag{8.98}$$

and the exponent $\alpha$ jumps to unity. At the crossover current density $J_x$ the probed length scale is the correlation length $\xi_{BKT}$; hence

$$J_x \simeq J_0\frac{\xi}{\xi_{BKT}} \; . \tag{8.99}$$

For currents $J > J_x$ the vortices are still bound on the probed length scales and the current-voltage characteristic is algebraic. The phase transition has been experimentally mapped out in a set of beautiful studies by Kadin, Epstein, and Goldman (1983) using Hg-Xe alloy films and by Fiory, Hebard, and Glaberson (1983) on In/In-O films.

Focusing now on layered material, we see a variety of new features appearing in the discussion. The simplest situation is that of a decoupled stack of parallel films. Due to the screening effects provided by neighboring lay-

ers, the interaction potential of a vortex pair in an individual layer remains logarithmic to all length scales [see Eq. (8.32)]. Therefore a true BKT transition can be expected to take place in a decoupled system. Turning on the Josephson interaction between the layers will change this simple picture considerably (Hikami and Tsuneto, 1980; Glazman and Koshelev, 1990). First of all, we have to distinguish between the two cases of strongly and weakly coupled layered materials. Such a distinction can be made on the basis of a comparison of the relative width of the 2D fluctuation regime $\tau_f^{2D} = (T_{c_0} - T_f^{2D})/T_{c_0}$ and the relative width $\tau_{cr} = (T_{c_0} - T_{cr})/T_{c_0}$ of the 3D bulk coupled regime around the mean-field transition temperature $T_{c_0}$. For a strongly coupled material, the 3D bulk regime is large, $\tau_{cr} \gg \tau_f^{2D}$, and the crossover from 3D bulk to 2D layered behavior can be discussed within a mean-field description. Here we are interested in weakly coupled material with $\tau_{cr} \ll \tau_f^{2D}$, where the transition is strongly influenced by the 2D fluctuations. Whereas the conventional superconductors as well as the YBCO compound ($\tau_{cr} \approx 0.15$) belong to the first class of materials, the strongly layered Bi- and Tl-based materials, in which we are mainly interested within this section, clearly are members of the second group with $\tau_{cr} \sim 10^{-3}$.

Let us look, then, at a weakly coupled layered superconductor for which the behavior of an individual layer provides a good starting point. Due to the coupling between the layers, the logarithmic interaction between a vortex pair is replaced by a linear confinement potential on scales $R > \Lambda$ [see Eq. (8.42)], which leads to a cutoff in the BKT behavior of the system. However, the cutoff in the present situation is of an entirely different origin and has drastically different consequences from the cutoff of the BKT transition due to finite screening in a thin-film superconductor, encountered before. In the film, the logarithmic interaction is replaced by a $1/R$ power-law *decay* such that pairs become *free* on large scales, leading to a stabilization of the high-temperature phase. In the coupled layer system, the logarithmic interaction is replaced by a linearly *increasing* potential leading to the *confinement* of vortex pairs and inducing a 3D bulk transition into a superconducting state possessing a finite order parameter and true off-diagonal long-range order. Obviously, this 3D bulk transition (which we denote by $T_c$) occurs when the BKT coherence length becomes of the order of $\Lambda$; hence

$$ T_c = T_{BKT} + \frac{b(T_{c_0} - T_{BKT})}{\{\ln[\Lambda/\xi(T_{BKT})]\}^2} . \tag{8.100} $$

Above $T_c$ the vortex plasma is rather dense, with a mean vortex separation less than $\Lambda$; hence the system behaves in an essentially two-dimensional way. This scenario is confirmed by numerical simulations (Minnhagen and Olsson, 1991a; Weber and Jensen, 1991).

The width $\delta T_f^{3D}$ of the 3D fluctuational regime can be estimated from the condition (Feigel'man, 1979)

$$ \delta T_f^{3D} |(\partial_T \xi_{BKT})| \simeq \Lambda , $$

and we obtain

$$ \delta T_f^{3D} \simeq \frac{2(T_c - T_{BKT})}{\ln[\Lambda/\xi(T_{BKT})]} = \frac{2b(T_{c_0} - T_{BKT})}{\{\ln[\Lambda/\xi(T_{BKT})]\}^3} . \tag{8.101} $$

Below the bulk transition at $T_c$, and outside the 3D fluctuation regime, the system still develops strong 2D fluctuations. On length scales $R < \Lambda$, the interlayer coupling is not yet effective, and a 2D description in terms of the (renormalized) Gaussian part of Eq. (8.75) is appropriate. The phase correlator of the order parameter is given by Eq. (8.79),

$$ \langle [\varphi(\mathbf{R}) - \varphi(0)]^2 \rangle \simeq \frac{T}{\nu_s \varepsilon_0 d} \ln \frac{R}{\xi} . \tag{8.102} $$

Strong 2D phase fluctuations are present on scales $R \lesssim \Lambda$ at temperatures above $T_f^{2D}$, which we define by the condition

$$ \langle [\varphi(\Lambda) - \varphi(0)]^2 \rangle |_{T = T_f^{2D}} \sim 1 . \tag{8.103} $$

Using (8.102), we easily find

$$ T_f^{2D} \simeq T_{c_0} - \frac{1}{2}(T_{c_0} - T_{BKT}) \ln \frac{\Lambda}{\xi(T_{BKT})} , $$

$$ \simeq T_{c_0} \left[ 1 - \frac{T_{c_0}}{\nu_s d \varepsilon_0(0)} \ln \frac{\Lambda}{\xi(T_{BKT})} \right] . \tag{8.104} $$

Note that Eq. (8.104) describing fluctuations in the phase is larger than the result for the fluctuation regime obtained by Bulaevskii, Ginzburg, and Sobyanin (1988) on the basis of a Ginzburg criterion,

$$ G_i^{2D} = \frac{T_{c_0}}{\sqrt{2}\varepsilon_0(0)d} \simeq \tau_f^{2D} . \tag{8.105} $$

In summary, a layered system goes through various regimes when the temperature $T$ is lowered; (see Fig. 38). At $T_{c_0}$ the local order parameter $\rho$ increases rapidly out of the fluctuating background (finite mean-field order pa-
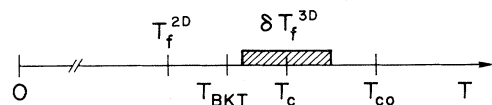


FIG. 38. Arrangement of the various (zero-field) temperature regimes in a strongly layered superconductor. A finite mean-field order parameter is established at $T_{c_0}$ within the individual layers. When the temperature is decreased, the 2D-BKT transition building up below $T_{c_0}$ is cut off at $T_c$ due to the finite interlayer Josephson coupling, and a 3D superconducting state is established. The region of strong 3D fluctuations is denoted by $\delta T_f^{3D}$. In an equivalent uncoupled system a true BKT transition would appear at $T_{BKT}$. Strong 2D fluctuations survive down to the temperature $T_f^{2D}$.

rameter). Then the system starts to undergo a Berezinskii-Kosterlitz-Thouless transition on approaching $T_{\mathrm{BKT}} < T_{c_o}$. This transition, however, is interrupted by the transition into a 3D bulk superconducting state at $T_c$ with $T_{\mathrm{BKT}} < T_c < T_{c_o}$. Strong 3D superconducting fluctuations are present within a region $\delta T_f^{3\mathrm{D}}$ around $T_c$. Outside this regime, strong 2D fluctuations persist until the temperature $T_f^{2\mathrm{D}} < T_{\mathrm{BKT}}$ is reached. Below $T_f^{2\mathrm{D}}$, finally, only weak 2D fluctuations are present in the system. Numerical estimates for the various temperatures for a strongly layered BiSCCO superconductor are [$T_{c_o} \approx 100$ K, $d \approx 15$ Å, $\xi_{\mathrm{BCS}} \approx 25$ Å, $\lambda_L \approx 2000$ Å, $\varepsilon \approx 1/150$, resulting in $\varepsilon_0(0)d \approx 1500$ K, and we choose $\nu_s \sim 1$]

$$T_{c_o} - T_{\mathrm{BKT}} \approx 13 \text{ K} ,$$

$$T_c - T_{\mathrm{BKT}} \approx b \text{ K} ,$$

$$\delta T_f^{3\mathrm{D}} \approx 0.5b \text{ K} , \qquad\qquad (8.106)$$

$$T_{c_o} - T_f^{2\mathrm{D}} \approx 25 \text{ K} .$$

The results depend strongly on the chosen numerical values for the material parameters, and our poor knowledge of the parameter $b$ renders the estimate for the position of the bulk transition temperature $T_c$ very uncertain.

An interesting proposal regarding the transition of a layered material into its bulk superconducting state was offered by Friedel (1988), who suggested that the proliferation of low-energy in-plane Josephson vortex-loop excitations should lead to a decoupling of the layers above some critical temperature $T_c$. In particular, it was conjectured that this transition should approach zero temperature as the coupling $E_J = j_J \Phi_0 / 2\pi c = \varepsilon^2 \varepsilon_0 / \pi d$ between the layers vanished, allowing for the possibility of pure 2D behavior of the decoupled layer system within the temperature interval $T_c < T < T_{\mathrm{BKT}} < T_{c_o}$. Later, Korshunov (1990) showed, however, that this interesting scenario is never realized and the bulk transition temperature $T_c$ is *always finite* and *above* the Berezinskii-Kosterlitz-Thouless transition temperatures $T_{\mathrm{BKT}}$ (see also Minnhagen and Olsson, 1991b). In fact, it turns out that the statistical mechanics of a system of Josephson loops can be mapped to a Coulomb gas problem with charges interacting logarithmically both within the individual layers and in different layers (Korshunov, 1990). The transition turns out to be very similar to the BKT transition in a purely two-dimensional system, with a transition temperature $T_J$ determined implicitly by the relation $T_J = 4\varepsilon_0(T_J)d > T_{\mathrm{BKT}}$; hence the zero-field decoupling transition into a set of independent two-dimensional superconducting layers is never realized. The results of Korshunov (1990) were later confirmed by Horovitz (1991), who also extended the analysis to include the disordering effect of pancake vortices, which

tend to suppress the effective coupling between the layers.

The 3D coupling of the layers turns the system into a bulk superconductor below $T_c$. In the absence of fluctuations (thermal or quantum), the system is expected to have a finite critical current density. Indeed, on scales $R > \Lambda$, the Lorentz force $jd\Phi_0/c$ has to compete with the confinement force $2\varepsilon_0\varepsilon$ [see Eq. (8.41); the confinement is simply due to the two Josephson strings created during the expansion of the pair], and we obtain the (planar) critical current density (see also Glazman and Koshelev, 1990; Jensen and Minnhagen, 1991)

$$j_{\mathrm{con}} \sim j_0 \frac{\xi}{\Lambda} . \qquad\qquad (8.107)$$

The critical current density along the $c$ axis is given by the Josephson coupling $j_J$ [see Eq. (8.8)] and is reduced by a factor $\varepsilon$ as compared with the above result for the confinement critical current density $j_{\mathrm{con}}$. As the (planar) current density is increased beyond $j_{\mathrm{con}}$, we are probing length scales smaller than $\Lambda$, and the current-voltage characteristic becomes algebraic. At finite temperatures, dissipation due to vortex-loop creation will lead to an additional experimentally small voltage $\propto \exp(-j_T/j)$, $j_T \sim j_0(\varepsilon_0\varepsilon\xi/T)$, in the system. Strong 2D fluctuations above $T_f^{2\mathrm{D}}$ will produce an additional temperature dependence in the bulk screening length $\lambda$ and in the critical current densities $j_{\mathrm{con}}$ and $j_J$, as can be found in the work of Glazman and Koshelev (1990). Evidence for BKT-type behavior in YBCO and in Bi- and Tl-based high-temperature superconductors has been reported by Stamp, Forro, and Ayache (1988; see also Yeh and Tsuei, 1989), Artemenko, Gorlova, and Latyshev (1989a, 1989b; see also Gorlova and Latyshev, 1990), Kim *et al.* (1989), and Martin *et al.* (1989). Surprisingly, in the work of Artemenko *et al.* the algebraic form of the current-voltage characteristic remains present even for low current densities, $j < j_{\mathrm{con}}$, where the theoretical analysis predicts an exponential behavior.

### 3. BKT-type vortex-lattice melting ($H > 0$)

As already mentioned in Sec. VIII.B.1, the 2D crystal in general, and thus the 2D vortex lattice in particular, is a further example exhibiting a Berezinskii phase at low temperature and a Kosterlitz-Thouless transition into a liquid phase at some elevated temperature. In this system, the role of the logarithmically interacting topological excitations is played by the edge dislocations. Using a continuum description, we find that the displacement field belonging to an edge dislocation with a Burgers vector $\mathbf{b} = (b,0)$ pointing along the $x$ axis is given by (Nabarro, 1979; Brandt, 1986b)

$$\mathbf{u} = \frac{b}{2\pi} \left[ \frac{xy}{R^2} + \arctan \frac{y}{x} , -\frac{x^2}{R^2} \right] , \qquad (8.108)$$

and the energy associated with this defect is

$$e_d(R) = d \int_{R_o}^{R} d^2 R' \frac{c_{66}}{2} (\nabla_\perp \mathbf{u})^2$$

$$= \frac{db^2}{2\pi} c_{66} \ln \frac{R}{R_o} \ . \tag{8.109}$$

The lower cutoff $R_o$ is provided by the lattice constant $a_o$ of the vortex lattice, whereas the upper cutoff $R$ is given either by the sample dimension $L$ ($\rightarrow$ self-energy of the topological defect) or by the distance $R$ to the nearest dislocation with an opposite Burgers vector ($\rightarrow$ logarithmic interaction between two oppositely "charged" topological excitations). Note that the distortion (8.108) does not involve compression ($\nabla \mathbf{u} = 0$) but only shear, which is a consequence of the incompressibility of the vortex lattice, $c_{11} \gg c_{66}$. For an elementary dislocation, the Burgers vector ($=$ misfit vector when encircling the dislocation) is equal to a unit lattice vector, and $e_d(R)$ becomes

$$e_d(R) = \frac{\varepsilon_o d}{4\sqrt{3}\pi} \ln \frac{R}{a_o} \ , \tag{8.110}$$

which is a factor $4\pi\sqrt{3} \approx 7\pi$ smaller than the corresponding energy for the vortex excitation itself. The BKT-type dislocation-mediated melting transition of the 2D vortex lattice then takes place at a temperature (Huberman and Doniach, 1979)

$$T_m^{2D} = \frac{da_\Delta^2 c_{66}}{4\pi} \simeq \frac{d\varepsilon_o}{8\sqrt{3}\pi} \ll T_{BKT} \ . \tag{8.111}$$

Of course, the presence of bound dislocation pairs again leads to a renormalization of the shear modulus $c_{66}$. From here on we do not explicitly note this renormalization of the coupling constants in the formulas, but we remind the reader that such effects are present. Equation (8.111) is also in agreement with the general equation for the melting temperature of a 2D crystal as obtained by Kosterlitz and Thouless (1973) and by Halperin and Nelson (1978; see also Nelson and Halperin, 1979, and Fisher, 1980),

$$T_m^{2D} = \frac{da_\Delta^2}{4\pi} \frac{c_{66}(c_{11} - c_{66})}{c_{11}} \ . \tag{8.112}$$

Taking into account that the vortex lattice is essentially incompressible, $c_{66} \ll c_{11}$, and using $c_{66} = \varepsilon_o / 4a_o^2$, we recover Eq. (8.111). The observation of dislocation-mediated melting in thin $Nb_3Ge$ films has been reported by Berghuis, van der Slot, and Kes (1990).

Let us estimate the 2D melting temperature $T_m^{2D}$ in the strongly layered Bi- and Tl-based compounds. Since $T_m^{2D} \ll T_{BKT}$, we have to take into account the change in the coupling constant $\varepsilon_o(T)$ due to the temperature dependence of $\lambda$,

$$T_m^{2D} \simeq \frac{T_{BKT}}{4\sqrt{3}\pi} \frac{T_{c_o} - T_m^{2D}}{T_{c_o} - T_{BKT}}$$

$$= \frac{T_{BKT}}{4\sqrt{3}\pi} \frac{1}{1 - T_{BKT}/T_{c_o}} \simeq 25 \text{ K} \ . \tag{8.113}$$

We briefly summarize the new additional elements relevant in the discussion of BKT behavior in a 2D crystal (Nelson and Halperin, 1979; Strandburg, 1988). First, we should point out that the basic Hamiltonian of the system is slightly more complicated than our prototype Hamiltonian (8.75), owing to the fact that the "charge" is now a vectorial quantity (Burgers vector) and owing to the appearance of an additional angular term in the Hamiltonian. As a consequence, several results will be slightly modified with respect to the standard theory, such as the exponent $\eta$ and the coherence length $\xi_{BKT}^m$ (see below).

The low-temperature phase is characterized by topological order, with a density-density correlator decaying algebraically (Jancovici, 1967; Imry and Gunther, 1971; Nelson and Halperin, 1979),

$$g^t(\mathbf{K}_\nu, \mathbf{r}) = \langle \rho_\mathbf{K}(\mathbf{R}) \rho_\mathbf{K}^*(0) \rangle \propto R^{-\eta_\mathbf{K}(T)} \ , \tag{8.114}$$

where the density wave $\rho_\mathbf{K}(\mathbf{R})$ is given by

$$\rho_\mathbf{K}(\mathbf{R}) = e^{i\mathbf{K}[\mathbf{R} + \mathbf{u}(\mathbf{R})]} \tag{8.115}$$

and

$$\eta_\mathbf{K}(T) = \frac{T\mathbf{K}_\nu^2(c_{11} + c_{66})}{4\pi c_{66} c_{11}} \simeq \frac{T\mathbf{K}_\nu^2}{4\pi c_{66}} \ . \tag{8.116}$$

This algebraic decay is a consequence of logarithmic divergence in the displacement field $\langle [\mathbf{u}(\mathbf{R}) - \mathbf{u}(0)]^2 \rangle \propto \ln R$ [see Eq. (3.131); the factor of 2 discrepancy between Eq. (3.131) and the above result is due to the different model used for the elastic manifold in Sec. III.E, where the displacement is transverse to the manifold]. As a result, the $\delta$-function Bragg peaks present in the structure factor of a crystal exhibiting true long-range order are replaced by power-law singularities,

$$S(\mathbf{K}) \propto |\mathbf{K} - \mathbf{K}_\nu|^{-2 + \eta_\mathbf{K}(T)} \ . \tag{8.117}$$

Whereas true long-range order is absent in the position (density) of the atoms, it is present, however, in the orientation order parameter $\Psi_n(\mathbf{R}) = \exp[in\theta(\mathbf{R})]$, with the bond-angle field $\theta(\mathbf{R})$ given by $\theta(\mathbf{R}) = (\partial_x u_y - \partial_y u_x)/2$ (for a triangular lattice, $n = 6$). The orientational correlator

$$g^o(6, \mathbf{r}) = \langle \Psi_6(\mathbf{R}) \Psi_6^*(0) \rangle \tag{8.118}$$

approaches a nonzero constant value asymptotically, $g^o(6, R \rightarrow \infty) \simeq \exp(-9T/2\pi\varepsilon_o d)$. The melting of the crystal then proceeds in two steps (Nelson and Halperin, 1979): First, the dislocations unbind at $T_m^{2D}$, as given by Eq. (8.111). Within the resulting phase, the density-density correlator decays exponentially, $g^t(\mathbf{K}_\nu, \mathbf{R}) \propto \exp[-R/\xi_{BKT}^m(T)]$, with $\xi_{BKT}^m$ given by the modified expression

$$\xi_{BKT}^m(T) \propto \exp\left[b\frac{T_m^{2D}}{T - T_m^{2D}}\right]^\nu, \quad \nu \approx 0.36963 \ . \tag{8.119}$$

The gas of free dislocations allows the shear stress to relax in this phase, and we obtain a finite viscosity

$$\nu \propto \xi_{BKT}^{m}{}^{2}(T) \; ; \tag{8.120}$$

hence the resulting phase is indeed a liquid. On the other hand, the orientational order is not yet completely destroyed and decays only with a power law, $g^{o}(6, \mathbf{R}) \propto R^{-\eta_6(T)}$, with the exponent $\eta_6(T)$ determined by the stiffness $K_A$ (Franck constant) of the bond-angle field [see Eq. (4.166)], $\eta_6 = 18T/\pi K_A$. Due to the gas of free dislocations, the orientation stiffness $K_A(T)$ is strongly temperature dependent. On approaching the melting temperature $T_m^{2D}$ from above, the free dislocations bind into pairs [on the scale $\xi_{BKT}^{m}(T)$] and the stiffness $K_A(T \to T_m^{2D})$ diverges. As a result, the exponent $\eta_6$ goes to zero as $T \to T_m^{2D}$, and in this manner orientational long-range order is established. The intermediate phase above $T_m^{2D}$, lacking translational but still possessing orientational order, is called a hexatic liquid. Obviously, free dislocations are able to destroy the translational order completely, but are less effective in destroying orientational order. The excitations that do, however, destroy orientational order are the disclinations, topological defects that rotate the triangular unit cell by $\pm 60°$ when encircling the defect. A dislocation can be viewed as a tightly bound pair of (oppositely "charged") disclinations and hence does not influence the bond-orientational order. Within the hexatic phase all disclinations are paired up and form a gas of free dislocations. The interaction between two disclinations is again logarithmic, with the coupling constant $\mathcal{J}$ in Eq. (8.75) given by the Franck constant, $\mathcal{J} = K_A/36$. Hence, on approaching the temperature $T_h^{2D} = \pi K_A/72$, the disclinations unbind, and orientational order disappears. At the transition the exponent $\eta_6$ takes the universal value $\eta_6 = \frac{1}{4}$. Above the hexatic transition the BKT correlation length shows the usual exponential behavior, $\xi_{BKT}^{h}(T) \propto \exp[(bT_h^{2D})/(T - T_h^{2D})]^{1/2}$, with the disclinations bound into pairs on scales $R < \xi_{BKT}^{h}(T)$ and the correlator $g^{o}(6, \mathbf{R}) \propto \exp[-R/\xi_{BKT}^{h}(T)]$ decaying exponentially with distance. Hence, at temperatures $T > T_h^{2D}$, a true liquid is established with all correlations decaying exponentially with distance.

As we move on to layered superconductors, the melting transition of the 3D vortex lattice can retain the 2D character of the melting transition in the layers. Let us remind ourselves about the Lindemann criterion for the melting of the vortex lattice as discussed in Sec. V.A, saying that thermal fluctuations will melt the lattice when the mean displacement $\langle u^2 \rangle_{th}^{1/2}$ grows beyond a fraction $c_L$ of the lattice constant $a_o$,

$$\langle u^2(T_m) \rangle_{th} \approx c_L^2 a_o^2 \; . \tag{8.121}$$

Inspection of the derivation of $\langle u^2 \rangle_{th}$ [see Eq. (4.83)] shows that the main contribution to thermal displacement $\langle u^2 \rangle_{th}^{1/2}$ originates from wave vectors near the Brillouin-zone boundary $K \simeq K_{BZ}$, with $k_z$ related to $K$

via

$$k_z \simeq \left[ \frac{c_{66}}{c_{44}} \right]^{1/2} K_{BZ} \; . \tag{8.122}$$

For wave vectors close to the Brillouin-zone boundary, the tilt modulus $c_{44}$ is dominated by the single-vortex limit $(\varepsilon^2 \varepsilon_o/2a_o^2)\ln(H_{c_2}/B)$ (Glazman and Koshelev, 1991a), and, using the standard expression (3.32) for the shear modulus, we obtain

$$k_z \simeq \frac{1}{\varepsilon a_o} \left[ \frac{2\pi}{\ln[H_{c_2}/B]} \right]^{1/2} \tag{8.123}$$

for the relevant wave vectors in the $z$ direction. From Eq. (8.123) we can extract a crossover field $B_{2D}$,

$$B_{2D} \approx \pi \frac{\Phi_o}{\Lambda^2} \ln \frac{\Lambda}{\xi} \; , \tag{8.124}$$

below which $k_z$ is small, $k_z < \pi/d$, and layering is unimportant. Within this weak-field regime, $B < B_{2D}$, the interaction of pancake vortices along the $z$ axis (as measured by the tilt energy) is larger than the in-plane (shear) interaction; hence the pancake vortices constitute well defined vortex lines. The melting transition can then be described via the usual Lindemann criterion, and we obtain a melting line of the form (Glazman and Koshelev, 1991a)

$$T_m(B) \approx \left[ \frac{\pi}{2} \ln \frac{H_{c_2}}{B} \right]^{1/2} \varepsilon \varepsilon_o c_L^2 \left[ \frac{\Phi_o}{B} \right]^{1/2} \; ,$$
$$B < B_{2D} \tag{8.125}$$

(see Fig. 39). Note that in Eq. (8.125) we have accounted for the strong suppression of the melting line far below the mean-field critical line $H_{c_2}$, rendering the single-vortex contribution to the tilt modulus dominant. At higher fields, $B > B_{2D}$, the planar interaction between the pancake vortices is dominant, and the melting transition becomes essentially 2D in character, with a field-independent melting line given by

$$T_m^{2D} \approx \frac{d\varepsilon_o}{8\sqrt{3}\pi}, \quad B_{2D} < B \tag{8.126}$$

(see Fig. 39). The matching of the two melting lines (8.125) and (8.126) at $(T_m^{2D}, B_{2D})$ provides us with an estimate for the Lindemann number,

$$c_L \approx \frac{1}{5} \; . \tag{8.127}$$

The crossover field $B_{2D}$ not only separates the two regimes where the character of the melting changes between 3D and 2D behavior, but, as would be expected, also sets the boundary between the regimes of 3D and 2D fluctuations in the vortex lattice. Whereas the fluctuations $\langle u^2 \rangle_{th}^{1/2}$ saturate in a 3D lattice [see Eq. (4.85)],
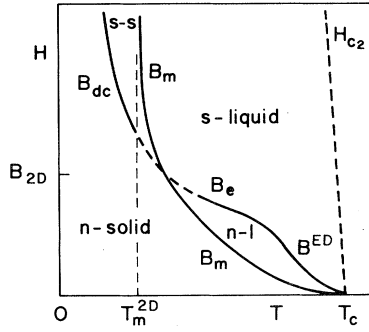
FIG. 39. Equilibrium phase diagram of a strongly layered high-temperature superconductor. The melting line $B_m(T)$ and the corresponding transition is 3D like below $B_{2D}$ and of quasi-two-dimensional character above $B_{2D}$. The low-field/low-temperature phase is a normal solid with a longitudinal superconducting response and a broken continuous translational symmetry transverse to the field direction. When $T$ is increased, the solid melts into a line liquid (normal liquid), which transforms to a point liquid (superfluid liquid) at even higher temperatures. $B_e$ and $B^{ED}$ denote the vortex evaporation line and the 3D disentangled-entangled transition line, respectively. At large fields, $B > B_{2D}$, the layers first decouple and the system transforms into a superfluid solid with a normal metallic response, even in the field direction, but still broken continuous translational symmetry transverse to the field. When the temperature across the melting line is increased, the supersolid transforms to a superliquid phase, which is equivalent to the normal-metal phase.

$$\langle u^2(\mathbf{R}) \rangle_{\text{th}} \simeq \frac{1}{4\sqrt{\pi}} \frac{T}{c_{66}\varepsilon a_0} a_0^2 \ , \tag{8.128}$$

they grow logarithmically in 2D,

$$\langle u^2(\mathbf{R}) \rangle_{\text{th}} \simeq \frac{T}{4\pi c_{66}d} \ln\left[\frac{R}{a_0}\right] . \tag{8.129}$$

The finite Josephson coupling between the layers will cut off the logarithmic growth in (8.129) at a distance $R \simeq \Lambda$. Hence we find that at small fields, $B < B_{2D}$, the fluctuations are given by Eq. (8.128) and are of a 3D nature, whereas at high fields the fluctuations are of a 2D character $(a_0 < \Lambda)$ and given by Eq. (8.129). At crossover $(B \simeq B_{2D}$ and hence $a_0 \simeq \Lambda)$, the fluctuations are equal, thus providing an alternative (and equivalent) criterion for the determination of $B_{2D}$. Note, too, that up to logarithmic corrections, $B_{2D} \simeq H_\Lambda$ as defined in Eq. (8.57). For the Bi-based compounds with $\varepsilon \simeq 1/150$ and $d \simeq 15$ Å, typical values for the crossover field $B_{2D}$ are of the order of $B_{2D} \approx 0.5$ T. The exact value of the crossover field $B_{2D}$ depends sensitively on the anisotropy parameter $\varepsilon$. The experiments by Martínez *et al.* (1992) indicate that $\varepsilon$ could be as small as $\varepsilon < 1/150$.

It has been argued (Fischer, 1992) that the 3D-2D crossover at $B_{2D}$ is suppressed by the magnetic interlayer coupling, which renders the system always 3D-like. This conclusion was reached by a comparison of the magnetic interlayer energy with the 2D vortex-lattice melting temperature $T_m^{2D}$. In particular, a thermal distortion of the vortex lattice by $u \sim a_0/2$ between neighboring planes costs a magnetic energy of the order of $\mathcal{E}_{em} \simeq 2d\varepsilon_0(d/\lambda)\ln(a_0/2\xi)$ (two vortex-antivortex pairs of size $R \sim a_0/2$ placed in adjacent layers). This energy contains the small factor $d/\lambda$ and is not important in the discussion of the BKT-like transition into the superconducting state. However, the melting temperature (8.126) contains the small numerical factor $1/8\sqrt{3}\pi$ and can be even smaller than $\mathcal{E}_{em}$; thus one could argue that the electromagnetic coupling is always important for the 2D vortex-lattice melting transition. The problem with this argument is that one is comparing two energy scales belonging to two different systems. The BKT melting temperature refers to dislocations in the 2D vortex lattice which, as already pointed out, live on an energy scale reduced by a factor of $\sim 7\pi$ with respect to the planar vortex-vortex interaction scale itself. On the other hand, the magnetic interlayer coupling energy considered by Fischer refers to the vortices themselves and not to the dislocations; hence one should not compare these two quantities, which refer to different objects, dislocations, and vortices. The correct procedure involves a comparison of energy scales on the level of vortices or on the level of dislocations. With the former method, we have to compare the Josephson interaction energy and the magnetic interaction energy between the vortices, with the result that the Josephson term is dominant; thus the above analysis leading to the crossover field $B_{2D}$ seems to be correct. The alternative is to compare the interaction energies between two *dislocations* in different planes due to Josephson and magnetic coupling, which is a much more difficult task.

In a further step, we can determine the upward shift of the 2D melting line (8.126) due to Josephson coupling between the layers. The present discussion is completely analogous to that of the BKT-like transition in layered superconductors (see Sec. VIII.B.2), where the coupling between the layers leads to a cutoff of the 2D transition at $T_c > T_{BKT}$ and the occurrence of a true 3D transition with a finite order parameter. Consider the high-temperature liquid phase at large fields, $T > T_m^{2D}$ and $B > B_{2D}$. Under these conditions the vortex liquid is a liquid of 2D pancake vortices (rather than of vortex lines, as is expected at lower fields, $B < B_{2D}$). The largest interaction energy in the system is the in-plane repulsion between the pancake vortices. When the temperature is lowered towards the melting temperature $T_m^{2D}$, the gas of free dislocations in each plane starts to bind into pairs on scales $R < \xi_{BKT}^m$. Lattice coherent regions of size $\xi_{BKT}^m$ can couple via the Josephson interaction between the layers and gain an energy of the order of $E_J(\xi_{BKT}^m)^2$, where $E_J = j_J\Phi_0/2\pi c = \varepsilon^2\varepsilon_0/\pi d$ is the coupling energy density between two layers. As this energy becomes comparable to $T$, the 2D melting transition starts to couple into the third dimension, and we obtain a 3D transition. This

coupling into the third dimension then leads to an upward shift of the melting line, and we obtain the corrected result (see Fig. 39)

$$T_m(B) \approx T_m^{2D} \left\{ 1 + \frac{b}{[\ln(B/B_{2D})]^{1/\nu}} \right\}, \quad B_{2D} < B .$$

(8.130)

Here we have ignored a possible downward renormalization of the Josephson-coupling energy density $E_J$ due to thermal fluctuations (see Sec. VIII.B.4).

The high-temperature phase above $T_m(B)$ is expected to be quite different in the two field regimes below and above $B_{2D}$. Whereas a liquid of vortex lines is expected to exist below $B_{2D}$, a liquid of 2D pancakes will be more appropriate for describing the high-field phase at $B > B_{2D}$. Some hexatic order is expected to survive in both of these liquids up to the disclination unbinding temperature (Marchetti and Nelson, 1990a). The vortex lines surviving the melting transition in the low-field regime, $B < B_{2D}$, are expected to break up into individual pancake vortices at a temperature $T_e$ [evaporation temperature (see Sec. VIII.A.2); note, however, that here we have to take into account the presence of other vortices]. An estimate for this evaporation temperature is obtained from the condition $\langle [u(0,d) - u(0,0)]^2 \simeq a_\circ^2$ and the use of Eq. (3.131), from which we find $T_e(B) \sim \varepsilon^2 \varepsilon_\circ a_\circ^2 / d$. At $B_{2D}$ the evaporation temperature should be equal to the melting temperature, $T_e(B_{2D}) \simeq T_m^{2D}$; combining these two results, we obtain (see also Glazman and Koshelev, 1991a)

$$T_e(B) \simeq T_m(B) \left[ \frac{B_{2D}}{B} \right]^{1/2} .$$

(8.131)

The resistivity changeover observed in artificial multilayers by White, Kapitulnik and Beasley (1991) may find a natural explanation in terms of this vortex evaporation phenomenon.

Equation (8.131) is expected to describe well the situation close to the crossover field $B_{2D}$. At low magnetic fields the condition $\langle [u(0,d) - u(0,0)]^2 \rangle \simeq a_\circ^2$ is too stringent. Since the line $T_e(B)$ describes nothing but the loss of superconducting coherence along the field direction, we expect $T_e(B)$ to merge into the disentangled-entangled vortex-liquid transition line at low fields, where the anisotropic description works well (see Sec. V.B and Fig. 39).

The above scenario for the melting transition in layered superconductors agrees quite well with the experimental analysis of the melting line in layered BiSCCO superconductors by Gammel et al. (1988) and by Durán et al. (1991) and with the results of Monte Carlo simulations of the melting of the vortex lattice in layered superconductors by Ryu et al. (1992).

Finally, the existence and the character of the (finite-temperature) melting transition in a two-dimensional vortex system seem not to be completely settled yet. In particular, O'Neill and Moore (1992) do not find evidence for a finite-temperature transition into the vortex-lattice phase in their recent Monte Carlo simulations. On the other hand, a finite-temperature melting transition far below the mean-field upper critical-field line $H_{c_2}(T)$ has been found by Tešanović and Xing (1991) in their analysis of critical fluctuations in (quasi-) two-dimensional superconductors; however, from their results they cannot conclude whether the transition is continuous (BKT-type) or weakly first order. In very recent work, Kato and Nagaosa (1993) report finding a first-order melting transition for the two-dimensional vortex lattice close to the transition temperature $T_m^{2D}$ predicted by the BKT scenario.

### 4. Decoupling transition

Quite a while ago it was proposed that thermal fluctuations of the vortex lattice lead to a destruction of superconducting long-range order in the Abrikosov phase above $H_{c_1}$ (Maki and Takayama, 1971). This suggestion was recently reconsidered by Moore (1989, 1992), who found that the phase correlator $\langle \varphi^2(r) \rangle_{th} = \langle [\varphi(r) - \varphi(0)]^2 \rangle$ diverges in fewer than four dimensions. In three dimensions the decay of the order-parameter correlator

$$\langle \Psi(r)\Psi^*(0) \rangle \sim e^{-\langle \varphi^2(r) \rangle_{th}/2}$$

(8.132)

was found to be highly anisotropic and faster along the direction perpendicular to the field, where it takes the form

$$\langle \Psi(r)\Psi^*(0) \rangle \sim e^{-R/L_\circ} ,$$

(8.133)

with $L_\circ \sim \varepsilon_\circ a_\circ \lambda / T$. Typical values for $L_\circ$ are of the order of millimeters; thus the destruction of the off-diagonal long-range order would take place only on very large length scales. The results of Moore (1989) and of Maki and Takayama (1971) have been criticized by Houghton, Pelcovits, and Sudbo (1990) who argue that the appropriate quantity to study is the gauge-invariant correlator $\langle \tilde{\Psi}(r)\tilde{\Psi}^*(0) \rangle \propto \exp[S(r)]$, with

$$S(r) = \frac{1}{2} \left\langle \left| \varphi(r) - \varphi(0) + \frac{2\pi}{\Phi_\circ} \int^r A \, dl \right|^2 \right\rangle .$$

(8.134)

The origin of the divergence in the phase correlator, found by Moore, is easily traced to the singular behavior of the long-wavelength modes of the phase field $\varphi(r)$ under (shear) distortions $u(R)$ of the vortex lattice,

$$\delta\varphi(k) = 2\pi i \frac{B}{\Phi_\circ} \frac{[u(k) \wedge K] \cdot n}{k^2} .$$

(8.135)

The correlator of the phase fluctuations $\delta\varphi$ can be related to the correlator of the transverse lattice distortions [see Eq. (4.82)], and the result is

$$\langle [\delta\varphi(\mathbf{r})-\delta\varphi(\mathbf{0})]^2\rangle$$
$$=2T\left[\frac{2\pi}{a_\circ^2}\right]^2\int\frac{d^3k}{(2\pi)^3}\frac{K^2}{k^4}\frac{1-\cos\mathbf{k}\mathbf{r}}{c_{66}K^2+c_{44}(\mathbf{k})k_z^2} \ .$$

$$(8.136)$$

Due to the additional factor $K^2/k^4$, the phase correlator turns out to be more singular than the displacement correlator, and the possibility arises of obtaining a divergence in $\langle [\delta\varphi(\mathbf{r})-\delta\varphi(\mathbf{0})]^2\rangle$ while the vortex lattice still preserves translational long-range order, $\langle [\mathbf{u}(\mathbf{r})-\mathbf{u}(\mathbf{0})]^2\rangle<\infty$. Houghton, Pelcovits, and Sudbo (1990) argued that, by going over to a gauge-invariant phase $\tilde{\varphi}$, the divergence in $\delta\tilde{\varphi}=\delta\varphi+(2\pi/\Phi_\circ)\int\delta\mathbf{A}\,dl$ is removed and the gauge-invariant phase correlator remains finite in three dimensions. However, the results of Houghton, Pelcovits, and Sudbo (1990) are at variance with the more recent findings of Glazman and Koshelev (1991a, 1991b) and of Moore (1992), who report obtaining divergences in the gauge-invariant phase correlators, too; thus the situation is rather confusing at present. [Definition (8.134) of the phase correlator is not unproblematic either, as this quantity is divergent even in the Meissner phase if all fluctuations are accounted for. In order to avoid overcounting, one should fix a gauge, say, $\nabla\mathbf{A}=0$. This particular choice produces just the phase correlator for the (geometric) phase of the order parameter; see Moore (1992) for more details.] Furthermore, the physical meaning of the phase correlator itself and of its possible divergence is somewhat unclear in the following sense: Within the mixed phase of a type-II superconductor, the relevant objects that determine the physics of the system are the vortices, and their spatial fluctuations can be understood as representing topological fluctuations of the phase field. The phase field as defined Eq. (8.135) is tied to the position of the vortices and hence does not represent an additional degree of freedom in the system. In fact, restricting ourselves to two dimensions, we can *construct* an equivalent "phase correlator" $\langle [\delta\theta(\mathbf{r})-\delta\theta(\mathbf{0}]^2\rangle$ in the following way (see Landau and Lifshitz, 1959a): We idealize the vortex lattice as being incompressible; hence $\nabla\mathbf{u}=0$, and $\mathbf{u}$ is a pure transverse field. Thus there exists a scalar field $\theta(\mathbf{R})$ such that $\mathbf{u}(\mathbf{K})=\mathbf{K}_\perp\theta(\mathbf{K})$, where $\mathbf{K}_\perp=(K_y,-K_x)$. The scalar field $\theta(\mathbf{K})$, being just a mathematical construct for expressing the vector field $\mathbf{u}$ in terms of a scalar field $\theta$, has the same properties as the phase field $\delta\varphi$, but should *not* be interpreted as a new and independent degree of freedom in the system. In particular, the $\langle [\delta\theta(\mathbf{R})]^2\rangle$ correlator diverges at infinity, but has no relation whatsoever with a thermodynamic phase transition in the vortex system. Moreover, Gaussian (as opposed to topological) fluctuations cannot relax the strain in the phase field and hence cannot lead to dissipation of energy (cf. Huse, Fisher, and Fisher, 1992). A somewhat different point of view was proposed by Moore (1992): Instead of taking the finiteness of the displacement correlator $\langle u^2\rangle_{\rm th}$ as evidence for the *stability* of the vortex lattice against thermal fluc-

tuations, and hence arguing that a vortex-lattice phase indeed exists, one could take the divergence of the phase correlator as evidence for the nonexistence of a vortex-lattice phase. In fact, such an argument is based on the result obtained by O'Neill and Moore (1992), who reported finding no vortex lattice at all in a 2D system (see the discussion above).

Whereas the properties of the long-range behavior of the phase correlator $\langle [\delta\varphi(\mathbf{r})-\delta\varphi(\mathbf{0})]^2\rangle$ and its physical interpretation are still rather unclear at present, the short-distance analogy of this quantity is much more useful. In particular, in layered superconductors the phase correlator $\langle [\delta\varphi(0,d)-\delta\varphi(0,0)]^2\rangle$ gives information on the effective coupling strength between two neighboring superconducting layers. With increasing temperature, thermal fluctuations of the vortex positions can lead to a reduction of the interlayer coupling and even to a phase transition in which the layers decouple and the superconducting coherence along the field direction ($z$ axis) is lost. A simple derivation of the decoupling temperature proceeds as follows (Glazman and Koshelev, 1991b): The elastic energy density contained in the shear motion of the vortex lattice is

$$\delta E(\mathbf{K})\simeq c_{66}dK^2\left[\frac{\mathbf{u}\wedge\mathbf{K}}{K}\right]^2 \ .$$

$$(8.137)$$

Substitution of Eq. (8.135) for the displacement field $\mathbf{u}$ leads to the expression

$$\delta E(\mathbf{K})\simeq c_{66}d(a_\circ K)^4\left[\frac{\delta\varphi}{2\pi}\right]^2 \ .$$

$$(8.138)$$

Calculating the phase correlator along the field direction in the path-integral formulation and using Eq. (8.138), we obtain the estimate

$$\langle [\delta\varphi(0,d)-\delta\varphi(0,0)]^2\rangle\sim\frac{T}{c_{66}da_\circ^4}\int_{K_{\rm min}}\frac{dK}{K^3} \ ,$$

$$(8.139)$$

with the lower cutoff $K_{\rm min}$ determined by the requirement that the planar shear mode not couple into the third dimension. This is the case if $\delta E(K,\delta\varphi\sim1)>E_J=\varepsilon^2\varepsilon_\circ/\pi d$, from which we obtain the condition $K>K_{\rm min}\simeq1/\sqrt{a_\circ}\Lambda$. The final result for the phase correlator then reads

$$\langle [\delta\varphi(0,d)-\delta\varphi(0,0)]^2\rangle\sim\frac{T}{T_{dc}^G(B)} \ ,$$

$$(8.140)$$

with the decoupling temperature

$$T_{dc}^G(B)\simeq\varepsilon\varepsilon_\circ a_\circ\simeq T_m^{2D}\left[\frac{B_{2D}}{B}\right]^{1/2} \ , \quad B_{2D}<B \ .$$

$$(8.141)$$

As the temperature $T$ increases beyond $T_{dc}^G(B)$, the thermal phase fluctuations become large and the individual layers start to decouple. Since this phenomenon is tied to the discreteness of the material along the $z$ axis, the decoupling is expected to be restricted to the high-field regime, $B>B_{2D}$. The decoupling temperature

$T_{dc}^G(B) \simeq T_m^{2D}(B_{2D}/B)^{1/2}$ lies below the 2D melting line and joins the melting line at $B \simeq B_{2D}$ (see Fig. 39).

The existence of a true phase transition where the long-range superconducting coherence along the field direction disappears above some critical temperature is more difficult to show. Glazman and Koshelev (1991a) have analyzed the behavior of the thermal phase correlator

$$\delta S(\mathbf{r}) = \frac{1}{2} \left\langle \left[ \delta \varphi(\mathbf{r}) - \delta \varphi(0) + \frac{2\pi}{\Phi_o} \int^{\mathbf{r}} \delta \mathbf{A} \, dl \right]^2 \right\rangle \quad (8.142)$$

at large distances and obtained some evidence for the existence of a decoupling phase transition. Unfortunately, the physical meaning of the phase correlator $\delta S$ is rather unclear, and a consistent interpretation of the results is difficult. A more appropriate quantity for studying the presence of absence of longitudinal superconductivity probably is the correlator $D_{zz}(\mathbf{K}) = \langle A_z(\mathbf{K}) A_z(-\mathbf{K}) \rangle$ (see Sec. V.B), but such an analysis for a layered material at high fields is still missing.

The decoupling transition described above is driven by *Gaussian* fluctuations of the vortex lattice. Even before Glazman and Koshelev's work, a decoupling transition based on *topological* excitations of the vortex lattice had been proposed to exist in layered superconductors (Feigel'man, Geshkenbein, and Larkin, 1990). In order to understand this defect-induced decoupling transition, we have to analyze in some detail the structure of dislocations in the 2D and in the 3D vortex lattice. Let us first consider the purely two-dimensional situation. Topological defects in the vortex lattice are edge dislocations where an additional half-row of vortices is introduced into the lattice. The edge dislocation can move within its gliding plane (see Fig. 40). Two oppositely "charged" dislocations with a distance $R_g$ between their (parallel running) gliding planes introduce or remove $(2R_g/\sqrt{3}a_\Delta)$ vortices from the lattice. Such dislocation pairs with a finite distance $R_g > 0$ between the gliding planes constitute low-energy topological excitations of the 2D vortex lattice.

Let us turn now to a layered system with a finite inter-layer Josephson coupling $E_J > 0$. As already pointed out in Sec. VIII.A.2, introducing additional vortices into a plane requires an infinite (in the thermodynamic limit) amount of energy. In a continuous bulk superconductor, this restriction corresponds to the requirement that the dislocation loops always lie within the gliding planes of their edge dislocations and thus do not add flux to or remove flux from the vortex system (Campbell and Evetts, 1972). Hence the allowed dislocation pair excitations either must have a common gliding plane such that $R_g = 0$ or must couple to a second pair that removes (adds) all the flux introduced (removed) by the first pair. The resulting object consisting four edge dislocations is called a quartet (see Fig. 40). The analogous object in a bulk superconductor is a pair of parallel running (and "oppositely charged") dislocation loops bound together. Whereas
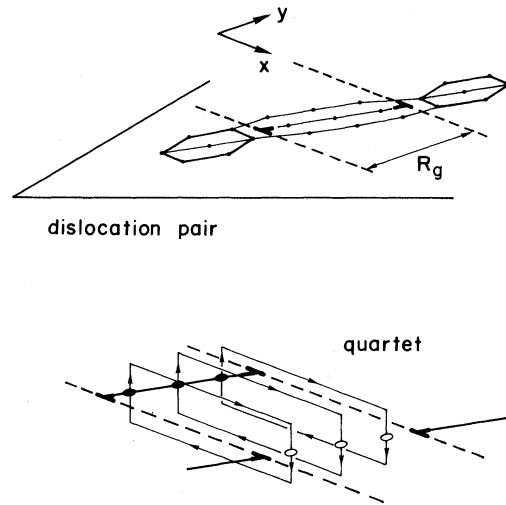


dislocation pair



quartet

FIG. 40. Dislocation pair and quartet in a (two-dimensional) Abrikosov vortex lattice. The dislocation pair encloses an additional flux $\Phi_{dp} = 2R_g \Phi_o / \sqrt{3} a_\Delta$ between the two gliding planes separated by $R_g$. In a coupled layered superconductor, such a dislocation pair costs an extensive amount of energy, and only pairs with $R_g = 0$ or pairs combined into a quartet are thermodynamic objects with a finite energy of creation. In a continuous anisotropic superconductor, the additional transverse flux (Josephson vortices) is introduced by pairs of screw dislocations interconnecting the edge dislocations. A single dislocation loop in a 3D vortex lattice cannot add or remove flux from the system.

the edge dislocations are connected by Josephson strings in the layered material, they are connected by screw dislocations for the case of a vortex lattice in a 3D bulk superconductor (see, for example, Marchetti and Nelson, 1990a, for a picture of a single dislocation loop). The binding energy of a quartet is provided by the Josephson strings connecting the additional and the removed flux in the plane. For a small quartet (one flux quantum added and removed; distance $R$ between the pairs less than $\Lambda$), the binding energy can be estimated from Eq. (8.39) to be

$$\mathcal{E}_q \simeq \varepsilon_o d \left[ \frac{R}{\Lambda} \right]^2 . \quad (8.143)$$

With increasing temperature, the density of quartets increases and an unbinding transition leading to a decoupling of the planes becomes possible. The mean distance $R$ between the (small) pairs is estimated to be $R \simeq 1/\sqrt{n_p}$, with $n_p \simeq (1/a_o^2) \exp(-2\mathcal{E}_c/T)$, and $\mathcal{E}_c \simeq \varepsilon_o d /4\pi\sqrt{3}$ is the core energy of a dislocation. At the decoupling transition, we have $\mathcal{E}_q \simeq T$, and we obtain the estimate

$$T_{dc}^t(B) \simeq \frac{T_m^{2D}}{\ln(B/B_{2D})} . \quad (8.144)$$

Equation (8.144) does not take into account the down-ward renormalization of the interlayer coupling due to

thermal fluctuations of the vortex lines. In the end, probably both Gaussian and topological fluctuations of the quasi-two-dimensional vortex lattice are important in the decoupling transition. The situation, in fact, resembles the BKT phase transition: the Gaussian fluctuations renormalize the stiffness of the phase, whereas the topological fluctuations trigger the phase transition itself. Since the interlayer coupling is strongly renormalized above $T_{dc}^G(B)$ (and hence $\Lambda \to \infty$), we can expect the true decoupling phase-transition line $T_{dc}(B)$ to be close to $T_{dc}^G(B)$.

Similar ideas have been put forward by Nelson (1991) and by Frey, Nelson, and Fisher (1994). Instead of studying quartets in layered superconductors, they consider interstitial-vacancy loops within an Abrikosov flux lattice. Such interstitial-vacancy loops are direct generalizations of the quartets to the continuous situation. They can be viewed as a combination of four ($\to$quartets) dislocations, with one pair introducing an interstitial and the other a vacancy into the vortex array. Within the vortex-lattice phase, the energy for creating this defect scales linearly with its total length, and thus free interstitials or vacancies are not thermodynamic quantities at low temperatures. However, with increasing temperatures, the entropic contribution to the free energy, which also scales linearly with the length of the defect, can neutralize the line energy, and vacancy-interstitial loops of all length scales start to proliferate. If this transition takes place below the melting temperature of the crystal, the resulting phase will be an entangled vortex lattice, showing translational long-range order in the vortex positions and normal metallic properties in the direction parallel to the vortices. In the phraseology of boson systems we then have a *supersolid* quantum crystal. The bosons make up a 2D phase-coherent crystal with a finite density of interstitials and/or vacancies forming a superfluid.

In order to be more specific, we introduce the two relevant correlation functions, $g^t(\mathbf{K}_\nu, \mathbf{r})$ describing the translational correlations,

$$g^t(\mathbf{K}_\nu, \mathbf{r}) = \langle\langle e^{i\mathbf{K}[\mathbf{u}(\mathbf{r}) - \mathbf{u}(0)]} \rangle\rangle \ , \qquad (4.150)$$

and $g^\phi(\mathbf{R}, \mathbf{R}'; z, z')$ describing the boson coherence,

$$g^\phi(\mathbf{R}, \mathbf{R}'; z, z') = \langle \phi(\mathbf{R}, z)\phi^*(\mathbf{R}', z') \rangle \ , \qquad (8.145)$$

where $\phi(\mathbf{R}, z)$ and $\phi^*(\mathbf{R}, z)$ are destruction and creation operators for either 2D bosons moving in imaginary time [see Eq. (5.35)] or flux lines extending along $z$. Within the vortex picture, the correlator $g^\phi(\mathbf{R}, \mathbf{R}'; z, z')$ describes the termination of a vortex line at $(\mathbf{R}, z)$ and the creation of a new line at $(\mathbf{R}', z')$. For $z < z'$, a vacancy is introduced into the vortex system, whereas the case $z > z'$ describes an interstitial. The two end points of the vortex lines correspond to magnetic monopoles. A typical realization of these types of defects can easily be envisaged for a layered superconductor in a parallel-field configuration [see Blatter, Rhyner, and Ivlev (1991) and Sec. VIII.B.5].

In analogy with the above discussion, we introduce the

temperature $T_{dc}^d$ at which the free energy $f_d = e_d - (T/l_o)\ln W$ of the line defect turns negative and the defects (interstitials/vacancies) start to proliferate. Here, $e_d$ is the line energy of the defect, $l_o$ is the (longitudinal) length scale for (transverse) fluctuations, and $W$ denotes the number of available positions.

Let us consider the various possible phases and their properties. Within the solid phase ($T < T_m$), the correlator $g^t$ shows a finite asymptotic value, indicating the presence of translational long-range order, whereas $g^t$ decays exponentially to zero in the liquid phase above $T_m$. On the other hand, $g^\phi \sim \exp[-f_d l/T]$, with $l = \sqrt{(\mathbf{R} - \mathbf{R}')^2 + (z - z')^2}$ the length of the defect, decays exponentially in the low-temperature phase, $T < T_{dc}^d$. Above $T_{dc}^d$, $f_d$ changes sign and off-diagonal long-range order is established in the boson system. Following the discussion in Sec. V.B.3, the corresponding vortex phase shows a normal (dissipative) response along the magnetic field. The arrangement of these two transitions possess an interesting question. The conventional scenario is to assume that the defect energy will turn negative at the melting transition, and hence longitudinal superconductivity and translational long-range order will be lost at the same time. In boson language, the translational order is lost at the same temperature $T_m$ where quantum coherence appears. On the other hand, an interesting alternative appears when the defect proliferation temperature $T_{dc}^d$ is smaller than the melting temperature $T_m$, $T_{dc}^d < T_m$. In this case, boson coherence appears while the translational order is still present, and the resulting phase in which both correlators exhibit long-range order is a supersolid. In vortex language, this phase exhibits a vortex lattice that is entangled (due to the presence of vacancies/interstitials) and thus is not superconducting along the field direction. The corresponding phase diagram shows similarities to the phase diagram of a type-II superconductor. In both cases an intermediate phase with line defects appears before the underlying broken symmetry disappears at higher temperatures—in a type-II superconductor, the underlying broken symmetry is that of gauge, and the defected phase is the Schubnikov phase; in the present case, the underlying broken symmetry is the translational lattice order, and the defected phase is the supersolid. On the other hand, the situation in which translational order is lost at the same temperature $T_m$ as quantum coherence appears produces a phase diagram that is similar to that of a type-I superconductor where no intermediate phase is present.

The above melting scenario involving an intermediate supersolid phase corresponds to the existence of a decoupling transition below the melting transition for the vortex lattice, as discussed above for a layered superconductor. When viewed in this manner we obtain $T_{dc}^d \equiv T_{dc}^t \equiv T_{dc}^G \equiv T_{dc}$. In fact, calculating $T_{dc}^d$ from the sign change in the defect free energy $f_d$ for high-field situation, $B > B_{2D}$, in a layered superconductor ($e_d \simeq \alpha \varepsilon_o$; $\alpha$ a prefactor of order 0.1; $l_o \simeq d$; $W = \Lambda^2/a_o^2$), we obtain

$$f_d \simeq \alpha \varepsilon_o - \frac{T}{d} \ln \frac{B_{2D}}{B} \; ; \qquad (8.146)$$

and using the definition $f_d(T_{dc}^d, B) = 0$, we reproduce the result (8.144) up to a numerical factor. The existence of a supersolid phase depends critically on the defect line free energy. In a layered superconductor, there is an additional length scale present (the interlayer distance $d$), which helps in the creation of these topological defects. No corresponding scale is present within a continuous anisotropic superconductor, and the chances for this intermediate phase to exist in this case are low. In fact, calculations of the defect energies in a continuous anisotropic superconductor by Frey, Nelson, and Fisher (1994) do not support the existence of a supersolid phase for this case.

Let us finally summarize the present views regarding the various phases and phase transitions appearing in the vortex system of a continuous anisotropic superconductor as well as in a discrete layered superconductor. In Sec. V.B we saw that we have to destroy *two* types of order when going from the low-temperature Abrikosov phase to the high-temperature normal-metal phase. These two types of order are the translational long-range order in a vortex lattice *perpendicular* to the field direction and the superconducting long-range order *along* the field. In Sec. V.B we discussed the possibility that these two properties are lost sequentially in two transitions: within a continuous anisotropic superconductor, first the translational order is lost ($\rightarrow$disentangled liquid), and in a second transition the longitudinal superconductivity disappears ($\rightarrow$entangled vortex liquid). A moment of thought shows that the decoupling transition discussed above is nothing but the inversion of the order of these two transitions. While the longitudinal superconductivity is lost at $T_{dc}(B)$, the lattice translational order persists until we reach the higher temperature $T_m(B) > T_{dc}(B)$. This sequence of transitions is realized within a layered superconductor at high fields, $B > B_{2D}$. For low fields, $B < B_{2D}$, the conventional 3D picture seems to apply, and lattice order is lost before the longitudinal superconductivity disappears. Quite naturally, then, in a layered superconductor, the transition lines for loss of translational order and for loss of longitudinal superconductivity cross at the point $[T_m(B_{2D}), B_{2D}]$ in the phase diagram (see Fig. 39). Whether a similar crossing can be realized in a continuous anisotropic superconductor remains an open problem. A simple and consistent nomenclature for the various phases we expect to exist in a layered superconductor can be obtained by combining the vortex picture and its 2D-boson analogy. The longitudinal superconductivity is described in the Bose picture: *superfluidity* of bosons is equivalent to normal longitudinal response in the vortex lattice, whereas a *normal* Bose liquid is tantamount to superconducting coherence along the field. The perpendicular lattice order is described in the vortex picture: we have a *solid*, if translational long-range order exists, and a *liquid* in its absence.

We then encounter the following phases in a layered superconductor as we raise the temperature. At low fields we start out with a *normal solid*, which first transforms to a *normal liquid* and, afterwards, to a *superliquid* (see Sec. V.B). At high fields, $B > B_{2D}$, the system also starts out in a *normal-solid* phase, then goes over into a *supersolid* phase at $T_{dc}(B)$, and finally transforms to the high-temperature *superliquid* phase. Though this picture is still quite speculative, it provides a very consistent and complete phase diagram for the layered superconductors, emphasizing again the richness we can expect to encounter in the phenomenology of high-temperature superconductors.

### 5. Parallel magnetic fields

As discussed in Sec. VIII.A.2, layered superconductors are potentially ideal BKT systems with an infinite-range logarithmic interaction in the limit of zero interlayer coupling. The hope that a decoupling transition in zero field below $T_{BKT}$ could take place due to the proliferation of Josephson-loop excitations (Friedel, 1988) was never realized (Korshunov, 1990). The question then arose whether such a decoupled state could be reached with the help of a magnetic field applied parallel to the layers, which tends to suppress the interlayer coupling. The first to address this interesting question was Efetov (1979), who indeed found a decoupled state under high-field conditions, $H > H_J = \Phi_o / d\Lambda$, by means of a high-temperature expansion. The two phases found by Efetov can be described as a vortex solid and a smectic vortex liquid at low and at high temperatures, respectively (Blatter, Ivlev, and Rhyner, 1991). The low-energy excitations of the system consist of double-kink excitations in which a finite segment of a Josephson vortex is thrown over to a neighboring layer, thereby creating two oppositely "charged" pancake vortices. Moving these pancake vortices around in the plane leaves behind a trail of dislocations in the vortex lattice. Within the low-temperature solid phase, the dislocation string has a linear energy and the excitation is confined, whereas in the high-temperature phase the string has "melted" and the linear interaction between the pancakes turns logarithmic, leading to true BKT behavior (Blatter, Ivlev, and Rhyner, 1991).

The question of whether there indeed exists a finite-temperature decoupling transition in the parallel-field configuration apparently remains open. This question is related to the presence of a finite-temperature glass transition (as opposed to a glass phase extending over all temperatures) in the $(1+1)$-dimensional vortex model (see the discussion in Sec. VII.A.3). According to Mikheev and Kolomeisky (1991), a vortex lattice that is intrinsically pinned by the layered structure cannot melt via a *second-order* phase transition. Qualitatively, the intrinsic pinning leads to a dimensional reduction of the fluctuational degrees of freedom, as the vortices can move only along one direction, that parallel to the planes. Similar

results have been reported by Korshunov and Larkin (Korshunov, 1991; Korshunov and Larkin, 1992). Here we concentrate on the analysis presented by Mikheev and Kolomeisky (1991), who consider the low-density limit of the problem, where the intraplanar repulsion between the vortices is provided by collisions due to line wandering. Whereas some consensus seems to exist on this low-density result, the high-density situation is less obvious (Nelson, 1993).

We consider a $(1+1)$-dimensional array of lines described within a continuum elastic model by the functional

$$\mathcal{H} = \frac{1}{2} \int d^2R \left[ c_{44}(\partial_y u)^2 + c_{11}(\partial_x u)^2 \right] . \qquad (8.147)$$

The Hamiltonian (8.147) accounts for the tilt and the compression energy in the system, with $u = u_x(\mathbf{R})$ denoting the displacement field directed along the $x$ axis and with the strings pointing in the $y$ direction. The compression modulus originating from the entropic repulsion takes the form (Pokrovsky and Talapov, 1979)

$$c_{11} = \frac{\pi^2 T^2 n_l^4}{c_{44}} \frac{1}{(1 - Dn_l)^2} , \qquad (8.148)$$

where $n_l$ denotes the mean line density. The second factor represents a correction due to the finite collision length $D$ (=interaction range) of two lines. Rescaling the coordinate $y, y \rightarrow y(c_{11}/c_{44})^{1/2}$, one arrives at the isotropic Hamiltonian

$$\mathcal{H} = \int d^2R \frac{C}{2} (\nabla u)^2 , \qquad (8.149)$$

with

$$C = (c_{11}c_{44})^{1/2} = \pi T n_l^2 \frac{1}{1 - Dn_l} . \qquad (8.150)$$

The displacement correlator $\langle u^2(R) \rangle_{\text{th}}$ for this 2D elastic model grows logarithmically [see Eq. (3.131)],

$$\langle u^2(R) \rangle_{\text{th}} = \frac{T}{\pi C} \ln(n_l R) , \qquad (8.151)$$

so that the planar density-density correlator $[\rho = \exp(2\pi i u n_l)]$ decays only algebraically,

$$\langle \rho(\mathbf{R})\rho^*(0) \rangle_{\text{th}} = e^{-(2\pi n_l)^2 \langle u^2(R) \rangle_{\text{th}}/2} = R^{-\eta} , \qquad (8.152)$$

with the exponent $\eta$ given by

$$\eta = 2\pi T n_l^2 / C = 2(1 - Dn_l) . \qquad (8.153)$$

For a planar array of vortices within a layered superconductor, the tilt modulus is given by $c_{44} = n_l \varepsilon_l = n_l \varepsilon \varepsilon_0$ and the mean line density is $n_l = 1/a_{\parallel}$, with $a_{\parallel} = a_0/\sqrt{\varepsilon}$ the in-plane lattice constant. The interaction range between two Josephson vortices is $D = \lambda/\varepsilon$. Calculating perturbatively the interaction energy between two neighboring layers of vortices, we obtain

$$\mathcal{E}_J \propto \int d^2R \langle \rho(\mathbf{R})\rho^*(0) \rangle_{\text{th}} = \int dR \, R^{1-\eta} . \qquad (8.154)$$

For $\eta > 2$ the integral is finite, and once the temperature $T$ can compete with $\mathcal{E}_J$, the layers should decouple into a system of independent 2D superconductors.

In this low-density analysis the exponent $\eta$ appears to be bounded by 2, and we find that no decoupling transition takes place—the coupling between the layers, no matter how weak, always remains relevant. The above simple arguments are in agreement with the more elaborate renormalization-group arguments by Mikheev and Kolomeisky (1991). We thus have to conclude that, at least in the weak-field limit, the parallel vortex lattice in a layered superconductor cannot transform to a smectic vortex liquid via a second-order phase transition.

The main factor responsible for the above result is the dependence of the compression modulus $c_{11}$ on temperature, $c_{11} \propto T^2$ at low fields, a consequence of the entropic repulsion between the lines. Using a renormalization-group analysis, we find that the generalization of the above result to higher densities takes the form (Nelson and Seung, 1989; Nelson, 1993)

$$c_{11} = \frac{\pi T^2 n_l^4}{c_{44}} \left[ 1 + \frac{n_l D}{\bar{v}} (\pi - \bar{v}) \right]^{-1} \qquad (8.155)$$

with $\bar{v} = v_0 \varepsilon_l D / T^2$. The parameter $v_0$ is the interaction parameter [corresponding to $u_0$ in Eq. (5.29)]; for Josephson vortices with a line energy $\varepsilon \varepsilon_0$ and a range $D = \lambda/\varepsilon$, $v_0 \simeq \varepsilon_0 \lambda$. For large densities the compression modulus scales to $c_{11} = n_l^2 v_0$, and the exponent $\eta$ can become larger than 2, suggesting a finite-temperature glass transition in the disordered $1+1$ model (quasiglass→quasisolid) as well as the existence of a finite-temperature decoupling transition in a layered superconductor (3D solid→3D smectic). Equation (8.155) was obtained within the lowest-order $\varepsilon = 2 - d$ expansion; however, the small thermal renormalization of the high-density result is expected always to be correct.

On the other hand, no such transition was obtained by Korshunov (1991) or by Korshunov and Larkin (1992), who investigated the possibility of a parallel-vortex-lattice melting transition due to a proliferation of dislocations in the crystal at intermediate and at high magnetic-field values. Both an approximate local elastic description and the nonlocal description accounting for the long-range nature of the vortex-vortex interaction led to the result that a potential melting transition lies *above* the bulk phase transition into the superconducting state in the absence of the field, $T_m > T_c$. In fact, it remains to be shown whether the finite-temperature glass transition or the solid-to-smectic transition discussed above really take place below $T_c$ if real vortices are considered in the line model.

Finally, we mention the work of Horovitz (1991), who studies the transition regime in the $(H, T)$ plane via a mapping to a fermionic problem. Within this formulation, the vortex lines are mapped onto chains of fermions that are separated $l$ layers apart, with $l$ determined by the strength of the applied field. Thus the system splits into

superlayers of thickness $ld$, where the individual super-layer is free from vortices, whereas neighboring super-layers are separated by an array of Josephson vortices. Again, the decoupling transition due to fluctuating Josephson vortices competes with the BKT transition due to the unbinding of "pancake" vortices, where the "pancake" vortices now refer to the superlayers and thus extend over a distance $ld$. The two (bare) transition temperatures turn out to scale differently with the superlayer thickness $ld$: whereas decoupling takes place at $T_J(l) = \varepsilon_0 d \sqrt{2l}$, the BKT transition temperature for $l$ layers is $T_{\mathrm{BKT}}(l) = \varepsilon_0 dl/2$. Hence, for $l < 8$, we have $T_{\mathrm{BKT}} < T_J$ and the transition is always three dimensional. On the other hand, for $l > 8$, the decoupling temperature drops below the BKT transition temperature, $T_J < T_{\mathrm{BKT}}$, implying that a narrow 2D regime exists close to $T_c$, where the system decouples into a set of internally coherent superlayers. Note that this scenario can work only if the coupling between the layers is not too weak, so that the 3D transitions are close to $T_J(l)$.

In summary, the question of the existence of a decoupling transition for the parallel-field configuration in a layered superconductor and the related problem of a finite-temperature glass transition in the $1+1$ model have yet to be definitely settled. Whereas agreement between the various approaches exists in the dilute limit, the question remains controversial at high fields. The crucial question in this context is how the interaction between the vortices scales, where the interaction is a combination of bare, thermal, and disorder-induced.

## C. Intrinsic pinning and creep

In this section we concentrate on the phenomenon of strong intrinsic pinning in layered superconductors. Intrinsic pinning in the oxides is a consequence of the layered structure of the material, with strong superconductivity present in the metallic CuO planes and only weak or vanishing superconductivity found in the intermediate buffer layers. Therefore the superconducting order parameter (and, together with it, the condensation energy) is expected to exhibit strong oscillations with period $d$, the interlayer distance. With the magnetic-field **H** aligned parallel to the $ab$ planes ($y$ axis), the vortex lattice tries to accommodate itself to the layer structure so that the vortex cores come to lie in between the strongly superconducting CuO planes. A current density $j$ ($\parallel x$ axis) flowing along the planes will exert a Lorentz force on the vortices which is pointing along the $c$ axis ($z$ axis of the coordinate system). In order to move, the vortices have to cross the strongly superconducting layers, which involves a large expenditure of condensation energy, thus creating the intrinsic pinning barriers. It is this special geometry and its consequences in which we are interested in this section. Note that a current density running along the $c$ axis will push the vortices to move along the planes ($x$ axis) where no barriers are inhibiting the flow. In this

case, point defects are essential for producing a finite critical current density.

In Sec. VIII.C.1 we first evaluate the intrinsic critical current density $j_c^{\mathrm{in}}$, following Tachiki and Takahashi (1989), Barone, Larkin, and Ovchinnikov (1990), and Ivlev and Kopnin (1989, 1990a). The determination of $j_c^{\mathrm{in}}$ will allow us to obtain the intrinsic pinning potential $U_{\mathrm{in}}$ from which we can find the commensurability condition for a vortex lattice with a layered structure. In Sec. VIII.C.2, we shall discuss the problem of creep, both for the case of weak layering (Ivlev and Kopnin, 1990b), where we can make use of the results obtained in Sec. III.E, and for the strongly layered situation, where we shall mainly follow the analysis of Chakravarty, Ivlev, and Ovchinnikov (1990a, 1990b).

### 1. Intrinsic pinning

The first quantitative analysis of intrinsic pinning in layered superconductors was that of Tachiki and Takahashi (1989). In their model the modulus of the order parameter $\Psi = f \exp(i\varphi)$ is assumed to exhibit a periodic spatial variation of the form

$$f(z) = f_0 + f_1 \cos 2\pi \frac{z}{d} \, , \qquad (8.156)$$

with $0 < f_1 < f_0$. The strength of the layering is parametrized by the ratio $\delta = f_1/f_0$. A vortex running parallel to the planes ($y$ direction) and positioned at a height $z = z_0$ will modify the order parameter according to

$$f_v(\mathbf{r}; z_0) = f(z) \tanh \left[ \left[ \frac{x}{\xi} \right]^2 + \left[ \frac{z - z_0}{\varepsilon \xi} \right]^2 \right]^{1/2} , \qquad (8.157)$$

leading to a periodically changing cost in the condensation energy density $(H_c^2/8\pi)\{1 - [f_v(\mathbf{r}; z_0)/f(z)]^2\}$. A simple integration in the $xz$ plane provides the intrinsic pinning potential $u_{\mathrm{in}}$, and the intrinsic pinning force $f_{\mathrm{in}}(z_0)$ is obtained by taking the derivative $f_{\mathrm{in}}(z_0) = -du_{\mathrm{in}}(z_0)/dz_0$. The intrinsic critical current density, finally, is determined by the maximum pinning force and takes the form

$$j_c^{\mathrm{in}} = \frac{3\sqrt{3}}{8} \eta \frac{\Lambda}{\xi} \left[ 1 - \frac{B}{H_{c_2}} \right] j_0 \, , \qquad (8.158)$$

with the parameter $\eta$ depending on the modulation parameter $\delta$ and on the length ratio $\xi/\Lambda$. The factor $1 - B/H_{c_2}$ originates from the suppression of the order parameter on approaching the upper critical field $H_{c_2}$. Note that the length ratio $\Lambda/\xi = d/\varepsilon\xi$ strongly depends on the anisotropy $\varepsilon$ of the system. Assuming $\delta \approx 0.4$–$0.8$ and using $\Lambda/\xi \approx 4$ appropriate to YBCO, the numerical parameter $\eta$ is of the order of 0.2 and the intrinsic depinning current density $j_c^{\mathrm{in}}$ is close to the depairing current density $j_0$, $j_c^{\mathrm{in}} \approx (j_0/2)(1 - B/H_{c_2})$.

A more microscopic approach to the intrinsic pinning problem of a single vortex has been taken by Barone, Larkin, and Ovchinnikov (1990), who base their analysis on the Lawrence-Doniach model [Eq. (8.1)]. Such an approach allows one to relate the parameters of the theory more directly to the experimentally accessible (phenomenological) parameters of the layered material. For the case of weak layering with $\Lambda \ll \xi$, the structure $\Psi_v(x,z)$ of the vortex can be calculated in the continuum anisotropic approximation. The intrinsic pinning energy is then obtained by inserting the solution $\Psi_v(x,z-z_0)$ back into the discrete Lawrence-Doniach free-energy expression (8.1) and determining its variation with the parameter $z_0$. Since the order parameter $\Psi_v$ is a smooth function of position, the energy difference between the continuum anisotropic free energy (giving no intrinsic pinning) and the discrete layered free energy is exponentially small in the parameter $\xi/\Lambda$; we obtain an exponentially small pinning energy

$$U_{\text{in}} \approx 5.10^2 \varepsilon \varepsilon_0 \left[\frac{\xi}{\Lambda}\right]^{5/2} e^{-2\pi\alpha\xi/\Lambda}, \quad \Lambda \ll \xi, \quad (8.159)$$

with the factor $\alpha \approx 2.51$. The intrinsic critical current density is then small, too,

$$j_c^{\text{in}} \approx 4.10^3 \left[\frac{\xi}{\Lambda}\right]^{7/2} e^{-2\pi\alpha\xi/\Lambda} j_0, \quad \Lambda \ll \xi, \quad (8.160)$$

with $j_0$ denoting the depairing critical current density (2.30). In the opposite case of strong layering with $\Lambda \gg \xi$, the critical current density is of the order of the depairing current density $j_0$ itself. An expression for $j_c^{\text{in}}$ is obtained by looking for the largest possible in-plane current flow across a Josephson vortex that still allows for a static solution of the Ginzburg-Landau equations. Hereby the suppression of the order parameter within the layers due to the current flow is taken into account. Such a calculation leads to the estimate

$$j_c^{\text{in}} \approx j_0 \left[1 - \left[\frac{\xi}{\Lambda}\right]^{1/3}\right], \quad \xi \ll \Lambda, \quad (8.161)$$

for the intrinsic critical current density in a strongly layered situation.

The problem of intrinsic pinning in large fields, $B \lesssim H_{c_2}(T)$, has been studied by Ivlev and Kopnin (1989, 1990a; see also Ivlev and Kopnin, 1990b). The basis of their analysis is again the Lawrence-Doniach-model free energy (8.1). Both the weakly layered system with $d \ll \varepsilon\xi$ ($\Lambda \ll \xi$) and the more strongly layered case ($d \lesssim \varepsilon\xi$ or $\Lambda \lesssim \xi$) have been studied. In the vicinity of the upper critical-field line $H_{c_2}(T)$, the order parameter $\Psi_n(\mathbf{R})$ can be obtained from the solution of a linear eigenvalue problem, where the lowest eigenvalue determines the upper critical field $H_{c_2}$ itself. For a field $\mathbf{B}$ pointing along the $y$ axis and a current density $j$ directed along the $x$ axis, we can make the ansatz

$$\Psi_n(x) = \sum_{l=1}^{N} c_l e^{2\pi i n l/N} \psi_p \left[x + \frac{\Phi_0}{Bd}\frac{l}{N}\right], \quad (8.162)$$

where we assume that the vortex lattice relaxes to a state that is commensurate ($a_\perp = a_0\sqrt{\varepsilon} \approx Nd$ = lattice constant along the $c$ axis) with the layer structure. The Bloch functions $\psi_p$ satisfy the Schrödinger equation

$$\frac{\hbar^2}{2m}\left[-\frac{d^2}{dx^2} + \frac{1}{\Lambda^2}\left[1 - \cos 2\pi\frac{Bxd}{\Phi_0}\right]\right]\psi_p(x) = e(p)\psi_p(x). \quad (8.163)$$

Equation (8.163) has been solved in the two limits of weak $[\Lambda \ll \xi(T)]$ and intermediate $[\Lambda \lesssim \xi(T)]$ layering. In the case of weak layering, the potential term in (8.163) is dominant, and $\psi_p$ can be expanded into Wannier functions. On the other hand, for intermediate layering, a free-electron ansatz is appropriate,

$$\psi_p(x) = \begin{cases} \sum_m e^{ipx_m}\phi(x - x_m), & \Lambda \ll \xi(T), \\ u_p(x)e^{ipx}, & \Lambda \lesssim \xi(T), \end{cases} \quad (8.164)$$

with $x_m = m\Phi_0/Bd$. For weak layering, we can approximate the potential term as a harmonic well and use the lowest eigenfunction of the harmonic oscillator,

$$\phi(x) \propto e^{-\pi x^2/a_\parallel^2}, \quad (8.165)$$

with $a_\parallel = a_0/\sqrt{\varepsilon}$ the planar lattice constant, for the Wannier function $\phi(x)$. Due to the small overlap of the neighboring "atomic" functions, the lowest eigenvalue $e_0 = \hbar^2\pi/ma_\parallel^2$ broadens into a narrow band,

$$e(p) = \frac{\hbar^2\pi}{ma_\parallel^2}\left[1 - \frac{8\sqrt{2}}{\pi}\frac{a_\parallel}{\Lambda}e^{-(4/\pi)(a_\parallel^2/\Lambda^2)}\cos\frac{\Phi_0 p}{Bd}\right]. \quad (8.166)$$

The lowest eigenvalue determines the upper critical field $H_{c_2}$; in the absence of a current flow, $e(0) = |\alpha|$, leading to

$$H_{c_2} = \frac{\Phi_0}{2\pi\varepsilon\xi^2}. \quad (8.167)$$

The planar current density flowing in the system is determined by the quasimomentum $\hbar p$ of the wave function,

$$j = 2e\langle|\Psi_n|^2\rangle\frac{1}{\hbar}\frac{de(p)}{dp}, \qu(8.168)$$

where the normalization $\langle|\Psi_n|^2\rangle$ of the order parameter is determined by the quartic term $(\beta/2)|\Psi_n|^4$ in Eq. (8.1) (Ivlev and Kopnin, 1990b),

$$\langle|\Psi_n|^2\rangle = \sum_{l=1}^{N}|c_l|^2 = \frac{B^2}{8\pi}\frac{1}{e_0}\frac{\varepsilon^2}{\kappa^2\beta_A}\frac{H_{c_2} - B}{B}, \quad (8.169)$$

with $\beta_A = \langle|\Psi_n|^4\rangle/\langle|\Psi_n|^2\rangle^2 \approx 1.16$. The intrinsic critical current density close to $H_{c_2}$ can be calculated as the

maximum value of Eq. (8.168), and the result is

$$j_c^{\text{in}} \approx \left[ \frac{8\xi}{\Lambda} \right]^2 \left[ 1 - \frac{B}{H_{c_2}} \right] e^{-8(\xi/\Lambda)^2} j_\circ \ . \tag{8.170}$$

Obviously, reducing the layering by increasing the length ratio $\xi/\Lambda$ leads to an exponential decrease of the intrinsic critical current density.

The same analysis can be carried out for the more strongly layered situation [$\Lambda \lesssim \xi(T)$; see Ivlev and Kopnin, 1989]. In this case we can use a nearly-free-electron approximation for the wave function $\psi_p(x)$, with a periodic part $u_p(x) \sim 1$ and a free-electron-like spectrum $e(p) \sim \text{const} + \hbar^2 p^2 / 2m$. On approaching the limiting value $2\xi^2 = \Lambda^2$, the upper critical field $H_{c_2}$ diverges according to

$$H_{c_2} = \frac{\Phi_\circ}{2\pi\varepsilon\xi^2} \frac{1}{\sqrt{1 - \Lambda^2/2\xi^2}} \ ,$$

and the superconducting state becomes Pauli limited (see Klemm, Luther, and Beasley, 1975). The intrinsic critical current density is given by

$$j_c^{\text{in}} = \frac{8}{\beta_A} \left[ \frac{\xi}{\Lambda} \right]^9 \left[ 1 - \frac{\Lambda^2}{2\xi^2} \right]^{3/2} \left[ 1 - \frac{B}{H_{c_2}} \right]^{3/2} j_\circ \ . \tag{8.171}$$

Note the different field dependence for the intrinsic critical current densities in the weakly layered [Eq. (8.170)] and in the more strongly layered [Eq. (8.171)] cases. Extending the above analysis to the time-dependent situation allows us to study the problem of flux flow near the upper critical field, and we refer the reader to the work of Ivlev and Kopnin (1989, 1990c, 1991a) for details.

Having determined the intrinsic critical current density, we can immediately proceed to obtain the pinning potential $U_{\text{in}}$ acting on the vortex lattice. For the weakly layered case, we have [see Eqs. (8.166) and (8.168)]

$$j = j_c^{\text{in}} \sin \left[ \frac{\Phi_\circ p}{Bd} \right] \ . \tag{8.172}$$

We can easily generalize Eq. (8.172) to the situation in which the vortex lattice is shifted by $u_z$ along the $c$ axis. Such a shift changes the vector potential by $\delta \mathbf{A} = \mathbf{u} \wedge \mathbf{B}$, and for $\mathbf{u} = (0, 0, u_z)$ we obtain $\delta A_x = -u_z B_y$. Replacing the quasimomentum $\hbar p$ in (8.172) by its gauge-invariant form $\hbar p + (2e/c) \mathbf{A}$, we obtain

$$j = j_c^{\text{in}} \sin \left[ \frac{\Phi_\circ p}{Bd} - 2\pi \frac{u_z}{d} \right] \ . \tag{8.173}$$

Finally, making use of the relation $j = 2e \partial U_{\text{in}}/\partial \hbar p$, we obtain the intrinsic pinning potential

$$U_{\text{in}}(p, u_z) = -\frac{j_c^{\text{in}} Bd}{2\pi c} \cos \left[ \frac{\Phi_\circ p}{Bd} - 2\pi \frac{u_z}{d} \right] \ . \tag{8.174}$$

Having determined $U_{\text{in}}$, we can go back one step and check the validity of our initial assumption of having a commensurate vortex lattice. When we denote by $a_\| = a_\Delta/\sqrt{\varepsilon}$ and $a_\perp = a_\Delta\sqrt{\varepsilon}$ the lattice constants along the $x$ and $z$ axes, the condition for finding a commensurate vortex lattice is

$$|a_\perp - Nd| < u_z(a_\perp) \ , \tag{8.175}$$

where the maximal possible shear displacement $u_z(z_\circ)$ is determined by the energy balance

$$c_{66}^\perp \left[ \frac{u_z}{a_\|} \right]^2 \simeq U_{\text{in}} \ . \tag{8.176}$$

Using Eqs. (3.41) for the hard shear mode, $c_{66}^\perp = c_{66}(1-b)^2/\varepsilon$, as well as Eq. (8.174), we obtain the region of attraction for the commensurate state with lattice constant $Nd$ along $z$,

$$\left| \frac{a_\perp}{d} - N \right|$$
$$< \frac{8N}{(\sqrt{\pi}\beta_A)^{1/2}} \left[ \frac{\xi}{\Lambda} \right]^{1/2} \left[ 1 - \frac{B}{H_{c_2}} \right]^{-1/2} e^{-4(\xi/\Lambda)^2} \ , \tag{8.177}$$

with $a_\perp = a_\Delta\sqrt{\varepsilon} \approx Nd$. Here we have also accounted for the suppression of the shear mode close to the upper critical-field line $H_{c_2}$ (see Sec. III.A). For fields such that (8.177) is fulfilled for some integer $N$, one expects that the critical current density will reach a large value close to Eq. (8.170). In a similar way, the higher-order commensurability condition for the case $a_\perp \approx (K/N)d$, $K, N = \text{integers}$, is expected to provide a local maximum in the depinning current density.

The intrinsic pinning potential ($U_{\text{in}}$) as given by Eq. (8.174) applies to the weakly layered case. For strongly layered superconductors, the vortices develop sharp kinks as they cross a superconducting layer, which requires an expenditure of energy $\varepsilon_\circ d \ln(\Lambda/\xi)$ for the formation of a pancake vortex. In the following section we make use of these results in our determination of the creep rate for a parallel field in a layered superconductor.

## 2. Creep

Let us first concentrate on a weakly layered superconductor. To simplify matters, we shall restrict ourselves to the case of a thin sample with a thickness $L$ small as compared with the extent of the vortex bundle along the $c$ axis, $L < d(c_{11}/U_{\text{in}})^{1/2}$. We can then neglect variations of $u_z$ along the $c$ axis, and the problem becomes effectively two dimensional (Ivlev and Kopnin, 1990a, 1990b). The free energy describing this situation is

$$\mathcal{F} = L \int d^2R \left[ \frac{c_{66}^\perp}{2}(\partial_x u)^2 + \frac{c_{44}^\perp}{2}(\partial_y u)^2 + U_{\rm in}(u) \right] .$$

$$(8.178)$$

For weak enough layering we can neglect the dispersion in $c_{44}^\perp$, allowing us to isotropize the free energy such that

$$\mathcal{F} = L \int d^2R \left[ \frac{C}{2}(\nabla u)^2 + \tilde{U}_{\rm in}(u) \right] , \qquad (8.179)$$

with $C = (c_{66}^\perp c_{44}^\perp)^{1/2}$ and $\tilde{U}_{\rm in} = (c_{44}^\perp / c_{66}^\perp)^{1/2} U_{\rm in}$. The free energy (8.179) describes nothing but the energy of a two-dimensional elastic manifold subject to a periodic potential, a problem which we discussed in detail in Sec. III.E. Carrying over the results (3.108) and (3.121), we immediately obtain the expressions for the creep activation energy near $j_c^{\rm in}$ and at low current densities, $j \ll j_c^{\rm in}$,

$$U(j) = \frac{d^2 L}{\kappa} \frac{H_{c_2}(H_{c_2} - B)}{8\pi} \begin{cases} \dfrac{1}{\sqrt{2}}\left[1 - \dfrac{j}{j_c^{\rm in}}\right], & j \lesssim j_c^{\rm in} , \\[2mm] \dfrac{4\sqrt{2}}{\pi^2} \dfrac{j_c^{\rm in}}{j}, & j \ll j_c^{\rm in} . \end{cases}$$

$$(8.180)$$

At low current densities, $j \ll j_c^{\rm in}$, we obtain a glassy behavior with a barrier diverging according to $U(j \to 0) \propto 1/j$. The two (weak-pinning) conditions for the applicability of the above results are

$$L < L_{\max} = d \left[ \frac{c_{11}}{U_{\rm in}} \right]^{1/2}$$

$$= \lambda \left[ \frac{\Lambda}{\xi} \right]^{3/2} \left[ \frac{H_{c_2}}{H_{c_2} - B} \right]^{1/2} e^{4(\xi/\Lambda)^2} \qquad (8.181)$$

(thin enough sample thickness $L$) and

$$\frac{\kappa}{\varepsilon} \left[ \frac{\xi}{\Lambda} \right]^{3/2} \frac{H_{c_2}}{H_{c_2} - B} e^{-4(\xi/\Lambda)^2} \ll 1 \qquad (8.182)$$

[neglect of dispersion, $k_x = (c_{44}^\perp / c_{66}^\perp) L_{\max}^{-1} \ll \varepsilon/\lambda_{\rm eff}$, with $\lambda_{\rm eff}^2 = \lambda^2/(1 - B/H_{c_2})$ the effective screening length near the upper critical field $H_{c_2}$].

For a stronger intrinsic pinning potential (and for weak enough fields), the possibility of single-vortex pinning arises. We are then back to the pinning problem of an isolated string in a periodic potential and thus can make use of the results obtained in Sec. III.E.1. In particular, close to $j_c^{\rm in}$, we obtain for the relevant quantities describing creep the activation barrier

$$U(j) = \frac{24 \times 2^{1/4}}{5\pi} d \sqrt{\varepsilon_l^\perp U_{\rm in}} \left[ 1 - \frac{j}{j_c^{\rm in}} \right]^{5/4}$$

$$\simeq T_c \sqrt{(1-t)/Gi} \left[ \frac{\Lambda}{\xi} \right]^{3/2} \left[ \frac{j_c^{\rm in}}{j_0} \right]^{1/2} \left[ 1 - \frac{j}{j_c^{\rm in}} \right]^{5/4} ,$$

$$(8.183)$$

and the effective action

$$S_E^{\rm eff}(j) = \frac{24}{25 \times 2^{1/4}\pi} \frac{\hbar^2}{e^2} \left[ \frac{\Lambda}{\xi} \right]^2 \frac{\varepsilon d}{\rho_n} \sqrt{\varepsilon_l^\perp / U_{\rm in}} \left[ 1 - \frac{j}{j_c^{\rm in}} \right]^{3/4}$$

$$\simeq \frac{\hbar}{Qu} \left[ \frac{\Lambda}{\xi} \right]^{5/2} \left[ \frac{j_0}{j_c^{\rm in}} \right]^{1/2} \left[ 1 - \frac{j}{j_c^{\rm in}} \right]^{3/4} , \qquad (8.184)$$

where we have used Eqs. (3.136), (3.116), and (8.20), as well as the definitions of $Gi$ [Eq. (2.48)] and $Qu$ [Eq. (2.167)]. The out-of-plane elasticity $\varepsilon_l^\perp$ is given by $\varepsilon_l^\perp \simeq \varepsilon_0 / \varepsilon$. The above results, in particular, the numerical prefactor in (8.184), were obtained by Ivlev, Ovchinnikov, and Thompson (1991). The opposite limit $j \to 0$ produces a nondivergent activation barrier,

$$U(j \ll j_c^{\rm in}) = \frac{8}{\pi} d \sqrt{\varepsilon_l^\perp U_{\rm in}} \qquad (8.185)$$

[see Eq. (3.121)], whereas the Euclidean action takes the form

$$S_E(j \ll j_c^{\rm in}) = \frac{8}{\pi^2} d^2 \sqrt{\varepsilon_l^\perp m_l^\perp} \frac{j_c^{\rm in}}{j} \qquad (8.186)$$

for the case of a massive string [see Eq. (3.122) and use $U_{\rm in} = j_c \Phi_0 d / 2\pi c$]. The dissipative limit is more difficult to obtain, and the result for the action diverges according to (Morais-Smith *et al.*, 1995)

$$S_E^{\rm eff}(j \ll j_c^{\rm in}) = \frac{2}{\pi^2} \frac{\hbar^2}{e^2} \left[ \frac{\Lambda}{\xi} \right]^2 \frac{\varepsilon d}{\rho_n} \sqrt{\varepsilon_l^\perp / U_{\rm in}} \frac{j_c^{\rm in}}{j} \ln \frac{j_c^{\rm in}}{j} .$$

$$(8.187)$$

The results for the massive and the dissipative cases agree up to logarithmic corrections, which arise from the different dynamical terms $\sim M \int dt (\partial_t u)^2$ and $\sim \eta \int dt \, dt' (\partial_t u)(\partial_{t'} u) \ln|t - t'|$ in the action; the appearance of such logarithmic corrections for the dissipative case may be a general feature. Note that, very close to $j_c^{\rm in}$ and in the limit $j \to 0$, the interaction between vortices always becomes relevant and the single-vortex behavior will cross over to the pinning of a higher-dimensional manifold.

Finally, let us turn to the strongly layered case with $\xi \lesssim \Lambda$. Depending on the size of the driving current density, creep can again proceed via the activation of a single-vortex line or via the formation of an activated vortex bundle. We begin with a (relatively) high current density and thus concentrate on single-vortex creep. The activated nucleus consists of a double-kink excitation in which a line segment is thrown to the adjacent layer, thereby creating two (oppositely "charged") pancake vortices. The energy of formation $\mathcal{E}_p$ of these pancake vortices plays the role of the intrinsic pinning potential here $[\mathcal{E}_p = \varepsilon_0 d \ln(\Lambda/\xi) \leftrightarrow E_k = d \sqrt{\varepsilon_l U_{\rm in}}]$. The free energy describing this situation is (see Fig. 41)

$$\mathcal{F}(R) = V_{K,-K}^{\rm int}(R) - \frac{1}{c}(j - j_b)\Phi_0 dR , \qquad (8.188)$$

where $V_{K,-K}^{int}$ is the interaction energy between two oppositely "charged" kinks as given by Eq. (8.43). The confinement current density $j_b$ is determined by a combination of the compression and shear energies in the vortex lattice arising from local distortion due to the activated nucleus. Both energies can be obtained from simple dimensional estimates. Using the dispersive limit for $c_{11}$, we obtain a compressional energy per unit area,

$$c_1 = \frac{1}{2} c_{11}(k_z \sim 1/a_\perp) \left[ \frac{d}{a_\perp} \right]^2 a_\perp = \pi \sqrt{\varepsilon} \varepsilon_0 \frac{d^2}{a_o^3} , \qquad (8.189)$$

and the corresponding shear energy is

$$c_6 = \frac{1}{2} c_{66}^\perp \left[ \frac{d}{a_\parallel} \right]^2 a_\parallel = \frac{1}{8\sqrt{\varepsilon}} \varepsilon_0 \frac{d^2}{a_o^3} . \qquad (8.190)$$

Here we have assumed that, due to the strong layering, the deformation $u = d$ is limited to the minimal possible distances, which are the lattice constant $a_\perp = a_o \sqrt{\varepsilon}$ along the $c$ axis in the case of compression and $a_\parallel = a_o /\sqrt{\varepsilon}$, the planar lattice constant, for shear distortion. The elastic
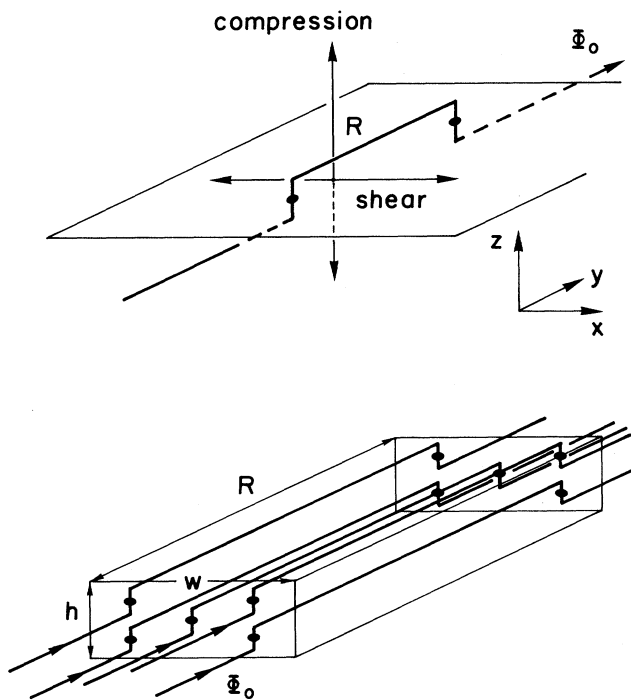


FIG. 41. Nuclei for flux motion across the intrinsic pinning barrier in a strongly layered superconductor: Top, double-kink excitation of a single-vortex line involving shear and compression in addition to the double-kink formation energy. Bottom, vortex bundle excitation relevant at low current densities, where the single-vortex excitation is forbidden due to its (relatively) large compression and shear energies. Whereas the compression, shear, and tilt (=kink formation) energies grow only with the bundle surface, the gain out of the Lorentz force grows with the volume of the bundle. The intrinsic creep at low current densities leads to a glassy response with an exponent $\mu = 2$.

confinement energy for the single-vortex activation is given by

$$\frac{1}{c} j_b \Phi_o dR \approx (c_1 a_\parallel + c_6 a_\perp) R$$

$$\approx \pi R \varepsilon_0 \left[ \frac{d}{a_o} \right]^2 , \qquad (8.191)$$

leading to the current density

$$j_b \approx \frac{3\sqrt{3}\pi}{4} \frac{\xi}{d} \left[ \frac{d}{a_o} \right]^2 j_o , \qquad (8.192)$$

below which single-vortex creep becomes impossible and creep proceeds via the activation of vortex bundles. For large current densities $j$ with $j_b < j \ll j_c^{in} \approx j_o$, the critical size $R_c$ of the nucleus is given by the condition $\partial_R \mathcal{F}(R)|_{R=R_c} = 0$. Using Eq. (8.43) for the potential $V_{K,-K}^{int}$, we obtain (Chakravarty, Ivlev, and Ovchinnikov, 1990a)

$$R_c = \xi \begin{cases} \dfrac{1}{I}, & \dfrac{\xi}{\Lambda} < I \ll 1 , \\[2ex] \dfrac{1}{2} \left[ \dfrac{\Lambda}{\xi I} \right]^{1/2}, & \dfrac{\Lambda}{\xi} \dfrac{\varepsilon^2}{\kappa^2} < I < \dfrac{\xi}{\Lambda} , \\[2ex] \dfrac{\kappa}{\varepsilon} \ln \left[ \dfrac{\varepsilon^2}{\kappa^2} \dfrac{\Lambda}{\xi I} \right], & 0 < I < \dfrac{\Lambda}{\xi} \dfrac{\varepsilon^2}{\kappa} , \end{cases} \qquad (8.193)$$

where we have introduced the current ratio

$$I = \frac{2}{3\sqrt{3}} \frac{j - j_b}{j_o} . \qquad (8.194)$$

The corresponding activation energies are

$$U(j) = 2\varepsilon_0 d \begin{cases} \ln \dfrac{1}{I} - 1, & \dfrac{\xi}{\Lambda} < I \ll 1 , \\[2ex] \ln \dfrac{\Lambda}{\xi} - \left[ \dfrac{\Lambda I}{\xi} \right]^{1/2}, & \dfrac{\Lambda}{\xi} \dfrac{\varepsilon^2}{\kappa^2} < I < \dfrac{\xi}{\Lambda} , \\[2ex] \ln \dfrac{\Lambda}{\xi} - \dfrac{\kappa I}{\varepsilon} \ln \left[ \dfrac{\varepsilon^2}{\kappa^2} \dfrac{\Lambda}{\xi I} \right], & 0 < I < \dfrac{\Lambda}{\xi} \dfrac{\varepsilon^2}{\kappa} . \end{cases}$$

$$(8.195)$$

As the current density drops below $j_b$, a single-vortex line can no longer be activated, due to the confinement energy provided by the vortex lattice. The nucleus for creep-type motion of the flux then becomes a vortex bundle, the idea being that the expenditure in elastic energy grows only with the surface of nucleus, whereas the energy gain due to the Lorentz force is a volume term. The appropriate free energy to be studied can be written as (see Fig. 41)

$$\mathcal{F}(w,h,R) \approx 2c_4 wh + 2c_1 wR + 2c_6 hR - \frac{1}{c} jBdwhR , \qquad (8.196)$$

where $w$ denotes the width (along $x$), $h$ the height (along

$z$), and $R$ the length (along $y$) of the bundle. The "tilt" energy per unit area $c_4$ is due to the creation of pancake vortices and therefore takes the value $c_4 = (\varepsilon_0 d / a_0^2) \ln(\Lambda / \xi)$. The dimensions $w$, $h$, and $R$ of the vortex bundle are easily found by minimization of Eq. (8.196),

$$R = \frac{3\sqrt{3}}{2} \xi \frac{j_0}{j} \ln \frac{\Lambda}{\xi} ,$$

$$w = \frac{1}{8} \frac{d}{a_\perp} \frac{1}{\ln(\Lambda / \xi)} R \ll R , \qquad (8.197)$$

$$h = 8\pi\varepsilon w .$$

These results combine into an activation energy

$$U(J) \simeq \varepsilon_0 d \ln \frac{\Lambda}{\xi} \left[ \frac{j_b}{j} \right]^2 , \quad j < j_b , \qquad (8.198)$$

and we find a typical low-current glassy behavior with an exponent $\mu = 2$.

## D. Collective pinning and creep

Collective pinning and creep in layered superconductors require special discussion, as the discreteness of the structure can modify the results obtained for an anisotropic (i.e., continuous) description. The problem of pinning and creep in two-dimensional systems, i.e., thin films, also deserves special attention due to its technological relevance and because of the appearance of new physical effects. Again we assume that pinning is weak and is due to the collective action of point defects such as oxygen vacancies (see Sec. III.C). Depending on the strength $\gamma$ of the pinning and on the direction and magnitude of the magnetic field **B**, the collectively pinned object and the nucleus for creep-type motion can take any form from a zero-dimensional pancake vortex for a three-dimensional vortex bundle in a layered superconductor. To be specific, consider a weak magnetic field **B** directed along the $c$ axis such that each vortex line is pinned individually. Since in this geometry the line tension $\varepsilon_l \simeq \varepsilon^2 \varepsilon_0$ remains unchanged as compared with a continuous anisotropic description [see Eqs. (8.47) and (8.48)], the length of the collectively pinned segment is given by Eq. (2.149), $L_c^c \simeq (\varepsilon_0^2 \xi^2 \varepsilon^4 / \gamma)^{1/3}$. For weak enough pinning ($\gamma$ small), we will have $L_c^c > d$, and the collectively pinned object is a line segment. On the other hand, in order to neglect the interaction between the vortex lines, the magnetic field has to be weak enough that $L_c^c < \varepsilon a_0$ [see Eq. (2.154)]. Putting these limits together, we find the requirements for single-vortex line pinning to be

$$d < L_c^c < \varepsilon a_0 , \quad \text{1D pinning} .$$

When we increase the magnetic field $B$ so that $\varepsilon a_0 < L_c^c$, the system enters the regime of 3D bulk pinning,

$$d, \varepsilon a_0 < L_c^c , \quad \text{3D pinning} .$$

On the other hand, if we increase instead the pinning parameter $\gamma$ such that $L_c^c$ drops below the interlayer distance $d$, the system enters the single-pancake pinning regime. An additional condition for each pancake to be pinned individually is $c_{66} \xi^2 d < U_{pc} = \sqrt{\gamma d \xi^2}$; i.e., the interplanar interaction energy between the pancake vortices has to be smaller than the pinning energy $U_{pc}$ of an individual pancake vortex. Combining these results, we obtain the requirements for single-pancake pinning,

$$L_c^c < d < d \frac{U_{pc}}{\varepsilon_0 d} \left[ \frac{a_0}{\xi} \right]^2 , \quad \text{zero-dimensional pinning} .$$

With an increase in the magnetic field $B$ such that $a_0 < \xi \sqrt{d \varepsilon_0 / U_{pc}}$, the possibility of 2D collective pinning arises. In this case all the pancake vortices within a radius $R_c > a_0$ relax collectively to the underlying pinning potential. The collective pinning radius $R_c$ is obtained from the elastic-disorder energy balance, $c_{66} d (\xi / R_c)^2 R_c^2 \simeq (R_c / a_0) U_{pc}$; hence

$$R_c \simeq a_0 \frac{\varepsilon_0 d}{U_{pc}} \left[ \frac{\xi}{a_0} \right]^2 .$$

A second requirement for the existence of a 2D collective pinning regime is given by the smallness of the interlayer coupling

$$U_{\text{int}}^J \simeq c_{44}(\kappa \sim \pi / R_c)(\xi / d)^2 dR_c^2$$

$$\simeq \varepsilon_0 d (\xi / \Lambda)^2 (R_c / a_0)^4$$

as compared with the intraplanar energy $U_{\text{int}}^{2D} \simeq c_{66} d \xi^2$. The two conditions define the boundaries of the 2D collective pinning regime,

$$L_c^c < d, \quad a_0 < R_c < \sqrt{a_0 \Lambda}, \quad \text{2D pinning} .$$

For a thin film, $\Lambda \to \infty$ and $R_c$ can extend to arbitrary distances.

Finally, for even larger fields such that $R_c > \sqrt{a_0 \Lambda}$, we enter the 3D collective pinning regime,

$$L_c^c < d, \quad \sqrt{a_0 \Lambda} < R_c, \quad \text{3D pinning} .$$

This condition is equivalent to the previous condition $\varepsilon a_0 < L_c^c$. The boundary of the 3D collective pinning regime does not depend on the interlayer distance $d$ and is the same whether it is reached from the 1D or from the 2D pinning regime.

In summary, for **B**$\|c$, we find that at high fields, $\varepsilon a_0 < L_c^c$, pinning always involves 3D bundles. At small fields, however, the layering becomes important and pinning can involve either vortex lines, if the disorder is weak ($d < L_c^c$), or vortex points/planar vortex ensembles if the disorder is strong ($L_c^c < d$). Below, we first discuss the weak-pinning situation in which both pinning and creep involve only vortex lines (Sec. VIII.D.1). In Sec. VIII.D.2 we turn our attention to the case of strong disorder and analyze the regime of 2D pinning and creep. Finally, in Sec. VIII.D.3, we concentrate on the role of

dislocations and show how they destroy glassiness in the two-dimensional situation.

### 1. Single-vortex pinning and creep ($d < L_c^c$)

The problem of single-vortex pinning and creep (both classical and quantum) in layered superconductors was investigated by Blatter and Geshkenbein (1992) for the general case in which the magnetic field **B** encloses an angle $\vartheta$ with the *ab* plane. Within the angular regime $\varepsilon < \vartheta < \pi/2$, the results for a layered superconductor coincide with those obtained within an anisotropic continuum description, and therefore all the results obtained in Secs. II.C, II.D, III.A, and IV.D involving only single vortices can be applied directly to the layered case. This coincidence is based on two facts: First, within the angular regime $\vartheta > \varepsilon$, we have $\varepsilon_\vartheta \simeq |\sin\vartheta|$, and the single-line tensions given by Eqs. (8.47) and (8.48) agree with those obtained in a continuum anisotropic description [see Eqs. (2.144) and (2.146)]. Second, the pinning energy of a line segment of length $L$ involves only the pancake vortices and thus is given by $\mathscr{E}_{\rm pin}(L,\vartheta) \simeq (f_{\rm pin}^2 n_i \xi^2 L |\sin\vartheta|)^{1/2}\xi \simeq (\gamma L |\sin\vartheta|)^{1/2}\xi$, where we have used Eq. (2.43). Again, since $\varepsilon_\vartheta \simeq |\sin\vartheta|$, this pinning energy coincides with the continuum anisotropic result (2.147). Whereas in the anisotropic case the volume of the vortex core decreases with angle $\vartheta$ according to $L\xi^2\varepsilon_\vartheta$, for the layered case the concentration of the pinning to the pancakes has the same net effect of reducing the volume to $L\xi^2|\sin\vartheta|$.

The analysis becomes more difficult, however, as we go to the small-angle regime, $|\vartheta| < \varepsilon$. Let us concentrate first on the case $\vartheta = 0$, in which the field **B** is aligned with the *ab* planes. The presence of intrinsic pinning preventing vortex motion along the *c* direction is discussed in detail in Sec. VIII.C. Here we take the intrinsic pinning to be infinite and concentrate on the effect of point pins hampering vortex motion along the *ab* planes. We first have to determine the magnitude of the elementary pinning force acting on a Josephson vortex. We shall assume that the pinning is due to the presence of pointlike defects suppressing the magnitude of the order parameter within the superconducting CuO planes. As a reference, we shall use the elementary pinning force $f_{\rm pin}$ [see Eq. (2.43)] experienced by a vortex directed along the *c* axis (stack of pancake vortices). Pinning can be due to disorder in $T_c$ or in the mean free path $l$ (Larkin, 1970) and involves either the modulus $|\Psi|^2$ or the gradient term $|\nabla\Psi|^2$ of the order parameter [see Eqs. (2.33) and (2.34) and Sec. III.C]. Close to the center of an Abrikosov vortex, the order parameter $|\Psi_v|^2$ goes to zero on a scale $\xi$. On the other hand, a Josephson vortex only weakly perturbs the order parameter in the adjacent superconducting layers. As follows from the discussion in Sec. VIII.A.1, the order parameter is suppressed, Eq. (8.14), by a factor $\sim [1 - (\xi/\Lambda)^2]$ on a scale $\Lambda$. For the case of $\delta T_c$ pinning, we thus find that the condensation energy

gain due to the presence of a point defect is reduced by a factor $\sim (\xi/\Lambda)^2$ as compared with the Abrikosov vortex. In addition, the length scale on which the Josephson vortex can experience this (small) energy gain is $\Lambda$ and thus is a factor $\Lambda/\xi$ larger than for the Abrikosov vortex. Combining these factors, we therefore find that the elementary pinning force $f_{\rm pin}^J$ acting on a Josephson vortex is reduced by a factor $\sim (\xi/\Lambda)^3$ as compared with the force $f_{\rm pin}$ acting on an Abrikosov vortex. The same result is obtained for the case of $\delta l$ pinning, since the gradient acting on the phase of the order parameter leads to $|\nabla\Psi_v|^2 \simeq |\Psi_\infty|^2/\Lambda^2$, which is again reduced by a factor $(\xi/\Lambda)^2$ as compared with the corresponding result for the Abrikosov vortex. In summary, we find that the same point defect acts differently on a Josephson vortex than it does on an Abrikosov vortex, with the elementary pinning forces related via (Perruchoud, 1991)

$$\frac{f_{\rm pin}^J}{f_{\rm pin}}\bigg|_{\delta T_c} \approx \left[\frac{\xi}{0.66\Lambda}\right]^3 , \tag{8.199}$$

$$\frac{f_{\rm pin}^J}{f_{\rm pin}}\bigg|_{\delta l} \approx \left[\frac{\xi}{0.71\Lambda}\right]^3 . \tag{8.200}$$

Within the phenomenological approach, $f_{\rm pin}$ can be determined from a measurement of $j_c^c$ (the in-plane, single-vortex critical current density with **B**$\|c$, $B$ small), and $f_{\rm pin}^J$ can then be obtained by scaling, $f_{\rm pin}^J \approx (\xi/0.7\Lambda)^3 f_{\rm pin}$. Another source of pinning (which we do not consider here) is a spatial inhomogeneity in the Josephson coupling. Such a disorder will act only on the Josephson vortices and will not affect the pancake vortices in the system.

The knowledge of $f_{\rm pin}^J$ allows us to determine all the relevant quantities necessary for a description of the dynamic behavior of a Josephson vortex. Since here we assume the intrinsic pinning to be infinite, the only remaining degree of freedom is motion within the *ab* plane. The collective pinning length $L_c^J$ is obtained from the energy balance

$$\varepsilon_0\varepsilon\frac{\Lambda^2}{L_c^J} \simeq U_c^J = [(f_{\rm pin}^J)^2 n_i L_c^J \Lambda d]^{1/2}\Lambda , \tag{8.201}$$

where we have used the elasticity $e_J \simeq \varepsilon_0\varepsilon$, Eq. (8.16), of the Josephson vortex. The results for $L_c^J$, for the collective pinning energy $U_c^J$, and for the critical current density $j_c^J$ are

$$L_c^J \simeq \frac{L_c^c}{\varepsilon}\left[\frac{\Lambda}{\xi}\right]^2 , \tag{8.202a}$$

$$U_c^J \simeq U_c^c , \tag{8.202b}$$

$$j_c^J \simeq \varepsilon j_c^c\left[\frac{\xi}{\Lambda}\right]^3 , \tag{8.202c}$$

where we express the results in terms of the basic quantities $L_c^c$, $U_c^c$, and $j_c^c$ characterizing single-vortex pinning for **B**$\|c$.

The action for quantum creep involves the mass $m_J \simeq \varepsilon m_l^c$ and/or the viscous friction coefficient $\eta_J \simeq \varepsilon \eta_l^c (\xi / \Lambda)^2$ [see Eqs. (2.26) and (8.19)], of the Josephson vortex. Note that, in the calculation of $m_J$, the different (phase) core size $d\Lambda$ of the Josephson vortex from that of an equivalent Abrikosov vortex (core size $\varepsilon \xi^2$) exactly compensates for the reduced suppression of the order parameter, $\delta |\Psi_v|^2 \simeq (\xi / \Lambda)^2 |\Psi_\infty|^2$. Moreover, the electromagnetic contribution to the vortex mass, $M_{em} \simeq (\varepsilon \varepsilon_d / 2\pi d^2)(\hbar^2 / e^2)$, can become large for the Josephson vortex due to increased capacitive effects present in the layered structure (large dielectric constant $\varepsilon_d$ of the buffer layers). Following the steps outlined in Sec. II.A.5, we obtain the (effective) Euclidean action determining the quantum creep rate for a Josephson vortex,

$$S_E^J \simeq S_E^c \left[ \frac{\Lambda}{\xi} \right]^2 , \tag{8.203a}$$

$$S_E^{\mathrm{eff},J} \simeq S_E^{\mathrm{eff},c} \left[ \frac{\Lambda}{\xi} \right]^2 . \tag{8.203b}$$

Having discussed the angular regimes $\vartheta > \varepsilon$ and $\vartheta = 0$, we are left with the (usually small) intermediate region $0 < \vartheta < \varepsilon$, where the kinked structure of the vortex line is relevant. Since the vortex line breaks up into Josephson and pancake vortices, we should take into account the pinning of both types of segments. However, due to the smallness of the pinning forces acting on the Josephson vortex, the pinning of the pancake vortices is dominant over most of the angular region $0 < \vartheta < \varepsilon$. We therefore concentrate first on pinning of the pancake vortices and discuss later the crossover to Josephson vortex pinning at very small angles.

First of all, we have to determine the relevant mode of relaxation, which can involve either in-plane or out-of-plane motion of the pancake vortices (or a combination thereof). The two corresponding pinning lengths $L_c^{\|}$ and $L_c^{\perp}$ are determined by the energy balance between the elastic and the pinning energies,

$$\mathcal{E}_{\mathrm{el}}^{\|}(\vartheta) \simeq \varepsilon_l^{\|}(\vartheta) \xi^2 / L^{\|} ,$$

$$\mathcal{E}_{\mathrm{el}}^{\perp}(\vartheta) \simeq \varepsilon_l^{\perp}(\vartheta)(\xi \sin \vartheta)^2 / L^{\perp} ,$$

$$\mathcal{E}_{\mathrm{pin}}(\vartheta) \simeq (f_{\mathrm{pin}}^2 n_i \xi^2 L |\sin \vartheta|)^{1/2} \xi .$$

The elasticities $\varepsilon_l^{\|}(\vartheta)$ and $\varepsilon_l^{\perp}(\vartheta)$ are given by Eqs. (8.47) and (8.48). Note that only pancake vortices (with a total length $L |\sin \vartheta|$) contribute to the pinning energy. For out-of-plane relaxation, only the component $\xi |\sin \vartheta|$ along the $y'$ axis enters the elastic energy $\mathcal{E}_{\mathrm{el}}^{\perp}$. Dimensional estimates than provide the pinning lengths

$$L_c^{\|} \simeq \frac{L_c^c}{\varepsilon_\vartheta} \left[ \frac{\varepsilon_\vartheta}{|\sin \vartheta|} \right]^{1/3} , \tag{8.204a}$$

$$L_c^{\perp} \simeq \frac{L_c^c}{\varepsilon_\vartheta} \frac{|\sin \vartheta|}{\varepsilon_\vartheta} . \tag{8.204b}$$

Obviously, $L_c^{\|} \simeq L_c^{\perp} \simeq L_c(\vartheta)$ within the regime $\vartheta > \varepsilon$, as must be expected. On the other hand, for small angles, $|\vartheta| < \varepsilon$, we have $L_c^{\perp} / L_c^{\|} \simeq (|\vartheta| / \varepsilon)^{4/3} < 1$, and therefore out-of-plane relaxation becomes dominant. The relevant collective pinning length is $L_c(\vartheta) = L_c^{\perp}(\vartheta) \simeq L_c^c |\vartheta| / \varepsilon^2$, leading to a pinning energy $U_c(\vartheta) \simeq U_c^c |\vartheta| / \varepsilon$ and to critical current densities $j_c^{\|} \simeq j_c^c (\varepsilon / |\vartheta|)$ and $j_c^{\perp} \simeq \varepsilon j_c^c$. These results are valid, provided that the pinning length $L_c(\vartheta)$ is still enclosing many pancake vortices, $L_c(\vartheta) > d / |\vartheta|$; otherwise, each pancake vortex is pinned individually with an energy $U_{pc} = U_c^c (d / L_c^c)^{1/2}$. The critical current densities within the single-pancake pinning regime become $j_c^{\|} \simeq j_c^c (L_c^c / d)^{1/2}$ and $j_c^{\perp} \simeq j_c^c (L_c^c / d)^{1/2} |\vartheta|$. The condition for single-pancake pinning, $L_c(\vartheta) < d / |\vartheta|$, can be rewritten as $|\vartheta| < \varepsilon (d / L_c^c)^{1/2}$, with $d / L_c^c < 1$, the weak-pinning condition, applying throughout the present section. With a further decrease in the angle $\vartheta$, the total pinning force acting on the vortex due to the pinning of the pancake vortices becomes smaller, and the pinning of the Josephson vortex segments becomes relevant. As a crossover criterion, we can use the condition $j_c^J \simeq j_c^{\perp}$, which defines the angle $\vartheta_J \simeq \varepsilon (d / L_c^c)^{1/2} (\xi / \Lambda)^3$.

In summary, the *pinning* properties of a kinked vortex within the angular regime $0 < \vartheta < \varepsilon$ can be characterized as follows:

$$L_c(\vartheta) \simeq \begin{cases} \dfrac{L_c^c}{\varepsilon} \dfrac{|\vartheta|}{\varepsilon}, & \varepsilon \left[ \dfrac{d}{L_c^c} \right]^{1/2} < \vartheta < \varepsilon , \\[3ex] \dfrac{d}{|\vartheta|}, & |\vartheta| < \varepsilon \left[ \dfrac{d}{L_c^c} \right]^{1/2} , \end{cases} \tag{8.205}$$

$$U_c(\vartheta) \simeq \begin{cases} U_c^c \dfrac{|\vartheta|}{\varepsilon}, & \varepsilon \left[ \dfrac{d}{L_c^c} \right]^{1/2} < \vartheta < \varepsilon , \\[3ex] U_{pc} \simeq U_c^c \left[ \dfrac{d}{L_c^c} \right]^{1/2}, & |\vartheta| < \varepsilon \left[ \dfrac{d}{L_c^c} \right]^{1/2} , \end{cases} \tag{8.206}$$

$$j_c^{\|}(\vartheta) \simeq \begin{cases} j_c^c \dfrac{\varepsilon}{|\vartheta|}, & \varepsilon \left[ \dfrac{d}{L_c^c} \right]^{1/2} < \vartheta < \varepsilon , \\[3ex] j_c^c \left[ \dfrac{L_c^c}{d} \right]^{1/2}, & |\vartheta| < \varepsilon \left[ \dfrac{d}{L_c^c} \right]^{1/2} , \end{cases} \tag{8.207}$$

$$j_c^{\perp}(\vartheta) \simeq \begin{cases} \varepsilon j_c^c, & \varepsilon \left[ \dfrac{d}{L_c^c} \right]^{1/2} < \vartheta < \varepsilon , \\[3ex] \varepsilon j_c^c \left[ \dfrac{L_c^c}{d} \right]^{1/2} \dfrac{|\vartheta|}{\varepsilon}, & \vartheta_J < \vartheta < \varepsilon \left[ \dfrac{d}{L_c^c} \right]^{1/2} . \end{cases} \tag{8.208}$$

For very small angles, $|\vartheta| < \vartheta_J = \varepsilon (d / L_c^c)^{1/2} (\xi / \Lambda)^3$, Eqs. (8.202) for the Josephson vortex apply. The angular dependence of the critical current density in layered superconductors has also been treated by Pokrovsky, Lyuksyutov, and Nattermann (1992).

It remains to study the creep process at small angles, $|\vartheta| < \varepsilon$. In the following, we first derive the results for the case of classical creep and then present the main results for the quantum case. For a derivation and a complete list of the quantum results, we refer the reader to the work of Blatter and Geshkenbein (1992). Creep can again proceed either along the planes (driving current $j \| y'$ axis) or in the out-of-plane direction (driving current density $j$ in the $ab$ plane). Since relaxation to the pinning potential involves mainly out-of-plane motion, the corresponding activation energy for creep is given simply by the collective pinning energy. On the other hand, for the case of in-plane motion, we have to recalculate the optimal segment $L_h^{\|}$ for the hop. Equating the elastic energy density involved in the hop, $\varepsilon_l^{\|}(\vartheta)(\xi/L_h^{\|})^2$, with the elastic energy density $\varepsilon_l^{\perp}(\vartheta)(\xi\vartheta/L_c^{\perp})^2$ of the relaxed vortex, we obtain the hopping length

$$L_h^{\|} \simeq \frac{\varepsilon}{|\vartheta|} L_c^{\perp} \simeq \frac{L_c^c}{\varepsilon} , \qquad (8.209)$$

which exceeds the collective pinning length $L_c(\vartheta)$.

Therefore the activation energy for in-plane creep differs from the collective pinning energy $U_c(\vartheta)$ and reads $U_c(\vartheta)(L_h^{\|}/L_c^{\perp}) \simeq U_c^c$. Note that, due to the increase in the length of the hopping segment $L_h^{\|}$, the regime of collective creep involving many pancakes extends down to smaller angles. For angles $|\vartheta| < \varepsilon(d/L_c^c)^{1/2}$, pinning is due to single vortices with a mean pinning energy density $U_c^c(d/L_c^c)^{1/2}|\vartheta|/d$. Equating this energy density to the elastic energy density involved in the hop, we obtain $L_h^{\|}/L_c^{\perp} \simeq (|\vartheta|/\varepsilon)^{1/2}(L_c^c/d)^{3/4}$, where $L_c^{\perp} \simeq d/|\vartheta|$. The resulting activation energy becomes

$$U_c^c(d/L_c^c)^{1/2}(L_h^{\|}/L_c^c) \simeq U_c^c(L_c^c/d)^{1/4}(|\vartheta|/\varepsilon)^{1/2}$$

and is valid down to the single-pancake creep regime at $|\vartheta| < \varepsilon(d/L_c^c)^{3/2}$, where the length of the hopping segment $L_h^{\|}$ becomes larger than the separation $d/|\vartheta|$ between two pancakes. Within the single-pancake creep regime, the activation energy is $U_c^c(d/L_c^c)^{1/2}$, independent of the angle and of the direction of motion. We can thus summarize the activation energies for classical creep in the small-angle regime:

$$U^{\perp}(\vartheta) \simeq \begin{cases} U_c^c \dfrac{|\vartheta|}{\varepsilon}, & \varepsilon \left[\dfrac{d}{L_c^c}\right]^{1/2} < \vartheta < \varepsilon , \\[12pt] U_c^c \left[\dfrac{d}{L_c^c}\right]^{1/2}, & |\vartheta| < \varepsilon \left[\dfrac{d}{L_c^c}\right]^{1/2} , \end{cases} \qquad (8.210)$$

$$U^{\|}(\vartheta) \simeq \begin{cases} U_c^c, & \varepsilon \left[\dfrac{d}{L_c^c}\right]^{1/2} < \vartheta < \varepsilon , \\[12pt] U_c^c \left[\dfrac{L_c^c}{d}\right]^{1/4} \left[\dfrac{|\vartheta|}{\varepsilon}\right]^{1/2}, & \varepsilon \left[\dfrac{d}{L_c^c}\right]^{3/2} < \vartheta < \varepsilon \left[\dfrac{d}{L_c^c}\right]^{1/2} , \\[12pt] U_{\mathrm{pc}} \simeq U_c^c \left[\dfrac{d}{L_c^c}\right]^{1/2}, & \vartheta_J < \vartheta < \varepsilon \left[\dfrac{d}{L_c^c}\right]^{3/2} . \end{cases} \qquad (8.211)$$

The determination of the quantum creep rate proceeds along the same lines. Again, we have to distinguish between out-of-plane ($\perp$) and in-plane ($\|$) motion, and the results for a mass-dominated dynamics are

$$S_E^{\perp}(\vartheta) \simeq \begin{cases} S_E^c \left[\dfrac{|\vartheta|}{\varepsilon}\right]^{3/2}, & \varepsilon \left[\dfrac{d}{L_c^c}\right]^{1/2} < \vartheta < \varepsilon , \\[12pt] S_E^c \left[\dfrac{d}{L_c^c}\right]^{3/4}, & |\vartheta| < \varepsilon \left[\dfrac{d}{L_c^c}\right]^{1/2} , \end{cases} \qquad (8.212)$$

$$S_E^{\|}(\vartheta) \simeq \begin{cases} S_E^c, & \varepsilon \left[\dfrac{d}{L_c^c}\right]^{3/2} < \vartheta < \varepsilon , \\[12pt] S_E^c \left[\dfrac{d}{L_c^c}\right]^{3/4} \left[\dfrac{\varepsilon}{|\vartheta|}\right]^{1/2}, & \vartheta_J < \vartheta < \varepsilon \left[\dfrac{d}{L_c^c}\right]^{3/2} . \end{cases} \qquad (8.213)$$

The corresponding results in the dissipative limit are

$$S_E^{\mathrm{eff}^\perp}(\vartheta) \simeq \begin{cases} S_E^{\mathrm{eff},c}\left[\dfrac{\vartheta}{\varepsilon}\right]^2, & \varepsilon\left[\dfrac{d}{L_c^c}\right]^{1/2} < \vartheta < \varepsilon, \\[4mm] S_E^{\mathrm{eff},c}\dfrac{d}{L_c^c}, & |\vartheta| < \varepsilon\left[\dfrac{d}{L_c^c}\right]^{1/2}, \end{cases} \tag{8.214}$$

$$S_E^{\mathrm{eff}^\parallel}(\vartheta) \simeq \begin{cases} S_E^{\mathrm{eff},c}\dfrac{|\vartheta|}{\varepsilon}, & \varepsilon\left[\dfrac{d}{L_c^c}\right]^{1/2} < \vartheta < \varepsilon, \\[4mm] S_E^{\mathrm{eff},c}\left[\dfrac{d}{L_c^c}\right]^{1/4}\left[\dfrac{|\vartheta|}{\varepsilon}\right]^{1/2}, & \varepsilon\left[\dfrac{d}{L_c^c}\right]^{3/2} < \vartheta < \varepsilon\left[\dfrac{d}{L_c^c}\right]^{1/2}, \\[4mm] S_E^{\mathrm{eff},c}\dfrac{d}{L_c^c}, & \varepsilon\left[\dfrac{\xi}{\Lambda}\right]^2 < \vartheta < \varepsilon\left[\dfrac{d}{L_c^c}\right]^{3/2}, \\[4mm] S_E^{\mathrm{eff},c}\dfrac{d}{L_c^c}\left[\dfrac{\xi}{\Lambda}\right]^2\dfrac{\varepsilon}{|\vartheta|}, & \vartheta_J < \vartheta < \varepsilon\left[\dfrac{\xi}{\Lambda}\right]^2. \end{cases} \tag{8.215}$$

One should point out that all the above results usually apply to a very narrow angular regime, and it may be very difficult to distinguish between the different behaviors. On the other hand, the analysis presented here illustrates what elements enter the discussion of pinning and creep in layered superconductors and what types of new results we can expect to find in the small-angle regime, $0 < \vartheta < \varepsilon$, where the discreteness of the structure is really important.

Finally, a word concerning the regime of applicability of the above results. Within the large-angle regime, $\vartheta > \varepsilon$, the continuum anisotropic description can be applied, and thus the single-vortex pinning regime is restricted to fields $B < \beta_{sb}H_{c_2}(\vartheta)(j_c^c/j_0)$ with $\beta_{sb} \approx 5$. Repeating the corresponding analysis at small angles, $|\vartheta| < \varepsilon$, leads to the same result. Note that creep processes involving larger length scales (e.g., in-plane creep or creep at small current densities) already couple to neighboring vortices at smaller fields.

## 2. 2D collective pinning and creep ($L_c^c < d$)

The problem of collective pinning and creep in thin films and in strongly layered superconductors has been analyzed by Feigel'man, Geshkenbein, and Larkin (1990), by Koshelev (1990), and by Vinokur, Kes, and Koshelev (1990). Throughout the following discussion we shall restrict ourselves to the case in which the magnetic field is pointing along the $c$ axis. To begin with, let us consider a weak magnetic field so that we can neglect the interaction between the vortices within the plane (the "strong" pinning condition $L_c^c < d$ allows us to ignore the interaction between neighboring pancake vortices in different layers). An estimate for the intraplanar vortex-vortex in-

teraction is given by the shear energy buildup during the relaxation process and involves mutual displacements between the vortices of the order of $u \simeq \xi$,

$$U_{\mathrm{int}}^{2D} \simeq c_{66}d\left[\dfrac{\xi}{a_0}\right]^2 a_0^2 \simeq \varepsilon_0 d\left[\dfrac{\xi}{2a_0}\right]^2. \tag{8.216}$$

For the "strong" pinning situation $U_{pc} > U_{\mathrm{int}}^{2D}$, we can neglect all interactions between the vortices, and each pancake vortex is pinned individually. The collective pinning energy for a single pancake vortex is

$$U_{pc} \simeq (\gamma\xi^2 d)^{1/2}, \tag{8.217}$$

and the planar critical current density becomes equal to

$$j_{pc} \simeq j_0\dfrac{U_{pc}}{\varepsilon_0 d}. \tag{8.218}$$

Expressing the activation energy $U_{pc}$ via the Ginzburg number $Gi$ and the experimentally accessible critical current density $j_{pc}$, we obtain

$$U_{pc} \simeq T_c\sqrt{(1-t)/Gi}\,\dfrac{\Lambda}{\xi}\dfrac{j_{pc}}{j_0} \simeq T_c\dfrac{1-t}{Gi^{2D}}\dfrac{j_{pc}}{j_0}. \tag{8.219}$$

Note that the applicability of the weak-collective-pinning idea to single pancakes requires $U_{pc}$ to be small in the sense $U_{pc} < \varepsilon_0 d$, whereas neglect of all interactions necessitates strong pinning with $U_{pc} > \varepsilon_0 d\,(\xi/\Lambda)^2$ (from $L_c^c < d$) and $U_{pc} > \varepsilon_0 d\,(\xi/2a_0)^2$ (from $U_{pc} > U_{\mathrm{int}}^{2D}$). Hence the conditions for (collective) single-pancake pinning are

$$\varepsilon_0 d\left[\dfrac{\xi}{\min(2a_0,\Lambda)}\right]^2 < U_{pc} < \varepsilon_0 d. \tag{8.220}$$

With increasing magnetic field, the intraplanar interaction becomes increasingly important, and the vortex system crosses over to 2D collective pinning. In this case all

pancake vortices within the radius $R_c > a_0$ are pinned collectively. The collective pinning radius $R_c$ is obtained by balancing the total pinning energy $U_{pc}(R_c/a_0)$ against the elastic energy $U_{int}^{2D}$, and we obtain

$$R_c \simeq a_0 \frac{\varepsilon_0 d}{U_{pc}} \left[ \frac{\xi}{2a_0} \right]^2 . \tag{8.221}$$

The resulting critical current density for the 2D collective pinning regime is

$$j_c^{2D} \simeq j_{pc} \frac{a_0}{R_c} \simeq j_0 \left[ \frac{U_{pc}}{\varepsilon_0 d} \right]^2 \left[ \frac{2a_0}{\xi} \right]^2 \simeq j_0 \left[ \frac{j_{pc}}{j_0} \right]^2 \left[ \frac{2a_0}{\xi} \right]^2 . \tag{8.222}$$

The magnetic field $B_b^{2D}$ limiting the single-pancake pinning regime is determined by the condition $U_{pc} \simeq U_{int}^{2D}$ (which is equivalent to $R_c \simeq a_0$),

$$B_b^{2D} \simeq \beta_b \frac{U_{pc}}{\varepsilon_0 d} H_{c_2}^c \simeq \beta_b \frac{j_{pc}}{j_0} H_{c_2}^c , \tag{8.223}$$

where $\beta_b$ is a numerical factor of the order of 10.

With a further increase in the field, the collective pinning radius $R_c$ grows and, together with it, the Josephson coupling of the 2D bundle to the neighboring layers. An estimate for the energy coupling the collectively pinned area into the third dimension is obtained from the tilt energy

$$U_{int}^J \simeq dc_{44} \left[ \frac{\xi}{d} \right]^2 R_c^2 \simeq d\varepsilon_0 \left[ \frac{\xi}{\Lambda} \right]^2 \left[ \frac{R_c}{a_0} \right]^4 , \tag{8.224}$$

where we have used the nonlocal limit $c_{44} \simeq (B^2/4\pi)(\varepsilon R_c/\pi\lambda)^2$ for the tilt modulus. The 2D collective pinning region is limited by the condition $U_{int}^{2D} \simeq U_{int}^J$, from which we obtain the crossover field $B_b^{3D}$ to the regime of three-dimensional collectively pinned bundles,

$$B_b^{3D} \simeq B_b^{2D} \left[ \frac{\Lambda^2}{\xi^2} \frac{U_{pc}}{\varepsilon_0 d} \right]^{1/3} \simeq B_b^{2D} \left[ \frac{d}{L_c^c} \right]^{1/2} . \tag{8.225}$$

The size of the 2D collectively pinned vortex bundles is restricted by the condition $R_c < \sqrt{a_0} \Lambda \simeq a_0 (d/L_c^c)^{1/2}$; i.e., the strong-pinning parameter $d/L_c^c > 1$ determines the maximal number of 2D collectively pinned vortices. For fields $B > B_b^{3D}$, the relevant length scale along the $c$ axis is larger than the interlayer spacing $d$, and the results of the continuum anisotropic description (see Sec. IV.D.2) can be applied. Note that in the above formulas the length $L_c^c$ plays the role of a disorder parameter and has no direct physical meaning. Within a phenomenological approach, the ratio $L_c^c/d$ can be determined from a measurement of $j_{pc}$ [see Eqs. (8.217) and (8.218) and the definition (2.149) in terms of the disorder parameter $\gamma$],

$$\frac{L_c^c}{d} \simeq \left[ \frac{j_0}{j_{pc}} \right]^{2/3} \left[ \frac{\xi}{\Lambda} \right]^{4/3} . \tag{8.226}$$

Now, let us generalize the above results to include the smoothing of the disorder potential due to thermal fluctuations of the vortices. First, the effective length scale $r_p(T)$ of the disorder potential becomes temperature dependent,

$$r_p^2(T) \simeq \xi^2 + \langle u^2 \rangle_{th} . \tag{8.227}$$

Second, from Eq. (2.119) we find that the pinning energy scales with the thermal displacement $\langle u^2 \rangle_{th}^{1/2}$ according to $\mathcal{E}_{pin}^2 \simeq \gamma d\xi^4/\langle u^2 \rangle_{th}$, and we obtain the temperature dependence of $U_{pc}$,

$$U_{pc}(T) \simeq \frac{U_{pc}}{(1+\langle u^2 \rangle_{th}/\xi^2)^{1/2}} . \tag{8.228}$$

The strength of thermal fluctuations $\langle u^2 \rangle_{th}$ is given by [see Eqs. (8.128) and (8.129)]

$$\langle u^2 \rangle_{th} \simeq \xi^2 \frac{T}{T_{dp}} , \tag{8.229}$$

with the depinning temperature

$$T_{dp} \simeq \frac{\beta_b}{2} U_{pc} \begin{cases} \dfrac{\sqrt{BB_{2D}}}{B_b^{2D}}, & B < B_{2D} , \\[3mm] \dfrac{B}{B_b^{2D}}, & B_{2D} < B . \end{cases} \tag{8.230}$$

Here we neglect the small corrections on $\langle u^2 \rangle_{th}$ due to logarithmic dependence on distance, which is relevant at large fields, $B > B_{2D}$. These have been taken into account in the work of Koshelev (1990) and of Vinokur, Kes, and Koshelev (1990). The temperature dependence of the 2D collective pinning radius $R_c(T)$ is given by

$$R_c(T) \simeq R_c \left[ 1 + \frac{T}{T_{dp}} \right]^{3/2} , \tag{8.231}$$

and the critical current density $j_c^{2D}(T)$ becomes

$$j_c^{2D}(T) \simeq j_c^{2D} \left[ 1 + \frac{T}{T_{dp}} \right]^{-5/2} . \tag{8.232}$$

Finally, the criterion $R_c(T) < \sqrt{a_0} \Lambda$ limiting the regime of 2D collective pinning can be written in the form

$$T_b^{3D}(B) \simeq \frac{\beta_b}{2} \frac{U_{pc}}{B_b^{2D}} \left[ \left[ \frac{B_b^{3D}}{B} \right]^{1/2} - 1 \right] \begin{cases} \sqrt{BB_{2D}}, & B < B_{2D} , \\[2mm] B, & B_{2D} < B . \end{cases} \tag{8.233}$$

The high-field expression develops a maximum of $T_b^{3D} \simeq U_{pc}(d/L_c^c)^{1/2}$ at $B \simeq B_b^{3D}/4$, whereas the low-field expression approaches the finite value $T_b^{3D} \simeq (\beta_b/2)U_{pc}(d/L_c^c)^{1/4}(B_{2D}/B_b^{2D})^{1/2}$ at vanishing field. The regime of applicability of Eq. (8.233) is bounded by the single-pancake pinning regime $T < U_{pc}$ at low temperatures and by the melting line $T_m$ at high temperatures. Taking typical parameters for BiSCCO [see Eq. (2.135)] and assuming a zero-field/low-temperature critical current density of the order of $j_{pc} \simeq 10^6$ A cm$^{-2}$, we obtain the following set of estimates: $j_o \simeq 2 \times 10^8$ A cm$^{-2}$, $U_{pc} \simeq 10$ K, $d/L_c^c \simeq 10$, $B_b^{2D} \simeq 5$ T, and $B_b^{3D} \simeq 10$ T. The high-field expression for the 2D-3D crossover line $T_b^{3D}(B)$ then has its maximum at $B \simeq 2.5$ T, where $T_b^{3D} \simeq 3U_{pc}$. A qualitative phase diagram is shown in Fig. 42.

Let us turn next to the problem of 2D collective creep. Consider a field large enough that $R_c > a_o$. The following analysis proceeds along the lines introduced in Sec. III.F. With decreasing current density $j \ll j_c^{2D}$, both the size of the 2D bundle and the hopping distance between metastable minima become large. Due to the compression of the vortex lattice during creep, the transverse size $R_\perp(j)$ becomes different from the longitudinal size $R_\parallel(j)$. Let us calculate first $R_\perp(j)$. Using the results characterizing the behavior of an elastic manifold subject to a disorder potential, we can relate the hopping distance $u$ and the size $R_\perp$ of the bundle,

$$u(R_\perp) \simeq \xi \left[\frac{R_\perp}{R_c}\right]^{\zeta_{2,2}} . \tag{8.234}$$
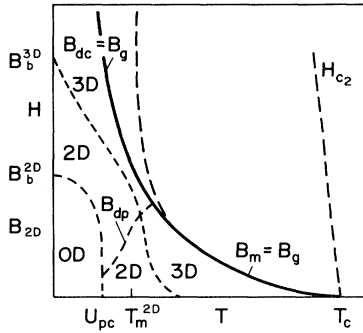


FIG. 42. Equilibrium phase diagram for a strongly layered superconductor including effects of thermal and of quenched disorder. The vortex-glass transition line follows the melting line $B_m(T)$ at low fields, $B < B_{2D}$, and the decoupling line $B_{dc}(T)$ at large fields, $B > B_{2D}$ [the high-field part of the melting line $B_m(T) > B_{2D}$ marks only a crossover line below which pinning effects increase rapidly]. Also shown are the various collective pinning regimes for the case in which disorder is rather strong, $L_c^c < d$. A single-pancake pinning regime at low temperatures and fields (zero dimension) is followed by a regime of 2D collective pinning, which in turn crosses over to 3D bundle pinning above the line $B_b^{3D}(T)$. Below the depinning line $B_{dp}(T)$, thermal fluctuations smooth the pinning potential and the critical current density $j_c(T)$ decreases rapidly with increasing temperature.

Using Eq. (3.164) for the wandering exponent $\zeta_{2,2}$, we obtain $\zeta_{2,2} = 2/5$. The length scales $u$ and $R_\perp$ can be related to the current density $j$ by determining the saddle of the effective free-energy density,

$$F \simeq \frac{c_{66}d}{2}\left[\frac{u}{R_\perp}\right]^2 - \frac{1}{c}jB\, du ,$$

and we find

$$u(j) \simeq \xi \left[\frac{j_c^{2D}}{j}\right]^{1/4} , \quad R_\perp(j) \simeq R_c \left[\frac{j_c^{2D}}{j}\right]^{5/8} . \tag{8.235}$$

The longitudinal length $R_\parallel(j)$ is obtained by balancing the shear and compression energies [see also Sec. IV.B.2; here we follow the analysis proposed by Koshelev (1994)], $\mathcal{E}_{shear} \simeq c_{66}d(u/R_\perp)^2 R_\perp R_\parallel$ and

$$\mathcal{E}_{comp} \simeq \frac{d\hat{c}_{11}}{\lambda_{eff}^2}\int d^2r d^2r' \ln[|r-r'|/\xi](\nabla u)(\nabla' u)$$

$$\simeq d\hat{c}_{11}\frac{R_\perp^2}{\lambda_{eff}^2}u^2 ,$$

and we obtain

$$R_\parallel \simeq \frac{R_\perp^3}{a_o^2} . \tag{8.236}$$

Note that in a thin film the screening length is exceedingly large, $\lambda_{eff} = 2\lambda^2/d$, and the dispersive regime extends to very large scales. Combining the above results we obtain the activation energy for creep,

$$U(j) \simeq \begin{cases} U_{sb}^{2D}\left[\dfrac{j_c^{2D}}{j}\right]^{7/4} , & j_{CDW}^{2D} < j \ll j_c^{2D} , \\[14pt] U_{CDW}^{2D}\dfrac{j_{CDW}^{2D}}{j}\ln\dfrac{j_{CDW}^{2D}}{j}, & j < j_{CDW}^{2D} , \end{cases} \tag{8.237}$$

with $U_{sb}^{2D} \simeq \varepsilon_o d(\varepsilon_o d/U_{pc})^2(\xi/a_o)^6$ and $U_{CDW}^{2D} \simeq \varepsilon_o d(\varepsilon_o d/U_{pc})^2(a_o/\xi)$. At the current density $j_{CDW}^{2D} \simeq j_c^{2D}(\xi/a_o)^4$ the hopping distance $u$ increases beyond the lattice constant $a_o$ and the system enters the CDW-type creep regime. The transverse length $R_\perp$ then scales with current density according to $R_\perp(j) \simeq R_c(a_o/\xi)^{5/2}(j^{2D}/j)^{1/2}$. Note that in the absence of dispersion the barriers for creep grow only logarithmically (Nattermann, 1990); here we have accounted for the compression energy involved in the creep which together with the long range interaction potential between the vortices (dispersion in $c_{11}$) leads to the more singular growth $U(j) \propto (1/j)\ln(1/j)$ of the activation barrier.

For the case of a layered material (as opposed to a thin film) the coupling into the third dimension usually cuts off the two-dimensional behavior before the CDW-type creep regime has been reached. Using the tilt energy (4.132) with $L^b \simeq d$ as an estimate for the interlayer coupling energy and comparing this expression with the intralayer shear energy above, we obtain the condition

$R_\perp \simeq (a_\circ^2 \Lambda)^{1/3}$ for the crossover to the 3D collective creep regime [note the difference to the crossover condition $R_\perp \simeq (a_\circ \Lambda)^{1/2}$ to the 3D collective *pinning* regime]. The corresponding current density takes the value $j_c^{2D}(R_c^3/a_\circ^2 \Lambda)^{8/15}$.

The result of the above analysis, particularly the glass exponent $\mu = 7/4$ in Eq. (8.236), differs from the original result obtained by Feigel'man, Geshkenbein, and Larkin (1990) and by Vinokur, Kes, and Koshelev (1990) due to the oversimplified treatment in the determination of the superbundle dimension in the original papers (see Sec. IV.B.2 for a more detailed discussion of this point): The exponent $\mu = 9/8$ in the original papers should be substituted by the value $\mu = 7/4$ derived above following the correct treatment of the compression energy as proposed by Koshelev (1994).

In the above discussion we have explicitly assumed that the magnetic field is large or that the disorder is weak enough to guarantee that $R_c > a_\circ$. On the other hand, for weak fields, $B < B_b^{2D}$, and small temperatures, $T < U_{pc}$, the system may well start out within the single-pancake pinning regime, as is the case in the above example for a Bi-based superconductor, provided that $B \lesssim 4$ T and $T \lesssim 20$ K. As the current $j$ drops below its critical value $j_c^{2D}$, we expect creep to involve only single pancakes, so that the activation energy $U(j)$ remains constant, $U(j) \simeq U_{pc}$. However, this seems to be in contradiction with the results of experiments carried out in this strong-pinning regime, where an increase in the activation barrier $U(j)$ with decreasing current density has been observed (van der Beek, Kes, Maley, *et al.*, 1992). The question then poses itself how the individual pancake vortices can be coupled to a 2D elastic manifold. The basic idea leading to the coupling of the pancake vortices into an elastic plane with decreasing current density is the concept of variable-range hopping (VRH; Mott, 1969; for a detailed review, see Shklovskii and Efros, 1984). Due to randomness in the energies of the metastable states, the pancake vortices will hop a larger distance $U$ as the current density $j$ decreases. Such long-distance jumps produce a larger interaction energy $c_{66}du^2$, and the pancake vortex starts to couple to its neighbors as $u$ becomes large enough. For a qualitative analysis, let us assume a distribution of final-state energies characterized by the density of states $g \simeq 1/U_{pc}\xi^2$. The typical energy difference $\delta\mathcal{E}$ that a pancake vortex hopping a distance $U$ has to overcome is of the order of $\delta\mathcal{E} \simeq 1/gu^2 \simeq U_{pc}(\xi/u)^2$. In the presence of a current density $j$, this energy can be provided by the Lorentz force, $\delta\mathcal{E} \simeq j\Phi_\circ du/c$, from which we find the optimal hopping distance

$$u \simeq \xi \left[ \frac{j_{pc}}{j} \right]^{1/3} . \qquad (8.238)$$

The barrier that the pancake vortex has to overcome remains independent from $j$, $U(j) \simeq U_{pc}$. However, the interaction energy $c_{66}du^2$ grows with decreasing current

density $j$ and becomes equal to the disorder energy $U_{pc}$ when

$$u \simeq u_{VRH} \simeq a_\circ \left[ \frac{U_{pc}}{\epsilon_\circ d} \right]^{1/2} < a_\circ ,$$

$$j \simeq j_{VRH} \simeq j_{pc} \left[ \frac{\xi^2}{a_\circ^2} \frac{\epsilon_\circ d}{U_{pc}} \right]^{3/2} \simeq j_{pc} \left[ \frac{R_c}{a_\circ} \right]^{3/2} < j_{pc} . \qquad (8.239)$$

Below $j_{VRH}$, the pancake vortices are coupled to a 2D elastic medium, and creep proceeds via the activation of vortex bundles. In summary, starting out at low fields/low temperatures, the vortex system first goes through a VRH regime, which is followed by a 2D collective creep regime at lower current densities,

$$u(j) \simeq \begin{cases} \xi \left[ \dfrac{j_{pc}}{j} \right]^{1/3} , & u_{VRH} < j < j_{pc} , \\[3mm] u_{VRH} \left[ \dfrac{j_{VRH}}{j} \right]^{1/4} , & j_{CDW}^{2D} < j < j_{VRH} , \end{cases} \qquad (8.240)$$

$$R_\perp(j) \simeq \begin{cases} a_\circ , & j_{VRH} < j < j_{pc} , \\[3mm] a_\circ \left[ \dfrac{j_{VRH}}{j} \right]^{5/8} , & j_{CDW}^{2D} < j < j_{VRH} , \end{cases} \qquad (8.241)$$

$$U(j) \simeq \begin{cases} U_{pc} , & j_{VRH} < j < j_{pc} , \\[3mm] U_{pc} \left[ \dfrac{j_{VRH}}{j} \right]^{7/4} , & j_{CDW}^{2D} < j < j_{VRH} , \end{cases} \qquad (8.242)$$

with $j_{CDW}^{2D} \simeq j_{VRH}(u_{VRH}/a_\circ)^4$.

We close this section with a few remarks concerning quantum creep in the single-pancake pinning limit and for the case of 2D collective pinning (see also Glazman and Fogel, 1984; Fisher, Tokuyasu, and Young, 1991). For the (physically more relevant) dissipative limit, we obtain the following expression for the effective action: For a single pancake vortex, the tunneling time is determined by the energy balance $\eta_l d\xi^2/t_c \simeq U_{pc}$, whereas for a 2D collectively pinned bundle we have $\eta d\xi^2/t_c \simeq c_{66}d(\xi/R_c)^2$ with $\eta = \eta_l/a_\circ^2$. For a single pancake, we then obtain

$$\frac{S_E^{eff}}{\hbar} \simeq \frac{t_c U_{pc}}{\hbar} \simeq \frac{\hbar}{e^2} \frac{d}{\rho_n} \simeq \frac{1}{Qu} \frac{\Lambda}{\xi} = \frac{S_{pc}}{\hbar} , \qquad (8.243)$$

which agrees with the previously obtained result (8.214) within the angular regime where the pancakes are pinned individually. Creep at low current densities is described by

$$S_E^{eff}(j) \simeq \begin{cases} S_{pc} \left[ \dfrac{j_{pc}}{j} \right]^{1/3} , & j_{VRH} < j < j_{pc} , \\[3mm] S_{pc} \left[ \dfrac{a_\circ}{R_c} \right]^{1/2} \left[ \dfrac{j_{VRH}}{j} \right]^{11/4} , & j_{CDW}^{2D} < j < j_{VRH} , \end{cases}$$

$$\qquad (8.244)$$

where $R_c/a_o \simeq (\varepsilon_o d/U_{\rm pc})(\xi/2a_o)^2 < 1$ should be understood only as a convenient parameter. In the case of 2D collective creep $(R_c > a_o)$, we have

$$\frac{S_E^{\rm eff}}{\hbar} \simeq \frac{t_c c_{66} d}{\hbar} \left[ \frac{\xi}{R_\perp} \right]^2 R_\perp R_\parallel \simeq \left[ \frac{R_c}{a_o} \right]^4 \frac{S_{\rm pc}}{\hbar} \ , \quad (8.245)$$

and the dependence on small driving forces is given by

$$S_E^{\rm eff}(j) \simeq S_{\rm pc} \left[ \frac{R_c}{a_o} \right]^4 \left[ \frac{j_c^{\rm 2D}}{j} \right]^{11/4} , \quad j_{\rm CDW}^{\rm 2D} < j \ll j_c^{\rm 2D} \ . \tag{8.246}$$

In the CDW regime the exponent decreases to the value $\mu_S = 2$.

## 3. Absence of glassiness in 2D

As we pointed out in Sec. VIII.B.4 (see Fig. 40), in a 2D vortex lattice the structure of allowed topological excitations is very different from the 3D bulk case. In fact, in a 2D vortex lattice, dislocation pairs adding or removing flux from the vortex lattice are energetically allowed, whereas the corresponding object would acquire an infinite energy in a bulk superconductor. A dislocation pair with gliding planes (directed along the $x$ axis) separated by a distance $R_g$ encloses a total additional flux $\Phi_{\rm dp}$, which, under the action of an external current density $j$, is given with the force

$$f_x = \frac{1}{c} j_y \Phi_{\rm dp} \ . \tag{8.247}$$

Ignoring any pinning of the dislocations for the time being, we find that the motion of the flux $\Phi_{\rm dp}$ is determined by the viscosity in the system. Assuming a density $n_{\rm dp}$ of dislocation pairs with size $R_g$ moving with a velocity $v_{\rm dp}$, we can determine the resulting electric field,

$$E = \frac{1}{c} \Phi_o n_{\rm dp} \sum_i v_{i,x} = \frac{1}{c} n_{\rm dp} \Phi_o v_{\rm dp} \sum_i \partial_x u_{i,x}$$

$$= \frac{1}{c} n_{\rm dp} v_{\rm dp} \Phi_{\rm dp} \ , \tag{8.248}$$

as well as the dissipated energy,

$$W = \eta_l n_{\rm dp} \sum_i v_i^2 = \eta_l n_{\rm dp} v_{\rm dp}^2 \sum_i (\partial_x \mathbf{u}_i)^2$$

$$\simeq \frac{1}{2\sqrt{3}\pi} \eta_l n_{\rm dp} v_{\rm dp}^2 \ln \frac{R_g}{a_o} \ , \tag{8.249}$$

with $\eta_l = \Phi_o H_{c_2}/\rho_n c^2$. Here we have used

$$\sum_i \partial_x u_{i,x} = \frac{1}{a_o^2} \int d^2 R \, \partial_x u_x$$

$$= \frac{1}{a_o^2} \int dy \, \Delta u_x = \frac{\Phi_{\rm dp}}{\Phi_o} \ ,$$

$$\sum_i (\partial_x \mathbf{u}_i)^2 = \frac{1}{a_o^2} \int d^2 R \, (\partial_x \mathbf{u})^2 \simeq \frac{1}{2\sqrt{3}\pi} \ln \frac{R_g}{a_o} \ ,$$

where the latter sum is dominated by the near-field distortion $(\partial_x \mathbf{u})^2 = (a_\Delta/\pi)^2 (xy/R^3)^2$ [see Eq. (8.108)], which has to be cut off at a distance $R_g$. The resistivity $\rho$ in the system is easily obtained from $\rho = E^2/W$, and, using the above results for $E$ and $W$, we find

$$\rho = \rho_{\rm flow} 4\pi \left\langle \frac{n_{\rm dp} R_g^2}{\ln(R_g/a_o)} \right\rangle \ , \tag{8.250}$$

with $\rho_{\rm flow} \simeq \rho_n B/H_{c_2}$. The concentration of pairs of size $R_g$ is

$$n_{\rm dp} \simeq a_o^{-2} e^{-2e_d(R_g)/T - 2\mathscr{E}_c/T} \ , \tag{8.251}$$

with $e_d(R) = (\varepsilon_o d/4\sqrt{3}\pi) \ln(R/a_o)$ and $2\mathscr{E}_c$ the interaction and core energies of the two dislocations. The expectation value of the moment $\langle n_{\rm dp} R_g^2/\ln(R_g/a_o) \rangle$ becomes

$$\left\langle \frac{n_{\rm dp} R_g^2}{\ln(R_g/a_o)} \right\rangle \simeq e^{-2\mathscr{E}_c/T} \int \frac{d^2 R}{a_o^2} \left[ \frac{R}{a_o} \right]^{2 - 4T_m^{\rm 2D}/T}$$

$$\simeq \frac{T}{T_m^{\rm 2D} - T} e^{-2\mathscr{E}_c/T} \ , \tag{8.252}$$

leading to the final result for the dislocation-pair-induced resistivity

$$\rho(T) \simeq \alpha \rho_{\rm flow} \frac{T}{T_m^{\rm 2D} - T} e^{-2\mathscr{E}_c/T} \ , \tag{8.253}$$

with the numerical factor $\alpha$ of the order of 10.

Thus at low temperatures we obtain an activated resistivity $\rho \sim \rho_{\rm flow} \exp(-2\mathscr{E}_c/T)$, which becomes large on approaching the 2D melting temperature $T_m^{\rm 2D}$ and goes over into the flux-flow resistivity $\rho \sim \rho_{\rm flow}$ above $T_m^{\rm 2D}$. The core energy $2\mathscr{E}_c \simeq \varepsilon_o d/2\sqrt{3}\pi$ plays the role of a plastic creep barrier in the system, which we should compare with the elastic barriers $U(j)$ for 2D collective creep found in Sec. VIII.D.2. As the current density drops below $j_{\rm pl}$, where $(j_{\rm pl}) \simeq 2\mathscr{E}_c$, plastic creep becomes dominant and the finite plastic barrier cuts off the glassiness in the system. The absence of a finite-temperature glass transition in 2D has its implications for a layered superconductor, too. Assuming a magnetic field $B > B_{\rm 2D}$ and lowering the temperature $T$ below the melting transition $B_m(T)$, we find that the system remains decoupled and hence effectively two dimensional until we reach the decoupling transition line, $B_{\rm dc}(T) < B_m(T)$. Hence for $B > B_{\rm 2D}$ the melting transition transforms into a crossover line, where the pinning properties become strong, and the true phase transition into the vortex glass takes place at the lower transition line $B_{\rm dc}(T)$; see Fig. 42. It appears that the experiments of Safar, Gammel, Bishop, *et al.* (1992; see also van der Beek, Kes, Maley, *et al.*, 1992) on BiSCCO single crystals showing evidence for a glass transition are in good agreement with this scenario.

In the above analysis we have ignored all the effects of energy barriers restricting the free motion of the dislocations. In fact, the Peierls barriers experienced by the

dislocations will lead to an additional reduction in the resistivity $\rho$, which can be accounted for via a (small) correction of the core energy $\mathscr{E}_c$, $\mathscr{E}_c \to \mathscr{E}_c + \mathscr{E}_{\text{Peierls}}$. In addition, the disorder potential will also lead to an additional pinning barrier for the dislocation pairs. For a small pair with $R_g \simeq a_0$, this disorder-induced barrier is of the order of $\delta U \simeq U_{\text{pc}}(a_0/\xi)^{1/2}$ [moving the pair a distance $a_0$ produces a displacement field $\delta u \simeq a_0(a_0/R)^2$ such that all vortices within the radius $R \simeq a_0(a_0/\xi)^{1/2}$ shift by more than $\xi$]. With $U_{\text{pin}} \ll \varepsilon_0 d$, the main temperature dependence in the resistivity is again due to the plastic barrier $2\mathscr{E}_c$.

An additional consequence of the disorder potential is the creation of a finite density of dislocation pairs even at zero temperature. The local concentration of small pairs with $R_g \simeq a_0$ (flux vacancies or interstitials) is given by $n_{\text{dp}} \simeq a_0^{-2} \exp[-(2\mathscr{E}_c + \delta U)/T]$. Taking an average over the disorder field (Balatskii and Vinokur, 1984), one obtains

$$n_{\text{dp}} \simeq a_0^{-2} e^{-2\mathscr{E}_c/T + \sigma^2/2T^2} , \qquad (8.254)$$

with $\sigma = \langle(\delta U)^2\rangle^{1/2} \simeq U_{\text{pc}}(a_0/\xi)^{1/2}$ the variance of the random pinning potential experienced by the dislocation pair. Upon a lowering of the temperature, the correction to $n_{\text{dp}}$ due to the quenched disorder becomes as important as the thermal disorder at a value $T \simeq \sigma^2/4\mathscr{E}_c$, for $T < \sigma^2/4\mathscr{E}_c$, disorder-induced dislocations will dominate, resulting in a low-temperature dislocation-pair density

$$n_{\text{dp}} \simeq a_0^{-2} e^{-8\mathscr{E}_c/\sigma^2} \qquad (8.255)$$

and a corresponding resistivity

$$\rho \simeq \rho_{\text{flow}} e^{-8\mathscr{E}_c/\sigma^2 - \sigma/T} \qquad (8.256)$$

An instability of the 2D vortex lattice subject to a quenched pinning potential against formation of dislocations has also been found by Shi and Berlinsky (1991), and their contribution to the dynamic response of the vortex system has been investigated analytically as well as numerically (Jensen *et al.*, 1990; Shi and Berlinsky, 1991).

Finally, let us consider the zero-temperature limit of the problem. It has been proposed that a zero-temperature vortex-glass phase could exist in two dimensions (Fisher, 1989; Fisher, Fisher, and Huse, 1991), and a detailed analysis of the low-temperature behavior of a strongly disordered system has been given by Fisher, Tokuyasu, and Young (1991). Recent experiments by Dekker *et al.* (1992) on thin YBCO films provide the first experimental evidence for a finite two-dimensional vortex-glass correlation length that diverges on approaching zero temperature, indicating the possible existence of a $T=0$ vortex-glass phase. From the above arguments, one would expect that, due to the presence of disorder, the density of dislocation pairs in the 2D vortex lattice would not vanish at $T=0$. The question then arises how these defects will move as the temperature de-

creases. First, the classical thermally activated motion will be replaced by some kind of tunneling motion. Due to the presence of disorder, a variable-range hopping type of motion (Shklovskii and Efros, 1984) is expected to take place at low but finite temperatures, leading to a vanishing of the resistivity $\rho(T \to 0) \to 0$ which is different from the classical Arrhenius behavior. The exact form of $\rho(T)$ depends on the details of the saddle-point configuration describing the creep-type motion and involves taking into account the interaction between different dislocation pairs as well as the appropriate expression for the tunneling dynamics (massive or dissipative dynamics).

## IX. STRONG PINNING

Whereas in the previous sections we have concentrated on weak pointlike pins (uncorrelated disorder), here we focus our interest on the pinning properties of extended defects (correlated disorder). Typical examples of such extended pinning centers are one-dimensional screw dislocations, like those observed in thin films of YBCO (Hawley *et al.*, 1991; Schlom *et al.*, 1992; Mannhart *et al.*, 1992), and the artificially produced columnar defect structure resulting from energetic heavy-ion irradiation (Roas, Hensel *et al.*, 1990; Civale *et al.*, 1991; Hardy *et al.*, 1991; Konczykowski, Rullier-Albenque *et al.*, 1991; Gerhäuser *et al.*, 1992). Examples of planar defect structures are the twin boundaries in YBCO and, in a wider sense, also the layering in the strongly anisotropic Bi- and Tl-based compounds (intrinsic pinning). The main feature setting apart these extended defects from the previously discussed pointlike defects is their extensive pinning character, i.e., the pinning energy grows *linearly* with the distance along the vortex for the case in which the vortex system is properly *aligned* with the defect structure. This strong anisotropic pinning has to be contrasted with the weak isotropic pinning produced by pointlike defects that compete with one another, leading to a mere square-root growth of the pinning energy along the vortex line.

Enhanced pinning due to the presence of twin boundaries has been observed in a variety of experiments. When the magnetic field is aligned with the twinning planes, enhanced pinning due to twin boundaries shows up as a drop in the resistivity within the thermally assisted flux-flow regime (Kwok *et al.*, 1990; Iye *et al.*, 1990; Fleshler *et al.*, 1992), and as an increase in the critical density in the glassy regime, measured in a torque experiment (Gyorgy *et al.*, 1990). Furthermore, a magnetization anisotropy is observed in the glassy regime for fields directed normal to the $c$ axis, with stronger pinning (larger magnetization) realized when the field is parallel to the twinning planes (Liu *et al.*, 1991; see also Swartzendruber *et al.*, 1990 and Roitburd *et al.*, 1990). The enhancement of pinning due to the presence of twin boundaries has been investigated by Blatter, Rhyner, and Vinokur (1991) within the framework of weak collective

pinning theory. Enhanced pinning by twin boundaries and its consequences for resistivity in the vortex-liquid state has been considered by Marchetti and Nelson (1990). Finally, the properties of vortices trapped by twin boundaries and subject to a transverse force (current parallel to the twinning planes) have been investigated by Nelson (1991), by Nelson and Vinokur (1992, 1993), and by Marchetti and Vinokur (1994).

The most prominent type of strong pinning to date is pinning by columnar defects. Whereas the twinning phenomenon is particular to YBCO, columnar defects can be introduced artificially into every material and are thus much more versatile. Furthermore, it appears that suppression of the order parameter within the columnar tracks produced by the irradiation beam is much stronger than perturbation of the order parameter due to the presence of twinning planes. As a consequence, the introduction of columnar defects leads to a marked increase in the critical current density and also shifts the experimentally observed irreversibility line towards higher temperatures and fields (Civale *et al.*, 1991; Konczykowski, Rullier-Albenque *et al.*, 1991). Note that proton irradiation producing either pointlike defects or defect clusters leads to an increase in the critical current density but leaves the irreversibility line unchanged (Civale *et al.*, 1990). Recent experiments by Worthington *et al.* (1992) on heavy-ion-irradiated samples suggest that the thermodynamic phase-transition line into the glass state itself remains unaffected. The experimentally measured shift in the irreversibility line, then, could be due to a change in the nonlinear behavior of the system upon irradiation. Since the experiments are usually carried out at finite frequencies and/or finite amplitude, this change would easily manifest itself as an apparent shift of the irreversibility line.

Similar results have been obtained for strongly layered BiSCCO material subject to heavy-ion irradiation (Gerhäuser *et al.*, 1992; Thompson *et al.*, 1992). The columnar defect structure produces an enhanced critical current density, and a shift in the irreversibility line has been observed by Thompson *et al.* (1992). However, the angular sensitivity of the magnetization loop with respect to the field-track orientation turns out to be much weaker for the BiSCCO compound (Thompson *et al.*, 1992) than for YBCO, on which the identical experiment was carried out (Civale *et al.*, 1991). The different behavior between the anisotropic YBCO and the layered BiSCCO superconductor has been attributed to the large difference in anisotropy between these materials, with each pancake vortex being pinning individually for the case of the BiSCCO compound (Gerhäuser *et al.*, 1992; Brandt, 1992a and 1992b). The interplay between the vortex system and a columnar defect structure has been analyzed by Nelson and Vinokur (1992 and 1993), by Lyuksyutov (1992), and by Brandt (1992a, 1992b). The competition between point disorder and columnar defects has been investigated by Hwa, Nelson, and Vinokur (1993). In the following we first study the effects of twin boundaries and

then those of the columnar defects on the pinning properties of the oxides.

## A. Twin boundaries

The first observations that twin boundaries do influence the pinning of vortices in YBCO go back to Vinnikov *et al.* (1988) and to Dolan *et al.* (1989). In their Bitter decoration analysis of the low-field vortex structure, the attraction of the vortices to the twinning planes manifests itself directly in a higher concentration of flux lines within the twin planes than in the bulk. The attraction of the vortices to the twin boundaries produces a variety of interesting effects, such as vortex trapping and locking when the field is turned towards the direction of the twin boundary planes, enhanced pinning for vortex motion orthogonal to the twin planes, and interesting creep phenomena (Marchetti and Vinokur, 1994). Below we shall discuss in some detail the origin and the magnitude of the attractive twin boundary potential well, the associated trapping and locking phenomena, as well as transverse pinning and creep.

Not only are the vortices attracted to the twin boundaries; their motion *along* the twin planes seems to be influenced by the twin boundaries as well. In particular, for both the field and the current density directed along the *ab* plane (i.e., Lorentz force and hence vortex motion directed along the *c* axis) the motion of the flux lines appears to be more strongly hindered than in the bulk, an effect which we attribute to the presence of *enhanced* pinning within the twin planes. This conclusion can be drawn from the experiments of Kwok *et al.* (1990), who observe a sharp ($\sim 5°$ wide) drop in resistivity within the TAFF regime when the magnetic field is aligned with the twin boundaries. The same conclusion can be obtained from the torque experiments of Gyorgy *et al.* (1989) and from the magnetization experiments of Liu *et al.* (1991), who observe an increase in the critical current density within the glass regime whenever the field is directed along the twinning planes. On the other hand, for a magnetic field directed along the *c* axis, recent experiments of Durán *et al.* (1992) suggest that the pinning along the twin boundaries is *reduced*. This conclusion is based on the analysis of real-time imaging experiments of flux profiles, which suggest that the twinning planes provide favorable channels for flux penetration into the sample. Recent magneto-optical experiments by Vlasko-Vlasov *et al.* (1994) show that the twin boundaries act as obstacles for the flux entering the sample, leading to an accumulation of vortices along one side of the twinning planes and a depletion on the other (shadowing effect). Whereas some flux enters the sample in a narrow channel along the twin boundary potential well, their main effect is to *guide* the vortices on one side of the twin planes into the sample.

It thus appears that vortices trapped in the potential well of a twin boundary and moving along the twin planes experience enhanced pinning in one case (e.g.,

Kwok *et al.*, 1990), and reduced pinning in other situations. In fact, the following two phenomena affect the in-plane pinning strength of the twin boundaries in opposite ways. Due to the reduction of the order parameter in the twin plane (which follows from the observed attraction of the vortices to the plane), the vortex core is elongated along the plane (Gurevich, 1992), and hence pinning is reduced. On the other hand, thermal fluctuations (which are particularly important in these materials) leading to a smearing of the pinning potential at high temperatures, are reduced when the vortex is trapped in the potential well of the twin boundary, leading to an enhanced pinning force in the planes. Whereas the thermal effect should be dominant at high temperatures, reduced pinning may be more relevant at low temperatures. The direction of motion (along or perpendicular to the *c* axis) may influence the result as well, since in one case the intrinsic pinning potential of the layered structure is relevant. Below we shall discuss in more detail the dimensional reduction of thermal fluctuations, leading to an enhanced pinning force along the twin planes.

Enhanced pinning by twin boundaries, as observed in the experiments of Kwok *et al.*, Gyorgy *et al.*, and Liu *et al.*, can be understood as a two-step process: Consider a magnetic field directed along the *ab* planes. As the vortices are turned towards the twinning planes, the attractive interaction between the vortices and the twin boundaries leads to a deformation of the vortices, with increasingly large segments $r(\varphi)$ of the vortices trapped in the potential wells of the twin boundaries; see Fig. 43. Under the action of a driving current $\mathbf{j} \| ab$, the vortices are forced to move along the *c* direction, with the trapped segments moving within the twin boundary potential well. Due to the partial trapping of the vortex in the potential well, transverse thermal fluctuations of the vortex line are suppressed (dimensional reduction of the fluctuations), leading quite naturally to enhanced pinning for those vortex segments trapped by the twin boundaries.

In the following we first discuss the accommodation of the vortices to the twin boundaries (Sec. IX.A.1) and determine the trapping angle $\varphi_t$ below which the vortex starts to deform. The size of the trapping angle $\varphi_t$ is determined by the ratio of the twin boundary potential-well depth and the vortex line energy. In Sec. IX.A.2 we discuss in more detail the origin and size of the twin boundary potential well. Section IX.A.3 is devoted to a discussion of enhanced pinning due to the dimensional reduction of thermal fluctuations. Finally, in Sec. IX.A.4 we treat the problem of pinning and creep for the special case in which the vortex line is aligned with the twin boundary and the driving force acts to liberate the vortex line from its trapping potential.

### 1. Vortex trapping

We consider an idealized situation with a periodic array of twin boundaries (with spacing $d_{\mathrm{TP}}$) and a magnetic field **H** applied parallel to the *ab* plane, enclosing an angle $\varphi$ with the twin planes. We neglect the influence of point pins for the time being and concentrate on the accommodation of the vortices to the attractive potential of the twinning array. This situation is closely related to the problem of intrinsic pinning in a layered superconductor, with the twinning planes playing the role of the buffer regions between superconducting planes and the magnetic field tilted an angle $\vartheta$ away from the planes.

To begin with, consider a single vortex line. In order to minimize its energy, the flux line will deform and gain energy from the attractive potential wells produced by the twinning array; see Fig. 43. The attraction of the vortex by the twin planes can be described in terms of a reduction $\varepsilon_{\mathrm{TP}}$ in the vortex line energy. The energy gain $-r\varepsilon_{\mathrm{TP}}$ of a trapped segment of length $r$ is balanced by the energy cost $e_l(0)r + e_l(\varphi')s - e_l(\varphi)t$ due to elastic deformation ($\varphi'$ denotes the angle between a segment of length $s$ and the twin planes). The elastic energy can be rewritten as the product of the line tension and the total length change, such that we have to optimize the energy,

$$\mathscr{E}(r,\varphi) = (r + s - t)\varepsilon_l(\varphi) - r\varepsilon_{\mathrm{TP}} , \tag{9.1}$$

with respect to the length $r$ of the trapped segment (for the present case with $\mathbf{H} \perp c$ the line energy $e_l$ does not depend on the angle $\varphi$, and thus the line energy $e_l = \varepsilon\varepsilon_0 \ln(\kappa/\varepsilon)$ is equal to the line tension $\varepsilon_l$). From simple trigonometry we have $t = d_{\mathrm{TP}}/\sin\varphi$ and $s = [d_{\mathrm{TP}}^2 + (d_{\mathrm{TP}}/\tan\varphi - r)^2]^{1/2}$, and expanding Eq. (9.1) for small angles $\varphi$ we arrive at

$$\mathscr{E}(r,\varphi) \approx \frac{1}{2}\varepsilon_l \left[ \frac{1}{r} - \frac{\varphi}{d_{\mathrm{TP}}} \right]^{-1} \varphi^2 - r\varepsilon_{\mathrm{TP}} . \tag{9.2}$$

The final result (9.2) expressed in terms of the line tension $\varepsilon_l$ is general and applicable in other cases; see Sec. IX.B.4 below. Variation of Eq. (9.2) with respect to $r$ at fixed angle $\varphi$ provides us with an expression for the trapped length $r(\varphi)$,
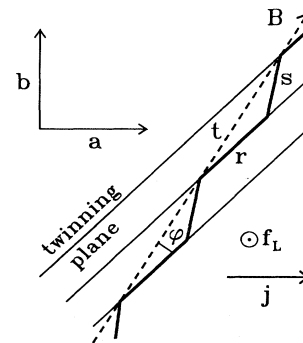


FIG. 43. Accommodation of an individual vortex line to an array of twinning planes. With both the magnetic field **B** and the current **j** directed along the *ab* planes, the Lorentz force $\mathbf{f}_L$ acts in the direction of the *c* axis.

$$r(\varphi) \approx d_{\text{TP}} \left[ \frac{1}{\varphi} - \frac{1}{\varphi_t} \right] \Theta(\varphi_t - \varphi) . \tag{9.3}$$

Inserting this result back into Eq. (9.2), we obtain the energy gain

$$\mathcal{E}[r(\varphi), \varphi] \approx - \frac{1}{2} \varepsilon_l d_{\text{TP}} \frac{(\varphi_t - \varphi)^2}{\varphi} \Theta(\varphi_t - \varphi) . \tag{9.4}$$

The critical trapping angle $\varphi_t$ below which the vortex starts to deform is given by

$$\varphi_t = \left[ \frac{2\varepsilon_{\text{TP}}}{\varepsilon_l} \right]^{1/2} \tag{9.5}$$

and becomes smaller as the attraction $\varepsilon_{\text{TP}}$ turns weaker.

The accommodation of the vortex line to the twinning array and the concomitant lowering of energy leads to a lock-in transition. We consider a finite but small density of vortices such that our result (9.4) is still applicable. Due to the presence of the twinning planes we then obtain an additional contribution,

$$E(\varphi) = \frac{1}{a_0^2 t} \mathcal{E}[r(\varphi), \varphi]$$

$$\approx - \frac{1}{2} \frac{\varepsilon_l}{a_0^2} (\varphi_t - \varphi)^2 \Theta(\varphi_t - \varphi) , \tag{9.6}$$

to the total free-energy density $g$ of the vortex system,

$$g = \frac{B^2}{8\pi} + \frac{\Phi_0 B \varepsilon_\vartheta}{2(4\pi\lambda)^2} \ln\left[ \frac{H_{c_2}^c}{\varepsilon_\vartheta B} \right]$$

$$- \frac{B}{\Phi_0} \frac{\varepsilon_l}{2} (\varphi_t - \varphi)^2 \Theta(\varphi_t - \varphi)$$

$$- \frac{BH}{4\pi} \cos(\varphi - \varphi_H) . \tag{9.7}$$

Minimization of $g$ with respect to $\varphi$ provides us with the dependence $\varphi(\varphi_H)$ of the internal field direction $\varphi$ on the direction $\varphi_H$ of the external field,

$$\varphi \approx \begin{cases} 0, & \varphi_H < \varphi_L , \\ \dfrac{\varphi_H - \varphi_L}{1 - 4\pi\varepsilon_l / \Phi_0 H}, & \varphi_L < \varphi_H < \varphi_t , \\ \varphi_H, & \varphi_t < \varphi_H . \end{cases} \tag{9.8}$$

The lock-in angle $\varphi_L$ is given by

$$\varphi_L = \frac{4\pi\varepsilon_l}{\Phi_0 H} \varphi_t . \tag{9.9}$$

This transition is analogous to a second-order phase transition, with $\varphi$ and $\varphi_H$ playing the roles of the order parameter and of the external driving variable, respectively. The lock-in transition goes hand in hand with a divergence of the tilt modulus for angles $\varphi \to 0$, both effects arising from the linear term in (9.6),

$$E(\varphi) = \text{const} + \frac{1}{a_0^2} \sqrt{2\varepsilon_l \varepsilon_{\text{TP}}} |\varphi| + O(\varphi^2) . \tag{9.10}$$

This linear term corresponds to the deformation energy density produced by the kinked vortex structure. With the kink energy given by $E_k \simeq d_{\text{TP}} \sqrt{\varepsilon_l \varepsilon_{\text{TP}}}$, the number of kinks per vortex $L|\varphi|/d_{\text{TP}}$, and the volume per vortex $La_0^2$ ($L$ = sample dimension along the field), we can immediately reproduce the linear term in (9.10). In the related problem of a lock-in transition due to intrinsic pinning (see Sec. VIII.A.3), the kink energy is much larger, $E_k \simeq d\varepsilon_0$ (with $d$ denoting the layer distance here), and hence the lock-in angle becomes much larger. Note, however, that demagnetization effects much be taken into account in a discussion of the lock-in transition due to intrinsic pinning, where the magnetic field moves out of the superconducting planes (see Sec. VIII.A.3 above and Maslov and Pokrovski, 1991). These demagnetizing effects are irrelevant in the present discussion, where the field always remains aligned with the planes.

The above analysis describes well the situation for low magnetic fields, where the vortices relax individually to the twinning array without any further restrictions due to interaction with other vortices. At high magnetic fields, we have to take into account the interaction between the flux lines and we have to analyze the relaxation of the whole lattice. The simplest quantity to determine is the trapping angle $\varphi_t$. Near $\varphi_t$, the elastic deformation energy is compensated for by the energy gain due to trapping of the flux lines by the twin boundaries, and we find the condition

$$\frac{1}{2} c_{44}^{\parallel}(\mathbf{k}) \varphi_t^2 \simeq \frac{\varepsilon_{\text{TP}}}{a_0^2} f , \tag{9.11}$$

with $f$ the fraction of trapped vortices. For large fields with $a_0/\sqrt{\varepsilon} \ll d_{\text{TP}}$, the fraction of trapped vortices is $f \simeq a_0/(d_{\text{TP}}\sqrt{\varepsilon})$, and the relevant wave vector is given by $K \simeq \pi/d_{\text{TP}}$ (K perpendicular to the twinning planes). Using Eq. (3.58) for the in-plane tilt modulus, we obtain a reduced critical angle

$$\varphi_t \approx \left[ \frac{2\varepsilon_{\text{TP}}}{\varepsilon_l} \right]^{1/2} \left[ \ln\left[ \frac{\kappa}{\varepsilon} \right] \left[ \frac{a_0}{d_{\text{TP}}\sqrt{\varepsilon}} \right]^3 \right]^{1/2} . \tag{9.12}$$

For small fields with $a_0/\sqrt{\varepsilon} > d_{\text{TP}}$, the result (9.12) goes over to the single-vortex result (9.5).

### 2. Twin boundary pinning potential

An evaluation of the size of the critical trapping angle $\varphi_t$ requires knowledge of the potential-well depth $\varepsilon_{\text{TP}}$ produced by the twinning planes. An estimate of the ratio $\varepsilon_{\text{TP}}/\varepsilon_l$ can be obtained from analysis of the decoration experiments by Dolan *et al.* (1989). The increased repulsive energy between the more densely spaced vortices in the twin planes has to be compensated for by the attractive potential $\varepsilon_{\text{TP}}$, hence,

$$\varepsilon_{TP} \simeq V(a_o^{TP}) - V(a_o^b) \ , \qquad (9.13)$$

where $V(R) = 2\varepsilon_o K_0(R/\lambda)$ is the repulsive interaction energy between two straight vortices ($K_0$ is the modified Bessel function of order zero) and where $a_o^{TP}$ and $a_o^b$ are the separations between neighboring vortex lines in the twinning planes and in the bulk, respectively. In the experiment of Dolan *et al.* (1989; see also Vinnikov *et al.*, 1990), the field $H = 40$ G is directed along the $c$ axis, and the mean vortex separations are $a_o^{TP} \approx 0.7$ $\mu$m and $a_o^b \approx 1.3$ $\mu$m; hence

$$\frac{\varepsilon_{TP}}{\varepsilon_l}(\mathbf{H}\|c, T = 4.2 \ \text{K}) \simeq \frac{2K_0(5)}{\ln\kappa} \simeq 2 \times 10^{-3} \ . \quad (9.14)$$

The result (9.14) applies to low temperatures and to magnetic fields pointing along the $c$ axis. In order to obtain the dependence of $\varepsilon_{TP}$ on temperature and on the direction of the magnetic field, we have to adopt some model assumptions for the origin of the vortex attraction to the twin boundary. Here we assume that the creation of an attractive potential well is due to a (weak) suppression of the order parameter at the twin boundary. A vortex aligned parallel to the twin boundary and placed a distance $x$ away experiences an energy gain (per unit length)

$$\varepsilon_{TP}(x) \approx \frac{H_c^2}{8\pi} \delta 2\sqrt{2}\xi \int dy \, [1 - |\psi_v(x,y)|^2]$$

$$\approx \frac{\varepsilon_o \delta\sqrt{2}\xi}{\sqrt{x^2 + 2\xi^2}}, \quad x < \lambda \ , \qquad (9.15)$$

where $\delta \simeq 1 - |\Psi^{TP}|^2/|\Psi_\infty|^2$ quantifies the (small) relative suppression of the order parameter at the twinning planes and where we have assumed that this suppression affects a region of width $\sim\sqrt{2}\xi$ away from the plane. The suppression of the order parameter due to the vortex has been modeled by the variational ansatz described by Schmid (1966) [see Eq. (2.34)]. In the following we use the abbreviation $\varepsilon_{TP} = \varepsilon_{TP}(x = 0) \approx \varepsilon_o \delta$. Turning the field direction into the plane, then simply rescaling (see Sec. III.A) results in a reduction of the potential well by a factor $\varepsilon$ combined with an enhanced range $|x| < \lambda/\varepsilon$. Since the line energy $e_l \simeq \varepsilon\varepsilon_o$ also picks up an additional factor $\varepsilon$, the ratio $\varepsilon_{TP}/e_l$ remains unchanged [note that $\varepsilon_{TP}/e_l \simeq \varepsilon_{TP}/\varepsilon_l$ for $\mathbf{H}\perp c$, whereas the corresponding result is more complicated when $\mathbf{H}\|c$; see Eq. (3.44)].

Next, we wish to discuss the temperature dependence of the result (9.14). The magnitude of the suppression of the order parameter is determined by the boundary condition $d\Psi/dx \simeq \Psi/b$ at the twin boundary. Here the length parameter $b$ is roughly given by $b \approx \xi^2(0)/a$, with $a$ the lattice constant of the crystal lattice (de Gennes, 1966). For $b/\xi(T) \gg 1$, the suppression of the order parameter is weak, $|\Psi^{TP}/\Psi_\infty| \simeq 1$ and $\delta \ll 1$, whereas for $b/\xi(T) \ll 1$ the suppression can become large, $|\Psi^{TP}/\Psi_\infty| \simeq b/\xi(T)$ and $\delta \lesssim 1$. It has been pointed out (Deutscher and Müller, 1987) that due to the smallness of the coherence length $\xi$ in the high-temperature superconductors the latter case can become relevant over an ap-

preciable regime of temperatures close to $T_c$, in particular for a boundary perpendicular to the $c$ axis. For the present case of twin boundaries running parallel to the $c$ axis we can expect a rather weak temperature dependence of $\delta$ at low temperatures and an increase on approaching $T_c$.

A second source of temperature dependence in the pinning potential $\varepsilon_{TP}$ is the presence of thermal fluctuations smoothing the twin boundary potential well. In order to estimate this effect, we make use of the analogy between the statistical mechanics of a vortex line and the quantum mechanics of a particle in 2D, introduced in Sec. V.B above. The statistical mechanics ($T$) of the present single-vortex problem is mapped to the quantum mechanics ($\hbar = T$) of a particle of mass $m = \varepsilon_l$ ($\varepsilon_l$ denotes the elasticity of the vortex line) trapped in a one-dimensional potential well $U(x) = \varepsilon_{TP}(x)$. Along the twinning plane ($y$ axis) the problem is translation invariant; see Fig. 44. For a field directed along the $c$ axis the elasticity is $\varepsilon_l \simeq \varepsilon^2\varepsilon_o$, whereas for a field parallel to the planes we have $\varepsilon_l \simeq \varepsilon\varepsilon_o$. Note that the possibility of such a "vortex$\leftrightarrow$particle" mapping arises as a consequence of the translational invariance of the pinning potential along the direction of the vortex line. Furthermore, translational invariance along $y$ renders the particle problem effectively one-dimensional. The simplest approach to finding the binding energy makes use of the perturbation result for a one-dimensional shallow well (Landau and Lifschitz, 1958a),

$$E_B \approx \frac{m}{2\hbar^2} \left[ \int dx \, U(x) \right]^2 \ . \qquad (9.16)$$

The long-range nature of the potential (9.15) can be accounted for by cutting the integral in (9.16) at $|x| = \sqrt{2}\xi U(0)/E_B$. Making use of the above transcription rules, we obtain the result
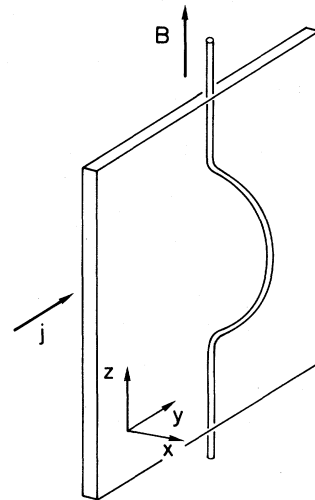


FIG. 44. Half-loop excitation of a vortex line out of the twin-boundary potential well for the case in which the driving current density **j** is parallel to the twinning plane.

$$\varepsilon_{\mathrm{TP}}(T) \simeq \begin{cases} \varepsilon_{\mathrm{TP}}, & T < T_{\mathrm{dp}}^{\mathrm{TP}} , \\ \varepsilon_{\mathrm{TP}} \left[ \dfrac{\tilde{T}_{\mathrm{dp}}^{\mathrm{TP}}}{T} \right]^2 \left[ \ln \left[ \dfrac{T}{\tilde{T}_{\mathrm{dp}}^{\mathrm{TP}}} \right]^2 \right]^2 , & T_{\mathrm{dp}}^{\mathrm{TP}} < T . \end{cases} \tag{9.17}$$

Here we have to distinguish between the parameter $\tilde{T}_{\mathrm{dp}}^{\mathrm{TP}}(T)$, which is a function of temperature,

$$\tilde{T}_{\mathrm{dp}}^{\mathrm{TP}} \simeq 2\xi \sqrt{\varepsilon_l \varepsilon_{\mathrm{TP}}} , \tag{9.18}$$

and the actual depinning temperature $T_{\mathrm{dp}}^{\mathrm{TP}}$, which is determined by the implicit equation

$$\begin{aligned} T_{\mathrm{dp}}^{\mathrm{TP}} &= \tilde{T}_{\mathrm{dp}}^{\mathrm{TP}}(T_{\mathrm{dp}}^{\mathrm{TP}}) \simeq 2\xi \sqrt{\varepsilon_l \varepsilon_{\mathrm{TP}}} \\ &\simeq T_c \left[ \frac{\delta}{2Gi} \right]^{1/2} \left[ 1 - \frac{T_{\mathrm{dp}}^{\mathrm{TP}}}{T_c} \right]^{1/2} . \end{aligned} \tag{9.19}$$

In a more elaborate approach (see also Sec. IX.B.1 below) one solves the differential equation

$$\left[ \partial_x^2 + \frac{\beta}{\sqrt{x^2 + x_\circ^2}} - \kappa^2 \right] \Psi(x) = 0 , \tag{9.20}$$

with

$$\beta x_\circ = (2m x_\circ^2 / \hbar^2) U(0) = (\tilde{T}_{\mathrm{dp}}^{\mathrm{TP}} / T)^2 \ll 1 ,$$

$$\kappa^2 = (2m / \hbar^2) E_B ,$$

$$x_\circ = \sqrt{2}\xi ,$$

in the three regions

$$|x| < x_\circ \quad [\Psi \sim \cos(\sqrt{\beta / x_\circ}\, x)] ,$$

$$x_\circ < x < x^* = \beta / \kappa^2 \quad (\Psi \sim \sqrt{x}\, [J_1(2\sqrt{\beta x})$$

$$+ C N_1(2\sqrt{\beta x})]) ,$$

$$x^* < x \quad [\Psi \sim \exp(-\kappa x)] ,$$

and equates the logarithmic derivatives $d \ln\Psi/dx$ at the various boundaries (with $C$ an integration constant and $J_1$ and $N_1$ are Bessel functions). This procedure leads (up to numerical factors of order unity) to the same result as the previous simplified approach (note that quasiclassical approximation is not applicable to this problem). The result (9.17) differs only in the appearance of logarithmic correction factors from the result obtained on the basis of the most simple model assumption using a square-well potential of depth $U = \varepsilon_{\mathrm{TP}}$ and extent $a = 2\sqrt{2}\xi$.

When the field is turned into the *ab* plane, $\varepsilon_{\mathrm{TP}}$ picks up an additional factor $\varepsilon$, and the product $\varepsilon_l \varepsilon_{\mathrm{TP}}$ remains invariant. Using the result (9.14) ($\delta/\ln\kappa \simeq 2 \times 10^{-3}$, $Gi \simeq 10^{-2}$), we obtain the numerical estimate $T_{\mathrm{dp}}^{\mathrm{TP}} \approx 0.5 T_c$. Combining Eqs. (9.5), (9.17), and (9.19), we obtain for the trapping angle the expression

$$\varphi_t \simeq \begin{cases} \dfrac{\sqrt{2\delta}}{\sqrt{\ln\kappa}}, & T < T_{\mathrm{dp}}^{\mathrm{TP}} , \\ \dfrac{\delta}{\sqrt{Gi \ln\kappa}} \left[ 1 - \dfrac{T}{T_c} \right]^{1/2} , & T_{\mathrm{dp}}^{\mathrm{TP}} < T , \end{cases} \tag{9.21}$$

resulting in a trapping angle of the order of a few degrees at low temperatures. Close to $T_c$ we have to expect two competing effects to occur, an increase in $\delta$ due to a larger suppression of the order parameter at the twin boundary and a smoothing of the potential due to thermal fluctuations of the vortex line. A more precise estimate requires more detailed knowledge of the temperature dependence of $\delta$. Regarding the field dependence of the trapping angle, we can assume the typical distance between the twinning planes to be of the order of $d_{\mathrm{TP}} \sim 10^3$ Å and a further decrease of the critical angle $\varphi_t$ has to be expected for fields above $\sim 1$ T. These results are in good qualitative agreement with the experiments of Kwok *et al.* (1990), Iye *et al.* (1990), Gyorgy *et al.* (1990), and Fleshler *et al.* (1992), who observe a change in resistivity or critical current density (torque) when the magnetic field is aligned with the twin planes within a few degrees.

### 3. Longitudinal motion: enhanced pinning and dimensional reduction

Having discussed the relaxation of the vortices to the twinning array, we now study their dynamic behavior in an applied force field directed parallel to the twinning planes. The situation in which the vortices are locked to the twinning planes and the current flow is directed along the twin boundaries (force acting perpendicular to the twinning planes) is discussed in Sec. IX.A.4 below. With the force acting parallel to the twin planes, the presence of twin boundaries alone does not lead to a pinning of the flux lines—in order to prevent the vortices from flowing we have to introduce additional pinning sites breaking the translation invariance along the planes. This type of enhanced pinning by twin boundaries has also been considered by Marchetti and Nelson (1990), who describe a vortex fluid flowing in channels parallel to the twinning array. Within their hydrodynamic formulation of the problem the twin boundaries produce a zero-velocity boundary condition on the flow due to enhanced pinning along the planes. In the following we concentrate on the case in which the field is along the CuO planes and the force is directed along the *c* axis, the situation realized in many of the above experiments, and discuss the interplay between twin boundary trapping and generic pinning due to point defects.

Enhanced pinning of vortices moving along the twin boundaries can have an extrinsic as well as an intrinsic origin. Extrinsically, the strain fields associated with the twin boundaries make them probable locations for atomic defects. The enhanced density of point-pinning centers then directly leads to the increased pinning properties of the twin boundaries. The intrinsic enhancement of the pinning forces acting within the twinning planes has its origin in the (dimensionally reduced) thermal fluctuations, which tend to smooth the pinning potential. Consider the case of single-vortex collective pinning at temperatures $T > T_{\mathrm{dp}}^s$, where the mean-squared amplitude of

thermal fluctuations becomes large, $\langle u^2(T)\rangle_{\text{th}} > \xi^2$. According to the discussion in Sec. II.C above, the smoothing of the pinning potential and the resulting decrease in the critical current density with increasing temperature depends strongly on the dimensionality of the system. In two dimensions, corresponding to a vortex trapped within the twin boundary potential well, the critical density decays only algebraically, $j_c^{2D}(T) \simeq j_c^{2D}(0)(\tilde{T}_{\text{dp}}^s/T)^7$. On the other hand, a single vortex line is only marginally pinned in three dimensions, and therefore the critical current density decays exponentially fast in this case, $j_c^{3D}(T) \simeq j_c^{3D}(0)\exp[-(T/\tilde{T}_{\text{dp}}^s)^3]$. Hence, due to a dimensional reduction of the thermal fluctuations, one expects to find enhanced pinning for a vortex line trapped within a twin boundary, as compared with one pinned in the bulk, as soon as $T > T_{\text{dp}}^s$. From Eq. (2.130) we can estimate a value $T_{\text{dp}}^s \simeq 50$ K for the depinning temperature in YBCO.

Enhanced pinning by the twin boundaries manifests itself in a rather sharp structure in the angular dependence of the resistivity, for the geometry in which the vortex lines are moving along the twin boundaries (Kwok *et al.*, 1990). Let us denote by $\eta^b$ and $\eta^{\text{TP}}$ the effective friction coefficients for a vortex line moving in the bulk and within the twin boundary potential well, respectively. The friction force experienced by a vortex moving parallel (along $c$) to the twin planes is

$$f_{\text{fr}} = \frac{r\eta^{\text{TP}} + s\eta^b}{r+s}v, \qquad (9.22)$$

with $r$ and $s$ denoting the lengths of the trapped and free vortex segments, respectively. In writing Eq. (9.22) we take into account that the resistive measurements by Kwok *et al.* were carried out in the ohmic regime. Note that the $\eta$'s denote effective friction coefficients enhanced by pinning; see Eq. (6.34). Assuming for simplicity that the critical trapping angle $\varphi_t$ is small, one obtains for the angular dependence of the effective friction

$$\eta^{\text{eff}} = \eta^b \frac{|\varphi|}{\varphi_t} + \eta^{\text{TP}}\left[1 - \frac{|\varphi|}{\varphi_t}\right]. \qquad (9.23)$$

Since the resistivity $\rho \propto 1/\eta^{\text{eff}}$, one immediately finds the angular behavior of the resistivity at small angles, $\varphi \ll \varphi_t$,

$$\rho(\varphi) \propto \frac{1}{\eta^{\text{TP}}}\left[1 - \left[1 - \frac{\eta^b}{\eta^{\text{TP}}}\right]\frac{|\varphi|}{\varphi_t}\right]^{-1}$$

$$\simeq \frac{1}{\eta^{\text{TP}}}\left[1 + \left[1 - \frac{\eta^b}{\eta^{\text{TP}}}\right]\frac{|\varphi|}{\varphi_t}\right]. \qquad (9.24)$$

A quantitative analysis requires that we take dynamic effects into account as well (Fleshler *et al.*, 1992).

Finally, we concentrate on the problem of (longitudinal, i.e., parallel to the twinning planes) vortex creep and ask ourselves if and under what conditions the vortex line remains trapped by the twin boundary potential during vortex motion. As an alternative, the vortex line could

jump out of the twin boundary potential well and continue its creep-type motion within the bulk, in which case the enhanced pinning properties of the twin boundaries would be rendered ineffective. According to the general theory outlined in Sec. III.F.2, creep motion within the planes is determined by the activation barriers $U^{2D}(j) \simeq U_c(j_c^{2D}/j)^{1/4}$. On the other hand, the motion in the bulk would proceed via jumps of optimal segments of length $L_{\text{opt}}^{3D}(j) \simeq L_c(j_c^{3D}/j)^{5/7}$. In order for the vortex to move in the bulk, a segment of length $L_{\text{opt}}^{3D}(j)$ has to be liberated from the twinning planes, requiring the vortex to overcome a barrier $U_{\text{lib}}(j) \simeq L_{\text{opt}}^{3D}(j)\varepsilon_{\text{TP}}$. For large current densities, $j > j_{\text{esc}}$, such that $U_{\text{lib}}(j) < U^{2D}(j)$, the vortex escapes from the twin boundary and moves within the bulk, where it is less pinned. The criterion for this dynamic instability is obtained from the condition $U_{\text{lib}}(j_{\text{esc}}) \simeq U^{2D}(j_{\text{esc}})$, and we find

$$j_{\text{esc}} \simeq j_c^{2D}\left[\frac{j_c^{3D}}{j_c^{2D}}\right]^\alpha \left[\frac{L_c\varepsilon_{\text{TP}}}{U_c}\right]^{\alpha'}, \qquad (9.25)$$

with $\alpha = 20/13 \approx 3/2$ and $\alpha' = 28/13 \approx 2$. An estimate for the escape current density $j_{\text{esc}}$ can be obtained by expressing the collective pinning energy $U_c$ due to point defects in terms of the elastic energy $\varepsilon_l\xi^2/2L_c$. The factor $L_c\varepsilon_{\text{TP}}/U_c$ measuring the relative strength of the trapping energy in the twin-boundary potential well versus the collective pinning energy due to the point defects becomes

$$\frac{L_c\varepsilon_{\text{TP}}}{U_c} \simeq \frac{2\varepsilon_{\text{TP}}}{\varepsilon_l}\left[\frac{L_c}{\xi}\right]^2 \simeq 2\pi\varphi_t^2\frac{H_{c_2}^c}{\varepsilon B}, \qquad (9.26)$$

where the last equation is fulfilled at the depinning temperature $T_{\text{dp}}^s$. The critical current-density ratio $j_c^{2D}/j_c^{3D}$ can be estimated from the experiments of Liu *et al.* (1991) to be of the order of 2, whereas Gyorgy *et al.* (1989) obtain a somewhat larger value $\sim 6$ from their torque measurements. For a field $B \simeq 1$ T, we can conclude that at $T_{\text{dp}}^s$ the escape current density is large, of the order of the critical current density $j_c^{2D}$, and thus creep proceeds with the vortices remaining trapped inside the potential well of the twin boundaries. With increasing temperature, the collective pinning length increases rapidly, and one expects the effects of trapping by the twin boundaries to become stronger. However, a more quantitative discussion would require us to take into account the formation of collectively pinned vortex bundles.

### 4. Transverse motion: critical current density and creep

In this section we concentrate on transverse pinning and creep as it results from a geometrical arrangement with the magnetic field parallel to the $c$ axis and a planar current density $j$ running parallel to the twinning planes. This geometry has been investigated by Nelson (1991) and by Nelson and Vinokur (1993). The low-temperature critical current density for this configuration is easily calculated to be

$$j_c^{\text{TP}} \simeq \frac{\varepsilon_{\text{TP}}}{\varepsilon_o} j_o , \quad T < T_{\text{dp}}^{\text{TP}} , \tag{9.27}$$

and we can make use of the result (9.14) to find that the critical current density is of the same order of magnitude as the depinning current density expected due to the collective pinning action of the pointlike oxygen defects. At large temperatures thermal fluctuations lead to a renormalization of the pinning energy [see Eq. (9.17)], as well as the pinning length. The latter is given by the thermal fluctuation amplitude

$$\langle u^2(T) \rangle_{\text{th}}^{1/2} \simeq \xi \left[ \frac{T}{\tilde{T}_{\text{dp}}^{\text{TP}}} \right]^2 , \quad T_{\text{dp}}^{\text{TP}} < T < T_{\text{dl}} , \tag{9.28}$$

as determined from the quantum analog $l^2 \simeq \hbar^2/mE_B$ [here we ignore the logarithmic correction factors obtained in Eq. (9.17)]. The resulting critical current density decays only algebraically with increasing temperature,

$$j_c^{\text{TP}} \simeq \frac{\varepsilon_{\text{TP}}}{\varepsilon_o} \left[ \frac{\tilde{T}_{\text{dp}}^{\text{TP}}}{T} \right]^4 j_o , \quad T_{\text{dp}}^{\text{TP}} < T < T_{\text{dl}} , \tag{9.29}$$

as opposed to the exponential dependence on temperature obtained for pinning by point disorder (see Sec. II.B), rendering the twin-boundary pinning increasingly important at higher temperatures. As the temperature rises beyond the delocalization temperature $T_{\text{dl}}$, as defined by the condition $\langle u^2(T_{\text{dl}}) \rangle_{\text{th}} \simeq d_{\text{TP}}^2$, the vortex samples an ensemble of twinning planes and is only pinned by the fluctuations in the pinning potential. The fluctuation amplitude $l_{\text{loc}} \simeq \langle u^2 \rangle_{\text{th}}^{1/2}$ is obtained by balancing the elastic energy $T^2/\varepsilon_l \langle u^2 \rangle_{\text{th}}$ obtained from the quantum-kinetic energy $\hbar^2/ml_{\text{loc}}^2$ (see Sec. IX.B.2 for more details) against the pinning energy $\varepsilon_{\text{TP}} \sqrt{l_{\text{loc}}/d_{\text{TP}}} (\xi/l_{\text{loc}})$, where the first factor accounts for the random addition of the $l_{\text{loc}}/d_{\text{TP}}$ twin-boundary potential wells and the second factor for the relative contribution of each twin-boundary potential well over the distance $l_{\text{loc}}$. The resulting fluctuation amplitude grows with temperature according to

$$\langle u^2 \rangle_{\text{th}}^{1/2} = l_{\text{loc}} \simeq d_{\text{TP}} \left[ \frac{\xi}{d_{\text{TP}}} \right]^{2/3} \left[ \frac{T}{\tilde{T}_{\text{dp}}^{\text{TP}}} \right]^{4/3} , \quad T_{\text{dl}} < T , \tag{9.30}$$

where the delocalization temperature $T_{\text{dl}}$ is given as the solution of the implicit equation

$$T_{\text{dl}} = \tilde{T}_{\text{dl}}(T_{\text{dl}}) \simeq \left[ \frac{d_{\text{TP}}}{\xi} \right]^{1/2} \tilde{T}_{\text{dp}}^{\text{TP}} . \tag{9.31}$$

The critical current density follows from balancing the Lorentz force $j_c \Phi_o/c$ against the pinning force (the relevant length scale is $l_{\text{loc}}$), and we obtain again an algebraic decrease with temperature,

$$j_c^{\text{TP}} \simeq \frac{\varepsilon_{\text{TP}}}{\varepsilon_o} \frac{\xi}{d_{\text{TP}}} \left[ \frac{\tilde{T}_{\text{dp}}^{\text{TP}}}{T} \right]^2 j_o , \quad T_{\text{dl}} < T . \tag{9.32}$$

In order to discuss creep we can again use the "vortex↔particle" analogy introduced in Sec. IX.A.2 above. The vortex motion (creep) away from the twin boundary proceeds via a half-loop excitation of the vortex line out of the potential well; see Fig. 44. The corresponding process in the particle picture is the field-induced emission of the particle (ionization) out of its trapping potential, whereby the driving current density $j$ producing a Lorentz force $f_L = j\Phi_o/c$ maps to the electronic field $\mathscr{E}$ producing a force $F = e\mathscr{E}$ on the particle. The half-loop excitation of the vortex itself maps to the instanton solution for the field-emission process. We thus have to solve the quantum-mechanical problem of a charged particle trapped in a (shallow) rectangular potential well $U(x)$ and subject to an external electric field $\mathscr{E}$,

$$\frac{\hbar^2}{2m} \frac{d^2\Psi}{dx^2} + [E - U(x) + Fx]\Psi = 0 . \tag{9.33}$$

In the absence of the electric field, the solution is

$$E_B = U_o - E = \frac{mU_o^2 a^2}{2\hbar^2} , \tag{9.34}$$

$$\Psi_o(x > 0) = \sqrt{k} \exp(-kx) , \tag{9.35}$$

$$k = \frac{1}{\hbar}(2mE_B)^{1/2} = \frac{mU_o a}{\hbar^2} , \tag{9.36}$$

where the potential well has been placed between $x = -a$ and $x = 0$. For a finite electric field we can again solve the problem in the quasiclassical approximation and obtain for the wave function

$$\Psi(x) = \begin{cases} \dfrac{C}{\sqrt{q}} \exp\left[ \displaystyle\int_x^{x_1} |q| dx \right], & x < x_1 , \\[3mm] \dfrac{C}{\sqrt{q}} \exp\left[ i\dfrac{\pi}{4} + i \displaystyle\int_{x_1}^x q\, dx \right], & x_1 < x , \end{cases} \tag{9.37}$$

where $q^2 = 2mFx/\hbar^2 - k^2$ and $x_1 = E_B/F$. The normalization constant $C$ is obtained by requiring $\Psi(0) \simeq \Psi_o(0)$. The ionization rate is given by $w = |\Psi(x_1)|^2 \hbar q/m$, and the final result is

$$w \approx \frac{2E_B}{\hbar} \exp\left[ -\frac{4}{3} \frac{\sqrt{2m}}{\hbar F} E_B^{3/2} \right] . \tag{9.38}$$

Transforming back to the vortex picture, we obtain the activation probability per unit length of the trapped vortex,

$$w \approx \frac{2\varepsilon_{\text{TP}}(T)}{T} \exp\left[ -\sqrt{6} \frac{\xi \sqrt{\varepsilon_l \varepsilon_{\text{TP}}(T)}}{T} \frac{\varepsilon_{\text{TP}}(T)}{\varepsilon_o} \frac{j_o}{j} \right] . \tag{9.39}$$

Of course, to exponential accuracy, the result (9.39) can be most simply obtained by dimensional estimates; see Sec. IX.B.3 below. A comparison of the probability (9.39) with the bulk activation rate $w \propto \exp[-(U_{\text{sv}}/T)(j_{\text{sv}}$

$/j)^{1/7}$] shows that, at low enough current density, liberation from the twin boundary is always the limiting factor in creep motion.

## B. Columnar defects

Pinning in a type-II superconductor can be optimized by introducing defects that trap the individual vortex lines all along their linear dimensions while simultaneously destroying a minimal-volume fraction of the superconducting material itself. Clearly, a defect structure reaching this goal can be obtained by introducing columnar defects into the material with cylinders of nonsuperconducting material of diameter $\sim \xi$, the vortex core size. The resulting pinning properties will be highly anisotropic, with optimal pinning obtained for a configuration in which the magnetic field is aligned with the linear defect structure. For this situation each trapped vortex gains an energy $U_r = \alpha H_c^2 \xi^2 L$, where $L$ is the size of the system along the direction of the magnetic field and $\alpha$ is a geometry factor. For fields weak enough that defects outnumber vortices and the interaction between vortices is negligible compared to $U_r$, we can expect to obtain a critical current density $j_c \simeq \alpha j_0$, $\alpha \sim 0.1-1$, of the order of the depairing current density $j_0$. Second, since thermal softening of the linear pinning potential is much more gradual than for the pointlike pins, one can also expect less of a decrease in the critical current density with increasing temperature. Both these effects have been observed by Civale et al. (1991) and by Konczykowski, Rullier-Albenque et al. (1991) on samples of YBCO irradiated with high-energy ($\sim$GeV) Sn and Pb ions. The fast heavy ions produce linear tracks of damaged material due to their large ionization energy-loss rate, exceeding a few keV/Å. High-resolution electron microscopy indeed confirms the formation of linear tracks of highly defected material aligned with the beam direction. The resulting defect structure can be modeled as a random array of parallel normal cylinders of diameter 50–70 Å embedded in a matrix of superconducting material. The density of these columns is conveniently measured in terms of the field $B_\Phi$ (the "matching field") producing an equivalent density of vortex lines in the superconductor. Typical irradiation doses used in the experiments produce values for $B_\Phi$ between 1 and 5 T.

From a theoretical point of view, we can distinguish between two major limiting cases regarding the importance of the vortex-vortex interaction in our discussion of the pinning problem: (i) If the interaction of the individual vortex lines with the columnar defects outweighs the intervortex interaction, we essentially are dealing with a single-vortex problem, which is conveniently mapped to the problem of a single particle in two dimensions moving in a random potential; see Sec. V.B. Due to the translation invariance of the defect structure along the direction of the magnetic field, the resulting random potential as seen by the 2D particle is a *static* one. (ii) When the vortex-vortex interaction becomes essential for

high values of the magnetic field, the quantum-mechanical analog of the vortex pinning problem is the pinning of a 2D Wigner crystal. Note that the extent of the above "single-vortex" and "many-vortex" pinning regimes depends on the question under consideration, whether it is a static or a dynamic one. We start out with a description of the vortex/2D-boson analogy (Sec. IX.B.1; the exchange of two particles involves Bose rather than Fermi statistics) and then proceed to determine the pinning potential and the critical current density for various temperature and field regimes (Sec. IX.B.2). Section IX.B.3 is devoted to the problem of creep. In Sec. IX.B.4 we discuss various aspects of the Bose-glass transition, its shift with respect to the melting line in a pure system, and the application of Bose-glass scaling laws to a continuous phase transition. Finally, in Sec. IX.B.5, we concentrate on the lock-in phenomenon originating from directed pinning due to columnar defects and the stability of the Bose-glass phase when the magnetic field is tilted away from the tracks.

### 1. Vortex/2D-boson analogy

We consider a system of vortex lines in the presence of a columnar defect structure. For small and intermediate values of the magnetic field, $B \ll H_{c_2}$, we can make use of the London approximation and write the energy of the vortex system in terms of the trajectories $\mathbf{s}_\mu(z) = (\mathbf{R}_\mu(z), z)$ (see also Sec. V.B),

$$\mathcal{H}[\mathbf{s}_\mu(z)] = \int_0^L dz \left\{ \sum_\mu \left[ \frac{\varepsilon_l}{2} \left[ \frac{d\mathbf{R}_\mu(z)}{dz} \right]^2 - \mu \right] \right.$$
$$+ \frac{1}{2} \sum_{\mu \neq \nu} V^{\text{int}}[\mathbf{R}_\mu(z) - \mathbf{R}_\nu(z)]$$
$$\left. + \sum_\mu U_r[\mathbf{R}_\mu(z)] \right\}, \qquad (9.40)$$

where $\varepsilon_l$ is the tilt modulus of the individual vortex lines, $\mu = H\Phi_0/4\pi - \varepsilon_0 \ln\kappa$ is the chemical potential, $V^{\text{int}}(\mathbf{R})$ denotes the interaction between the vortex lines and $U_r(\mathbf{R})$ is the z-independent random pinning potential due to the rods of damaged material. $L$ is the thickness of the sample along the z direction. To simplify matters we choose an interaction potential local in $z$, say, $V^{\text{int}}(R) \simeq 2\varepsilon_0 K_0(R/\lambda)$, which is appropriate in the limit of small fluctuations with $(\partial_z \mathbf{R})^2 \ll 1/\varepsilon^2$. To make these ideas explicit, we concentrate on the case of an isotropic material [$\varepsilon_l = \varepsilon_0 \ln(1/k_z \xi)$] or on the situation in which the field is aligned with the c axis of the anisotropic material [$\varepsilon_l = \varepsilon^2 \varepsilon_0 \ln(1/k_z \varepsilon \xi)$]—the results for the general anisotropic case can be obtained by means of the scaling method described in Sec. III.A. Note that the line tension $\varepsilon_l(k_z)$ is dispersive, and we should use the relevant longitudinal length scale as a cutoff in the logarithm.

We model the pinning potential $U_r(\mathbf{R})$ by a random array of identical cylindrical traps of average spacing $d_r$,

effective radius

$$b_0 = \max(r_r, \sqrt{2}\xi) ,$$ (9.41)

and a potential-well depth $\varepsilon_r$ ($r_r$ is the geometrical radius of the normal cylinder). The columnar defects are assumed to pass through the entire sample. When the vortices wander over many rods, pinning will be due to fluctuations in the rod density only and hence be similar in nature to the collective pinning of vortices by pointlike defects. It is convenient to describe this situation in terms of the correlation function for the pinning potential,

$$\langle U_r(\mathbf{R})U_r(\mathbf{R}')\rangle = \Delta_r \delta(\mathbf{R}-\mathbf{R}') ,$$ (9.42)

where the weight $\Delta_r$ can be expressed in terms of the above parameters characterizing the defect structure,

$$\Delta_r \simeq \varepsilon_r^2 b_0^4 / d_r^2$$ (9.43)

[in terms of a pinning energy density the correlator is $\langle E_{r,\mathrm{pin}}(\mathbf{R})E_{r,\mathrm{pin}}(\mathbf{R}')\rangle = (\varepsilon_r^2/d_r^2)(b_0^2/a_0^2)\delta(\mathbf{R}-\mathbf{R}')$; see Eq. (4.4) and use $U_{r,\mathrm{pin}}=U_r/b_0^2$]. Note that quantitative accuracy requires the pinning to be weak in the sense $\varepsilon_r \ll \varepsilon_l$, in which case a simple description of the vortex elasticity in terms of an expansion in the small quantity $(\partial_z \mathbf{R})^2$ is appropriate. However, we assume that for a qualitative analysis we can still use such a description, even for somewhat stronger pinning, with $\varepsilon_r \simeq \varepsilon_0$, as is the case for rods with a radius $r_r$ exceeding the vortex core radius. For the anisotropic case the regime of validity of the elastic theory requires only $(\partial_z \mathbf{R})^2 \lesssim 1/\varepsilon^2$ instead of the more stringent condition $(\partial_z \mathbf{R})^2 \lesssim 1$ (Brandt, 1992b). The enhanced regime of applicability can be easily understood within the scaling approach, which maps the angle $\tan\theta = \partial_z R \simeq 1/\varepsilon$ back to unity ($\tan\tilde{\theta}=\varepsilon\tan\theta, \theta=$ angle measured from the $c$ axis) in the isotropized system. Therefore the analysis presented below is also qualitatively correct for the case of maximal trapping energy $\varepsilon_r \simeq \varepsilon_0$ in the anisotropic situation, where strong deformations $(\partial_z \mathbf{R})^2 \sim 1/\varepsilon^2$ of the vortex line have to be expected. In all the results below the anisotropy is contained in the line tension $\varepsilon_l \propto \varepsilon^2$.

Following the ideas outlined in Sec. V.B, we note that the classical statistical mechanics of the system (9.40) is equivalent to the quantum mechanics of interacting bosons in two dimensions subject to a static random potential $U_r(\mathbf{R})$. However, here we are also interested in the case of finite sample thickness with $L < \infty$, corresponding to a finite temperature $T^B > 0$ in the Bose system. We then have to make sure that the periodic boundary conditions imposed on the Bose system do not dominate the physics of the problem. Here we should point out that the vortex/2D-boson analogy will be used mainly as a guideline to our results, whereas the actual calculations will be done within the vortex picture. On the other hand, it turns out that the results obtained within the original formulation, in terms of vortices, agree with those expressions obtained by mapping the final results in

the Bose problem back to the vortex system via the usual substitution of parameters $\hbar^2 \to T$, $\hbar^B/T^B \to L$, $m^B \to \varepsilon_l$. In this sense, the present discussion can be understood as indicating that the vortex/2D-boson analogy has an even wider regime of applicability than one might expect.

In the following, we first look at the magnetic-field regime where the interaction between vortices does not strongly affect a possible shift of a vortex line by the mean spacing $d_r$ between rods. Second, we consider pinning and creep at higher fields, where the intervortex interaction plays an important role. Pinning and creep then involve vortex bundles and can be both plastic and collective in nature. In order to obtain an estimate for the crossover field $B_{\mathrm{rb}}$ separating the single-vortex regime from the bundle regime, we can compare the shear energy per unit length $c_{66}(d_r/a_0)^2 a_0^2$ due to a displacement $d_r$ with the pinning energy $\varepsilon_r$. Making use of Eq. (3.32) for the shear modulus $c_{66}$, we find

$$B_{\mathrm{rb}} \approx \frac{4\varepsilon_r}{\varepsilon_0} B_\Phi ,$$ (9.44)

where $B_\Phi = \Phi_0/d_r^2$ is the field-equivalent irradiation dose (matching field). The result (9.44) applies to low temperatures; with increasing temperatures we have to take into account not only the temperature dependence of the pinning potential well $\varepsilon_r$ but also its thermal renormalization; see below. For fields $B < B_{\mathrm{rb}}$, each vortex can adjust to the pinning potential (which involves displacements $u < d_r/2$ on average) without interference with the other vortices present in the system. The field $B_{\mathrm{rb}}$ thus separates that portion of the $H$-$T$ plane where the vortices are individually pinned (by one or by many tracks) from the region where the pinning involves vortex bundles; see Fig. 45. Assuming a pinning efficiency $\alpha \approx \varepsilon_r/\varepsilon_0 \approx j_c/j_0 \sim 0.1$, we have $B_{\mathrm{rb}} \lesssim B_\Phi = \Phi_0/d_r^2$, and thus the rods outnumber the vortices for fields $B < B_{\mathrm{rb}}$.

Within the field range $B < B_{\mathrm{rb}}$ the vortices can accommodate freely to the pinning sites, and therefore the boson Hamiltonian associated with Eq. (9.40) can be replaced by a tight-binding model defined on a lattice of sites determined by the positions $\mathbf{R}_\mu^r$ of the rods,

$$\mathcal{H} = -\sum_\mu \mu^B a_\mu^\dagger a_\mu - \sum_{\mu \neq \nu} t_{\mu\nu}(a_\mu^\dagger a_\nu + a_\nu^\dagger a_\mu)$$
$$+ \sum_\mu u_0 n_\mu n_\mu .$$ (9.45)

Here $a_\mu^\dagger$ and $a_\mu$ are boson creation and annihilation operators at the site $\mathbf{R}_\mu^r$, $n_\mu = a_\mu^\dagger a_\mu$ is the number operator, $\mu^B = \mu$ is the chemical potential that fixes the vortex line density in the original model, and $u_0 = \Phi_0^2/4\pi$ is the on-site interaction potential. An estimate for the hopping matrix element $t_{\mu\nu}$ connecting the sites $\mathbf{R}_\mu^r$ and $\mathbf{R}_\nu^r$ separated by a distance $d_{\mu\nu} = |\mathbf{R}_\mu^r - \mathbf{R}_\nu^r|$ is given by the expression
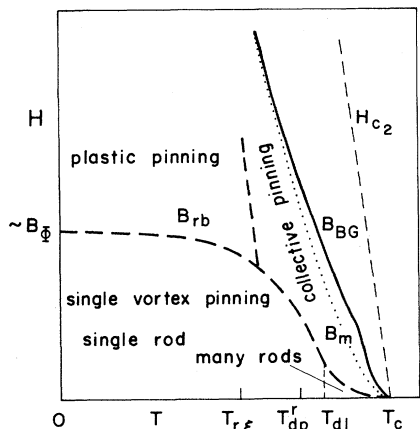
FIG. 45. Equilibrium and pinning diagram of a high-temperature superconductor taking into account thermal fluctuations and correlated quenched disorder (columnar defects). The melting line $B_m(T)$ of the pure sample is transformed into a Bose-glass transition line in the presence of a correlated static disorder potential. Also shown are the various pinning regimes with a single-vortex/single-rod pinning region at low fields and temperatures, followed by a region where the individual flux lines are pinned collectively by an assembly of rods at high temperatures, $T > T_{dl}$. Above the crossover line $B_{rb}(T)$, the largest energy in the problem is the intervortex interaction, and pinning involves vortex bundles.

$$t_{\mu\nu} \simeq 2\varepsilon_r(T) \left[\frac{2T}{\pi E_{\mu\nu}}\right]^{1/2} e^{-E_{\mu\nu}/T} . \tag{9.46}$$

Here $E_{\mu\nu} = d_{\mu\nu}[2\varepsilon_l \varepsilon_r(T)]^{1/2}$ is the kink energy involved in the activation process where the vortex jumps between the rods at $\mathbf{R}_\mu^r$ and $\mathbf{R}_\nu^r$, and $\varepsilon_r(T)$ denotes the effective pinning potential as renormalized by thermal fluctuations. Note that we distinguish between the unrenormalized quantity $\varepsilon_r$ (where $\varepsilon_r$ itself depends on temperature through the usual $1 - T/T_c$ dependence of the GL parameters) and the renormalized energy $\varepsilon_r(T)$.

The effective depth $\varepsilon_r(T)$ of the potential well and the hopping matrix element $t_{\mu\nu}$ can be determined by solving the two quantum-mechanical problems of a particle trapped within a potential well in two dimensions and of a particle tunneling between two wells separated by a distance $d_{\mu\nu}$ (see, for example, Landau and Lifshitz, 1958a; Baz', Zeldovich, and Perelomov, 1969; Nelson, 1991; Nelson and Vinokur, 1993). The binding energy $E_B$ for a particle of mass $m$ trapped in a potential $U(R)$ of depth $U_0$ and extent $a$ is given by

$$E_B \simeq U_0 \left[1 - c\frac{\hbar^2}{2ma^2}\right] , \tag{9.47}$$

with $c$ a constant of order unity. If the potential is shallow, the corresponding result is (Landau and Lifshitz, 1958a)

$$E_B \approx \frac{\hbar^2}{ma^2} e^{-\hbar^2/m\mathcal{A}} , \tag{9.48}$$

with

$$\mathcal{A} = \int_0^\infty dR\, R|U(R)| .$$

Using the transcription $\hbar \to T$, $m \to \varepsilon_l$, $U_0 \to \varepsilon_r$, and $a \to 2b_0$, we obtain the pinning potential $\varepsilon_r(T)$ renormalized due to thermal fluctuations,

$$\varepsilon_r(T) \simeq \varepsilon_r f\left[\frac{T}{\tilde{T}_{dp}^r}\right] , \tag{9.49}$$

with

$$\tilde{T}_{dp}^r(T) \simeq b_0 \sqrt{\varepsilon_l \varepsilon_r} \tag{9.50}$$

and

$$f(x) = \begin{cases} 1 - x^2, & x < 1 , \\ x^2 e^{-x^2}, & x > 1 . \end{cases}$$

At temperatures $T > \tilde{T}_{dp}^r(T)$ the effective potential depth goes rapidly to zero, and we call the solution $T_{dp}^r$ of the self-consistency equation $T_{dp}^r = \tilde{T}_{dp}^r(T_{dp}^r)$ the depinning temperature [note that we distinguish between the temperature-dependent depinning energy $\tilde{T}_{dp}^r(T)$ and the depinning temperature $T_{dp}^r$]. In the above transcription the quantum fluctuations leading to a decrease in binding energy transform into thermal (entropic) fluctuations of the vortex line. The loss in entropy due to the confining potential then leads to a reduction in the pinning energy for the vortex. The result (9.49) applies to a short-range potential that can be modeled as a local potential well of finite extent. Below we derive a more accurate expression for the pinning potential $\varepsilon_r(R)$ produced by a columnar defect, which turns out to be long range, $\varepsilon_r(R) \propto 1/R^2$. As a consequence, the effect of thermal fluctuations is reduced, with a potential renormalization given by $f_{lr}(x > 1) = \exp(-x)$.

The hopping matrix element $t$ for a two-column system separated by a distance $d$ can be found by solving for the ground state $-E_{dw}$ of the corresponding quantum-mechanical double-well tunneling problem: For a square-well potential, the wave function away from the tracks (tracks positioned at the origin and in $\mathbf{R}_d$) is given by

$$\Psi(\mathbf{R}) = K_0(\kappa R) + K_0(\kappa|\mathbf{R} - \mathbf{R}_d|) ,$$

$$\approx -\ln(\kappa R) + \left[\frac{2}{\pi\kappa d}\right]^{1/2} e^{-\kappa d} , \tag{9.51}$$

whereas we assume $\Psi(\mathbf{R}) \approx 1$ inside the (shallow) well. The ground-state energy $-E_{dw}$ is related to the wave vector $\kappa$ via the usual relation, $E_{dw} = \hbar^2\kappa^2/2m$. Integration of the Schrödinger equation inside the well determines the derivative at the well boundary,

$$\frac{d\Psi}{dR}\bigg|_{R=a} = \frac{2m}{\hbar^2 a} \int_0^a dR\, RU(R) , \tag{9.52}$$

and matching the (logarithmic) derivatives at the bound-

ary $a$ provides us with the implicit equation for $\kappa$,

$$-\ln(\kappa d)+\left[\frac{2}{\pi\kappa d}\right]^{1/2}e^{-\kappa d}=\frac{\hbar^2}{ma^2U_\circ} . \qquad (9.53)$$

For the single-well problem we can neglect the small exponential correction, and we recover the binding energy for the shallow well (9.48). Inserting this solution in Eq. (9.53) and expanding, we obtain the binding energy for the double-well problem,

$$E_{\mathrm{dw}}=E_B\left[1+2\left[\frac{2\hbar}{\pi E_k}\right]^{1/2}e^{-E_k/T}\right], \quad E_k=d\sqrt{2mE_B} . \qquad (9.54)$$

The hopping matrix element $t$ is then given by the energy difference $t=E_{\mathrm{dw}}-E_B$. Using the above transformation rules we easily recover the result (9.46).

The system described by a Hamiltonian of the form (9.45) with the positions $\mathbf{R}_\mu^r$ on a *regular* lattice but with on-site (i.e., diagonal) randomness has been discussed by Fisher *et al.* (1989) within the context of boson localization. Fisher *et al.* present qualitative arguments giving strong evidence for a localization of the Bose particles and propose a phase diagram involving a superfluid phase, a Mott insulator (number of sites = number of particles), and what has been called a Bose-glass phase, separating the first two phases. The corresponding three phases are expected to occur in the vortex system as well: starting with the localized phase, the vortex system considered here is characterized by structural (i.e., off-diagonal) disorder, and thus some kind of localization of the vortices to the tracks is expected to occur, leading to a Bose-glass phase at low enough temperatures. As we shall show below, this localization phenomenon gives rise to the occurrence of infinite barriers against vortex motion in the system, and hence the term "Bose glass" seems to be appropriate for the description of a vortex system localized on the columnar defects, too. At higher temperatures we expect a delocalization of the vortex system from the tracks, resulting in a vortex-liquid phase, the analog of the superfluid phase in the Bose system. The Mott insulator, finally, corresponds to a vortex density in which every columnar defect is occupied by a single vortex line. As a result, the vortex density is pinned over some field regime $B \approx B_\Phi$, leading to a Meissner-Ochsenfeld-like effect at a finite magnetic field. Note that the Bose-glass phase introduced here within the context of correlated disorder is quite distinct from the vortex-glass phase discussed in Sec. VII above. Whereas the dynamic properties of the two glass phases are similar (albeit, with different exponents $\mu$ involved), their statistical mechanics properties are very different. The uncorrelated disorder in the vortex-glass phase induces line wandering, whereas the correlated disorder due to columnar defects or due to twin boundaries promotes localization of the vortex lines.

After this general discussion, let us now go into more

detail and determine the dynamic properties of the vortex system subject to an aligned columnar defect structure.

### 2. Pinning potential and critical current density

To begin with, let us consider the simplest case which is realized at low temperatures $T<T_{\mathrm{dp}}^r$ and fields $B<B_{\mathrm{rb}}$, where each vortex is pinned by its own individual rod (no jumps of the vortex between rods). In order to obtain an estimate for the pinning potential $\varepsilon_r$ and for the critical current density $j_c$ we have to compare the total vortex line energies in the presence and absence of a columnar defect. Consider first the case $\sqrt{2}\xi<r_r$, the situation at low temperatures. In this case we can use the analysis of Mkrtchyan and Schmidt (1972), who determined the pinning force acting on a vortex due to the presence of a cylindrical cavity[10] with radius $r_r$, $\sqrt{2}\xi<r_r<\lambda$, within the London approximation. The energy gain (per unit length) of the vortex at a distance $R>r_r$ away from the center of the cylinder is

$$\varepsilon_r(R)=-\varepsilon_\circ\ln\left[1-\left[\frac{r_r}{R}\right]^2\right] , \qquad (9.55)$$

from which the maximal pinning force per unit length of the vortex line is easily found to be

$$f_{\mathrm{pin}}=-\left.\frac{\partial\varepsilon_r(R)}{\partial R}\right|_{R=r_r+\sqrt{2}\xi}=\frac{\varepsilon_\circ}{\sqrt{2}\xi} . \qquad (9.56)$$

Hence we find that the critical current density $j_c$ is indeed given by the depairing current density $j_\circ$,

$$j_c=\frac{3\sqrt{3}}{4\sqrt{2}}j_\circ \approx j_\circ , \qquad (9.57)$$

and an upper estimate for the pinning potential $-\varepsilon_r(R)$ is

$$\varepsilon_r(R)\approx\begin{cases}\varepsilon_\circ\ln\dfrac{r_r}{\sqrt{2}\xi}, & R<r_r , \\[2mm] -\varepsilon_\circ\ln\left[1-\left[\dfrac{r_r}{R+\xi/\sqrt{2}}\right]^2\right], & r_r<R<\lambda .\end{cases} \qquad (9.58)$$

At low temperatures, where the pinning energy $\varepsilon_r$ is of the order of $\varepsilon_\circ$, the field $B_{\mathrm{rb}}$ limiting the regime where the individual vortices can freely accommodate to the defect structure is roughly given by the matching field $B_\Phi$, $B_{\mathrm{rb}}\simeq B_\Phi$.

At higher temperatures we have $r_r<\sqrt{2}\xi$ and the energy gain for the vortex can be simply calculated from the reduction in the order parameter as given by (2.34), leading to a pinning potential $-\varepsilon_r(R)$ of the form

---

[10]This analysis provides an upper estimate for the pinning energy/force/critical current density.

$$\varepsilon_r(R) \approx \frac{H_c^2}{8\pi} \pi r_r^2 [1 - |\Psi(R)|^2]$$

$$= \frac{\varepsilon_0}{2} \frac{r_r^2}{R^2 + 2\xi^2}, \quad 0 < R < \lambda . \tag{9.59}$$

A useful interpolation formula for the depth of the pinning potential $\varepsilon_r = \varepsilon_r(R = 0)$ is given by

$$\varepsilon_r \approx \frac{\varepsilon_0}{2} \ln \left[ 1 + \frac{r_r^2}{2\xi^2} \right] . \tag{9.60}$$

Both the low-temperature expression (9.58) and the high-temperature result (9.59) are characterized by a long tail, $\varepsilon_r(R) \simeq \varepsilon_0 r_r^2 / R^2$, $b_0 < R < \lambda$. The critical current density $j_c$ can be estimated from the force balance equation, and we obtain

$$j_c = \frac{27\sqrt{2}}{64} \left[ \frac{r_r}{2\xi} \right]^2 j_0, \quad T_{r\xi} < T . \tag{9.61}$$

The crossover temperature separating the low- and high-temperature limits, (9.58) and (9.59), is defined by the relation $\sqrt{2}\xi(T_{r\xi}) = r_r$,

$$\frac{T_{r\xi}}{T_c} = 1 - \frac{2\xi^2(0)}{r_r^2} . \tag{9.62}$$

Using parameters appropriate for YBCO [$\xi(0) \approx 12$ Å, $r_r \approx 35$ Å], we obtain the estimate $T_{r\xi} \approx 0.76 T_c \approx 70$ K. Note the different scaling behavior of $\varepsilon_r$ with temperature; on approaching $T_c$ the potential depth $\varepsilon_r$ scales according to $\varepsilon_r(R = 0) \propto (T_c - T)^2$, and hence the crossover field $B_{rb}$ limiting the free accommodation of the individual vortex lines to the columnar pins decreases above $T_{r\xi}$,

$$B_{rb} \approx \left[ \frac{r_r}{\xi} \right]^2 B_\Phi \propto \left[ 1 - \frac{T}{T_c} \right]^2 . \tag{9.63}$$

At large temperatures, $T > T_{dp}^r$, the single-vortex pinning potential energy is strongly renormalized by thermal fluctuations. Taking account of the slow decay of the pinning potential, $-\varepsilon_r(R) \simeq -\varepsilon_0 r_r^2 / R^2$, we should cut off the radial integral in (9.48) at a distance $R^* = b_0 \sqrt{U(0)/E_B}$, leading to a renormalization of the pinning energy by a factor $\sim \exp(-T/\tilde{T}_{dp}^r)$. For an accurate determination of the depinning energy $\tilde{T}_{dp}^r$, this simple analysis is not sufficient. After mapping the vortex problem to the corresponding 2D quantum problem, we need to solve the Schrödinger equation for a particle in a shallow, long-range potential,

$$\left[ \partial_R^2 + \frac{\beta}{R^2 + R_0^2} - \kappa^2 \right] \Psi(R) = 0 , \tag{9.64}$$

with

$$\beta = (2mR_0^2/\hbar^2)U(0) = (r_r\sqrt{\varepsilon_l\varepsilon_0}/T)^2 \ll 1 ,$$

$$\kappa^2 = (2m/\hbar^2)E_B ,$$

$$R_0 = \sqrt{2}\xi$$

(here we assume that $T > T_{r\xi}$). Again, simple quasiclassical approximation is not applicable, and we have to solve (9.64) explicitly. For $R < R_0$ we can approximate $\beta/(R^2 + R_0^2) - \kappa^2 \approx \beta/R_0^2$ and obtain the solution $\Psi(R) \sim J_0(\sqrt{\beta}R/R_0)$. The solution in the intermediate regime $R_0 < R < R^* = \sqrt{\beta}/\kappa$, where we can use $\beta/(R^2 + R_0^2) - \kappa^2 \approx \beta/R^2$, is given by $\Psi(R) \sim \cos[\sqrt{\beta}\ln(R/R_0) + \delta]$, with the phase $\delta \approx \sqrt{\beta}/2 \ll 1$ determined by equating the logarithmic derivatives of $\Psi(R)$ at $R_0$. In the region $R > R^*$, we can neglect the potential term in Eq. (9.64), and the solution is $\Psi(R) \sim K_0(\kappa R)$. Again equating logarithmic derivatives at $R^*$, we find the relation

$$-\frac{1}{\sqrt{\beta}} \frac{1}{\ln(\kappa R^*/2)} = \tan\left[ \sqrt{\beta} \ln \frac{\sqrt{\beta}}{\kappa R_0} + \delta \right] . \tag{9.65}$$

With $-\sqrt{\beta}\ln\sqrt{\beta} \ll 1$ the left-hand side of Eq. (9.65) is large, and using $\delta \ll 1$ we obtain the binding energy

$$E_B \approx \frac{\hbar^2\beta}{4m\xi^2} e^{-\pi/\sqrt{\beta}} . \tag{9.66}$$

Transcribing back to the vortex language, we obtain the thermally renormalized pinning energy

$$\varepsilon_r(T) \approx \varepsilon_r e^{-T/\tilde{T}_{dp}^r} , \tag{9.67}$$

with the depinning energy given by

$$\tilde{T}_{dp}^r \approx \frac{r_r}{\pi} \sqrt{\varepsilon_l\varepsilon_0} = \frac{\sqrt{2}}{\pi} b_0 \sqrt{\varepsilon_l\varepsilon_r} . \tag{9.68}$$

The result (9.68) differs from the short-range result (9.50) only by the numerical factor $\sqrt{2}/\pi$. More importantly, the exponent in Eq. (9.49) changes from $(T/\tilde{T}_{dp}^r)^2$ to $T/\tilde{T}_{dp}^r$, reducing the effect of thermal fluctuations for the long-range potential $\varepsilon_r(R) \sim \varepsilon_r r_r^2 / R^2$. A $T^2$-type dependence in the exponent is only recovered when the amplitude of thermal fluctuations (or, correspondingly, the extent of the wave function) grows beyond the range $\lambda$ of the potential.[11]

The renormalization of the pinning energy due to thermal fluctuations implies a corresponding reduction in the crossover field,

$$B_{rb}(T) \approx \frac{r_r^2}{\xi^2} B_\Phi e^{-T/\tilde{T}_{dp}^r} . \tag{9.69}$$

Similarly, thermal fluctuations lead to a strong reduction in the critical current density. Increasing the temperature beyond the depinning temperature $T_{dp}^r$, we find that the vortex line starts to wander away from its columnar defect. In order to find the mean amplitude of thermal fluctuations $\langle u^2(T) \rangle_{th}$, we consider again the 2D quantum problem of a particle trapped in a shallow potential

---

[11]The influence of the long-range nature of the pinning potential on its thermal renormalization was not accounted for in the preprint version of this work.

well (Nelson, 1991). The binding energy $E_B$ is easily converted to a localization length $l_{loc}$ for the wave function, $l_{loc}^2 \simeq \hbar^2/mE_B$, and using our mapping rules connecting the 2D Bose system and the vortex system, we immediately obtain

$$\langle u^2(T)\rangle_{th}^{1/2} = l_{loc} \simeq b_o \frac{T}{\tilde{T}_{dp}^r} e^{T/2\tilde{T}_{dp}^r} . \qquad (9.70)$$

Combining Eqs. (9.67) and (9.70), we obtain the fluctuation-corrected critical current density, for $T_{r\xi} > T_{dp}^r$,

$$j_c \simeq \frac{r_r^2}{\xi^2} \frac{\tilde{T}_{dp}^r}{T} e^{-(3/2)(T/\tilde{T}_{dp}^r)} j_o , \quad T_{dp}^r < T < T_{dl} . \quad (9.71)$$

As the thermal amplitude $\langle u^2(T)\rangle_{th}^{1/2}$ grows beyond the mean rod spacing $d_r$, the vortex line cannot be pinned by an individual rod any longer, but rather is pinned collectively by fluctuations in the density of columnar defects; see Fig. 46. The temperature at which $\langle u^2(T)\rangle_{th} \simeq d_r^2$ is called the delocalization temperature $T_{dl}$ and can be estimated from the implicit equation

$$T_{dl} = \tilde{T}_{dl}(T_{dl}) \simeq \tilde{T}_{dp}^r(T_{dl}) \ln \frac{d_r^2}{b_o^2} . \qquad (9.72)$$

We then have to determine the amplitude $\langle u^2(T)\rangle_{th}^{1/2}$ (localization length) within the high-temperature regime $T > T_{dl}$, and we do so by using the method of dimensional estimates. Going over to the 2D quantum analog of the vortex problem, our task is to find the localization length of a particle satisfying the Schrödinger equation (Nelson, 1991)

$$\left[ -\frac{T^2}{2\varepsilon_l}(\nabla^{(2)})^2 + U_r(\mathbf{R}) \right] \Psi(\mathbf{R}) = e\Psi(\mathbf{R}) , \qquad (9.73)$$

with $U_r(\mathbf{R})$ the random potential set up by the columnar defect structure. The localization length $l_{loc}$ can be obtained by balancing the kinetic energy $T^2/2\varepsilon_l l_{loc}^2$ against the mean potential energy $\varepsilon_r(b_o/l_{loc})^2(l_{loc}/d_r)$, where



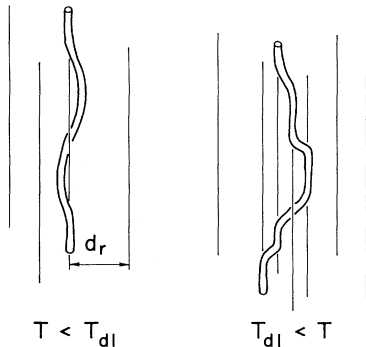FIG. 46. Vortex line pinned by an individual columnar defect $(T < T_{dl}, \langle u^2\rangle_{th}^{1/2} < d_r)$ and by the collective action of many rods $(T > T_{dl}, \langle u^2\rangle_{th}^{1/2} > d_r)$. In the latter case, only fluctuations in the track density are able to pin the vortex.

the factor $(b_o/l_{loc})^2$ describes the relative contribution from each rod and the second factor arises from the random addition of the $(l_{loc}/d_r)^2$ rods within the localization area (note that the individual rods compete with each other, hence the energy grows only with the square root of the number of relevant rods. Here, the pinning energy involves the unrenormalized potential-well depth $\varepsilon_r$). The final result for the localization length $l_{loc}$ and hence for the mean amplitude of thermal fluctuations is

$$\langle u^2(T)\rangle_{th}^{1/2} = l_{loc} \simeq d_r \left[ \frac{T}{\tilde{T}_{dl}} \right]^2 , \quad T > T_{dl} . \qquad (9.74)$$

Above $T_{dl}$ the pinning energy decreases only slowly with temperature,

$$\varepsilon_{pin} \simeq \varepsilon_r \left[ \frac{b_o}{d_r} \right]^2 \left[ \frac{\tilde{T}_{dl}}{T} \right]^2 , \quad T > T_{dl} . \qquad (9.75)$$

The critical current density for temperatures $T > T_{dl}$ can be most simply obtained by means of dimensional estimates. Comparing the pinning energy (9.75) with the energy gain $j_c\Phi_o\langle u^2\rangle_{th}^{1/2}/c$ due to the Lorentz force acting on the vortex line, we obtain the critical current density

$$j_c(T) \simeq \frac{\varepsilon_r}{\varepsilon_o} \frac{\xi}{d_r} \left[ \frac{b_o}{d_r} \right]^2 \left[ \frac{\tilde{T}_{dl}}{T} \right]^4 j_o , \quad T > T_{dl} . \quad (9.76)$$

Equations (9.57), (9.61), (9.71), and (9.76) describe the decrease of the *single-vortex critical current density* with increasing temperature. At low temperatures, $T < T_{r\xi}$, the critical current density is of the order of the depairing current density Eq. (9.57). Above $T_{r\xi}$, the critical current density decreases, first due to the reduction in $\varepsilon_r$, Eq. (9.61), then, above $T_{dp}^r$, due to thermal fluctuations, Eq. (9.71), and finally, above $T_{dl}$, due to delocalization from the individual rods and crossover to collective pinning by many rods, Eq. (9.76).

Before turning to a discussion of the high-field regime with $B > B_{rb}$, we briefly estimate the various crossover temperatures introduced above and determine the crossover field $B_{rb}$ at high temperatures. The above results for the pinning potential $\varepsilon_r(R)$ allow us to calculate a more reliable estimate for the depinning temperature $T_{dp}^r$. Assuming $T_{dp}^r > T_{r\xi}$ and making use of the result Eq. (9.68), we obtain the following implicit equation for $T_{dp}^r$:

$$T_{dp}^r = \tilde{T}_{dp}^r(T_{dp}^r) = \frac{1}{\pi} r_r \sqrt{\varepsilon_l \varepsilon_o}$$

$$\approx \frac{r_r}{2\sqrt{2}\pi\xi(0)} T_c \left[ \frac{\ln(L/\varepsilon\xi)}{Gi} \right]^{1/2} \left[ 1 - \frac{T_{dp}^r}{T_c} \right] .$$

$$(9.77)$$

The length scale $L$ of the thermal fluctuations is determined by the relation $\varepsilon_l l_{loc}^2/L^2 \simeq \varepsilon_r(T)$, balancing the elastic energy against the pinning energy. The localization length $l_{loc}$ and the binding energy $\varepsilon_r(T)$ are given by Eqs. (9.70) and (9.49), respectively. Evaluating the length

$L$ at the depinning temperature $T_{dp}^r$, we obtain the result $L \simeq \sqrt{2}\varepsilon\xi\sqrt{\ln(L/\varepsilon\xi)}$, of the order of $\varepsilon\xi$, and we can drop the logarithmic correction in Eq. (9.77). For small temperatures (where $b_o = r_r$), a similar result with a slightly different numerical prefactor is obtained. Using parameters appropriate for YBCO, $Gi \simeq 10^{-2}$, $\xi(0) \simeq 12$ Å, and choosing the defect radius $r_r \approx 35$ Å, we obtain the estimate $T_{dp}^r \approx 0.77 T_c \approx 70$ K for the depinning temperature. Combining Eqs. (9.77) and (9.72) and using the same parameters as above (we choose $d_r \approx 400$ Å corresponding to $B_\Phi \approx 1$ T), we obtain the estimate $T_{dl} \approx 0.93 T_c \approx 85$ K for the delocalization temperature. Note that these estimates assume maximal pinning, i.e., $\alpha = 1$. Experimentally one finds $j_c/j_o \sim 0.1$ in the low-temperature/weak-field regime, indicating that $\alpha < 1$ and thus also reducing the above estimates for $T_{dp}^r$ and for $T_{dl}$.

The single-vortex pinning regime extends up to fields where the thermal amplitude of the individual lines $\langle u^2(T)\rangle_{th}^{1/2}$ remains smaller than the thermal amplitude of fluctuations of the vortex lattice as given by (4.85). Making use of Eq. (4.85) for the vortex lattice, we find that the regime of single-vortex collective pinning is limited by the condition

$$B < B_{rb} \simeq B_\Phi \left[\frac{b_o}{d_r}\right]^2 \frac{\varepsilon_r}{\varepsilon_o} \left[\frac{\tilde{T}_{dl}}{T}\right]^6, \quad T > T_{dl} . \quad (9.78)$$

In the vicinity of $T_c$ we can use $b_o \simeq \sqrt{2}\xi$, $\varepsilon_r \simeq \varepsilon_o(r_r/2\xi)^2$ and obtain the following scaling behavior close to $T_c$:

$$B_{rb} \approx \frac{1}{2\pi^6 Gi^3} B_\Phi \left[\frac{r_r}{d_r}\right]^2 \left[\frac{r_r}{\sqrt{2}\xi(0)}\right]^6$$
$$\times \left[\ln\frac{d_r}{\sqrt{2}\xi}\right]^6 \left[1 - \frac{T}{T_c}\right]^6 . \quad (9.79)$$

The result (9.78) can be obtained equally well by comparing the shear energy involving a displacement $\langle u^2(T)\rangle_{th}^{1/2}$ with the total pinning energy as given by Eq. (9.75). To summarize, we find a crossover field $B_{rb}$ of the order of the matching field $B_\Phi$ at low temperatures. Above $T_{r\xi}$, the field $B_{rb}$ decreases with temperature as described by Eq. (9.63). Within the small-temperature interval $T_{dp}^r < T < T_{dl}$, the crossover line $B_{rb}(T) \approx (4\varepsilon_r(T)/\varepsilon_o)B_\Phi$ decreases exponentially with increasing temperature until it reaches the high-temperature branch as given by Eq. (9.78); see Fig. 45.

It is both instructive and useful to check the above results obtained via simple dimensional estimates by means of the dynamic approach. Following the steps outlined in Sec. III.D and applying them to the case of a single vortex subject to a columnar defect structure, one arrives at the following expression for the relative correction $\delta v/v$ to the vortex velocity $v$:

$$\frac{\delta v}{v} = \frac{\gamma_r}{\eta_l} \int \frac{d^2K}{(2\pi)^2} dz\, dt\, G(z,t) K^2 K_v |p(K)|^2$$
$$\times \frac{\sin K_v vt}{v} e^{-K^2\langle u_{th}^2(z,t)\rangle/2}, \quad (9.80)$$

with the mean-squared amplitude of thermal fluctuations given by [see Eq. (3.131)]

$$\langle u_{th}^2(z,t)\rangle \approx \frac{T}{\pi\varepsilon_l} \left[z^2 + \frac{\varepsilon_l}{\eta_l}t\right]^{1/2} \quad (9.81)$$

and the single-vortex Green's function in real space,

$$G(z,t) = \Theta(t) \frac{\exp[-\eta_l z^2/4\varepsilon_l t]}{\sqrt{4\pi\varepsilon_l\eta_l t}} . \quad (9.82)$$

Here we have expressed the pinning potential $U_r(\mathbf{R})$ via the usual convolution of the disorder potential $U_{r,pin}(\mathbf{R})$ and the form factor $p(\mathbf{R})$ of an individual vortex,

$$U_r(R) = \int d^2 R'\, U_{r,pin}(\mathbf{R}')p(\mathbf{R} - \mathbf{R}') . \quad (9.83)$$

The correlator for the potential $U_{r,pin}(\mathbf{R}')$ takes the form

$$\langle U_{r,pin}(\mathbf{R})U_{r,pin}(\mathbf{R}')\rangle = \gamma_r\delta(\mathbf{R} - \mathbf{R}') , \quad (9.84)$$

with $\gamma_r$ and $\Delta_r$ related via

$$\gamma_r \simeq \frac{\Delta_r}{b_o^4} \simeq \frac{\varepsilon_r^2}{d_r^2} . \quad (9.85)$$

We first perform the integration over $z$, neglecting the $z$ dependence in $\langle u^2\rangle_{th}$, and obtain

$$\frac{\delta v}{v} = \frac{\gamma_r}{\eta_l} \int \frac{d^2K}{(2\pi)^2} dt\, K^2 K_v |p(K)|^2$$
$$\times \frac{\sin K_v vt}{v}\exp\left[-\frac{K^2 T}{2\pi}\sqrt{t/\varepsilon_l\eta_l}\right] . \quad (9.86)$$

The large wave-vector cutoff is provided by the Debye-Waller factor, $K < K_{max}$, with

$$K_{max} \simeq \left[\left[\frac{2\pi}{T}\right]^2 \frac{\varepsilon_l\eta_l}{t}\right]^{1/4} . \quad (9.87)$$

The main contribution to the $K$ integral comes from the region of large wave vectors, $K \sim K_{max}$. Second, we perform the integration over time $t$, which again is dominated by large times, the cutoff being provided by the factor $\sin K_v vt$ at $K_{max}vt_{max} \sim 1$, hence

$$t_{max} \simeq \left[\left[\frac{T}{2\pi}\right]^2 \frac{1}{\varepsilon_l\eta_l v^4}\right]^{1/3} . \quad (9.88)$$

The final result reads

$$\frac{\delta v}{v} \simeq \Delta_r \left[\frac{\varepsilon_l^2}{\eta_l v T^4}\right]^{2/3} . \quad (9.89)$$

The condition

$$\frac{\delta v}{v}\bigg|_{v=v_c}=1 \qquad (9.90)$$

determines the critical velocity $v_c$, and using $j_c=c\eta_l v_c/\Phi_0$ we recover the expression (9.76) for the critical current density $j_c$.

Analyzing the origin of Eq. (9.89) in more detail, we can independently rederive many of the previously stated results. First of all, an alternative derivation of Eq. (9.72) for the delocalization temperature $T_{dl}$ proceeds as follows. As we decrease the temperature, the main contribution to the $K$ integral comes from progressively larger wave vectors $K_{max}$. With $K_{max}$ increasing beyond $1/d_r$, the condition for the applicability of collective pinning is violated, and we enter the single-vortex/single-rod pinning regime. The characteristic crossover temperature $T_{dl}$ can be obtained from the condition

$$K_{max}(T=T_{dl})\simeq\frac{1}{d_r}, \qquad (9.91)$$

with the relevant time scale $t$ given by $t_{max}(v=v_c)\simeq T^6\eta_l/\varepsilon_l^3\Delta_r^2$. Using the definition (9.87) of $K_{max}$, we obtain the delocalization temperature

$$T_{dl}\simeq(\varepsilon_l^2\Delta_r d_r^2)^{1/4}\simeq b_0\sqrt{\varepsilon_l\varepsilon_r}, \qquad (9.92)$$

which agrees up to logarithmic accuracy with the estimate (9.72) for $T_{dl}$. Second, an expression for the delocalization length $l_{loc}$ is obtained again from the cutoff $K_{max}$. Defining $l_{loc}\simeq1/K_{max}$ and inserting the relevant time scale $t_{max}(v=v_c)$ given above, we recover the result (9.74) for $l_{loc}$, thus confirming the correctness of the previous derivation of the localization length.

Finally, let us leave the single-vortex pinning regime and consider fields $B_{rb}<B<B_{BG}$ intermediate between the crossover field $B_{rb}$ and the Bose-glass line $B_{BG}(T)$ (see Fig. 45), where the lattice is not yet melted (see Sec. IX.B.4 for a discussion of the Bose-glass line). Within this field regime the vortices form a lattice, and the interaction between flux lines is dominant, leading either to weak collective pinning of vortex bundles or to plastic pinning. Let us first consider the case of collective pinning at low temperatures. Balancing the elastic energy $c_{66}(u/R)^2R^2$ against the pinning energy

$$\mathcal{E}_{r,pin}(R,u)\simeq\left[\frac{b_0^2}{a_0^2}\gamma_r R^2\right]\frac{u}{b_0} \qquad (9.93)$$

[see Eq. (4.29)], we obtain the disorder-induced displacement field

$$u(R)\simeq\frac{\varepsilon_r}{\varepsilon_0}\frac{a_0}{d_r}R, \quad R<b_0. \qquad (9.94)$$

Using the definition $u(R_c)\simeq b_0$, we find the collective pinning radius

$$R_c\simeq d_r\frac{\varepsilon_0}{\varepsilon_r}\frac{b_0}{a_0}. \qquad (9.95)$$

The critical current density $j_c$ is obtained by balancing the Lorentz force $j_c BR_c^2/c$ against the elastic force $c_{66}b_0$, and we find the low-temperature/high-field result $(B_{r_r}=\Phi_0/r_r^2)$

$$j_c\simeq\frac{\varepsilon_r}{\varepsilon_0}\frac{\xi}{b_0}\frac{B_{rb}}{B}j_0\simeq\begin{cases}\left[\dfrac{B_{r_r}}{H_{c_2}}\right]^{1/2}\dfrac{B_{rb}}{B}j_0, & T<T_{r\xi}, \\[4mm] \dfrac{H_{c_2}}{B_{r_r}}\dfrac{B_{rb}}{B}j_0, & T_{r\xi}<T.\end{cases} \qquad (9.96)$$

For temperatures $T>T_{r\xi}$, Eq. (9.96) matches the low-field result (9.61) at $B=B_{rb}$.

At low temperatures, $T<T_{r\xi}$, the collective pinning radius $R_c\simeq r_r(d_r/a_0)$ is of the order of $r_r\ll d_r$ at the crossover field $B_{rb}\simeq B_\Phi$ and becomes large (of the order of $d_r$) only at very high fields, $B_{r_r}=\Phi_0/r_r^2$. Within the intermediate-field regime $B_{rb}<B<B_{r_r}$ the vortex lattice is plastically pinned. The fraction $B_\Phi/B$ of the vortices is firmly pinned by columnar defects, whereas the rest is merely fixed by the shear force within the lattice. The Lorentz force $j_{pl}Bd_r^2(1-B_\Phi/B)/c$ acting on the remaining vortices competes with the pinning force $c_{66}a_0$ produced by the shear and leads to the critical current density

$$j_{pl}\simeq\begin{cases}j_0, & B_{rb}\lesssim B, \\[3mm]\dfrac{a_0\xi}{d_r^2}j_0\simeq\dfrac{B_{rb}}{\sqrt{BH_{c_2}}}, & B_{rb}<B<B_{r_r}.\end{cases} \qquad (9.97)$$

Equation (9.97) approaches the depairing current at the low-field boundary $B_\Phi$ and correctly matches the collective pinning result (9.96) at the upper boundary $B_{r_r}$.

At higher temperatures we should take the thermal smearing of the potential into account. The appropriate criterion is given by $\langle u^2\rangle_{th}>b_0^2$, and for $T>T_{r\xi}$ we recover the usual lattice depinning temperature $T_{dp}\simeq\varepsilon\varepsilon_0\xi^2/a_0$. At high temperatures, $T>T_{dp}$, the pinning energy $\mathcal{E}_{r,pin}$ is reduced by the factor $b_0/\langle u^2\rangle_{th}^{1/2}$ [see Eq. (2.118)]. Balancing $\mathcal{E}_{r,pin}$ against the shear energy $c_{66}\langle u^2\rangle_{th}$, we obtain the collective pinning radius

$$R_c\simeq d_r\frac{\varepsilon_0}{\varepsilon_r}\frac{\langle u^2\rangle_{th}^{3/2}}{a_0\xi^2}\simeq d_r\frac{\langle u^2\rangle_{th}^{3/2}}{a_0r_r^2}. \qquad (9.98)$$

Rewriting $\langle u^2\rangle_{th}\simeq a_0r_r(T/\tilde{T}_{dp}^r)$, we find that

$$R_c\simeq d_r\left[\frac{a_0}{r_r}\right]^{1/2}\left[\frac{T}{\tilde{T}_{dp}^r}\right]^{3/2}, \qquad (9.99)$$

hence $R_c>d_r$ for temperatures $T>T_{dp}^r$ and plastic pinning is irrelevant in this regime. The critical current density then takes the form

$$j_c \simeq \frac{a_o^2}{d_r^2} \frac{r_r^4}{\xi^4} \left[ \frac{\xi^2}{\langle u^2 \rangle_{\text{th}}} \right]^{5/2} j_o \simeq \begin{cases} \dfrac{r_r^2}{d_r^2} \left[ \dfrac{\xi}{d_r} \right]^{1/2} \left[ \dfrac{B}{B_{\text{rb}}} \right]^{1/4} \left[ \dfrac{\widetilde{T}_{\text{dp}}^r}{T} \right]^{5/2} j_o , & T_{\text{dp}}^r < T < T_{\text{dl}} , \\[3ex] \dfrac{\xi r_r^2}{d_r^3} \left[ \dfrac{B}{B_{\text{rb}}} \right]^{1/4} \left[ \dfrac{\widetilde{T}_{\text{dp}}^r}{T} \right]^4 j_o , & T_{\text{dl}} < T , \end{cases}$$

(9.100)

where we have neglected small logarithmic corrections in the last formulas. Using $\langle u^2 \rangle_{\text{th}} \simeq T a_o / \varepsilon \varepsilon_o$, we obtain the temperature/field dependence $j_c \propto B^{1/4}/T^{5/2}$ [note that $B_{\text{rb}} \propto T^{-6}$ in the high-temperature regime $T > T_{\text{dl}}$; see Eq. (9.78)].

Equation (9.100) likewise follows from the dynamic approach. The relative correction $\delta v / v$ to the flow velocity in the dynamic approach, for a vortex lattice in the presence of a columnar defect structure, is given by

$$\frac{\delta v}{v} = \frac{\gamma_r}{\eta a_o^2} \int \frac{d^2 K}{(2\pi)^2} dz\, dt\, G(z,t) K^2 K_v |p(K)|^2$$
$$\times \frac{\sin K_v v t}{v} S(\mathbf{K}, z, t) ,$$

(9.101)

with $G(z,t)$ and $S(K,z,t)$ the Green's function and the dynamic structure factor for the vortex lattice. We express the Green's function $G(\mathbf{r},t)$ by its Fourier representation $G(\mathbf{q},\omega)$. Again neglecting $z$ dependence in the structure factor and performing the integrations over $z$ and $t$, we obtain

$$\frac{\delta v}{v} = \frac{\gamma_r}{a_o^2} \int \frac{d^2 K}{(2\pi)^2} \frac{d^2 Q}{(2\pi)^2} \frac{K^2 K_v^2 e^{-K^2 \langle u^2 \rangle_{\text{th}}/2}}{(c_{66} Q^2)^2 + (jBK_v/c)^2} .$$

(9.102)

The remaining integrations over $\mathbf{Q}$ and $\mathbf{K}$ can easily be done, and we find for the relative velocity correction

$$\frac{\delta v}{v} \simeq \frac{c \Delta_r}{c_{66} j \Phi_o \langle u^2 \rangle_{\text{th}}^{5/2}} ,$$

(9.103)

resulting in a critical current density

$$j_c \simeq \frac{c \Delta_r}{\varepsilon_o B \langle u^2 \rangle_{\text{th}}^{5/2}} ,$$

(9.104)

in agreement with Eq. (9.100) above. Note that, due to the translational invariance of the problem along the $z$ axis, the tilt mode is not relevant in the relaxation of the vortex lattice to the pinning potential. In particular, the dimension along the $z$ axis of the collectively pinned bundle is simply $L$. Therefore the dispersion is not relevant in the present problem of a vortex lattice pinned by columnar defects, and we do not have to distinguish between small and large collectively pinned bundles in our discussion of the critical current density (dispersion does, however, become relevant in the problem of creep of vortex bundles; see below).

### 3. Vortex creep at $j \ll j_c$

Here we discuss the response of the vortex system to a small current density, $j \ll j_c$, applied transverse to the field direction. Again we shall find various regimes of different behavior as the current density probes different length scales in the system. We shall also consider samples of finite thickness $L$. Hence the barriers against motion will always be cut off at small current densities, due to the finiteness of the sample. True Bose-glass behavior with diverging barriers in the limit $j \to 0$ will be found only in the limit $L \to \infty$. We first concentrate on single-vortex creep and then treat the creep of vortex bundles.

The liberation of a vortex line from its rod takes place via thermal activation of a finite segment of length $l_{\text{hl}}$ out of the pinning well, creating a half-loop excitation of the string; see Fig. 47. It is interesting to compare the present situation with the problem of pinning in a periodic potential, as discussed in Sec. III.E above. The important difference is that in this problem the transverse size $u_{\text{hl}}$ of the half-loop is not simply given by the periodicity $u_o$, but is determined by competition between the elastic energy $\varepsilon_l u_{\text{hl}}^2 / l_{\text{hl}}$ and the pinning energy $\varepsilon_r(T) l_{\text{hl}}$. As a result we shall find that a vortex trapped by a columnar defect will show glassiness, whereas a string trapped in a
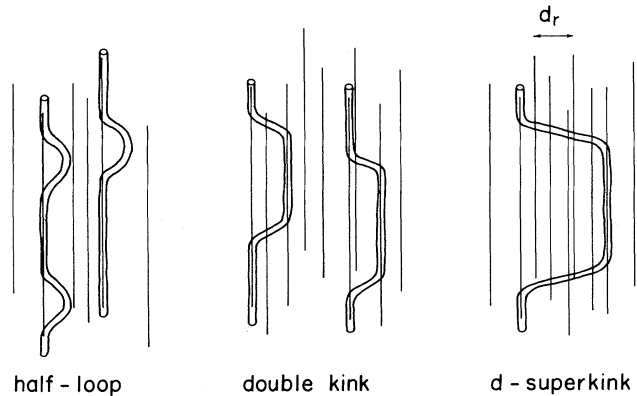


FIG. 47. Typical excitations of a vortex line from its pinning track, leading to vortex creep. The half-loop excitations are relevant at high current densities $j$, where the critical nucleus does not yet reach out to the neighboring columns. With decreasing current density, the nucleus grows, and double-kink excitations to the neighboring track become relevant. Finally, dispersion in the pinning energies becomes important for small current densities and large sample length $L$, and the vortex motion proceeds, via the formation of double-superkink excitations, to the next optimal track (variable-range hopping).

periodic potential does not.

The geometrical *shape* of all the possible half-loop excitations is given by the relation $u_{hl} \simeq [\varepsilon_r(T)/\varepsilon_l]^{1/2} l_{hl}$. It remains to determine the *size* of the loop excitation. This is obtained by balancing the cost in elastic energy against the energy gain from the Lorentz force, $j\Phi_0 l_{hl} u_{hl}/c$. The final results for the size and the activation energy of the critical nucleus are

$$l_{hl}(j) \simeq \xi \left[ \frac{\varepsilon_l \varepsilon_r(T)}{\varepsilon_0^2} \right]^{1/2} \frac{j_0}{j} , \quad (9.105)$$

$$u_{hl}(j) \simeq \xi \frac{\varepsilon_r(T)}{\varepsilon_0} \frac{j_0}{j} , \quad (9.106)$$

$$U_{hl}(j) \simeq \varepsilon_r(T) \xi \left[ \frac{\varepsilon_l \varepsilon_r(T)}{\varepsilon_0^2} \right]^{1/2} \frac{j_0}{j} . \quad (9.107)$$

At low temperatures $T < T_{r\xi}$ and for an isotropic situation we obtain a circular half-loop excitation ($u_{hl} \simeq l_{hl}$), whereas for the anisotropic case with $l_{hl} \simeq \varepsilon u_{hl}$ the form of the nucleus changes to an ellipse [see also Brandt (1992b) for a detailed discussion of the shape of the critical nucleus]. The rescaling of the length $l_{hl}$ along the $z$ axis follows trivially from the scaling rule (3.12). The above analysis works in a regime of currents $j > j_d$ such that the presence of other columnar defects is irrelevant, which is the case for $u_{hl}(j) < d_r$. The relation $u_{hl}(j_d) \simeq d_r$ then determines the crossover current density $j_d$,

$$j_d \simeq \frac{\xi}{d_r} \frac{\varepsilon_r(T)}{\varepsilon_0} j_0 . \quad (9.108)$$

At $j \simeq j_d$, the activation energy $U(j_d)$ becomes equal to the mean kink energy

$$E_k \simeq d_r \sqrt{\varepsilon_l \varepsilon_r(T)} , \quad (9.109)$$

and hence we can write instead of (9.107)

$$U_{hl}(j) \simeq E_k \frac{j_d}{j} , \quad j_d < j \ll j_c . \quad (9.110)$$

The half-loop barrier increases with decreasing current density $j$, and hence the system exhibits a glassy response ($\mu = 1$) with a strongly nonlinear current-voltage characteristic,

$$E \propto \exp \left[ -\frac{E_k}{T} \frac{j_d}{j} \right] , \quad j_d < j \ll j_c . \quad (9.111)$$

For strongly anisotropic (layered) material such as the Bi- and Tl-based compounds, the size $l_{hl}(j > j_d)$ $< d_r \sqrt{\varepsilon_l/\varepsilon_r(T)}$ of the critical nucleus can drop below the interlayer distance $d$, resulting in (nonglassy) creep and thermal depinning of individual pancakes (see also Brandt, 1992a, 1992b).

A more quantitative analysis of the liberation of a single vortex from a columnar defect can be done by mapping the problem to the quantum mechanics of a charged particle in two dimensions, trapped by a compact defect and subject to an electric field. The problem is analogous to that encountered above in the discussion of the liberation of a vortex from twin boundaries; see Sec. A.4. We shall not go into the details of the calculation here, which proceeds along the same lines, but merely give the result for the activation probability of the vortex line per unit length,

$$w \approx \frac{\sqrt{2\pi}}{3\sqrt{3}} \frac{j}{j_0} \frac{1}{\varepsilon\xi} \left[ \frac{\varepsilon_0}{\varepsilon_r(T)} \right]^{1/2}$$

$$\times \exp \left[ -\frac{\sqrt{3}}{\sqrt{2}} \frac{\varepsilon\xi\varepsilon_r(T)}{T} \left[ \frac{\varepsilon_r(T)}{\varepsilon_0} \right]^{1/2} \frac{j_0}{j} \right] . \quad (9.112)$$

The simple estimate (9.111) reproduces the exponential dependence of (9.112) very accurately.

For currents $j \ll j_d$, the transverse displacement $u_{hl}(j)$ of the liberated vortex segment exceeds the mean distance $d_r$ between the rods (see Fig. 47), and the motion of the vortex line from one rod to another takes place via a thermally activated critical nucleus with dimensions $d_r$ (transverse to the columns) and $d_r \sqrt{\varepsilon_l/\varepsilon_r(T)} \ln(j_c/j)$ (along the columns). The *finite* activation energy $U \simeq 2E_k$ is determined by the kink energy $E_k$, as given by Eq. (9.109). The individual kinks have a width $w_k \simeq d_r \sqrt{\varepsilon_l/\varepsilon_r(T)}$, and the logarithmic factor appearing in the longitudinal extent of the critical nucleus has its origin in the weak attraction between the two kinks (see Landauer and Büttiker, 1981; here we shall neglect this logarithmic correction). Since the activation energy for the nucleus is finite for this case, we will not obtain a glassy behavior within this regime. Once such a critical nucleus has been formed, the nucleus expands and the vortex moves to the next rod. Hence the dynamics of an elementary hop from one rod to the next is completely analogous to the motion of the vortex line in a periodic pinning potential, as discussed in Sec. III.E above, if we simply substitute $d_r$ for $u_0$. However, this type of vortex motion is only possible if the neighboring track provides a favorable final state, e.g., one with a lower energy than the original defect. Otherwise, the nucleus cannot expand, and the vortex remains trapped. We then have to consider dispersion in the energy levels provided by the columnar defects. Such a spread in the distribution of trapping energies arises, for example, from randomness in the irradiation process generating the tracks (intrinsic dispersion). Let us assume that the well depths $\varepsilon_r$ are distributed around some mean value $\varepsilon_{r_0}$ with a width $\gamma$.

We then can distinguish between two regimes of small and large dispersion $\gamma$, where the nature of the vortex motion turns out to be quite different. For small dispersion, $\gamma L < E_k$, the activated nucleus can expand, and the motion will proceed via nearest-neighbor hopping. On the other hand, for a large dispersion, $\gamma L > E_k$, the neighboring track does not provide a favorable final state, and the vortex line has to find a better low-energy track a further distance away. The optimal jump will then involve a compromise in finding a good final-state

configuration at a larger distance, while spending the least possible amount of elastic energy for the creation of the nucleus reaching this state. The resulting dynamical behavior of the vortices then shows all the features of the variable-range hopping motion first introduced by Mott (1969) for the description of electronic transport in disordered semiconductors. In the following we discuss these two types of motion in more detail.

Let us first consider the simpler case with weak dispersion, $\gamma L < E_k$. We then can neglect the fluctuations in $\varepsilon_r$ altogether and assume that all rods have the same potential well depth. Disorder is purely structural, with only the distances $d_{\mu\nu}$ being random quantities. The randomness in the distances produces randomness in the activation energies $E_k(d_{\mu\nu}) \simeq d_{\mu\nu}[\varepsilon_l\varepsilon_r(T)]^{1/2}$, and hence the vortex motion is equivalent to the nearest-neighbor percolative hopping conductivity in a 2D semiconductor (see, for example, Shklovskii and Efros, 1984). The resulting vortex velocity and the current-voltage characteristic are given by

$$E \propto j \exp\left[-\frac{c_p E_k}{T}\right], \quad j \ll j_d, \quad (9.113)$$

where the constant $c_p$ is obtained explicitly from 2D percolation theory (Shklovskii and Efros, 1984). With Eq. (9.113) we find that the glassy behavior above $j_d$ is replaced by an ohmic characteristic below $j_d$ if the dispersion $\gamma$ or the sample thickness $L$ is small, $\gamma L < E_k$; hence such a sample is not in a glassy phase. The precise value of $c_p$ depends on the distribution of distances $d_{\mu\nu}$ and on the type of lattice chosen to model the positions of the rods. Assuming a uniform distribution of activation energies $E_k(d_{\mu\nu})$ between zero $(d_{\mu\nu}=0)$ and $2E_k \simeq 2d_r[\varepsilon_l\varepsilon_r(T)]^{1/2}(d_{\mu\nu}=2d_r)$, we obtain a constant $c_p = 1$ if we model the sites of the rods by a square lattice and $c_p = 0.695$ for a triangular lattice; thus we can expect a constant $c_p$ of order unity.

Now let us consider the case of larger samples/larger dispersion, where $\gamma L > E_k$ and small currents $j \ll j_d$. Before discussing the dynamic properties of this system, we wish to analyze in more detail the origin of the dispersion $\gamma$ in the energy well depths. It is interesting to note that in addition to the intrinsic dispersion $\gamma_i$ arising from the randomness of the irradiation process, there is a second intrinsic source of dispersion, of an entropic origin, which arises due to structural disorder in the positions of the irradiation tracks. Consider a thermodynamically large system in equilibrium. A typical equilibrium configuration of a vortex line consists of long straight segments trapped by different rods and interconnected by kinks. The probability per unit length for a kink to occur is proportional to $\exp(-E_k/T)$, hence the mean separation $l_k$ between kinks depends exponentially on the kink energy, $l_k \propto \exp(E_k/T)$. As the kink energy depends on the distance $d_{\mu\nu}$ between the rods, $E_k(d_{\mu\nu}) \simeq d_{\mu\nu}[\varepsilon_l\varepsilon_r(T)]^{1/2}$, the (negative) contribution to the free energy of a vortex line due to the entropy is larg-

est for those vortices localized at two neighboring rods with minimal spacing $d_{\mu\nu}$. The structural disorder in the rod separations $d_{\mu\nu}$ therefore leads to an intrinsic (temperature-dependent) dispersion in the free binding energies for the vortices. The phenomenon described above is an exact transcription of Lifshitz localization in a quantum system, where the breakdown of the resonances and the level repulsion due to the presence of structural disorder lead to the localization of the wave function. We can obtain an estimate for the dispersion $\gamma$ in terms of the bandwidth $t$ appearing in the boson Hamiltonian (9.45) by evaluating the hopping matrix element $t_{\mu\nu}$ for a typical distance $d_{\mu\nu} \simeq d_r$ between the rods and at high temperatures where tunneling is effective,

$$t(d_r) \simeq \varepsilon_r(T)\left[\frac{T}{E_k}\right]^{1/2} e^{-cE_k/T}. \quad (9.114)$$

The dispersion $\gamma$ then is given by the combination of the site disorder $\gamma_i$ and the structural disorder $t(d_r)$,

$$\gamma \simeq \gamma_i + t(d_r). \quad (9.115)$$

The dispersion $\gamma$ in the well energies gives rise to a variable-range hopping (VRH) transport of the vortex lines, similar to the phenomenon of the quantum VRH conductivity in a doped semiconductor (Mott, 1969; Ambegaokar, Halperin, and Langer, 1971; Shklovskii, 1972a; Shklovskii and Efros, 1984). This variable-range hopping concept can be applied to the charge carriers in a doped semiconductor, as originally done by Mott (1969), or, alternatively, we can derive all the results remaining always in the vortex picture. Since below we wish to generalize Mott's idea to take into account interaction effects (Coulomb gap; see, for example, Shklovskii and Efros, 1984), we choose here to present first a brief description of Mott's original argument. Consider a doped semiconductor with localized impurity states in the gap (without external bias applied). The task is to calculate the mobility of the electrons at the Fermi level. This is determined by optimal hops to unoccupied neighbors. At low temperatures, thermal activation to the conduction band is exponentially suppressed, and the motion proceeds via tunneling. The tunneling probability to a level a distance $r$ away is given by $p_t \propto \exp(-2r/l_{loc})$, with $l_{loc}$ the localization length of the impurity state. The process can happen only if an equal-energy final state is available (dissipation-free tunneling is assumed). Such unoccupied equal-energy states are rare, and hence the hop necessarily involves a large distance $r$. On the other hand, thermal activation followed by a tunneling process to a closer state involving an energy difference $\delta E$ enhances $p_t$ but reduces the total probability by the thermal factor $\exp(-\delta E/T)$. The optimal hop arises out of competition between the tunneling component and the thermal activation process. The missing energy $\delta E$ depends on the jump distance. Within the volume $r^d$ the number of available states per energy interval is $gr^d$, where $g$ denotes the density of states at the Fermi level. The

mean level separation within this volume then is $\delta E(r) \simeq 1/gr^d$, and the optimal hop is obtained by maximizing the total probability (per unit time) $p \simeq \nu \exp[-2r/l_{loc} - \delta E(r)/T]$ with respect to the distance $r$. The result for the optimal hopping distance is $r_{opt} \simeq (l_{loc}/gT)^{1/(d+1)}$. Defining the diffusion coefficient $D \simeq p(r_{opt})r_{opt}^2$, one obtains the famous Mott conductivity law $\sigma \propto \exp[-(T_o/T)^{1/(d+1)}]$ via the usual Einstein relation $\mu = eD/T$ for the mobility $\mu$.

The above hopping mechanism can be *transcribed* to the problem of vortex creep in the presence of columnar defects; on the other hand, we can equally well derive the same results while always remaining in the vortex picture. Let us briefly go through the derivation. Whereas the original conductivity problem involves the electrons located at the Fermi level, in the vortex system the VRH motion involves the most weakly bound flux lines with all the lower-energy states filled (here we again assume that repulsive intervortex interaction effectively excludes double occupancy of pinning sites). The vortex motion requires hopping of a vortex segment (via double superkink formation; see Fig. 47) to an optimal, in general distant, defect with nearly the same energy. The activation energy involved in the hopping process is given by $2u[\varepsilon_l \varepsilon_r(T)]^{1/2} \simeq 2(u/d_r)E_k$, with $u$ the distance to the chosen rod. This term is also an exact transcription of the tunneling term $2r/l_{loc}$ in the original Mott problem (the kinks along the $z$ axis correspond to the imaginary-time tunneling paths in the particle problem). The characteristic energy difference between initial and final vortex states is given by $\delta E \simeq L/gu^2$, with $g$ the density of states that has to be determined from the Hamiltonian (9.45) (alternatively we can use the transcription $T \rightarrow 1/L$ between the bosons and vortices to arrive at the same result). A simple estimate for the density of states $g$ is given in terms of the energy dispersion $\gamma$ [see Eq. (9.115)],

$$g \simeq \frac{1}{\gamma d_r^2} \ . \tag{9.116}$$

The optimal jump distance is found by minimizing the effective free energy,

$$\mathcal{F}[u] = 2\frac{u}{d_r}E_k + \frac{L}{gu^2} \ , \tag{9.117}$$

giving

$$u_{Mott}(L) \simeq \left[ \frac{Ld_r}{gE_k} \right]^{1/3} \simeq d_r \left[ \frac{\gamma L}{E_k} \right]^{1/3} \tag{9.118}$$

and the corresponding energy

$$U_{Mott}(L) \simeq 2E_k \frac{u_{Mott}(L)}{d_r} \simeq 2E_k \left[ \frac{\gamma L}{E_k} \right]^{1/3} \ . \tag{9.119}$$

Let us go one step further and generalize these results to the case in which the system is driven by an applied

current density $j$. The corresponding semiconductor transport problem involves an electric field leading to a nonlinear current-voltage characteristic, investigated first by Shklovskii (1972b). Here we present the derivation in the vortex picture: The energy involved in the creation of a loop of dimensions $u$ (hopping distance) and $l$ (hopping segment) takes the form

$$\mathcal{F}[u,l] = 2\frac{u}{d_r}E_k + \frac{l}{gu^2} - \frac{\Phi_o}{c}jul \ . \tag{9.120}$$

The critical loop size has been reached when both forces $\partial_u \mathcal{F}$ and $\partial_l \mathcal{F}$ turn negative. First consider the condition $\partial_l \mathcal{F} = 1/gu^2 - \Phi_o ju/c = 0$, saying that the loop can expand along the $z$ axis as soon as the current density $j$ can provide the "missing energy" $L/gu^2$. We then obtain the current-dependent hopping distance

$$u_{VRH}(j) \simeq \left[ \frac{c}{g\Phi_o j} \right]^{1/3} \simeq d_r \left[ \frac{j_v}{j} \right]^{1/3} \ , \tag{9.121}$$

with the current density $j_v$ given by

$$j_v = \frac{c}{g\Phi_o d_r^3} \simeq \frac{\xi}{\varepsilon_o g d_r^3}j_o \ . \tag{9.122}$$

The activation energy for the hop depends only on the hopping distance $u_{VRH}$,

$$U_{VRH}(j) \simeq E_k \left[ \frac{j_v}{j} \right]^{1/3} \ . \tag{9.123}$$

Second, we have to make sure that the loop does not collapse in the transverse direction. The condition $\partial_u \mathcal{F} = 2E_k/d_r - 2l/gu^3 - \Phi_o jl/c = 0$ then defines the critical length $l_{VRH}$ of the loop

$$l_{VRH}(j) \simeq l_{hl}(j) \simeq L\frac{j_L}{j} \simeq d_r \frac{E_k}{d_r \varepsilon_r} \frac{j_d}{j}, \quad j_L < j \ , \tag{9.124}$$

with the current density $j_L$ given by

$$j_L \simeq \frac{cE_k}{d_r \Phi_o L} \simeq \frac{\xi}{L} \frac{E_k}{d_r \varepsilon_o}j_o \ . \tag{9.125}$$

As the current density $j$ drops below $j_L$, the sample width $L$ cuts off the loop, and we obtain a crossover to the ohmic Mott regime. Note that by inserting Eq. (9.125) into (9.123) we recover the original Mott law (9.119), using a derivation based solely on the vortex picture.

In summary, at high current densities, $j_L < j$, the vortex motion involves the creation of a critical loop of dimensions $u_{VRH}$ and $l_{VRH}$ requiring an activation energy $U_{VRH}$ and producing a non-Ohmic current-voltage characteristic

$$E \propto \exp\left[ -\frac{E_k}{T} \left[ \frac{j_v}{j} \right]^{1/3} \right], \quad j_L < j \ . \tag{9.126}$$

For small current densities, $j < j_L$, on the other hand, the vortex has to be thermally activated to its final state a

distance $u_{\mathrm{Mott}}$ away, and the barrier $U_{\mathrm{Mott}}$ does not depend on the current density $j$, resulting in an ohmic current-voltage characteristic

$$E \propto j \exp\left[-\left[\frac{L}{L_T}\right]^{1/3}\right], \quad j < j_L, \tag{9.127}$$

with

$$L_T \simeq \frac{T^3}{\gamma E_k^2}. \tag{9.128}$$

As $L \to \infty$ in the thermodynamic limit, $j_L \to 0$, and glassiness [Eq. (9.126)] with the characteristic exponent $\mu = \frac{1}{3}$ extends down to vanishing current densities.

The crossover between the variable-range hopping regime at low current densities and the half-loop regime at high current densities depends on the ratio $j_d/j_v \simeq \varepsilon_r(T)d_r^2 g \simeq \varepsilon_r(T)/\gamma$. For a *strongly dispersive* situation with $\varepsilon_r(T)/\gamma < 1$, the activation energy for the VRH process drops below the activation energy for the half-loop process at the crossover current density $j_{xs}$,

$$j_{xs} \simeq \left[\frac{\varepsilon_r(T)}{\gamma}\right]^{1/2} j_d \simeq \left[\frac{\varepsilon_r(T)}{\gamma}\right]^{3/2} j_v, \tag{9.129}$$

with $j_{xs} < j_d < j_v$; hence the crossover from half-loops to VRH takes place below $j_d, j_v$. For small sample thickness, $L < L_{xs} = l_{\mathrm{hl}}(j_{xs}) = w_k[\gamma/\varepsilon_r(T)]^{1/2}$, and small current densities, $j < j_L$, the creep process involves a rigid translation of a vortex segment [the activation energy $L\varepsilon_r(T)$ for a rigid translation is smaller than the half-loop activation energy $E_k(j_d/j)$ up to lengths $L_{xs}$]. No nearest-neighbor hopping regime exists in the strongly dispersive case. The various creep regimes are summarized in Fig. 48.

For the case of *weak dispersion* with $\varepsilon_r(T)/\gamma > 1$, we have the sequence $j_v < j_d < j_{xs}$, and the VRH activation energy drops below the half-loop energy even above $j_v, j_d$. However, the hopping distance needed in the process of superkink formation becomes large enough $(u_{\mathrm{VRH}} > d_r)$ only below $j_v$, and thus the crossover between the VRH and half-loop regimes takes place only at $j_v$. For small enough sample length, $L < E_k/\gamma = w_k[\varepsilon_r(T)/\gamma]$, a nearest-neighbor hopping regime is realized. Here $w_k \simeq E_k/\varepsilon_r(T)$ is the extent of an individual kink along the vortex axis. This nearest-neighbor hopping regime extends down to the length $L \simeq w_k$, below which creep again proceeds via a rigid translation of vortices. Note that $l_{\mathrm{hl}}(j_d) \simeq w_k$ and $l_{\mathrm{hl}}(j_v) \simeq w_k[\varepsilon_r(T)/\gamma]$. The creep regimes for the weakly dispersive situation are illustrated in Fig. 49.

Finally, let us return to the original free energy (9.120) and consider the effect of vortex-vortex interactions. For large hopping distances $u$ we have to account for the competition between the shear energy $\varepsilon_o(u/a_o)^2$ involving neighboring vortices and the disorder energy $1/gu^2$. The crossover to the regime where vortex interactions become relevant takes place as the hopping distance $u$

grows beyond the value

$$u_b \simeq \sqrt{a_o d_r}\left[\frac{\gamma}{\varepsilon_o}\right]^{1/4}, \tag{9.130}$$

producing a crossover current density

$$j_{xb} \simeq \left[\frac{d_r}{a_o}\right]^{3/2}\left[\frac{\varepsilon_o}{\gamma}\right]^{3/4} j_v \simeq \left[\frac{d_r}{a_o}\right]^{3/2}\left[\frac{\gamma\varepsilon_o}{\varepsilon_r^2(T)}\right]^{3/4} j_{xs} \tag{9.131}$$

and a crossover length

$$L_b \simeq \frac{E_k}{\gamma}\left[\frac{a_o}{d_r}\right]^{3/2}\left[\frac{\gamma}{\varepsilon_o}\right]^{3/4}. \tag{9.132}$$

The two criteria match at the boundary $j_L(L), j_L(L_b) \simeq j_{xb}$; see Figs. 48 and 49.
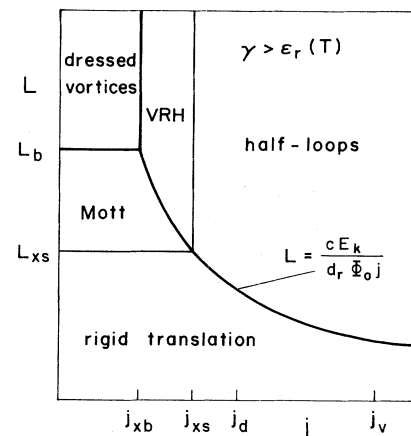
FIG. 48. Creep diagram for the strongly dispersive case $\gamma > \varepsilon_r(T)$. For large currents and not too thin samples, the creep motion proceeds through the generation of half-loop excitations. When the current density is decreased at small sample length, $L < L_{xs} = w_k[\gamma/\varepsilon_r(T)]^{1/2}$, the energy for the half-loop excitation grows beyond that for a rigid translation and creep proceeds via rigid motion of vortex segments. When the current density is decreased at large sample size, $L > L_{xs}$, the half-loop excitations extend beyond the separation $d_r$ between rods, and creep proceeds via the variable-range hopping (VRH) mechanism, where the vortex chooses an optimal neighbor. At even smaller current densities it is more profitable to provide the missing energy $L/gR^2$ through thermal activation of the vortex line rather than via the Lorentz-force, and the system enters the Mott regime. Finally, the interactions between the vortex lines become important as the hopping distance grows beyond the critical value $u_b \simeq \sqrt{a_o d_r}(\gamma/\varepsilon_o)^{1/4}$. These interactions can be accounted for via a renormalization of the density of available pinning sites (Coulomb gap), leading to the notion of "dressed" vortices. Here $E_k = d_r\sqrt{\varepsilon_l\varepsilon_r(T)}$ is the kink energy, $j_d$ and $j_v$ are the relevant current scales for half-loop and VRH motion, $j_{xs}$ is the crossover current density where the half-loop activation energy grows beyond the VRH activation energy, and at the crossover current density $j_{xb}$ the transverse loop size has reached the critical distance $u \simeq u_b$ where interactions between the vortices become relevant.
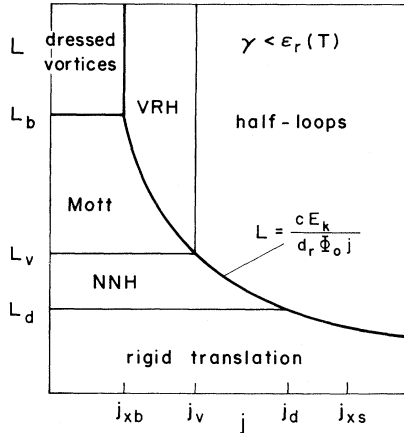
FIG. 49. Creep diagram for the weakly dispersive case $\gamma < \varepsilon_r(T)$. An additional intermediate regime arises for sample lengths $L_d = w_k < L < L_v = w_k[\varepsilon_r(T)/\gamma]$, where creep proceeds via nearest-neighbor percolative hopping. Here $w_k$ is the extent of a kink along the vortex axis.

Once the hopping distance increases beyond $u_b$ we cannot neglect the interaction between the vortices any longer. In this case we have to take into account the presence of the neighboring vortices in our description of vortex creep, and we refer the reader to the discussion following Eq. (9.150), where interaction effects are discussed in more detail.

At very low temperatures the possibility of quantum creep arises, and we briefly discuss this possibility before turning to large magnetic fields and interaction effects. We first consider the case of a half-loop nucleus. For dissipative dynamics we determine the tunneling time $t$ by balancing the dynamic term $\eta_l u^2/t$ against the elastic energy $\varepsilon_l u^2/l^2$, thus relating the tunneling time $t$ to the length $l$ of the half-loop,

$$t_{hl} \simeq \frac{\eta_l}{\varepsilon_l} l_{hl}^2 .$$ (9.133)

The length $l$ is given by Eq. (9.105). Combining Eq. (9.133) and the half-loop energy (9.107) we obtain the action

$$S_E^{\text{eff},c}(j) \simeq t_{hl} U_{hl} \simeq S_{hl} \left[ \frac{j_0}{j} \right]^3 ,$$ (9.134)

with $S_{hl} \simeq (\hbar/e^2)(\varepsilon \xi/\rho_n)$. Here we have used $\varepsilon_r \simeq \varepsilon_0$ at the low temperatures where quantum tunneling is relevant. At low current densities a crossover to the variable-range tunneling regime takes place. The action for the tunneling process then is given by the expression $S_E^{\text{eff}} \simeq v_{\max}^{-1} \varepsilon_r l_{\text{VRH}} u_{\text{VRH}}$, with the short-wavelength limit of the velocity determined by the tunneling process to the neighboring column, $v_{\max} \simeq \varepsilon_0/\eta d_r$ (see Sec. II.A.5). Making use of the results (9.121) and (9.124), we find the tunneling action

$$S_E^{\text{eff},c}(j) \simeq S_{hl} \frac{d_r^3}{\xi^3} \frac{\varepsilon_0}{\gamma} \left[ \frac{j_v}{j} \right]^{4/3} .$$ (9.135)

The two equations (9.134) and (9.135) match at a current density $j'_{xs} \simeq j_v(\varepsilon_0/\gamma)^{6/5}$, marking the crossover from half-loop tunneling to the variable-range tunneling regime. Equation (9.135) differs from that obtained by Vinokur (1993), who followed our earlier approach to the quantum collective creep problem (see the detailed discussion at the end of Sec. II.A.5).

The above results are valid as long as the vortex-vortex interaction is negligible, i.e., within a temperature-field regime bounded by the condition $B < B_{rb}(T)$, as well as for large enough current densities. Our remaining task, then, is to investigate the various regimes where the intervortex interaction dominates the creep process. In close analogy to the discussion of the critical current density in the previous subsection, we have to consider various types of creep—plastic, collective, and CDW-type. We can take advantage of the translation invariance along the $z$ axis and map the present classical 3D creep problem to the problem of quantum creep of a 2D system, where the imaginary-time axis of the quantum problem maps to the $z$ axis of the classical one. The appropriate dynamics for the quantum problem is given by the tilt energy density and hence involves a dispersive mass. Rewriting the free energy for the creation of a nucleus as the action of a 2D quantum creep problem, we obtain the functional [see Eq. (3.180)]

$$\mathcal{F} = \int d^2R \, dz \left\{ \frac{c_{44}}{2} [\partial_z u]^2 + \frac{c_{11}}{2} [\partial_x u]^2 + \frac{c_{66}}{2} [\partial_y u]^2 \right. $$
$$\left. + E_{\text{pin}}(\mathbf{R}, \mathbf{u}) + \bar{E}_{\text{pin}} \right\} .$$ (9.136)

Here the term $\bar{E}_{\text{pin}}$ accounts for the lowering of the vortices' energy as they are trapped in a metastable state of the pinning potential. For the case of plastic pinning, $\bar{E}_{\text{pin}} \simeq c_{66} a_0^2/d_r^2$, whereas for collective pinning $\bar{E}_{\text{pin}} \simeq c_{66} r_p^2/R_c^2$. After replacing the integration over the $z$ axis by one along the displacement $u$, we find that the random potential $E_{\text{pin}}$ drops out of the problem, and we arrive at the following estimate for the activation energy:

$$U_b \simeq \frac{1}{v_{\max}} \bar{E}_{\text{pin}} u R_\parallel R_\perp$$
$$\simeq \sqrt{c_{44} \bar{E}_{\text{pin}}} \, u R_\parallel R_\perp ,$$ (9.137)

where $v_{\max}$ denotes the short-wavelength limit of the "velocity" $|\partial_z u|$,

$$v_{\max} \simeq \left[ \frac{\bar{E}_{\text{pin}}}{c_{44}} \right]^{1/2} .$$

The hopping distance $u$ is determined by the competition between the elasticity of the vortex lattice and the pinning potential. For the case of plastic creep, the next favorable metastable state is a distance $u \simeq a_0$ away,

whereas for a short-range correlated 2D disorder potential the distance to the next optimal state depends on the bundle size $R_\perp$,

$$u(R_\perp) \simeq \begin{cases} u_\circ \left[ \dfrac{R_\perp}{R_\circ} \right]^{2/5} , & u < a_\circ , \\ a_\circ \ln \dfrac{R_\perp}{R_\circ} , & a_\circ < u \end{cases} \qquad (9.138)$$

[see Eq. (3.143), $\zeta_{2,2} = \frac{2}{5}$, and (4.38), $\zeta_{2,2} = 0$; the logarithmic growth of the displacement with increasing distance holds for any dimension $2 \le d < 4$ (Nattermann, 1990)]. The parameters $u_\circ$ and $R_\circ$ depend on the specific situation and a few examples are mentioned below.

The competition between the shear and compression energies determines the relation between the transverse dimensions $R_\perp$ and $R_\parallel$ of the bundle. Following the analysis suggested by Koshelev (1994; see also the discussion in Sec. IV.B.2), we can estimate the compression energy involved in the hop: Taking the 2D limit $L^b \to \infty$ in the compression modulus (4.124b) we find

$$\mathcal{E}_{\text{comp}} \simeq \frac{\hat{c}_{11}}{\lambda^2} \int d^2r \, d^2r' e^{-|\mathbf{r}-\mathbf{r}'|/\lambda} \ln(|\mathbf{r}-\mathbf{r}'|/\xi)(\nabla \mathbf{u})(\nabla' \mathbf{u})$$

from which we obtain the following result for the bundle size $R_\parallel$,

$$R_\parallel \simeq \begin{cases} \dfrac{R_\perp^3}{a_\circ^2} , & a_\circ < R_\perp < (a_\circ^2 \lambda)^{1/3} , \\ \left[ \dfrac{\lambda R_\perp^3}{a_\circ^2} \right]^{1/2} , & (a_\circ^2 \lambda)^{1/3} < R_\perp < \lambda , \\ \dfrac{\lambda}{a_\circ} R_\perp , & \lambda < R_\perp . \end{cases} \qquad (9.139)$$

Finally, the required elastic energy $c_{66} u^2/R_\perp^2$ has to be provided by the energy gain from the Lorentz force, allowing us to relate the various lengths to the driving current density $j$,

$$R_\perp \simeq \sqrt{u} \, \xi \left[ \frac{j_\circ}{j} \right]^{1/2} . \qquad (9.140)$$

The creep process for vortex bundles in the presence of columnar disorder is illustrated in Fig. 50. As usual, dispersion in the elastic moduli $c_{44}(\mathbf{k})$ and $c_{11}(\mathbf{k})$ has to be taken into account (note, however, that $c_{44}$ involves the smallest length scale in the problem, whereas the dispersion in $c_{11}$ involves the larger scales $R_\perp$ and $R_\parallel$).
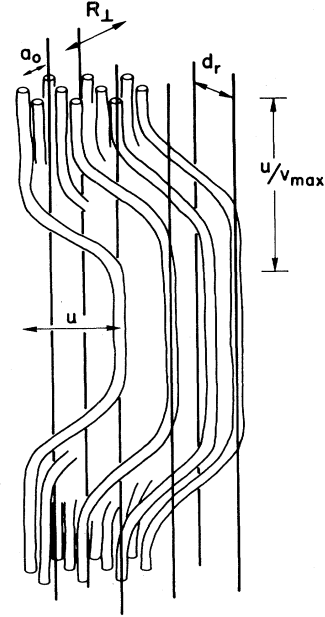


FIG. 50. Double-kink configuration for the creep of vortex bundles. The jump length $u$ is determined by the distance between optimal 2D configurations and scales with the bundle dimension $R_\perp$ like $u \propto R_\perp^{\zeta_{2,2}}$. The kink shape is determined by the competition between the tilt and the pinning energy density. The Lorentz force balances the energy difference between the initial and final states of the vortex bundle arising from the shear deformation of the 2D bundle. Once the double-kink configuration has been created, the nucleus expands and the bundle moves to the final state.

Let us first consider the case of plastic creep which is realized at high fields and low temperatures. Using $u \simeq a_\circ$ in Eq. (9.140) we obtain the following relation between the transverse dimension $R_\perp$ and the current density $j$:

$$R_\perp(j) \simeq d_r \left[ \frac{j_{\text{pl}}}{j} \right]^{1/2} , \qquad (9.141)$$

with $j_{\text{pl}} \simeq (a_\circ \xi / d_r^2) j_\circ$ the plastic critical current density found above, Eq. (9.97). Taking the dispersion in $c_{44}$ and $c_{11}$ into account $[c_{44}(1/d_r) \simeq \varepsilon^2 \varepsilon_\circ d_r^2/a_\circ^4]$ and using Eq. (9.137) we find the plastic barrier

$$U_{\text{pl}}(j) \simeq \varepsilon \varepsilon_\circ d_r \left[ \frac{B}{B_{\text{rb}}} \right]^{3/2} \left[ \frac{j_{\text{pl}}}{j} \right]^2 . \qquad (9.142)$$

For larger bundles with $(a_\circ^2 \lambda)^{1/3} < R_\perp < \lambda$ and in the nondispersive regime $R_\perp > \lambda$ the corresponding results are

$$U_{\text{pl}}(j) \simeq \begin{cases} \varepsilon \varepsilon_\circ d_r \left[ \dfrac{\lambda}{d_r} \right]^{1/2} \dfrac{B}{B_{\text{rb}}} \left[ \dfrac{j_{\text{pl}}}{j} \right]^{5/4} , & (a_\circ^2 \lambda)^{1/3} < R_\perp < \lambda , \\ \varepsilon \varepsilon_\circ \lambda \dfrac{B}{B_{\text{rb}}} \dfrac{j_{\text{pl}}}{j} , & R_\perp > \lambda . \end{cases} \qquad (9.143)$$

Note that plastic creep crosses over to collective—in fact CDW-type—creep when $R_\perp > d_r$.

Second, we turn to collective creep of vortex bundles. Combining Eqs. (9.140) and (9.138), we can relate the transverse bundle dimension $R_\perp$ to the current density $j$,

$$R_\perp(j) \simeq R_0 \left[ \frac{j_{xb}}{j} \right]^{5/8} , \qquad (9.144)$$

where the (crossover) current density $j_{xb}$ can be expressed in terms of $u_0$ and $R_0$,

$$j_{xb} \simeq \frac{\xi u_0}{R_0^2} j_0 . \qquad (9.145)$$

Again, taking the dispersion in the elastic moduli into account (we assume here that $R_c < \lambda/\varepsilon$ and hence $c_{44}(1/R_c) \simeq \varepsilon^2 \varepsilon_0 R_c^2/a_0^4$ ) and making use of Eq. (9.137), we obtain the activation energy in terms of the parameters $u_0$, $R_0$, and $j_{xb}$,

$$U(j) \simeq \varepsilon \varepsilon_0 r_p \frac{u_0 R_0^4}{a_0^5} \begin{cases} \left[ \dfrac{j_{xb}}{j} \right]^{11/4} , & a_0 < R_\perp < (a_0^2 \lambda)^{1/3} , \\[2ex] \left[ \dfrac{a_0^2 \lambda}{R_0^3} \right]^{1/2} \left[ \dfrac{j_{xb}}{j} \right]^{29/16} , & (a_0^2 \lambda)^{1/3} < R_\perp < \lambda , \\[2ex] \dfrac{a_0 \lambda}{R_0^2} \left[ \dfrac{j_{xb}}{j} \right]^{3/2} , & \lambda < R_\perp . \end{cases} \qquad (9.146)$$

Finally, for the CDW-type creep the corresponding expressions for the transverse bundle dimension $R_\perp(j)$ and for the crossover current density $j_{xb}$ are

$$R_\perp(j) \simeq R_0 \left[ \frac{a_0}{u_0} \right]^{5/2} \left[ \frac{j_{xb}}{j} \right]^{1/2} \qquad (9.147)$$

with

$$j_{xb} \simeq \frac{a_0 \xi}{R_0^2} \left[ \frac{u_0}{a_0} \right]^5 j_0 \qquad (9.148)$$

(we neglect logarithmic corrections here and in the following). When calculating the activation energy, one needs to be careful from which regime the CDW-type creep is entered. Coming from the collective creep regime the activation energy is given by the expression

$$U(j) \simeq \varepsilon \varepsilon_0 r_p \frac{R_0^4}{a_0^4} \begin{cases} \left[ \dfrac{a_0}{u_0} \right]^{10} \left[ \dfrac{j_{xb}}{j} \right]^2 , & a_0 < R_\perp < (a_0^2 \lambda)^{1/3} , \\[2ex] \left[ \dfrac{a_0^2 \lambda}{R_0^3} \right]^{1/2} \left[ \dfrac{a_0}{u_0} \right]^{25/4} \left[ \dfrac{j_{xb}}{j} \right]^{5/4} , & (a_0^2 \lambda)^{1/3} < R_\perp < \lambda , \\[2ex] \dfrac{a_0 \lambda}{R_0^2} \left[ \dfrac{a_0}{u_0} \right]^5 \dfrac{j_{xb}}{j} , & \lambda < R_\perp . \end{cases} \qquad (9.149)$$

Entering the CDW-type creep region from the plastic creep regime we have to substitute the plastic deformation energy $\overline{E}_{pin} \simeq c_{66} a_0^2/d_r^2$ for $\overline{E}_{pin} \simeq c_{66} r_p^2/R_c^2$. The result (9.149) then is still applicable if we choose $r_p \simeq a_0$ for the pinning length. If $R_c > \lambda/\varepsilon$ the tilt modulus is no longer dispersive, and Eqs. (9.146) and (9.149) have to be multiplied by the factor $\lambda/\varepsilon R_c$; as expected, the anisotropy drops out (the corresponding crossover for the plastic → CDW creep regime when $d_r > \lambda/\varepsilon$ is rather unrealis-

tic as the appropriate irradiation doses turn out to be extremely small).

Let us consider a few prominent examples of the above general results. At high fields, $B > B_{rb}$, we start out from the bundle pinning regime. At low temperatures, plastic creep involves displacements $u_0 \simeq a_0$ and we obtain a crossover to CDW creep with decreasing current density. Using Eq. (9.149) with $u_0 \simeq a_0$, $R_0 \simeq d_r$, and $j_{xb} \simeq j_{pl}$ we reproduce the result (9.142) for the CDW creep regime.

For large temperatures $T > T_{dp}^r$, creep starts out from the collective pinning regime with $u_o^2 = \langle u^2 \rangle_{th} \simeq a_o r_r (T/\tilde{T}_{dp}^r)$, $R_o = R_c \simeq d_r \langle u^2 \rangle_{th}^{3/2}/a_o r_r^2$, producing [see (9.145)] the crossover current density $j_{xb} \simeq j_c$. The collective creep barrier at high temperatures $T > T_{dp}^r$ and fields $B > B_{rb}(T)$ then takes the form

$$U(j) \simeq T \frac{B}{B_{rb}(T)} \left[ \frac{j_c}{j} \right]^{11/4} , \qquad (9.150)$$

where we have again dropped small logarithmic corrections. With decreasing current density the barrier changes according to the general results (9.146) and (9.149). The derivation of the activation barriers for the high-field creep problem producing Eqs. (9.142), (9.146), and (9.149) differs from that presented by Nelson and Vinokur (1993) based on our previous approach to the quantum collective creep problem (see the detailed discussion at the end of Sec. II.A.5).

Finally, let us turn to low fields with $B < B_{rb}(T)$. Here we concentrate on the low-temperature regime, where each vortex is individually pinned by a single defect. For small current densities, $j < j_{xb}$ [see Eq. (9.131)], and thick samples, $L > L_b$ [see Eq. (9.132)], we have to take into account in our description of variable-range hopping of vortex lines the interaction effects between the vortices. Usually the presence of other vortices has been accounted for by going over to the creep of vortex bundles; see Sec. IV.B.3. However, in the present (weak-field) situation the pinning potential is neither weak nor short-range correlated, and a straightforward generalization of the conventional approach seems difficult. Alternatively, we can appeal to the previously mentioned equivalence between the present vortex creep problem and the problem of hopping conductivity in a doped semiconductor. In the latter case the interaction between charged particles is taken into account by a renormalization of the density of states near the Fermi surface, leading to the appearance of a Coulomb gap (see, for example, Shklovskii and Efros, 1984). Similarly, we can treat the interaction with other vortices in the present case by an appropriate renormalization of $g$. Let us briefly repeat the original Coulomb gap argument for a general algebraic interaction $V^{int}(r) = V_o (r_o/r)^\sigma$ between the particles. An excitation involving displacement of a particle by a distance $r$ (equivalent to creating a particle-hole excitation of extent $r$) involves an energy $\delta E - V_o (r_o/r)^\sigma > 0$, with $\delta E$ the difference between the single-particle energies. An upper bound on the density of states within a bandwidth $\delta E$ is then given by $n \simeq 1/r^d \simeq (\delta E/V_o)^{d/\sigma}/r_o^d$. Taking the derivative with respect to $\delta E$, we obtain the density of states $g(\delta E) \simeq g_o (\delta E/V_o)^n$ with $g_o \simeq 1/V_o r_o^d$ and $n = d/\sigma - 1 > 0$. For a Coulomb interaction, $\sigma = 1$ and $g(\delta E)$ is strongly suppressed at low excitation energies (Coulomb gap ), so that $g \propto (\delta E)^2$ ($g \propto |\delta E|$) in $d = 3$ ($d = 2$) dimensions. Repeating the Mott argument with this energy-dependent density of states, we find that the optimal hopping distance takes the form

$r_{opt} \simeq l_{loc}(V_o/T)^{(n+1)/(n+1+d)}(r_o/l_{loc})^{d/(n+1+d)}$. [The missing energy $\delta E(r)$ to be paid in a hop of range $r$ is determined by the relation $\delta E(r) \simeq 1/g(\delta E)r^d$, and we obtain $\delta E(r) \simeq V_o(g_o V_o r^d)^{-1/(n+1)}$; the optimal distance is obtained by minimizing the expression $2r/l_{loc} - \delta E(r)/T$.] For $n = 0$ we reproduce the result for the noninteracting case, whereas we obtain the simple expression $r_{opt} \simeq l_{loc}(V_o/T)^{1/(1+\sigma)}(r_o/l_{loc})^{\sigma/(1+\sigma)}$ independent of the dimension $d$ for the interacting case.

Going over to the vortex problem, we should replace the algebraic form of the interaction by a logarithmic one and correspondingly take the limit $\sigma = 0$ in the above relations. The interaction energy and distance scales are given by $V_o \simeq c_{66}u_b^2 \simeq \varepsilon_o(u_b/a_o)^2$ and $r_o \simeq d_r$, with the hopping distance $u_b$ at crossover given by Eq. (9.130). The asymptotic density of states remains $g(\delta E > V_o) = g_o \simeq 1/\gamma d_r^2$. The optimal hopping distance then is found to be (note that $\hbar/T \to L$)

$$u_{Mott}(L) \simeq u_b \frac{L}{L_b}, \quad u_b < u_{Mott} , \qquad (9.151)$$

with the crossover length $L_b$ given by Eq. (9.132). Equation (9.151) replaces (9.118) for the noninteracting case as the hopping distance grows beyond $u_b$. Similarly, we can generalize Eq. (9.121) to the interacting case [the missing energy $\delta E(r) \to c_{66}u_b^2(u_b/u)^{2/(n+1)}$ now is provided by the Lorentz force and $u_{VRH}(j) \propto j^{-(n+1)/(n+1+d)}$] and obtain

$$u_{VRH}(j) \simeq u_b \frac{j_{xb}}{j}, \quad u_b < u_{VRH} , \qquad (9.152)$$

with the crossover current density $j_{xb}$ given by Eq. (9.131). The crossover current density separating the ohmic Mott regime from the non-ohmic VRH regime is given again by $j_L$; see Eq. (9.125). The activation energies for the creep of these "dressed" vortices take the form

$$U_{Mott}(L) \simeq U_{Mott}(L_b) \frac{L}{L_b}, \quad L_b < L , \qquad (9.153)$$

and

$$U_{VRH}(j) \simeq U_{VRH}(j_{xb}) \frac{j_{xb}}{j}, \quad j < j_{xb} , \qquad (9.154)$$

generalizing the results (9.119) and (9.123) to the interacting case. The increase of the exponents from $\frac{1}{3}$ to unity is a consequence of the vortex interactions. Instead of isolated vortex hops, the creep in the present regime leads to a rearrangement of the environment, producing the "dressing" of the hopping vortex. The situation is similar to the creep of vortex bundles; however, in the present case, the excitation involves a plastic deformation of the lattice. This concludes our discussion of creep in the interacting vortex system.

Let us make a few concluding remarks. Equation (9.127) for the *resistivity* in the system looks like the original Mott law for the *conductivity* in the semiconducting

analog. In fact, it turns out that using the transcription

| 2D bosons | $\leftrightarrow$ | Vortices |
|---|---|---|
| $\sigma$ | $\leftrightarrow$ | $\rho$ |
| $E$ | $\leftrightarrow$ | $j$ |
| $j$ | $\leftrightarrow$ | $E$ |
| $\hbar$ | $\leftrightarrow$ | $T$ |
| $\hbar/T$ | $\leftrightarrow$ | $L$ |
| $m$ | $\leftrightarrow$ | $\varepsilon_l$ |

$$\text{(9.155)}$$

between the 2D-particle and vortex systems, we can map the results obtained in the particle system to the corresponding results in the vortex system. (Note that the time coordinate in the vortex picture has no analog within the Bose picture, and hence we cannot determine the preexponential factor in any dynamic quantity for the vortices. That is, the determination of dynamic quantities is limited to the saddle-point approximation.) Hence we find that, as long as Bose statistics play no essential role, the mapping of the vortex system to a 2D-particle system works well and produces the correct results irrespective of the boundary conditions.

A second remark concerns an experimental consequence of VRH-type vortex motion. The relevant quantity determining the vortex motion is the kink or superkink energy, which grows with increasing distance between the defects. Hence we obtain the interesting result that the creep rate will *increase* with an increase in the density of rods, as long as the creep is dominated by the hopping transport mechanism. Such an increase in the creep rate with increasing ion fluence has been observed recently by Konczykowski *et al.* (1994).

### 4. Bose-glass transition

In the previous paragraphs we have concentrated on the low-temperature *Bose-glass* phase of the vortex system, which is characterized by the *localization* of the vortex lines onto a single columnar defect or into an assembly of rods. This has to be contrasted with the usual low-temperature *vortex-glass* phase due to the presence of pointlike disorder, which is characterized by the enhanced *wandering* of the vortex lines. According to the analogy between our vortex system and the physics of 2D bosons subject to a (static) disorder potential (Fisher *et al.*, 1989), we expect a phase transition to occur at higher temperatures when the vortex system goes over into an entangled vortex-liquid phase (superfluid bosons). In order to find the position of the phase transition line $B_{BG}(T)$, we have to consider the relative importance of the pinning potential and the interaction between the vortices.

At very low magnetic fields $B \lesssim \Phi_0/\lambda^2$ the intervortex interaction is short range $[V(r) \propto \exp(-r/\lambda)]$, and we can consider the motion of an individual vortex in the presence of columnar tracks. For temperatures $T > T_{dl}$, each vortex is localized within a tube of radius $l_{loc} \simeq d_r(T/\tilde{T}_{dl})^2$; see Eq. (9.74). Delocalization of the vortex lines takes place as these tubes start to overlap with increasing field, providing us with an estimate for the Bose-glass transition line via the condition $a_0 \simeq l_{loc}(T_{BG})$,

$$B_{BG}(T) \simeq \frac{B_\Phi}{Gi^2}\left[\frac{r_r}{\xi(0)}\right]^4\left[\frac{T_c}{T}\right]^4\left[1-\frac{T}{T_c}\right]^4. \tag{9.156}$$

At higher fields, $B > \Phi_0/\lambda^2$, Eq. (9.79) shows that close to the "melting" line the interaction between the vortices is the main energy in the problem. We can then use a perturbative scheme to find the (upward) shift from the melting line in an unirradiated system to the Bose-glass line in the strongly disordered system. As a first step we reformulate the usual Lindemann criterion $\langle u^2(T_m)\rangle \approx c_L^2 a_0^2$ into an equivalent energy criterion.

Consider a vortex trapped in the potential well created by its surrounding neighbors. In the Bose language, the thermal fluctuations of this vortex correspond to the zero-point oscillations of a particle trapped in a well. Within a harmonic approximation $[V(R)=fR^2/2]$ the ground-state energy of the particle (with mass $m$) is given by $\hbar\omega/2$, $\omega=\sqrt{f/m}$, and its fluctuation amplitude is $\langle R^2\rangle \simeq \hbar\omega/f$. For the vortex problem the corresponding quantities are $f \to \varepsilon_0/a_0^2$, $m \to \varepsilon_l$, $\hbar \to T$, $\omega \to \sqrt{\varepsilon_0/\varepsilon_l}/a_0 \approx 1/\varepsilon a_0$, producing a thermal energy

$$\varepsilon_{th} \simeq \frac{T}{\varepsilon a_0} \tag{9.157}$$

and a mean-squared amplitude

$$\langle R^2\rangle \simeq \frac{T}{\varepsilon\varepsilon_0 a_0}a_0^2 . \tag{9.158}$$

The Lindemann criterion $\langle R^2\rangle \approx c_L^2 a_0^2$ produces the melting temperature $T_m \simeq c_L^2 \varepsilon\varepsilon_0 a_0$, in agreement with Eq. (4.105). On the other hand, we can make use of an equivalent energy argument: The vortex lattice melts as the thermal energy $\varepsilon_{th}$ grows beyond the fraction $c_L^2\varepsilon_0$ of the potential barrier $\varepsilon_0$ produced by the neighboring vortices. Indeed, the condition

$$\varepsilon_{th}(T_m) \approx c_L^2\varepsilon_0 \tag{9.159}$$

reproduces the above expression for $T_m$.

The energy criterion (9.159) can now easily be used for an estimate of the shift in the melting line due to columnar disorder. Consider first the weak-field situation with $c_L d_r < a_0 < \lambda$. The presence of columnar defects within the potential well leads to a lowering of the ground-state energy. Within the area $\langle R^2\rangle$ the $\langle R^2\rangle/d_r^2$ defects pro-

duce the pinning energy $\varepsilon_r \sqrt{\langle R^2 \rangle / d_r^2}(b_o^2 / \langle R^2 \rangle)$, where the last factor gives the relative contribution of each trap. The Lindemann criterion then reads

$$\varepsilon_{th}(T_{BG}) \approx \frac{T_{BG}}{\varepsilon a_o} - \frac{\varepsilon_r b_o^2}{d_r \sqrt{\langle R^2 \rangle}} \approx c_L^2 \varepsilon_o , \qquad (9.160)$$

resulting in a Bose-glass line $T_{BG}$ shifted to higher temperatures as compared to the melting temperature $T_m$ in the unirradiated material,

$$T_{BG} = T_m \left[ 1 + \frac{\pi^2}{2} \frac{c_L a_o}{d_r} \frac{\tilde{T}_{dp}^{r2}}{T_m^2} \right] . \qquad (9.161)$$

Rewriting the melting temperature in the form

$$T_m \simeq c_L^2 \frac{a_o}{\xi(0)} \frac{T_c}{\sqrt{Gi}} \left[ 1 - \frac{T}{T_c} \right] \left[ 1 - \frac{B}{H_{c_2}} \right] \qquad (9.162)$$

and making use of Eq. (9.77), we can cast the shift of the melting line in a convenient form containing only a single parameter $\gamma$ describing the effect of disorder,

$$T_{BG}(B) \approx \gamma T_m(B) + (1 - \gamma) T_c \left[ 1 - \frac{B}{H_{c_2}(0)} \right] , \qquad (9.163)$$

with the disorder parameter

$$\gamma = \left[ 1 + \frac{1}{16 c_L \sqrt{Gi}} \frac{r_r^2}{\xi(0) d_r} \right]^{-1} . \qquad (9.164)$$

Equation (9.163) shows all the correct limits, for $\gamma = 1, T_{BG}(B) = T_m(B)$ in the absence of disorder and for $\gamma \to 0, T_{BG}(B) \to T_{c_2}(B)$ in the presence of strong disorder, and is also in good agreement with experiments on irradiated YBCO single crystals (Krusin-Elbaum *et al.*, 1994).

The above analysis is valid as long as the vortex samples many traps within the potential well produced by its neighboring vortices, i.e., as long as $\langle R^2 \rangle \approx c_L^2 a_o^2 > d_r^2$. For higher fields, $a_o < d_r / c_L$, we have either none or of the order of one trap available in each vortex potential well. We then should expect the Bose-glass line to approach the original melting line in a smooth way. The mean energy lowering over many vortices due to the presence of columnar traps is given by $\varepsilon_r(\langle R^2 \rangle / d_r^2)(b_o^2 / \langle R^2 \rangle)$, where the second factor gives the probability of having a defect available and the last factor gives the mean contribution of this defect. Equation (9.163) is then reproduced with a field-dependent parameter $\gamma(a_o)$ given by

$$\gamma(a_o) = \left[ 1 + \frac{1}{16 \sqrt{Gi}} \frac{a_o}{\xi(0)} \frac{r_r^2}{d_r^2} \right]^{-1} \qquad (9.165)$$

At high fields $\gamma(a_o)$ goes to unity, and hence $T_{BG}(B)$ approaches $T_m(B)$. The expected shape for the Bose-glass line is illustrated in Fig. 45.

Next we turn to the scaling properties of the system close to the proposed Bose-glass transition line. At low

enough fields, where the disorder is relevant, we expect that the first-order melting line is replaced by a continuous Bose-glass transition. We can then construct a scaling theory of the dynamical behavior of the system in the vicinity of the transition, in close analogy with the vortex-glass scaling described in Sec. VII.B above. Following Nelson and Vinokur (1992, 1993), we introduce the two diverging length scales

$$l_\perp = l_{loc}(T) \propto (T_{BG} - T)^{-\nu_\perp} \qquad (9.166)$$

and

$$l_\parallel \sim l_\perp^2 / D_o , \qquad (9.167)$$

where $D_o$ is a short-distance "diffusion" constant. Hence we explicitly take into account here the possibility of anisotropic scaling, in contrast to the discussion of the vortex (gauge)-glass scaling in Sec. VII.B. In the simplest scenario, $D_o$ remains finite on approaching the phase transition, so that the scaling exponent of $l_\parallel$ takes the value $\nu_\parallel = 2\nu_\perp$. From numerical simulations (Krauth, Trivedi, and Ceperley, 1991; Sorensen *et al.*, 1992; Wallin *et al.*, 1994) one obtains the estimate $\nu_\perp \approx 1$. Second, we introduce the dynamic scaling exponent $z'$ via $\tau_{BG} \propto l_\perp^{z'}$.

Let us concentrate on the electric response of the system in the critical regime. The appropriate scaling combinations are $El_\perp^{1+z'}$ and $jl_\perp l_\parallel$ (from $E \propto \partial_t A$ and $j \propto \partial_A f$), and we obtain the scaling ansatz for the current-voltage characteristic

$$E \propto l_\perp^{-(z'+1)} e_\pm (jl_\perp^3) , \qquad (9.168)$$

with $e_+(x \to 0) \sim x$, $e_-(x \to 0) \sim \exp(-a / x^{1/3})$, and $e_\pm(x \to \infty) \sim x^\alpha$, $\alpha = (z'+1)/3$. The current-voltage characteristic at the transition is algebraic,

$$E \propto j^{(z'+1)/3} , \qquad (9.169)$$

and the resistivity in the thermally assisted flux-flow regimes vanishes according to

$$\rho \propto (T - T_{BG})^{\nu_\perp (z' - 2)} \qquad (9.170)$$

on approaching the transition. The crossover current densities separating the critical region explored at large current densities from the noncritical glassy (below $T_{BG}$) or TAFF (above $T_{BG}$) regimes at low current densities are

$$j_x^\pm \propto (l_\perp l_\parallel)^{-1} \propto |T - T_{BG}|^{3\nu_\perp} . \qquad (9.171)$$

These results have to be compared with those of the (isotropic) vortex-glass scaling, which read $E \propto j^{(z+1)/2}$, $\rho \propto (T - T_{BG})^{\nu(z-1)}$, and $j_z^\pm \propto |T - T_{BG}|^{2\nu}$, with $z$ and $\nu$ the vortex-glass scaling exponents introduced in Sec. VII.B above.

### 5. Lock-in transition

In close analogy with the lock-in transitions due to intrinsic pinning by the layered structure (Sec. VIII.A.3)

and due to trapping by an array of twin boundaries (Sec. IX.A), a lock-in transition is expected to occur due to the presence of a columnar defect structure. The analysis in the present case is completely analogous to that presented in Sec. IX.A above, and we simply can take over the results: The important quantity driving the singularity in the tilt modulus and leading to the lock-in transition is the linear contribution to the energy density gained from vortex trapping [see Eq. (9.6)],

$$E(\vartheta) \simeq \frac{1}{a_o^2} \sqrt{\varepsilon_l \varepsilon_r(T)} |\vartheta| \ . \tag{9.172}$$

The trapping $(\theta_t)$ and the lock-in angle $\theta_L$ then take the form [see Eq. (9.9)]

$$\theta_t = \left[ \frac{2\varepsilon_r(T)}{\varepsilon_l} \right]^{1/2} \quad \text{and} \quad \theta_L \simeq \frac{4\pi\varepsilon_l}{\Phi_o H} \theta_t \ , \tag{9.173}$$

where both angles are measured from the c axis. In the anisotropic case the trapping angle is larger than in the isotropic case, by a factor $1/\varepsilon$, which is a consequence of the reduced line tension (reduced kink energy) of the vortex lines. The relevant angle for pinning by columnar defects is the trapping angle rather than the lock-in angle. From the larger anisotropy in BiSCCO as compared with YBCO one would expect to find an enhanced angular pinning range due to columnar defects in the BiSCCO material. This expectation is confirmed by the experiments of Thompson et al. (1992) and of Civale et al. (1991), in which the magnetic hysteresis loop was measured for two samples of BiSCCO and of YBCO irradiated under a finite angle $\theta_{cd}$ away from the c axis. Choosing the direction of the magnetic field first to be aligned with the tracks $(\theta_H = \theta_{cd})$ and a second time symmetrically opposed $(\theta_H = -\theta_{cd})$ to the tracks, they found essentially no change in the magnetization loop in the case of the BiSCCO sample, whereas for the case of YBCO the magnetic loop was much reduced when the field was turned away from the columnar defects. Hence one concludes that in the case of BiSCCO the vortices still remain trapped by the defects and pinning remains large. Note that this effect can be easily understood in terms of the scaling approach. After rescaling $(\cot\tilde{\theta} = \varepsilon \cot\theta)$, the angle between the magnetic field and the columnar tracks becomes small and the vortices remain trapped by the columnar defects, even for the case in which the field and the tracks are symmetrically inclined with respect to each other.

The result (9.173) is valid for fields $B < B_{rb}$. At higher fields, $a_o \ll d_r$ and only a fraction of the vortex lines can gain energy from trapping by the columnar defect structure, leading to a reduction in the trapping and lock-in angles.

A further interesting feature is the stability of the Bose-glass phase under small tilts. The locking angle $\theta_L$, Eq. (9.173), translates into a transverse critical field

$$H_{c_1}^\perp = \theta_L H \simeq \frac{\sqrt{\varepsilon_l \varepsilon_r(T)}}{\varepsilon_o} H_{c_1} \tag{9.174}$$

below which the vortex system exhibits a transverse Meissner-Ochsenfeld effect, i.e., a transverse field $H_\perp < H_{c_1}^\perp$ is perfectly screened from the sample. As the Bose-glass transition is approached, the locking angle $\theta_L$ and thus also the transverse critical field $H_{c_1}^\perp$ vanishes according to

$$\frac{\theta_L(T)}{\theta_L} = \frac{H_{c_1}^\perp(T)}{H_{c_1}^\perp} \simeq \left[ 1 - \frac{T}{T_{BG}} \right]^{3\nu_\perp} \ . \tag{9.175}$$

This result follows from the scaling behavior of the transverse field $\mathbf{H}_\perp = \partial \mathbf{A}_\perp / \partial z \propto 1/l_\perp l_\parallel$, with $A_\perp \propto 1/l_\perp$ and $z \propto l_\parallel$, making $H_{c_1}^\perp l_\perp l_\parallel$ the appropriate scaling combination. The resulting cusp in the irreversibility line when traced as a function of angle distinguishes the Bose-glass phase from the vortex-glass phase, for which a smooth behavior is expected.

## X. THERMAL DIFFUSION OF VORTICES

Within the previous sections we have analyzed the dynamic properties of the vortex system on what we call the "microscopic" level. Typical objectives have been to calculate the critical current density $j_c$, separating the linear from the nonlinear part of the current-voltage characteristic, or the characteristic creep barriers $U_c$ or $S_E^{eff}$ for the cases of classical and quantum motion. The present section is devoted to the macroscopic description of the mixed state in type-II superconductors. Our principal objective is to solve the set of dynamic equations that describe the behavior of the vortex system on a macroscopic scale, i.e., on length and time scales exceeding the characteristic scales associated with pinning. The equations we have to deal with are the Maxwell equations

$$\nabla \cdot \mathbf{B} = 0 \ , \tag{10.1a}$$

$$\nabla \wedge \mathbf{E} = -\frac{1}{c} \frac{d\mathbf{B}}{dt} \ , \tag{10.1b}$$

$$\nabla \wedge \mathbf{B} = \frac{4\pi}{c} \mathbf{j} \ , \tag{10.1c}$$

combined with the materials equation $\mathbf{j}(\mathbf{E}, \mathbf{B})$ describing the electromagnetic response of a superconductor, which depends on the dynamic behavior of the vortex system.

The simplest situation is encountered in the flux-flow regime, where the barriers $U$ inhibiting vortex motion can be neglected, $U < T$, and the material can be characterized by the relation

$$E = \rho_{flow}(B) j \ , \tag{10.2}$$

with $\rho_{flow} \simeq \rho_n B / H_{c_2}$. On the other hand, within the activated regime the (creep) barriers are relevant, and the material is conveniently described by the set of equations

$$\mathbf{E} = \frac{1}{c} \mathbf{B} \wedge \mathbf{v} \ , \tag{10.3}$$

$$\mathbf{v} = \mathbf{v}_o e^{-U(j)/T} \ , \tag{10.4}$$

where the activation barriers $U$ additionally can depend on the magnetic field $B$ and on the temperature $T$; see Sec. IV. At very small temperatures Eq. (10.4) is replaced by its quantum analog

$$\mathbf{v} = \mathbf{v}_0 e^{-S(j)/\hbar} , \qquad (10.5)$$

with $S$ the appropriate action describing the tunneling motion of the vortices; see again Sec. IV. Note that the dynamic properties of the vortex system also depend on the time scale under consideration. For example, at high enough frequencies the intervalley motion considered above is replaced by the (dissipative) intravalley response of the vortices. The "microscopic" velocity $v_0$ can be estimated from the critical velocity $v_c = j_c B / c \eta \simeq j_c \rho_{\text{flow}} c / B$, $v_0 = \mathcal{A} v_c$. The numerical factor $\mathcal{A}$ is of order unity for a pointlike object. Its precise structure is as yet unknown for the general problem of an elastic manifold pinned by a random potential; however, based on the analysis of the thermally activated motion of a string in a periodic potential (Büttiker and Landauer, 1981), one would expect that $\mathcal{A}$ increases with the volume of the vortex bundle. A comparison of Eq. (10.4) with (10.5) shows that the two cases of classical and quantum motion are equivalent, and we shall restrict ourselves to thermally activated processes in the following. The results for the case of quantum tunneling can be obtained by the simple replacement $U \leftrightarrow S$ and $T \leftrightarrow \hbar$.

The problem posed by the set of equations (10.1) and (10.2) or (10.4) can be either linear or nonlinear. The crucial parameter distinguishing between these two cases is the quantity

$$\alpha = \left| \frac{\partial U(j)}{\partial j} \right| \frac{\delta j}{T} , \qquad (10.6)$$

where $\delta j$ denotes the typical current scale involved in the problem. For $\alpha \ll 1$, the problem is a linear one and the vortex dynamics is diffusive, whereas in the opposite case, $\alpha \gg 1$, we are confronted with a difficult nonlinear problem. Let us consider the system response at small current densities with both $\delta j$ and $j \simeq \delta j$ small. In an Anderson-Kim-type model with finite activation barriers, we have $\alpha \simeq (U_0 / T)(j/j_c)$, and the response is always linear (diffusive) at small enough current densities $j$. By contrast, for a glassy response $\alpha \simeq \mu U(j)/T$ always becomes large at small current densities $j$, rendering the response highly nonlinear. Below we first concentrate on the simpler linear behavior (Sec. X.A) and then come back to the discussion of the glassy response in Sec. X.B. Throughout the following discussion we should keep in mind that we are always solving the same problem [the set of equations (10.1) and (10.4) plus boundary conditions], but are using different approaches depending on the value of $\alpha$.

## A. Linear response: thermally assisted flux flow

The basic assumption on which the results of this section rely is the finiteness of the activation barrier $U(j)$ in

the small-current-density limit, $U(j \to 0) = U_0 < \infty$. Such behavior of the creep barriers is expected to be realized in a vortex liquid at high temperatures, $T > T_m$ (see Secs. VI.A.2 and VI.B), where the finite barriers against plastic motion cut off the diverging elastic barriers in the vortex system. At small current densities $j \to 0$ we can expand,

$$U(j) \approx U_0 + \frac{\partial U}{\partial j} \bigg|_{j=0} j , \qquad (10.7)$$

and the expression for the thermally activated velocity including both forward (current-assisted) and backward (current-impeded) hops takes the form

$$v = v_0 e^{-U_0/T} 2 \sinh \left[ \frac{\partial U}{\partial j} \bigg|_0 \frac{j}{T} \right] . \qquad (10.8)$$

The smallness of the parameter $\alpha = (\partial U/\partial j)(j/T)$ allows us to expand Eq. (10.8) and combining the result with (10.3) we obtain the ohmic response

$$E = \rho j , \qquad (10.9)$$

$$\rho = \frac{2 v_0 B}{cT} \frac{\partial U}{\partial j} \bigg|_0 e^{-U_0/T} , \qquad (10.10)$$

for a vortex system in the liquid state. When we use $v_0 = \mathcal{A} v_c$ and $(\partial U/\partial j)|_0 \simeq U_0 / j_c$, the result (10.10) further simplifies to

$$\rho \approx 2 \mathcal{A} \rho_{\text{flow}} \frac{U_0}{T} e^{-U_0/T} . \qquad (10.11)$$

With Eq. (10.9) the vortex system develops a diffusive dynamics that has been studied in detail by Kes *et al.* (1989) and by Brandt (1990, 1991, 1992d). The important point to be noted here is that the electrodynamics of a type-II superconductor in the TAFF regime where (10.9) is valid is nothing but the electrodynamics of a normal metal, albeit with an exponentially small resistivity (Geshkenbein, Vinokur, and Fehrenbacher, 1991).

In order to obtain the equation governing the behavior of the magnetic field $B$, we combine the Maxwell equations with Ohm's law and obtain

$$\partial_t B = \frac{c^2}{4\pi} \rho \Delta B . \qquad (10.12)$$

Equation (10.12) is a *linear* diffusion equation determining the spatio-temporal evolution of the magnetic field $B(\mathbf{r}, t)$. In the following we use Eq. (10.12) to analyze the response of a superconductor to the presence of a small ac field. This type of experiment has found widespread use in the field of high-temperature superconductivity as a means of determining the irreversibility line (or, with some provisos, melting line); see, for example, Malozemoff, Worthington *et al.* (1988).

It is well known that the electrodynamics of a normal metal in an ac field is governed by the skin effect; see, for example, Landau and Lifshitz (1959b). Assuming a perturbation $\propto \exp(i\omega t)$, Eq. (10.12) can be written as

$$\Delta B = -\frac{4\pi i\omega}{\rho c^2}B \ ,$$ (10.13)

from which we immediately obtain the basic length scale in the problem,

$$\delta_s = \left[\frac{\rho c^2}{2\pi\omega}\right]^{1/2} \ ,$$ (10.14)

the skin depth. Let us compare $\delta_s$ with the basic length scale of a superconducting electrodynamic response, the London penetration depth $\lambda$. For a BCS superconductor in the dirty limit we have (see Abrikosov, 1988)

$$\frac{\delta_s}{\lambda} = \left[\frac{2\pi\Delta}{\hbar\omega}\frac{\rho}{\rho_n}\tanh\frac{\Delta}{2T}\right]^{1/2} \ ,$$ (10.15)

where $\Delta$ denotes the superconducting gap. For a typical high-temperature superconductor we have $2\Delta \sim 10^{13}$ Hz, whereas typical experimental frequencies are in the range between $10^3$ Hz and $10^7$ Hz. With the resistivity ratio $\rho/\rho_n \sim 10^{-5}$–1 we find $\delta_s \gg \lambda$. Note that our use of the averaged equations (10.9) and (10.13) requires the scale $\delta_s$ to be larger than the microscopic length determining the resistivity. For very high frequencies ($\omega \sim$ GHz) the skin depth $\delta_s$ can drop below the London depth $\lambda$, and we should take the London screening into account. Also, at high frequencies the contribution of the vortices to the system response changes its nature from inter- to intra-valley dominated motion. A detailed analysis of the latter regimes has been given by Brandt (1991b, 1991c), Koshelev and Vinokur (1991), and Coffey and Clem (1991, 1992a, 1992b). Here we restrict ourselves to the low-frequency regime such that $\delta_s \gg \lambda$.

Depending on the value of the resistivity $\rho$ and hence on the temperature, the skin depth $\delta_s$ can be either larger (high-temperature $T$) or smaller (low $T$, small $\rho$) than the sample size. At the temperature where $\delta_s$ becomes of the order of the sample size $d$, the imaginary part of the susceptibility $\chi''$ measuring the absorption of the system develops a maximum. To be specific, let us consider the simplest case of a slab geometry, $0 \leq x \leq d, \mathbf{B}\|z$. Taking into account the boundary conditions $B(x=0,d;t)=h_{ac}\exp(-i\omega t)$ at the sample surfaces, we obtain for the ac component of the magnetic field inside the sample

$$B(x,t)=h_{ac}\frac{e^{ikx}+e^{ik(d-x)}}{1+e^{ikd}} \ ,$$ (10.16)

with $k=(1+i)/\delta_s$. The ac susceptibility $\chi$ is given by

$$4\pi\chi=\frac{1}{h_{ac}d}\int_0^d dx\, B(x)-1 \ ,$$ (10.17)

resulting in the real and imaginary parts

$$4\pi\chi'=\frac{1}{u}\frac{\sinh u+\sin u}{\cosh u+\cos u}-1 \ ,$$

(10.18)

$$4\pi\chi''=\frac{1}{u}\frac{\sinh u-\sin u}{\cosh u+\cos u} \ ,$$

with

$$u=\frac{d}{\delta_s}=\left[\frac{\omega}{\rho}\frac{2\pi d^2}{c^2}\right]^{1/2} \ .$$ (10.19)

In Fig. 51 we plot both $\chi'$ and $\chi''$ as a function of $\rho/\omega$ (as expressed in units of $2\pi d^2/c^2$). The absorptivity $\chi''$ attains a maximum at $u_{\text{peak}}\approx 2.25$, which transforms to the condition

$$\omega_{\text{peak}}\approx 0.8\frac{c^2}{d^2}\rho(H,T)$$ (10.20)

under the use of Eq. (10.19). The physical interpretation of the origin of the peak in $\chi''$ is very simple (Landau and Lifshitz, 1959b). For a large penetration depth $\delta_s \to \infty$ ($\rho$ large, $T$ high), the field penetrates the sample completely and the out-of-phase signal $\chi''$ disappears. In the opposite limit, $\delta_s \to 0$ ($\rho$ small, low temperature), the screening is complete, $\chi' \to -1/4\pi$, and $\chi''$ vanishes again. The result (10.20) contains only the measurable quantities $\omega_{\text{peak}}$, $\rho$, and $d$. Note that the slab geometry applies well to experiments carried out on high-temperature superconductors in the form of *platelike*-shaped single crystals for the case where the ac field is in the *ab* plane. The particular direction of the large dc component of the magnetic field is not important, as it enters the analysis only via the value of the resistivity $\rho(H,T)$.

Equation (10.20) can be used for a contact-free determination of the resistivity $\rho(H,T)$ by means of an ac absorption measurement. When $H$ and $T$ are kept fixed, the position of the peak in $\chi''(\omega)$ corresponds to a definition level of resistivity,

$$\rho(T,H)\approx 1.25\omega_{\text{peak}}\frac{d^2}{c^2} \ ,$$

(10.21)

$$\rho[\mu\Omega\,\text{cm}]\approx 7.6\times 10^{-3}d^2[\text{cm}^2]\nu_{\text{peak}}[\text{Hz}] \ ,$$

with $\nu=\omega/2\pi$. For $\nu \sim 1$, kHz and $d \sim 100\,\mu$m we obtain $\rho \sim 10^{-3}\,\mu\Omega$ cm. The half-width of the absorption peak corresponds to a drop in resistivity by a factor $\approx 0.06$ which, together with the exponential dependence of the resistivity on temperature, leads to a narrow absorption peak in $\chi''(T)$. With increasing field the resistive transi-
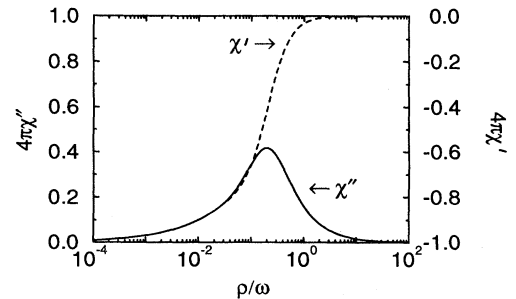


FIG. 51. Real ($\chi'$) and imaginary ($\chi''$) part of the ac susceptibility vs $\rho/\omega$ expressed in units of $2\pi d^2/c^2$ with $d$ the sample dimension.

tion broadens and so does the absorption peak in the ac response, in agreement with the experiments of Worthington, Gallagher, and Dinger (1987). By decreasing the measuring frequency $v$, one can extend the determination of the resistivity $\rho(H,T)$ to those regions where $\rho$ becomes too small to be determined in a direct transport experiment. Simultaneous measurements of $\rho$ using both direct resistive transport and ac absorption techniques have been carried out by Steel and Graybeal (1992), and good agreement between the results has been obtained.

Another type of experiment that is equivalent to the measurement of the ac absorption is the mechanical oscillator experiment (Gammel *et al.*, 1988, Gupta *et al.*, 1989, Kober *et al.*, 1991, Farrell *et al.*, 1991). In this case the dissipation is due to small rotations of the sample with respect to the magnetic field (Brandt, Esquinazi, and Weiss, 1989; Brandt, 1990, 1991a; Esquinazi, 1991). Within a reference frame moving with the sample, the magnetic field performs small angle-rotations of amplitude $\theta$, and hence the measurement corresponds to an absorption experiment with a transverse ac field

$$\mathbf{h}_{ac}\bot \mathbf{H}, \quad h_{ac}=H\theta\exp(2\pi i v t) \qquad (10.22)$$

and an ac frequency given by the period of the oscillator, $v=1/\tau_{vr}$. Keeping the measuring frequency $v$ fixed and determining the position of the absorption peak in the $(H,T)$ plane allows one to map out an irreversibility line $T_{irr}(H)$ along which the resistivity $\rho$ exhibits a constant (small) value. The limiting line for $v\to 0$ is often interpreted as the melting line of the vortex lattice (Gammel *et al.*, 1988; Durán *et al.*, 1991; Farrell *et al.*, 1991). However, since the experiment determines only the trace of a possible phase transition (vanishing of the linear resistivity $\rho$), such an interpretation is not compelling (Brandt, Esquinazi, and Weiss, 1989; Kleiman *et al.*, 1989; Esquinazi, 1991; Kober *et al.*, 1991).

More general experimental geometries involving magnetic fields inclined with the main axes of the crystal have been analyzed by Brandt (1992b). In this case the ac field component can penetrate the sample from different surfaces, and an appropriate sample dimension has to be substituted for the length $d$ in Eq. (10.20). Furthermore, subsequent full penetration of the various components of the ac field along the different axes can lead to the appearance of multiple (up to three) absorption peaks in the ac susceptibility, as the condition (10.20) is sequentially satisfied for individual field components. An analogous discussion applies to the mechanical oscillator experiments for the case in which the dc magnetic field is inclined with the sample axis. The appearance of two peaks and their transformation into each other with variation of the angle between the field and the crystal axes has indeed been observed experimentally (Durán *et al.*, 1991), and an interpretation along the above lines has been given by Brandt (1992b). Finally, a discussion of the absorption phenomenon for other sample shapes and sample field configurations can be found in the original

paper by Kes *et al.* (1988)[12] and in that of Landau and Lifshitz (1959b).[13] The analysis for the ellipsoidal geometry which comes closest to the usual sample shape seems not yet to be available.

The above analysis shows that the electromagnetic response of a high-temperature superconductor in the TAFF regime is not very different from that of a "chicken in a microwave oven." Of course, it is also very attractive to relate the appearance of sharp absorption peaks to the *direct* observation of a possible phase transition in the vortex system (Gammel *et al.*, 1988; Durán *et al.*, 1991; Farrel *et al.*, 1991). However, before doing so, one should rule out simple electrodynamical explanations like those offered above.

### B. Nonlinear response: self-organized criticality

Within the glassy regime at temperatures $T$ below the melting line $T_m(H)$ the system response is highly nonlinear, as the parameter $\alpha$ always diverges in the small-current-density limit. The linear diffusion equation (10.12) then has to be replaced by the nonlinear equation

$$\partial_t B = -\partial_x[v_0 B e^{-U(j)/T}], \qquad (10.23)$$

where we consider again a simple slab geometry with $\mathbf{B}\|z$, $\mathbf{E},\mathbf{j}\|y$, and $\mathbf{v}\|x$. Differentiation of (10.23) with respect to the coordinate $x$ provides us with a nonlinear diffusion equation for the current density $j$,

$$\partial_t j = \frac{c}{4\pi}\partial_x^2[v_0 B e^{-U(j)/T}]. \qquad (10.24)$$

Below we consider two types of (very commonly used) experimental situations, the magnetic relaxation experiment with a steplike change in time of the external magnetic field and the ac absorption experiment with a periodic change in time of the boundary conditions. In our discussion of magnetic relaxation we closely follow the analysis of Beasley, Labusch, and Webb (1969; they discuss the limit $j_c-j\ll j_c$), which we generalize to arbitrary values for the current density $j$ (see also Feigel'man, Geshkenbein, and Vinokur, 1991; Fischer and Nattermann, 1991). The highly nonlinear equations (10.23) and (10.24) can be solved perturbatively to logarithmic accuracy and in special cases $[U(j)\propto\ln(j_c/j)]$ even exactly (see below). To illustrate the main ideas we consider the simplest nontrivial situation of complete field penetration for the case of single-vortex pinning where the barrier $U(j)$ does not depend on the magnetic field. The subsequent extension to the general case poses no major additional difficulties.

Keeping in mind that for the Bean model the current density flowing in the sample is independent of $x$, we look for a solution of (10.24) of the form

---

[12]For a cylindrical sample with $\mathbf{h}_{ac}\|$cylinder axis; see also Clem, Kerchner, and Sekula (1976).

[13]For a sphere and cylinder with $\mathbf{h}_{ac}\bot$cylinder axis.

$$j(x,t)=j_0(t)+j_1(x,t), \quad |j_1| \ll j_0 . \tag{10.25}$$

Note that both the space and the time dependence of $j$ are a consequence of creep, which is neglected in the original Bean model. Substituting (10.25) into (10.24) and using the expansion $U(j) \approx U(j_0) + \partial_j U|_{j_0} j_1$, we arrive at the form

$$\partial_t j_0 \approx \frac{cv_0}{4\pi} e^{-U(j_0)/T} \partial_x^2 \left[ B \exp \left[ -\frac{\partial U}{\partial j} \Big|_{j_0} \frac{j_1}{T} \right] \right] , \tag{10.26}$$

which concentrates all of the space dependence into the second factor, hence

$$\partial_x^2 \left[ B \exp \left[ -\frac{\partial U}{\partial j} \Big|_{j_0} \frac{j_1}{T} \right] \right] = C_2(t) . \tag{10.27}$$

Combining the boundary condition $\partial_t B (x=0,t)=0$ with Eq. (10.23), we find

$$\partial_x \left[ B \exp \left[ -\frac{\partial U}{\partial j} \Big|_{j_0} \frac{j_1}{T} \right] \right] = 0$$

and therefore

$$j_1(x,t) \approx \frac{T}{|\partial_j U|} \ln \frac{C_1+(C_2/2)x^2}{B(x)} . \tag{10.28}$$

Finally, the boundary condition $B(x=0,t)=H$ [with $j_1(x=0,t)=0$] determines $C_1=H$, whereas the integration constant $C_2$ is fixed by the condition of flux conservation across the sample surface,

$$vH = \partial_t \int_0^d dx\, B(x) = -\frac{4\pi}{c} \int_0^d dx \int^x dx' \partial_t j , \tag{10.29}$$

from which we obtain $C_2=-8H/d^2$. The solution $j_1(x,t)$ takes the final form

$$j_1(x,t) \approx \frac{T}{|\partial_j U|} \ln \left[ \left[ 1-\frac{4x^2}{d^2} \right] \frac{H}{B(x)} \right] , \tag{10.30}$$

and the time evolution of $j_0(t)$ is given by

$$\partial_t j_0 \approx -\frac{2cv_0 H}{\pi d^2} e^{-U(j_0)/T} . \tag{10.31}$$

Note that $j_1 \sim T/(\partial_j U) \sim (T/U) j_0 \ll j_0$ in the strongly nonlinear regime discussed here (an exception is the narrow regime near the center of the sample, where $j$ changes sign), and hence the straight-line approximation for the field profile works well throughout most of the sample region (see also Griessen *et al.*, 1990; van der Beek, Nieuwenhuys, and Kes, 1991; van der Beek *et al.*, 1992b). Equation (10.31) has already been discussed in Sec. II.A.4 with an unknown prefactor $j_c/\tau_0$. Solving Eq. (10.31) to logarithmic accuracy with the initial condition $U[j_0(t=0)]=0$, we find

$$U[j_0(t)] \approx T \ln \left[ 1+\frac{t}{t_0} \right] \tag{10.32}$$

with

$$t_0 = \frac{\pi}{2} \frac{Td^2}{|\partial_j U| cv_0 H} . \tag{10.33}$$

The result (10.32) is the main equation governing the temporal evolution of the screening current $j_0$. Its physical interpretation is very simple and straightforward. Since we are dealing with an activated dynamics, $v \propto \exp[-U(j)/T]$, the barriers $U$ which can be overcome within the time $t$ are given by $U=T \ln(t/t_0)$. An important fact to be noticed is that the time scale $t_0$ in the problem is a *macroscopic* rather than a microscopic time. In particular, $t_0$ depends on the sample size $d$, which is the consequence of the magnetization's being proportional to the sample volume, whereas its rate of change is proportional to the surface area of the sample (any change in the total trapped flux involves vortices entering or leaving the sample through its surface). As a result the actual value for $t_0$ is much bigger than the microscopic time ($\sim 10^{-11}$ s) used in the analysis of the early relaxation experiments on giant flux creep (Yeshurun and Malozemoff, 1988; Malozemoff and Fisher, 1990). In fact, more recent experiments (Konczykowski, Malozemoff, and Holtzberg, 1991; Svedlindh *et al.*, 1991; Zavaritsky and Zavaritsky, 1991; Brawner, Ong, and Wang, 1993) produce much larger values for the time scale $t_0$, of the order of $\sim 10^{-6}$–1 s. This compares well with the theoretical estimate [see Eq. (10.33) and use $v_0 = \mathcal{A} v_c = \mathcal{A} j_c B/c\eta$]

$$t_0 \approx \frac{1}{\mathcal{A}} \frac{T}{U_c} \frac{d^2}{c^2 \rho_{\text{flow}}} , $$

$$t_0[s] \approx \frac{10^{-3}}{\mathcal{A}} \frac{T}{U_c} \frac{d^2[\text{cm}^2]}{\rho_{\text{flow}}[\mu\Omega\,\text{cm}]} , \tag{10.34}$$

which amounts to $t_0 \approx 10^{-6}$ for typical values $T/U_c \sim 10^{-1}$, $H_{c_2}/B \simeq 10^2$, $d \sim 0.1$ cm, $\rho_n \sim 100\ \mu\Omega$ cm. Note that, for the case in which the *remanent* magnetization is measured, we have $H=0$ and a direct application of Eq. (10.33) is not possible. However, it seems reasonable to estimate the effective value $H_{\text{eff}}$ to be inserted into the expression for $t_0$ as the value of the magnetic field a hopping distance $u$ away from the sample surface, $H_{\text{eff}} \simeq B(x \simeq u) \simeq (u/d) B_t$, where $B_t$ denotes the magnetic field trapped in the center of the sample. Obviously, the time constant $t_0$ is much larger in a measurement of the remanent magnetization than in a zero-field-cooled magnetic relaxation experiment. Such an effect has to be expected, since the rate of change of the magnetic field inside the sample is proportional to the number of vortices leaving (entering) the sample through its surface.

The relaxation of the screening current can be obtained from Eq. (10.32). Although the time constant $t_0$ depends on various parameters $(H,T,j_0)$, the correspond-

ing dependence appears only in the logarithm and thus can be neglected. For the case of full penetration, differentiation of Eq. (10.32) with respect to $\ln t$ provides us with the normalized relaxation rate

$$S = -\frac{1}{j}\frac{dj}{d\ln t} \simeq \frac{T}{j|\partial_j U|} . \tag{10.35}$$

On the other hand, assuming that all the temperature dependence in the problem is due to flux creep only (i.e., assuming that there is no intrinsic dependence on temperature for flux pinning), differentiation of Eq. (10.32) with respect to $T$ leads to

$$\frac{1}{j}\frac{dj}{dT} = \frac{\ln(1+t/t_\circ)}{j|\partial_j U|} , \tag{10.36}$$

and combining Eq. (10.35) with (10.36) we obtain the relation (Geshkenbein and Larkin, 1989)

$$\ln\frac{t}{t_\circ}\frac{dj}{d\ln t} = T\frac{dj}{dT} . \tag{10.37}$$

Equation (10.37) expresses the fact that the combination $T\ln(t/t_\circ)$ is a scaling variable. Independent measurement of $dj/d\ln t$ and $dj/dT$ allows for the determination of the important parameter $\ln(t/t_\circ)$. Moreover, since the relevant barrier $U$ is given by the combination $T\ln(t/t_\circ)$, the function $U(j)$ can be mapped out by changing either $T$ or the time window $\ln(t/t_\circ)$ (Maley *et al.*, 1990; van der Beek, Nieuwenhuys *et al.*, 1992).

The generalization of the above calculation to the case of partial penetration is very simple and requires the replacement of the sample size $d$ by the penetration depth $d_p = cH/4\pi j_0(t)$ in Eqs. (10.30), (10.31), and (10.33). In order to include an arbitrary field dependence of the activation barrier $U(B,j)$, one has to use the expansion

$$U(B,j) \approx U(B_0,j_0) + \frac{\partial U}{\partial B}B_1(x,t) + \frac{\partial U}{\partial j}j_1(x,t)$$

and solve self-consistently for the two corrections $B_1$ and $j_1 = (c/4\pi)\partial_x B_1$. The result for the relevant activation barriers then generalizes to

$$U(B,j) = T\ln\left|1+\frac{t}{t_\circ}\right| . \tag{10.38}$$

Note that for this general case the straight-line approximation for the magnetic-field profile in the sample breaks down. The quantity that remain constant throughout the sample is now the activation energy $U(B,j)$ rather than the current density $j$ (van der Beek, Nieuwenhuys, and Kes, 1991; van der Beek, Nieuwenhuys *et al.*, 1992).

From a very general point of view the dynamical behavior of the critical state in a type-II superconductor provides an example of self-organized criticality (De Gennes, 1966; Vinokur, Feigel'man, and Geshkenbein, 1991; Pla and Nori, 1991). Such phenomena have attracted much attention recently; see, for example, Bak, Tang, and Wiesenfeld (1988). The self-organization of the vortices is a consequence of the strongly nonlinear

(exponential) character of the diffusion equation (10.24). Near the critical current density the activation barriers in the system are given by $U(j) \simeq U_c(1-j/j_c)^\alpha$ [see Eq. (3.175)], so that at time $t = 0$ we have a Bean critical state with $j = j_c$; see Eq. (10.32). The decay of this state is regulated by the activation barriers $U(j)$. A local perturbation $\delta j < 0$ in the current density leads to an increase in the barrier, whereas in the opposite case, $\delta j > 0$, the barrier decreases. Correspondingly, a perturbation with $\delta j < 0$ "waits" until the average current level has decayed to the same value, whereas a perturbation $\delta j > 0$ decays faster until it reaches the average current level. The dynamical behavior of the system then tends to eliminate all the fluctuations in the system, so that the relaxation rate and hence $U(j)$ becomes constant throughout the sample. As a consequence, the straight-line approximation provides a good description of the field profile inside the sample [Griessen, 1990; van der Beek, Nieuwenhuys, and Kes, 1991; van der Beek, Nieuwenhuys *et al.*, 1992; see also the discussion above where we obtained $j_1(x,t) \ll j_0(t)$]. Interestingly, the nonlinear diffusion equation (10.24) can be solved *exactly* everywhere in the sample for the case of a logarithmic barrier dependence

$$U(j) = U_\circ \ln\frac{j_c}{j} , \tag{10.39}$$

thus providing an exact solution for a self-organizing critical system (Vinokur, Feigel'man, and Geshkenbein, 1991). A logarithmic dependence of the activation barrier on current density $j$ is close to a power law $(j_c/j)^\mu$ with $\mu \ll 1$ expected to describe single-vortex creep within weak collective creep theory and has also been measured experimentally by Zeldov *et al.* (1989). In this case the basic equations (10.23) and (10.24) can be written in the form

$$\partial_t b = \partial_x(\partial_x b|\partial_x b|^\sigma) , \tag{10.40}$$

$$\partial_t J = \partial_x^2(J|J|^\sigma) , \tag{10.41}$$

with $\sigma = U_\circ/T$, $b = \delta B/B_\circ$, $J = j/j_c$, and where we have introduced the dimensionless coordinates $x \to x/d_p$, $t \to tv_\circ/d_p$, $d_p = cB_\circ/4\pi j_c$. We have also introduced an additional factor $j/j_c$ in the expression for the velocity $v$,

$$v = v_\circ(j/j_c)\exp[-U(j)/T] = v_\circ J|J|^\sigma ,$$

in order to provide a gradual crossover to the viscous flux-flow regime $(v \propto J)$ at high temperatures, $T > U$. The two fields $B_\circ$ and $\delta B_\circ$ denote the underlying homogeneous induction in the sample and the small superimposed field $\delta B_\circ$ switched on at $t = 0$, respectively.

For the case of full penetration, $\delta B_\circ > H^* = 2\pi j_c d/c$, Eq. (10.41) can be solved by separating variables, and the solution for the current density takes the form $(\sigma \gg 1)$

$$J(x,t) \approx \left[\frac{1-4x^2/d^2}{1+t/t_\circ}\right]^{1/\sigma} , \tag{10.42}$$

with the time scale $t_\circ$ given by

$$t_\circ = \frac{d^2}{8\sigma} \to \frac{\pi}{2}\frac{Td^2 j_c}{U_\circ c v_\circ \delta B_\circ} \ . \tag{10.43}$$

The solution for the magnetic field is

$$b(x,t) \approx b_\circ - \frac{x}{(1+t/t_\circ)^{1/\sigma}}, \quad 0 \le x \le \frac{d}{2} \ . \tag{10.44}$$

Note that the result (10.42) is also valid in the sample center $(x = d/2)$ where the current density changes sign. The analysis of the magnetic relaxation data by Brawner, Ong, and Wang (1993) agrees very favorably with the scaling law (10.44).

For the case of partial field penetration, Eq. (10.40) can be solved with the help of the scaling ansatz

$$b(x,t) = b(\xi) \ , \tag{10.45}$$

with

$$\xi = \frac{x}{(1+t/t_{sc})^{1/(\sigma+2)}} \ . \tag{10.46}$$

The scale $t_{sc} \sim 1$ denotes the time needed to establish the scaling behavior of the system. The magnetic field is given by

$$b(x,t) = b_\circ - \frac{\xi}{x}\int_0^x dy\,[1 - C\xi^2(y)]^{1/\sigma} \ , \tag{10.47}$$

with $C = \sigma/2(\sigma+1)(\sigma+2)$ and develops a flux front $[b(x_f,t) = 0]$ at the position

$$x_f \approx (1+t/t_{sc})^{1/\sigma}b_\circ \ . \tag{10.48}$$

Taking the spatial derivative of (10.47), one obtains the screening current density

$$J(x,t) = \frac{(1-C\xi^2)^{1/\sigma}}{(1+t/t_{sc})^{1/(\sigma+2)}}\Theta[x_f(t)-x] \ . \tag{10.49}$$

The two flux fronts entering the sample from $x = 0$ and $x = d$ meet after a time

$$t^* = \frac{c}{4\pi}\frac{B_\circ}{j_c v_\circ}\left[\frac{2\pi d j_c}{c\delta B_\circ}\right]^\sigma \ , \tag{10.50}$$

and the solution goes over into the form (10.42) and (10.44).

Finally, let us discuss the second type of experiment in which an ac field is applied to a glassy vortex system. We first consider the small-amplitude response $(\alpha < 1)$, then close the section with a discussion of the behavior for large amplitudes.

Consider a sample put into the critical state at a time $t = 0$. We are interested in the dynamic evolution of a perturbation $\delta B$ on top of the field $B_\circ(x,t)$, which is the solution of Eq. (10.23) with constant boundary conditions. The linearized equation governing the evolution of $\delta B$ is

$$\partial_t \delta B = -\frac{c v_\circ}{4\pi}\partial_x\left[\frac{B_\circ}{T}\frac{\partial U(j)}{\partial j}\bigg|_{j_\circ}e^{-U(j_\circ)/T}\partial_x \delta B\right] \ , \tag{10.51}$$

with $j_\circ(x,t) = j_0(t) + j_1(x,t)$ the current density corresponding to the field $B_\circ(x,t)$ and given by Eqs. (10.31) and (10.30). Making use of this solution, we find that Eq. (10.51) takes the form (Geshkenbein, Feigel'man, and Vinokur, 1991)

$$\partial_t \delta B = \frac{c^2}{4\pi}\partial_x[\rho(x)\partial_x \delta B] \tag{10.52}$$

with the universal resistivity

$$\rho(x) = \frac{\pi}{2}\frac{d^2}{c^2}\frac{1}{t}\left[1 - \frac{4x^2}{d^2}\right] \ . \tag{10.53}$$

The resistivity $\rho(x)$ is entirely determined by the (self-organized critical) state of the vortex system and depends neither on the initial magnetic field nor on temperature or any intrinsic parameter of the superconductor, such as the critical current density $j_c$ or the activation barrier $U$. The evolution of the perturbation is determined completely by the geometry of the sample and by the characteristic time $t$ during which the initial critical state has decayed. The origin of the universal behavior of the perturbation $\delta B$ can be understood as follows: After a time $t$ the relevant barriers $U(j)$ in the system have grown to a value $T \ln(t/t_\circ)$. In order for the small perturbation $\delta B$ to evolve in time, the system has to diffuse over its relevant barriers, leading to a diffusion coefficient

$$D \propto \rho \approx (v_\circ B/cT)(U_\circ/j_c)\exp[-U(j)/T]$$

$$\propto (d^2/c^2)(1/t) \ .$$

Note that since $\rho \propto 1/t$, Eq. (10.52) has the form of a diffusion equation with respect to the "logarithmic time" $\tau = \ln t$ and thus resembles the equation governing the logarithmic decay of the critical state due to flux creep itself.

With the linear diffusion equation (10.52) we can immediately obtain the ac response of the superconductor by taking over the results from Sec. X.A; see Eq. (10.12). Consider the following experiment: After an initial critical state has been created at time $t = 0$ (e.g., by switching on a magnetic field after zero-field cooling), a small ac field $\delta B \propto \exp(-i\omega t)$ is turned on at time $t_w$ and the ac susceptibility is measured. For a frequency $\omega$ much bigger than the inverse waiting time $1/t_w$, the skin penetration depth (10.14) becomes $\delta_S = d/2\sqrt{\omega t_w} \ll d$, and for the ac susceptibility we obtain

$$4\pi\chi'' = \frac{1}{2\sqrt{\omega t_w}} \ , \tag{10.54}$$

explicitly exhibiting universal behavior. Note that in order for the system to evolve in the linear regime, both the perturbation $\delta B$ and the associated current density $\delta j$ have to be small in the sense $\delta j \ll (T/U)j_\circ$, where the latter condition (equivalent to $\alpha \ll 1$) is the more stringent one.

We now turn to the opposite case of a large ac amplitude, for which the response of the system is highly nonlinear. In this case the decay of the critical state com-

petes with the time scale imposed on the system by the external ac field. Consider than an experiment in which the sample is taken through a complete hysteretic loop within the time period $t = 2\pi/\omega$, where $t$ instead of being of the order of hours is now of the order of $\sim 10^{-6}$–$10^{-3}$ s (Campbell and Evetts, 1972). In this case the decay of the magnetization is cut on the time scale $t \sim 1/\omega$, so that the screening currents flowing in the sample are given by

$$U(j) = T \ln \frac{1}{\omega t_\circ} \ . \tag{10.55}$$

The hysteretic losses are proportional to the area of the magnetization loop, and the maximum in the susceptibility $\chi''$ will occur when the flux front reaches the center of the sample. Thus the discussion proceeds along the same lines as the Bean analysis of the critical state, except that the screening current density, instead of being the critical value $j_c$, is now reduced to $j(\omega) = U^{-1}[T \ln(1/\omega t_\circ)]$ due to creep. Accordingly the penetration depth for the flux profile is now given by

$$d_p = \frac{c}{4\pi} \frac{\hbar_{ac}}{j(\omega)} \tag{10.56}$$

and thus the position of the peak in $\chi''$ will strongly depend on the amplitude $h_{ac}$ of the ac field. The criterion for the peak in the susceptibility is

$$U \left[ j = \frac{c h_{ac}}{2\pi d} \right] = T \ln \frac{1}{\omega_{peak} t_\circ} \ . \tag{10.57}$$

At first sight, both the physical origin and the peak criterion (10.57) appear to be very different from the skin-effect approach and its result (10.20) derived for the TAFF regime in Sec. X.A. However, the two approaches in fact are very similar, and closer inspection of the criterion (10.20) shows that it can be rewritten in the form

$$U_\circ(H, T) = T \ln \frac{1}{\omega_{peak} t_\circ} \ , \tag{10.58}$$

which exactly coincides with the condition (10.57) for the nonlinear case. In the derivation of Eq. (10.58) we made use of Eqs. (10.10) and (10.33). The only difference between the two criteria (10.57) and (10.58) is that, for the case of linear diffusion, the barrier $U_\circ(H, T)$ does not depend on the amplitude of the ac field, while in the nonlinear regime the barrier $U(j, H, T)$ strongly depends on the current density and hence on the amplitude $h_{ac}$.[14] With decreasing amplitude $h_{ac}$, the energy $U(j)$ is increased and the temperature where the dissipation peak occurs is shifted to higher values, which is in agreement with experimental data of Krusin-Elbaum *et al.* (1991) and of Sagdahl *et al.* (1991). Note that, reversing the above argumentation, we can also say that Eq. (10.20) is

---

[14]Note that for maximal dissipation the current density $j_{peak} = (c/2\pi)(h_{ac}/d)$ in both cases, but $U = U(j)$ only in the glassy regime.

valid in the nonlinear case, but with a resistivity $\rho$ that depends on the amplitude $h_{ac}$ of the ac field.

In summary, by varying the frequency $\omega$ and the amplitude $h_{ac}$ of the ac field, one can use the results of the ac susceptibility to reconstruct the current-voltage characteristic of the sample (Krusin-Elbaum *et al.*, 1991). The general basic equation that describes both the linear and the nonlinear case is (van der Beek, Geshkenbein, and Vinokur, 1993)

$$U \left[ j = \frac{c h_{ac}}{2\pi d}, H, T \right] = T \ln \frac{1}{\omega_{peak} t_\circ} \ . \tag{10.59}$$

Plotting $-T \ln(\omega_{peak} t_\circ)$ versus the amplitude $c h_{ac}/2\pi d$, one can reconstruct the current dependence of the activation barrier $U(j)$. On the other hand, a plot of $j = c h_{ac}/2\pi d$ as a function of $-\ln \omega_{peak} t_\circ$ is nothing but a measurement of the magnetic relaxation $j(t) \propto (\ln t)^{-1/\mu}$. Using the ac method, one can overcome the usual difficulty in conventional relaxation measurements of having only a very limited time window (typically $1$–$10^4$ s) by extending the latter to smaller values $10^{-4}$–$10^{-2}$ s and thereby can increase the dynamic range of $\ln(t/t_\circ)$ considerably [note that $U(j, H, T) > U_c^b(H, T)$ is a limiting condition on the smallness of $\omega$]. It would be very interesting to combine both dc and ac methods within the same setup, which would allow us to measure the relaxation over roughly 10 decades in time and would make it possible to determine the exponent $\mu$ describing the dynamics of the glassy phase with high accuracy.

## XI. CONCLUSION

Since the main results discussed in this review have already been summarized in the introduction, we conclude this work with a list of the main unsolved problems in this field. Let us start with

(a) *Thermodynamics of the mixed state in pure type-II superconductors.* The major unsolved problems here concern the nature of the melting transition, as well as the physics of the resulting vortex-liquid phase(s); cf. the discussion in Sec. V above.

(i) An important issue is *the order of the phase transition;* is the melting a first-order transition or is it of second order, so that scaling concepts can be applied? Recent results of Monte Carlo simulations by Hetzel, Sudbø, and Huse (1992) seem to favor a first-order transition. Moreover, detailed investigations of the resistive transition by Safar, Gammel, Huse *et al.* (1992; see also Charalambous, 1992 and Charalambous *et al.*, 1993; Kwok *et al.*, 1994a and 1994b) exhibit a sharp and hysteretic behavior in $\rho(T)$, thus also providing evidence for a first-order transition. However, the identification of the observed hysteretic behavior with a possible melting transition still needs to be clarified.

(ii) Regarding the nature of the vortex-liquid phase, we need to explore *the possible existence of an intermediate disentangled phase.* Furthermore, in which respects

would such a disentangled liquid differ from the hexatic vortex-liquid phase proposed by Marchetti and Nelson (1990a, 1990b) and observed in the Monte Carlo simulations by Ryu *et al*. (1992). The results by Hetzel *et al*., Safar *et al*., and Kwok *et al*. could as well be interpreted as a first-order transition between such an intermediate (disentangled) vortex-liquid state and the high-temperature entangled vortex-liquid phase, which is thermodynamically equivalent to a normal metal. Direct experimental evidence for the existence of the proposed disentangled phase would involve simultaneous measurement of the response both parallel and transverse to the magnetic field **B**, with a determination of the zero-current asymptotics of the longitudinal and transverse resistivity $\rho^{\parallel}(j \to 0)$ and $\rho^{\perp}(j \to 0)$, respectively. The intermediate phase would then manifest itself by a finite $\rho^{\perp}(0) > 0$, while the longitudinal response would be superconducting, $\rho^{\parallel}(0) = 0$. Recent developments within this area are documented in the work of Steel, White, and Graybeal (1993), Safar *et al*. (1994), and Feigel'man and Ioffe (1995).

(iii) An analogous problem is posed by *the possible existence of a supersolid phase* in the case of layered superconductors at large enough fields $B > B_{2D}$. In this case, too, the existence of a phase intermediate between the low-temperature Abrikosov lattice phase and the high-temperature normal metal has been suggested (Feigel'man, Geshkenbein, and Larkin, 1990; Glazman and Koshelev, 1991a), but a reliable proof for its existence (see Sec. VII.B.4) is still missing. The characteristics of this supersolid intermediate phase differ from those of the normal-liquid phase discussed above. Here the phase constitutes a 3D lattice of pancake vortices without superconducting coherence between the layers, hence $\rho^{\parallel}(0) > 0$. Related experiments have been carried out by Safar, Gammel, Bishop, *et al*. (1992).

(iv) In layered materials a very interesting *crossover regime* could exist in the vicinity of $(T_m^{2D}, B_{2D})$, where the four phases (normal-solid, supersolid, normal-liquid, superliquid) join up. The details of this crossover regime have not as yet been addressed.

(b) The second group of open questions concerns the problematics of *quenched disorder, i.e., pinning*. Again, it is the further development in our understanding of the vortex-glass phase itself, as well as of the vortex-glass transition, which has to be mentioned first. The vortex-glass phase is formed at low temperatures due to the presence of quenched disorder, which can be either weak or strong. By weak disorder we refer to the situation in which the basic shape of the thermodynamic phase diagram, e.g., the melting line, is only weakly affected by the disorder and the new thermodynamic phases developed in the presence of disorder possess the same kind of short-range order as the "pure" phases from which they originate. By contrast, in a strongly disordered situation a significant change in the overall shape of the phase diagram is expected to occur. Whereas it seems that many single crystals of the new high-temperature superconduc-

tors belong to the first class of weakly disordered systems, the corresponding thin-film samples appear to belong to the second, strongly disordered case.

In the case of weak disorder, the remaining outstanding questions are: (i) Does the vortex-glass transition line at intermediate fields $H_{c_1} \ll B \ll H_{c_2}$ essentially (up to corrections of the order of $j_c / j_0$) coincide with the melting line of the pure system, or, on the contrary, does the transition shift below the melting line and approach the limit $T = 0$ for vanishing disorder strength $j_c / j_0 \to 0$? In Sec. VII.C we have presented arguments in favor of the first scenario. However, the subject is still controversial; see, for example, Dorsey, Huang, and Fisher (1992) and Worthington *et al*. (1992). A promising way to resolve this controversy would be to study in more detail the possible occurrence and the behavior of dislocation lines in a weakly pinned vortex lattice. (ii) How does the vortex-glass phase relate to gauge glass, which is supposed to exist in strongly disordered systems such as a random Josephson network in a magnetic field? This question is of very practical importance, since many Monte Carlo simulations have been carried out on the gauge-glass model and have been interpreted in relation to the vortex-glass problem. (iii) Is the vortex-glass phase essentially anisotropic with respect to the angle $\phi$ between the current density **j** and the magnetic field **B**? In particular, does the glass exponent $\mu$ depend on $\phi$? What are the consequences of such an anisotropy for the vortex-glass transition? (iv) Is the vortex-glass transition a first- or second-order transition or could it even be triggered to change between these two options by varying the strength of disorder?

For the strongly disordered case one has to distinguish between isotropic and anisotropic disorder. Examples of the latter are found in samples with columnar defects or twin planes. The first case (isotropic strong disorder) is probably irrelevant for the new oxide superconductors in single-crystal form, in which isotropic disorder always seems to be weak; however, it may be relevant for thin-film samples. It is still unclear what type of model system should be used to describe the latter case. Disorder due to columnar defects is a particularly important and interesting case, since it can be introduced in a controllable fashion and can also be theoretically investigated in a simpler way via the mapping to a 2D Bose system subject to static disorder. This system has already been studied quite extensively (Fisher *et al*. 1989), and the concept of the Bose-glass phase has been developed. On the other hand, the actual investigation of the Bose-glass problem in relation to the problem of pinning of vortices in type-II superconductors has only been undertaken recently (Nelson and Vinokur, 1992 and 1993; Brandt, 1992c; Lyuksyutov, 1992), and the number of accurate quantitative predictions is still quite limited.

(c) In the above we have concentrated on the theoretical problems related with thermal and quenched disorder in the *bulk* of a type-II superconductor in the mixed phase. However, as suggested by recent experiments

(Burlachkov, *et al.*, 1991; Konczykowski, Burlachkov, *et al.*, 1991, 1992; Chikumoto *et al.*, 1992a, 1992b), in some cases both pinning and creep seem to be dominated by surface effects. The theoretical investigation of surface-dominated flux creep at elevated temperatures is still in its infancy (Burlachkov *et al.*, 1991; Koshelev, 1992), and more work is needed in order to obtain a correct interpretation of the experimental results on magnetic relaxation. Interesting recent developments have been reported by Zeldov *et al.* (1994) and Schuster *et al.* (1994).

(d) A further problem, also related to the interpretation of experimental data, concerns the measurements of the response to *a weak ac magnetic field superimposed on a dc background field H*. Such measurements contain much valuable information about pinning and creep of vortices, particularly if the nonlinear, i.e., higher harmonic, response is also measured. However, at present no clear predictions for these kinds of experiments exist on the basis of collective creep or vortex-glass-like theories.

(e) The results concerning the (relative) strength of (static and thermal) disorder and the overall shape of the phase diagram depend on the *values of the phenomenological parameters of superconductivity*, such as the coherence length $\xi$, the penetration depth $\lambda$, and the anisotropy $\varepsilon$. However, it is less obvious that these dependencies can become quite subtle, i.e., a variation of the above parameters by 20% can easily result in a quantitative change of the vortex-glass/vortex-liquid phase diagram. Therefore a reliable comparison between theory and experiment requires not only an accurate knowledge of the numerical factors on the theoretical side but also a very precise determination of all the relevant phenomenological parameters of the superconductor.

(f) A number of topics have only been mentioned briefly or have not been discussed at all in the present review: A very interesting recent development concerns the *Hall motion of the vortices*. Here we have discussed the equation of motion and the phenomenon of Hall tunneling in a super-clean material (see Harris *et al.*, 1994, for evidence of superclean YBCO) but have left out other topics such as the observed sign change in the Hall voltage as the sample goes superconducting. The issues concerning ceramic or polycrystalline material have not been addressed. Finally, topics related more closely with the microscopic theory of superconductivity, such as the details of the vortex core structure or the possibility of unconventional superconductivity (see Wollman *et al.*, 1993; Brawner and Ott, 1994; Kirtley *et al.*, 1994), have not been touched upon.

*Note added.* Within the time span between the first preprint version of this work and its final printed version two major corrections have been introduced: (i) As discussed in more detail in Sec. II.A.5 we have revised our understanding of the quantum collective creep process. As a consequence, the scaling behavior of the action at small driving forces, $S(j \ll j_c) \simeq S_o(j_o/j)^{\mu_S}$, has been modified as compared to the preprint version of this text (Secs. II.A.5, III.F.2, IV.B.3, IV.D, VIII.D.2, and IX.B.3). (ii) As pointed out by Koshelev (1994) the simple estimates of the superbundle dimension based on the smallest length scale in the problem is not correct in the nonlocal regime and one has to take account of *all three different* lengths $R_{\parallel}$, $R_{\perp}$, and $L^b$ in the determination of the elastic tilt and shear energies (see the more detailed discussion in Sec. IV.B.2). As a consequence, the scaling behavior of the barriers and actions at low driving forces, $U(j \ll j_c) \simeq U_o(j_o/j)^{\mu}$ and $S(j \ll j_c) \simeq S_o(j_o/j)^{\mu_S}$ (in particular, the glass exponents $\mu$ and $\mu_S$), have been modified as compared with the preprint version (Secs. IV.B.2 and IV.B.3, IV.D, VIII.D.2, and IX.B.3). We thank Alex Koshelev for pointing out to us the error in the argument.

TABLE I. Basic formulas for a type-II superconductor.

| Description | Formal expression | Eq. |
|---|---|---|
| Coherence length | $\xi^2(T) = \dfrac{\hbar^2}{2m\lvert\alpha(T)\rvert} = \xi^2(0)\dfrac{1}{1-T/T_c}$ | (2.5) |
| BCS coherence length | $\xi_{\text{BCS}}^2 = \left[\dfrac{\hbar v_F}{\pi\Delta_{\text{BCS}}}\right]^2 = 1.85\xi^2(0)\dfrac{1}{\chi(\rho)}$ | (3.69) |
| GL penetration depth | $\lambda^2(T) = \dfrac{mc^2}{16\pi e^2\lvert\Psi_0(T)\rvert^2} = \lambda^2(0)\dfrac{1}{1-T/T_c}$ | (2.6) |
| London penetration depth | $\lambda_L^2 = \dfrac{mc^2}{4\pi ne^2} = 2\lambda^2(0)\chi(\rho)$ | (3.70) |
| Anisotropy | $\varepsilon^2 = m/M < 1$ | (2.2) |
| GL parameter | $\kappa = \lambda/\xi$ | |
| Energy scale | $\varepsilon_0 = \left[\dfrac{\Phi_0}{4\pi\lambda}\right]^2$ | (2.14) |
| Th. dyn. critical field | $H_c = \dfrac{\Phi_0}{2\sqrt{2}\pi\lambda\xi}$ | (2.7) |
| Lower critical field | $H_{c_1} = \dfrac{\Phi_0}{4\pi\lambda^2}\ln\dfrac{\lambda}{\xi}$ | (2.13) |
| Upper critical field | $H_{c_2} = \dfrac{\Phi_0}{2\pi\xi^2}$ | (2.17) |
| Ginzburg number | $Gi = \dfrac{1}{2}\left[\dfrac{T_c}{H_c^2(0)\varepsilon\xi^3(0)}\right]^2 = \dfrac{1-t}{8}\left[\dfrac{T_c}{\varepsilon\varepsilon_0\xi}\right]^2$ | (2.47) |
| Quantum resistance | $Qu = \dfrac{e^2}{\hbar}\dfrac{\rho_n}{\varepsilon\xi}$ | (2.167) |
| Lattice constant | $a_\Delta = \left[\dfrac{2}{\sqrt{3}}\right]^{1/2}\left[\dfrac{\Phi_0}{B}\right]^{1/2} \approx \left[\dfrac{\Phi_0}{B}\right]^{1/2} = a_0$ | (2.15) |
| Line tension | $\varepsilon_l = \varepsilon_0\ln\dfrac{\lambda}{\xi}$ | (2.13) |
| Dispersive line tension | $\varepsilon_l(k > 1/\lambda) = \varepsilon_0\ln\dfrac{1}{k\xi}$ | (2.18) |
| Friction coefficient | $\eta_l \simeq \dfrac{\Phi_0 H_{c_2}}{\rho_n c^2} = \eta a_0^2$ | (2.26) |
| Hall coefficient | $\alpha_l = \dfrac{\Phi_0}{c}\rho_s = \pi\hbar n$ | |
| Green's function | $G(q,\omega) = \dfrac{1}{-i\eta_l\omega + \varepsilon_l q^2}$ | (2.114) |
| Current density | $\mathbf{j} = -\dfrac{2e\hbar}{m}\lvert\Psi\rvert^2\left[\nabla\varphi + \dfrac{2\pi}{\Phi_0}\mathbf{A}\right]$ | (2.9) |
| Depairing current density | $j_0 = \dfrac{cH_c}{3\sqrt{6}\pi\lambda} = \dfrac{4}{3\sqrt{3}}\dfrac{c\varepsilon_0}{\xi\Phi_0}$ | (2.30) |

TABLE II. Single-vortex pinning.

| Description | Formal expression | Eq. |
|---|---|---|
| Disorder correlator | $\langle U_{\rm pin}(\mathbf{r})U_{\rm pin}(\mathbf{r}')\rangle = \gamma_U\delta(\mathbf{r}-\mathbf{r}')$ | (2.36) |
| Pinning potential | $\varepsilon_{\rm pin}(z,\mathbf{u}) = \int d^2R\ U_{\rm pin}(\mathbf{r})p(\mathbf{R}-\mathbf{u})$ | (2.33) |
| Form factors $(\delta T_c,\ \delta l)$ | $p(R)=1-|\psi_v(R)|^2,\ \ \xi^2|\nabla\psi_v(R)|^2$ | (2.34) |
| Pinning parameter $(\delta T_c)$ | $\gamma=2\pi\gamma_U=2\pi\dfrac{\gamma_a}{\alpha^2}\left[\dfrac{H_c^2}{4\pi}\right]^2$ | (2.38) |
| Pinning parameter $(\delta l)$ | $\gamma=\dfrac{14\pi}{15}\gamma_U=\dfrac{14\pi}{15}\dfrac{\gamma_m}{m^2}\left[\dfrac{H_c^2}{4\pi}\right]^2$ | (2.38) |
| Pinning parameter | $\gamma\simeq f_{\rm pin}^2 n_i\xi^2$ | (2.43) |
| Pinning energy | $\langle\mathcal{E}_{\rm pin}^2(L)\rangle\simeq\gamma\xi^2 L$ | (2.40) |
| Collective pinning length | $L_c\simeq\left[\dfrac{\varepsilon_0^2\xi^2}{\gamma}\right]^{1/3}\simeq\xi\left[\dfrac{j_0}{j_c}\right]^{1/2}$ | (2.45) |
| Collective pinning energy | $U_c\simeq(\gamma\varepsilon_0\xi^4)^{1/3}\simeq H_c^2\xi^3\dfrac{\xi}{L_c}\simeq T_c\sqrt{(1-t)/Gi}\left[\dfrac{j_c}{j_0}\right]^{1/2}$ | (2.46) |
| Critical current density | $j_c\simeq\dfrac{c}{\Phi_0}\left[\dfrac{\gamma}{L_c}\right]^{1/2}\simeq j_0\left[\dfrac{\xi}{L_c}\right]^2$ | (2.50) |
| Action | $\dfrac{S_E^{\rm eff}}{\hbar}\simeq\dfrac{\hbar}{e^2}\dfrac{\xi}{\rho_n}\left[\dfrac{j_0}{j_c}\right]^{1/2}\simeq\dfrac{1}{Qu}\left[\dfrac{j_0}{j_c}\right]^{1/2}$ | (2.90) |
| Activation barrier $(j\lesssim j_c)$ | $U(j)\simeq U_c(1-j/j_c)^\alpha$ | (2.58) |
| Activation barrier $(j\to 0)$ | $U(j)\simeq U_c(j_c/j)^\mu$ | (2.60) |
| Glass exponent | $\mu=(2\zeta-1)/(2-\zeta)$ | (2.68) |
| Relevant barrier after $t$ | $U(j)=T\ln\left[1+\dfrac{t}{t_0}\right],\quad t_0\simeq\dfrac{Td^2}{|\partial_j U|cv_0 H}$ | (2.57) |
| Line wandering $(L>L_c)$ | $u(L)\sim u_c\left[\dfrac{L}{L_c}\right]^\zeta,\ \ \mathcal{E}(L)\sim U_c\left[\dfrac{L}{L_c}\right]^{2\zeta-1}$ | (2.63) |
| Optimal hopping length | $L_{\rm opt}(j)\sim L_c(j_c/j)^{1/(2-\zeta)}$ | (2.66) |
| Wandering exponents | $\zeta_{1,1}=2/3,\ \ \zeta_{1,2}\approx 3/5$ | (2.66) |
| Relaxation | $j(t)\simeq j_c\left[1+\dfrac{\mu T}{U_c}\ln\left[1+\dfrac{t}{t_0}\right]\right]^{-1/\mu}$ | (2.72) |
| Relaxation rate | $S=-\dfrac{d\ln j}{d\ln t}\simeq\dfrac{T}{U_c+\mu T\ln(1+t/t_0)}$ | (2.77) |

TABLE III. Materials parameters, anisotropy.

| Description | Formal expression | Eq. |
|---|---|---|
| Material parameters (YBCO) | $\lambda_L \approx 1400$ Å,   $\xi_{BCS} \approx 12\text{--}18$ Å | |
| | $d \approx 12$ Å,   $\varepsilon \approx \frac{1}{5} - \frac{1}{7}$ | (2.134) |
| Material parameters (BiSCCO) | $\lambda_L \approx 1400\text{--}2000$ Å,   $\xi_{BCS} \approx 20\text{--}40$ Å | |
| | $d \approx 15$ Å,   $\varepsilon \approx \frac{1}{50} - \frac{1}{200}$ | (2.134) |
| Anisotropy parameter | $\varepsilon_\vartheta^2 = \varepsilon^2(\vartheta) = \varepsilon^2\cos^2\vartheta + \sin^2\vartheta$ | (2.137) |
| Scaling rule | $Q(\vartheta, H, T, \xi, \lambda, \varepsilon, \gamma) = s_Q \tilde{Q}\left[\varepsilon_\vartheta H, \dfrac{T}{\varepsilon}, \xi, \lambda, \dfrac{\gamma}{\varepsilon}\right]$ | (3.12) |
| Scaling factors | $s_V = s_E = s_S = s_T = \varepsilon$,   $s_B = s_H = \varepsilon_\vartheta^{-1}$ | (3.12) |
| Lower critical field (approximative) | $H_{c_1}(\theta_H) = \dfrac{\Phi_0}{4\pi\lambda^2} \dfrac{\varepsilon}{\varepsilon_{\theta_H}} \ln\left[\dfrac{\lambda}{\xi}\right]$ | (2.136) |
| Upper critical field | $H_{c_2}(\vartheta) = \dfrac{\Phi_0}{2\pi\varepsilon_\vartheta\xi^2}$ | (2.138) |
| Line tensions (approximative) | $\varepsilon_l^\perp(\vartheta) \simeq \varepsilon^2\varepsilon_0 / \varepsilon_\vartheta^3$,   $\varepsilon_l^\parallel(\vartheta) \simeq \varepsilon^2\varepsilon_0 / \varepsilon_\vartheta$ | (2.144) |
| Friction coefficients | $\eta_l^\parallel(\vartheta) = \varepsilon_\vartheta\eta_l^c$,   $\eta_l^\perp(\vartheta) = \eta_l^c/\varepsilon_\vartheta$ | (2.163) |
| Pinning energy | $\langle \mathcal{E}_{\mathrm{pin}}^2(L)\rangle \simeq \gamma\varepsilon_\vartheta\xi^2 L$ . | (2.147) |
| Collective pinning length | $L_c(\vartheta) \simeq \dfrac{L_c^c}{\varepsilon_\vartheta}$,   $L_c^c \simeq \varepsilon^{4/3} L_c^{\mathrm{iso}}$ | (2.149) |
| Collective pinning energy | $U_c^c \simeq \varepsilon^{2/3} U_c^{\mathrm{iso}} \simeq H_c^2\varepsilon\xi^3 \dfrac{\varepsilon\xi}{L_c^c} \simeq T_c\sqrt{(1-t)/Gi}\,\dfrac{\varepsilon\xi}{L_c^c}$ | (2.150) |
| Action | $\dfrac{S_E^{\mathrm{eff},c}}{\hbar} \simeq \varepsilon^{4/3}\dfrac{S_E^{\mathrm{eff,iso}}}{\hbar} \simeq \dfrac{\hbar}{e^2}\dfrac{\varepsilon\xi}{\rho_n}\left[\dfrac{j_0}{j_c^c}\right]^{1/2} \simeq \dfrac{1}{Qu}\left[\dfrac{j_0}{j_c^c}\right]^{1/2}$ | (2.166) |
| Critical current density | $j_c^\parallel \simeq j_c^c \simeq \varepsilon^{-2/3} j_c^{\mathrm{iso}} \simeq j_0\left[\dfrac{\varepsilon\xi}{L_c^c}\right]^2$ | (2.151) |
| Critical current density | $j_c^\perp(\vartheta) \simeq \varepsilon_\vartheta j_c^c$ | (2.152) |
| Optimal hopping length | $L_{\mathrm{opt}}(j) \simeq L_c(\vartheta)(j_c^c/j)^{5/7}$ | |
| Activation barrier | $U(j) \simeq U_c^c(j_c^c/j)^{1/7}$ | |
| Action | $S(j) \simeq S_E^{\mathrm{eff},c}(j_c^c/j)^{8/7}$ | |

TABLE IV. Single-vortex pinning: thermal fluctuations.

| Description | Formal expression | Eq. |
|---|---|---|
| Diffusion law | $\langle u^2(t) \rangle_{\mathrm{th}} \simeq T \left[ \dfrac{t}{\varepsilon_l \eta_l} \right]^{1/2}$ | (2.116) |
| Thermal displacement | $\langle u^2(L_c) \rangle_{\mathrm{th}} \simeq \dfrac{T L_c(T)}{\varepsilon_l}$ | (2.117) |
| Pinning energy | $\langle \langle \mathscr{E}_{\mathrm{pin}}(L_c) \rangle_t^2 \rangle \simeq \gamma L_c \left[ \dfrac{\xi^4}{\langle u^2(L_c) \rangle_{\mathrm{th}}} \right]^{n/2}$ | (2.118) |
| Collective pinning length $(1+1)$ | $L_c(T) \simeq \xi \left[ \dfrac{j_0}{j_c} \right]^{1/2} \left[ \dfrac{T}{\widetilde{T}^s_{\mathrm{dp}}} \right]^5$ | |
| Collective pinning length $(2+1)$ | $L_c(T) \simeq L_c(0) \dfrac{\widetilde{T}^s_{\mathrm{dp}}}{T} \exp\left[ c \left[ \dfrac{T}{\widetilde{T}^s_{\mathrm{dp}}} \right]^3 \right]$ | (2.127) |
| Depinning energy $(1+1)$ | $\widetilde{T}^s_{\mathrm{dp}} \simeq T_c \dfrac{1-t}{Gi^{2\mathrm{D}}} \dfrac{\xi}{d} \left[ \dfrac{j_c}{j_0} \right]^{1/2}, \quad Gi^{2\mathrm{D}} \simeq \dfrac{T_c}{\varepsilon_0(0)d}$ | |
| Depinning energy $(2+1)$ and anisotropy | $\widetilde{T}^s_{\mathrm{dp}} = \alpha^s_{\mathrm{dp}} T_c \sqrt{(1-t/Gi)} \left[ \dfrac{j_c}{j_0} \right]^{1/2}, \quad \alpha^s_{\mathrm{dp}} \approx 0.7$ | (2.128) |
| | $\widetilde{T}^s_{\mathrm{dp}} = \varepsilon^{2/3} \widetilde{T}^{s,\mathrm{iso}}_{\mathrm{dp}}$ | (2.179) |
| Depinning temperature | $T^s_{\mathrm{dp}} = \widetilde{T}^s_{\mathrm{dp}}(T^s_{\mathrm{dp}})$ | (2.130) |
| Collective pinning energy | $U_c(T) \simeq \dfrac{\varepsilon_0 \langle u^2(L_c) \rangle_{\mathrm{th}}}{L_c(T)} \simeq T$ | (2.131) |
| Critical-current density $(1+1)$ | $j_c(T) \simeq j_0 \left[ \dfrac{\xi}{L_c(0)} \right]^2 \left[ \dfrac{\widetilde{T}^s_{\mathrm{dp}}}{T} \right]^7$ | (2.132) |
| Critical current density $(2+1)$ | $j_c(T) \simeq j_c(0) \left[ \dfrac{T}{\widetilde{T}^s_{\mathrm{dp}}} \right]^2 \exp\left[ -\dfrac{3c}{2} \left[ \dfrac{T}{\widetilde{T}^s_{\mathrm{dp}}} \right]^3 \right]$ | (2.132) |

TABLE V. Boundaries of pinning regimes.

| Description | Formal expression | Eq. |
|---|---|---|
| Single-vortex pinning reg. | $a_\circ > L_c$ | (2.172) |
| | $B < B_{sb} = \beta_{sb} \dfrac{j_c}{j_\circ} H_{c_2}, \quad \beta_{sb} \approx 5$ | (2.173) |
| and anisotropy and temperature dependence | $L_c^c(T) < \dfrac{\varepsilon}{\sqrt{\varepsilon_\vartheta}} a_\circ$ | |
| | $B < B_{sb}(\vartheta, T)$ $= \beta_{sb} H_{c_2}(\vartheta) \dfrac{j_c^c}{j_\circ} \left[ 1 + \dfrac{T}{\widetilde{T}_{dp}^s} \right]^2 e^{-2c(\alpha + T/\widetilde{T}_{dp}^s)^3}$ | (2.178) |
| Temperature dependence | $T < T_{dp}^s \left[ \ln \dfrac{B_{sb}}{B} \right]^{1/3}$ | (2.133) |
| Current dependence | $j > j_{sb} = j_c \left[ \dfrac{L_c}{a_\circ} \right]^{2-\zeta} \simeq j_c \left[ \dfrac{B}{B_{sb}} \right]^{7/10}$ | (2.180) |
| and anisotropy and temperature dependence | $j > j_{sb}^\parallel(\vartheta, T) = j_c^c(T) \left[ \dfrac{\sqrt{\varepsilon_\vartheta}}{a_\circ} \dfrac{L_c^c(T)}{\varepsilon} \right]^{2-\zeta}$ | (2.181) |
| | $j > j_{sb}^\perp(\vartheta, T) = \varepsilon_\vartheta j_{sb}^\parallel(\vartheta, T)$ | (2.182) |
| Small-bundle pinning | $a_\circ > L_c \left[ \dfrac{1}{\widetilde{c}} \ln \dfrac{\lambda}{L_c} \right]^{-1/3}$ | (4.23) |
| | $B < B_{lb} \approx \beta_{lb} H_{c_2} \dfrac{j_{sv}}{j_\circ} \left[ \ln \left[ \kappa^2 \dfrac{j_{sv}}{j_\circ} \right] \right]^{2/3}, \quad \beta_{lb} \approx 2$ | (4.51) |
| and temperature dependence | $\dfrac{B_{lb}(T)}{H_{c_2}} \approx \dfrac{\beta_{lb} j_{sv}}{j_\circ} \left[ \dfrac{T_{dp}}{T_{dp} + T} \right]^2 \left\{ \ln \left[ \dfrac{\kappa^2 j_{sv}}{j_\circ} \left[ \dfrac{T_{dp}}{T_{dp} + T} \right]^2 \right] \right\}^{2/3}$ | (4.95) |
| and anisotropy $\mathbf{H} \parallel c$ | $\dfrac{B_{lb}(T)}{H_{c_2}} \approx \dfrac{\beta_{lb} j_{sv}}{j_\circ} \left[ \dfrac{T_{dp}}{T_{dp} + T} \right]^2 \left\{ \ln \left[ \dfrac{\kappa^2 j_{sv}}{\varepsilon^2 j_\circ} \left[ \dfrac{T_{dp}}{T_{dp} + T} \right]^2 \right] \right\}^{2/3}$ | |
| Depinning temperature | $T_{dp} \approx \dfrac{T_c}{\sqrt{Gi}} \left[ \dfrac{B}{\beta_{dp} H_{c_2}(0)} \right]^{1/2}, \quad \beta_{dp} \approx 8$ | (4.87) |

TABLE VI. Continuum elastic theory.

| Description | Formal expression | Eq. |
|---|---|---|
| Elastic energy | $\mathcal{F}[\mathbf{u}] = \dfrac{1}{2} \int_{BZ} \dfrac{d^3 k}{(2\pi)^3} u_\alpha(\mathbf{k}) \Phi_{\alpha\beta}(\mathbf{k}) u_\beta(-\mathbf{k})$ | (3.19) |
| Elastic matrix | $\Phi_{\alpha\beta}(\mathbf{k}) = [c_{11}(\mathbf{k}) - c_{66}] K_\alpha K_\beta + \delta_{\alpha\beta}[c_{66} K^2 + c_{44}(\mathbf{k}) k_z^2]$ | (3.28) |
| Green's function | $G_{\alpha\beta}(\mathbf{k}, \omega) = \dfrac{\mathcal{P}^L_{\alpha\beta}(\mathbf{K})}{-i\eta\omega + c_{11}(\mathbf{k})K^2 + c_{44}(\mathbf{k})k_z^2} + \dfrac{\mathcal{P}^T_{\alpha\beta}(\mathbf{K})}{-i\eta\omega + c_{66}K^2 + c_{44}(\mathbf{k})k_z^2}$ | (3.30) |
| Projectors | $\mathcal{P}^L_{\alpha\beta}(\mathbf{K}) = \dfrac{K_\alpha K_\beta}{K^2}, \quad \mathcal{P}^T_{\alpha\beta}(\mathbf{K}) = \dfrac{\delta_{\alpha\beta} - K_\alpha K_\beta}{K^2}$ | |
| Compression modulus | $c_{11}(\mathbf{k}) \simeq \dfrac{B^2}{4\pi} \dfrac{1}{1 + \lambda^2 k^2}$ | (3.31) |
| Tilt modulus | $c_{44}(\mathbf{k}) = c^\circ_{44}(\mathbf{k}) + c^c_{44}(\mathbf{k})$ | (3.34) |
| | $c^\circ_{44}(\mathbf{k}) \approx \dfrac{B^2}{4\pi} \dfrac{1}{1 + \lambda^2 k^2}$ | (3.31) |
| | $c^c_{44}(\mathbf{k} \to 0) = \dfrac{B(H - B)}{4\pi}$ | (3.35) |
| | $c^c_{44}(K \lesssim K_{BZ}, k_z) \approx \dfrac{\varepsilon_0}{2a_0^2} \ln \dfrac{\kappa^2}{1 + \lambda^2(K_{BZ}^2 + k_z^2)}$ | (3.35) |
| Shear modulus | $c_{66} \approx \dfrac{\Phi_0 B}{(8\pi\lambda)^2}$ | (3.32) |
| Small fields $\lambda < a_0$ | $c_{66} = \dfrac{1}{3} c_{11} = \left[ \dfrac{\pi}{6} \dfrac{\lambda}{a_0} \right]^{1/2} \dfrac{\varepsilon_0}{\lambda^2} e^{-a_0/\lambda}$ | (3.36) |

TABLE VII. Elastic moduli, anisotropic case.

| Description | Formal expression | Eq. |
|---|---|---|
| Conventions | $\parallel$:  displacement parallel to CuO planes | |
| | $\perp$:  displacement perpendicular to CuO planes | |
| Anisotropy parameter | $\varepsilon_\vartheta^2 = \varepsilon^2(\vartheta) = \varepsilon^2\cos^2\vartheta + \sin^2\vartheta$ | (2.137) |
| $\theta = \pi/2 - \vartheta$ | $\varepsilon_\theta^2 = \varepsilon^2\sin^2\vartheta + \cos^2\vartheta$ | (2.137) |
| Compression moduli (anisotropic) | $c_{11}^\parallel(\mathbf{k}) = c_{11}^\perp(\mathbf{k}) = c_{11}^{\parallel\perp}(\mathbf{k}) = \dfrac{1+(\varepsilon_\vartheta\lambda_c k)^2}{1+\lambda^2 k^2} c_{44}^{\circ\parallel}(\mathbf{k})$ | (3.45) |
| Tilt moduli (anisotropic) | $c_{44}(\mathbf{k}) = c_{44}^\circ(\mathbf{k}) + c_{44}^c(\mathbf{k}), \quad \lambda_c = \lambda_\varepsilon$ | |
| | $c_{44}^{\circ\parallel}(\mathbf{k}) = \dfrac{B^2}{4\pi} \dfrac{1}{1+\lambda^2 k^2 + (\lambda_c^2 - \lambda^2)K^2}$ | (3.42a) |
| | $c_{44}^{\circ\perp}(\mathbf{k}) = \dfrac{1+(\varepsilon_\theta\lambda_c k)^2}{1+\lambda^2 k^2} c_{44}^{\circ\parallel}(\mathbf{k})$ | (3.42b) |
| | $c_{44}^c(\mathbf{k}\to 0) = \dfrac{1}{4\pi} B(H-B)$ | |
| | $c_{44}^c(K \lesssim K_{\mathrm{BZ}}, k_z) \approx \dfrac{\varepsilon_0}{2a_0^2} \left[ \varepsilon^2 \ln \dfrac{\kappa_c^2}{1+\lambda_c^2 K_{\mathrm{BZ}}^2 + \lambda^2 k_z^2} \right.$ | |
| | $\left. + \dfrac{1}{\lambda^2 k_z^2} \ln \left[ 1 + \dfrac{\lambda^2 k_z^2}{1+\lambda^2 K_{\mathrm{BZ}}^2} \right] \right]$ | (3.43) |
| Single-vortex limit | $\varepsilon_l(k_z) \approx \varepsilon^2\varepsilon_0 \ln \left[ \dfrac{\kappa_c^2}{1+\lambda^2 k_z^2} \right]^{1/2} + \varepsilon_0 \dfrac{1}{\lambda^2 k_z^2} \ln(1+k_z^2\lambda^2)^{1/2}$ | (3.44) |
| Shear moduli (anisotropic) | $c_{66}^\parallel(\vartheta) = c_{66}\varepsilon_\vartheta^3, \quad c_{66}^\perp(\vartheta) = c_{66}/\varepsilon_\vartheta$ | (3.41) |
| Mixed compression-tilt moduli | $c_{14}^\perp(\mathbf{k}) = c_{14}^{\parallel\perp}(\mathbf{k}) = \dfrac{\sqrt{\varepsilon_\vartheta^2\varepsilon_\theta^2 - \varepsilon^2}\,\lambda_c^2 k^2}{1+\lambda^2 k^2} c_{44}^{\circ\parallel}(\mathbf{k})$ | (3.46) |
| Mixed shear-tilt moduli | $c_{64}^\parallel \simeq \dfrac{\sqrt{\varepsilon_\vartheta^2\varepsilon_\theta^2 - \varepsilon^2}}{\varepsilon_\vartheta^2} c_{66}^\parallel$ | (3.63) |

TABLE VIII. Microscopic origin of pinning.

| Description | Formal expression | Eq. |
|---|---|---|
| GL parameters | $\alpha = -\dfrac{12\pi^2}{7\zeta(3)}\dfrac{T_c}{\varepsilon_F}(T_c - T)$ | (3.64a) |
| | $\beta = \dfrac{18\pi^2}{7\zeta(3)}\dfrac{1}{N(\varepsilon_F)}\left[\dfrac{T_c}{\varepsilon_F}\right]^2$ | (3.64b) |
| | $m = \dfrac{m_e}{\chi(\rho)}, \quad \chi(\rho) = \dfrac{8}{7\zeta(3)}\sum_0^\infty \dfrac{1}{(2n+1)^2(2n+1+\rho)}$ | (3.64c) |
| | $\rho = \dfrac{\hbar v_F}{2\pi T_c l}, \quad \zeta(3) = 1.202$ | (3.66) |
| Order parameter | $|\Psi_0(T)|^2 = \dfrac{n}{2}(1 - T/T_c)$ | |
| Dimensionless pinning parameters | $\delta_\alpha = \dfrac{1}{2\pi}\dfrac{\gamma_\alpha}{\alpha^2\xi^3}, \quad \delta_m = \dfrac{7}{30\pi}\dfrac{\gamma_m}{m^2\xi^3}$ | (3.71) |
| Single-vortex pinning | $L_c^c = \varepsilon\xi\left[\dfrac{\delta}{\varepsilon}\right]^{-1/3}, \quad U_c^c = H_c^2\varepsilon\xi^3\left[\dfrac{\delta}{\varepsilon}\right]^{1/3}$ | |
| | $\dfrac{S_E^{\mathrm{eff},c}}{\hbar} = \dfrac{\hbar}{e^2}\dfrac{\varepsilon\xi}{\rho_n}\left[\dfrac{\delta}{\varepsilon}\right]^{-1/3}, \quad j_c^c = j_0\left[\dfrac{\delta}{\varepsilon}\right]^{2/3}$ | (3.74) |
| $\delta T_c$ pinning | $\dfrac{\delta_\alpha}{\varepsilon} = \dfrac{0.063}{\varepsilon}\left[\dfrac{n_i}{T_c}\dfrac{d^2 T_c}{dn_i^2}\right]^2\dfrac{1}{\xi_{\mathrm{BCS}}^5 d}\dfrac{1}{(1-t)^{1/2}} \simeq \dfrac{10^{-3}}{(1-t)^{1/2}}$ | (3.78) |
| $\delta T_c$ pinning | $\dfrac{\delta_\alpha}{\varepsilon} = \dfrac{0.4}{\varepsilon}\left[\dfrac{n_i}{T_c}\dfrac{dT_c}{dn_i}\right]^2\dfrac{1}{\xi_{\mathrm{BCS}}^3 n_i}\dfrac{1}{(1-t)^{1/2}} \simeq \dfrac{10^{-2}}{(1-t)^{1/2}}$ | (3.81) |
| $\delta l$ pinning | $\dfrac{\delta_m}{\varepsilon} = \dfrac{0.13}{\varepsilon}\dfrac{(1-t)^{3/2}}{\xi_{\mathrm{BCS}} l^2 n_i} \simeq (0.2-1)10^{-3}(1-t)^{3/2}$ | (3.83) |

TABLE IX. Dynamic approach, thermal displacements, Green's functions.

| Description | Formal expression | Eq. |
|---|---|---|
| Dynamic approach | $\delta\mathbf{v}=\dfrac{\gamma v}{\eta}\displaystyle\int dt'\,G(0,t-t')\sum_{\mu\nu}\langle(\nabla p\,[\mathbf{R}-\mathbf{R}_\mu(t')-\mathbf{v}t']\cdot\nabla)\nabla p\,[\mathbf{R}-\mathbf{R}_\nu(t)-\mathbf{v}t]\rangle_{\text{th}}$ | (3.96) |
| | $\dfrac{\delta v}{v}=\dfrac{\gamma v}{\eta a_0^2}\displaystyle\int\dfrac{d^2K}{(2\pi)^2}\,dt\,K^2 K_v\,|p(K)|^2 G(0,t)S(\mathbf{K},t)\dfrac{\sin(K_v vt)}{v}$ | (3.98) |
| Structure factor | $S(\mathbf{K},t)=\dfrac{1}{NL}\displaystyle\int dz\sum_{\mu\nu}\langle\exp\{i\mathbf{K}\cdot[\mathbf{R}_\mu(z,0)-\mathbf{R}_\nu(z,t)]\}\rangle_{\text{th}}$ | (3.99) |
| Washboard potential | $\dfrac{\delta v}{v}=\dfrac{V_0^2 k_0^3}{2\eta}\displaystyle\int d^dx\,dt\,G(\mathbf{x},t)\dfrac{\sin vk_0 t}{v}e^{-k_0^2\langle u_{\text{th}}^2(\mathbf{x},t)\rangle/2}$ | (3.126) |
| Mean thermal displacement | $\langle u_{\text{th}}^2(\mathbf{x},t)\rangle=4T\displaystyle\int\dfrac{d^dq}{(2\pi)^d}\dfrac{d\omega}{2\pi}[1-\cos(\mathbf{q}\mathbf{x}-\omega t)]\dfrac{1}{\omega}\,\text{Im}\,G(\mathbf{q},\omega)$ | (3.129) |
| Green's function (simple) | $G(\mathbf{q},\omega)=\dfrac{1}{-i\eta\omega+Cq^2}$ | |
| Mean thermal displacements | $\langle u_{\text{th}}^2(\mathbf{x},t)\rangle\approx\dfrac{T}{\pi C}[x^2+(C/\eta)t]^{1/2},\quad d=1$ | (3.130) |
| | $\langle u_{\text{th}}^2(\mathbf{x},t)\rangle\approx\dfrac{T}{\pi C}\ln\left[\dfrac{x^2+(C/\eta)t}{x_0^2}\right]^{1/2},\quad d=2$ | (3.130) |
| | $\langle u_{\text{th}}^2(\mathbf{x},t)\rangle\approx\dfrac{T}{\pi Cx_0},\quad d=3$ | (3.130) |
| Green's function (lattice) | $G(0,t)=\dfrac{\Theta(t)}{2\eta a_0^3}\left[\dfrac{t_{\text{th}}}{t}\right]^{1/2},\quad t<t_{\text{th}}$ | (6.11) |
| | $=\dfrac{\sqrt\pi}{4}\dfrac{\Theta(t)}{\eta a_0^3}\left[\dfrac{t_{\text{th}}}{t}\right]^2,\quad t_{\text{th}}\ll t\ll\left[\dfrac{\lambda}{a_0}\right]^2 t_{\text{th}}$ | (6.10) |
| | $=\dfrac{\Theta(t)}{4\sqrt\pi\eta\lambda a_0^2}\left[\dfrac{t_{\text{th}}}{t}\right]^{3/2},\quad\left[\dfrac{\lambda}{a_0}\right]^2 t_{\text{th}}\ll t$ | (6.8) |
| Thermal time | $t_{\text{th}}=\dfrac{\eta}{c_{66}K_{\text{BZ}}^2}=\dfrac{8\kappa^2 a_0^2}{c^2\rho_n}$ | (6.9) |

TABLE X. Elastic manifolds in quenched random media.

| Description | Formal expression | Eq. |
|---|---|---|
| Line wandering | $\langle\langle[\delta u(L)]^2\rangle\rangle \equiv \langle\langle[\mathbf{u(L)}-\mathbf{u(0)}]^2\rangle\rangle \propto L^{2\zeta_{d,n}}$ | (3.143) |
| Energy fluctuations | $\langle\langle[\delta\mathcal{F}(L)]^2\rangle\rangle \equiv \langle\langle[\mathcal{F}(L)-\langle\langle\mathcal{F}(L)\rangle\rangle]^2\rangle\rangle \propto L^{2\chi_{d,n}}$ | (3.144) |
| Energy exponent | $\chi_{d,n}=2\zeta_{d,n}+d-2$ | (3.146) |
| Random-field and random bond problems | RF: $\beta(n)=-n$,  RB: $\beta(n)=n$ | |
| Flory exponent | $\zeta_{d,n}^F=\dfrac{4-d}{4+\beta(n)}$,  $\beta<\beta_c$ | (3.158) |
| Short-range exponent | $\zeta_{d,n}^{SR}=\dfrac{2(4-d)}{8+n}$,  $\beta>\beta_c$ | (3.164) |
| Critical exponent | $\beta_c(n)=\dfrac{n}{2}$ | (3.163) |
| Classical creep | $\mathcal{F}(L)\simeq U_c\left[\left[\dfrac{L}{L_c}\right]^{\chi_{d,n}}-\dfrac{F}{F_c}\left[\dfrac{L}{L_c}\right]^{d+\zeta_{d,n}}\right]$ | (3.176) |
| Optimal hopping length | $L_{\mathrm{opt}}(F)\simeq L_c\left[\dfrac{F_c}{F}\right]^{1/(2-\zeta_{d,n})}$ | (3.177) |
| Optimal hopping distance | $u_{\mathrm{opt}}(F)\simeq\xi\left[\dfrac{F_c}{F}\right]^{\zeta_{d,n}/(2-\zeta_{d,n})}$ | (3.178) |
| Activation energy | $U(F)\simeq U_c\left[\dfrac{F_c}{F}\right]^{\mu}$,  $\mu=\dfrac{2\zeta_{d,n}+d-2}{2-\zeta_{d,n}}$ | (3.179) |
| Action | $S(F)\simeq S_c\left[\dfrac{F_c}{F}\right]^{\mu_S}$,  $\mu_S=\dfrac{\zeta_{d,n}+d}{2-\zeta_{d,n}}=\mu+1$ | (3.185) |
| Relaxation, classical | $F(t)\simeq F(t=0)\left[\dfrac{U_c}{T}\dfrac{1}{\ln(t/t_0)}\right]^{1/\mu}$ | (3.190) |
| Relaxation, quantum | $F(t)\simeq F(t=0)\left[\dfrac{S_c}{\hbar}\dfrac{1}{\ln(t/t_0)}\right]^{1/\mu_S}$ | (3.190) |

TABLE XI. Pinning of vortex lattice: statistical mechanics.

| Description | Formal expression | Eq. |
|---|---|---|
| Displacement | $\langle u^2(L) \rangle^{1/2} \simeq \xi \left[ \dfrac{L}{L_c} \right]^{3/2}, \quad u < \xi, \quad L < L_c$ | (4.1) |
| | $\langle u^2(L) \rangle^{1/2} \simeq \xi \left[ \dfrac{L}{L_c} \right]^{3/5}, \quad \xi < u < \xi \left[ \dfrac{a_\circ}{L_c} \right]^{3/5}, \quad L_c < L < a_\circ$ | (4.2) |
| | $\langle u^2(\mathbf{r}) \rangle^{1/2} \simeq \xi \left[ \dfrac{a_\circ}{L_c} \right]^{3/2} \left[ \left[ \dfrac{R^2}{\lambda^2} + \dfrac{a_\circ^2 L^2}{\lambda^4} \right]^{1/2} + \ln \left[ 1 + \dfrac{R^2}{a_\circ^2} + \dfrac{L}{a_\circ} \right] \right]^{1/2},$ $\quad u < \xi, \quad a_\circ < L_c$ | (4.17) |
| | $\langle u^2(\mathbf{r}) \rangle^{1/2} \simeq \xi \left\{ \left[ \dfrac{a_\circ}{L_c} \right]^3 \left[ \left[ \dfrac{R^2}{\lambda^2} + \dfrac{a_\circ^2 L^2}{\lambda^4} \right]^{1/2} + \ln \left[ 1 + \dfrac{R^2}{a_\circ^2} + \dfrac{L}{a_\circ} \right] \right] \right\}^{\zeta_{3,2}},$ $\quad \xi < u < a_\circ$ | (4.25) |
| | $\langle u^2(r) \rangle^{1/2} \simeq \dfrac{a_\circ}{2\sqrt{2}\pi} \ln \left[ 1 + \dfrac{R^2}{R_a^2} + \dfrac{a_\circ^2 L^2}{\lambda^2 R_a^2} \right], \quad a_\circ < u$ | (4.44) |
| Crossover lengths | $\langle u^2(R_c) \rangle \simeq \xi^2, \quad \langle u^2(L_c^b) \rangle \simeq \xi^2$ | (4.18) |
| | $R_c \simeq a_\circ e^{\tilde{c}(L_c/a_\circ)^3}, \quad a_\circ < R_c < \lambda, \quad L_c^b \simeq \dfrac{R_c}{a_\circ} R_c, \quad a_\circ < L_c^b < \dfrac{\lambda}{a_\circ} \lambda$ | (4.19) |
| | $R_c \simeq \lambda \left[ \dfrac{L_c}{a_\circ} \right]^3, \quad \lambda < R_c, \quad L_c^b \simeq \dfrac{\lambda}{a_\circ} R_c, \quad \dfrac{\lambda}{a_\circ} \lambda < L_c^b$ | (4.21) |
| Crossover lengths | $\langle u^2(R_a) \rangle \simeq a_\circ^2, \quad \langle u^2(L_a) \rangle \simeq a_\circ^2$ | (4.39) |
| | $R_a \simeq a_\circ e^{\tilde{c}(L_c/\xi)^3(a_\circ/\xi)^2}, \quad a_\circ < R_a < \lambda$ | (4.42) |
| | $R_a \simeq \lambda \left[ \dfrac{L_c}{\xi} \right]^3 \left[ \dfrac{a_\circ}{\xi} \right]^2, \quad \lambda < R_a$ | (4.43) |

TABLE XII. Pinning of vortex lattice: energy barriers.

| Description | Formal expression | Eq. |
|---|---|---|
| Collective pinning energy | $U_c \simeq c_{66}(\xi/R_c)^2 V_c$ | (4.45) |
| | $U_c \simeq U_{sv} \simeq H_c^2 \xi^3 \dfrac{\xi}{L_c}, \quad 1 < \dfrac{a_0}{L_c}$ | (4.46) |
| | $\simeq U_{sv} \dfrac{L_c}{a_0} \exp\left[ 2\tilde{c} \left[ \dfrac{L_c}{a_0} \right]^3 \right], \quad [\ln(\lambda/L_c)/\tilde{c}]^{-1/3} < \dfrac{a_0}{L_c} < 1$ | |
| | $\simeq U_{sv} \left[ \dfrac{\lambda}{a_0} \right]^2 \left[ \dfrac{L_c}{a_0} \right]^4, \quad \dfrac{a_0}{L_c} < [\ln(\lambda/L_c)/\tilde{c}]^{-1/3}$ | |
| Energy barriers $(j \sim 0)$ | $\dfrac{U(R)}{U_{av}} \simeq \left[ \dfrac{L}{L_c} \right]^{1/5}, \quad L_c < L < a_0$ | (4.47) |
| $(L_c < a_0)$ | $\simeq \left[ \dfrac{a_0}{L_c} \right]^{1/5} \left[ \dfrac{R}{a_0} \right]^2, \quad a_0 < R < \lambda$ | |
| | $\simeq \left[ \dfrac{a_0}{L_c} \right]^{1/5} \left[ \dfrac{\lambda}{a_0} \right]^2 \left[ \dfrac{R}{\lambda} \right]^{7/5}, \quad \lambda < R < R_a$ | |
| | $\simeq \left[ \dfrac{a_0}{L_c} \right]^{1/5} \left[ \dfrac{\lambda}{a_0} \right]^2 \left[ \dfrac{R_a}{\lambda} \right]^{7/5} \dfrac{R}{R_a}, \quad R_a < R$ | |
| Activation energy $(j \lesssim j_c)$ | $U_c^b \simeq c_{66}(\xi/R_c)^2 V_c \simeq (R_\parallel/R_c)(L^b/L_c^b)U_c$ | (4.57) |
| | $U(j) \simeq U_c^b \left[ 1 - \dfrac{j}{j_c} \right]^\alpha$ | (4.61) |
| | $U_c^b \simeq U_{sv} \simeq T_c \sqrt{(1-t)/Gi} \left[ \dfrac{j_{sv}}{j_0} \right]^{1/2}, \quad 1 < \dfrac{a_0}{L_c}$ | (4.58) |
| Anisotropic case, | $\simeq U_{sv} \dfrac{L_c}{a_0} \exp\left[ 5\tilde{c} \left[ \dfrac{L_c}{a_0} \right]^3 \right], \quad [\ln(\lambda/L_c)/3\tilde{c}]^{-1/3} < \dfrac{a_0}{L_c} < 1$ | |
| see (4.138) and (4.139) | $\simeq U_{sv} \dfrac{\lambda L_c}{a_0^2} \exp\left[ 2\tilde{c} \left[ \dfrac{L_c}{a_0} \right]^3 \right],$ | |
| | $\qquad\qquad [\ln(\lambda/L_c)/\tilde{c}]^{-1/3} < \dfrac{a_0}{L_c} < [\ln(\lambda/L_c)/3\tilde{c}]^{-1/3}$ | |
| | $\simeq U_{sv} \left[ \dfrac{\lambda}{a_0} \right]^3 \left[ \dfrac{L_c}{a_0} \right]^4, \quad \dfrac{a_0}{L_c} < [\ln(\lambda/L_c)/\tilde{c}]^{-1/3}$ | |
| Activation energy $(j \ll j_c)$ | $U(j) \simeq U_{sv} \left[ \dfrac{j_{sv}}{j} \right]^{1/7}, \quad j_{sb} < j \ll j_{sv}$ | (4.67) |
| | $\simeq U_{sb} \left[ \dfrac{j_{sb}}{j} \right]^{5/2}, \quad j_{sb}(a_0/\lambda)^{2/3} < j < j_{sb}$ | |
| | $\simeq U_{sb} \dfrac{\lambda}{a_0} \dfrac{j_{sb}}{j}, \quad j_{lb} < j < j_{sb}(a_0/\lambda)^{2/3}$ | |
| Anisotropic case, | $\simeq U_{lb} \left[ \dfrac{j_{lb}}{j} \right]^{7/9}, \quad j_{CDW} < j < j_{lb}$ | |
| see (4.146) and (4.147) | $\simeq U_{CDW} \left[ \dfrac{j_{CDW}}{j} \right]^{1/2}, \quad 0 < j < j_{CDW}$ | |
| | $U_{sb} \simeq U_{sv} \left[ \dfrac{a_0}{L_c} \right]^{1/5}, \quad U_{lb} \simeq U_{sb} \left[ \dfrac{\lambda}{a_0} \right]^3, \quad U_{CDW} \simeq U_{lb} \left[ \dfrac{a_0^2 L_c^3}{\xi^5} \right]^{7/5}$ | |

TABLE XIII. Pinning of vortex lattice: critical current densities, actions.

| Description | Formal expression | Eq. |
|---|---|---|
| Critical current density | $j_c \simeq cU_c/BV_c\xi \simeq (\xi/R_c)^2 j_\circ$ | (4.49) |
| | $j_c \simeq j_{sv} \simeq (\xi/L_c)^2 j_\circ, \quad 1 < a_\circ/L_c$ | (4.50) |
| | $\simeq j_{sv}\left[\dfrac{L_c}{a_\circ}\right]^2 \exp\left[-2\tilde{c}\left[\dfrac{L_c}{a_\circ}\right]^3\right], \quad [\ln(\lambda/L_c)/\tilde{c}]^{-1/3} < \dfrac{a_\circ}{L_c} < 1$ | |
| | $\simeq j_{sv}\left[\dfrac{a_\circ}{\lambda}\right]^2 \left[\dfrac{a_\circ}{L_c}\right]^4, \quad \dfrac{a_\circ}{L_c} < [\ln(\lambda/L_c)/\tilde{c}]^{-1/3}$ | |
| Relaxation | $j(t) \simeq j_{sv}\left[\dfrac{T}{U_c}\ln\dfrac{t}{t_\circ}\right]^{-7}, \quad j_{sb} < j \ll j_{sv}$ | (4.69) |
| | $\simeq j_{sb}\left[\dfrac{T}{U_{sb}}\ln\dfrac{t}{t_\circ}\right]^{-2/5}, \quad j_{sb}(a_\circ/\lambda)^{2/3} < j < j_{sb}$ | |
| | $\simeq j_{sb}\dfrac{\lambda}{a_\circ}\left[\dfrac{T}{U_{sb}}\ln\dfrac{t}{t_\circ}\right]^{-1}, \quad j_{lb} < j < j_{sb}(a_\circ/\lambda)^{2/3}$ | |
| | $\simeq j_{lb}\left[\dfrac{T}{U_{lb}}\ln\dfrac{t}{t_\circ}\right]^{-9/7}, \quad j_{CDW} < j < j_{lb}$ | |
| | $\simeq j_{CDW}\left[\dfrac{T}{U_{CDW}}\ln\dfrac{t}{t_\circ}\right]^{-2}, \quad 0 < j < j_{CDW}$ | |
| | $j_{sb} \simeq j_{sv}\left[\dfrac{L_c}{a_\circ}\right]^{7/5}, \quad j_{lb} \simeq j_{sb}\left[\dfrac{a_\circ}{\lambda}\right]^2, \quad j_{CDW} \simeq j_{lb}\left[\dfrac{\xi^5}{a_\circ^2 L_c^3}\right]^{9/5}$ | |
| Action ($j \lesssim j_c$) | $S_c^b \simeq t_c U_c^b \simeq \eta\xi^2 V_c(R_\parallel/R_c)(L^b/L_c^b)$ | (4.59) |
| | $S(j) \simeq S_c^b\left[1 - \dfrac{j}{j_c}\right]^{\alpha_S}$ | (4.62) |
| | $S_c^b \simeq S_{sv} \simeq \dfrac{\hbar}{Qu}\left[\dfrac{j_\circ}{j_{sv}}\right]^{1/2}, \quad 1 < \dfrac{a_\circ}{L_c}$ | (4.60) |
| Anisotropic case, | $\simeq S_{sv}\dfrac{a_\circ}{L_c}\exp\left[7\tilde{c}\left[\dfrac{L_c}{a_\circ}\right]^3\right], \quad [\ln(\lambda/L_c)/3\tilde{c}]^{-1/3} < \dfrac{a_\circ}{L_c} < 1$ | |
| see (4.140) and (4.141) | $\simeq S_{sv}\dfrac{\lambda}{L_c}\exp\left[4\tilde{c}\left[\dfrac{L_c}{a_\circ}\right]^3\right],$ | |
| | $\qquad\qquad [\ln(\lambda/L_c)/\tilde{c}]^{-1/3} < \dfrac{a_\circ}{L_c} < [\ln(\lambda/L_c)/3\tilde{c}]^{-1/3}$ | |
| | $\simeq S_{sv}\left[\dfrac{\lambda}{a_\circ}\right]^5 \left[\dfrac{L_c}{a_\circ}\right]^8, \quad \dfrac{a_\circ}{L_c} < [\ln(\lambda/L_c)/\tilde{c}]^{-1/3}$ | |
| Action ($j \ll j_c$) | $S(j) \simeq S_{sv}\left[\dfrac{j_{sv}}{j}\right]^{8/7}, \quad j_{sb} < j \ll j_{sv}$ | (4.68) |
| | $\simeq S_{sb}\left[\dfrac{j_{sb}}{j}\right]^{7/2}, \quad j_{sb}(a_\circ/\lambda)^{2/3} < j < j_{sb}$ | |
| | $\simeq S_{sb}\dfrac{\lambda}{a_\circ}\left[\dfrac{j_{sb}}{j}\right]^2, \quad j_{lb} < j < j_{sb}(a_\circ/\lambda)^{2/3}$ | |
| Anisotropic case, | $\simeq S_{lb}\left[\dfrac{j_{lb}}{j}\right]^{16/9}, \quad j_{CDW} < j < j_{lb}$ | |
| see (4.148) and (4.149) | $\simeq S_{CDW}\left[\dfrac{j_{CDW}}{j}\right]^{3/2}, \quad 0 < j < j_{CDW}$ | |
| | $S_{sb} \simeq S_{sv}\left[\dfrac{a_\circ}{L_c}\right]^{8/5}, \quad S_{lb} \simeq S_{sb}\left[\dfrac{\lambda}{a_\circ}\right]^5, \quad S_{CDW} \simeq S_{lb}\left[\dfrac{a_\circ^2 L_c^3}{\xi^5}\right]^{16/5}$ | |

TABLE XIV. Vortex lattice: thermal fluctuations.

| Description | Formal expression | Eq. |
|---|---|---|
| Thermal displacement | $\langle u^2 \rangle_{th} \approx \dfrac{\lambda T}{2a_o^2 \sqrt{c_{66}\hat{c}_{44}}} = \dfrac{1}{8\sqrt{\pi}} \dfrac{T}{c_{66}a_o^3} a_o^2 = \dfrac{1}{2\sqrt{\pi}} \dfrac{T}{\varepsilon_o a_o} a_o^2$ | (4.85) |
| Depinning condition | $\langle u^2(T_{dp}) \rangle_{th} \approx \xi^2$ | (4.76) |
| Depinning temperature | $T_{dp} \simeq 2\sqrt{\pi}\varepsilon_o \xi^2 \left[ \dfrac{B}{\Phi_o} \right]^{1/2}$ | (4.86) |
| | $\approx \dfrac{T_c}{\sqrt{Gi}} \left[ \dfrac{B}{\beta_{dp}H_{c_2}(0)} \right]^{1/2} \approx \left[ \dfrac{B}{B_{sb}} \right]^{1/2} \tilde{T}_{dp}^s$ | (4.87) |
| | $\simeq \left[ \dfrac{1}{Gi} \dfrac{j_{sv}(0)}{j_o(0)} \right]^{1/2} \left[ \dfrac{B}{B_{sb}(0)} \right]^{1/2} T_c, \quad \beta_{dp} \approx 8$ | |
| Single-vortex depinning | $T_{dp}^s \approx 0.7 \left[ \dfrac{1}{Gi} \dfrac{j_{sv}}{j_o} \right]^{1/2} T_c \ll T_c, \quad \dfrac{1}{Gi} \dfrac{j_{sv}(0)}{j_o(0)} < 1$ | (4.109) |
| | $T_{dp}^s \simeq T_c \left\{ 1 - \left[ Gi \dfrac{j_o(0)}{j_{sv}(0)} \right]^{3/2} \right\} \simeq T_c, \quad \dfrac{1}{Gi} \dfrac{j_{sv}(0)}{j_o(0)} > 1$ | (4.111) |
| Weak-pinning condition | $\left[ \dfrac{j_{sv}(0)}{j_o(0)} \right]^3 < Gi\, c_L^4 \dfrac{\beta_m}{\beta_{dp}} \approx \dfrac{5.6}{8} Gi\, c_L^4$ | (4.114) |
| Depinning field | $B_{dp} = \beta_{dp} Gi\, H_{c_2}(0) \left[ \dfrac{T}{T_c} \right]^2$ | (4.88) |
| | $\simeq Gi \dfrac{j_o(0)}{j_{sv}(0)} B_{sb}(0) \left[ \dfrac{T}{T_c} \right]^2, \quad \beta_{dp} \approx 8$ | |
| Melting condition | $\langle u^2(T_m) \rangle_{th} \approx c_L^2 a_o^2$ | (4.104) |
| Melting temperature | $T_m(B) \approx 2\sqrt{\pi}\varepsilon_o c_L^2 \left[ \dfrac{\Phi_o}{B} \right]^{1/2}$ | (4.105) |
| | $\approx \dfrac{c_L^2 T_c}{\sqrt{\beta_m Gi}} \left[ 1 - \dfrac{T_m}{T_c} - \dfrac{B}{H_{c_2}(0)} \right] \left[ \dfrac{H_{c_2}(0)}{B} \right]^{1/2}, \quad \beta_m \approx 5.6$ | |
| Melting field | $B_m(T) \approx \beta_m \dfrac{c_L^4}{Gi} H_{c_2}(0) \left[ 1 - \dfrac{T}{T_c} - \dfrac{B_m}{H_{c_2}(0)} \right]^2$ | (4.107) |
| | $\approx \dfrac{4\theta^2}{(1+\sqrt{1+4\theta T_s/T})^2} H_{c_2}(0),$ | (5.10) |
| | $\theta = c_L^2 \sqrt{\beta_m/Gi} \left[ \dfrac{T_c}{T} - 1 \right], \quad T_s = T_c c_L^2 \sqrt{\beta_m/Gi}$ | |

TABLE XV. Vortex-glass scaling.

| Description | Formal expression | Eq. |
|---|---|---|
| Correlation length | $\xi_{VG}(T) \propto |T - T_g|^{-\nu}$ | (7.25) |
| Relaxation time | $\tau_{VG}(T) \propto [\xi_{VG}(T)]^z \propto |T - T_g|^{-\nu z}$ | (7.26) |
| Typical exponents (exp.) | $\nu \simeq 1-2, \quad z \simeq 3-6$ | |
| Scaling laws | $E \propto \xi_{VG}^{-(z+1)} e_{\pm}(j\xi_{VG}^{d-1}, \omega\tau_{VG})$ | (7.38) |
| | $\sigma(\omega) \propto \xi_{VG}^{2+z-d} s_{\pm}(\omega\xi_{VG}^z)$ | (7.39) |
| Characteristic at $T_g$ | $E \propto j^{(z+1)/(d-1)}$ | (7.40) |
| Conductivity at $T_g$ | $\sigma(\omega) \propto (-i\omega)^{(d-z-2)/z}$ | (7.47) |
| Resistivity above $T_g$ | $\rho(T) \propto (T - T_g)^{\nu(z+2-d)}$ | (7.41) |
| Glassy response below $T_g$ | $E \propto e^{-c(j_c/j)^{\mu}}$ | (7.43) |
| Crossover current densities | $j_x^{\pm} \propto |T - T_g|^{\nu(d-1)}$ | (7.42) |
| Crossover frequency | $\Omega(T) \sim \dfrac{1}{\tau_{VG}} \propto (T - T_g)^{\nu z}$ | (7.48) |

TABLE XVI. Layered superconductors: Josephson and pancake vortices.

| Description | Formal expression | Eq. |
|---|---|---|
| Josephson length | $\Lambda = d \left[ \dfrac{M}{m} \right]^{1/2} = \dfrac{d}{\varepsilon}$ | (8.9) |
| Josephson current density | $j_J = \dfrac{c\Phi_0\varepsilon}{8\pi^2\lambda^2\Lambda} \simeq j_0 \dfrac{\varepsilon\xi}{\Lambda}$ | (8.8) |
| Deconfinement current density | $j_{con} \sim j_0 \dfrac{\xi}{\Lambda}$ | (8.107) |
| Line energy Josephson vortex | $e_J = \varepsilon\varepsilon_0 \left[ \ln\dfrac{\lambda}{d} + 1.12 \right]$ | (8.17) |
| Friction coefficient Josephson vortex | $\eta_J = 2.226 \dfrac{\Phi_0^2}{2\pi\rho_n^c c^2 \varepsilon\Lambda^2}$ | (8.19) |
| Pancake interaction | $V^{int}(R, z=0) \approx 2d\varepsilon_0 \ln\dfrac{R}{\xi}, \quad \xi < R < \Lambda$ <br> $\approx 2d\varepsilon_0 \dfrac{R}{\Lambda} - \dfrac{\Lambda}{4R}, \quad \Lambda < R < \lambda/\varepsilon$ <br> $\approx 2d\varepsilon_0 \dfrac{R}{\Lambda}, \quad \lambda/\varepsilon < R$ | (8.42) |
| Kink-antikink interaction | $V_{K,-K}^{int} \simeq 2d\varepsilon_0 \ln\dfrac{R}{\xi}, \quad \xi < R < \Lambda$ <br> $\approx 2d\varepsilon_0 \ln\dfrac{\Lambda}{\xi} - \dfrac{\Lambda}{4R}, \quad \Lambda < R < \lambda/\varepsilon$ <br> $\approx 2d\varepsilon_0 \ln\dfrac{\Lambda}{\xi}, \quad \lambda/\varepsilon < R$ | 8.43 |
| Kink-kink interaction | $V_{K,K}^{int} \simeq d\varepsilon_0 \dfrac{d}{2\lambda}\dfrac{R}{\lambda} + \dfrac{1}{2}\left[\dfrac{R}{\Lambda}\right]^2 \ln\dfrac{\Lambda}{R}, \quad \xi < R < \Lambda$ <br> $\approx d\varepsilon_0 \dfrac{\Lambda}{2R}, \quad \Lambda < R < \lambda/\varepsilon$ | (8.44) |
| Line tensions (approximative) | $\varepsilon_l^{\perp}(\vartheta) \simeq \dfrac{\varepsilon_0}{\varepsilon}\dfrac{1}{\cos^3\vartheta}, \quad 0 < \vartheta < \varepsilon$ <br> $\simeq \left[\dfrac{\varepsilon}{\sin\vartheta}\right]^3, \quad \varepsilon < \vartheta < \dfrac{\pi}{2}$ | (8.47) |
| | $\varepsilon_l^{\parallel}(\vartheta) \simeq \varepsilon\varepsilon_0\cos\vartheta, \quad 0 < \vartheta < \varepsilon$ <br> $\simeq \dfrac{\varepsilon}{\sin\vartheta}, \quad \varepsilon < \vartheta < \dfrac{\pi}{2}$ | (8.48) |
| Lock-in angle | $\vartheta_L \simeq 2v\dfrac{H_{c_1}^c}{H_a}\dfrac{\ln(\Lambda/\xi)}{\ln(\lambda/\xi)}, \quad v = \dfrac{L_z}{L_y}$ | (8.63) |

TABLE XVII. Layered superconductors: statistical mechanics.

| Description | Formal expression | Eq. |
|---|---|---|
| BKT temperature | $T_{\text{BKT}} = \dfrac{\nu_s^\infty}{2} \varepsilon_0(T_{\text{BKT}})d$ | (8.88) |
| | $T_{\text{BKT}} \approx T_{c_0}\left[1 - \dfrac{2T_{c_0}}{\nu_s^\infty d \varepsilon_0(0)}\right]$ | (8.89) |
| BKT coherence length | $\xi_{\text{BKT}}(T) \simeq \xi(T)\exp\left[\left[b\dfrac{T_{c_0}-T}{T-T_{\text{BKT}}}\right]^{1/2}\right]$ | (8.90) |
| BKT charact. $(T<T_{\text{BKT}})$ | $V = \rho I \propto \left[\dfrac{J}{J_0}\right]^\alpha, \quad \alpha(T)=1+\dfrac{\nu_s \varepsilon_0 d}{T}$ | (8.96) |
| Nonlinear resistivity $(T<T_{\text{BKT}})$ | $\rho = 2\pi\xi^2\rho_n n_v \propto \left[\dfrac{J}{J_0}\right]^{\nu_s \varepsilon_0 d/T}$ | (8.95) |
| BKT resistivity $(T>T_{\text{BKT}})$ | $\dfrac{\rho(T)}{\rho_n} \simeq 2\pi\left[\dfrac{\xi}{\xi_{\text{BKT}}}\right]^2 \simeq 2\pi\exp\left[-2\left[b\dfrac{T_{c_0}-T}{T-T_{\text{BKT}}}\right]^{1/2}\right]$ | (8.98) |
| 3D transition temperature | $T_c = T_{\text{BKT}} + \dfrac{b(T_{c_0}-T_{\text{BKT}})}{\{\ln[\Lambda/\xi(T_{\text{BKT}})]\}^2}$ | (8.100) |
| 3D fluctuation region | $\delta T_f^{3D} \simeq \dfrac{2(T_c-T_{\text{BKT}})}{\ln[\Lambda/\xi(T_{\text{BKT}})]} = \dfrac{2b(T_c-T_{\text{BKT}})}{\{\ln[\Lambda/\xi(T_{\text{BKT}})]\}^3}$ | (8.101) |
| 2D fluctuation region | $T_f^{2D} \simeq T_{c_0} - \dfrac{1}{2}(T_{c_0}-T_{\text{BKT}})\ln\dfrac{\Lambda}{\xi(T_{\text{BKT}})}$ | (8.104) |
| Numerical estimates (BiSCCO) | $T_{c_0}-T_{\text{BKT}} \approx 4.5$ K, $\quad T_c-T_{\text{BKT}} \approx b$ K | (8.106) |
| | $\delta T_f^{3D} \approx 0.8b$ K, $\quad T_{c_0}-T_f^{2D} \approx 5$ K | |
| 2D melting | $T_m^{2D} \approx \dfrac{da_\Delta^2 c_{66}}{4\pi} \simeq \dfrac{d\varepsilon_0}{8\sqrt{3}\pi} \ll T_{\text{BKT}}$ | (8.111) |
| | $T_m^{2D} \simeq \dfrac{T_{\text{BKT}}}{4\sqrt{3}\pi}\dfrac{T_{c_0}-T_m^{2D}}{T_{c_0}-T_{\text{BKT}}} \approx 25$ K | (8.113) |
| Crossover field | $B_{2D} \approx \pi\dfrac{\Phi_0}{\Lambda^2}\ln\dfrac{\Lambda}{\xi}$ | (8.124) |
| 3D melting | $T_m(B) \approx \left[\dfrac{\pi}{2}\ln\dfrac{H_{c_2}}{B}\right]^{1/2} \varepsilon\varepsilon_0 c_L^2 \left[\dfrac{\Phi_0}{B}\right]^{1/2}, \quad B<B_{2D}$ | (8.125) |
| | $\approx T_m^{2D}\left\{1+\dfrac{b}{[\ln(B/B_{2D})]^{1/\nu}}\right\}, \quad B_{2D}<B$ | (8.130) |
| Evaporation temperature | $T_e(B) \simeq T_m(B)\left[\dfrac{B_{2D}}{B}\right]^{1/2}, \quad B<B_{2D}$ | (8.131) |
| Decoupling temperature | $T_{dc}^G(B) \simeq \varepsilon\varepsilon_0 a_0 \simeq T_m^{2D}\left[\dfrac{B_{2D}}{B}\right]^{1/2}, \quad B_{2D}<B$ | (8.141) |

TABLE XVIII. Layered superconductors: pinning.

| Description | Formal expression | Eq. |
|---|---|---|
| *Single vortex intrinsic pinning* | | |
| Activation energy | $U(j \lesssim j_c) \simeq T_c \sqrt{(1-t)/Gi} \left[ \dfrac{\Lambda}{\xi} \right]^{3/2} \left[ \dfrac{j_c^{\mathrm{in}}}{j_\circ} \right]^{1/2} \left[ 1 - \dfrac{j}{j_c^{\mathrm{in}}} \right]^{5/4}$ | (8.183) |
| | $U(j \ll j_c^{\mathrm{in}}) \simeq T_c \sqrt{(1-t)/Gi} \left[ \dfrac{\Lambda}{\xi} \right]^{3/2} \left[ \dfrac{j_c^{\mathrm{in}}}{j_\circ} \right]^{1/2}$ | (8.185) |
| Action | $S_E^{\mathrm{eff}}(j \lesssim j_c) \simeq \dfrac{\hbar}{Qu} \left[ \dfrac{\Lambda}{\xi} \right]^{5/2} \left[ \dfrac{j_\circ}{j_c^{\mathrm{in}}} \right]^{1/2} \left[ 1 - \dfrac{j}{j_c^{\mathrm{in}}} \right]^{3/4}$ | (8.184) |
| | $S_E^{\mathrm{eff}}(j \ll j_c^{\mathrm{in}}) \simeq \dfrac{\hbar}{Qu} \left[ \dfrac{\Lambda}{\xi} \right]^{5/2} \left[ \dfrac{j_\circ}{j_c^{\mathrm{in}}} \right]^{1/2} \dfrac{j_c^{\mathrm{in}}}{j} \ln \dfrac{j_c^{\mathrm{in}}}{j}$ | (8.187) |
| *Bundle strong intrinsic pinning* | | |
| Activation energy | $U(j \ll j_c) \simeq \varepsilon_\circ d \ln \dfrac{\Lambda}{\xi} \left[ \dfrac{j_b}{j} \right]^2$ | (8.198) |
| *Single pancake pinning* | | |
| Activation energy | $U_{\mathrm{pc}} \simeq T_c \sqrt{(1-t)/Gi} \, \dfrac{\Lambda}{\xi} \dfrac{j_{\mathrm{pc}}}{j_\circ} \simeq T_c \dfrac{1-t}{Gi^{2D}} \dfrac{j_{\mathrm{pc}}}{j_\circ}$ | (8.219) |
| Action | $\dfrac{S_{\mathrm{pc}}}{\hbar} \simeq \dfrac{t_c U_{\mathrm{pc}}}{\hbar} \simeq \dfrac{\hbar}{e^2} \dfrac{d}{\rho_n} \simeq \dfrac{1}{Qu} \dfrac{\Lambda}{\xi}$ | (8.241) |
| *2D collective pinning* | | |
| Collective pinning radius | $R_c \simeq a_\circ \dfrac{\varepsilon_\circ d}{U_{\mathrm{pc}}} \left[ \dfrac{\xi}{2a_\circ} \right]^2$ | (8.221) |
| Activation energy | $U_c^b \simeq U_{\mathrm{pc}} \left[ \dfrac{R_c}{a_\circ} \right]^3, \quad a_\circ < R_c$ | |
| | $U(j) \simeq U_{\mathrm{sb}}^{2D} \left[ \dfrac{j_c^{2D}}{j} \right]^{7/4}, \quad j_{\mathrm{CDw}}^{2D} < j \ll j_c^{2D}$ | (8.237) |
| | $\simeq U_{\mathrm{CDW}}^{2D} \dfrac{j_{\mathrm{CDw}}^{2D}}{j} \ln \dfrac{j_{\mathrm{CDw}}^{2D}}{j}, \quad j < j_{\mathrm{CDw}}^{2D}$ | |
| | $U_{\mathrm{sb}}^{2D} \simeq \dfrac{(\varepsilon_\circ d)^3}{U_{\mathrm{pc}}^2} \left[ \dfrac{\xi}{a_\circ} \right]^6, \quad U_{\mathrm{CDW}}^{2D} \simeq \dfrac{(\varepsilon_\circ d)^3}{U_{\mathrm{pc}}^2} \dfrac{a_\circ}{\xi}$ | |
| | $j_c^{2D} \simeq j_{\mathrm{pc}} \dfrac{a_\circ}{R_c}, \quad j_{\mathrm{CDw}}^{2D} \simeq j_c^{2D} \left[ \dfrac{\xi}{a_\circ} \right]^4$ | |
| Action | $\dfrac{S_E^{\mathrm{eff}}}{\hbar} \simeq \dfrac{S_{\mathrm{pc}}}{\hbar} \left[ \dfrac{R_c}{a_\circ} \right]^4, \quad a_\circ < R_c$ | (8.245) |
| | $S_E^{\mathrm{eff}}(j) \simeq S_{\mathrm{pc}} \left[ \dfrac{R_c}{a_\circ} \right]^4 \left[ \dfrac{j_c^{2D}}{j} \right]^{11/4}, \quad j_{\mathrm{CDw}}^{2D} < j \ll j_c^{2D}$ | (8.246) |

TABLE XIX. Strong pinning: twinning planes.

| Description | Formal expression | Eq. |
|---|---|---|
| Pinning potential | $\varepsilon_{TP} \approx \varepsilon_0 \left[ 1 - \dfrac{\lvert \Psi^{TP} \rvert^2}{\lvert \Psi_\infty \rvert^2} \right]$ | |
| Renormalized pinning potential | $\varepsilon_{TP}(T) \simeq \varepsilon_{TP}, \quad T < T_{dp}^{TP}$ <br><br> $\simeq \varepsilon_{TP} \left[ \dfrac{\widetilde{T}_{dp}^{TP}}{T} \right]^2 \left[ \ln \left[ \dfrac{T}{\widetilde{T}_{dp}^{TP}} \right]^2 \right]^2, \quad T_{dp}^{TP} < T$ | (9.17) |
| Depinning energy | $\widetilde{T}_{dp}^{TP} \simeq 2\xi \sqrt{\varepsilon_l \varepsilon_{TP}} \simeq \dfrac{T_c}{\sqrt{2Gi}} \sqrt{\varepsilon_{TP}/\varepsilon_0} \left[ 1 - \dfrac{T}{T_c} \right]^{1/2}$ | (9.19) |
| Depinning temperature | $T_{dp}^{TP} = \widetilde{T}_{dp}^{TP}(T_{dp}^{TP})$ | (9.19) |
| Critical current density | $j_c^{TP} \simeq \dfrac{\varepsilon_{TP}}{\varepsilon_0} j_0, \quad T < T_{dp}^{TP},$ | (9.27) |
| | $\simeq \dfrac{\varepsilon_{TP}}{\varepsilon_0} \left[ \dfrac{\widetilde{T}_{dp}^{TP}}{T} \right]^4 j_0, \quad T_{dp}^{TP} < T < T_{dl},$ | (9.29) |
| | $\simeq \dfrac{\varepsilon_{TP}}{\varepsilon_0} \dfrac{\xi}{d_{TP}} \left[ \dfrac{\widetilde{T}_{dp}^{TP}}{T} \right]^2 j_0, \quad T_{dl} < T,$ | (9.32) |
| Creep | $U_{hl}(j) \simeq \xi \sqrt{\varepsilon_l \varepsilon_{TP}(T)} \dfrac{\varepsilon_{TP}(T)}{\varepsilon_0} \dfrac{j_0}{j}$ | (9.39) |
| Trapping angle | $\varphi_t = \left[ \dfrac{2\varepsilon_{TP}}{\varepsilon_l} \right]^{1/2}$ | (9.5) |
| Lock-in angle | $\varphi_L = \dfrac{4\pi\varepsilon_l}{\Phi_0 H} \varphi_t$ | (9.9) |

TABLE XX. Strong pinning: columnar defects.

| Description | Formal expression | Eq. |
|---|---|---|
| Pinning potential | $\varepsilon_r \approx \dfrac{\varepsilon_0}{2} \ln\left[1 + \dfrac{r_r^2}{2\xi^2}\right]$ | (9.60) |
| Renormalized pinning potential | $\varepsilon_r(T) \approx \varepsilon_r f_{lr}\left[\dfrac{T}{\tilde{T}_{dp}^r}\right]$ | (9.67) |
| | $f_{lr}(x) = 1 - x^2 \ (x < 1), \quad = e^{-x} \ (x > 1)$ | (9.67) |
| Energy dispersion | $\gamma \approx \gamma_i + t(d_r)$ | (9.115) |
| Depinning energy | $\tilde{T}_{dp}^r \approx \dfrac{r_r}{\pi}\sqrt{\varepsilon_l \varepsilon_0} = \dfrac{r_r}{2\sqrt{2}\pi\xi(0)} \dfrac{T_c}{\sqrt{Gi}}\left[1 - \dfrac{T}{T_c} - \dfrac{B}{H_{c_2}(0)}\right]$ | (9.77) |
| Depinning temperature | $T_{dp}^r = \tilde{T}_{dp}^r(T_{dp}^r)$ | |
| Delocalization temperature | $T_{dl} = \tilde{T}_{dl}(T_{dl}) \approx \tilde{T}_{dp}^r(T_{dl})\ln(d_r/b_0)^2$ | (9.72) |
| Single vortex regime | $B < B_{rb} \approx \dfrac{4\varepsilon_r(T)}{\varepsilon_0}B_\Phi, \quad T < T_{dl}$ | (9.44) |
| | $\simeq B_\Phi\left[\dfrac{b_0}{d_r}\right]^2 \dfrac{\varepsilon_r}{\varepsilon_0}\left[\dfrac{T_{dl}}{T}\right]^6, \quad T_{dl} < T$ | (9.78) |
| | $\propto B_\Phi\left[1 - \dfrac{T}{T_c}\right]^6, \quad T \to T_c$ | |
| *Single vortex properties* | | |
| Critical current densities | $j_c = \dfrac{3\sqrt{3}}{4\sqrt{2}}j_0 \approx j_0, \quad T < T_{r\xi}$ | (9.57) |
| | $= \dfrac{27\sqrt{2}}{64}\left[\dfrac{r_r}{2\xi}\right]^2 j_0, \quad T_{r\xi} < T < T_{dp}^r$ | (9.61) |
| | $= \dfrac{r_r^2}{\xi^2}\dfrac{\tilde{T}_{dp}^r}{T}\exp\left[-\dfrac{3}{2}\dfrac{T}{\tilde{T}_{dp}^r}\right]j_0, \quad T_{dp}^r < T < T_{dl}$ | (9.71) |
| | $= \dfrac{\varepsilon_r}{\varepsilon_0}\dfrac{\xi}{d_r}\left[\dfrac{b_0}{d_r}\right]^2\left[\dfrac{\tilde{T}_{dl}}{T}\right]^4 j_0, \quad T_{dl} < T$ | (9.71) |
| Creep | $U_{nn} \simeq E_k \simeq d_r\sqrt{\varepsilon_l \varepsilon_r(T)}$ | (9.113) |
| | $U_{hl}(j) \simeq E_k\dfrac{j_d}{j}, \quad j_d \simeq \dfrac{\xi}{d_r}\dfrac{\varepsilon_r(T)}{\varepsilon_0}j_0 < j \ll j_c$ | (9.110) |
| | $U_{VRH}(j) \simeq E_k\left[\dfrac{j_v}{j}\right]^{1/3}, \quad j_L < j < j_v \simeq \dfrac{\xi}{\varepsilon_0 g d_r^3}j_0$ | (9.123) |
| | $U_{Mott}(L) \simeq (\gamma L E_k^2)^{1/3}, \quad j < j_L \simeq \dfrac{\xi}{L}\dfrac{E_k}{d_r \varepsilon_0}j_0$ | (9.119) |
| Quantum creep | see (9.134) and (9.135) | |
| Crossover current density | $j_{xs} \simeq j_d[\varepsilon_r(T)/\gamma]^{1/2} \simeq j_v[\varepsilon_r(T)/\gamma]^{3/2}$ | (9.129) |
| Trapping/locking angle | $\theta_t = \left[\dfrac{2\varepsilon_r(T)}{\varepsilon_l}\right]^{1/2}, \quad \theta_L \simeq \dfrac{4\pi\varepsilon_l}{\Phi_0 H}\theta_t$ | (9.173) |
| *Vortage bundles* | | |
| Plastic pinning, $T < T_{r\xi}$ | $j_{pl} \simeq j_0, \quad B_{rb} \lesssim B$ | |
| | $\simeq \dfrac{a_0 \xi}{d_r^2}j_0 \simeq \dfrac{B_{rb}}{\sqrt{BH_{c_2}}}, \quad B_{rb} < B < B_{r_r}$ | (9.97) |

TABLE XX. (*Continued*).

| Description | Formal expression | Eq. |
|---|---|---|
| Collective pinning | $j_c \simeq \left[\dfrac{B_{r_r}}{H_{c_2}}\right]^{1/2} \dfrac{B_{rb}}{B} j_\circ, \quad T < T_{r\xi}$ | |
| | $\simeq \dfrac{H_{c_2}}{B_{r_r}} \dfrac{B_{rb}}{B} j_\circ, \quad T_{r\xi} < T$ | (9.96) |
| | $\simeq \dfrac{r_r^2}{d_r^2} \left[\dfrac{\xi}{d_r}\right]^{1/2} \left[\dfrac{B}{B_{rb}}\right]^{1/4} \left[\dfrac{\tilde{T}_{dp}^r}{T}\right]^{5/4} j_\circ, \quad T_{dp}^r < T < T_{dl}$ | |
| | $\simeq \dfrac{\xi r_r^2}{d_r^3} \left[\dfrac{B}{B_{rb}}\right]^{1/4} \left[\dfrac{\tilde{T}_{dp}^r}{T}\right]^4 j_\circ, \quad T_{dl} < T$ | (9.100) |
| Plastic creep | $U_{pl}(j) \simeq \varepsilon\varepsilon_\circ d_r \left[\dfrac{B}{B_{rb}}\right]^{3/2} \left[\dfrac{j_{pl}}{j}\right]^2, \quad R_\perp < (a_\circ^2\lambda)^{1/3}$ | (9.142) |
| | $\simeq \varepsilon\varepsilon_\circ d_r \left[\dfrac{\lambda}{d_r}\right]^{1/2} \dfrac{B}{B_{rb}} \left[\dfrac{j_{pl}}{j}\right]^{5/4}, \quad (a_\circ^2\lambda)^{1/3} < R_\perp < \lambda$ | |
| | $\simeq \varepsilon\varepsilon_\circ \lambda \dfrac{B}{B_{rb}} \dfrac{j_{pl}}{j}, \quad \lambda < R_\perp$ | (9.143) |
| Collective creep | $U(j) \simeq \varepsilon\varepsilon_\circ r_p \dfrac{u_\circ R_\circ^4}{a_\circ^5} \left[\dfrac{j_{xb}}{j}\right]^{11/4}, \quad a_\circ < R_\perp < (a_\circ^2\lambda)^{1/3}$ | |
| | $\simeq \varepsilon\varepsilon_\circ r_p \dfrac{u_\circ R_\circ^3}{a_\circ^4} \left[\dfrac{\lambda}{R_\circ}\right]^{1/2} \left[\dfrac{j_{xb}}{j}\right]^{29/16}, \quad (a_\circ^2\lambda)^{1/3} < R_\perp < \lambda$ | |
| | $\simeq \varepsilon\varepsilon_\circ r_p \dfrac{u_\circ \lambda R_\circ^2}{a_\circ^4} \left[\dfrac{j_{xb}}{j}\right]^{3/2}, \quad \lambda < R_\perp$ | (9.146) |
| with | $j_{xb} \simeq \dfrac{\xi u_\circ}{R_\circ^2} j_\circ$ | (9.145) |
| CDW creep | $U(j) \simeq \varepsilon\varepsilon_\circ r_p \dfrac{R_\circ^4}{a_\circ^4} \left[\dfrac{a_\circ}{u_\circ}\right]^{10} \left[\dfrac{j_{xb}}{j}\right]^2, \quad a_\circ < R_\perp < (a_\circ^2\lambda)^{1/3}$ | |
| | $U(j) \simeq \varepsilon\varepsilon_\circ r_p \dfrac{R_\circ^3}{a_\circ^3} \left[\dfrac{\lambda}{R_\circ}\right]^{1/2} \left[\dfrac{a_\circ}{u_\circ}\right]^{25/4} \left[\dfrac{j_{xb}}{j}\right]^{5/4}, \quad (a_\circ^2\lambda)^{1/3} < R_\perp < \lambda$ | |
| | $\simeq \varepsilon\varepsilon_\circ r_p \dfrac{\lambda R_\circ^2}{a_\circ^3} \left[\dfrac{a_\circ}{u_\circ}\right]^5 \dfrac{j_{xb}}{j}, \quad \lambda < R_\perp$ | (9.149) |
| with | $j_{xb} \simeq \dfrac{a_\circ \xi}{R_\circ^2} \left[\dfrac{u_\circ}{a_\circ}\right]^5 j_\circ$ | (9.148) |
| "dressed" vortices | $U_{VRH}(j) \simeq U_{VRH}(j_{xb}) \dfrac{j_{xb}}{j}, \quad j < j_{xb}$ | (9.154) |
| with | $j_{xb} \simeq \left[\dfrac{d_r}{a_\circ}\right]^{3/2} \left[\dfrac{\varepsilon_\circ}{\gamma}\right]^{3/4} j_v$ | (9.131) |
| "dressed" vortices | $U_{Mott}(L) \simeq U_{Mott}(L_b) \dfrac{L}{L_b}, \quad L_b < L$ | (9.153) |
| with | $L_b \simeq \dfrac{E_k}{\gamma} \left[\dfrac{a_\circ}{d_r}\right]^{3/2} \left[\dfrac{\gamma}{\varepsilon_\circ}\right]^{3/4}$ | (9.132) |

TABLE XX. (*Continued*).

| Description | Formal expression | Eq. |
|---|---|---|
| *Bose-glass transition* | | |
| Low magnetic fields | $B_{\mathrm{BG}}(T) \simeq \dfrac{B_\Phi}{Gi^2} \left[ \dfrac{r_r}{\xi(0)} \right]^4 \left[ \dfrac{T_c}{T} \right]^4 \left[ 1 - \dfrac{T}{T_c} \right]^4, \quad B < \dfrac{\Phi_0}{\lambda^2}$ | (9.156) |
| Shift of transition | $T_{\mathrm{BG}}(B) \approx \gamma T_m(B) + (1-\gamma)T_c \left[ 1 - \dfrac{B}{H_{c_2}(0)} \right]$ | (9.163) |
| intermediate fields | $\gamma = \left[ 1 + \dfrac{1}{16c_L \sqrt{Gi}} \dfrac{r_r^2}{\xi(0)d_r} \right]^{-1}, \quad d_r/c_L < a_0$ | (9.164) |
| high fields | $\gamma(a_0) = \left[ 1 + \dfrac{1}{16\sqrt{Gi}} \dfrac{a_0}{\xi(0)} \dfrac{r_r^2}{d_r^2} \right]^{-1}, \quad a_0 < d_r/c_L$ | (9.165) |
| *Bose-glass scaling* | | |
| Anisotropic scaling | $l_\perp = l_{\mathrm{loc}}(T) \propto (T_{\mathrm{BG}} - T)^{-\nu_\perp}, \quad \nu_\perp \sim 1$ | (9.166) |
| | $l_\parallel \sim l_\perp^2 / D_0$ | (9.167) |
| Dynamic scaling | $\tau_{\mathrm{BG}} \propto l_\perp^{z'}, \quad z' \sim 5-9$ | |
| Scaling laws | $E \propto l_\perp^{-(z'+1)} e_\pm(jl_\perp^3)$ | (9.168) |
| Characteristic at $T_{\mathrm{BG}}$ | $E \propto j^{(z'+1)/3}$ | (9.169) |
| Resistivity above $T_{\mathrm{BG}}$ | $\rho \propto (T - T_{\mathrm{BG}})^{\nu_\perp(z'-2)}$ | (9.170) |
| Crossover current densities | $j_x^\pm \propto (l_\perp l_\parallel)^{-1} \propto |T - T_{\mathrm{BG}}|^{3\nu_\perp}$ | (9.171) |

TABLE XXI. Macroscpic linear and nonlinear response.

| Description | Formal expression | Eq. |
|---|---|---|
| Nonlinearity parameter | $\alpha = \left\| \dfrac{\partial U(j)}{\partial j} \right\| \dfrac{\delta j}{T}$ | (10.6) |
| *Linear response* | | |
| *TAFF, $\alpha \ll 1$* | | |
| Resistivity | $\rho \approx 2 \mathcal{A} \rho_{\text{flow}} \dfrac{U_0}{T} \exp\left[ -\dfrac{U_0}{T} \right]$ | (10.11) |
| Diffusion equation | $\partial_t B = \dfrac{c^2}{4\pi} \rho\, \Delta B$ | (10.12) |
| Skin depth | $\delta_s = \left[ \dfrac{\rho c^2}{2\pi\omega} \right]^{1/2}$ | (10.14) |
| Peak frequency | $\omega_{\text{peak}} \approx 0.8 \dfrac{c^2}{d^2} \rho(H,T)$ | (10.20) |
| Resistivity | $\rho(T,H) \approx 1.25 \omega_{\text{peak}} \dfrac{d^2}{c^2}$ | |
| | $\rho[\mu\Omega\,\text{cm}] \approx 7.6 \times 10^{-3} d^2 [\text{cm}^2] \nu_{\text{peak}}[\text{Hz}]$ | (10.21) |
| *Nonlinear response, $\alpha \gg 1$* | | |
| Diffusion equations | $\partial_t B = -\partial_x [v_0 B e^{-U(j)/T}]$ | (10.23) |
| | $\partial_t j = \dfrac{c}{4\pi} \partial_x^2 [v_0 B e^{-U(j)/T}]$ | (10.24) |
| Solution $(j = j_0 + j_1)$ | $U[j_0(t)] \approx T \ln\left[ 1 + \dfrac{t}{t_0} \right]$ | (10.32) |
| | $j_1(x,t) \approx \dfrac{T}{\|\partial_j U\|} \ln\left[ \left[ 1 - \dfrac{4x^2}{d^2} \right] \dfrac{H}{B(x)} \right]$ | (10.30) |
| Characteristic time | $t_0 = \dfrac{\pi}{2} \dfrac{T d^2}{\|\partial_j U\| c v_0 H}$ | (10.33) |
| | $\approx \dfrac{1}{\mathcal{A}} \dfrac{T}{U_c} \dfrac{d^2}{c^2 \rho_{\text{flow}}}$ | |
| | $t_0[s] \approx \dfrac{10^{-3}}{\mathcal{A}} \dfrac{T}{U_c} \dfrac{d^2[\text{cm}^2]}{\rho_{\text{flow}}[\mu\Omega\,\text{cm}]}$ | (10.34) |
| Relevant barriers | $U(B,j) = T \ln\left[ 1 + \dfrac{t}{t_0} \right]$ | (10.38) |
| Self-organized critical state | $\partial_t b = \partial_x (\partial_x b \|\partial_x b\|^\sigma), \quad \partial_t J = \partial_x^2 (J\|J\|^\sigma)$ | (10.40) |
| Current, full penetration | $J(x,t) \approx \left[ \dfrac{1 - 4x^2/d^2}{1 + t/t_0} \right]^{1/\sigma}, \quad \sigma = \dfrac{U_0}{T}, \quad J = \dfrac{j}{j_c}$ | (10.42) |
| Field, full penetration | $b(x,t) \approx b_0 - \dfrac{x}{(1 + t/t_0)^{1/\sigma}}, \quad b = \delta B/B_0$ | (10.44) |
| General peak criterion | $U\left[ j = \dfrac{c h_{\text{ac}}}{2\pi d}, H, T \right] = T \ln \dfrac{1}{\omega_{\text{peak}} t_0}$ | (10.59) |

TABLE XXII. Some useful numerical expressions.

| Quantity | Numerical expression | Eq. |
|---|---|---|
| 1 eV | 11 605 K | |
| $\Phi_0$ [G] | $2.068 \times 10^{-7}$ | |
| $\sigma_n$ [s$^{-1}$] | $0.9 \times 10^{10} \dfrac{1}{\rho_n [\Omega\,\mathrm{cm}]}$ | |
| $\dfrac{e^2}{m_e}$ [cm$^3$ s$^{-2}$] | $2.5327 \times 10^8$ | |
| $\tau_r$ [s] | $3.9484 \times 10^{-9} \dfrac{m^* \sigma_n [\mathrm{s}]^{-1}}{n [\mathrm{cm}^{-3}]}, \quad m^* = \dfrac{m_{\mathrm{eff}}}{m_e}$ | |
| $k_F$ [cm$^{-1}$] | $\{3\pi^2 n [\mathrm{cm}^{-3}]\}^{1/3}$ | |
| $\varepsilon_F$ [eV] | $3.811 \times 10^{-16} \dfrac{(k_F[\mathrm{cm}^{-1}])^2}{m^*}$ | |
| $v_F$ [cm s$^{-1}$] | $1.158 \dfrac{k_F[\mathrm{cm}^{-1}]}{m^*}$ | |
| $l = v_F \tau_r$ [Å] | $10^8 v_F[\mathrm{cm/s}]\, \tau_r[\mathrm{s}]$ | |
| $\Delta_{\mathrm{BCS}}$ [eV] | $1.52 \times 10^{-4} T_c[\mathrm{K}]$ | |
| $\lambda_L$ [Å] | $5.134 \times 10^{13} \sqrt{m^*/n\,[\mathrm{cm}^{-3}]}$ | (3.70) |
| $\xi_{\mathrm{BCS}}$ [Å] | $2.095 \times 10^{-8} \dfrac{v_F[\mathrm{cm/s}]}{\Delta_{\mathrm{BCS}}[\mathrm{eV}]}$ | (3.69) |
| $H_{c\mathrm{BCS}}$ [G] | $\dfrac{\Phi_0}{\sqrt{2/3}\pi^2 \lambda_L \xi_{\mathrm{BCS}}} = \dfrac{2.566 \times 10^8}{\lambda_L[\mathrm{Å}]\,\xi_{\mathrm{BCS}}[\mathrm{Å}]}$ | |
| $\chi$ | 1 (clean limit), $\quad 1.33 \dfrac{l}{\xi_{\mathrm{BCS}}}$ (dirty limit) | (3.65) |
| $\lambda(0)$ [Å] | $\dfrac{1}{\sqrt{2\chi}} \lambda_L[\mathrm{Å}]$ | (2.6) |
| $\xi(0)$ [Å] | $0.7385\sqrt{\chi}\,\xi_{\mathrm{BCS}}[\mathrm{Å}]$ | (2.5) |
| $H_c(0)$ [G] | $\dfrac{\Phi_0}{2\sqrt{2}\pi\lambda(0)\xi(0)} = \dfrac{2.327.10^8}{\lambda(0)[\mathrm{Å}]\,\xi(0)[\mathrm{Å}]}$ | (2.7) |
| $H_{c_1}(0)$ [G] | $\dfrac{\Phi_0}{4\pi\lambda^2(0)}\ln\kappa = \dfrac{\ln\kappa}{\sqrt{2}\kappa} H_c(0), \quad \kappa = \dfrac{\lambda(0)}{\xi(0)}$ | (2.13) |
| $H_{c_2}(0)$ [G] | $\dfrac{\Phi_0}{2\pi\xi^2(0)} = \sqrt{2}\kappa H_c(0)$ | (2.17) |
| $R = \dfrac{\hbar}{e^2}$ [$\Omega$] | 4108.6 | |
| $H^2$ [G$^2$] | $7.253 \times 10^{-9}$ [KÅ$^{-3}$] | |
| $\varepsilon_0$ [K/Å] | $\dfrac{1.964 \times 10^8}{(\lambda[\mathrm{Å}])^2}$ | (2.14) |
| $Gi$ | $\dfrac{1}{8}\left[\dfrac{T_c}{\varepsilon\varepsilon_0(0)\xi(0)}\right]^2$ | (2.47) |
| $Qu$ | $\dfrac{e^2}{\hbar}\dfrac{\rho_n}{\varepsilon\xi} = 2.434 \times 10^4 \dfrac{\rho_n[\Omega\,\mathrm{cm}]}{\varepsilon\xi[\mathrm{Å}]}$ | (2.167) |
| $\nabla \wedge \mathbf{B} = \dfrac{4\pi}{c}\mathbf{j}$ | $B[\mathrm{G}], \quad j[\mathrm{A\,cm}^{-2}], \quad \text{length [cm]}, \quad c = 10$ | |
| $j_0$ [A cm$^{-2}$] | $\dfrac{cH_c}{3\sqrt{6}\pi\lambda} = 0.433 \dfrac{H_c[\mathrm{G}]}{\lambda\,[\mathrm{cm}]}$ | (2.30) |

# REFERENCES

Abrikosov, A. A., 1957, Zh. Eksp. Teor. Fiz. **32**, 1442 [Sov. Phys. JETP **5**, 1174 (1957)].

Abrikosov, A. A., 1988, *Fundamentals of the Theory of Metals* (North-Holland, Amsterdam).

Abrikosov, A. A., L. P. Gor'kov, and I. E. Dzyaloshinski, 1975, *Methods of Quantum Field Theory in Statistical Physics* (Dover, New York).

Affleck, I., and E. Brézin, 1985, Nucl. Phys. B **257**, 451.

Aharony, A., Y. Imry, and S.-k. Ma, 1976, Phys. Rev. Lett. **37**, 1364.

Ambegaokar, V., B. I. Halperin, and J. S. Langer, 1971, Phys. Rev. B **4**, 2612.

Ambegaokar, V., B. I. Halperin, D. R. Nelson, and E. D. Siggia, 1978, Phys. Rev. Lett. **40**, 783.

Ambegaokar, V., B. I. Halperin, D. R. Nelson, and E. D. Siggia, 1980, Phys. Rev. B **21**, 1806.

Anderson, P. W., 1962, Phys. Rev. Lett. **9**, 309.

Anderson, P. W., 1987, Science **235**, 1196.

Anderson, P. W., and Y. B. Kim, 1964, Rev. Mod. Phys. **36**, 39.

Andreev, A. F., and I. M. Lifshitz, 1969, Zh. Eksp. Teor. Fiz. **56**, 2057 [Sov. Phys. JETP **29**, 1107 (1969)].

Ao, P., and D. J. Thouless, 1993, Phys. Rev. Lett. **70**, 2158.

Ao, P., and D. J. Thouless, 1994, Phys. Rev. Lett. **72**, 132.

Artemenko, S. N., I. G. Gorlova, and Yu. I. Latyshev, 1989a, Pis'ma Zh. Eksp. Teor. Fiz. **49**, 566 [JETP Lett. **49**, 654 (1989)].

Artemenko, S. N., I. G. Gorlova, and Yu. I. Latyshev, 1989b, Phys. Lett. A **138**, 428.

Artemenko, S. N., I. G. Gorlova, and Yu. I. Latyshev, 1989c, Pis'ma Zh. Eksp. Theor. Fiz. **49**, 352 [JETP Lett. **49**, 403 (1989)].

Artemenko, S. N., and A. N. Kruglov, 1990, Phys. Lett. A **143**, 485.

Bak, P., C. Tang, and K. Wiesenfeld, 1988, Phys. Rev. A **38**, 364.

Balatskii, A. V., L. I. Burlachkov, and L. P. Gor'kov, 1986, Zh. Eksp. Teor. Fiz. **90**, 1478 [Sov. Phys. JETP **63**, 866 (1986)].

Balatskii, A. V., and V. M. Vinokur, 1984, Solid State Commun. **52**, 847.

Banks, T., C. Bender, and T. T. Wu, 1973, Phys. Rev. D **8**, 3366.

Bardeen, J., and R. Sherman, 1975, Phys. Rev. B **12**, 2634.

Bardeen, J., and M. J. Stephen, 1965, Phys. Rev. **140**, 1197A.

Barone, A., A. I. Larkin, and Yu. N. Ovchinnikov, 1990, J. Supercond. **3**, 155.

Baskaran, G., and P. W. Anderson, 1988, Phys. Rev. B **37**, 580.

Batlogg, B., 1990, in *The Phenomenology of Flux Motion in High Temperature Superconductivity,* Proceedings of the Los Alamos Symposium-1989, edited by K. S. Bedell, D. Coffey, D. E. Meltzer, D. Pines, and J. R. Schrieffer (Addison-Wesley, Redwood City, CA), p. 37.

Baz', A. I., Ya. B. Zel'dovich, and A. M. Perelomov, 1969, *Scattering, Reactions, and Decay in Nonrelativistic Quantum Mechanics* (Israel Program for Scientific Translations, Jerusalem).

Bean, C. P., 1962, Phys. Rev. Lett. **8**, 250.

Bean, C. P., 1964, Rev. Mov. Phys. **36**, 31.

Beasley, M. R., R. Labusch, and W. W. Webb, 1969, Phys. Rev. **181**, 682.

Beasley, M. R., J. E. Mooij, and T. P. Orlando, 1979, Phys. Rev. Lett. **42**, 1165.

Beck, R. G., D. E. Farrell, J. P. Rice, D. M. Ginsberg, and V.

G. Kogan, 1992, Phys. Rev. Lett. **68**, 1594.

Bednorz, J. G., and K. A. Müller, 1986, Z. Phys. **64**, 189.

Berezinskii, V. L., 1970, Zh. Eksp. Teor. Fiz. **59**, 907 [Sov. Phys. JETP **32**, 493 (1971)].

Berezinskii, V. L., 1971, Zh. Eksp. Teor. Fiz. **61**, 1144 [Sov. Phys. JETP **34**, 610 (1972)].

Berghuis, P., and P. H. Kes, 1993, Phys. Rev. B **47**, 262.

Berghuis, P., A. L. F. van der Slot, and P. H. Kes, 1990, Phys. Rev. Lett. **65**, 2583.

Bethe, H. A., 1931, Z. Phys. **71**, 205.

Bhatt, R. N., and A. P. Young, 1985, Phys. Rev. Lett. **54**, 924.

Binder, K., and A. P. Young, 1986, Rev. Mod. Phys. **58**, 801.

Blandin, A., 1978, J. Phys. (Paris) Colloq. **C6-39**, 1499.

Blatter, G., V. B. Geshkenbein, 1993, Phys. Rev. B **47**, 2725.

Blatter, G., V. B. Geshkenbein, and A. I. Larkin, 1992, Phys. Rev. Lett. **68**, 875.

Blatter, G., V. B. Geshkenbein, and A. I. Larkin, 1993, Phys. Rev. Lett. **71**, 302.

Blatter, G., V. B. Geshkenbein, and V. M. Vinokur, 1991, Phys. Rev. Lett. **66**, 3297.

Blatter, G., and B. I. Ivlev, 1993, Phys. Rev. Lett. **70**, 2621.

Blatter, G., and B. I. Ivlev, 1994, Phys. Rev. B **50**, 10 272.

Blatter, G., B. I. Ivlev, Y. Kagan, M. Theunissen, Y. Volokitin, and P. Kes, 1994, preprint.

Blatter, G., B. I. Ivlev, and J. Rhyner, 1991, Phys. Rev. Lett. **66**, 2392.

Blatter, G., J. Rhyner, and V. M. Vinokur, 1991, Phys. Rev. B **43**, 7826.

Bolle, C.A., P. L. Gammel, D. G. Grier, C. A. Murray, D. J. Bishop, D. B. Mitzi, and A. Kapitulnik, 1991, Phys. Rev. Lett. **66**, 112.

Bouchaud, J.-P., M. Mézard, and J. S. Yedidia, 1991, Phys. Rev. Lett. **67**, 3840.

Bouchaud, J.-P., M. Mézard, and J. S. Yedidia, 1992, Phys. Rev. B **46**, 14 686.

Brandt, E. H., 1977a, J. Low Temp. Phys. **26**, 709.

Brandt, E. H., 1977b, J. Low Temp. Phys. **26**, 735.

Brandt, E. H., 1977c, J. Low Temp. Phys. **28**, 263.

Brandt, E. H., 1977d, J. Low Temp. Phys. **28**, 291.

Brandt, E. H., 1986a, J. Low Temp. Phys. **64**, 375.

Brandt, E. H., 1986b, Phys. Rev. B **34**, 6514.

Brandt, E. H., 1989, Phys. Rev. Lett. **63**, 1106.

Brandt, E. H., 1990, Z. Phys. B **80**, 167.

Brandt, E. H., 1991a, Int. J. Mod. Phys. B **5**, 751.

Brandt, E. H., 1991b, Phys. Rev. Lett. **67**, 2219.

Brandt, E. H., 1991c, Physica C **185-189**, 270.

Brandt, E. H., 1992a, Europhys. Lett. **18**, 635.

Brandt, E. H., 1992b, Phys. Rev. Lett. **68**, 3769.

Brandt, E. H., 1992c, Phys. Rev. Lett. **69**, 1105.

Brandt, E. H., 1992d, Physica C **195**, 1.

Brandt, E. H., P. Esquinazi, and G. Weiss, 1989, Phys. Rev. Lett. **62**, 2330.

Brandt, E. H., and U. Essmann, 1987, Phys. Status Solidi B **144**, 13.

Brandt, E. H., and A. Sudbø, 1991a, Physica C **180**, 426.

Brandt, E. H., and A. Sudbø, 1991b, Phys. Rev. Lett. **66**, 2278.

Brawner, D. A., N. P. Ong, and Z. Z. Wang, 1993, Phys. Rev. B **47**, 1156.

Brawner, D. A., and H. R. Ott, 1994, Phys. Rev. B **50**, 6530.

Bray, A. J., and M. A. Moore, 1984, J. Phys. C **17**, L463.

Bray, A. J., and M. A. Moore, 1985, Phys. Rev. B **29**, 340.

Brézin, E., D. R. Nelson, and A. Thiaville, 1985, Phys. Rev. B **31**, 7124.

Brunner, O., L. Antognazza, J.-M. Triscone, L. Miéville, and O.

Fischer, 1991, Phys. Rev. Lett. **67**, 1354.

Büttiker, M., and R. Landauer, 1981, Phys. Rev. A **23**, 1397.

Bulaevskii, L. N., 1973, Zh. Eksp. Teor. Fiz. **64**, 2241 [Sov. Phys. JETP **37**, 1133 (1973)].

Bulaevskii, L. N., 1991, Phys. Rev. B **44**, 910.

Bulaevskii, L. N., and J. R. Clem, 1991, Phys. Rev. B **44**, 10 234.

Bulaevski, L. N., V. L. Ginzburg, and A. A. Sobyanin, 1988, Zh. Eksp. Teor. Fiz. **94**, 355 [Sov. Phys. JETP **68**, 1499 (1988)].

Bulaevskii, L. N., M. Ledvij, and V. G. Kogan, 1992, Phys. Rev. B **46**, 366.

Burkov, S. E., 1991, Phys. Rev. B **44**, 2850.

Burlachkov, L., M. Konczykowski, Y. Yeshurun, and F. Holtzberg, 1991, J. Appl. Phys. **70**, 5759.

Burton, W. K., N. Cabrera, and F. C. Frank, 1951, Philos. Trans. R. Soc. London, Ser. A **243**, 299.

Buzdin, A., and D. Feinberg, 1990, J. Phys. (Paris) **51**, 1971.

Buzdin, A. I., and A. Yu. Simonov, 1990, Pis'ma Zh. Eksp. Teor. Fiz. **51**, 168 [JETP Lett. **51**, 191 (1990)].

Caldeira, A. O., and A. J. Leggett, 1981, Phys. Rev. Lett. **46**, 211.

Caldeira, A. O., and A. J. Leggett, 1983, Ann. Phys. **149**, 374.

Callan, C. G., and S. Coleman, 1977, Phys. Rev. D **16**, 1762.

Campbell, A. M., and J. E. Evetts, 1972, Adv. Phys. **21**, 199.

Campbell, I. A., L. Fruchter, and R. Cabanel, 1990, Phys. Rev. Lett. **64**, 1561.

Campbell, L. J., M. M. Doria, and V. G. Kogan, 1988, Phys. Rev. B **38**, 2439.

Cardy, J. L., and S. Ostlund, 1982, Phys. Rev. B **25**, 6899.

Caroli, C., P. G. de Gennes, J. Matricon, 1964, Phys. Lett. **9**, 307.

Carton, J. P., 1991, J. Phys. I (Paris) **1**, 113.

Cataudella, V., and P. Minnhagen, 1990, Physica C **166**, 442.

Cava, R. J., B. Batlogg, C. H. Chen, E. A. Rietman, S. M. Zahurak, and D. Werder, 1987, Phys. Rev. B **36**, 5719.

Cava, R. J., B. Batlogg, R. B. van Dover, D. W. Murphy, S. Sunshine, T. Siegrist, J. P. Remeika, E. A. Rietman, S. Zahurak, and G. P. Espinosa, 1987, Phys. Rev. Lett. **58**, 1676.

Ceperley, D., 1978, Phys. Rev. B **18**, 3126.

Ceperley, D. M., and E. L. Pollock, 1989, Phys. Rev. B **39**, 2084.

Chakravarty, S., B. I. Ivlev, and Yu. N. Ovchinnikov, 1990a, Phys. Rev. B **42**, 2143.

Chakravarty, S., B. I. Ivlev, and Yu. N. Ovchinnikov, 1990b, Phys. Rev. Lett. **64**, 3187.

Charalambous, M., 1992, Ph.D. thesis (CRTPT, CNRS, Grenoble).

Charalambous, M., J. Chaussy, P. Lejay, and V. Vinokur, 1993, Phys. Rev. Lett. **71**, 436.

Chien, T. R., T. W. Jing, N. P. Ong, and Z. Z. Wang, 1991, Phys. Rev. Lett. **66**, 3075.

Chikumoto, N., M. Konczykowski, N. Motohira, and K. Kishio, 1992a, Physica C **199**, 32.

Chikumoto, N., M. Konczykowski, N. Motohira, and A. P. Malozemoff, 1992b, Phys. Rev. Lett. **69**, 1260.

Chudnovsky, E. M., 1986, Phys. Rev. B **33**, 245.

Chudnovsky, E. M., 1989, Phys. Rev. B **40**, 11 355.

Chudnovsky, E. M., 1990, Phys. Rev. Lett. **65**, 3060.

Chudnovsky, E. M., 1991, Phys. Rev. Lett. **67**, 1809.

Chui, S. T., and J. D. Weeks, 1976, Phys. Rev. B **14**, 4978.

Cieplak, M., J. R. Banavar, and A. Khurana, 1991, J. Phys. A **24**, L145.

Cieplak, M., J. R. Banavar, M. S. Li, and A. Khurana, 1992, Phys. Rev. B **45**, 786.

Civale, L., A. D. Marwick, M. W. McElfresh, T. K.

Worthington, A. P. Malozemoff, F. H. Holtzberg, J. R. Thompson, and M. A. Kirk, 1990, Phys. Rev. Lett. **65**, 1164.

Civale, L., A. D. Marwick, T. K. Worthington, M. A. Kirk, J. R. Thompson, L. Krusin-Elbaum, Y. Sun, J. R. Clem, and F. Holtzberg, 1991, Phys. Rev. Lett. **67**, 648.

Clem, J. R., 1975, J. Low Temp. Phys. **18**, 427.

Clem, J. R., 1991, Phys. Rev. B **43**, 7837.

Clem, J. R., and M. W. Coffey, 1990, Phys. Rev. B **42**, 6209.

Clem, J. R., M. W. Coffey, and Z. Hao, 1991, Phys. Rev. B **44**, 2732.

Clem, J. R., H. R. Kerchner, and T. S. Sekula, 1976, Phys. Rev. B **14**, 1893.

Coffey, M. W., 1994, Phys. Rev. B **49**, 9774.

Coffey, M. W., and J. R. Clem, 1991a, Phys. Rev. B **44**, 6903.

Coffey, M. W., and J. R. Clem, 1991b, Phys. Rev. Lett. **67**, 386.

Coffey, M. W., and J. R. Clem, 1992a, Phys. Rev. B **45**, 9872.

Coffey, M. W., and J. R. Clem, 1992b, Phys. Rev. B **45**, 10 527.

Coleman, S., 1977, Phys. Rev. D **15**, 2929.

Cook, J., and B. Derrida, 1989, J. Stat. Phys. **57**, 89.

Cook, J., and B. Derrida, 1990, J. Phys. A **23**, 1523.

Coppersmith, S. N., M. Inui, and P. B. Littlewood, 1990, Phys. Rev. Lett. **64**, 2585.

de Almeida, J. R. L., and D. J. Thouless, 1978, J. Phys. A **11**, 983.

de Gennes, P.-G., 1986, *Superconductivity of Metals and Alloys* (Addison-Wesley, Reading, MA).

Dekker, C., W. Eidelloth, and R. H. Koch, 1992, Phys. Rev. Lett. **68**, 3347.

Dekker, C., P. J. M. Wöltgens, R. H. Koch, B. W. Hussey, and A. Gupta, 1992, Phys. Rev. Lett. **69**, 2717.

Deutscher, G., and K. A. Müller, 1987, Phys. Rev. Lett. **59**, 1745.

Dinger, T. R., T. K. Worthington, W. J. Gallagher, and R. L. Sandstrom, 1987, Phys. Rev. Lett. **58**, 2687.

Dolan, G. J., G. V. Chandrashekhar, T. R. Dinger, C. Feild, and F. Holtzberg, 1989, Phys. Rev. Lett. **62**, 827.

Dong, M., M. C. Marchetti, A. A. Middleton, and V. M. Vinokur, 1993, Phys. Rev. Lett. **70**, 662.

Doniach, S., 1990, in *The phenomenology of flux motion in high temperature superconductors,* Proceedings of the Los Alamos Symposium—1989, edited by K.S. Bedell, D. Coffey, D. E. Meltzer, D. Pines, and J. R. Schrieffer (Addison-Wesley, Reading, MA), p. 406.

Doniach, S., and M. Inui, 1990, Phys. Rev. B **41**, 6668.

Dorsey, A. T., 1991, Phys. Rev. B **43**, 7575.

Dorsey, A. T., M. Huang, and M. P. A. Fisher, 1992, Phys. Rev. B **45**, 523.

Dotsenko, V. S., M. V. Feigel'man, and L. B. Joffe, 1990, Sov. Sci. Rev. A Phys. **15**, 1.

Duan, Ji-Min, and E. Šimánek, 1994, Phys. Lett. A **190**, 118.

Durán, C., P. L. Gammel, R. Wolfe, V. J. Fratello, D. J. Bishop, J. P. Rice, and D. M. Ginsberg, 1992, Nature **357**, 474.

Durán, C., J. Yazyi, F. de la Cruz, D. J. Bishop, D. B. Mitzi, and A. Kapitulnik, 1991, Phys. Rev. B **44**, 7737.

Ebner, C., and D. Stroud, 1985, Phys. Rev. B **31**, 165.

Eckern, U., G. Schön, and V. Ambegaokar, 1984, Phys. Rev. B **30**, 6419.

Edwards, S. F., and P. W. Anderson, 1975, J. Phys. F **5**, 965.

Efetov, K. B., 1979, Zh. Eksp. Teor. Fiz. **76**, 1781 [Sov. Phys. JETP **49**, 905 (1979)].

Efetov, K. B., and A. I. Larkin, 1977, Zh. Eksp. Teor. Fiz. **72**, 2350 [Sov. Phys. JETP **45**, 1236 (1977)].

Esquinazi, P., 1991, J. Low Temp. Phys. **85**, 139.

Farrell, D. E., S. Bonham, J. Foster, Y. C. Chang, P. Z. Jiang,

K. G. Vandervoort, D. J. Lam, and V. G. Kogan, 1989, Phys. Rev. Lett. **63**, 782.

Farrell, D. E., J. P. Rice, D. M. Ginsberg, 1991, Phys. Rev. Lett. **67**, 1165.

Farrell, D. E., J. P. Rice, D. M. Ginsberg, and J. Z. Liu, 1990, Phys. Rev. Lett. **64**, 1573.

Farrell, D. E., C. M. Williams, S. A. Wolf, N. P. Bansal, and V. G. Kogan, 1988, Phys. Rev. Lett. **62**, 2805.

Feigel'man, M. V., 1979, Zh. Eksp. Teor. Fiz. **76**, 784 [Sov. Phys. JETP **49**, 395 (1979)].

Feigel'man, M. V., 1983, Zh. Eksp. Teor. Fiz. **85**, 1851 [Sov. Phys. JETP **58**, 1076 (1983)].

Feigel'man, M. V., V. B. Geshkenbein, L. B. Ioffe, and A. I. Larkin, 1993, Phys. Rev. B **48**, 16 641.

Feigel'man, M. V., V. B. Geshkenbein, and A. I. Larkin, 1990, Physica C **167**, 177.

Feigel'man, M. V., V. B. Geshkenbein, A. I. Larkin, and S. Levit, 1993, Pis'ma Zh. Eksp. Teor. Fiz. **57**, 699 [JETP Lett. **57**, 711 (1993)].

Feigel'man, M. V., V. B. Geshkenbein, A. I. Larkin, and V. M. Vinokur, 1989, Phys. Rev. Lett. **63**, 2303.

Feigel'man, M. V., V. B. Geshkenbein, and V. M. Vinokur, 1990, Pis'ma Zh. Eksp. Teor. Fiz. **52**, 1141 [JETP Lett. **52**, 546 (1990)].

Feigel'man, M. V., V. B. Geshkenbein, and V. M. Vinokur, 1991, Phys. Rev. B **43**, 6263.

Feigel'man, M. V., and L. B. Ioffe, 1995, JETP Lett. (to be published).

Feigel'man, M. V., and V. M. Vinokur, 1990, Phys. Rev. B **41**, 8986.

Feigel'man, M. V., and K. Ziegler, 1992, Phys. Rev. B **46**, 6647.

Feinberg, D., and C. Villard, 1990, Phys. Rev. Lett. **65**, 919.

Feynman, R. P., 1972, *Statistical Mechanics,* Frontiers in Physics Lecture Notes No. 36 (Benjamin/Cummings, Reading, MA).

Fiory, A. T., A. F. Hebard, and W. I. Glaberson, 1983, Phys. Rev. B **28**, 5075.

Fischer, K. H., 1976, Solid State Commun. **18**, 1515.

Fischer, K. H., 1991, Physica C **178**, 161.

Fischer, K. H., 1992, Physica C **193**, 401.

Fischer, K. H., and J. A. Hertz, 1991, *Spin Glasses* (Cambridge University, Cambridge, England).

Fischer, K. H., and T. Nattermann, 1991, Phys. Rev. B **43**, 10 372.

Fisher, D. S., 1980, Phys. Rev. B **22**, 1190.

Fisher, D. S., 1986, Phys. Rev. Lett. **56**, 1964.

Fisher, D. S., M. P. A. Fisher, and D. A. Huse, 1991, Phys. Rev. B **43**, 130.

Fisher, D. S., and P. C. Hohenberg, 1988, Phys. Rev. B **37**, 4936.

Fisher, D. S., and D. A. Huse, 1986, Phys. Rev. Lett. **56**, 1601.

Fisher, D. S., and D. A. Huse, 1988a, Phys. Rev. B **38**, 386.

Fisher, D. S., and D. A. Huse, 1988b, Phys. Rev. B **38**, 373.

Fisher, D. S., and D. A. Huse, 1991, Phys. Rev. B **43**, 10 728.

Fisher, M. E., M. N. Barber, and D. Jasnow, 1973, Phys. Rev. A **8**, 1111.

Fisher, M. P. A., 1989, Phys. Rev. Lett. **62**, 1415.

Fisher, M. P. A., and D. H. Lee, 1989, Phys. Rev. B **39**, 2756.

Fisher, M. P. A., T. A. Tokuyasu, and A. P. Young, 1991, Phys. Rev. Lett. **66**, 2931.

Fisher, M. P. A., P. B. Weichmann, G. Grinstein, and D. S. Fisher, 1989, Phys. Rev. B **40**, 546.

Fleshler, S., W.-K. Kwok, U. Welp, V. M. Vinokur, M. K. Smith, J. Downey, and G. W. Crabtree, 1993, Phys. Rev. B **47**, 14 448.

Forrest, B. M., and L.-H. Tang, 1990, Phys. Rev. Lett. **64**, 1405.

Forster, D., D. R. Nelson, and M. J. Stephen, 1977, Phys. Rev. A **16**, 732.

Fradkin, E., B. A. Huberman, and S. H. Shenker, 1978, Phys. Rev. B **18**, 4789.

Freixa-Pascual, M., and H. Horner, 1990, Z. Phys. B **80**, 95.

Frey, E., D. R. Nelson, and D. S. Fisher, 1994, Phys. Rev. B **49**, 9723.

Friedel, J., 1988, J. Phys. (Paris) **49**, 1561.

Fruchter, L., A. P. Malozemoff, I. A. Campbell, J. Sanchez, M. Konczykowski, R. Griessen, and F. Holtzberg, 1991, Phys. Rev. B **43**, 8709.

Fujita, A., S. Hikami, and A. I. Larkin, 1991, Physica C **185-189**, 1883.

Fukuyama, H., and P. A. Lee, 1978, Phys. Rev. B **17**, 535.

Galffy, M., and E. Zirgiebl, 1988, Solid State Commun. **68**, 929.

Gammel, P. L., D. J. Bishop, G. J. Dolan, J. R. Kwo, C. A. Murray, L. F. Schneemeyer, and J. V. Waszczak, 1987, Phys. Rev. Lett. **59**, 2592.

Gammel, P. L., D. J. Bishop, J. P. Rice, and D. M. Ginsberg, 1992, Phys. Rev. Lett. **68**, 3343.

Gammel, P. L., L. F. Schneemeyer, and D. J. Bishop, 1991, Phys. Rev. Lett. **66**, 953.

Gammel, P. L., L. F. Schneemeyer, J. V. Waszczak, and D. J. Bishop, 1988, Phys. Rev. Lett. **61**, 1666.

Gerhäuser, W., G. Ries, H. W. Neumüller, W. Schmidt, O. Eibl, G. Saemann-Ischenko, and S. Klaumünzer, 1992, Phys. Rev. Lett. **68**, 879.

Geshkenbein, V. B., M. V. Feigel'man, and V. M. Vinokur, 1991, Physica C **185-189**, 2511.

Geshkenbein, V. B., L. B. Ioffe, and A. I. Larkin, 1993, Phys. Rev. B **48**, 9917.

Geshkenbein, V. B., and A. I. Larkin, 1989, Zh. Eksp. Teor. Fiz. **95**, 1108 [Sov. Phys. JETP **68**, 639 (1989)].

Geshkenbein, V., A. Larkin, M. Feigel'man, and V. Vinokur, 1989, Physica C **162-164**, 239.

Geshkenbein, V. B., V. M. Vinokur, and R. Fehrenbacher, 1991, Phys. Rev. B **43**, 3748.

Giamarchi, T., and P. Le Doussal, 1994, Phys. Rev. Lett. **72**, 1530.

Gingras, M. J. P., 1991a, Phys. Rev. B **43**, 13 747.

Gingras, M. J. P., 1991b, Phys. Rev. B **44**, 7139.

Gingras, M. J. P., 1992, Phys. Rev. B **45**, 7547.

Ginzburg, V. L., 1960, Fiz. Tverd. Tela **2**, 2031 [Sov. Phys. Solid State **2**, 1824 (1961)].

Ginzburg, V. L., and L. D. Landau, 1950, Zh. Eksp. Teor. Fiz. **20**, 1064.

Glazman, L. I., and N. Ya. Fogel, 1984, Fiz. Nizk. Temp. **10**, 95 [Sov. J. Low Temp. Phys. **10**, 51 (1984)].

Glazman, L. I., and A. E. Koshelev, 1990, Zh. Eksp. Teor. Fiz. **97**, 1371 [Sov. Phys. JETP **70**, 774 (1990)].

Glazman, L. I., and A. E. Koshelev, 1991a, Phys. Rev. B **43**, 2835.

Glazman, L. I., and A. E. Koshelev, 1991b, Physica C **173**, 180.

Gor'kov, L. P., 1959, Zh. Eksp. Teor. Fiz. **37**, 1407 [Sov. Phys. JETP **37**, 998 (1960)].

Gor'kov, L. P., and G. M. Éliashberg, 1968, Zh. Eksp. Teor. Fiz. **54**, 612 [Sov. Phys. JETP **27**, 328 (1968)].

Gor'kov, L. P., and N. B. Kopnin, 1973, Zh. Eksp. Teor. Fiz. **65**, 396 [Sov. Phys. JETP **38**, 195 (1974)].

Gorlova, I. G., and Yu. I. Latyshev, 1990, Pis'ma Zh. Eksp. Teor. Fiz. **51**, 197 [JETP Lett. **51**, 224 (1990)].

Grabert, H., and U. Weiss, 1984, Z. Phys. B **56**, 171.

Grabert, H., U. Weiss, and P. Hänggi, 1984, Phys. Rev. Lett. **52**, 2193.

Grier, D. G., C. A. Murray, C. A. Bolle, P. L. Gammel, D. J. Bishop, D. B. Mitzi, and A. Kapitulnik, 1991, Phys. Rev. Lett. **66**, 2270.

Griessen, R., 1990, Phys. Rev. Lett. **64**, 1674.

Griessen, R., J. G. Lensink, and H. G. Schnack, 1991, Physica C **185-189**, 337.

Griessen, R., J. G. Lensink, T. A. M. Schröder, and B. Dam, 1990, Cryogenics **30**, 563.

Grinstein, G., 1976, Phys. Rev. Lett. **37**, 944.

Grinstein, G., and S.-k. Ma, 1983, Phys. Rev. B **28**, 2588.

Grishin, A. M., A. Yu. Martynovich, and S. V. Yampolskii, 1990, Physica B **165&166**, 1103.

Gupta, A., P. Esquinazi, H. F. Braun, and H.-W. Neumüller, 1989, Phys. Rev. Lett. **63**, 1869.

Gurevich, A., 1992, Phys. Rev. B **46**, 3187.

Gyorgy, E. M., R. B. van Dover, K. A. Jackson, L. F. Schneemeyer, and J. V. Waszczak, 1989, Appl. Phys. Lett. **55**, 283.

Gyorgy, E. M., R. B. van Dover, L. F. Schneemeyer, A. E. White, H. M. O'Bryan, R. J. Felder, J. V. Waszczak, and W. W. Rhodes, 1990, Appl. Phys. Lett. **56**, 2465.

Hagen, C. W., and R. Griessen, 1989, Phys. Rev. Lett. **62**, 2857.

Hagen, S. J., C. J. Lobb, R. L. Greene, and M. Eddy, 1991, Phys. Rev. B **43**, 6246.

Haldane, F. D., and Y.-S. Wu, 1985, Phys. Rev. Lett. **55**, 2887.

Halperin, B. I., T. C. Lubensky, and S.-k. Ma, 1974, Phys. Rev. Lett. **32**, 292.

Halperin, B. I., and D. R. Nelson, 1978, Phys. Rev. Lett. **41**, 121.

Halperin, B. I., and D. R. Nelson, 1979, J. Low Temp. Phys. **36**, 599.

Halpin-Healy, T., 1989, Phys. Rev. Lett. **62**, 442.

Halpin-Healy, T., 1990, Phys. Rev. A **42**, 711.

Hänggi, P., P. Talkner, and M. Borkovec, 1990, Rev. Mod. Phys. **62**, 251.

Hao, H., and J. R. Clem, 1991, Phys. Rev. B **43**, 7622.

Hao, H., and J. R. Clem, 1992, Phys. Rev. B **46**, 5853.

Hao, H., and J. R. Clem, 1993, Phys. Rev. Lett. **71**, 301.

Hardy, V., D. Groult, J. Provost, M. Hervieu, B. Raveau, and S. Bouffard, 1991, Physica C **178**, 255.

Harris, A. B., 1974, J. Phys. C **7**, 1671.

Harris, J. M., Y. F. Yan, O. K. C. Tsui, Y. Matsuda, and N. P. Ong, 1994, Phys. Rev. Lett. **73**, 1711.

Harshman, D. R., L. F. Schneemeyer, J. V. Waszczak, G. Aeppli, R. J. Cava, B. Batlogg, L.W. Rupp, E. J. Ansaldo, and D. Ll. Williams, 1989, Phys. Rev. B **39**, 851.

Hawley, M., I. D. Raistrick, J. G. Beery, and R. J. Houlton, 1991, Science **251**, 1587.

Hazen, R. M., C. T. Prewitt, R. J. Angel, N. L. Ross, L. W. Finger, C. G. Hadidiacos, D. R. Veblen, P. J. Heaney, P. H. Hor, R. L. Meng, Y. Y. Sun, Y. Q. Wang, Y. Y. Xue, Z. J. Huang, L. Gao, J. Bechtold, and C. W. Chu, 1988, Phys. Rev. Lett. **60**, 1174.

Hetzel, R. E., A. Sudbø, and D. A. Huse, 1992, Phys. Rev. Lett. **69**, 518.

Hikami, S., A. Fujita, and A. I. Larkin, 1991, Phys. Rev. B **44**, 10400.

Hikami, S., and T. Tsuneto, 1980, Prog. Theor. Phys. **63**, 387.

Hida, K., 1985, Z. Phys. B **61**, 223.

Hohenberg, P. C., 1967, Phys. Rev. **158**, 383.

Horovitz, B., 1991, Phys. Rev. Lett. **67**, 378.

Houghton, A., R. A. Pelcovits, and A. Sudbø, 1989, Phys. Rev.

B **40**, 6763.

Houghton, A., R. A. Pelcovits, and A. Sudbø, 1990, Phys. Rev. B **42**, 906.

Hu, C. R., 1972, Phys. Rev. B **6**, 1756.

Huberman, B. A., and S. Doniach, 1979, Phys. Rev. Lett. **43**, 950.

Huse, D. A., M. P. A. Fisher, and D. S. Fisher, 1992, Nature **358**, 553.

Huse, D. A., and R. A. Guyer, 1979, Phys. Rev. Lett. **43**, 1163.

Huse, D. A., and C. L. Henley, 1985, Phys. Rev. Lett. **54**, 2708.

Huse, D. A., C. L. Henley, and D. S. Fisher, 1985, Phys. Rev. Lett. **55**, 2924.

Huse, D. A., and H. S. Seung, 1990, Phys. Rev. B **42**, 1059.

Hwa, T., D. R. Nelson, and V. M. Vinokur, 1993, Phys. Rev. B **48**, 1167.

Imbrie, J. Z., 1984, Phys. Rev. Lett. **53**, 1747.

Imbrie, J. Z., and T. Spencer, 1988, J. Stat. Phys. **52**, 609.

Imry, Y., 1991, private communication.

Imry, Y., and L. Gunther, 1971, Phys. Rev. B **3**, 3939.

Imry, Y., and S.-k. Ma, 1975, Phys. Rev. Lett. **35**, 1399.

Imry, Y., and M. Wortis, 1979, Phys. Rev. B **19**, 3580.

Ioffe, L. B., 1988, Phys. Rev. B **38**, 5181.

Ioffe, L. B., and M. V. Feigel'man, 1985, Zh. Eksp. Teor. Fiz. **89**, 654 [Sov. Phys. JETP **62**, 376 (1985)].

Ioffe, L. B., and V. Kalmeyer, 1991, Phys. Rev. B **44**, 750.

Ioffe, L. B., V. A. Kalmeyer, and P. Wiegmann, 1991, Phys. Rev. B **43**, 1219.

Ioffe, L. B., and A. I. Larkin, 1981, Zh. Eksp. Teor. Fiz. **81**, 707 [Sov. Phys. JETP **54**, 378 (1981)].

Ioffe, L. B., and A. I. Larkin, 1989, Phys. Rev. B **39**, 8988.

Ioffe, L. B., and V. M. Vinokur, 1987, J. Phys. C **20**, 6149.

Iordanskii, S. V., and A. M. Finkel'shtein, 1972, Zh. Eksp. Teor. Fiz. **62**, 403 [Sov. Phys. JETP **35**, 215 (1972)].

Israeloff, N. E., G. B. Alers, and M. B. Weissman, 1991, Phys. Rev. B **44**, 12613.

Ivlev, B. I., and L. J. Campbell, 1993, Phys. Rev. B **47**, 14514.

Ivlev, B. I., and N. B. Kopnin, 1989, J. Low Temp. Phys. **77**, 413.

Ivlev, B. I., and N. B. Kopnin, 1990a, Phys. Rev. Lett. **64**, 1828.

Ivlev, B. I., and N. B. Kopnin, 1990b, J. Low. Temp. Phys. **80**, 161.

Ivlev, B. I., and N. B. Kopnin, 1990c, Phys. Rev. B **42**, 10052.

Ivlev, B. I., and N. B. Kopnin, 1991a, Europhys. Lett. **15**, 349.

Ivlev, B. I., and N. B. Kopnin, 1991b, Phys. Rev. B **44**, 2747.

Ivlev, B. I., N. B. Kopnin, and V. L. Pokrovsky, 1990, J. Low Temp. Phys. **80**, 187.

Ivlev, B. I., N. B. Kopnin, and M. M. Salomaa, 1991, Phys. Rev. B **43**, 2896.

Ivlev, B. I., Yu. N. Ovchinnikov, and V. L. Pokrovsky, 1990, Europhys. Lett. **13**, 187.

Ivlev, B. I., Yu. N. Ovchinnikov, and V. L. Pokrovsky, 1991, Mod. Phys. Lett. B **5**, 73.

Ivlev, B. I., Yu. N. Ovchinnikov, and R. S. Thompson, 1991, Phys. Rev. B **44**, 7023.

Iye, Y., S. Nakamura, and T. Tamegai, 1989a, Physica C **159**, 433.

Iye, Y., S. Nakamura, and T. Tamegai, 1989b, Physica C **159**, 616.

Iye, Y., S. Nakamura, T. Tamegai, T. Terashima, K. Yamamoto, and Y. Bando, 1990, Physica C **166**, 62.

Iye, Y., T. Tamegai, H. Takeya, and H. Takei, 1987, Jpn. J. Appl. Phys. Part 2 **26**, L1057.

Iye, Y., T. Tamegai, H. Takeya, and H. Takei, 1988, in *Superconducting Materials*, Jpn. J. Appl. Phys. Series 1, edited by S.

Nakajima and H. Fukuyama (Publication Office, Japanese Journal of Applied Physics, Tokyo).

Iye, Y., T. Terashima, and Y. Bando, 1991, Physica C **177**, 393.

Jain, J. K., and S. Kivelson, 1987, Phys. Rev. A **36**, 3467.

Jain, J. K., and S. Kivelson, 1988, Phys. Rev. B **37**, 4111.

Jakob, G., T. Hahn, C. Stölzel, C. Tomé-Rosa, and H. Adrian, 1992, Europhys. Lett. **19**, 135.

Jancovici, B., 1967, Phys. Rev. Lett. **19**, 20.

Jensen, H. J., A. Brass, A.-C. Shi, and A. J. Berlinsky, 1990, Phys. Rev. B **41**, 6394.

Jensen, H. J., and P. Minnhagen, 1991, Phys. Rev. Lett. **66**, 1630.

John, S., and T. Lubensky, 1985, Phys. Rev. Lett. **34**, 1014.

John, S., and T. Lubensky, 1986, Phys. Rev. B **34**, 4815.

José, J. V., L. P. Kadanoff, S. Kirkpatrick, D. R. Nelson, 1977, Phys. Rev. B **16**, 1217.

Kadin, A. M., K. Epstein, and A. M. Goldman, 1983, Phys. Rev. B **27**, 6691.

Kapitulnik, A., 1991, in *Phenomenology and Applications of High-Temperature Superconductors*, Proceedings of the Los Alamos Symposium—1991, edited by K. S. Bedell, M. Inui, D. Meltzer, J. R. Schrieffer, and S. Doniach (Addison-Wesley, Reading, MA).

Kardar, M., 1985, Phys. Rev. Lett. **55**, 2923.

Kardar, M., 1987a, Nucl. Phys. B **290**, 582.

Kardar, M., 1987b, J. Appl. Phys. **61**, 3601.

Kardar, M., and D. R. Nelson, 1985, Phys. Rev. Lett. **55**, 1157.

Kardar, M., G. Parisi, and Y.-C. Zhang, 1986, Phys. Rev. Lett. **56**, 889.

Kardar, M., and Y.-C. Zhang, 1987, Phys. Rev. Lett. **58**, 2087.

Kato, Y., and N. Nagaosa, 1993, Phys. Rev. B **47**, 2932.

Kes, P. H., J. Aarts, J. van den Berg, C. J. van der Beek, and J. A. Mydosh, 1989, Supercond. Sci. Technol. **1**, 242.

Kes, P. H., J. Aarts, V. M. Vinokur, and C. J. van der Beek, 1990, Phys. Rev. Lett. **64**, 1063.

Kes, P. H., and R. Wördenweber, 1987, J. Low Temp. Phys. **67**, 1.

Kim, Y. B., C. F. Hempstead, and A. R. Strnad, 1962, Phys. Rev. Lett. **9**, 306.

Kim, D. H., A. M. Goldman, J. H. Kang, and R. T. Kampwirth, 1989, Phys. Rev. B **40**, 8834.

Kim, J. M., and J. M. Kosterlitz, 1989, Phys. Rev. Lett. **62**, 2289.

Kirzhnits, D. A., and Ya. A. Nepomnyashii, 1970, Zh. Eksp. Teor. Fiz. **59**, 2203 [Sov. Phys. JETP **32**, 1191 (1971)].

Kleiman, R. N., P. L. Gammel, L. F. Schneemeyer, J. V. Waszczak, and D. J. Bishop, 1989, Phys. Rev. Lett. **62**, 2331.

Klemm, R. A., 1990, Phys. Rev. B **41**, 117.

Klemm, R. A., 1993, Phys. Rev. B **47**, 14 630.

Klemm, R. A., and J. R. Clem, 1980, Phys. Rev. B **21**, 1868.

Klemm, R. A., A. Luther, and M. R. Beasley, 1975, Phys. Rev. B **12**, 877.

Kober, J., A. Gupta, P. Esquinazi, H. F. Braun, and E. H. Brandt, 1991, Phys. Rev. Lett. **66**, 2507.

Koch, R. H., V. Foglietti, and M. P. A. Fisher, 1990, Phys. Rev. Lett. **64**, 2586.

Koch, R. H., V. Foglietti, W. J. Gallagher, G. Koren, A. Gupta, and M. P. A. Fisher, 1989, Phys. Rev. Lett. **63**, 1511.

Kogan, V. G., 1981, Phys. Rev. B **24**, 1572.

Kogan, V. G., 1988, Phys. Rev. B **38**, 7049.

Kogan, V. G., and L. J. Campbell, 1989, Phys. Rev. Lett. **62**, 1552.

Kogan, V. G., and J. R. Clem, 1981, Phys. Rev. B **24**, 2497.

Kolomeisky, E. B., 1992, Phys. Rev. B **45**, 7094.

Konczykowski, M., L. I. Burlachkov, Y. Yeshurun, and F. Holtzberg, 1991, Phys. Rev. B **43**, 13 707.

Konczykowski, M., L. I. Burlachkov, Y. Yeshurun, and F. Holtzberg, 1992, Physica C **194**, 155.

Konczykowski, M., N. Chikumoto, V. M. Vinokur, and M. V. Feigel'man, 1994, submitted to Phys. Rev. B.

Konczykowski, M., A. P. Malozemoff, F. Holtzberg, 1991, Physica C **185-189**, 2203.

Konczykowski, M., F. Rullier-Albenque, E. R. Yacoby, A. Shaulov, Y. Yeshurun, and P. Lejay, 1991, Phys. Rev. B **44**, 7167.

Kopnin, N. B., and V. E. Kravtsov, 1976a, Pis'ma Zh. Eksp. Teor. Fiz. **23**, 631 [JETP Lett. **23**, 578 (1976)].

Kopnin, N. B., and V. E. Kravtsov, 1976b, Zh. Eksp. Teor. Fiz. **71**, 1644 [Sov. Phys. JETP **44**, 861 (1976)].

Kopnin, N. B., and M. M. Salomaa, 1991, Phys. Rev. B **44**, 9667.

Korshunov, S. E., 1990, Europhys. Lett. **11**, 757.

Korshunov, S. E., 1991, Europhys. Lett. **15**, 771.

Korshunov, S. E., 1993, Phys. Rev. B **48**, 3969.

Korshunov, S. E., and A. I. Larkin, 1992, Phys. Rev. B **46**, 6395.

Koshelev, A. E., 1990, Pis'ma Zh. Eksp. Teor. Fiz. **51**, 210 [JETP Lett. **51**, 238 (1990)].

Koshelev, A. E., 1992, Physica C **191**, 219.

Koshelev, A. E., 1994, private communication.

Koshelev, A. E., and V. M. Vinokur, 1991, Physica C **173**, 465.

Koshelev, A. E., and V. M. Vinokur, 1993, "Low angle resistivity anomaly in a layered superconductor," Argonne National Laboratory preprint.

Kosterlitz, J. M., 1974, J. Phys. C **7**, 1046.

Kosterlitz, J. M., and D. J. Thouless, 1973, J. Phys. C **6**, 1181.

Kramers, H. A., 1940, Physica (Utrecht) **7**, 284.

Krauth, W., T. Trivedi, and D. Ceperley, 1991, Phys. Rev. Lett. **67**, 2307.

Krusin-Elbaum, L., L. Civale, G. Blatter, A. D. Marwick, F. Holtzberg, and C. Feild, 1994, Phys. Rev. Lett. **72**, 1914.

Krusin-Elbaum, L., L. Civale, F. Holtzberg, A. P. Malozemoff, and C. Feild, 1991, Phys. Rev. Lett. **67**, 3156.

Krusin-Elbaum, L., L. Civale, V. M. Vinokur, and F. Holtzberg, 1992, Phys. Rev. Lett. **69**, 2280.

Krusin-Elbaum, L., R. L. Greene, F. Holtzberg, A. P. Malozemoff, and Y. Yeshurun, 1989, Phys. Rev. Lett. **62**, 217.

Kupriyanov, M. Yu., and K. K. Likharev, 1975, Zh. Eksp. Teor. Fiz. **68**, 1506 [Sov. Phys. JETP **41**, 755 (1975)].

Kwok, W. K., J. Fendrich, S. Fleshler, U. Welp, J. Downey, and G. W. Crabtree, 1994a, Phys. Rev. Lett. **72**, 1092.

Kwok, W. K., J. Fendrich, U. Welp, S. Fleshler, J. Downey, and G. W. Crabtree, 1994b, Phys. Rev. Lett. **72**, 1088.

Kwok, W. K., S. Fleshler, U. Welp, V. M. Vinokur, J. Downey, G. W. Crabtree, and M. M. Miller, 1992, Phys. Rev. Lett. **69**, 3370.

Kwok, W. K., U. Welp, G. W. Crabtree, K. G. Vandervoort, R. Hulscher, and J. Z. Liu, 1990, Phys. Rev. Lett. **64**, 966.

Kwok, W. K., U. Welp, V. M. Vinokur, S. Fleshler, J. Downey, and G. W. Crabtree, 1991, Phys. Rev. Lett. **67**, 390.

Labusch, R., 1967, Phys. Status Solidi **19**, 715.

Labusch, R., 1969, Phys. Status Solidi **32**, 439.

Lairson, B. M., J. Z. Sun, T. H. Geballe, M. R. Beasley, and J. C. Bravman, 1991, Phys. Rev. B **43**, 10 405.

Landau, L. D., and E. M. Lifshitz, 1958a, *Quantum Mechanics*, Course in Theoretical Physics Vol. 3 (Pergamon, London/-Paris).

Landau, L. D., and E. M. Lifshitz, 1958b, *Statistical Physics*,

Course in Theoretical Physics Vol. 5 (Pergamon, London/-Paris).

Landau, L. D., and E. M. Lifshitz, 1959a, *Theory of Elasticity,* Course in Theoretical Physics Vol. 7 (Pergamon, London/-Paris).

Landau, L. D., and E. M. Lifshitz, 1959b, *Electrodynamics of Continuous Media,* Course in Theoretical Physics Vol. 8 (Pergamon, London/Paris).

Langer, J. S., 1967, Ann. Phys. **41**, 108.

Langer, J. S., and M. E. Fisher, 1976, Phys. Rev. Lett. **19**, 560.

Larkin, A. I., 1970, Zh. Eksp. Teor. Fiz. **58**, 1466 [Sov. Phys. JETP **31**, 784 (1970)].

Larkin, A. I., and Yu. N. Ovchinnikov, 1973, Zh. Eksp. Teor. Fiz. **65**, 1704 [Sov. Phys. JETP **38**, 854 (1974)].

Larkin, A. I., and Yu. N. Ovchinnikov, 1979, J. Low Temp. Phys. **34**, 409.

Larkin, A. I., and Yu. N. Ovchinnikov, 1983a, Pis'ma Zh. Eksp. Teor. Fiz. **37**, 322 [JETP Lett. **37**, 382 (1983)].

Larkin, A. I., and Yu. N. Ovchinnikov, 1983b, Phys. Rev. B **28**, 6281.

Larkin, A. I., and Yu. N. Ovchinnikov, 1986, in *Nonequilibrium Superconductivity,* edited by D. N. Langenberg and A. I. Larkin (Elsevier Science, New York/Amsterdam), p. 493.

Larkin, A. I., Yu. N. Ovchinnikov, and A. Schmid, 1988, Physica B **152**, 266.

Lawrence, W. E., and S. Doniach, 1971, in *Proceedings of the Twelfth International Conference on Low Temperature Physics,* Kyoto, Japan, edited by E. Kanda (Keigaku, Tokyo), p. 361.

Lee, K. H., and D. Stroud, 1991, Phys. Rev. B **44**, 9780.

Lee, P. A., and T. M. Rice, 1979, Phys. Rev. B **19**, 3970.

Lefloch, F., J. Hamman, M. Ocio, and E. Vincent, 1992, Europhys. Lett. **18**, 647.

Lensink, J., C. F. J. Flipse, J. Roobeek, R. Griessen, and B. Dam, 1989, Physica C **162-164**, 663.

Levitov, L. S., 1991, Phys. Rev. Lett. **66**, 224.

Lifshitz, I. M., and Yu. Kagan, 1972, Zh. Eksp. Teor. Fiz. **62**, 385 [Sov. Phys. JETP **35**, 206 (1972)].

Lifshitz, E. M., and L. P. Pitaevskii, 1981, *Physical Kinetics,* Course in Theoretical Physics Vol. 10 (Pergamon, London/Paris).

Li, Q., X. X. Xi, X. D. Wu, A. Inam, S. Vadlamannati, W. L. McLean, T. Benkatesan, R. Ramesh, D. M. Hwang, J. A. Martinez, and L. Nazar, 1990, Phys. Rev. Lett. **64**, 3086.

Li, Y.-H., and S. Teitel, 1991, Phys. Rev. Lett. **66**, 3301.

Li, Y.-H., and S. Teitel, 1993, Phys. Rev. B **47**, 359.

Likharev, K. K., 1979, Rev. Mod. Phys. **51**, 101.

Lindemann, F., 1910, Phys. Z. (Leipzig) **11**, 69.

Liu, K., and M. E. Fisher, 1973, J. Low Temp. Phys. **10**, 655.

Liu, Y., D. B. Haviland, L. I. Glazman, and A. M. Goldman, 1992, Phys. Rev. Lett. **68**, 2224.

Liu, J. Z., Y. X. Jia, R. N. Shelton, and M. J. Fluss, 1991, Phys. Rev. Lett. **66**, 1354.

Liu, J. N., K. Kadowaki, M. J. V. Menken, A. A. Menovsky, and J. J. M. Franse, 1989, Physica C **161**, 313.

Lobb, C. J., 1987, Phys. Rev. B **36**, 3930.

Lowndes, D. H., D. P. Norton, and J. D. Budai, 1990, Phys. Rev. Lett. **65**, 1160.

Lyuksyutov, I., 1992, Europhys. Lett. **20**, 273.

Ma, H.-r., and S. T. Chui, 1991, Phys. Rev. Lett. **67**, 505.

Maki, K., and H. Takayama, 1971, Prog. Theor. Phys. **26**, 1651.

Maley, M. P., J. O. Willis, H. Lessure, and M. E. McHenry, 1990, Phys. Rev. B **42**, 2639.

Malozemoff, A. P., 1991, Physica C **185-189**, 264.

Malozemoff, A. P., and M. P. A. Fisher, 1990, Phys. Rev. B **42**,

6784.

Malozemoff, A. P., L. Krusin-Elbaum, D. C. Cronemeyer, Y. Yeshurun, and F. Holtzberg, 1988, Phys. Rev. B **38**, 6490.

Malozemoff, A. P., T. K. Worthington, Y. Yeshurun, F. Holtzberg, and P. H. Kes, 1988, Phys. Rev. B **38**, 7203.

Malozemoff, A. P., T. K. Worthington, E. Zeldov, N. C. Yeh, M. W. McElfresh, and F. Holtzberg, 1989, in *Strong Correlation and Superconductivity,* Springer Series in Solid-State Sciences No. 89, edited by H. Fukuyama, S. Maekawa, and A. P. Malozemoff (Springer, Berlin), p. 267.

Mannhart, J., D. Anselmetti, J. G. Bednorz, A. Catana, Ch. Gerber, K. A. Müller, and D. G. Schlom, 1992, Z. Phys. B **86**, 177.

Marchetti, M. C., 1991, Phys. Rev. B **43**, 8012.

Marchetti, M. C., and D. R. Nelson, 1990a, Phys. Rev. B **41**, 1910.

Marchetti, M. C., and D. R. Nelson, 1990b, Phys. Rev. B **42**, 9938.

Marchetti, M. C., and D. R. Nelson, 1991, Physica C **174**, 40.

Marchetti, M. C., and V. M. Vinokur, 1994, Phys. Rev. Lett. **72**, 3409.

Martin, S., A. T. Fiory, R. M. Fleming, G. P. Espinosa, and A. S. Cooper, 1989, Phys. Rev. Lett. **62**, 677.

Martin, S., A. T. Fiory, R. M. Fleming, L. F. Schneemeyer, and J. V. Waszczak, 1988, Phys. Rev. Lett. **60**, 2194.

Martin, S., A. T. Fiory, R. M. Fleming, L. F. Schneemeyer, and J. V. Waszczak, 1990, Phys. Rev. B **41**, 846.

Martínez, J. C., S. H. Brongersma, A. Koshelev, B. Ivlev, P. H. Kes, R. P. Griessen, D. G. de Groot, Z. Tarnavski, and A. A. Menovsky, 1992, Phys. Rev. Lett. **69**, 2276.

Martinis, J. M., M. H. Devoret, and J. Clarke, 1987, Phys. Rev. B **35**, 4682.

Maslov, S. S., and V. L. Pokrovsky, 1991, Europhys. Lett. **14**, 591.

McMillan, W. L., 1984a, J. Phys. C **17**, 3179.

McMillan, W. L., 1984b, Phys. Rev. B **29**, 4026.

McMillan, W. L., 1984c, Phys. Rev. B **30**, 476.

Medina, E., T. Hwa, M. Kardar, and Y.-C. Zhang, 1989, Phys. Rev. A **39**, 3053.

Mermin, N. D., and H. Wagner, 1966, Phys. Rev. Lett. **17**, 1133.

Mézard, M., 1990, J. Phys. (Paris) **51**, 1831.

Mézard, M., and G. Parisi, 1991, J. Phys. I (Paris) **1**, 809.

Mézard, M., G. Parisi, N. Sourlas, G. Toulouse, and M. Virasoro, 1984a, Phys. Rev. Lett. **52**, 1156.

Mézard, M., G. Parisi, N. Sourlas, G. Toulouse, and M. Virasoro, 1984b, J. Phys. (Paris) **45**, 843.

Mézard, M., G. Parisi, and M. A. Virasoro, 1987, *Spin Glass Theory and Beyond,* World Scientific Lecture Notes in Physics No. 9 (World Scientific, Singapore).

Mikheev, L. V., and E.B. Kolomeisky, 1991, Phys. Rev. B **43**, 10431.

Minnhagen, P., 1981, Phys. Rev. B **24**, 6758.

Minnhagen, P., 1987, Rev. Mod. Phys. **59**, 1001.

Minnhagen, P., and P. Olsson, 1991a, Phys. Rev. Lett. **67**, 1039.

Minnhagen, P., and P. Olsson, 1991b, Phys. Rev. B **44**, 4503.

Mitin, A. V., 1987, Zh. Eksp. Teor. Fiz. **93**, 590 [Sov. Phys. JETP **66**, 335 (1987)].

Mkrtchyan, G. S., and V. V. Schmidt, 1972, Sov. Phys. JETP **34**, 195.

Moore, M. A., 1989, Phys. Rev. B **39**, 136.

Moore, M. A., 1992, Phys. Rev. B **45**, 7336.

Morais-Smith, C., B. I. Ivlev, V. B. Geshkenbein, and G. Blatter, 1995, "Quantum Intrinsic Creep," ETH preprint.

Morgenstern, I., K. A. Müller, and J. G. Bednorz, 1987, Z. Phys. B **69**, 33.

Morris, B. W., S. G. Colborne, M. A. Moore, A. J. Bray, and J. Canisius, 1986, J. Phys. C **19**, 1157.

Mota, A. C., G. Juri, P. Visani, A. Pollini, T. Teruzzi, K. Aupke, and B. Hilti, 1991, Physica C **185-189**, 343.

Mota, A. C., A. Pollini, G. Juri, P. Visani, and B. Hilti, 1990a, Physica A **168**, 298.

Mota, A. C., A. Pollini, P. Visani, G. Juri, and J. J. M. Franse, 1990b, in *Progress in High Temperature Superconductivity*, Proceedings of the International Conference on Transport Properties of Superconductors, Vol. 25, edited by R. Nicolsky (World Scientific, Singapore).

Mota, A. C., A. Pollini, P. Visani, K. A. Müller, and J. G. Bednorz, 1988, Phys. Scr. **37**, 823.

Mota, A. C., P. Visani, and A. Pollini, 1988, Phys. Rev. B **37**, 9830.

Mott, N. F., 1969, Philos. Mag. **19**, 835.

Müller, K. A., M. Takashige, and J. G. Bednorz, 1987, Phys. Rev. Lett. **58**, 1143.

Murray, C. A., P. L. Gammel, D. J. Bishop, D. B. Mitzi, and A. Kapitulnik, 1990, Phys. Rev. Lett. **64**, 2312.

Nabarro, F. R. N., 1979, *Dislocations in Solids* (North-Holland, Amsterdam), Vol. 1.

Nattermann, T., 1985, J. Phys. C **18**, 6661.

Nattermann, T., 1990, Phys. Rev. Lett. **64**, 2454.

Nattermann, T., M. Feigel'man, and I. Lyuksyutov, 1991, Z. Phys. B **84**, 353.

Nattermann, T., and H. Leschhorn, 1991, Europhys. Lett. **14**, 603.

Nattermann, T., and R. Lipowsky, 1988, Phys. Rev. Lett. **61**, 2508.

Nattermann, T., and I. Lyuksyutov, 1992, Phys. Rev. Lett. **68**, 3366.

Nattermann, T., I. Lyuksyutov, and M. Schwartz, 1991, Europhys. Lett. **16**, 295.

Nattermann, T., Y. Shapir, and I. Vilfan, 1990, Phys. Rev. B **42**, 8577.

Naughton, M. J., R. C. Yu, P. K. Davies, J. E. Fischer, R. V. Chamberlin, Z. Z. Wang, T. W. Jing, N. P. Ong, and P. M. Chaikin, 1988, Phys. Rev. B **38**, 9280.

Negele, J. W., and H. Orland, 1988, *Quantum Many-Particle Systems* (Addison-Wesley, Reading, MA).

Nelson, D. R., 1988, Phys. Rev. Lett. **60**, 1973.

Nelson, D. R., 1991, in *Phenomenology and Applications of High-Temperature Superconductors*, Proceedings of the Los Alamos Symposium—1991, edited by K. S. Bedell, M. Inui, D. Meltzer, J. R. Schrieffer, and S. Doniach (Addison-Wesley, Reading, MA).

Nelson, D. R., 1993, unpublished.

Nelson, D. R., and B. I. Halperin, 1979, Phys. Rev. B **19**, 2457.

Nelson, D. R., and J. M. Kosterlitz, 1977, Phys. Rev. Lett. **39**, 1201.

Nelson, D. R., and P. Le Doussal, 1990, Phys. Rev. B **42**, 10 113.

Nelson, D. R., M. Rubinstein, and F. Spaepen, 1982, Philos. Mag. A **46**, 105.

Nelson, D. R., and H. S. Seung, 1989, Phys. Rev. B **39**, 9153.

Nelson, D. R., and V. M. Vinokur, 1992, Phys. Rev. Lett. **68**, 2398.

Nelson, D. R., and V.M. Vinokur, 1993, Phys. Rev. B **48**, 13 060.

Obukhov, S. P., and M. Rubinstein, 1990, Phys. Rev. Lett. **65**, 1279.

Obukhov, S. P., and M. Rubinstein, 1991, Phys. Rev. Lett. **66**, 2279.

Ogielski, A. T., 1985, Phys. Rev. B **32**, 7384.

Ogielski, A. T., and I. Morgenstern, 1985, Phys. Rev. Lett. **54**, 928.

Olsson, H. K., R. H. Koch, W. Eidelloth, and R. P. Robertazzi, 1991, Phys. Rev. Lett. **66**, 2661.

O'Neill, J. A., and M. A. Moore, 1992, Phys. Rev. Lett. **69**, 2582.

Ossandon, J. G., J. R. Thompson, D. K. Christen, B. C. Sales, Y. Sun, and K. W. Lay, 1992, Phys. Rev. B **46**, 3050.

Palmer, R. G., D. L. Stein, E. Abrahams, and P. W. Anderson, 1984, Phys. Rev. Lett. **53**, 958.

Palstra, T. T. M., B. Batlogg, L. F. Schneemeyer, R. B. van Dover, and J. V. Waszczak, 1988a, Phys. Rev. B **38**, 5102.

Palstra, T. T. M., B. Batlogg, L. F. Schneemeyer, and J. V. Waszczak, 1988b, Phys. Rev. Lett. **61**, 1662.

Palstra, T. T. M., B. Batlogg, R. B. van Dover, L. F. Schneemeyer, and J. V. Waszczak, 1989, Appl. Phys. Lett. **54**, 763.

Palstra, T. T. M., B. Batlogg, R. B. van Dover, L. F. Schneemeyer, and J. V. Waszczak, 1990, Phys. Rev. B **41**, 6621.

Parisi, G., 1979, Phys. Rev. Lett. **43**, 1754.

Parisi, G., 1980, J. Phys. A **13**, 1101.

Parisi, G., and N. Sourlas, 1979, Phys. Rev. Lett. **43**, 744.

Pearl, J., 1964, Appl. Phys. Lett. **5**, 65.

Pearl, J., 1965, in *Proceedings of the Ninth International Conference on Low Temperature Physics*, edited by J. G. Daunt, D. V. Edwards, F. J. Milford, and M. Yaqub (Plenum, New York), Part A, p. 566.

Pentegov, V., and M. V. Feigel'man, 1988, Zh. Eksp. Teor. Fiz. **94**, 345 [Sov. Phys. JETP **67**, 2154 (1988)].

Perruchoud, D., 1991, Diploma Thesis (Eidgenössische Technische Hochschule, Zürich, Switzerland).

Pla, O., and F. Nori, 1991, Phys. Rev. Lett. **67**, 919.

Pokrovsky, V. L., I. Lyuksyutov, and T. Nattermann, 1992, Phys. Rev. B **46**, 3071.

Pokrovsky, V. L., and A. L. Talapov, 1979, Phys. Rev. Lett. **42**, 65.

Pokrovskii, V. L., and G. V. Uimin, 1973, Zh. Eksp. Teor. Fiz. **65**, 1691 [Sov. Phys. JETP **38**, 847 (1974)].

Popov, V. N., 1972, Theor. Math. Phys. (Engl. Transl.) **11**, 565.

Popov, V. N., 1983, *Functional Integrals in Quantum Field Theory and Statistical Physics* (Reidel, Dordrecht).

Popov, V. N., 1987, *Functional Integrals and Collective Excitations* (Cambridge University, Cambridge).

Pollock, E. L., and D. M. Ceperley, 1987, Phys. Rev. B **36**, 8343.

Rammal, R., G. Toulouse, and M. A. Virasoro, 1986, Rev. Mod. Phys. **58**, 765.

Reger, J. D., T. A. Tokuyasu, A. P. Young, and M. P. A. Fisher, 1991, Phys. Rev. B **44**, 7147.

Renz, W., and T. Nattermann, 1990, unpublished.

Rhyner, J., and G. Blatter, 1989, Phys. Rev. B **40**, 829.

Roas, B., B. Hensel, S. Henke, S. Klaumünzer, B. Kabius, W. Watanabe, G. Saemann-Ischenko, L. Schultz, and K. Urban, 1990, Europhys. Lett. **11**, 669.

Roas, B., L. Schultz, and G. Saemann-Ischenko, 1990, Phys. Rev. Lett. **64**, 479.

Roitburd, A., L. J. Swartzendruber, D. L. Kaiser, F. W. Gayle, and L. H. Bennett, 1990, Phys. Rev. Lett. **64**, 2962.

Rossel, C., O. Peña, H. Schmitt, and M. Sergent, 1991, Physica C **191**, 363.

Ryu, S., S. Doniach, G. Deutscher, and A. Kapitulnik, 1992, Phys. Rev. Lett. **68**, 710.

Safar, H., P. L. Gammel, D. J. Bishop, D. B. Mitzi, and A. Kapitulnik, 1992, Phys. Rev. Lett. **68**, 2672.

Safar, H., P. L. Gammel, D. A. Huse, D. J. Bishop, J. P. Rice, and D. M. Ginsberg, 1992, Phys. Rev. Lett. **69**, 824.

Safar, H., P. L. Gammel, D. A. Huse, D. J. Bishop, W. C. Lee, and D. M. Ginsberg, 1993, Phys. Rev. Lett. **70**, 3800.

Safar, H., P. L. Gammel, D. A. Huse, S. N. Majumdar, L. F. Schneemeyer, and D. J. Bishop, 1994, Phys. Rev. Lett. **72**, 1272.

Sagdahl, L. T., T. Laegreid, K. Fossheim, M. Murakami, H. Fujimoto, S. Gotoh, K. Yamaguchi, H. Yamauchi, N. Koshizuka, and S. Tanaka, 1991, Physica C **172**, 495.

Sandvold, E., and C. Rossel, 1992, Physica C **190**, 309.

Sardella, E., 1992, Phys. Rev. B **45**, 3141.

Schilling, A., H. R. Ott, and Th. Wolf, 1992, Phys. Rev. B **46**, 14 253.

Schlom, D. G., D. Anselmetti, J. G. Bednorz, R. F. Broom, A. Catana, T. Frey, Ch. Gerber, H.-J. Güntherodt, H. P. Lang, and J. Mannhart, 1992, Z. Phys. B **86**, 163.

Schmid, A., 1966, Phys. Konden. Mater. **5**, 302.

Schmid, A., and W. Hauger, 1973, J. Low Temp. Phys. **11**, 667.

Schmitt, P., P. Kummeth, L. Schulz, and G. Saemann-Ischenko, 1991, Phys. Rev. Lett. **67**, 267.

Schönenberger, A., V. B. Geshkenbein, and G. Blatter, 1993, Phys. Rev. B **48**, 15 914.

Schuster, Th., M. V. Indenbom, H. Kuhn, E. H. Brandt, M. Konczykowski, 1994, Phys. Rev. Lett. **73**, 1424.

Sengupta, S., C. Dasgupta, H. R. Krishnamurthy, G. I. Menon, and T. V. Ramakrishnan, 1991, Phys. Rev. Lett. **67**, 3444.

Senoussi, S., M. Ousséna, G. Collin, and I. A. Campbell, 1988, Phys. Rev. B **37**, 9792.

Sherrington, D., and S. Kirkpatrick, 1975, Phys. Rev. Lett. **35**, 1972.

Shklovskii, B. I., 1972a, Fiz. Tekh. Poluprovodn. **6**, 1197 [Sov. Phys.-Semicond. **6**, 1053 (1973)].

Shklovskii, B. I., 1972b, Fiz. Tekh. Poluprovodn. **6**, 2335 [Sov. Phys.-Semicond. **6**, 1964 (1973)].

Shklovskii, B. I., and A. L. Efros, 1984, *Electronic Properties of Doped Semiconductors*, Springer Series in Solid-State Sciences No. 45 (Springer, Berlin).

Shi, A.-C., and A. J. Berlinsky, 1991, Phys. Rev. Lett. **67**, 1926.

Shih, W. Y., C. Ebner, and D. Stroud, 1984, Phys. Rev. B **30**, 134.

Sompolinsky, H., 1981, Phys. Rev. Lett. **47**, 935.

Sompolinsky, H., G. Kotliar, and A. Zippelius, 1984, Phys. Rev. Lett. **52**, 392.

Sorensen, E. S., M. Wallin, S. M. Girvin, and A. P. Young, 1992, Phys. Rev. Lett. **69**, 828.

Southern, B. W., and A. P. Young, 1977, J. Phys. C **10**, 2179.

Stamp. P. C. E., L. Forro, and C. Ayache, 1988, Phys. Rev. B **38**, 2847.

Steel, D. G., and J. M. Graybeal, 1992, Phys. Rev. B **45**, 12 643.

Steel, D. G., W. R. White, and J. M. Graybeal, 1993, Phys. Rev. Lett. **71**, 161.

Stollman, G. M., B. Dam, J. H. P. M. Emmen, and J. Pankert, 1989, Physica C **162-164**, 1191.

Strandburg, K. J., 1988, Rev. Mod. Phys. **60**, 161.

Sudbø, A., and E. H. Brandt, 1991a, Phys. Rev. Lett. **66**, 1781.

Sudbø, A., and E. H. Brandt, 1991b, Phys. Rev. B **43**, 10 482.

Sudbø, A., and E. H. Brandt, 1991c, Phys. Rev. Lett. **67**, 3176.

Suenaga, M., A. K. Ghosh, Y. Xu, and D. O. Welch, 1991, Phys. Rev. Lett. **66**, 1777.

Suhl, H., 1965, Phys. Rev. Lett. **14**, 226.

Sunshine, S. A., T. Siegrist, L. F. Schneemeyer, D. W. Murphy, R. J. Cava, B. Batlogg, R. B. van Dover, R. M. Fleming, S. H. Glarum, S. Nakahara, R. Farrow, J. J. Krajewski, S. M. Zahurak, J. V. Waszczak, J. H. Marshall, P. Marsh, L. W. Rupp, Jr., and W. F. Peck, 1988, Phys. Rev. B **38**, 893.

Svedlindh, P., C. Rossel, K. Niskanen, P. Norling, P. Nordblad, L. Lundgren, and G. V. Chandrashekar, 1991, Physica C **176**, 336.

Swartzendruber, L. J., A. Roitburd, D. L. Kaiser, F. W. Gayle, and L. H. Bennett, 1990, Phys. Rev. Lett. **64**, 483.

Tachiki, M., and S. Takahashi, 1989, Solid State Commun. **70**, 291.

Tamegai, T., L. Krusin-Elbaum, L. Civale, P. Santhanam, M. J. Brady, W. T. Masselink, F. Holtzberg, and C. Feild, 1992, Phys. Rev. B **45**, 8201.

Tešanović, Z., 1991, Phys. Rev. B **44**, 12 635.

Tešanović, Z., and L. Xing, 1991, Phys. Rev. Lett. **67**, 2729.

Theodorakis, S., 1990, Phys. Rev. B **42**, 10 172.

Thompson, J. R., Y. R. Sun, and F. Holtzberg, 1991, Phys. Rev. B **44**, 458.

Thompson, J. R., Y. R. Sun, H. R. Kerchner, D. K. Christen, B. C. Sales, B. C. Chakoumakos, A. D. Marwick, L. Civale, and J. O. Thomson, 1992, Appl. Phys. Lett. **60**, 2306.

Thouless, D., 1975, Phys. Rev. Lett. **34**, 949.

Thuneberg, E. V., 1984, J. Low Temp. Phys. **57**, 415.

Thuneberg, E. V., 1989, Cryogenics **29**, 236.

Thuneberg, E. V., J. Kurkijärvi, and D. Rainer, 1984, Phys. Rev. B **29**, 3913.

Tinkham, M., 1988a, Phys. Rev. Lett. **61**, 1658.

Tinkham, M., 1988b, Helv. Phys. Acta **61**, 443.

Toner, J., 1991a, Phys. Rev. Lett. **66**, 2523.

Toner, J., 1991b, Phys. Rev. Lett. **67**, 2537.

Toner, J., 1991c, Phys. Rev. Lett. **67**, 1810.

Toner, J., 1992, Phys. Rev. Lett. **68**, 3367.

Tozer, S. W., A. W. Kleinsasser, T. Penney, D. Kaiser, and F. Holtzberg, 1987, Phys. Rev. Lett. **59**, 1768.

Triscone, J-M., O. Fischer, O. Brunner, L. Antognazza, A. D. Kent, and M. G. Karkut, 1990, Phys. Rev. Lett. **64**, 804.

Triscone, J.-M., M. G. Karkut, L. Antognazza, O. Brunner, and O. Fischer, 1989, Phys. Rev. Lett. **63**, 1016.

Tsai, Y.-C., and Y. Shapir, 1992, Phys. Rev. Lett. **69**, 1773.

Tsuei, C. C., J. R. Kirtley, C. C. Chi, Lock See Yu-Jahnes, A. Gupta, T. Shaw, J. Z. Sun, and M. B. Ketchen, 1994, Phys. Rev. Lett. **73**, 593.

Tuominen, M., A. M. Goldman, Y. C. Chang, and P. Z. Jiang, 1990, Phys. Rev. B **42**, 8740.

Uemura, Y. J., G. M. Luke, B. J. Sternlieb, J. H. Brewer, J. F. Carolan, W. N. Hardy, R. Kadono, J. R. Kempton, R. F. Kiefl, S. R. Kreitzman, P. Mulhern, T. M. Riseman, D. Ll. Williams, B. X. Yang, S. Uchida, H. Takagi, J. Gopalakrishnan, A. W. Sleight, M. A. Subramanian, C. L. Chien, M. Z. Cieplak, Gang Xiao, V. Y. Lee, B. W. Statt, C. E. Stronach, W. J. Kossler, and X. H. Yu, 1989, Phys. Rev. Lett. **62**, 2317.

Urbach, J. S., W. R. White, M. R. Beasley, and A. Kapitulnik, 1992, Phys. Rev. Lett. **69**, 2407.

Usui, N., T. Ogasawara, and K. Yasukochi, 1968, Phys. Lett. A **27**, 140.

Usui, N., T. Ogasawara, K. Yasukochi, and S. Tomoda, 1969, J. Phys. Soc. Jpn. **27**, 574.

van Beelen, H., J. P. Van Braam Houckgeest, H. M. Thomas, C. Stolk, and R. De Bruyn Ouboter, 1967, Physica **36**, 241.

van der Beek, C. J., V. B. Geshkenbein, and V. M. Vinokur, 1993, Phys. Rev. B **48**, 3393.

van der Beek, C. J., and P. H. Kes, 1991, Phys. Rev. B **43**, 13 032.

van der Beek, C. J., P. H. Kes, M. P. Maley, M. J. V. Menken, and A. A. Menovsky, 1992, Physica C **192**, 307.

van der Beek, C. J., G. J. Nieuwenhuys, and P. H. Kes, 1991, Physica C **185-189**, 2241.

van der Beek, C. J., G. J. Nieuwenhuys, P. H. Kes, H. G. Schnack, and R. Griessen, 1992, Physica C **197**, 320.

Villain, J., 1986, Europhys. Lett. **2**, 871.

Vinen, W. F., 1969, in *Superconductivity*, edited by R. D. Parks (Marcel Dekker, New York), p. 1167.

Vinen, W. F., and A. C. Warren, 1967, Proc. Phys. Soc. London **91**, 409.

Vinnikov, L. Ya., L. A. Gurevich, G. A. Emelchenko, and Yu. A. Ossipyan, 1988, Solid State Commun. **67**, 421.

Vinnikov, L. Ya., I. V. Grigor'eva, L. A. Gurevich, and A. E. Koshelev, 1990, Sverkhprovodimost' Fiz. Khim. Tekh. **3**, 1434 [Supercond. Phys. Chem. Technol. **3**, 1121 (1990)].

Vinokur, V. M., 1993, Physica A **200**, 384.

Vinokur, V. M., M. V. Feigel'man, and V. B. Geshkenbein, 1991, Phys. Rev. Lett. **67**, 915.

Vinokur, V. M., M. V. Feigel'man, V. B. Geshkenbein, and A. I. Larkin, 1990, Phys. Rev. Lett. **65**, 259.

Vinokur, V. M., V. B. Geshkenbein, A. I. Larkin, and M. V. Feigel'man, 1991, Z. Eksp. Teor. Fiz. **100**, 1104 [Sov. Phys. JETP **73**, 610 (1991)].

Vinokur, V. M., V. B. Geshkenbein, M. V. Feigel'man, and G. Blatter, 1993, Phys. Rev. Lett. **71**, 1242.

Vinokur, V. M., L. B. Ioffe, A. I. Larkin, and M. V. Feigel'man, 1987, Zh. Eksp. Teor. Fiz. **93**, 343 [Sov. Phys. JETP **66**, 198 (1987)].

Vinokur, V. M., P. H. Kes, and A. E. Koshelev, 1990, Physica C **168**, 29.

Vlasko-Vlasov, V. K., L. A. Dorosinskii, A. A. Polyanskii, V. I. Nikitenko, U. Welp, B. W. Veal, and G. W. Crabtree, 1994, Phys. Rev. Lett. **72**, 3246.

Volovik, G. E., 1972, Pis'ma Zh. Eksp. Teor. Fiz. **15**, 116 [JETP Lett. **15**, 81 (1972)].

Volovik, G. E., 1993, Pis'ma Zh. Eksp. Teor. Fiz. **57**, 233 [JETP Lett. **57**, 244 (1993)].

Wallin, M., E. S. Sørensen, S. M. Girvin, and A. P. Young, 1994, Phys. Rev. B **49**, 12 115.

Weber, H., and H. J. Jensen, 1991, Phys. Rev. B **44**, 454.

Welp, U., W. K. Kwok, G. W. Crabtree, K. G. Vandervoort, and J. Z. Liu, 1989, Phys. Rev. Lett. **62**, 1908.

Weissman, M. B., N. E. Israeloff, and G. B. Alers, 1992, J. Magn. Magn. Mater. **114**, 87.

Wiegmann, P. B., 1978, J. Phys. C **11**, 1583.

White, W. R., A. Kapitulnik, and M. R. Beasley, 1991, Phys. Rev. Lett. **66**, 2826.

Wolf, D. E., and J. Kertész, 1987, Europhys. Lett. **4**, 651.

Wollman, D. A., D. J. Van Harlingen, W. C. Lee, D. M. Ginsberg, and A. J. Leggett, 1993, Phys. Rev. Lett. **71**, 2134.

Wördenweber, R., and P. H. Kes, 1985, Physica B **135**, 136.

Wördenweber, R., and P. H. Kes, 1986, Phys. Rev. B **34**, 494.

Wördenweber, R., and P. H. Kes, 1987, J. Low Temp. Phys. **67**, 1.

Worthington, T. K., M. P. A. Fisher, D. A. Huse, J. Toner, A. D. Marwick, T. Zabel, C. A. Feild, and F. H. Holtzberg, 1992, Phys. Rev. B **46**, 11 854.

Worthington, T. K., W. J. Gallagher, and T. R. Dinger, 1987, Phys. Rev. Lett. **59**, 1160.

Worthington, T. K., F. H. Holtzberg, and C. A. Feild, 1990, Cryogenics **30**, 417.

Worthington, T. K., E. Olsson, C. S. Nichols, T. M. Shaw, and D. R. Clarke, 1991, Phys. Rev. B **43**, 10 538.

Xing, L., and Z. Tešanović, 1990, Phys. Rev. Lett. **65**, 794.

Xu, Y., M. Suenaga, A. R. Moodenbaugh, and D. G. Welch, 1989, Phys. Rev. B **40**, 10 882.

Yeh, N.-C., D. S. Reed, W. Jiang, U. Kriplani, F. Holtzberg, A. Gupta, B. D. Hunt, R. P. Vasquez, M. C. Foote, and L. Bajuk, 1992, Phys. Rev. B **45**, 5654.

Yeh, N.-C., and C. C. Tsuei, 1989, Phys. Rev. B **39**, 9708.

Yeshurun, Y., and A. P. Malozemoff, 1988, Phys. Rev. Lett. **60**, 2202.

Yeshurun, Y., A. P. Malozemoff, F. H. Holtzberg, and T. R. Dinger, 1988, Phys. Rev. B **38**, 11 828.

Yeshurun, Y., A. P. Malozemoff, T. K. Worthington, R. M. Yandrofski, L. Krusin-Elbaum, F. H. Holtzberg, T. R. Dinger, and G. V. Chandrashekhar, 1989, Cryogenics **29**, 258.

Young, A. P., 1984, J. Phys. C **17**, L517.

Zavaritsky, V. N., 1992, in *Electronic Properties and Mechanisms of High-$T_c$ Superconductors*, edited by T. Oguchi, K. Kadowaki, and T. Sasaki (North-Holland, Amsterdam), p. 267.

Zavaritsky, V. N., and N. V. Zavaritsky, 1991, Physica C **185-189**, 2141.

Zeldov, E., A. I. Larkin, V. B. Geshkenbein, M. Konczykowski, D. Majer, B. Khaykovich, V. M. Vinokur, and H. Shtrikman, 1994, Phys. Rev. Lett. **73**, 1428.

Zeldov, E., N. M. Amer, G. Koren, A. Gupta, R. J. Gambino, and M. W. McElfresh, 1989, Phys. Rev. Lett. **62**, 3093.

Zhang, Y.-C., 1990, Phys. Rev. B **42**, 4897.